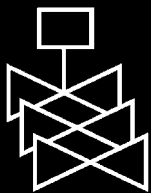
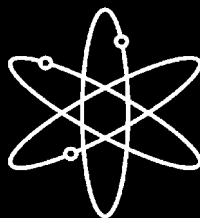
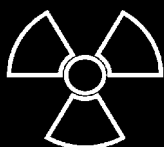
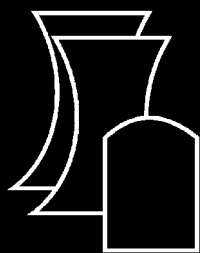


Thermal-Hydraulic Evaluation of Pressurized Thermal Shock



**U.S. Nuclear Regulatory Commission
Office of Nuclear Regulatory Research
Washington, DC 20555-0001**



AVAILABILITY OF REFERENCE MATERIALS IN NRC PUBLICATIONS

NRC Reference Material

As of November 1999, you may electronically access NUREG-series publications and other NRC records at NRC's Public Electronic Reading Room at <http://www.nrc.gov/reading-rm.html>.

Publicly released records include, to name a few, NUREG-series publications; *Federal Register* notices; applicant, licensee, and vendor documents and correspondence; NRC correspondence and internal memoranda; bulletins and information notices; inspection and investigative reports; licensee event reports; and Commission papers and their attachments.

NRC publications in the NUREG series, NRC regulations, and Title 10, Energy, in the *Code of Federal Regulations* may also be purchased from one of these two sources:

1. The Superintendent of Documents
U.S. Government Printing Office
Mail Stop SSOP
Washington, DC 20402-0001
Internet: bookstore.gpo.gov
Telephone: 202-512-1800
Fax: 202-512-2250
2. The National Technical Information Service
Springfield, VA 22161-0002
www.ntis.gov
1-800-553-6847 or, locally, 703-605-6000

A single copy of each NRC draft report for comment is available free, to the extent of supply, upon written request as follows:

Address: Office of the Chief Information Officer
Reproduction and Distribution
Services Section
U.S. Nuclear Regulatory Commission
Washington, DC 20555-0001

Email: DISTRIBUTION@nrc.gov
Facsimile: 301-415-2289

Some publications in the NUREG series that are posted at NRC's Web site address <http://www.nrc.gov/reading-rm/doc-collections/nuregs> are updated periodically and may differ from the last printed version. Although references to material found on a Web site bear the date the material was accessed, the material available on the date cited may subsequently be removed from the site.

Non-NRC Reference Material

Documents available from public and special technical libraries include all open literature items, such as books, journal articles, and transactions, *Federal Register* notices, Federal and State legislation, and Congressional reports. Such documents as theses, dissertations, foreign reports and translations, and non-NRC conference proceedings may be purchased from their sponsoring organization.

Copies of industry codes and standards used in a substantive manner in the NRC regulatory process are maintained at—

The NRC Technical Library
Two White Flint North
11545 Rockville Pike
Rockville, MD 20852-2738

These standards are available in the library for reference use by the public. Codes and standards are usually copyrighted and may be purchased from the originating organization or, if they are American National Standards, from—

American National Standards Institute
11 West 42nd Street
New York, NY 10036-8002
www.ansi.org
212-642-4900

Legally binding regulatory requirements are stated only in laws; NRC regulations; licenses, including technical specifications; or orders, not in NUREG-series publications. The views expressed in contractor-prepared publications in this series are not necessarily those of the NRC.

The NUREG series comprises (1) technical and administrative reports and books prepared by the staff (NUREG-XXXX) or agency contractors (NUREG/CR-XXXX), (2) proceedings of conferences (NUREG/CP-XXXX), (3) reports resulting from international agreements (NUREG/IA-XXXX), (4) brochures (NUREG/BR-XXXX), and (5) compilations of legal decisions and orders of the Commission and Atomic and Safety Licensing Boards and of Directors' decisions under Section 2.206 of NRC's regulations (NUREG-0750).

Thermal-Hydraulic Evaluation of Pressurized Thermal Shock

Manuscript Completed: April 2005

Date Published: May 2005

Prepared by
David E. Bessette
Advanced Reactors and Regulatory Effectiveness Branch
Division of Systems Analysis and Regulatory Effectiveness
Office of Nuclear Regulatory Research
U.S. Nuclear Regulatory Commission
Washington, DC 20555-0001

William Arcieri, C. Don Fletcher, and Robert Beaton
Information Systems Laboratories, Inc.
11140 Rockville Pike
Rockville, MD 20852

David E. Bessette, NRC Project Manager

Prepared for
Division of Systems Analysis and Regulatory Effectiveness
Office of Nuclear Regulatory Research
U.S. Nuclear Regulatory Commission
Washington, DC 20555-0001



ABSTRACT

In 2000, the U.S. Nuclear Regulatory Commission began a new research program to develop the technical basis for revising the Pressurized Thermal Shock (PTS) rule, set forth in Title 10, Section 50.61, of the Code of Federal Regulations (10 CFR 50.61). Since the first research program in the early 1980s, analytical methods have continued to improve allowing for more realistic analysis of PTS risk. The research program was coordinated among probabilistic fracture mechanics, probabilistic risk assessment, and thermal-hydraulics analysts. The thermal-hydraulic analysis was performed with the Fifth Version of the Reactor Excursion and Leak Analysis Program (RELAP5) code. Thermal-hydraulic information was supplied by RELAP5 as boundary conditions to the Fracture Analysis of Vessels: Oak Ridge (FAVOR) probabilistic fracture mechanics analysis code. An accompanying effort was made to demonstrate the applicability and uncertainty of RELAP5 to calculate a broad spectrum of transients of possible PTS significance. Assessment of RELAP5 to specific PTS applications was performed and showed the code to be applicable and to be reasonably accurate. Uncertainty in the code calculations was also quantified and the main source of uncertainty to the thermal-hydraulic analyses was from plant boundary conditions rather than from physical models in the code. This report demonstrates the applicability and uncertainty of RELAP5 for PTS applications.

FOREWORD

The reactor pressure vessel is exposed to neutron radiation during normal operation. Over time, the vessel steel becomes progressively more brittle in the region adjacent to the core. If a vessel had a preexisting flaw of critical size *and* certain severe system transients occurred, this flaw could propagate rapidly through the vessel, resulting in a through-wall crack. The severe transients of concern, known as pressurized thermal shock (PTS), are characterized by rapid cooling (i.e., thermal shock) of the internal reactor pressure vessel surface that may be combined with repressurization. The simultaneous occurrence of critical-size flaws, embrittled vessel, and a severe PTS transient is a very low probability event. The current study shows that U.S. pressurized-water reactors do not approach the levels of embrittlement to make them susceptible to PTS failure, even during extended operation well beyond the original 40-year design life.

Advancements in our understanding and knowledge of materials behavior, our ability to realistically model plant systems and operational characteristics, and our ability to better evaluate PTS transients to estimate loads on vessel walls have shown that earlier analyses, performed some 20 years ago as part of the development of the PTS rule, were overly conservative, based on the tools available at the time. Consistent with the NRC's Strategic Plan to use best-estimate analyses combined with uncertainty assessments to resolve safety-related issues, the NRC's Office of Nuclear Regulatory Research undertook a project in 1999 to develop a technical basis to support a risk-informed revision of the existing PTS Rule, set forth in Title 10, Section 50.61, of the *Code of Federal Regulations* (10 CFR 50.61).

Two central features of the current research approach were a focus on the use of realistic input values and models and an *explicit* treatment of uncertainties (using currently available uncertainty analysis tools and techniques). This approach improved significantly upon that employed in the past to establish the existing 10 CFR 50.61 embrittlement limits. The previous approach included unquantified conservatisms in many aspects of the analysis, and uncertainties were treated *implicitly* by incorporating them into the models.

This report is one of a series of 21 reports that provide the technical basis that the staff will consider in a potential revision of 10 CFR 50.61. The risk from PTS was determined from the integrated results of the Fifth Version of the Reactor Excursion and Leak Analysis Program (RELAP5) thermal-hydraulic analyses, fracture mechanics analyses, and probabilistic risk assessment. As part of the integrated PTS reevaluation, the RELAP5 code was used to calculate the thermal-hydraulic response of three nuclear power plants of the three pressurized water reactor vendors for a wide range of transients and accidents. The RELAP5 calculations provided boundary conditions to the fracture mechanics analyses. This report addresses the main issues involving the accuracy and uncertainty in the application of RELAP5 for determining the boundary conditions to the fracture mechanics analysis. The results showed that RELAP5 can be used with confidence for calculating plant responses to PTS transients.



Brian W. Sheron, Director
Office of Nuclear Regulatory Research
U.S. Nuclear Regulatory Commission

CONTENTS

	Page
Abstract	iii
Foreword	v
Executive Summary	xiii
Abbreviations	xvii
Nomenclature	xix
1. Introduction	1-1
1.1 Purpose and Summary	1-1
1.2 Report Organization	1-4
1.3 Interface Between Thermal-Hydraulics, Fracture Mechanics, and Probabilistic Risk Assessment	1-6
1.4 Modeling Issues	1-9
2. Thermal-Hydraulic Analysis Overview	2-1
2.1 Top-Down Scaling Approach	2-1
2.2 PTS Figure of Merit	2-2
2.3 Vessel Time Constants	2-4
3. Thermal-Hydraulic Phenomenology	3-1
3.1 Overview	3-1
3.2 Energy and Inventory	3-3
3.3 Classification of PTS Scenarios	3-10
3.4 LOCA-Induced Cooling of the Reactor Coolant System Scenario Description .	3-11
3.4.1 Cold Leg Behavior	3-13
3.4.2 Downcomer Behavior	3-19
3.4.3 Secondary Side Induced Cooling of the Reactor Coolant System . .	3-19
4. RELAP5 Assessment and Uncertainties for PTS Analyses	4-1
4.1 Introduction	4-1
4.2 Thermal-Hydraulic Parameters of Interest	4-2
4.3 Employment of the Experiments for the Assessments	4-3
4.4 Assessments Performed	4-4
4.5 Assessment Results: Reactor Vessel Downcomer Pressure	4-6
4.6 Assessment Results: Reactor Vessel Downcomer Fluid Temperature	4-8

4.7	Assessment Results: Reactor Vessel Wall Inside-Surface Heat Transfer Coefficient	4-10
4.7.1	Effect of Heat Transfer Coefficient on Wall Heat Flux	4-11
4.7.2	Comparison of Measured and RELAP5-Calculated Reactor Vessel Wall Heat Transfer Data	4-12
4.7.3	Comparison of RELAP5-Calculated and CFD-Calculated Downcomer Flows	4-21
4.7.4	Sensitivity of Fracture Mechanics Results to Variations in the Fluid Cooldown Rate and Heat Transfer Coefficient	4-21
4.8	Other Assessment and Uncertainty Topics	4-21
4.8.1	PTS Phenomena Identification and Ranking Table	4-22
4.8.2	Use of Thermal-Hydraulic Uncertainties in Developing Event Sequence Bins	4-24
4.9	Assessment Conclusions	4-24
5.	Uncertainty Effects of Thermal-Hydraulic Boundary Conditions	5-1
5.1	Objective	5-1
5.2	Results	5-2
5.3	Impact of Uncertainties in Calculated Boundary Conditions	5-3
5.3.1	Pressure	5-12
5.3.2	Heat Flux	5-12
5.4	Sensitivity Studies on the Impact of Heat Flux	5-14
5.4.1	Effect of h on Wall-to-Fluid ΔT	5-14
5.4.2	Sensitivity Study on $h_{dc}(t)$	5-16
5.4.3	Sensitivity Study Varying Both $T_{dc,f}(t)$ and $h_{dc}(t)$	5-16
5.5	Sensitivity of Probabilistic Fracture Mechanics Analysis Results to Imposed Thermal Plumes in the Downcomer	5-18
6.	Conclusions	6-1
7.	References	7-1

Appendices

	<u>Page</u>
A. RELAP5 Modeling for PTS Analysis	A-1
B. Fluid Temperature Distribution in the Downcomer	B-1
C. Numerics	C-1
D. Qualitative Assessment Criteria	D-1
E. RELAP5 Assessment Comparisons for Reactor Vessel Downcomer Pressure and Fluid Temperature	E-1
F. Wall Heat Transfer Modeling in RELAP5	F-1
G. Effect of Heat Transfer Coefficient on Wall Heat Flux	G-1
H. Comparison of Measured and RELAP5-Calculated Reactor Vessel Wall Heat Transfer	H-1
I. Comparison of RELAP5-Calculated and CFD-Calculated Downcomer Flows ...	I-1
J. Sensitivity of Fracture Mechanics Results to Variations in the Fluid Cooldown Rate and Heat Transfer Coefficient	J-1
K. PTS Phenomena Identification and Ranking Table	K-1
L. Use of Thermal-Hydraulic Uncertainties in Developing Event Sequence Bins .	L-1
M. Examples of Combined Thermal-Mechanical Results	—1
N. Applicability of 1994 FAVOR Results to Current PTS Reevaluation	—1

Figures

		<u>Page</u>
1-1	Basic Flow Diagram for PTS Analysis	1-7
2-1	FAVOR Computational Modules and Data Flow.	2-4
2-2	Conditional Probability of Failure as a Function of RT_{PTS}	2-5
2-3	Distribution of Depths at Which Cracks Initiate (FAVOR Version 3.1)	2-7
2-4	Vessel Wall Temperature Profile for Short Time Intervals Wall Boundary $T=20\text{ }^{\circ}\text{C}$ Applied	2-10
2-5	Vessel Wall Temperature Profile for Long Time Intervals Wall Boundary $T=20\text{ }^{\circ}\text{C}$ Applied	2-10
3-1	Conditional Probability of Failure as a Function of Break Size (Border Between Slow and Fast Transients is ~ 6 inches)	3-3
3-2	Effect of Break Size on Time to Vessel Failure	3-4
3-3	Temperature-Pressure Characteristics of Transients Contributing to Probability of Failure	3-4
3-4	Simplified Representation of the Reactor Coolant System Control Volume (Top-Down) Approach to System Evaluation	3-6
3-5	Natural Circulation Flow as a Function of Decay Heat Level	3-10
3-6	RCS Pressure as a Function of Break Size for Oconee	3-11
3-7	Palisades 2-inch Hot Leg Break	3-12
3-8	Schematic of B&W Design Showing Local Phenomena in Cold Leg and Downcomer .	3-15
3-9	Regional Mixing Model	3-17
3-10	Comparison of RELAP5 Calculation of Downcomer Temperature to Exponential Decay Function	3-18
4-1	UPTF 1-21 Downcomer Velocities at Bottom-Core Elevation Measured, Turbine Meters, Clockwise from Cold Leg 2	4-15
4-3	UPTF 1-21 Wall Temperature Minus Fluid Temperature Under Cold Leg 2 at Core-Top Elevation	4-17
4-4	UPTF Test 1-21 Wall Temperatures at 25 mm Depth Vessel Wall in Orientation of Cold Leg 2	4-18
4-5	APEX-CE-5 Measured and RELAP5 Fluid Temperatures 4D Below and Centered on the Cold Leg 4 Nozzle	4-20
4-6	APEX-CE-5 Measured and RELAP5 Wall Temperatures 4D Below and Centered on the Cold Leg 4 Nozzle	4-20
4-7	Creare Data Compared to Dittus-Boelter	4-21

5-1	Relationship Between PRA (Event Frequency) Uncertainty, Binning Process Uncertainty, and Thermal-Hydraulic Epistemic Uncertainty	5-3
5-2	Palisades Small-Break LOCA Bin	5-5
5-3	Palisades Medium-Break LOCA Bin	5-5
5-4	Oconee Small-Break LOCA Bin	5-6
5-5	Oconee Medium-Break LOCA Bin	5-6
5-6	Beaver Valley Small-Break LOCA Bin	5-7
5-7	Beaver Valley Medium-Break LOCA Bin	5-7
5-8	Oconee Stuck-Open SRV Bin (Full-Power)	5-8
5-9	Oconee Stuck-Open SRV Bin (Low-Power)	5-8
5-10	Beaver Valley Stuck-Open SRV Bin (1 and 2 Valves)	5-9
5-11	Cooldown Transients for Palisades	5-17
5-12	Plume Strengths Used in Sensitivity Study	5-20
5-13	Effect of Plumes on Conditional Probability of Vessel Failure	5-21

Tables

	<u>Page</u>	
1-1	Report Organization with Descriptions of Chapters and Appendices	1-4
1-2	Thermal-Hydraulic Phenomena Identified by the PTS PIRT	1-9
2-1	Methodology for Hierarchical Two-Tiered Scaling Analysis	2-1
3-1	Energy Source/Sink Magnitudes for Oconee	3-12
3-2	Classification of Two-Phase Transients	3-13
4-1	Experimental Facilities Used for Assessment	4-4
4-2	Statistical Evaluation of Assessment Results for Pressure	4-7
4-3	Statistical Evaluation of Assessment Results for Downcomer Fluid Temperature	4-9
4-4	Abbreviated PIRT for the Current PTS Thermal-Hydraulic Analyses	4-24
5-1	PWR LOCA Frequencies	5-3
5-2	Comparison of LOCA Frequencies	5-4
5-3	Range of Temperature and Pressure Variation Within Bins	5-4
5-4	Palisades Transients Used as Basis for Sensitivity Studies	5-13
5-5	Summary of Effect of h on ΔT	5-13
5-6	Effect of h on ΔT	5-13
5-7	Percent Contribution of Individual Transients to TWCF and CPF (60 EFPY)	5-15

5-8	Sensitivity Analysis for Exponential Temperature Decay Transients Solution	5-16
5-9	Sensitivity Studies on Plumes	5-18
5-10	Plume Strengths Observed in Experimental Facilities	5-19

EXECUTIVE SUMMARY

This report demonstrates the applicability and uncertainty of the Fifth Version of the Reactor Excursion and Leak Analysis Program (RELAP5) thermal-hydraulic modeling computer code for performing pressurized thermal shock (PTS) analysis. This conclusion is based on four key analysis results:

- (1) Event sequence selection uncertainty dominates the calculation of vessel failure probabilities.
- (2) The methodology used for event sequence selection is sound.
- (3) Thermal-hydraulic code calculations predict PTS conditions within an acceptable band of uncertainty and are realistic in nature.
- (4) Data used to benchmark thermal-hydraulic codes for PTS are extensive, appropriate, and of high quality.

These four key analysis results represent the culmination of 5 years of research in the Office of Nuclear Regulatory Research. This research was motivated by the fact that new information has resulted in improved analytical capability to evaluate PTS events since the NRC completed its previous integrated PTS study in 1984. This includes improved embrittlement correlations; greatly improved knowledge to estimate original flaw density, size, orientation, and distribution; and refinement of the Fracture Analysis of Vessels: Oak Ridge (FAVOR) probabilistic fracture mechanics analysis code. In the intervening years, advances were also made in probabilistic risk assessment (PRA) and thermal-hydraulics, such as improved understanding of criteria for flow interruption and stagnation (including fluid mixing behavior in the downcomer). The PTS reevaluation work is intended to provide technical basis to support revision of relevant NRC regulations and regulatory guidance. The following paragraphs will describe the methodology employed by the staff to analyze PTS and how each four key analysis results were arrived at.

The staff used an iterative and integrated analysis methodology to evaluate the consequences of PTS on the conditional probability of failure (CPF) of the reactor vessel. The PTS evaluation procedure included four main components:

- (1) A PRA was conducted to identify event sequences that could lead to PTS of the reactor vessel, and those event sequences were binned into common families of similar events.
- (2) The RELAP5 Mod. 3.2 thermal-hydraulics code was used to analyze conditions in the reactor vessel downcomer for the binned sequences of interest, which was then supplied as input to the fracture mechanics evaluation of the reactor vessel.
- (3) The Fracture Analysis of Vessels: Oak Ridge (FAVOR) probabilistic fracture mechanics analysis code was used to calculate the CPFs for each binned sequence of interest.
- (4) An uncertainty analysis was conducted in parallel to guide selection of boundary conditions and quantify the bias and uncertainty in the code calculation results.

Event sequence selection uncertainty dominates the calculation of vessel failure probabilities

The University of Maryland performed an uncertainty evaluation of the RELAP5 calculations to derive the required uncertainty estimates for the calculated parameters of temperature, pressure, and heat transfer. The range of thermal-hydraulic conditions in a given bin is much larger than the RELAP5 physical modeling uncertainty. That is, the aleatory part of the problem dominates over the epistemic. The boundary conditions (aleatory), such as break flow, therefore, are the principal source of uncertainty. For example, the factor of 10 range in break size within a given bin overwhelms other sources of uncertainty contributed by physical models in RELAP5 (epistemic). The challenge in this problem, therefore, was not in the thermal-hydraulic modeling of the system, rather, it was in selecting the transients and boundary conditions that cover all the possibilities that can lead to failure of the vessel.

The methodology used for event sequence selection is sound

Plant behavior is adequately resolved from the number of thermal-hydraulic calculations and corresponding bins defined by the PRA. A close relationship between the PRA binning process and thermal-hydraulic uncertainty analysis was maintained throughout this study. The definition of bins was achieved through an interactive feedback between PRA and thermal-hydraulics analysts.

Thermal-hydraulic code calculations predict PTS conditions within an acceptable band of uncertainty and are realistic in nature

RELAP5 was able to adequately predict downcomer fluid temperature, pressure, and heat transfer coefficient (HTC) based on comparisons between code results and facility data. The comparisons of RELAP5 with data yielded the following findings:

Pressure:	bias (RELAP5 - Experiment) = -0.093 MPa (-13 psi)
	standard deviation (1σ) = 0.32 MPa (46 psi)
Temperature:	bias (RELAP5 - Experiment) = -1 °C (2 °F)
	standard deviation (1σ) = 10 °C (18 °F)
HTC:	bias (RELAP5 - Experiment) = 1114 W/m ² -K
	standard deviation (1σ) = 1389 W/m ² -K

Since RELAP5 was developed and validated for use in thermal-hydraulic accident scenarios involving rapid primary system cooldown such as a loss-of-coolant accident (LOCA), it was well suited for use to analyze potential PTS scenarios. Pressurized thermal shock is most likely to be initiated by a LOCA or similar transient such as a Main Steam Line Break. RELAP5 and its supporting experimental data base were design for analyses under the conditions found in LOCAs. Because of the nature of the PTS transients, the uncertainties found in typical LOCA analysis of peak cladding temperature are larger than those found in PTS transients. This is largely because the conditions in the downcomer are basically single phase for the most part of the PTS transient and these conditions are far easier to predict.

The RELAP5 models, which used two-dimensional downcomer nodalization was found appropriate for modeling the downcomer behavior. Consistent nodalization was used for the three plant models, as well as the various experimental facilities used to assess RELAP5, which included the Upper Plenum Test Facility (UPTF), Loss-of-Fluid Test (LOFT) Facility, Rig of Safety Assessment (ROSA), Advanced Plant Experiment Facility (APEX), and Creare.

Based on the uncertainty in the RELAP5 prediction of nominal downcomer temperature, we defined a plume as a temperature variation of greater than 10 °C (20 °F), which was the 1 σ uncertainty in RELAP5. Temperature variations (circumferentially or axially) of less than this number are not significant to the analysis because they fall within the nominal predictive capability of RELAP5. That is, such temperature variations are less than the standard deviation of RELAP5 comparisons with experimental data. Review of integral system test data showed no temperature variations (i.e., variations <10 °C), either axially or azimuthally, in the downcomer that exceeded the predictive capability of RELAP5. Integral test facilities exhibit additional driving forces for mixing that are not present in separate effects tests. In addition, sensitivity studies performed with stronger plumes showed little impact on the probability of vessel failure.

Data used to benchmark thermal-hydraulic codes for PTS are extensive, appropriate, and of high quality

RELAP5 was assessed against a wide variety of integral system test data from UPTF, LOFT, ROSA, APEX, and the Multi-Loop Integral System Test (MIST). The APEX facility at Oregon State University was used to generate PTS-specific experimental data. This was a new experimental program to generate both integral and separate effects data in an integral facility. The information generated on loop flow stagnation, cold leg stratification, and downcomer mixing allowed better justification of the treatment of downcomer flows using RELAP5. The UPTF, LOFT, ROSA, APEX, and MIST facilities are geometrically similar to the three pressurized-water reactor vendor designs analyzed in this study. Power-to-volume scaling of 1:1 was used for all the integral test facilities. The geometric similitude and the energy/inventory (power-to-volume) scaling ensured that the experiments provided prototypic data for PTS. This ensured that the experiments provided prototypic data for PTS applications. A set of experiments was chosen that included scenarios similar to the risk-dominant PTS sequences.

The experiments consistently show large thermal stratification in the cold leg, however, these temperature differences do not carry over into the downcomer. Strong mixing occurs as the flow enters the downcomer from the cold leg as a result of buoyancy-driven flows in the downcomer. Based on data from three different facilities (UPTF, APEX-CE, and Creare), downcomer mass flows exceed the emergency core cooling (ECC) injection flows by a factor of 20. The flows calculated by RELAP5 for UPTF and APEX-CE are consistent with the experimental data. The HTCs that RELAP5 calculated for these two facilities either agree with those derived from the experimental data, or are conservative with respect to the data.

ABBREVIATIONS

ADS	Automatic Depressurization System
ADV	Atmospheric Dump Valve
APEX	Advanced Plant Experiment
B&W	Babcock and Wilcox
CE	Combustion Engineering
CFD	Computational Fluid Dynamics
CFR	<i>Code of Federal Regulations</i>
CL	Cold Leg
CMT	Core Makeup Tank
CPF	Conditional Probability of Failure
CSAU	Code Scaling, Applicability, and Uncertainty
ECC	Emergency Core Cooling
EFPY	Effective Full-Power Year(s)
FAVOR	Fracture Analysis of Vessels: Oak Ridge
Fo	Fourier Number
H2TS	Hierarchal Two-Tiered Scaling
HL	Hot Leg
HPI	High-Pressure Injection
HTC	Heat Transfer Coefficient
IPTS	Integrated Pressurized Thermal Shock
LOCA	Loss-of-Coolant Accident
LOFT	Loss-of-Fluid Test
LPI	Low-Pressure Injection
MBLOCA	Medium-Break Loss-of-Coolant Accident
MSLB	Main Steam Line Break
MIST	Multi-Loop Integral System Test
ORNL	Oak Ridge National Laboratory
PIRT	Phenomena Identification and Ranking Table
PORV	Power-Operated Relief Valve
PRA	Probabilistic Risk Assessment
PTS	Pressurized Thermal Shock
PWR	Pressurized-Water Reactor
RCP	Reactor Coolant Pump
RCS	Reactor Coolant System
RELAP	Reactor Excursion Leak and Analysis Program
ROSA	Rig of Safety Assessment
RT	Reference Temperature
SBLOCA	Small-Break Loss-of-Coolant Accident
SG	Steam Generator
SRV	Safety/Relief Valve
TWCF	Through-Wall Cracking Frequency
UPTF	Upper Plenum Test Facility

NOMENCLATURE

α	thermal diffusivity, m^2/s
β	bulk coefficient of expansion, $1/\text{C}$
μ	dynamic viscosity, $\text{kg}/\text{m}\cdot\text{s}$
ν	kinematic viscosity, m^2/s
ρ	density, kg/m^3
σ	stress, kg/ms^2
σ	standard deviation
τ	characteristic time
Δ	difference
C_p	heat capacity, $\text{m}^2/\text{s}^2\cdot\text{C}$
g	gravitational acceleration, m/s^2
h	convective heat transfer coefficient, $\text{W}/\text{m}^2\cdot\text{C}$
h	enthalpy, J/kg (m^2/s^2)
D	diameter, m
F	Fahrenheit
J	joules, $\text{kg}\cdot\text{m}^2/\text{s}^2$
K	Stress factor
k	conductivity, $\text{W}/\text{m}\cdot\text{C}$
l	length, m
P	pressure, $\text{kg}/\text{m}\cdot\text{s}^2$
Q	Volumetric flow, m^3/s
q	heat flux, W/m^2
s	seconds
t	thickness, m
t	time, s
u	velocity, m/s
T	temperature, C
W	mass flow, kg/s
W	watts, $\text{kg}\cdot\text{m}^2/\text{s}^3$

Subscripts

f	fluid
l	liquid
w	wall

1. INTRODUCTION

1.1 Purpose and Summary

This report demonstrates the applicability and uncertainty of the Fifth Version of the Reactor Excursion and Leak Analysis Program (RELAP5) thermal-hydraulic modeling computer code for performing pressurized thermal shock (PTS) analyses. As part of establishing the validation of RELAP5 for PTS applications, the report discusses several important thermal-hydraulic phenomenon and uncertainty considerations that contributed to the determination. This includes the investigation of the controlling thermal-hydraulic processes important to PTS, quantifying the uncertainties of RELAP5 and evaluating their impact, use of consistent noding between the three plant analyses and the code assessment, and determining the impact of simplifying assumptions such as temperature distributions in the downcomer.

The thermal-hydraulic analysis to support the PTS reevaluation centered on the application of RELAP5 to characterize a large number of potential PTS scenarios identified by probabilistic risk assessment (PRA). These calculations provided boundary conditions to the probabilistic fracture mechanics analyses. RELAP5 is highly flexible, and is designed to be applicable to the entire spectrum of postulated scenarios to which it was applied. The challenge rested with establishing the applicability and uncertainty of RELAP5 for calculating downcomer conditions, for the very broad spectrum of postulated scenarios. Establishing code applicability and uncertainty for PTS was in distinct contrast to past thermal-hydraulic uncertainty studies, which have been scenario-specific.

All PTS transients involve relatively rapid cooling of the reactor vessel. The original Integrated PTS (IPTS) study conducted in the early 1980s focused on transients that remained at relatively high pressure, based on the assumption that pressure was required to drive a crack all the way through the wall. The largest loss-of-coolant accidents (LOCAs) treated were small breaks up to 2 inches.

The current evaluation began with the same premise; however, it gradually became apparent that the conditional probability of failure (CPF) predicted for the reactor vessel was continuing to increase with break size. Therefore, the range of breaks was extended to include the full spectrum of LOCAs. Additionally, high-pressure scenarios involving reclosure of a stuck-open pressurizer valve received increased attention. In all, far more sequences (i.e., at least an order of magnitude) were analyzed with RELAP5 and the Fracture Analysis of Vessels: Oak Ridge (FAVOR) probabilistic fracture mechanics analysis code than in the IPTS study.

Similar to the IPTS study, the current effort focused on three plants from the three pressurized-water reactor (PWR) vendors:

- (1) Oconee-1 has the most embrittled of Babcock and Wilcox (B&W) reactors.
- (2) Palisades is a Combustion Engineering (CE) design that is of current interest from the perspective of the present PTS screening criteria.
- (3) Beaver Valley is a Westinghouse three-loop plant similar in design to H.B. Robinson, but with a more embrittled vessel.

Overall results from the PTS reevaluation are described in [1], including thermal-hydraulics, fracture mechanics, and PRA. This report is one of six supporting reports providing additional information on the thermal-hydraulics contributions. The conclusion that RELAP5 is applicable for use in analyzing PTS is based on the following four key analysis results:

- (1) Event sequence selection uncertainty dominates the calculation of vessel failure probabilities.
- (2) The methodology used for event sequence selection is sound.
- (3) Thermal-hydraulic code calculations predict PTS conditions within an acceptable band of uncertainty and are realistic in nature.
- (4) Data used to benchmark thermal-hydraulic codes for PTS are extensive, appropriate, and of high quality.

Event sequence selection uncertainty dominates the calculation of vessel failure probabilities

The University of Maryland performed an uncertainty evaluation of the RELAP5 calculations [2] to derive the required uncertainty estimates for the calculated parameters of temperature, pressure, and heat transfer. The range of thermal-hydraulic conditions in a given bin specified by the PRA group is much larger than the RELAP5 physical modeling uncertainty. That is, the aleatory part of the problem dominates over the epistemic. The boundary conditions (aleatory), such as break flow, therefore, are the principal source of uncertainty. For example, the factor of 10 range in break size within a given bin overwhelms other sources of uncertainty contributed by physical models in RELAP5 (epistemic). The challenge in this problem, therefore, was not in the thermal-hydraulic modeling of the system, rather, it was in selecting the transients and boundary conditions that cover all the possibilities that can lead to failure of the vessel.

The methodology used for event sequence selection is sound

Plant behavior is adequately resolved from the number of thermal-hydraulic calculations and corresponding bins defined by the PRA. A close relationship between the PRA binning process and thermal-hydraulic uncertainty analysis was maintained throughout this study. The definition of bins was achieved through an interactive feedback between PRA and thermal-hydraulics analysts.

Thermal-hydraulic code calculations predict PTS conditions within an acceptable band of uncertainty and are realistic in nature.

RELAP5 was able to adequately predict downcomer fluid temperature, pressure, and heat transfer coefficient (HTC) based on comparisons between code results and facility data. The comparisons of RELAP5 with data yielded the following findings:

Pressure:	bias (RELAP5 - Experiment) = -0.093 MPa (-13 psi)
	standard deviation (1σ) = 0.32 MPa (46 psi)
Temperature:	bias (RELAP5 - Experiment) = -1 °C (2 °F)
	standard deviation (1σ) = 10 °C (18 °F)
HTC:	bias (RELAP5 - Experiment) = 1114 W/m ² -K
	standard deviation (1σ) = 1389 W/m ² -K

Since RELAP5 was developed and validated for use in thermal-hydraulic accident scenarios involving rapid primary system cooldown such as a LOCA, it was well suited for use to analyze potential PTS scenarios. Pressurized thermal shock is most likely to be initiated by a LOCA or similar transient such as a main steam line break. RELAP5 and its supporting experimental data base were design for analyses under the conditions found in LOCAs. Because of the nature of the PTS transients, the uncertainties found in typical LOCA analysis of peak cladding temperature are larger than those found in PTS transients. This is largely because the conditions in the downcomer are basically single phase for the most part of the PTS transient and these conditions are far easier to predict.

The RELAP5 models, which used two-dimensional downcomer nodalization was found appropriate for modeling the downcomer behavior. Consistent nodalization was used for the three plant models, as well as the various experimental facilities used to assess RELAP5, which included the Upper Plenum Test Facility (UPTF), Loss-of-Fluid Test (LOFT) Facility, Rig of Safety Assessment (ROSA), Advanced Plant Experiment Facility (APEX), and Creare.

Based on the uncertainty in the RELAP5 prediction of nominal downcomer temperature, we defined a plume as a temperature variation of greater than 10 °C (20 °F), which was the 1 σ uncertainty in RELAP5. Temperature variations (circumferentially or axially) of less than this number are not significant to the analysis because they fall within the nominal predictive capability of RELAP5. That is, such temperature variations are less than the standard deviation of RELAP5 comparisons with experimental data.

Review of integral system test data showed no temperature variations (i.e., variations <10 °C), either axially or azimuthally, in the downcomer that exceeded the predictive capability of RELAP5. Integral test facilities exhibit additional driving forces for mixing that are not present in separate effects tests. In addition, sensitivity studies performed with stronger plumes showed little impact on the probability of vessel failure.

Data used to benchmark thermal-hydraulic codes for PTS are extensive, appropriate, and of high quality

RELAP5 was assessed against a wide variety of integral system test data from UPTF, LOFT, ROSA, APEX, and the Multi-Loop Integral System Test (MIST). The APEX facility at Oregon State University was used to generate PTS-specific experimental data [3, 4]. This was a new experimental program to generate both integral and separate effects data in an integral facility.

The information generated on loop flow stagnation, cold leg stratification, and downcomer mixing allowed better justification of the treatment of downcomer flows using RELAP5. The UPTF, LOFT, ROSA, APEX, and MIST facilities are geometrically similar to the three PWR vendor designs analyzed in this study. Power-to-volume scaling of 1:1 was used for all the integral test facilities. The geometric similitude and the energy/inventory (power-to-volume) scaling ensured that the experiments provided prototypic data for PTS. This ensured that the experiments provided prototypic data for PTS applications. A set of experiments was chosen that included scenarios similar to the risk-dominant PTS sequences.

The experiments consistently show large thermal stratification in the cold leg (up to 200C), however, these temperature differences do not carry over into the downcomer. Strong mixing occurs as the flow enters the downcomer from the cold leg as a result of buoyancy-driven flows in the downcomer. Based on data from three different facilities (UPTF, APEX-CE, and Creare), Downcomer flow rates in the experiments were a factor of 20 greater than the emergency core cooling (ECC) injection flow rates. Applying the ratio of mass flows to the maximum value of cold leg stratification, as follows:

$$\frac{\dot{m}_{ECC}}{\dot{m}_{dc}} \times 200C = 10C$$

yields values of maximum downcomer temperature variation comparable to the maximum observed in experiments. The flows calculated by RELAP5 for UPTF and APEX-CE are consistent with the experimental data. The HTCs that RELAP5 calculated for these two facilities either agree with those derived from the experimental data, or are conservative with respect to the data.

1.2 Report Organization

This report is organized into seven Chapters and thirteen Appendices. The seven chapters in the main body of this report provide a high-level view of the comprehensive thermal-hydraulic and uncertainty analyses, while the Appendices provide the technical details by which the key analysis results were obtained. Table 1-1 is a list of the Chapters and Appendices that comprise this report with short descriptions of their contents.

Table 1-1 Report Organization with Descriptions of Chapters and Appendices

Section	Description
Chapter 1	Background to the current PTS investigation, including a description of the interface between the three main components of the analysis (i.e., thermal-hydraulics, fracture mechanics, and probabilistic risk assessment)
Chapter 2	Overview of PTS thermal-hydraulic phenomenology and modeling issues. A scenario description is provided for the main contributors to PTS risk. The modeling of PTS scenarios is presented from the standpoint of energy and inventory, and the control volume approach to analyzing thermodynamic problems. Key RELAP5 modeling issues are summarized.
Chapter 3	Summary of the general phenomenology associated with the thermal-hydraulic evaluation of PTS.
Chapter 4	RELAP5 assessment and uncertainty performed for the three thermal-hydraulic figures of merit. Comparisons are made to integral system experimental data. Specific comparisons of RELAP5 to experimental data are shown. Sensitivity studies are presented to illustrate the significance of downcomer heat transfer uncertainties.
Chapter 5	Summary of the uncertainties in the thermal-hydraulic boundary conditions, relating them to their impact on the probability of vessel failure, and to uncertainties in PRA event frequencies.
Chapter 6	Summary of this report and conclusions.
Appendix A	Describes the RELAP5 input models used for the three plants for the PTS calculations. Important plant data are shown, and results of the analyses are summarized.

Section	Description
Appendix B	Discusses fluid temperature distribution in the downcomer. It presents experimental data from key experimental facilities used to study downcomer mixing. Sensitivity study results are shown that indicate the probability of vessel failure is not affected significantly by temperature variations, should they exist.
Appendix C	Discusses numerical issues that were encountered during the analyses and how they were treated.
Appendix D	Describes qualitative assessment criteria developed for past research programs used to judge comparisons of the code with experimental data.
Appendix E	Presents the results of RELAP5 assessments used to derive statistical comparisons of the code with experimental data, for pressure and downcomer temperature.
Appendix F	Describes the heat transfer modeling employed by RELAP5 for convective heat transfer in the downcomer.
Appendix G	Shows the results of a sensitivity study on wall heat flux as a function of the convective heat transfer coefficient. The study shows the effect on heat flux of variations in h to be highly damped because the heat transfer process is limited by the conductivity of the vessel wall.
Appendix H	Compares RELAP5 predictions of heat transfer with integral system test data for downcomer heat transfer. The comparisons made indicated RELAP5 to be realistic-to-conservative.
Appendix I	Compares RELAP5 calculations to computational fluid dynamics (CFD) calculations for the downcomer flow field. The RELAP5 predictions of downcomer velocity were similar in magnitude to the CFD calculations.
Appendix J	Gives the results of a sensitivity study of variations in the downcomer cooldown rate and HTC.
Appendix K	Presents the PTS Phenomena Identification and Ranking Table (PIRT).
Appendix L	Discusses the binning from a thermal-hydraulic perspective.
Appendix M	Gives examples of combined thermal-mechanical results that relate thermal-hydraulic boundary conditions to fracture mechanics results.
Appendix N	Shows applicability of plume sensitivity study using early version of FAVOR (94.1) to current version of FAVOR (04.1) used for the PTS reevaluation.

1.3 Interface Between Thermal-Hydraulics, Fracture Mechanics, and Probabilistic Risk Assessment

Figure 1-1 is an outline of the process used for performing PTS analysis. Evaluation of the risk-significance of PTS required considerable interaction and coordination throughout the study among the three disciplines of PRA, thermal-hydraulics, and fracture mechanics:

- (1) A comprehensive search was made for scenarios which were both probabilistically credible and physically significant. The starting point was an event tree, from which some 10^4 to 10^5 fault tree event sequences (transients) were delineated for each plant. Scenario screening was performed utilizing information from the three disciplines to render the number of sequences to be analyzed to be more manageable. An iterative process was used to eliminate events that were clearly not PTS-significant. This screening process excluded events where reactor coolant system (RCS) temperature remained above $\sim 200\text{C}$ (400F), as indicated by thermal-hydraulic analysis. Excluded as well were sequences of too low a probability to be of significance (e.g., $< 10^{-8}$).

The remaining sequences were categorized into “bins” consisting of events of similar nature, meaning similar sequences with relatively similar thermal-hydraulic outcomes. For example, PRA resolved the complete spectrum of LOCAs into four bins for small-break, medium-break, large-break, and repressurization events. The latter concerned all break LOCAs that repressurized from isolating the break, and the sequences were represented by stuck-open pressurizer safety/relief valves (SRVs) that reclosed. From this screening and binning process, for each plant approximately 100 transient sequences were identified for thermal-hydraulic analysis.

- (2) After screening, the remaining PTS sequences were analyzed using RELAP5 [5]. The thermal-hydraulic analysis is a transfer function to provide a *signature of boundary conditions* of a specific PRA scenario for fracture mechanics analysis. Thermal-hydraulic boundary conditions $[T_{dc}(t), P(t), h_{dc}(t)]$ determined by RELAP5 were applied to the FAVOR probabilistic fracture mechanics analysis code.
- (3) The FAVOR code calculated the conditional probability of through-wall cracking (CPF), which is the outcome measure of the combined fluid-structure analysis. The CPF for each scenario was then multiplied by its event frequency to obtain the PTS risk number, which is the product of CPF multiplied by the frequency of the occurrence (f), summed over all transients:

$$risk = \sum_i (f_i \times CPF_i)$$

It is noteworthy that the PTS analyses were not limited per se by the ability to carry out RELAP5 runs to characterize all PRA bins, as necessary. A one-to-one correspondence was, in effect, achieved between the thermal-hydraulics analysis and the binned PRA events. That is, it would have been inappropriate to further refine PRA bins because information is lacking to define probabilities on a finer scale. The sizing of bins was a tradeoff between the accuracy and uncertainty to which its frequency could be estimated. The probability of a bin depends on its size.

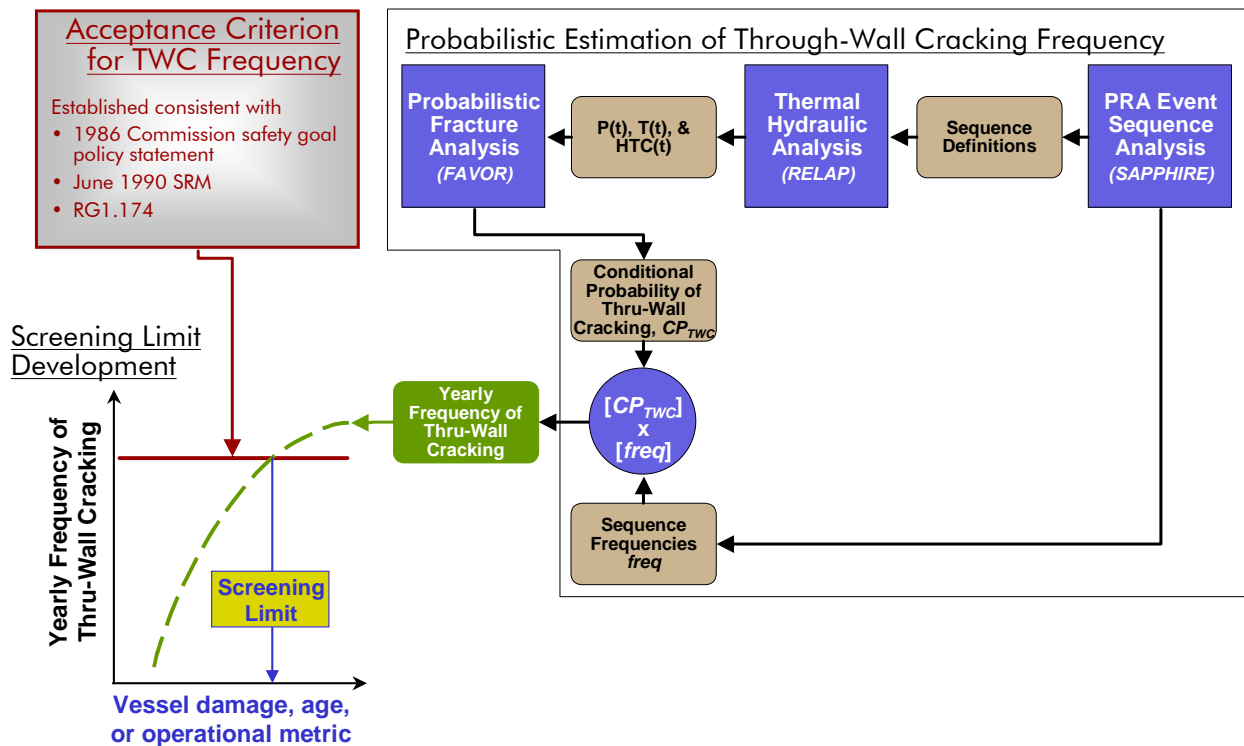


Figure 1-1. Basic Flow Diagram for PTS Analysis

If a bin is subdivided, its total probability is apportioned to the newly created sub-bins. As bins are made smaller, the probability of each sub-bin becomes progressively smaller, and the uncertainty in its frequency of occurrence increases

Evaluation of thermal-hydraulic uncertainties considered two distinct aspects. The first was the uncertainty associated with the content, or scope, of a given PRA bin (aleatory). That is, a particular bin comprises a family of possible transients similar, but not identical, in nature with respect to their thermal-hydraulic signature. For example, the small-break LOCA bin comprises all small-break LOCAs less than 4-inches in diameter. The break size may fall anywhere within that range, anywhere in location, and may encompass various equipment failures or operator actions, as well as various other aspect of plant operations. The uncertainty analyses, therefore, considered the *variation within a bin*.

The second category of thermal-hydraulic uncertainty was the physical modeling capability of the RELAP5 (epistemic). The method used was to rank the most important phenomena and processes modeled by RELAP5. The Phenomena Identification and Ranking Table (PIRT) technique was used to identify and rank the phenomena/processes and boundary conditions. The contributions of the highly ranked phenomena/processes to uncertainty were then evaluated. The two components of uncertainty, aleatory and epistemic, were treated together.

To evaluate the variation within a bin, a large number of RELAP5 sensitivity studies were performed for each critical bin, where the definition of a critical bin is one that contributed substantially to PTS risk. These sensitivity studies mapped the range of conditions that may occur within the given bin.

From this mapping, a number of specific scenarios were selected that represented the range of behavior exhibited by a particular bin. The frequency of occurrence (f) assigned by PRA to the bin, was broken down and apportioned to the scenarios used to represent the bin. The RELAP5 calculations of these scenarios were supplied as boundary conditions to the FAVOR analyses. Therefore, from a family of deterministic RELAP5 calculations, an uncertainty distribution of a given bin was developed, from the distribution of failure probabilities determined by FAVOR.

In summary, the uncertainty of a given bin was characterized in a three-step process [2]:

- (1) A large number of sensitivity studies performed with RELAP5 to vary each influencing factor to characterize the effect of each on the figure of merit]. The parameter used as the figure of merit was downcomer temperature. One-factor-at-a-time was varied between its nominal value, high value, and low value. The high and low values were chosen to be representative of the uncertainty distribution of each parameter.
- (2) Using a separate Monte Carlo code, the results from the individual one-factor-at-a-time RELAP5 sensitivity studies were combined to generate a probability density function. From this in turn, a cumulative distribution was generated.
- (3) RELAP5 calculations were chosen to represent the range of outcomes described by the cumulative distribution function. The probabilities of the individual sequences that characterize a bin were assigned by PRA as a subdivided probability of the total bin.

The dominant contribution to uncertainty was found to be the range of event sequences within a given PRA bin. Because a bin is defined broadly, the range of behavior that describes a given bin is mainly attributable to boundary conditions (aleatory) rather than physical models in RELAP5 (epistemic). For example, for LOCAs, the key factor is the size of the break:

Small-break bin:	1.4 inch – 4 inches:	factor of 8 variation in break size area
Medium-break bin:	4 inches – 8 inches:	factor of 4 variation in break size area
Large-break bin:	8 inches – 30 inches:	factor of 10 variation in break size area

The large range in break flow coupled with ECC injection flow dominates the state of the RCS. By comparison, the physical modeling of RELAP5 is relatively accurate compared to the range of plant behavior that falls within a given bin, which RELAP5 is required to model. That is, RELAP5 as a measuring tool is accurate compared that which it must measure. Since the uncertainty in RELAP5 predictions of $T_{dc}(t)$, $P(t)$, $h_{dc}(t)$ are small compared to the range of behavior within a given bin (as shown in the uncertainty analysis in Chapter 5), then the calculations properly map the bin.

1.4 Modeling Issues

The thermal-hydraulic analysis was centered on the calculation of potential PTS scenarios with the RELAP5 code. The role of the RELAP5 analyses was to supply boundary conditions to the FAVOR probabilistic fracture mechanics analysis code. FAVOR could only accept, in effect, point or averaged values for these three parameters. This gave rise to two basic considerations:

- (1) What is the accuracy and uncertainty in RELAP5 calculations of RCS pressure and average downcomer temperature and HTC?
- (2) Is an average value downcomer temperature and heat transfer appropriate, or are there significant variations around the downcomer?

These high-level issues devolved into the following lower-level issues:

- The modeling in RELAP5 of important physical phenomena identified through the PIRT technique. One issue that received particular scrutiny was the modeling of convective heat transfer.
- Whether phenomena not modeled by RELAP5 are important to the calculated results. In particular, this included the inability of a nodal-averaged code to calculate fluid-fluid mixing and stratification. The use of a uniform temperature distribution in the downcomer is a simplifying assumption used in the PTS analyses. This is the modeling approach used in FAVOR. One-dimensional modeling of pipes and volume averaging are inherent limitations of RELAP5 and other thermal-hydraulic systems codes.
- Numerical methods introduce an additional consideration to the solution of a physical/mathematical problem. In particular, the possible effects of numerically driven flows was evaluated. This is discussed in Appendix C.

Table 1-2 lists the physical phenomena identified by the PTS PIRT, along with their relative ranking in terms of importance with respect to the current PTS analysis. These are discussed in more detail Chapter 4 (Table 4-4).

Table 1-2. Thermal-Hydraulic Phenomena Identified by the PTS PIRT

Importance Rank	Phenomenon
1	Accumulator injection
2	Break flow/break size
3	Reactor vessel wall heat conduction
4	Jet behavior, flow distribution and mixing in downcomer
5	Jet behavior, flow distribution and mixing in cold leg
6	Wall-fluid heat transfer in downcomer
7	Natural circulation flow and loop flow resistance
8	Downcomer-upper plenum bypass
9	Upper head heat transfer
10	Liquid/vapor interface in upper downcomer
11	Steam generator (SG) heat transfer
N.R.	Condensation during ECC injection
N.R.	Condensation during repressurization

2. THERMAL-HYDRAULIC ANALYSIS OVERVIEW

2.1 Top-Down Scaling Approach

Establishing the applicability and uncertainty of RELAP5 for PTS was in distinct contrast to past thermal-hydraulic uncertainty studies, which have been scenario-specific and restricted to a few scenarios. For example, a single value of peak clad temperature is the figure of merit for large-break LOCAs, while a single value of minimum vessel inventory is used for small-break LOCAs. For the PTS analysis, it was necessary to consider the time-dependent downcomer fluid temperature, reactor system pressure, and downcomer fluid to vessel wall temperature ($T_{dc}(t)$, $P(t)$, and $h_{dc}(t)$) for the very broad spectrum of postulated scenarios.

The established method for analyzing code uncertainty is a methodology called Code Scaling, Applicability, and Uncertainty (CSAU) [6, 7, 8]. The CSAU methodology was developed for a single specific scenario in a single specific plant. However, the current application had to consider a large number of sequences in multiple plants. The complexity necessitated a top-down scaling approach to evaluate code applicability and uncertainty for PTS. In addition, the controlling processes of the PTS problem had to be identified, particularly from the perspective of thermal-hydraulic modeling and uncertainly analysis.

The methodology used to evaluate code applicability and uncertainty is Hierarchical Two-Tiered Scaling (H2TS) [9]. The H2TS methodology is shown in Table 2-1 and is a top-down, general approach for solving complex problems, of which PTS is an example. The H2TS methodology begins with determining the hierarchical structure of the problem to be solved. It specifies the *amount* of the given constituent and phase in the given geometrical system (initial conditions). Second, the *transfer area* or *transfer rate* is identified for the particular critical transfer process. Third, the *characteristic time* constants are identified for the critical system components and physicochemical processes.

Table 2-1 Methodology for Hierarchical Two-Tiered Scaling Analysis

Stage 1: System Decomposition	Stage 2: Scale Identification	Stage 3: Top-Down Processes and Scaling	Stage 4: Bottom-Up Process and Scaling
<u>Provide:</u> System Hierarchy	<u>Provide Hierarchy for:</u> Volumetric concentrations	<u>Provide:</u> Conservation equations	<u>Perform:</u> Detailed scaling analysis for important processes
<u>Identify:</u> Characteristic concentrations geometries processes	Area concentrations Process time scales	<u>Derive:</u> Scaling groups Characteristic time ratios	<u>Derive and Validate:</u> Scaling groups
		<u>Establish:</u> Scaling hierarchy	
		<u>Identify:</u> Identify important processes to be addressed in bottom-up scaling analyses	

[9 p. 17 NUREG/CR-5809]

H2TS proceeds with the determination of the length and time scales that govern the processes. These scales are needed to determine the mesh size (nodalization) and time step size. H2TS emphasizes integration of experiments, analyses, and uncertainty quantification. Finally, it specifies the use of the PIRT technique as part of the bottom-up determination to guide uncertainty analyses, assessment of code adequacy, and scaling of experiments.

The evaluation begins by identifying the key parameter, that is, the figure of merit, in the overall analysis. The figure of merit is the highest-level relation (first hierarchical tier), or controlling parameter, that governs the problem at hand. Then, the controlling phenomena, or parameters, that determine the predicted values of the figure of merit are identified (second hierarchical tier). The process continues to lower hierarchical levels as required, until it reaches the levels at which the code(s) (RELAP5) analyze(s) the problem.

A PIRT is developed to identify the most important phenomena, processes, and boundary conditions. The means by which these phenomena, processes, and boundary conditions were modeled are then described. Finally, the validity of the predictions is assessed. Specifically RELAP5 is validated as an appropriate tool to perform the necessary PTS plant calculations.

The PTS evaluation combines thermal-hydraulics with fracture mechanics and material properties to determine the probability of vessel failure. Uncertainty analysis must be part of a combined fluid-structure analysis. Uncertainties in the fracture mechanics analysis and in the thermal-hydraulics analyses are expressed in the CPF values. The fluid-structure analysis determines whether the magnitude and uncertainty of thermal-hydraulic parameters are of significance. While thermal-hydraulic uncertainties can be studied to some extent independently of the structural analysis, the bottom line answer can only be obtained through a combined analysis. In other words, the effects of variations and uncertainties in thermal-hydraulic analyses can only be evaluated in combination with fracture mechanics analyses.

On this basis, a physical explanation that describes the PTS results was developed. It was derived following the H2TS process to identify the *dominant processes/phenomena* of the PTS process and their *characteristic length and time scales*. It is based on the following factors:

- thermal response of the reactor vessel
- thermal response of the RCS

Quantitative values for the figure of merit are determined by the fracture mechanics analyses performed using the FAVOR code, and in particular by calculating the applied stress and the material fracture toughness. The thermal-hydraulic analyses are used to characterize the thermal response of the RCS.

2.2 PTS Figure of Merit

The figure of merit characterizes the overall analyses, which include both the thermal-hydraulic and fracture mechanics analyses. The figure of merit is not the thermal-hydraulic parameters pressure (P), temperature (T), and heat transfer coefficient (h), which reside at the next lower hierarchical level. Rather, it is the fracture mechanics relation, K-ratio (K_R):

$$K_R = \frac{K_I}{K_{IC}} \frac{\text{applied stress intensity}}{\text{minimum critical stress for crack initiation}}$$

K_R is the ratio of the applied stress intensity K_I attributable to the transient, to the minimum critical stress intensity for crack initiation K_{IC} . The value of K_R is specific to a given crack. The numerator is the applied stress (K_I) to a given flaw, or more generally, to a distribution of flaw sizes and locations. The value of K_I is determined from the stress field in the vessel wall created by temperature gradient across the vessel wall and RCS pressure.

As shown in Figure 2-1, FAVOR comprises three computational modules, including (1) a deterministic load generator (FAVLoad), (2) a Monte Carlo PFM module (FAVPFM), and (3) a post-processor (FAVPost). Figure 2-1 also indicates the nature of the data streams that flow through these modules.

FAVLoad takes as input the time histories of pressure, temperature, and heat transfer coefficient defined by the RELAP TH analysis. These inputs are used along with a 1D transient heat conduction equation to estimate the time-dependent variation of temperature through the vessel wall. These time-dependent temperature profiles are used, along with the RELAP pressure history, in a linear elastic stress analysis to estimate the time history of applied-KI, which is passed to FAVPFM for further analysis.

The FAVPFM module implements the logical specification of the PFM model within a series of nested loops. These loops step through the TH time history and implement the Monte-Carlo trials necessary to estimate the conditional probabilities of crack initiation and through-wall cracking. The probabilities estimated by FAVOR (complete with uncertainties) are conditional in the sense that, within the FAVPFM module, the TH transients are assumed to occur.

In the PTS reevaluation program, the FAVOR code was used to calculate the probability of vessel failure. In this mode, FAVOR did not calculate specific values of K_R . The FAVOR calculations involved distributions of crack sizes, locations, and material properties. K_{IC} is a distributed variable dependent on the material properties and their uncertainties. K_I depends on the flaw size, geometry, location, and orientation. In a FAVOR calculation, a distribution is normally used. However, FAVOR can also calculate K_I and K_{IC} for a specific crack size, location, and vessel properties. K_R must exceed 1 for the probability of a pre-existing flaw to begin to run, that is, for the probability to be non-zero. The more the value of K_R exceeds one, the more the probability of crack initiation increases.

The applied stress intensity K_I is a function of thermal stress and pressure stress. K_{IC} is an expression of fracture toughness. For a given set of vessel conditions, the fracture toughness is a function of temperature.

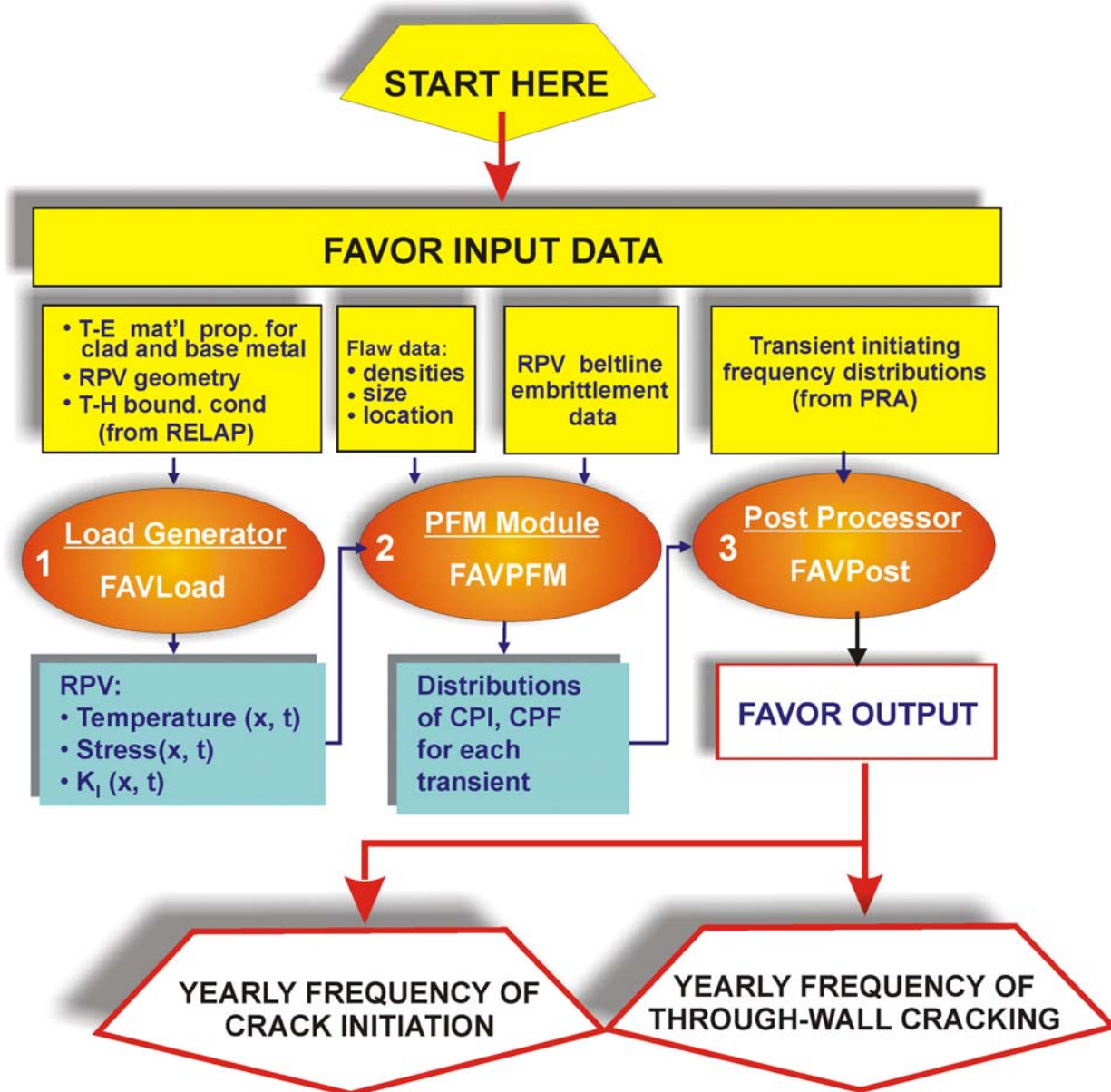


Figure 2-1. FAVOR Computational Modules and Data Flow

Temperature effects, therefore, appear in both the numerator K_I and denominator K_{IC} of the K_R equation. The larger the temperature gradient, the higher the thermal stress, while the lower the absolute temperature, the lower the toughness. Therefore, the response of the vessel to changes in temperature is **amplified** by the combined effects on stress and fracture toughness. In contrast, the effect of pressure is felt only in the numerator of the K_R equation. Vessel stress, and hence K_R , is **proportional** to pressure.

The sensitivity of K_{IC} to temperature is particularly pronounced over a certain range of temperatures. Figure 2-2 shows that CPF changes by 8 orders of magnitude (10^8) for a change in reference temperature of 200 °F. Reference temperature (RT) is a characteristic temperature used to locate the transition curve of a ferritic steel on the temperature axis.

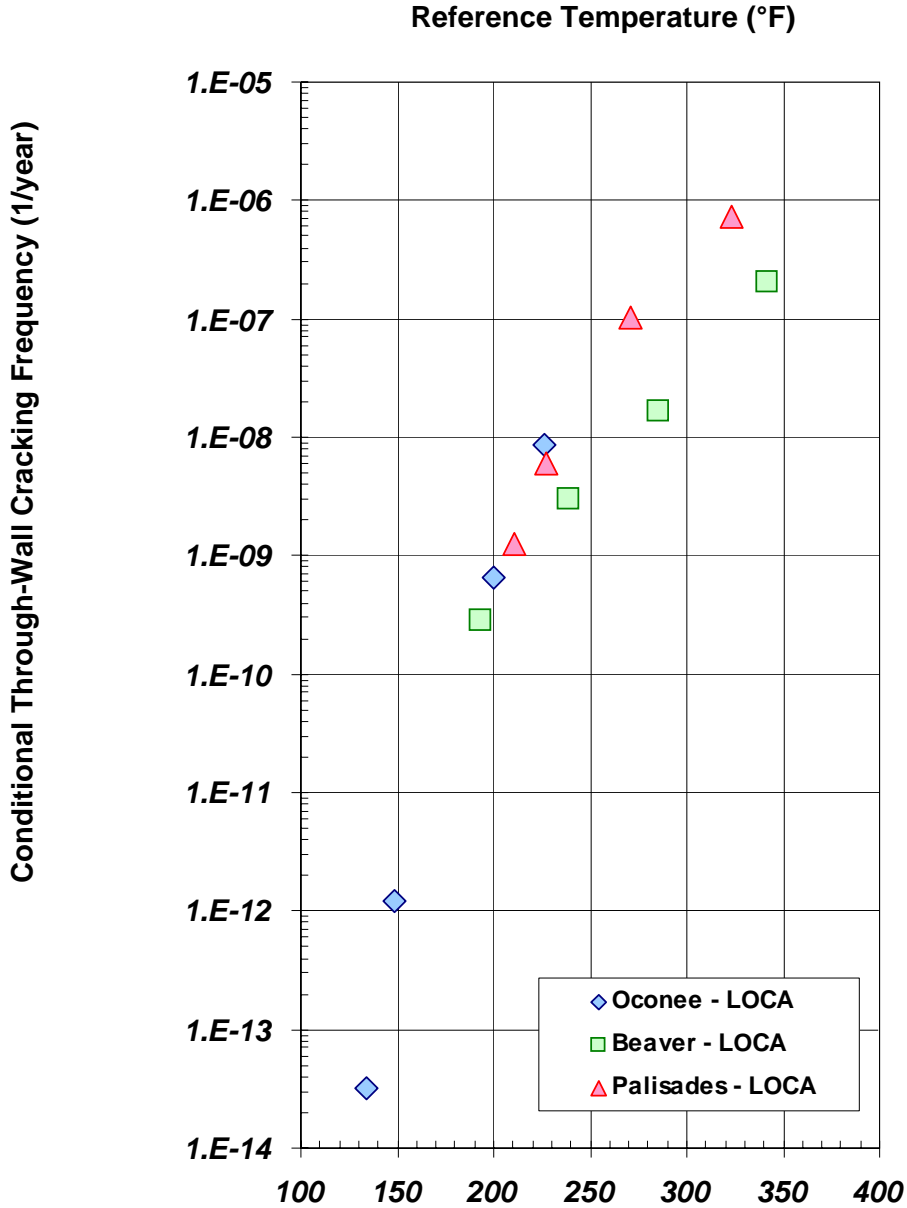


Figure 2-2. Conditional Probability of Failure as a Function of RT_{PTS} ¹

¹ RT_{NDT} is the reference temperature (RT) of the vessel under any condition, evaluated as a function of irradiation. RT_{PTS} is the RT_{NDT} at end of license irradiation.

2.3 Vessel Time Constants

The Biot number indicates the degree to which a heat transfer process involving both fluids and solids is controlled by conduction or convection. Thus, it shows the importance of magnitude and uncertainty of the convective heat transfer coefficient. It is the ratio of internal resistance to boundary layer resistance, expressed as

$$Bi = \frac{hL}{k}$$

where L is the characteristic length
k is the wall conductivity
h is the convective heat transfer coefficient

If Biot $\gg 1$ (e.g., >10), then the heat transfer is conduction limited. The term "L" may be taken as the vessel wall thickness, which is approximately 0.2 m (~8 inches). Evaluating the Biot number for the vessel wall, and solving for h gives,

$$\begin{aligned} \text{For } Bi = 1, \quad h &= 200 \text{ W/m}^2\text{-C} \\ \text{For } Bi = 10, \quad h &= 2000 \text{ W/m}^2\text{-C} \end{aligned}$$

Therefore, for heat transfer coefficients $h > 2000 \text{ W/m}^2\text{-C}$, the heat transfer process is conduction controlled. For conditions of loop flow stagnation or natural circulation, hand calculations of the expected range of convective heat transfer coefficients in the downcomer yield values in the range 1000 to 3000 $\text{W/m}^2\text{-C}$, which places the heat transfer generally in the conduction controlled region. RELAP5 calculated results for a variety of LOCA scenarios provides similar numbers.

The heat transfer in a solid, and therefore the vessel time constant, can be considered by the Fourier number (Fo):

$$Fo = \frac{\alpha t}{L^2}$$

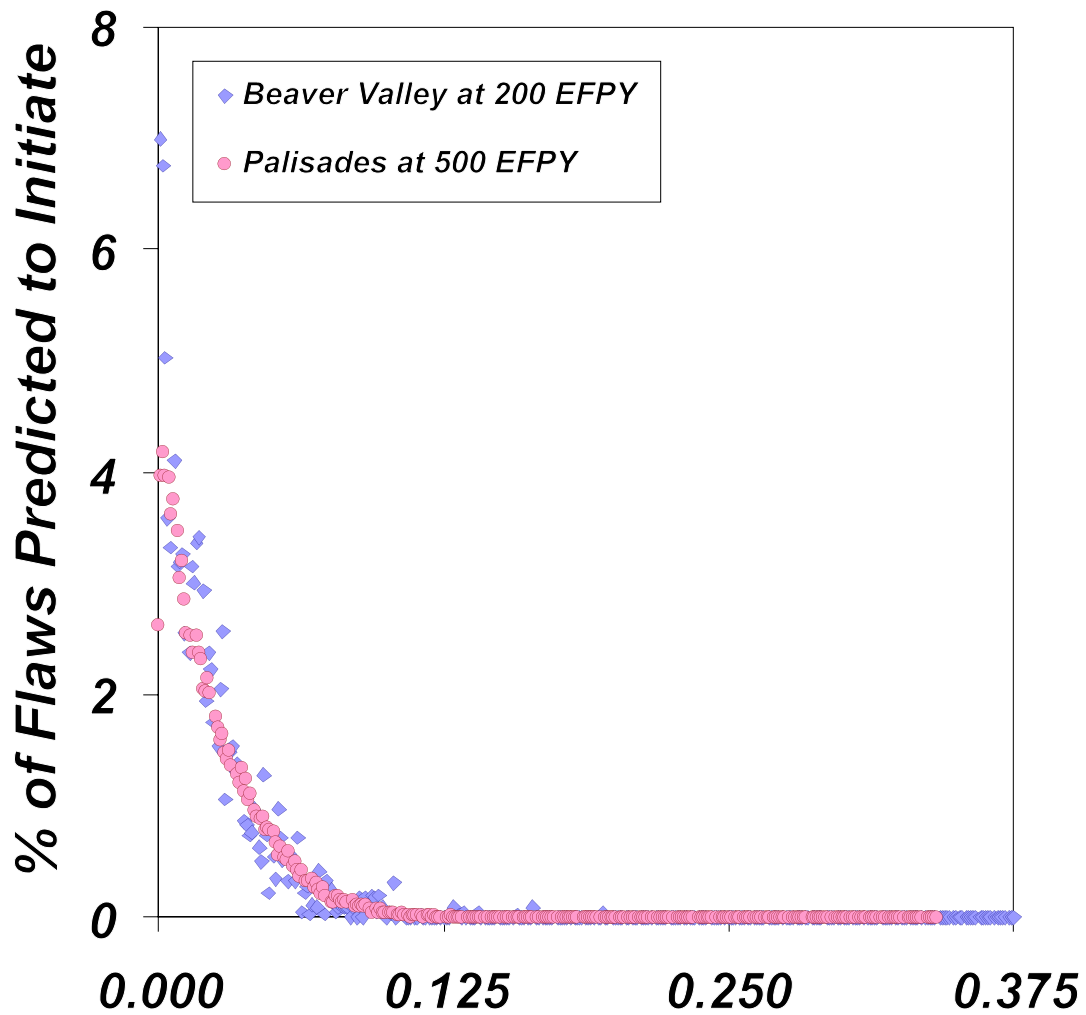
where the thermal diffusivity (α) is calculated as follows:

$$\alpha = \frac{k}{\rho C_p}$$

where ρ is the density (of steel)
 C_p is the specific heat capacity (of steel)

Initially, it was thought that the heat transfer across the vessel wall-downcomer fluid interface would be conduction-limited. However, consider Figure 2-3, which shows the results of FAVOR calculations for Beaver Valley and Palisades. The y-axis is normalized failures, while the x-axis is percent of total vessel wall thickness, as measured from the inside wall of the vessel. Most of the flaws that contribute to the probability of vessel failure are within ~1 cm (~ 1/2 inch) of the vessel inner surface. In this respect, it is useful to examine the vessel wall time constants (assuming Fo = 1) assuming the length scale L is equal to the wall thickness or 1 cm:

$$\begin{aligned} t \sim 3000\text{s}, \quad x &= 25.6 \text{ cm} \\ t \sim 12\text{s}, \quad x &= 1 \text{ cm} \end{aligned}$$



Fraction of Vessel Wall Thickness From Inside Surface

Figure 2-3. Distribution of Depths at Which Cracks Initiate (FAVOR Version 3.1)

and for

$$\begin{aligned}
 Bi = 1, \quad h \sim 3,000 \text{ W/m}^2\text{-C}, \quad x = 1 \text{ cm} \\
 Bi = 10, \quad h \sim 30,000 \text{ W/m}^2\text{-C}, \quad x = 10 \text{ cm}
 \end{aligned}$$

The latter heat transfer coefficient (30,000 W/m²-C) is of the same magnitude as when the reactor coolant pumps (RCPs) are operating.

In terms of flaws that can lead to vessel failure, the thermal analyses (based on the calculation of the Biot and Fourier numbers) shows that heat transfer is not simply conduction controlled. Times of the order of 10s are significant with respect to influencing the fracture toughness in the region where flaws are located that contribute to the probability of vessel failure.

Therefore, two characteristic time scales and length scales must be considered for the vessel. One is more relevant to local fracture toughness (K_{IC}) near the inside surface of the vessel where most of the flaws that contribute to vessel failure are located, while the other is more relevant to the temperature distribution throughout the vessel wall, and thus the applied stress (K_I). Changes in K_{IC} for near surface flaws may occur with a time scale of the order of 10s. On the other hand, K_I is a function of the overall thermal gradient in the vessel, and responds over a time scale of the order of 1000s. Both views of the thermal time constant are appropriate as the short time scale is applicable to temperature-driven transients such as large-break LOCAs while the long time scale is applicable to transients involving stuck-open SRVs that reclose, resulting in system repressurization. Since heat flux is affected by both by a change in fluid temperature or by a change in HTC, the uncertainty in each must be considered.

The one-dimensional conduction equation was solved using the following vessel properties:

L	0.256 m
T_i	285 °C
T_f	20 °C
k	48 W/m-C @ 325 °C 57 W/m-C @ 125 °C
ρ	7830 kg/m ³
C_p	0.584 kJ/kg-C @ 300 °C 0.537 kJ/kg-C @ 200 °C 0.490 kJ/kg-C @100 °C
α	<u>1.24 x 10⁻⁵ m²/s</u>

Figures 2-4 and 2-5 show solutions to conduction equation for different lengths of time, in which a temperature of 20 °C was applied at the inner wall of the vessel. This is equivalent to a step change in fluid temperature combined with an infinite value for h. The two figures show results for short and long time intervals, respectively. As seen in the figures, a step change in temperature at the surface is propagated to depths of ~2 cm in ~20 s. Much longer times are required (~1 hour) for the vessel wall as a whole to equilibrate. To summarize:

- K_I is a proportional function of temperature and pressure. While wall stress responds essentially instantaneously to changes in pressure, the thermal stress is a function of the entire time-temperature history. The characteristic time scale for temperature is of the order of 1000s and characteristic length scale is the vessel wall thickness (0.2 m). The characteristic time scale for the vessel stress to respond to a change in RCS pressure is very short ($\ll 1$ s; speed of sound).
- K_{IC} is an amplified function of temperature (over a certain range of temperatures). The characteristic time scale for temperature is on the order of 10 s and length scale is ~1 cm.

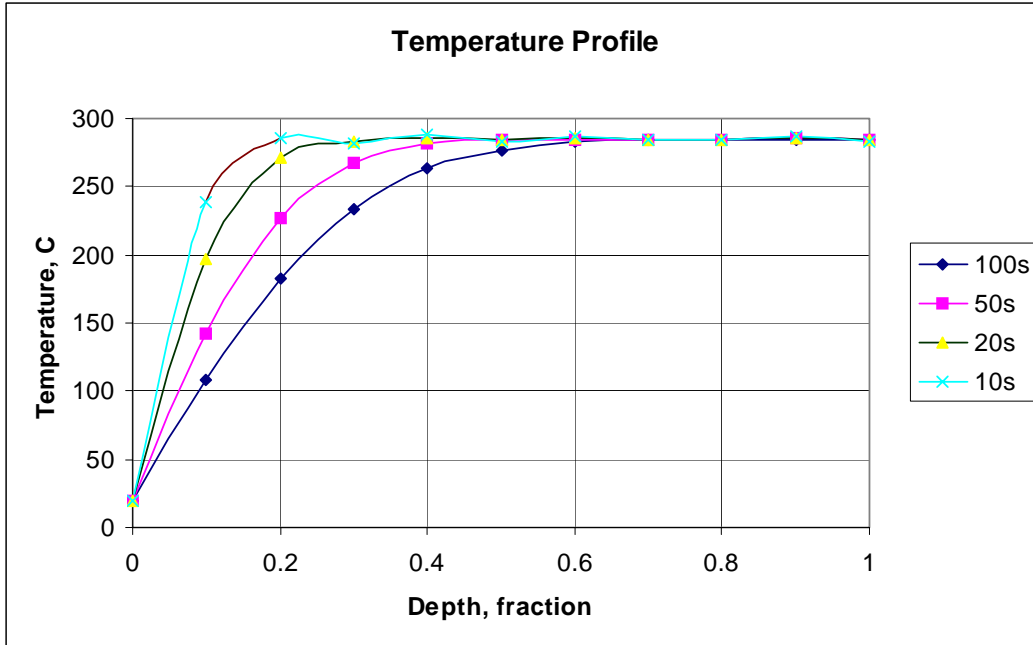


Figure 2-4. Vessel Wall Temperature Profile for Short Time Intervals
Wall Boundary T=20 °C Applied

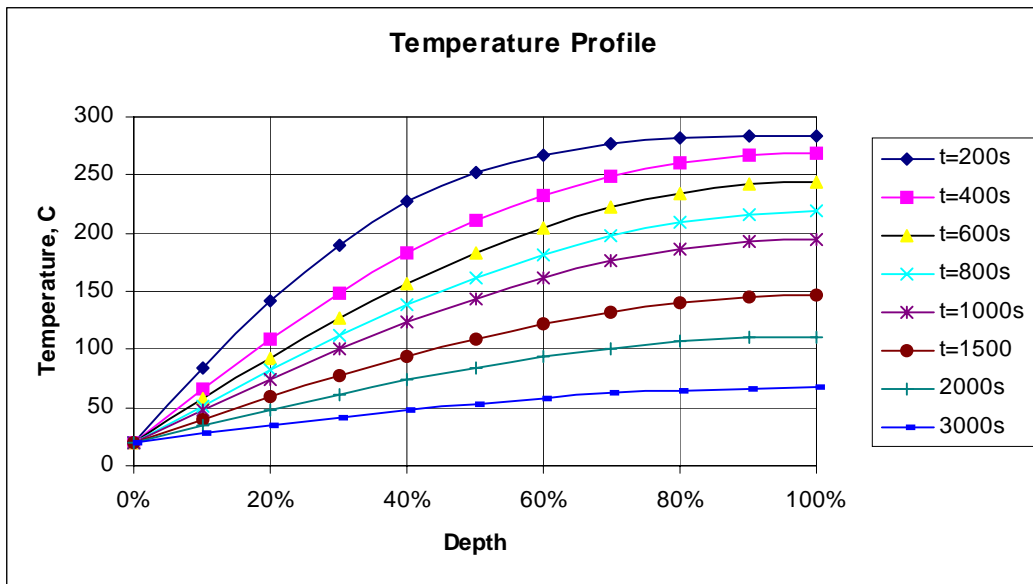


Figure 2-5. Vessel Wall Temperature Profile for Long Time Intervals
Wall Boundary T=20 °C Applied

Therefore, temperature effects are amplified, especially near the inside surface of the vessel. Vessel wall stress is the sum of the thermal stress and the pressure force,

$$\sigma = \sigma_T + \sigma_P$$

where σ is stress
subscripts T and P refer to thermal and pressure components

Thermal stress (σ_T) is derived from the temperature distribution through the vessel wall, $T(x, t)$. Temperature distribution is a cumulative function of the heat flux, q'' , from the vessel to the downcomer fluid.

In addition, the heat flux and resulting change in wall temperature has a strong influence on the fracture toughness in the vessel material. While RELAP5 itself calculates $T(x, T)$, this information was not used in FAVOR. Neither was the RELAP5 calculation of heat flux fed directly from RELAP5 to FAVOR. Instead, it was broken down according to,

$$q''(t) = h_{dc}(t) [T_w(t) - T_f(t)]$$

where q'' is the heat flux
 h is the convective heat transfer coefficient
 T is temperature
subscripts w and f refer to wall and fluid, respectively

The one-dimensional conduction equation was solved to obtain the temperature distribution across the wall. Thus, a uniform heat flux boundary condition was assumed to apply to the inner wall of the vessel. The boundary conditions actually supplied by RELAP5 were $h_{dc}(t)$ and $T_{dc,f}(t)$ from which FAVOR calculated q'' and T_w and solved the one-dimensional conduction equation

$$q'' = -k \frac{dT}{dx}$$

In terms of the vessel, the pressure stress (σ_P) is effectively an instantaneous quantity. Time dependent pressure $P(t)$ in the RCS is, however, a cumulative function of the flow of energy out of the RCS. Thus, the combined thermal-hydraulic/structural analysis is time-dependent for both quantities and cannot be separated.

3. THERMAL-HYDRAULIC PHENOMENOLOGY

This chapter summarizes the general phenomenology associated with the thermal-hydraulic evaluation of PTS.

Nearly all PTS risk results from LOCAs and stuck-open pressurizer valves that reclose. The latter class of events merely comprises small LOCAs that are later isolated, such that repressurization occurs. These events all share inherently similar characteristic responses in terms of global behavior of the RCS. For example, flow stagnation occurs for all LOCAs of PTS significance. Furthermore, the response of the RCS from plant to plant is similar for these classes of events.

3.1 Overview

PTS analysis of different scenarios requires coupled thermal-hydraulics/fracture mechanics calculations to obtain the CPF values for the vessel. RELAP5 was used to perform the thermal-hydraulic analysis, while FAVOR was used to perform the fracture analysis. The FAVOR CPF calculations were then combined with PRA frequency (f_i) to generate the probability of vessel failure:

$$risk = \sum_i (f_i \times CPF_i)$$

The coupled RELAP5-FAVOR analysis yielded the temperature distribution across the vessel as a function of time. The temperature distribution determines the local fracture toughness of the material and the thermal stress across the vessel wall. The fluid-structure analysis determined whether the magnitude and uncertainty of thermal-hydraulic parameters were significant. Of overriding importance to this combined analysis were the following coupled factors:

- time constant of the total RCS fluid energy (T_{RCS} or T_{dc}), from which one obtains $P(t)$ and $T_{dc}(t)$
- time constant of the reactor vessel wall (T_{vessel}), from which one obtains $T_{wall}(x, t)$

The time constants of the vessel wall T_{vessel} were discussed in Chapter 2. The time constant of the total RCS fluid energy T_{dc} and, therefore, $T_{dc}(t)$, is a function of thermal response T_{RCS} of the entire RCS. The characteristic time of the RCS fluid thermal transient is a function of the size of the break. A *fast* transient is one in which the change in downcomer temperature is rapid compared to the thermal response of the reactor vessel. Such is the case for a large-break LOCA. Conversely, a *slow* transient is one in which the rate of change in downcomer fluid temperature is slow compared to the characteristic time of the vessel, as is the case with small-break LOCAs. In this regard, main steam line breaks (MSLBs) fall into the category of a fast transient, while stuck-open SRVs are simply small-break LOCAs.

In terms of the vessel, the most severe thermal transient is one that has a high rate of change in downcomer fluid temperature, and in which the downcomer temperature drops to the lowest value. In the extreme, this is a step change in temperature applied to the vessel inner wall. Such a transient results in the highest vessel thermal stress and the lowest absolute vessel wall temperature. The characteristic time of the fluid energy in the RCS is as follows:

$$\tau = \frac{\int m_l h_l + m_v h_v + m_s C_{ps}}{\dot{m} h_{break}} \frac{\text{initial system energy - liquid + vapor + steel}}{\text{break energy flow}}$$

The fluid time constant, and hence $T_f(t)$, is approximated by break energy flow, which is a function of break size, over initial energy. This behavior will be similar from plant-to-plant. This is because different plants are designed with similar *power-to-volume* ratios, meaning that the ratio:

$$\frac{\text{thermal power}}{\text{reactor coolant system volume}}$$

is similar from plant-to-plant and from vendor-to-vendor.

Figures 3-1 and 3-2 show the outcome of fast and slow transients in terms of vessel failure potential. Figure 3-1 is a plot of CPF as a function of break size. The use of CPF eliminates the frequency of the initiating event as a variable. As break size increases from ~2 inches to ~4 inches, the CPF rises sharply by three orders of magnitude, Then the failure probability curve begins to flatten, reaching an asymptotic maximum of 10^{-4} .

Figure 3-2 shows the relation between break size and the most probable failure time based on FAVOR results for the Palisades dominant transients. The time to failure is much larger for small breaks (< ~6 inches) than for large breaks (> ~6 inches). Thus, the knee in the curve in Figure 3-1 at a break size of ~6-inch is evident in Figure 3-2 at the time $t = \sim 1000$ s. For breaks > ~6 inch, the break/ECC injection flow is so large, and the cooldown of the RCS is so rapid, that the thermal transient in the vessel wall is “strictly” conduction controlled. Wall heat flux is controlled by wall conduction rather than the fluid convection. Larger breaks (larger break flow) do not result in the thermal transient in the reactor vessel being appreciably faster. The vessel temperature distribution, therefore, becomes insensitive to further changes in break flow. The characteristic time of the fluid is no longer controlling, instead, it is the thermal time constant of the reactor vessel.

On this basis, for the purpose of PTS analysis, we classified breaks as follows:

- ≥ 8 inches large breaks (asymptotic CPF region)
- 4 inches to 8 inches medium breaks (transition region)
- ~1.4 inch to < 4 inches small breaks (sharply rising CPF region)
- $\leq \sim 1.4$ inch very small breaks were screened out because the downcomer does not cool below normal operating initial conditions (CPF = 0)

Pressure is not an important factor for LOCAs because RCS pressure is low (< 2 MPa) at the time the vessel is most likely to fail. For the subclass of small-break LOCAs consisting of stuck-open SRVs, however, pressure plays a dominant role. For SRV scenarios, downcomer temperature does

not fall as low as risk-significant LOCAs because the SRV break size is small (~1.7 inch). However, RCS pressure at the most probable time of vessel failure rises to the SRV set point (~2450 psi). Therefore, the tensile stress generated by RCS pressure is comparable to the stress generated by the thermal gradient through the vessel wall.

Figure 3-3 is a plot of RCS pressure versus downcomer temperature for all transients that contributed >0.1% to total vessel failure probability, for all three plants. The cluster of points below 100 °C and 5 MPa are LOCAs. The points clustered from 16 to 18 MPa are SRVs that reclose, along with MSLBs in which high-pressure injection (HPI) is actuated and not throttled. This illustrates that to generate a possibility of failure, low T_{dc} is required for failure to occur; however, P may be high or low for failure to occur.

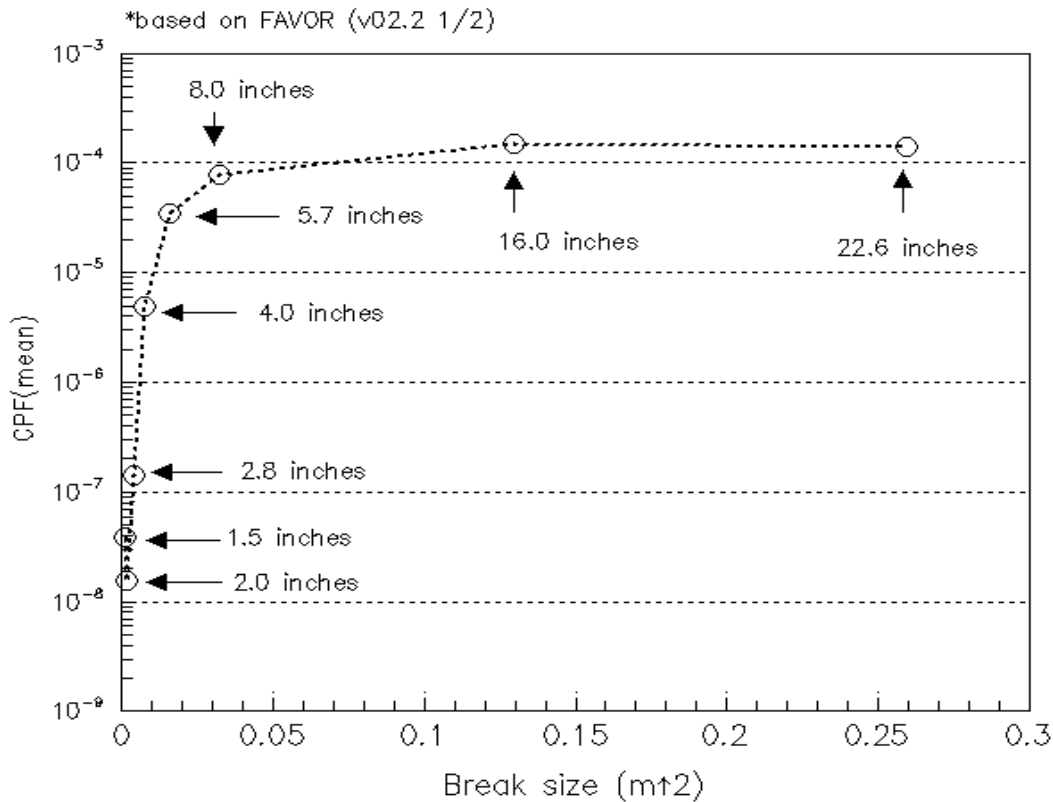


Figure 3-1. Conditional Probability of Failure as a Function of Break Size (Border Between Slow and Fast Transients is ~ 6 inches)

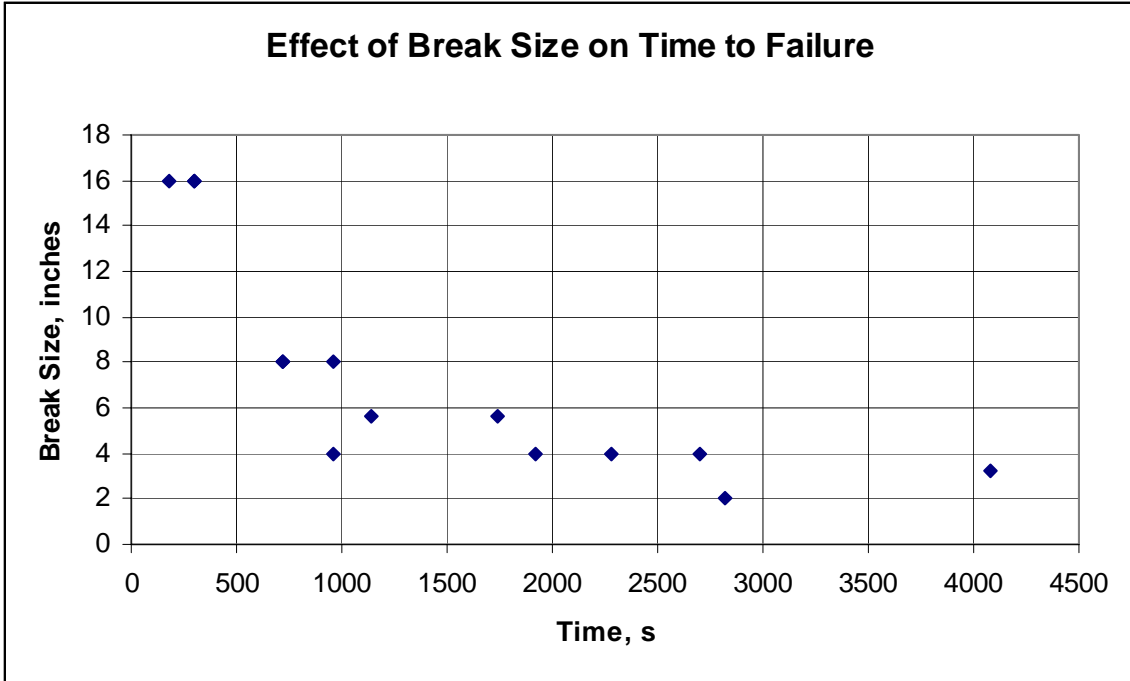


Figure 3-2. Effect of Break Size on Time to Vessel Failure

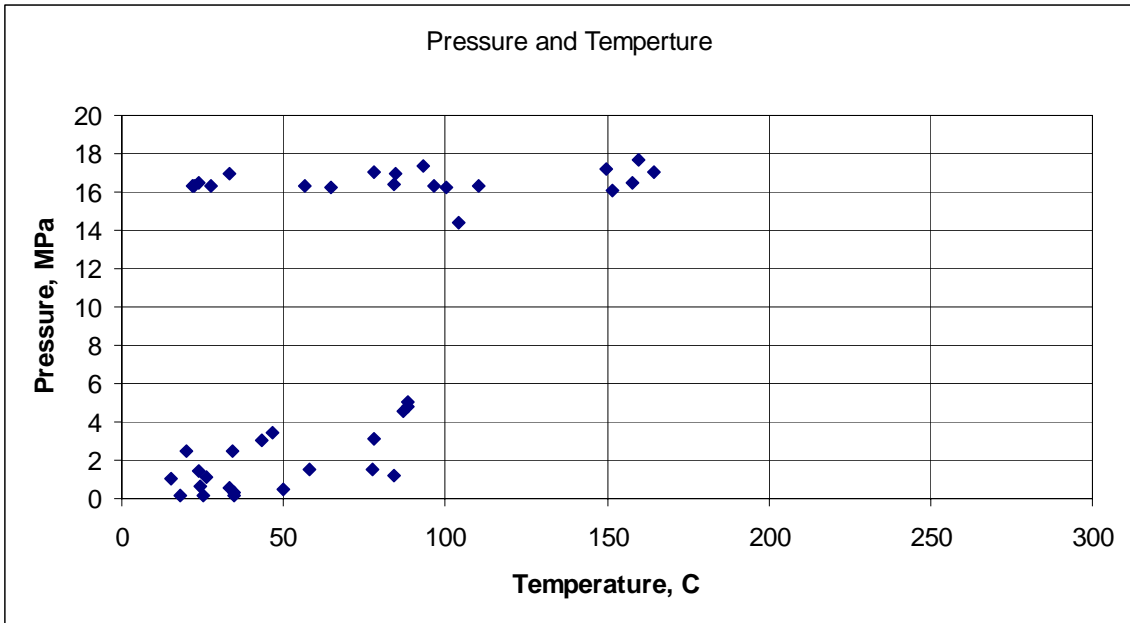


Figure 3-3. Temperature-Pressure Characteristics of Transients Contributing to Probability of Failure

3.2 Energy and Inventory

Pressure and temperature are closely interrelated, global measures of RCS energy. RCS pressure is determined by the hottest water in the RCS (unless the RCS is pumped water solid by HPI). When the RCS is well mixed, T and P are directly linked by the saturation curve. There are inherent limits to the degree of non-equilibrium of downcomer temperature conditions. This is based on the nature of PTS-significant transients and natural circulation flows.

Thermal-hydraulic problems can be treated using *controls volume* and their associated boundary conditions and initial conditions, as is illustrated in Figure 3-4 for the RCS. Analysis of any thermal-hydraulic control volume problem consists of four elements:

- (1) Establishing the control volume. The RCS can be treated as a single thermodynamic control volume with its accompanying initial and boundary conditions.
- (2) Defining its initial conditions. The initial conditions are defined by the mass and energy contained within the RCS at time zero. RCS mass and energy are reflected in the initial coolant inventory and temperature distribution. The initial conditions are the total initial energy of the control volume upon which the cooling transient acts.
- (3) Defining its boundary conditions.
- (4) Analyzing the transient effects on the control volume from mass and energy flows through its boundaries. The boundary conditions of the control volume are defined by the boundary flows that occur during the given transient, as follows:
 - Heat transfer across solid structures, which in turn consists of the following:
 - decay heat
 - stored heat in the metal structures that comprise the RCS
 - heat transfer to and from the steam generators
 - Mass/energy flows in/out. Flow out of the RCS is defined by a break in the RCS. Two types of breaks were considered:
 - those that may be isolated (such as a stuck-open pressurizer SRV)
 - those that cannot be isolated (that is, LOCAs induced by a pipe break)

From the perspective of thermal-hydraulic analysis and uncertainty evaluation, there is very little difference between the two subcategories of whether or not a break is later isolated. Break flow is a function of break location and break area. For LOCAs, neither the break location or break size can be defined a priori, so the analysis must consider the spectrum of possibilities. Once a given break size is specified, however, an uncertainty in the break flow model can be given. For stuck-open valves, the break area is defined by the valve characteristics. An equivalent diameter is defined as an input to the code from a design value or measured flow rate.

Flow into the control volume is defined by the ECC system characteristics:

- high-pressure injection (HPI) system
- low-pressure injection (LPI) system
- accumulators

HPI and LPI are characterized by flow rate (mass), which is an input to the code from pump curves used in the different plants. The second parameter is the ECC temperature (energy), which is a defined input. Accumulator flows are similar. Rather than pumps, accumulator mass flow is driven by prepressurization, while accumulator temperature is a defined input.

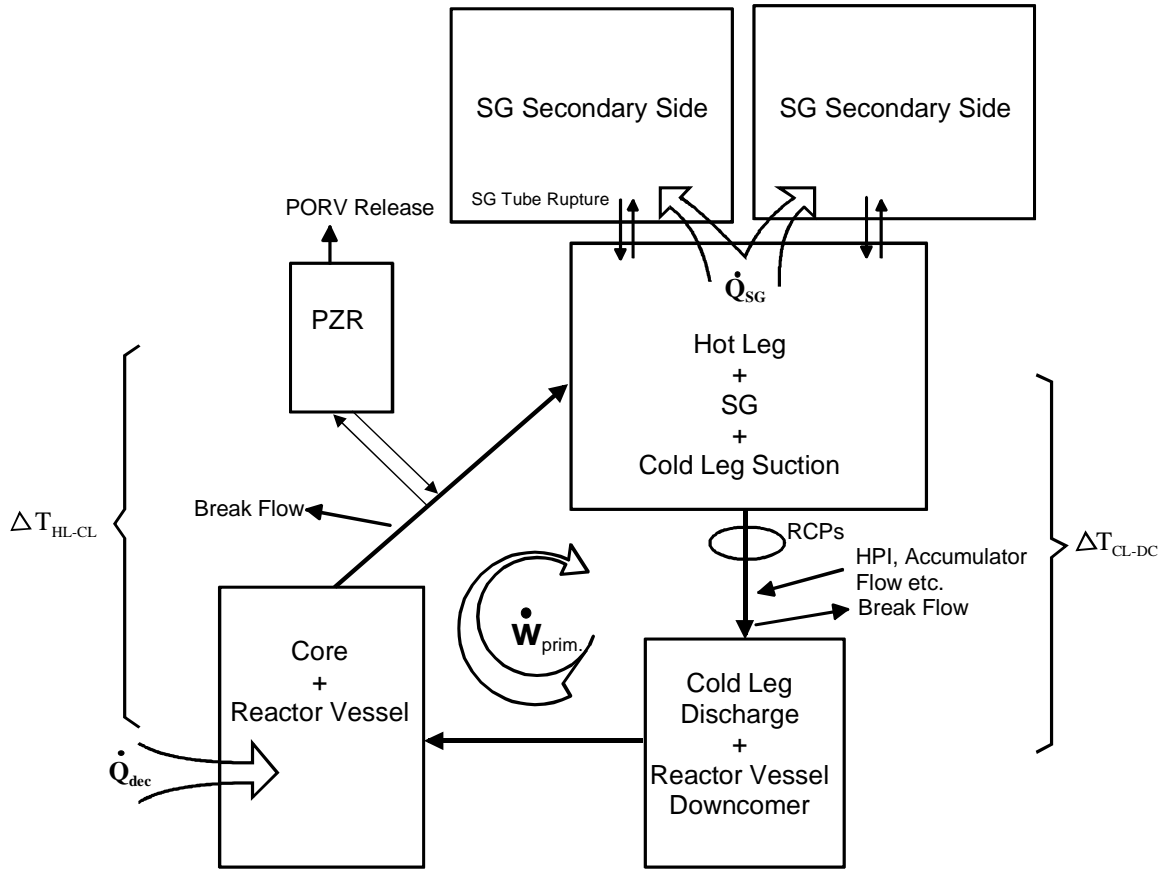


Figure 3-4. Simplified Representation of the Reactor Coolant System Control Volume (Top-Down) Approach to System Evaluation

The downcomer fluid temperature is the key fluid condition for PTS. The fluid time constant τ for the downcomer for LOCAs can be estimated by considering the volumetric flow rate of ECC flow and the control volume upon which the ECC acts. For this purpose, the downcomer control volume can be viewed as a subset of the entire RCS. It is taken to be the mixing volume available to the ECC following loop flow stagnation, and consists of the vessel + cold legs, which we call V_{vessel} , and which is $\sim 100 \text{ m}^3$. The time constant for the downcomer can be estimated as

$$\tau = \frac{V_{vessel}}{Q_{ECC}}$$

The ECC injection flows are approximately (within an order of magnitude)

HPI	0.06 m ³ /s
Accumulator	1 m ³ /s
LPI	0.36 m ³ /s

The downcomer fluid time constants for the three characteristic ECC injection rates are

$$\tau_{HPI} = 1700s, \quad \tau_{ACC} = 100s, \quad \tau_{LPI} = 280s$$

These times are measured from the onset of flow stagnation. Note that these estimates of fluid time constants are consistent with the failure data shown above in Figure 3-2. For breaks > ~6 inch, the RCS depressurizes within ~1000s to allow accumulator injection and LPI. Once these systems begin to inject, the characteristic time to cool the downcomer falls sharply from ~1700s to ~200s.

The time fluid time constants are important in the relation they play to the vessel time constants, as shown in Figures 3-1 and 3-2, and the Fourier number. A large break results in rapid depressurization and early initiation of accumulator injection and LPI. Larger breaks (i.e., >~6 inch) shift the fluid time constant by an order of magnitude from ~2000s to ~200s because of the large ECC injection rates from the accumulator and LPI. This results in rapid cooling of the downcomer relative to the vessel time constant (Fourier number). For small breaks (i.e., <~3 inch) the ECC flow is primarily or solely HPI. The fluid time constant is of the same order or longer than the vessel time constant (Fourier number).

One of the three important boundary flows is heat transfer across the steam generators (decay heat and RCS heat structures are the other two). For secondary side transients, the energy flow out of the RCS is via a secondary side break instead of an RCS break. Events that involve the secondary side are a major part of the ~10⁴ PTS sequences defined by PRA. Secondary side events consist of mass/energy flows in and out of the steam generators. Such events influence the RCS through heat transfer across the steam generator. From the perspective of thermal-hydraulic analyses, the main difference between secondary side events and LOCAs is that *natural circulation is enhanced* by secondary side breaks.

Similar to the RCS, mass/energy flows out of the secondary side result from a stuck-open valve or a break. Secondary side valves consist of steam generator SRVs, atmospheric release valves, and steam dump valves. As with stuck-open pressurizer SRVs, for stuck-open secondary side valves, the break area is defined by the valve characteristics. From a design value or measured flow rate, an equivalent diameter is defined as an input to the code.

Breaks may occur in steam lines or feed lines. Again, as for LOCAs, neither the break location or break size can be defined a priori, so the analysis must consider the spectrum of possibilities. Once a given break size is specified, however, an uncertainty in the break flow model can be given.

Feedwater flow is defined by the characteristics of the main or auxiliary feedwater pumps, which are inputs to the code from pump curves used in the different plants. The feedwater flow may be further specified as part of the event sequence involving failures of the level control system or operator errors. The second input parameter is the feedwater temperature, which is a predetermined input as well.

3.3 Classification of PTS Scenarios

There are two ways to approach the definition, classification, and evaluation of PTS scenarios. One is from the PRA perspective. In this bottom-up approach, the plant design is examined from the standpoint of the network of active (pumps and valves) and passive components. All possibilities of failures of components are considered, including failures of vital support systems such as power supplies, air supplies, water supplies, etc.

From the thermal-hydraulic perspective, it is advantageous to view the problem in a top-down manner. The RCS is seen as a control volume, as illustrated in Figure 3-4. This treats the solution as a problem of thermodynamics. The control volume must be cooled relatively rapidly and severely to generate a PTS risk potential. The boundary conditions acting on the control volume determine the problem to be solved, and play a dominant role in its solution. From this approach, classification of accident space begins with two categories, based on whether energy removal from the RCS is (1) direct by means of a break, or (2) indirect by means of heat transfer across a surface (i.e., steam generators), as follows:

- (1) Direct energy removal from the RCS involves transients that originate by a primary side break (LOCAs). LOCAs may occur either from a pipe break or a stuck-open pressurizer valve. The PTS risk from LOCAs is dominated by low vessel temperature. Since the RCS depressurizes, pressure is not a major factor in these scenarios. The possible locations of pipe break LOCAs can be subdivided into hot leg breaks and cold leg breaks. The sizes of breaks considered included the complete spectrum.

The subgroup of LOCAs consisting of stuck-open relief valves includes pressurizer power-operated relief valves (PORVs) and safety/relief valves (SRVs). Feed-and-bleed is a type of stuck-open relief valve scenario. Not only must the valve open to begin with, it must stick open, remain open for a sufficiently long time to cool the RCS, and then reclose at an inopportune time.

If a valve recloses early, there is no risk because the RCS does not have time to cool sufficiently. If the valve stays open, there is no PTS risk. This is because SRVs are small breaks, so the RCS cooling by itself is not so severe as to generate risk. When the valve closes, the RCS refills under the action of HPI. If the operator controls HPI to prevent the RCS from becoming water solid, there is no risk because RCS pressure remains controlled. Only those transients for which the valve remains open for a substantial period of time (1 to 2 hours), recloses, and HPI is not controlled generate substantial risk among SRV sequences. For these scenarios, high RCS pressure plays a vital role in determining the risk-significance.

- (2) Transients that originate by a secondary side break. Such transients cool down one or more steam generators and remove heat from the RCS across the heat exchanger surface. Examples are steam line breaks, stuck-open steam dump valve(s), stuck-open steam generator SRVs, and stuck-open atmospheric release valves.

The current studies show that both a steam line break and continuation of feedwater to the broken steam generator are required to generate PTS risk. Neither a steam line break by itself, nor a simple steam generator overfeed, will cool the RCS sufficiently.

The ECC injection rate increases as pressure decreases. In general, the rate of increase is a gradual function of pressure. There are, however, one or more important **step functions** in the process. These step functions in the relation between ECC flow and pressure at times **amplify** the effect of small differences in pressure. Such amplified response is noticeable when comparing RELAP5 predictions to experimental data, or comparing the results of sensitivity studies.

The first step change in ECC injection flow is associated with the safety injection signal that starts the ECC pumps. At that time, HPI flow begins. At first because of the high pressures, ECC flows are from HPI alone. In CE plants, the shutoff head of the HPI pumps is ~1200 psi, which is lower than the SI setting, so there is a time delay before injection begins while the RCS is depressurizing.

The next step to occur in the ECC injection process corresponds to the accumulator pressure. In Westinghouse and B&W plants this pressure is ~4.4 MPa (600 psi), while in some CE plants it is ~1.5 MPa (200 psi). The characteristic flow rates during accumulator injection depend on the RCS depressurization rate, but are generally much higher (order of magnitude) than HPI flow.

The final step corresponds to the shutoff head of the LPI pumps, which is 1.5 MPa (~200 psi) for all three vendors. The LPI flow rates are ~6 times greater than HPI flows.

Therefore, it is evident that larger breaks lead to much larger ECC injection flows than small breaks. This is the main reason that larger breaks are more severe. Break sizes of ~2.8 inches and greater are sufficient to cause accumulator injection and LPI. Breaks of 1.5 to 2 inches are sufficiently large to allow accumulator injection (Westinghouse and B&W), but not LPI. At lower pressures characteristic of medium and large breaks, ECC water enters at a high rate and quickly cools the downcomer.

3.4 LOCA-Induced Cooling of the Reactor Coolant System Scenario Description

LOCAs, including stuck-open SRVs, constitute a family of transients whose behavior is to a first approximation, similar and self-consistent. Specifically, their general behavior can be normalized on the basis of energy/inventory, instead of plotting against time. The predominant effect in terms of energy/inventory of increasing the break size is to make the transient proceed more rapidly.

The spectrum of LOCAs is considered from the perspective of PTS and the associated important thermal-hydraulic phenomena. From this standpoint, there are three possible, distinct, regimes of mass flux the RCS may experience:

- **Reactor coolant pumps on.** Mass flow is approximately 20,000 kg/s (400,000 gpm), with cold leg velocities ~15 m/s and downcomer velocities ~7 m/s.
- **Natural circulation.** The characteristic flow rates for natural circulation are of the order of 3% of pumped flow. Figure 3-5 shows the relation between natural circulation flow rate and decay heat [10] for steady state conditions (i.e., RCS temperature is held constant). At 3% of forced flow, natural circulation flow is ~600 kg/s, and the loop flow velocities decrease by a factor of 30 compared to pumped flow. Therefore, velocities in the cold leg and downcomer are ~0.5 m/s and 0.25 m/s.
- **Loop flow stagnation** (i.e., there is no longer a complete flow circuit throughout the RCS).

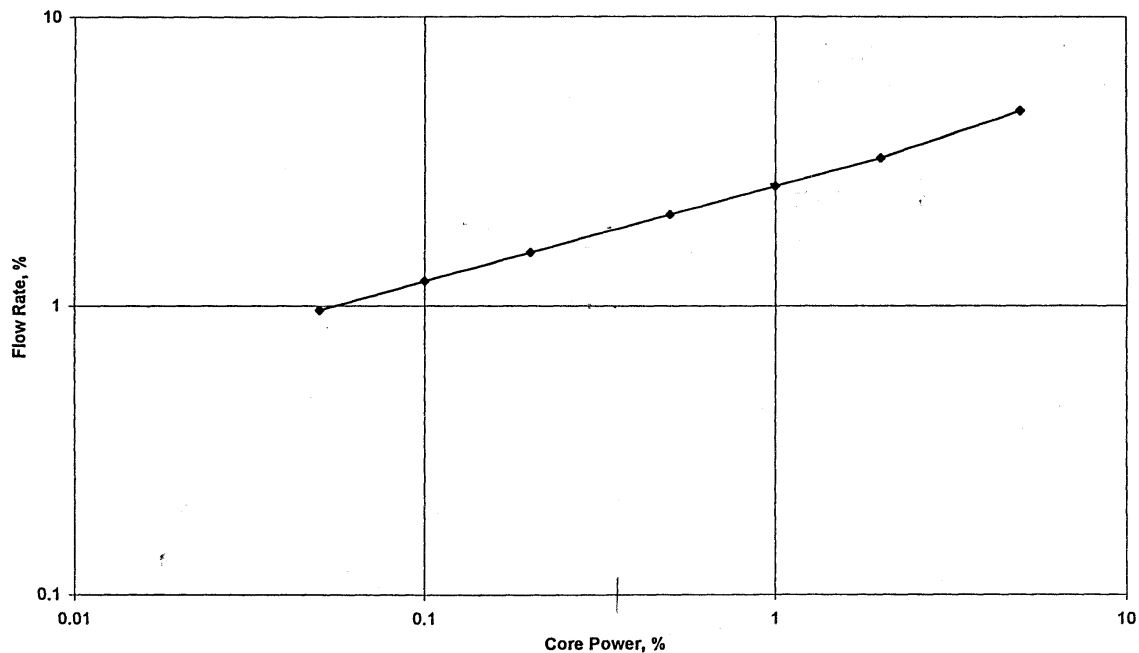


Figure 3-5. Natural Circulation Flow as a Function of Decay Heat Level [10]

The characteristic loop flow rates differ considerably among the three system flow regimes, as do the hydrodynamics of the loop flow. The following effects are of current interest:

- energy distribution throughout the primary system
- convective heat transfer coefficient
- fluid-fluid mixing and stratification in the cold legs and the downcomer

From the complete LOCA break spectrum, we first screen out very small LOCAs, which are defined for PTS purposes, as follows:

- Breaks < ~1.4 inch equivalent diameter

This class of very small-break LOCAs generates no PTS risk because the downcomer never cools. For LOCAs, loop flow stagnation is a precursor to developing downcomer conditions conducive to PTS. For very small breaks, forced flow is maintained (that is, RCPs remain running). Thus, the range of break sizes of PTS significance is bounded from below by breaks too small to decouple the primary side from the secondary side to cause cessation of forced flow.

The boundary region for break size between very small and small LOCAs is determined by whether or not HPI capacity is sufficient to compensate for break flow. The location of this boundary differs somewhat from plant to plant depending on the capacity of HPI and the core power. Generally, it is approximately 1.4 inch equivalent-diameter, given full-power initial conditions and full availability of HPI. Therefore, LOCAs >1.4 inch will cause loop flow stagnation.

Following break initiation, coolant is lost from the RCS, causing pressurizer level and pressure to fall. When the safety injection set point is reached, the ECC injection system is automatically started. The safety injection signal set point differs somewhat amongst the vendors, but is generally ~13 MPa (~1800 to 1900 psia). The small differences do not matter in the current context. If HPI flow can compensate for break flow (very small breaks), then the pressurizer will not empty. Inventory and pressure control is, therefore, maintained. Also, subcooling in the loops is maintained, and the RCPs remain running. Figure 3-6 shows the relationship between break size and RCS pressure.

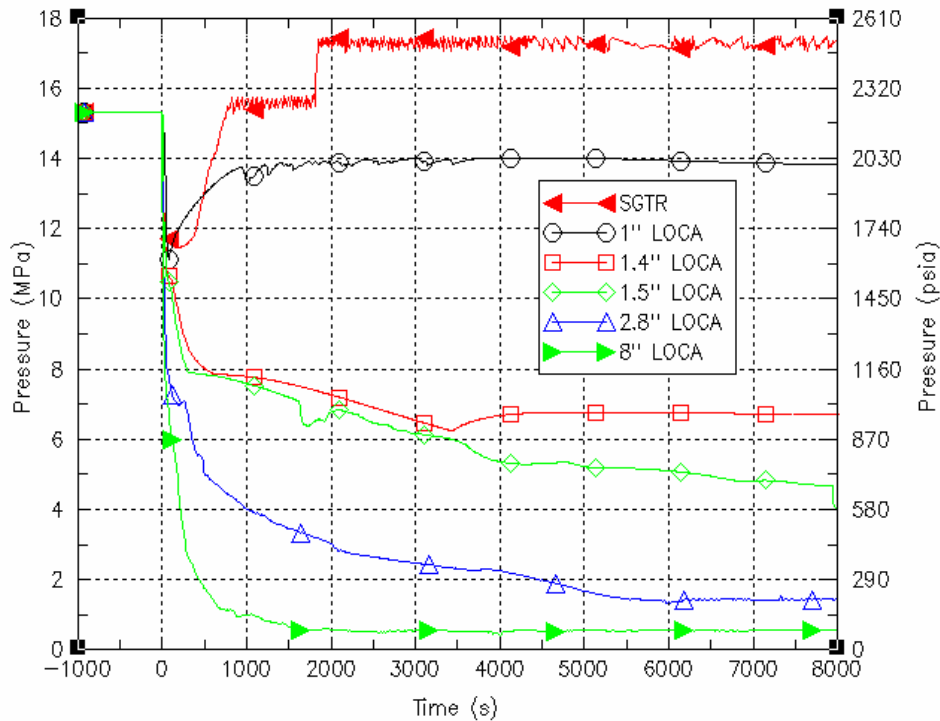


Figure 3-6. RCS Pressure as a Function of Break Size for Oconee
(Pressure control maintained for 1-inch break, but lost for 1.5-inch break.)

Once the pressurizer is completely empty, hot leg subcooling is lost. Upon loss of subcooling in the hot leg, operator procedures call for tripping the RCPs. The criteria for RCP trip differ somewhat from vendor to vendor, but the impact on the transient progression of these minor differences is immaterial. When the RCPs trip, the RCS quickly transitions from forced to natural circulation flow as the pumps coast down (which takes less than a minute). Following coastdown, natural circulation conditions may exist for some time interval, the length of which depends on the particular transient. The larger the break size, the less time is spent in natural circulation

Loss of natural circulation only occurs under conditions of LOCA (or steam generator dryout - loss of heat sink). If a break is sufficiently large that it results in the loss of pressurizer pressure and level control, the break is also large enough to remove decay heat. In fact, either the break flow or HPI flow alone are sufficient to remove decay heat (see Table 3-1). That being so, the steam generators are not needed as a heat sink.

Table 3-1. Energy Source/Sink Magnitudes for Oconee-1

Time after Trip (s)	System P* Bar (psi)	HPI Flow Rate (kg/s)	Decay Heat* (MW)	HPI Sensible Heat (MW)	Downcomer + Cold Leg HPI Fill Time (s)	SG Energy Removal Rate $\Delta T=6\text{ }^{\circ}\text{C}$ (MW)
1000	60 (870)	67	48	-70	400	150
2000	46 (670)	71	40	-74	380	125
4000	20 (290)	77	33	-81	350	115
2000	170 (2460)**	30	40 + 20*	-31	900	325

Above $\sim 7.1\text{ MPa}$ ($\sim 287\text{ }^{\circ}\text{C}$, saturated conditions), which is a typical steam generator secondary pressure, primary system pressure exceeds secondary side pressure, assuring natural circulation conditions. Once hot leg temperature (or pressure) drops below the secondary side temperature, natural circulation ceases:

$$T_{\text{hot leg}} < T_{\text{secondary}} \text{ or}$$

$$P_{\text{primary}} < P_{\text{secondary}} \text{ (upon loss of hot leg subcooling)}$$

Figure 3-7 shows, for example, the RELAP5 calculation of a 2-inch hot leg break in Palisades, indicating the onset of flow stagnation when primary pressure falls below secondary. Table 3-2 classifies transients according to whether or not flow stagnation occurs. Therefore, during LOCAs, the range of interest for evaluating downcomer conditions is $\sim 7\text{ MPa}$ to 0.2 MPa .

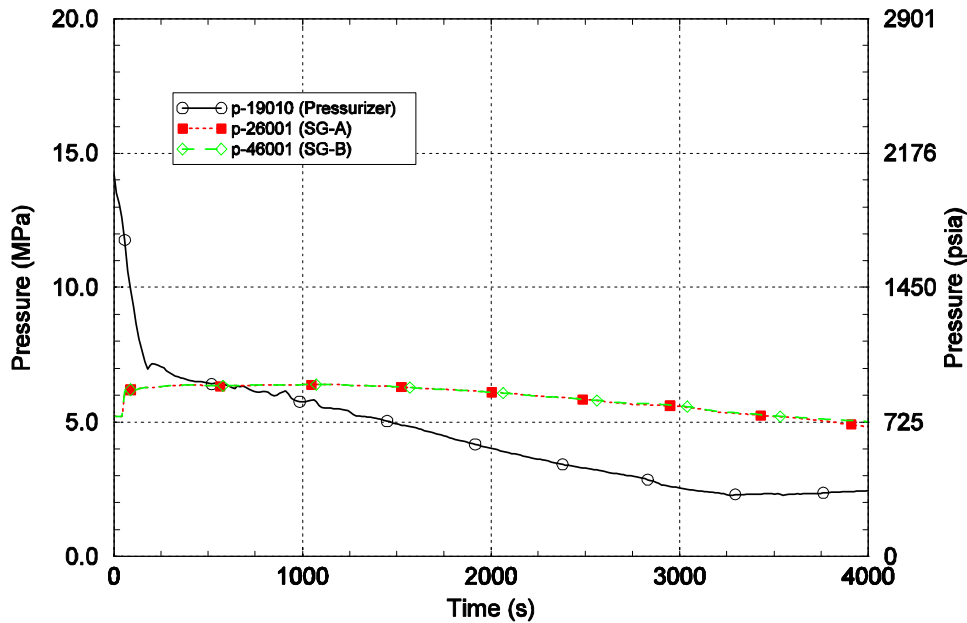


Figure 3-7. Palisades 2-inch Hot Leg Break
(Natural circulation ceases at $\sim 700\text{ s}$ when RCS pressure falls below steam generator pressure, which is onset of flow stagnation.)

Table 3-2. Classification of Two-Phase Transients

Break Energy/Mass Flow Rate		Energy/Mass Sources	Flow Stagnation
$\frac{\dot{Q}_{brk} - \dot{Q}_{HPI}}{\dot{W}_{brk}}$	<	$\frac{\dot{Q}_{dec}}{\dot{W}_{HPI}}$	No flow stagnation
$\frac{\dot{Q}_{brk} - \dot{Q}_{HPI}}{\dot{W}_{brk}}$	< >	$\frac{\dot{Q}_{dec}}{\dot{W}_{HPI}}$	Flow stagnation possible, but brief
$\frac{\dot{Q}_{brk} - \dot{Q}_{HPI}}{\dot{W}_{brk}}$	~ >	$\frac{\dot{Q}_{dec}}{\dot{W}_{HPI}}$	Flow stagnation possible and could be prolonged
$\frac{\dot{Q}_{brk} - \dot{Q}_{HPI}}{\dot{W}_{brk}}$	>> >>	$\frac{\dot{Q}_{dec}}{\dot{W}_{HPI}}$	Flow stagnation with rapid decrease of P
$\dot{Q}_{HPI} = \dot{W}_{HPI} \times [h_f(T_{sat}) - h_f(T_{HPI})]$			
* Add 20 MW to decay heat if RCPs are running			

During the depressurization and loss of inventory phase of LOCAs, the inherent tendency is for the level in the RCS to fall until reaching the break elevation [11]. This is normally the elevation of the hot and cold legs. Should the break occur in a branch line, it is equivalent to the break occurring where the branch connects to the main hot or cold leg, that is, the off take to the main coolant pipes. This elevation also corresponds closely to the entrance of the ECC injection line to the cold leg. When the loss of inventory phase of the LOCA is complete, an interface level will generally form at the loop elevation as the break partially uncovers.

3.4.1 Cold Leg Behavior

Under low flow conditions, cold leg stratification occurs. The onset of stratification in the cold leg may begin during natural circulation. As illustrated in Figure 3-6, the following important phenomena occur in the cold legs under flow stagnation conditions:

- Following interruption of natural circulation during LOCAs, there is a period of time required for the primary side of the steam generators to drain. Until the primary side is empty, reverse heat transfer occurs within the tube bundle region. Of the water in the primary side of U-tube steam generators, half drains into the cold legs, where it tends to mix with the HPI water. For once-through steam generators (B&W), all the primary side water drains into the cold legs.
- Local fluid mixing and the onset of thermal stratification in the cold leg.
- Stratification and mixing in the ECC injection line. Cold ECC water is injected through the ECC injection line into each cold leg. Depending on the injection flow rate, Froude number analysis indicates the potential for back-flow of warm water from the cold leg into the ECC injection line. The phenomenon was observed in a visual experimental facility conducted as part of the APEX-CE PTS testing.
- Backflow of ECC to loop seal volume. The loop seals participate as part of the mixing volume during ECC injection under conditions of loop flow stagnation. This tends to mitigate the cooldown rate. This effect is generally not present in B&W designs because the cold legs have a high point at the RCP, as shown in Figure 3-8. At the RCP discharge, the cold legs slope downwards before becoming horizontal and entering the vessel. The HPI is into the sloped part of the cold leg, so the ECC water flows toward the vessel and away from the loop seal.
- Reverse flow from upper downcomer into cold legs. Experiments have routinely shown that warm water flows from the upper downcomer into the cold legs, countercurrent to the flow of cold ECC water toward the vessel.
- Condensation. Direct contact condensation of vapor on the injected ECC water may occur in the cold legs during LOCAs. The propensity for condensation to occur depends on the orientation of the break and the ECC injection line. It is a maximum for a break on the bottom of the cold leg and ECC entrance at the top of the cold leg. Conversely, it is minimum for top breaks and bottom entry ECC lines. From the PTS perspective, condensation has a positive effect in that it (1) lowers the RCS pressure, (2) raises the temperature of the cold ECC injection water, and (3) promotes vigorous mixing within the RCS, which brings the overall fluid conditions toward equilibrium. CE plants have top-entry ECC injection. The HPI in B&W designs in the sloped part of the cold leg also enhances condensation potential. The ECC orientation in Westinghouse plant varies.

These phenomena all act to mix the ECC liquid before it enters the downcomer, so the downcomer does not reach the ECC injection temperature.

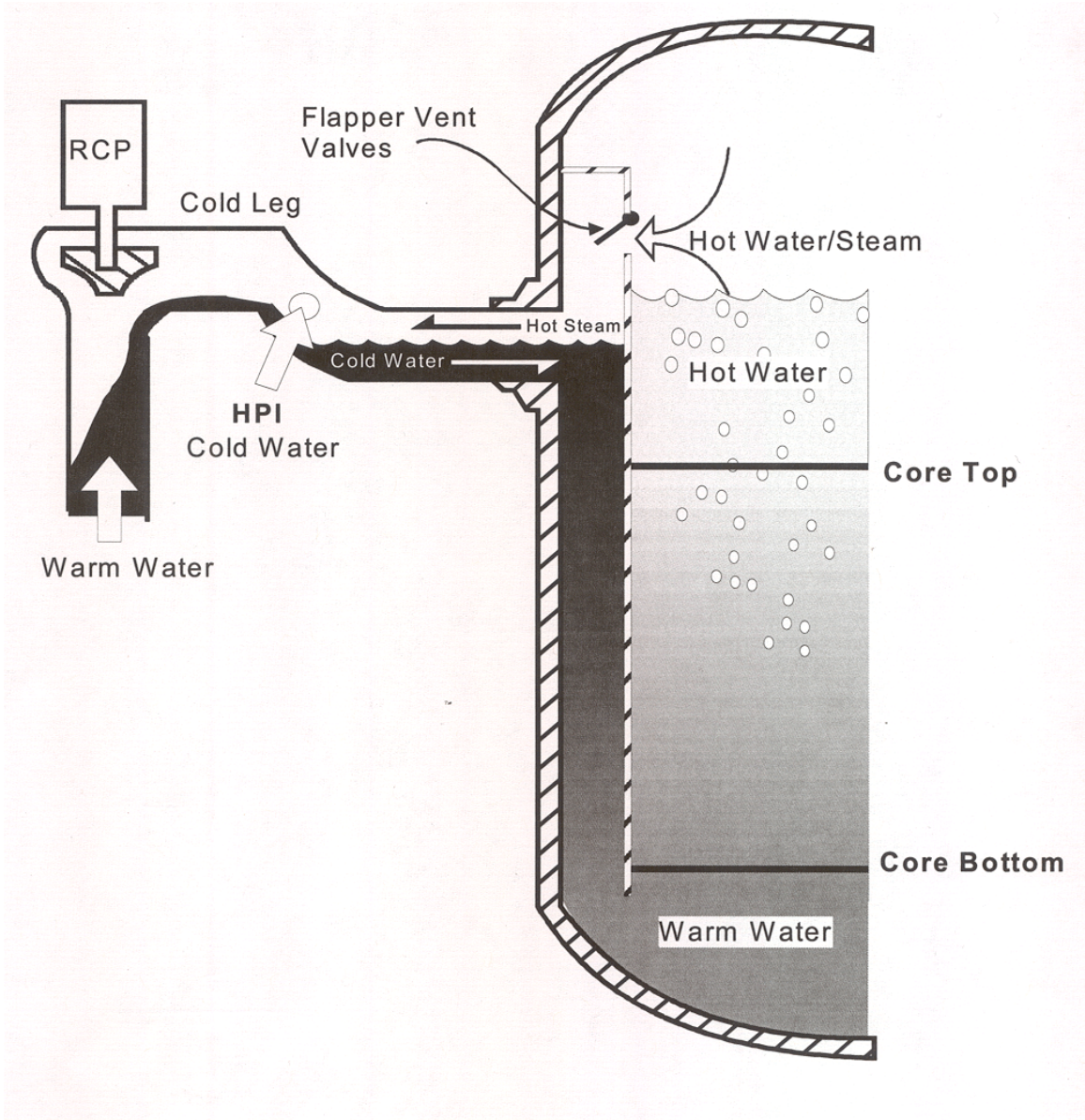


Figure 3-8. Schematic of B&W Design Showing Local Phenomena in Cold Leg and Downcomer

Following onset of flow stagnation, the cooling of the downcomer is approximated by the mixing cup (back-mixed) model, where the flow into the downcomer consists of ECC flow and the flow out of the downcomer is related to the break flow. Although loop flow has ceased, there are still driving forces for in-vessel flows, as illustrated in Figure 3-8, including the following:

- ECC injection flow in the cold legs
- break flow (hot leg or cold leg)
- buoyancy-driven natural circulation cells within the downcomer
- heat transfer across the core barrel and from the vessel to the downcomer fluid
- in-vessel buoyancy-driven natural circulation flows driven by core decay heat and ECC injection
- condensation

3.4.2 Downcomer Behavior

Following cessation of loop flow, there is an exponential temperature decay in a well mixed ambient volume. The mixing region that incorporates the downcomer and the ECC injection is shown in Figure 3-9. In this region, the temperature decay rate is a function of the break size and the associated ECC injection rate. It is possible to represent the temperature history in the downcomer by a simple exponential cooldown and, therefore, to determine an appropriate time constant.

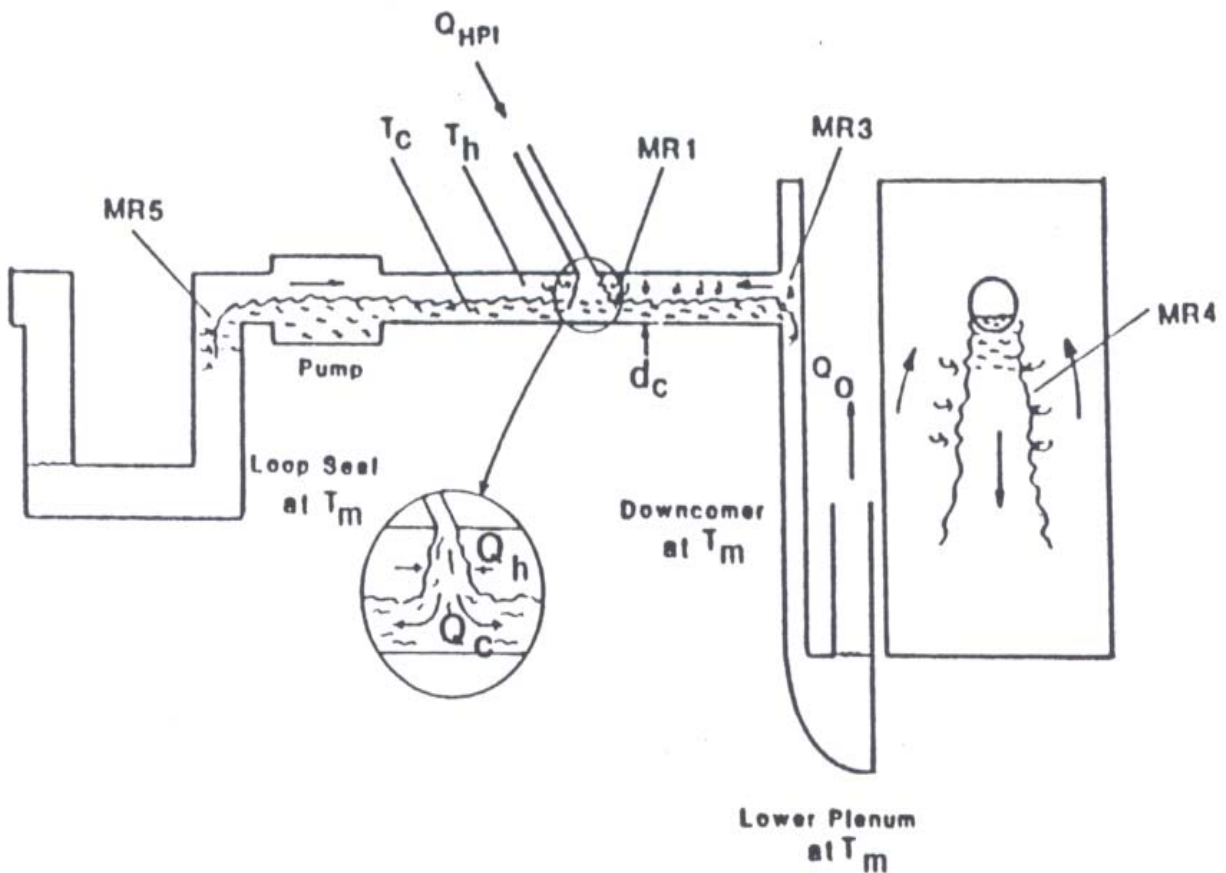


Figure 3-9. Regional Mixing Model

Figure 3.10 plots two temperature curves. The first is the RELAP5 calculation of downcomer temperature for a stuck-open pressurizer SRV in Palisades. The second curve is the solution to the following equation:

$$T(t) = T_{ECC} + (T_0 - T_{ECC})e^{-t/\tau}$$

where $T_{ECC} = 40 \text{ }^\circ\text{C}$

$T = 333\text{s}$ (time constant)

This equation expresses the cooldown of an ideally mixed (back-mixed, mixing cup) volume. The value for β was chosen to fit the RELAP5 calculation. The overlay of the RELAP5 calculation using a full plant model of Palisades with the exponential decay function, shows that the analysis in essence is an evaluation of energy/inventory. The RELAP5 solution method is based on conservation of mass and energy, which reduces to a thermodynamic control volume problem.

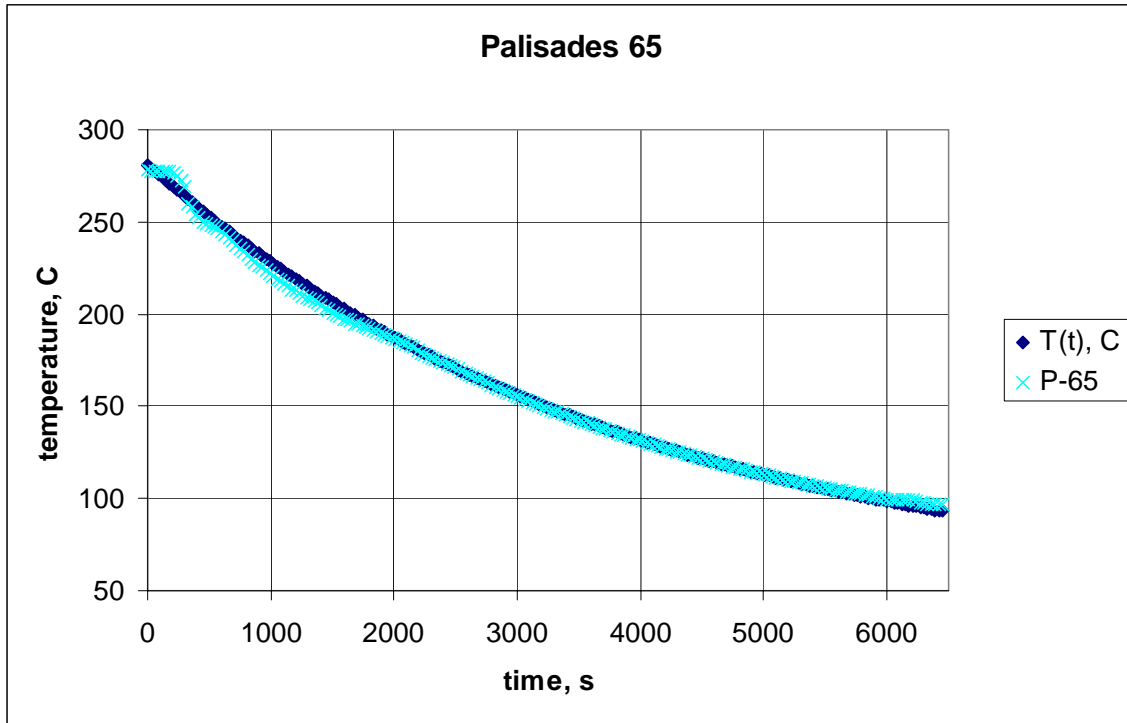


Figure 3-10. Comparison of RELAP5 Calculation of Downcomer Temperature to Exponential Decay Function (Ideally mixed volume).
*The curve with the symbol P-65 is the RELAP5 calculation of a Palisades small-break LOCA transient (two stuck-open SRVs that reclose at 6000s, low-power conditions).
 The curve with the symbol T(t) is the exponential decay equation, where T was chosen to best-fit RELAP5.*

3.4.3 Secondary Side Induced Cooling of the Reactor Coolant System

Secondary side transients of possible interest to PTS are all overcooling events involving some combination of excess steam flow and continuing feedwater flow. These events essentially produce sufficiently rapid and extensive cooldown and shrinkage of the coolant in the RCS, such that the pressurizer empties, HPI actuates, and subcooling is lost. In fact, secondary side events (MSLBs) are similar to LOCAs in terms of their global impact on the RCS.

The flow condition in the RCS for these events is predominantly natural circulation. Flow stagnation will not occur because the steam generators remain as the heat sink. In fact, natural circulation flow rates are enhanced as a result of the secondary side cooldown. The strong heat sink provided by one or more depressurized steam generators enhances natural circulation loop flows through the RCS. The downcomer does not get as cold for secondary side events as it does for LOCAs.

4. RELAP5 ASSESSMENT AND UNCERTAINTIES FOR PTS ANALYSES

4.1 Introduction

Coupling of the probabilistic fracture mechanics, deterministic thermal-hydraulics, and probabilistic risk assessment analyses into the process for evaluating the risk of vessel failure has been discussed in previous chapters. In this framework, thermal-hydraulics analysis provides the time-histories of pressure, temperature, and heat transfer needed as input parameters for the fracture mechanics analyses. RELAP5 was the thermal-hydraulic analysis tool used to model the prototype power plants.

The RELAP5 code models the conservation of mass, momentum and energy for the flow of single-phase liquid or vapor and two-phase flow of liquid and steam/noncondensable gas mixtures. The basic code formulation was developed for the one-dimensional flow within systems of piping and vessels. The code is non-equilibrium (allowing different temperatures between the phases) and non-homogeneous (allowing different liquid and vapor velocities).

The RELAP5 code also includes capabilities for the modeling of structural components and for thermal coupling between fluid and structures, as well as control systems with capabilities for modeling the automatic and operator-induced control functions of the prototype plants. The code is applied by developing a facility "input" model which represents the configuration of the fluid volumes, flow paths, structures and control systems of the prototype system. The input model breaks the fluid system up into a nodalization of discrete calculational fluid cells, which are connected together by junctions.

Although the basic RELAP5 code formulation is one-dimensional, the facility nodalizations may themselves be made multidimensional, with the understanding that the code does not fully represent all aspects of multidimensional flow. A top-level assumption with RELAP5 is that within each fluid cell the liquid and vapor phases may each have only one temperature and one velocity.

This section addresses the question, "How well does RELAP5 predict the reactor vessel downcomer pressure, temperature, and heat transfer coefficient responses that are needed as input for the fracture mechanics analyses?" The question is answered using assessments of the RELAP5 computer code for predicting the behavior observed during tests in instrumented experimental facilities. The assessment process involves developing a RELAP5 nodalization for the experimental facility, simulating a test in the facility and then comparing the response of measured data from the test with the RELAP5-calculated data for the parameters of interest for PTS.

Section 4.2 describes the thermal-hydraulic parameters of interest for PTS. Section 4.3 describes how the experiments are used to assess the capabilities of RELAP5 for predicting the thermal-hydraulic parameters of interest. Section 4.4 lists the experiments used in the assessments. Sections 4.5, 4.6, and 4.7 present the assessment results for the PTS parameters of interest, including reactor vessel downcomer pressure, fluid temperature, and wall inside-surface heat transfer coefficient, respectively. Additional assessments and uncertainties are discussed in Section 4.8 and assessment conclusions are given in Section 4.9.

4.2 Thermal-Hydraulic Parameters of Interest

The thermal-hydraulic analysis provides the information necessary for determining the PTS figure of merit, K_R (see Section 4.3). The high-level thermal-hydraulic parameters of interest are defined by the information required to evaluate K_R . That is, the parameters of interest are the boundary conditions necessary to perform the structural analysis. The boundary conditions are (1) RCS pressure, and (2) heat flux from the vessel wall to the downcomer fluid. These parameters define the stress field in the vessel (which is a function of pressure and temperature distribution in the wall) and its material properties. Heat flux is not fed directly from RELAP5 to FAVOR. Instead, it is broken down according to the following relation; all terms are functions of time, t :

$$q''(t) = h_{dc}(t) [(T_w(t) - T_f(t))]$$

where q'' is heat flux,

T is temperature, with subscripts w and f referring to wall and fluid, respectively and h_{dc} is the average vessel wall-to-fluid heat transfer coefficient in the downcomer

The boundary conditions supplied from RELAP5 to FAVOR are $P(t)$, $h_{dc}(t)$ and $T_f(t)$. FAVOR then calculates $T_w(x,t)$, where x spans the thickness of the vessel wall. The two important characteristics of $T_f(t)$ are the integrated change in T_f and its rate of change, dT_f/dt .

The fluid system response must be known in order to provide the boundary conditions of heat flux and pressure necessary to calculate K_R . The validation of RELAP5 for PTS analysis must first and foremost consider its ability to accurately calculate the thermal-hydraulic figures of merit, including the time histories of RCS pressure $P(t)$, fluid temperature in the downcomer $T_{dc}(t)$, and wall-to-fluid heat transfer coefficient in the downcomer $h_{dc}(t)$.

This chapter summarizes the supporting information that establishes the basis for the applicability of RELAP5 for PTS analyses. As described in previous chapters, pressure and temperature are global system parameters that are the most relevant measure of energy/inventory. The calculation of these parameters by RELAP5 is based on conservation of mass and energy. It follows that the assessment and validation of RELAP5 for calculating $P(t)$ and $T_f(t)$ were based on comparisons to experiments from scaled integral systems test facilities. The assessment of RELAP5 predictions of h_{dc} are based on limited numbers of these same experiments that had suitable measurements of downcomer fluid and wall temperatures and downcomer fluid velocity measurements.

Beyond the general ability of RELAP5 to calculate energy and inventory, and therefore temperature and pressure, the principal RELAP5 modeling and validation issue with respect to temperature was the one-dimensional formulation for pipe flow. The code treats fluid-fluid mixing as, in effect, ideal in each individual cell or node. The code does not represent possible temperature distributions within nodes.

The code must be shown to provide a reasonable approximation of multidimensional fluid conditions in the downcomer. In Section 4.5, we compare RELAP5 to experimental data on temperature distributions in the cold leg and downcomer. The data show the reactor vessel downcomer to be well-mixed despite large thermal stratification in the horizontal cold legs. The RELAP5 predictions of downcomer temperature are shown to be in good agreement with the data. Given the capabilities for representing the downcomer flows, the code must then be shown capable of reasonably representing the reactor vessel wall inside-surface heat transfer.

4.3 Employment of the Experiments for the Assessments

The assessment process involves developing a RELAP5 nodalization for an experimental facility, simulating a test performed in the facility with RELAP5 and then comparing the measured data from the test with the RELAP5-calculated data for the parameters of interest. As described in Section 4.2, for PTS the parameters of interest are the reactor vessel downcomer pressure, fluid temperature and wall inside-surface heat transfer coefficient.

When performing assessments it is important that the computer code and model nodalizations employed in the assessment calculations are consistent with those used in the plant application. Along with employing tests performed in experimental facilities that are correctly scaled to the prototype plants and that simulate behavior pertinent for PTS accident scenarios, this approach assures that judgements made in assessing RELAP5 for predicting plant behavior are correct.

The same version of the RELAP5 code (RELAP5/MOD3.2.2γ) was used for all the assessment studies and for all the plant calculations. In addition, consistent nodalization schemes were employed among the various experimental and prototype plant facility models. The reactor vessel downcomer nodalization scheme generally features a two-dimensional azimuthal cell layout on each axial level. For certain experimental facilities this two-dimensional layout was not used because, for example, the downcomer region is represented using a small pipe. Table 1-2 in [12] compares the nodalization schemes used in each of the experimental facility and plant models used in the PTS evaluation study.

The comparison methods used when assessing the code performance become an issue when one considers that the measured and calculated parameters both vary in time and that there is no clear figure of merit (for example, the lowest temperature attained) to use for the comparisons. Instead, for the PTS assessments both qualitative and quantitative comparisons were made between the measured and calculated data for the parameters of interest.

The qualitative comparisons were made using a standard set of criteria (previously applied in several other NRC projects) that judges whether the comparison between the measured and calculated data is excellent, reasonable, minimal or insufficient. These criteria are provided in Appendix C. The qualitative approach looks at measures of agreement (such as trends and rates of change) that go beyond quantitative measures.

For the quantitative comparisons of reactor vessel pressure and fluid temperature, the measured pressures and temperatures from the experiments are compared directly with the appropriate RELAP5-calculated pressures and fluid temperatures. The mean and standard deviations for the difference between the measured and calculated parameters are taken over the length of the comparison period.

For the reactor vessel wall heat transfer coefficient, quantitative comparisons are more difficult because heat transfer coefficients are not directly measured in the experiments. Further, since most of the test facilities were designed to study core-coolability safety issues and not vessel downcomer overcooling issues, instrumentation related to downcomer wall heat transfer (wall and fluid thermocouples, wall heat fluxes and downcomer fluid velocities) is, in general, very limited. Quantitative assessments for heat transfer coefficient and other parameters associated with the wall heat transfer process were made as feasible using the limited available data. A variety of other

investigations into reactor vessel wall heat transfer in general and RELAP5 capabilities in particular were also performed.

The results of the qualitative and quantitative comparisons between measured and calculated data are provided for downcomer pressure, downcomer fluid temperature and downcomer wall heat transfer in Sections 4.5, 4.6 and 4.7, respectively.

4.4 Assessments Performed

The assessments were performed using data from experimental facilities that represent the configurations of the three main reactor designs for U.S. power plants, including Westinghouse, CE, and B&W. The experimental facilities used for code assessment are the best available from the NRC thermal-hydraulic data base. They included ROSA [13], APEX-CE [3,4], MIST [14], LOFT [15], UPTF [16, 17], and MARVIKEN [18, 19]. Taken together, the facilities provide a range of scales from reduced size to full scale. Some were full height, some reduced height. Similarly, some were full temperature and pressure, while some were reduced. While they varied considerably in their basic geometrical scaling approach, they shared the common scaling principal of maintaining a power-to-volume ratio of 1:1. Table 4-1 lists the main attributes of the facilities. Brief facility descriptions follow.

Table 4-1. Experimental Facilities Used for Assessment

Facility	Height	Pressure/ Temperature	Volume	Aspect Ratio
ROSA-IV	Full	Full	1:48	1:7
ROSA-AP600	Full	Full	1:30	1:5.5
APEX-CE	1:3.5	210 °C	1:276	1:4
MIST	Full	Full	1:817	1:29
LOFT	1:2	Full	1:50	1:5
UPTF	Full	190 °C	1:1	1:1
MARVIKEN	Full	Full	1:1	1:1

ROSA-IV (Rig of Safety Assessment) was an integral test facility scaled to Westinghouse 4-loop plants. It was full-height, full-pressure, 1:48 volume scale. The four loops were combined into two in ROSA, which doubled their size. The hot and cold legs were 21 cm (8.2 inches) in diameter. The downcomer gap was 4.6 cm (1.8 inches). The vessel diameter was 0.64 m (2.1 ft). Each steam generator had 131 tubes.

The facility was of sufficient scale to minimize the impact of distortions attributable to facility heat loss or atypical heat flux from the metal structures to the fluid. Because of its scaling and instrumentation, it is in general the world's best available integral system test facility. ROSA had more than 2,000 instrument channels. The cold legs and downcomer were instrumented to measure local temperatures. The facility has been subject to detailed scaling analysis [20, 21].

ROSA/AP600 was a modified version of ROSA-IV used to perform AP600 experiments. With respect to the prototype, it was 1:30 volume scaled. The inclusion of the two ROSA/AP600 tests

is valuable in that the experiments start off as cold leg break LOCAs, but end up as hot leg break LOCAs as well, once the Automatic Depressurization System opens.

APEX-CE (Advanced Plant Experiment) was a 1:3.5 height, reduced pressure 2.75 MPa (400 psia), reduced temperature (210 °C, 400 °F), 1:276 volume facility, scaled to Palisades. APEX-CE had the same 2 x 4 coolant-loop arrangement as the plant, with 2 hot legs and steam generators, and 4 cold legs. The vessel diameter was 0.635 m (25 inches), nearly the same as ROSA. The downcomer gap was 6.4 cm (2.5 inches), which is similar to ROSA and LOFT. An important feature of APEX-CE is that the downcomer aspect ratio scale is 1:1 compared to Palisades. The cold leg diameters were 9 cm (3.5 inches). The facility heat losses were also nearly exactly scaled to the prototype.

MIST (Multi-Loop Integral System Test) was an integral test facility scaled according to the B&W lowered-loop plants. It was the only integral system test facility scaled according to the B&W geometry. MIST had two hot legs and four cold legs. It was full-height full-pressure, 1:817 volume scale. MIST had an external pipe downcomer. The other integral facilities all had annular downcomers. Of all the facilities used for RELAP5 assessment, MIST is the only one where distortions attributable to facility heat loss were a potential concern.

LOFT (Loss-of-Fluid Test) was an integral, full-pressure, full-temperature facility with a nuclear core. The volume scale was 1:50, the same as ROSA. The length scaling was ~1:2. The facility had one intact loop, which represented three loops of a four-loop Westinghouse plant, and one broken loop. The broken loop had a steam generator simulator, while the intact loop had a representative steam generator. The downcomer gap was 5 cm (2 inches), which was similar to ROSA and APEX. The vessel diameter was 1.46 m (4.8 ft). The cold leg diameter was 28 cm (11.2 inches). The test facility was power-to-volume scaled, which provides optimum similitude for representing system mass and energy for LOCAs.

UPTF (Upper Plenum Test Facility) was a full-scale test facility scaled to the Kraftwerk Union 1300 MWe four-loop design. The facility had full scale hot and cold legs. It operated at reduced pressure and at a reduced temperature of 190 °C (375 °F). The facility had a core simulator and simulated steam generators.

MARVIKEN was constructed as a boiling-water reactor. It operated briefly before being shut down. The facility was used for a number of experimental test programs, one of which was for LOCA blowdowns. The reactor vessel was full PWR scale, with a volume of 420 m³ (compared to ~250 m³ for the RCS of a PWR), an inside diameter of 5.22 m (17 ft) and height of 24.55 m (81 ft). The facility operated from full-temperature initial conditions. This facility was used to assess the RELAP5 modeling of depressurization and break flow.

Tests in these experimental facilities were selected so as to cover the range of the types of accidents and transients that were found to be important contributors to the overall PTS risk:

- small-break LOCAs
- medium-break LOCAs
- large-break LOCAs
- cold leg breaks
- hot leg breaks

- stuck-open pressurizer SRVs

While each of the experimental facilities is unique, data suitable for assessing RELAP5 code capabilities for representing the reactor vessel downcomer pressure and fluid temperature are generally available. However, as indicated in Section 4.3, heat transfer coefficient data measurements are not directly available. Further, sufficient and compatible fluid and wall temperature data needed to assess the RELAP5 wall heat transfer process are very limited.

The specific tests in the above experimental facilities used for assessing RELAP5 pressure, fluid temperature and wall heat transfer prediction capabilities are listed below in the assessment results sections for those parameters.

4.5 Assessment Results: Reactor Vessel Downcomer Pressure

RCS pressure, $P(t)$, is a global system state parameter and is often determined by the temperature of saturated water in the RCS. Pressure is essentially the same everywhere in the RCS, excepting minor effects of gravity head or when the RCPs are operating. Pressure is calculated by RELAP5 essentially based on the energy conservation equation.

In comparisons between code and experiment, the codes normally predict this parameter well, providing that the break flow calculation is accurate. In fact, the starting point of any code assessment performed against integral system experiments is the accurate prediction of break flow. Absent such good agreement for other key phenomena generally will not be obtained.

Table 4-2 provides a statistical summary of pressure comparisons for the 15 assessment cases that were carried out. A brief analysis and plotted comparisons between the measured and RELAP5-calculated system pressures is provided for each assessment case in Appendix D. RELAP5 on the average slightly under predicted the RCS pressure. The nominal bias for the set of 15 experiments was

$$\text{RELAP5 - Experiment} = -0.093 \text{ MPa (-13 psi)}$$

with a nominal standard deviation of

$$1\sigma = 0.32 \text{ MPa (46 psi)}$$

$$2\sigma = 0.64 \text{ MPa (92 psi)}$$

Note: 1σ contains 68% of the comparison points
 2σ contains 95.5% of the comparison points
 2.58σ contains 99.7% of the comparison points

Table 4-2. Statistical Evaluation of Assessment Results for Pressure

Facility	Test	Transient	Bias, MPa $P_{\text{RELAP}} - P_{\text{exp}}$	σ , MPa	Vessel Stress, psi @ Full P	% Stress
ROSA	AP-CL-03	1-inch cold leg LOCA	-0.26	0.61	-665	2.8

	AP-CL-09	1-inch cold leg, failure of core makeup tanks (CMTs), ½ automatic depressurization system (ADS)	-0.07	0.28	-111	0.5
	SB-CL-18	6-inch cold leg LOCA	0.14	0.27	+253	1.1
	SB-HL-06	2-inch hot leg LOCA	-0.38	0.66	-601	2.5
APEX-CE	13	stuck-open SRV recloses at 3600 s	-0.04	0.17		
	5	flow stagnation HPI cooldown	-0.15	0.05		
MIST	4100B2	4.4-inch cold leg LOCA	-0.25	0.26	-396	1.6
	360499	feed and bleed	0.03	0.40	-32	0.1
	3109AA	1.4-inch cold leg LOCA	0.47	0.46		
LOFT	L2-5	200% cold leg LOCA	-0.11	0.30	-174	0.7
	L3-1	4-inch cold leg LOCA	0.04	0.18		
	L3-7	1-inch cold leg LOCA	-0.43	0.50		
MARVIKEN	22	large-break LOCA	-0.21	0.24	-332	1.4
	24	large-break LOCA	-0.25	0.26	-396	1.7
UPTF	6-131	condensation	-0.05	0.10		
Average			-0.093	0.32	-206	0.9

The equivalent effect on vessel stress from uncertainty in the prediction of RCS pressure is given in the last column as calculated from the following equation:

$$\sigma = \frac{PD}{2L}$$

where P is pressure

D is the vessel diameter, which for Palisades is 5.3125 m

L is the vessel wall thickness, which for Palisades is 0.2201 m

The bias in the RELAP5 prediction of pressure expressed as a bias in vessel wall stress is 156 psi. At the 2σ level, the uncertainty in the RELAP5 prediction of vessel wall stress is 1104 psi. These numbers can be compared to the vessel stress at a normal operating pressure of 2200 psia:

$$\sigma = 24,000 \text{ psi}$$

and at the SRV setting of 2,500 psia:

$$\sigma = 27,500 \text{ psi}$$

The bias in the RELAP5 pressure prediction is equivalent to 0.6% of the operating stress, while the nominal 2σ pressure uncertainty is 4.5% of the operating stress. This agreement is considered excellent. The RELAP5 calculation bias and uncertainty have little impact on the value of K₁ and therefore the differences between the measured and RELAP5-calculated data for RCS pressure are small with respect to the effect on the vessel wall stress, K_r.

4.6 Assessment Results: Reactor Vessel Downcomer Fluid Temperature

The fluid temperature in the downcomer, to a first order approximation, is also a global parameter. The RCS can be considered as consisting of two regions, where (1) the “hot side” consists of the core, reactor vessel upper plenum and upper head, hot legs, and entrance to the steam generators, and (2) the “cold side” consists of the exit to the steam generators, cold legs, reactor vessel downcomer and lower plenum.

If the RCS were well-mixed, temperature and pressure would be directly linked. This is true for secondary-side events, such as main steam line breaks, for which primary-side coolant loop natural circulation is maintained. For LOCAs, however, coolant loop flow stagnation will result in differences between the cold and hot side temperatures. There are inherent limitations to the magnitude of uncertainty in downcomer temperature. Upper and lower bounding limits to downcomer temperature are described as follows.

For primary side breaks (LOCAs, including stuck-open SRVs), the temperature of the downcomer region is bounded from above by the saturation line and from below by the ECC injection temperature. Variations in the ECC injection rate have a direct, nearly linear, effect on downcomer temperature.

For secondary side breaks, the temperature in the downcomer region is bounded by the boiling point of water at the secondary-side pressure. Steam line breaks outside containment are low consequence PTS events because of the small combined probability of the break occurring coincident with the failure of both main steam isolation valves. Also, such events would normally not lead to tripping the RCPs. For steam line breaks inside containment, there is nothing to prevent blowdown of the secondary system of the affected steam generator. Such breaks also cause a containment isolation signal, which stops component cooling water flow to the RCPs. This causes the pumps to trip, which tends to enhance primary side cooling for two reasons. First, pump heat (~20 MW) is no longer added to the primary system. Second, the loop or loops that contain intact steam generators may stagnate, so reverse heat transfer from the intact steam generator(s) to the primary system may be lessened. For secondary side cooldown events, therefore, the minimum downcomer temperature attainable is approximately 125 °C (260 °F) corresponding to a containment pressure of ~2 to 2.5 bar. Note that the RELAP5 calculations are approximately 25 °C (14 °F) conservative (i.e., too cold) because the pressurization of the containment was not modeled.

The ability of RELAP5 to predict downcomer temperatures was assessed by comparison with integral system test data. The experiments selected were similar to PTS sequences, and the same as those used for the code-data pressure comparisons. The fluid temperature comparison results are shown in Table 4-3. A brief analysis and plotted comparisons between the measured and RELAP5-calculated reactor vessel downcomer fluid temperatures are provided for each assessment case in Appendix E.

Table 4-3. Statistical Evaluation of Assessment Results for Downcomer Fluid Temperature

Facility	Case	Transient	Bias, °C	
			$T_{RELAP} - T_{EXP}$	σ , °C
ROSA	AP-CL-03	1-inch cold leg LOCA, ADS actuation (becomes large hot leg break)	2	25
	AP-CL-09	1-inch cold leg LOCA, failure of CMTs, failure of ½ ADS	1	10
	SB-HL-06	2-inch hot leg LOCA, PORV opens later in transient	-9	14

	SB-CL-18	6-inch cold leg LOCA	2	4
APEX	CE-5	loop flow stagnation cooldown	-5	7
	CE-13	stuck-open SRV that reclosed at 3600s	-2	8
MIST	4100B2	4.4-inch cold leg LOCA	0	12
	360499	feed and bleed	4	4
	3109AA	1.4-inch cold leg LOCA	10	6
LOFT	L2-5	large cold leg LOCA	2	9
	L3-1	4-inch cold leg LOCA	-12	9
	L3-7	1-inch cold leg LOCA	-8	4
UPTF	6-131	Condensation	-4	16
Average			-1	10

Note: 1σ contains 68% of the comparison points
 2σ contains 95.5% of the comparison points
 2.58σ contains 99.7% of the comparison points

The overall average bias between RELAP5 and the experimental data was $-1\text{ }^{\circ}\text{C}$ ($-2\text{ }^{\circ}\text{F}$) with a nominal standard deviation $\sigma = 10\text{ }^{\circ}\text{C}$ ($18\text{ }^{\circ}\text{F}$). This difference can be further described in terms of dimensionless temperature, as follows:

$$T_{err}^* = \frac{T_{err}}{T_0 - T_{ECC}}$$

where $T_{err}^* = 1\text{ C}$

$$T_0 - T_{ECC} = 285\text{C} - 20\text{C} = 265\text{C}$$

The nominal bias (T_{err}^*) between RELAP5 and the data is less than 1%. RELAP5, therefore, has effectively no bias in the prediction of downcomer temperature. The 1σ uncertainty of $10\text{ }^{\circ}\text{C}$, while seemingly small, can still affect the determination of K_R . Based on the uncertainty in the RELAP5 prediction of nominal downcomer temperature, we define a plume as a temperature variation of greater than 1σ , or $10\text{ }^{\circ}\text{C}$. Temperature variations, either circumferentially or axially of less than this number are not of significance to the analysis because they fall within the nominal predictive capability of RELAP5.

4.7 Assessment Results: Reactor Vessel Wall Inside-Surface Heat Transfer Coefficient

For the reactor vessel wall heat transfer coefficient, quantitative comparisons are more difficult than for RCS pressure and downcomer fluid temperature because heat transfer coefficients are not directly measured in the experiments. Further, since most of the test facilities were designed to study core-coolability safety issues and not vessel downcomer overcooling issues, experiment instrumentation related to downcomer wall heat transfer (wall and fluid thermocouples, wall heat fluxes and downcomer fluid velocities) is in general very limited. Quantitative assessments of RELAP5 capabilities for predicting the vessel wall heat transfer coefficient and other heat transfer-related parameters are provided in this section to the extent feasible considering the limited available data. A variety of other investigations into reactor vessel wall heat transfer in general and

RELAP5 capabilities in particular are also presented here to support the assessment conclusions regarding the wall heat transfer coefficient.

The heat transfer package in RELAP5 has considerable flexibility and complexity, since it must be applicable to the entire range of heat transfer conditions expected when simulating reactor transients. Thus the RELAP5 heat transfer models cover the full spectrum of wall-to-fluid heat transfer regimes, including conduction through stagnant fluid, natural and forced convection, subcooled and saturated nucleate boiling, critical heat flux, and transition and film boiling.

When modeling with RELAP5, the geometric configuration and materials of the physical heat structures are represented using RELAP5 heat structure models. The analyst, through input, connects each heat structure model with the appropriate hydrodynamic fluid cell. As described in Section 4.1, within each fluid cell RELAP5 assumes that the fluid conditions for each phase are homogenized. Within each fluid cell, the steam and liquid phases may each possess only one velocity and one fluid temperature.

The RELAP5 heat transfer package couples the heat structure model (which calculates temperatures within the wall based on the solution for conduction heat transfer) to the liquid and vapor in the associated hydrodynamic fluid cell. The heat transfer package includes heat transfer models representing the various heat transfer regimes (convection to a steam-water mixture, subcooled nucleate boiling, saturated nucleate boiling, film boiling, etc.). RELAP5 selects the heat transfer regime based upon the current structure temperatures and fluid conditions (liquid and vapor temperatures, void fractions, liquid and vapor velocities, mass fluxes, etc.). Each heat transfer regime (see Appendix F for more information on heat transfer regimes) is assigned a number which is referred to as the RELAP5 heat transfer "mode." For each heat transfer regime, RELAP5 includes heat transfer correlation models that are also selected based upon the wall temperatures and fluid conditions.

As discussed later in this section, for the PTS application the wall heat transfer regime of most interest is for wall-to-fluid convection for Reynolds numbers toward the low end of the turbulent range. This regime corresponds to the reactor vessel downcomer situation during periods with very low coolant-loop natural circulation flow or periods after the coolant-loop flows have stagnated as a result of voiding in the upper regions of the RCS (generally caused by draining during LOCA events). Other heat transfer regimes are also experienced during portions of the PTS transient accident scenarios. Highly-turbulent forced convection is experienced when RCPs are operating or when there is robust coolant-loop natural circulation flow. Saturated and subcooled nucleate boiling are generally experienced for events where the RCS rapidly depressurized, the fluid saturation temperature quickly drops and the hot vessel wall passes heat to a flashing and boiling fluid. Attention is given here to the regime for convection at the low end of the turbulent range because it (1) is frequently encountered in the PTS application scenarios, and (2) results in a relatively low heat transfer coefficient that can dominate the wall-to-fluid heat transfer process. The other regimes (highly-turbulent convection and boiling) result in large heat transfer coefficients for which the wall heat transfer process is instead dominated by conduction through the wall.

The heat transfer regime for which the uncertainty has the greatest significance for the PTS application is therefore moderately-turbulent convection. This regime is modeled in RELAP5 using forced-convection and free-convection heat transfer correlations; the code calculates a value for each correlation and uses the maximum of the two. Appendix E describes the RELAP5 heat

transfer correlations used in the PTS applications for the moderately-turbulent ($3 \times 10^5 < Re < 3 \times 10^6$) wall-to-fluid heat transfer.

The remainder of this section describes wall heat transfer assessment evaluations related to applying RELAP5 for the PTS application.

4.7.1 Effect of Heat Transfer Coefficient on Wall Heat Flux

During normal steady plant operation, the reactor vessel wall temperature is the same as the downcomer fluid temperature (which is the reactor vessel inlet temperature). During accident scenarios that are pertinent for PTS the fluid temperature falls. The manner in which the changing fluid temperature affects thermal response of the initially hot reactor vessel wall is of significance. The RCS cooldowns experienced in the PTS accident scenarios generally fall into three categories of (1) secondary-side LOCA events, such as main steam line breaks, (2) small primary-side LOCAs, such as cold leg breaks or stuck-open pressurizer relief valve events, and (3) large primary-side LOCAs, such as double-ended cold leg breaks. Each of these event categories is now separately discussed.

For secondary-side LOCA events, the RCS is rapidly cooled by overcooling to the steam generators but the RCS remains at high pressure and, often, forced flow of coolant through the RCS loops continues. The RCS fluid cools, but the extent of the cooldown is limited because the ultimate heat sink temperature is the saturation temperature at atmospheric pressure, which represents the final state in the secondary coolant system. The reactor vessel wall heat transfer coefficient remains high as a result of pump-forced flow or a robust coolant-loop natural circulation flow for cases where the RCPs are tripped. As a result, the wall-to-fluid heat transfer process is controlled by heat conduction through the reactor vessel wall.

For small primary-side LOCAs, the RCS depressurizes at a rate that is inversely related to the break size. Fluid flashing caused by the RCS depressurization cools the RCS fluid as the saturation temperature falls. The ECC systems add very cold water to the RCS at rates that are inversely related to the RCS pressure. This pressure dependency results because the ECC systems are made up of (1) tanks (accumulators, core flood tanks and safety injection tanks) with cold water inventory stored at intermediate pressures and (2) centrifugal pump systems (HPI, LPI, etc.) for which no flow is delivered above the pump shutoff heads and for which lower RCS pressures lead to greater cold water injection flow rates.

For the small LOCAs, the system pressure is defined by the RCS mass and energy balances associated with core heat addition, cold water injection, steam generator heat removal and the break flow. For the small LOCAs, there is much interdependence among the PTS parameters of interest (pressure, fluid temperature, and heat transfer coefficient). A slightly larger break size leads to lower pressures (which tend to mitigate the PTS risk) while at the same time it leads to higher ECC injection rates and lower fluid temperatures (which tend to increase the PTS risk).

Further, the variations in the injection flow rate can directly affect the break flow (which in turn affects RCS pressure) and the RCS inventory, which affects tripping of RCPs, coolant loop natural circulation and stagnation, vessel downcomer velocities and wall heat transfer coefficients. For the small primary-side LOCA events, the PTS potential is caused by the incomplete RCS depressurization and the RCS draining which causes the stagnation of the coolant loop natural circulation flows and leads to the pooling of very cold water in the cold leg and downcomer regions.

For small breaks the injection of cold ECC water is at a low rate. The RCS cooldown experienced for this category of LOCA events is relatively slow and there is a feedback between the heat transfer from the wall to the fluid and the fluid temperature itself.

For this category of events, the downcomer wall heat transfer regimes generally fall into the range of turbulent forced convection from wall to subcooled liquid (even following coolant loop flow stagnation, the downcomer flow rates remain sufficiently high to resemble forced convection). However, in this situation the heat transfer process may be controlled at the wall-to-fluid interface rather than by conduction within the wall.

For large primary-side LOCA events, the RCS completely depressurizes and the injections of cold ECC water from the HPI, LPI, and accumulator systems are at very high rates. The rapid decline in the fluid saturation temperature leads to fluid flashing and boiling on the hot vessel wall. The very large wall heat transfer coefficient during boiling causes rapid declines in the wall temperatures and the heat transfer process is controlled by conduction within the wall. As a result of the large-break size, the RCS cannot repressurize from the ECC injection. The high injection rate floods the cold legs and vessel regions with cold water and this quickly terminates the boiling process.

Appendix F presents a study quantifying the effects of variations in the vessel wall inside-surface heat transfer coefficient on the wall heat flux (and thereby on the wall temperatures). The study further discusses and quantifies the top-level vessel wall heat transfer aspects of the PTS accident categories described above.

4.7.2 Comparison of Measured and RELAP5-Calculated Reactor Vessel Wall Heat Transfer Data

Only limited pertinent data are available for assessing RELAP5 reactor vessel wall-to-fluid heat transfer for geometries consistent with the plants and the conditions present in the PTS accident scenarios. In the integral test facilities instruments are not available for directly measuring heat transfer coefficient or heat flux. However, downcomer fluid and vessel wall thermocouple data along with fluid velocity data are occasionally available that allow for making a quantified comparison between the measured and RELAP5-calculated wall heat transfer process. This section presents vessel wall-to-fluid heat transfer comparisons pertinent to PTS for tests performed in the UPTF, APEX-CE, and Create test facilities. These assessments, which are summarized here, are described in detail in Appendix G.

UPTF Test 1 Run 21

The Upper Plenum Test Facility (UPTF, see Section 4.4) featured a full-scale representation of the reactor vessel, downcomer and cold legs of a PWR. Test 1 Run 21 consisted of injecting cold HPI water into one of the four cold legs (Cold Leg 2) of a system that was initially filled with hot pressurized water. The experimental conditions are comparable to those experienced in a PWR following stagnation of the coolant loop natural circulation flow. This experimental facility and test were modeled with RELAP5 and the calculated results were compared with the measured test data. The RELAP5 model included a two-dimensional nodalization scheme, comparable to those employed in the PTS plant analyses.

The measured velocity data at the core-bottom elevation in the downcomer exhibited a downward flow below Cold Leg 2 and upward flows through other azimuthal sectors of the downcomer as shown in Figure 4-1 (the direction of positive velocity is downward). The RELAP5 simulation also showed a downward water flow below Cold Leg 2 (Figure 4-2), but with the cold water spreading into sectors adjacent to Cold Leg 2 by the time the flow reached the core bottom elevation. As a result, the RELAP5-calculated velocities are seen in these figures to be lower than the measured velocities. The fluid velocities in the downcomer (in both the test and calculation) were much greater than the superficial fluid velocity based on only the HPI flow in the downcomer. The test data indicated that the downcomer velocity is ~16 times the downcomer HPI superficial velocity.

An assessment of the RELAP5-calculated vessel wall heat transfer coefficient was made using fluid and wall thermocouple data. In downcomer regions away from Cold Leg 2, RELAP5 was found to under predict the rates of decline in both the fluid and vessel wall temperatures by a similar extent and therefore to well predict (by within ~15%) the heat transfer coefficient. Under Cold Leg 2, RELAP5 was found to under predict the wall-to-fluid differential temperature of the test as shown in Figure 4-3 and to also under predict the wall-to-fluid heat flux (as indicated by the slower cooldown rate at the location of a thermocouple embedded 25 mm (1 inch) into the vessel wall at the core top elevation, see Figure 4-4). Since the RELAP5 under prediction of the differential temperature was much greater than the RELAP5 under prediction of the heat flux, RELAP5 was found to over predict the wall-to-fluid heat transfer coefficient under Cold Leg 2 for UPTF Test 1-21 by a factor of ~2.

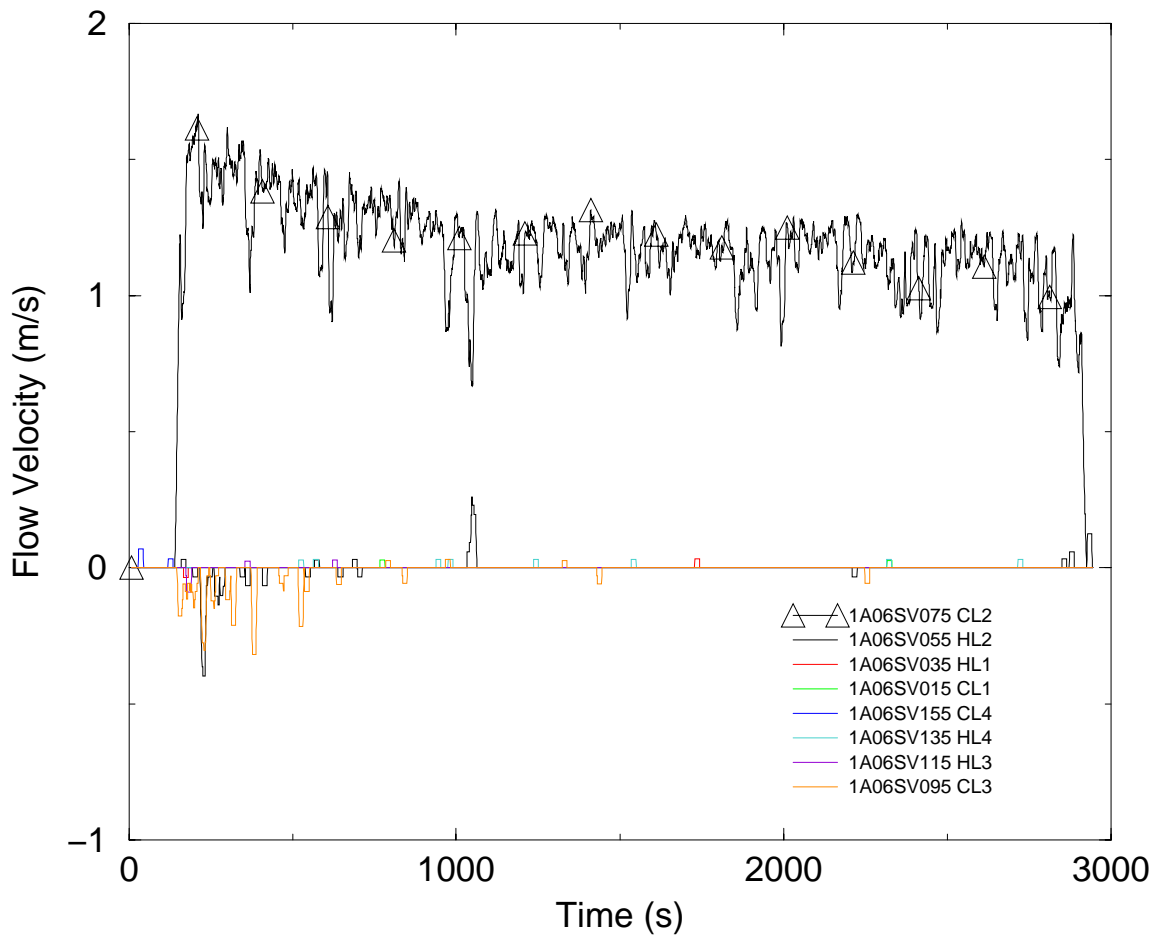


Figure 4-1. UPTF 1-21 Downcomer Velocities at Bottom-Core Elevation Measured, Turbine Meters, Clockwise from Cold Leg 2

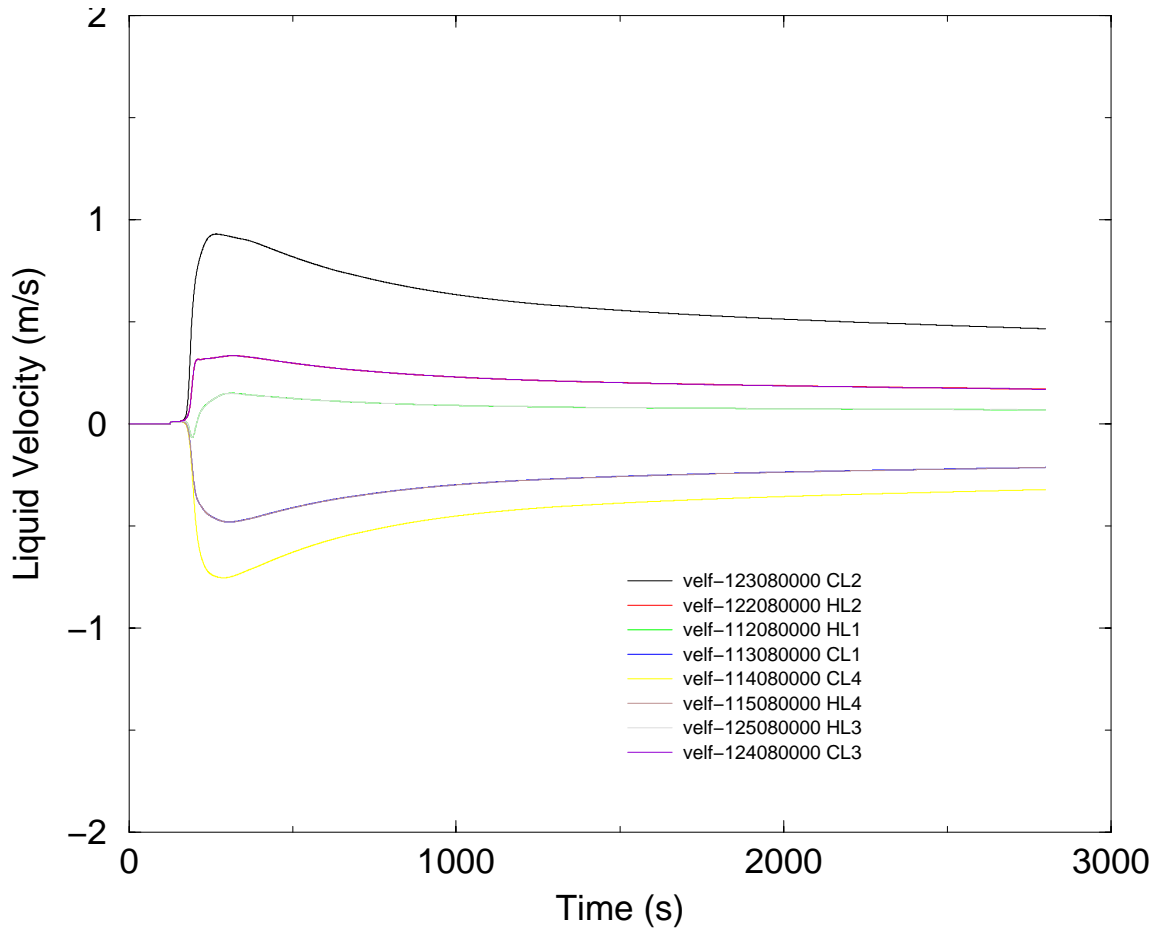


Figure 4-2. UPTF 1-21 Downcomer Velocities at Bottom-Core Elevation RELAP5-Calculated, Clockwise from Cold Leg 2

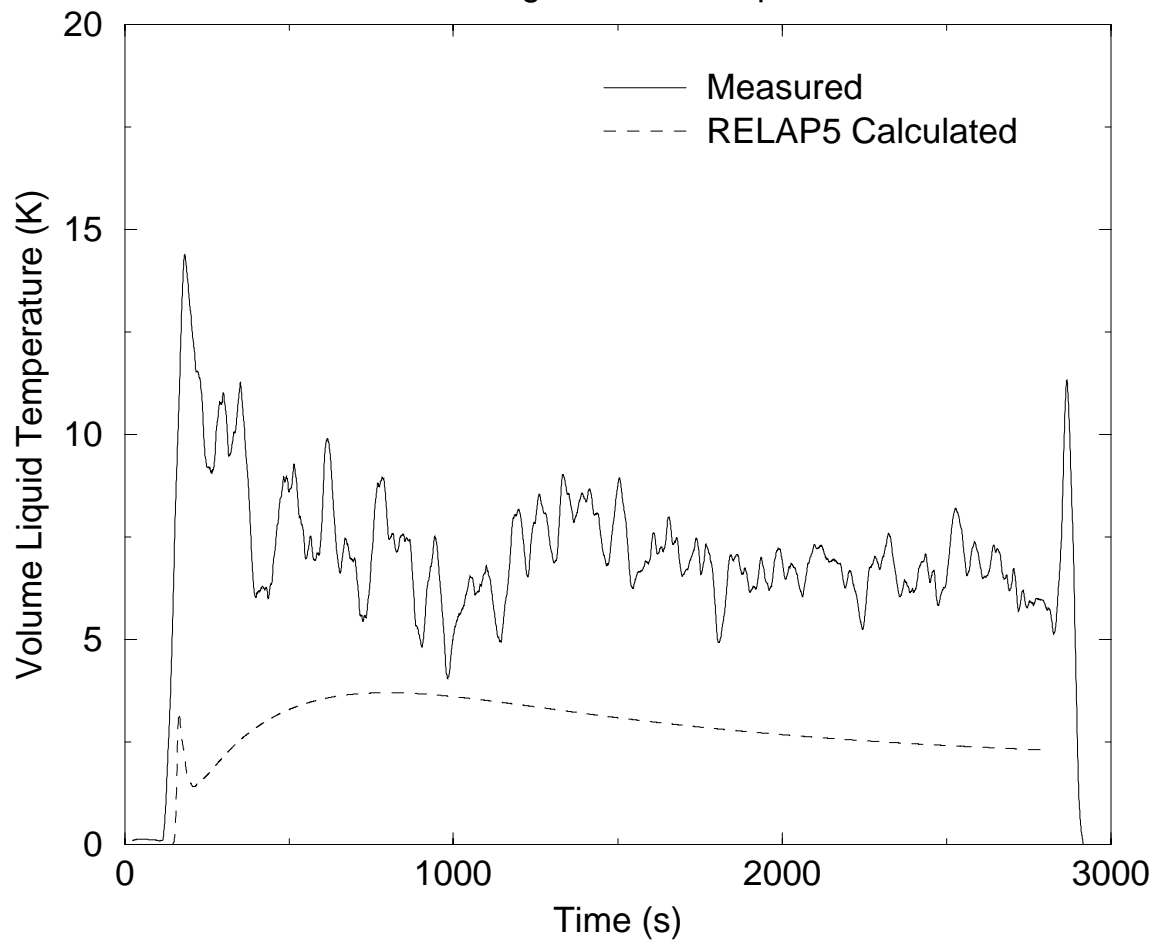


Figure 4-3. UPTF 1-21 Wall Temperature Minus Fluid Temperature Under Cold Leg 2 at Core-Top Elevation

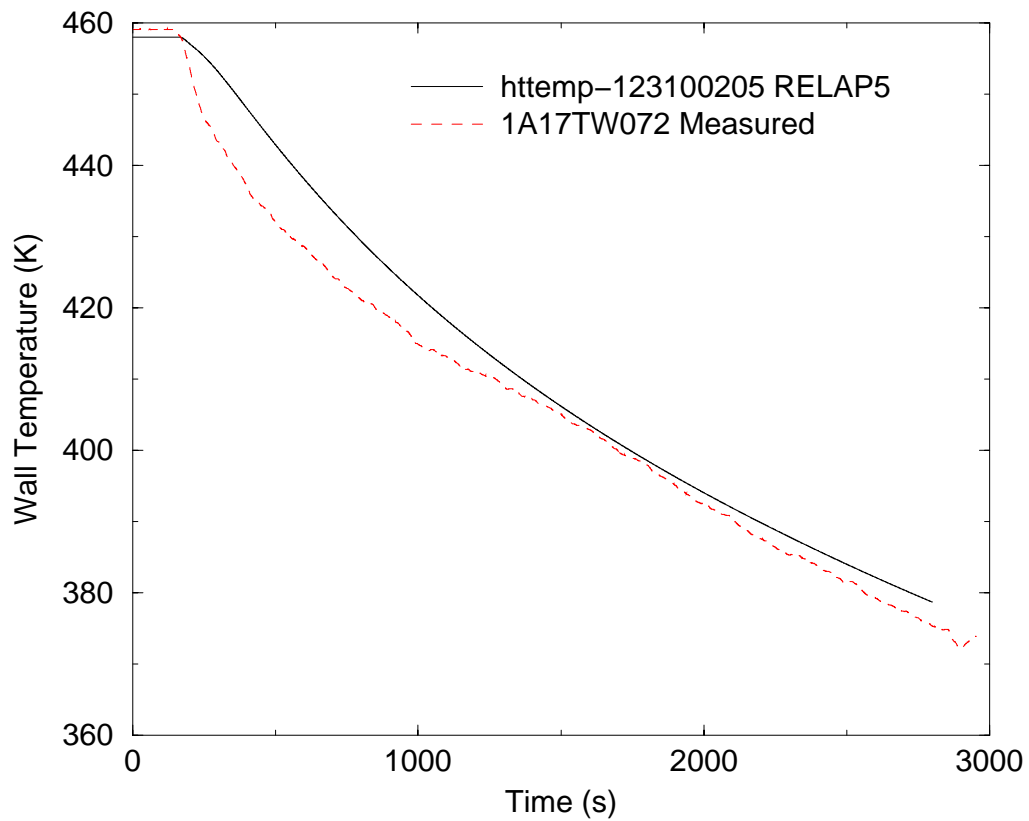


Figure 4-4. UPTF Test 1-21 Wall Temperatures at 25 mm Depth Vessel Wall in Orientation of Cold Leg 2

APEX-CE Test 5

The Advanced Plant Experiment facility (APEX-CE, see Section 4.4) is a reduced-height, pressure and temperature facility scaled to Palisades, a CE-design plant. The test consisted of injecting cold HPI water into all four cold legs of a system that was initially filled with hot pressurized water. The experimental conditions are comparable to those experienced in a PWR following stagnation of the coolant loop natural circulation flow. This experimental facility and test were modeled with RELAP5 and the calculated results were compared with the measured test data. The RELAP5 model included a two-dimensional nodalization scheme, comparable to those employed in the PTS plant analyses.

The RELAP5 assessment concentrated on the first 1,700 s of the test period, when there was excellent agreement between measured and calculated fluid and wall temperatures as shown in Figures 4-5 and 4-6. The excellent match between the measured and calculated wall temperatures indicated that RELAP5 is also excellently predicting the wall heat flux. However a comparison between the measured and calculated wall-to-fluid differential temperatures indicated that RELAP5 under predicted the test differential temperature by a factor of ~2 and therefore over predicted the wall-to-fluid heat transfer coefficient for APEX-CE-5 by the same factor.

There are no direct measurements for downcomer flow velocity in the APEX-CE facility, but flow velocity indications were derived from thermocouple data. The calculations indicated that the RELAP5 and measured flow velocities are in good agreement and that (after scaling up for a full-height downcomer) the data indicate that the downcomer circulating flow velocity is a factor of ~20 greater than the superficial velocity of the HPI flowing alone in the downcomer region.

Creare Fluid Mixing Tests

Creare performed experiments in a one-half linear scale facility to investigate fluid mixing in a downcomer region for a stagnant coolant-loop situation. The facility represents the region of a single cold leg and one-fourth of the reactor vessel downcomer. The downcomer configuration included a thermal shield which was installed in the center of the downcomer span. Two NRC tests, MAY105 and MAY106 were performed to simulate cold water injection into an initially-hot downcomer (RELAP5 simulations for these tests were not performed). Velocity measurements for two tests indicated velocity ratios (downcomer velocity to superficial downcomer velocity based on HPI flow) of 21 and 26. The downcomer flow was found to contain regions of up-flow and down-flow, with the down-flow velocities greater than the up-flow velocities. The downcomer flow pattern was found to be buoyancy-induced.

Figure 4-7 shows that the heat transfer data for the Creare tests are proportional with the Dittus-Boelter correlation. An enhancement of the heat transfer by a factor of ~1.55 above the Dittus-Boelter correlation is seen in the figure for downflow regions but not elsewhere. The enhancement is attributed to entrance effects to which the thermal shield configuration may contribute.

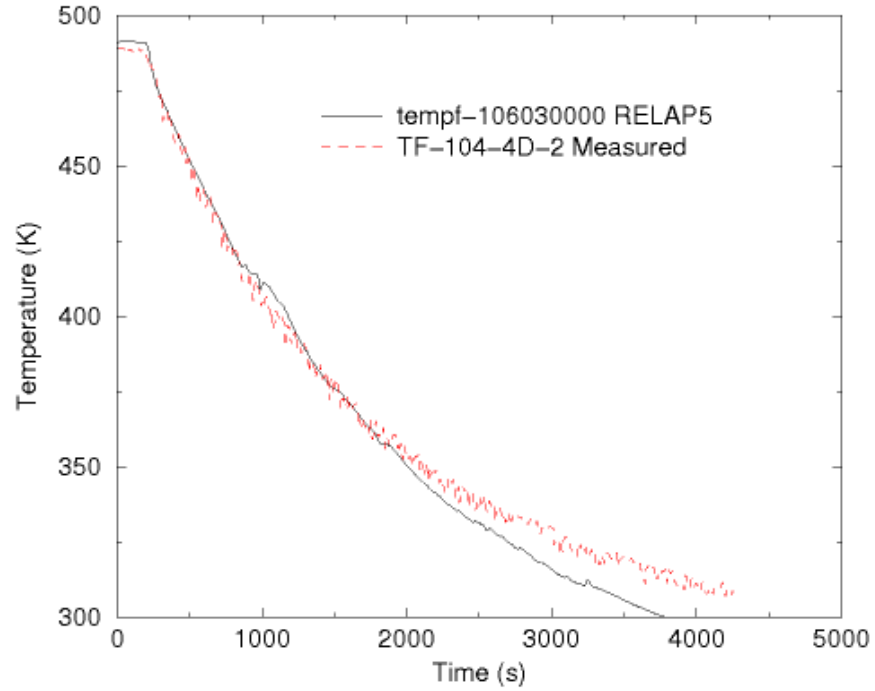


Figure 4-5. APEX-CE-5 Measured and RELAP5 Fluid Temperatures 4D Below and Centered on the Cold Leg 4 Nozzle

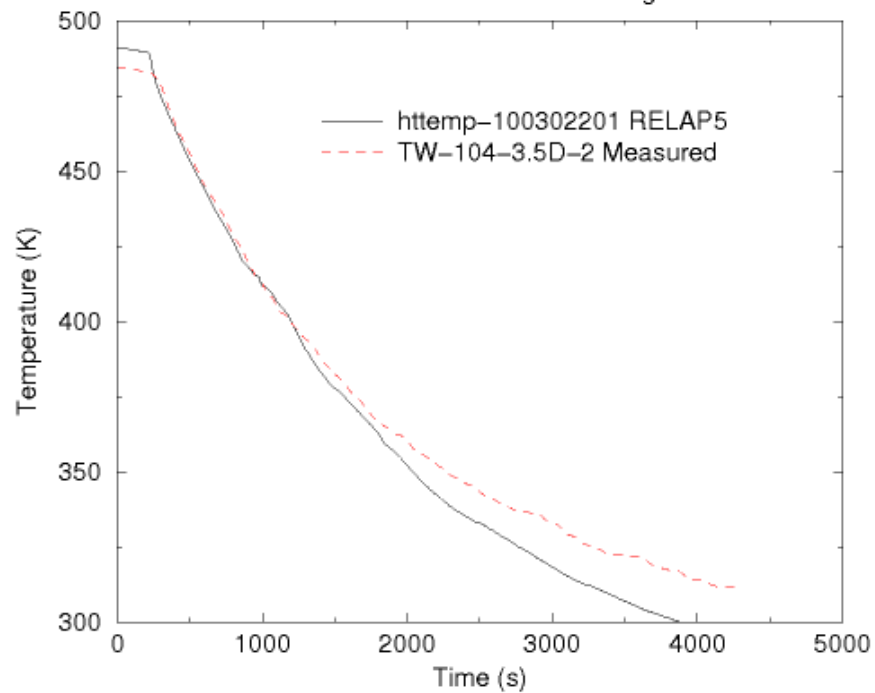


Figure 4-6. APEX-CE-5 Measured and RELAP5 Wall Temperatures 4D Below and Centered on the Cold Leg 4 Nozzle

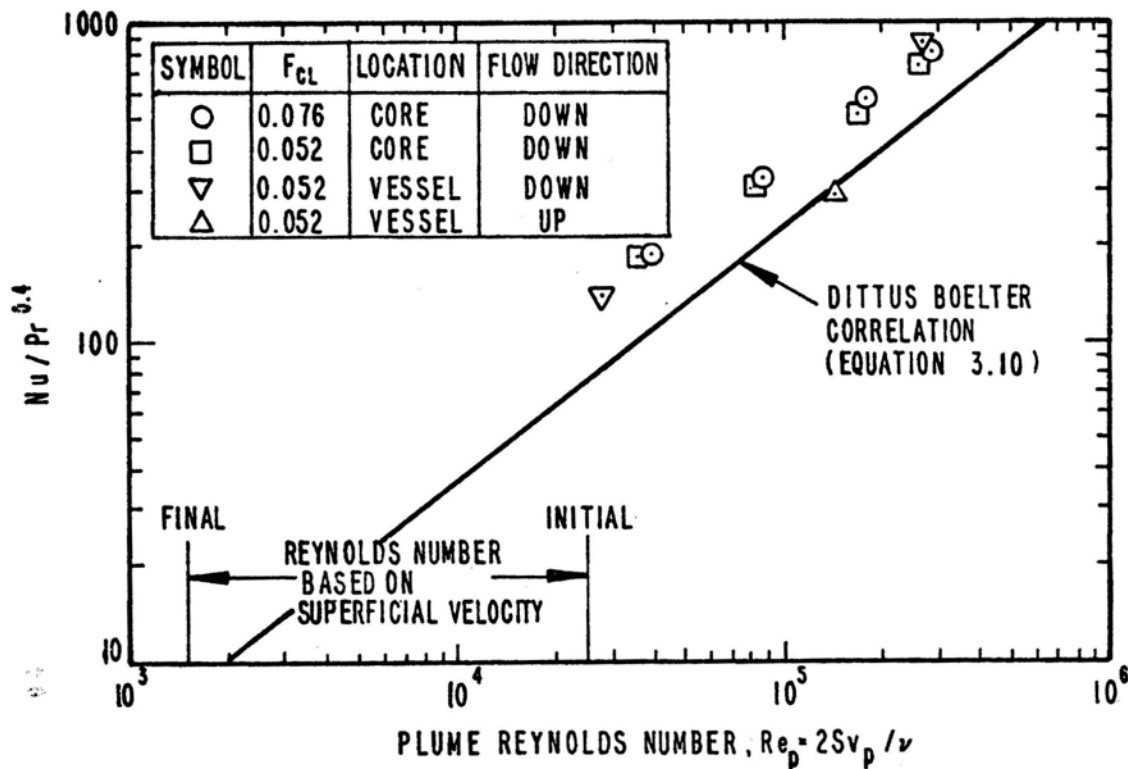


Figure 4-7. Creare Data Compared to Dittus-Boelter

Summary and Discussion

Three sets of experiments related to injection of cold water into stagnant initially hot water in the reactor vessel downcomer region of a PWR have been described in this section. The situation represented in these tests is consistent with that following coolant-loop stagnation in many of the PTS accident scenario categories. The experiments all indicate that the buoyancy effects of cold water entering the downcomer through the cold legs sets up a circulation within the downcomer region. The downcomer circulation velocities are seen to be larger than the superficial velocity (that which would result in the downcomer from the ECC injection flow alone) by factors of ~16 to 26.

In the UPTF and APEX-CE assessments, RELAP5 with a two-dimensional downcomer nodalization is seen to be able to capture on a first-order basis the flow pattern and velocities in the downcomer region. Based on comparison between measured and RELAP5-calculated wall and fluid temperature data, RELAP5 is seen to provide reasonable representations of the vessel wall inside surface heat transfer coefficient. For the UPTF test, RELAP5 is seen to provide a good representation (within ~15%) of the heat transfer coefficient for downcomer regions away from Cold Leg 2 (the only cold leg through which the cold water enters the vessel) and to over predict the heat transfer coefficient by a factor of ~2 for the region under Cold Leg 2. For the APEX-CE test (for which cold water enters the vessel through all cold legs), RELAP5 is seen to over predict the heat transfer coefficient for all downcomer regions, again by a factor of ~2.

4.7.3 Comparison of RELAP5-Calculated and CFD-Calculated Downcomer Flows

A comparison was made between RELAP5 and COMMIX CFD code solutions for the flow patterns experienced in the reactor vessel downcomer. The comparison was made during the coolant-loop flow stagnation period following a 2-inch hot-side break accident scenario in a three-loop Westinghouse plant.

The comparison indicated that RELAP5 adequately captured the overall flow patterns but not finer-scale eddy-flow behavior seen in the COMMIX run. The flow velocities from the COMMIX and RELAP5 calculations were similar and on the order of 0.5 to 1.0 m/s. The comparison between RELAP5 and COMMIX calculations is provided in Appendix H.

4.7.4 Sensitivity of Fracture Mechanics Results to Variations in the Fluid Cooldown Rate and Heat Transfer Coefficient

Sensitivity studies were performed using the FAVOR probabilistic fracture mechanics analysis code to calculate the CPF for the reactor vessel. A base FAVOR calculation was first performed using the RELAP5-calculated pressure, temperature, and vessel wall heat transfer coefficient for a stuck-open pressurizer SRV accident scenario at the Palisades plant. The FAVOR sensitivity calculations were then performed using variations in the fluid temperature and reactor vessel inside-wall heat transfer coefficient around those provided by RELAP5 for the base run.

For the fluid temperature variations, an exponential curve fit was made to the RELAP5 base case calculation cooldown behavior. The cooldown time constant for the base case was 3450 s. The FAVOR calculation was then rerun with the cooldown time constant varied from 2439 s to 4762 s. This range of time constants resulted in a spread in fluid temperatures of about 45 °C (80 °F). The FAVOR results showed the expected sensitivity to the cooldown rate; faster cooldowns led to larger CPFs. The CPF varied by an order of magnitude over the range of cooldowns evaluated.

Variations in the RELAP5-calculated base case heat transfer coefficient were then applied to the same set of cooldown curves. The heat transfer coefficients were varied by applying multipliers of 0.7 to 1.56 on the base case heat transfer coefficients. When using the revised heat transfer coefficients, the CPFs varied from 0.67 to 1.38 of the base-case CPF.

From these sensitivity studies, it was concluded that the CPF is much more sensitive to variations in the rate and extent of the fluid cooldown than it is to variations in the wall-to-fluid heat transfer coefficient. More information on these sensitivity studies is provided in Appendix I.

4.8 Other Assessment and Uncertainty Topics

The previous sections in this chapter concentrated on RELAP5 capabilities and uncertainties in predicting the parameters of interest for PTS (i.e., reactor vessel downcomer pressure, fluid temperature, and heat transfer coefficient). This section describes investigations into other aspects of RELAP5 application for PTS. Section 4.8.1 describes the PIRT activities performed regarding the PTS issue for PWRs and investigations into various phenomena, processes, and parameters that were performed as a result of the PIRT. Section 4.8.2 describes investigations into uncertainties in the thermal-hydraulic response that are used in binning event sequences.

4.8.1 PTS Phenomena Identification and Ranking Table

This section describes PIRT activities performed regarding the PWR PTS issue and investigations into various phenomena, processes, and parameters that were performed as a result of the PIRT. The current PTS PIRT is the result of two prior PTS PIRTs, one for a 2-inch diameter equivalent cold leg break in the H. B. Robinson Unit 2 plant and one for a scaled 2.8-inch diameter equivalent cold leg break in Yankee Rowe. These two previous PIRTs were found to have similar results and were combined together into a single PIRT for use in the current PTS evaluation.

The PIRT is performed in order to describe which phenomena, processes, and parameters could be of significance for the plant behavior during PTS accidents. As indicated earlier, the main parameters of interest for PTS are the reactor vessel downcomer pressure, fluid temperature and wall inside-surface heat transfer coefficient. These are the output parameters from RELAP5 which are passed to the fracture mechanics analysts and are used as input to the FAVOR code. The PIRT evaluates which other parameters could influence these primary parameters of interest and ranks the likely magnitudes of those influences. The PIRT is then used to initiate investigations into sensitivities and modeling capabilities regarding the PIRT parameters that may, if particularly uncertain, significantly influence the primary parameters of interest.

Table 4-4 shows an abbreviated version of the current PTS PIRT with the parameters ranked from most to least important. The complete PIRT and the discussions, analyses, and assessments related to the PIRT parameters appear in Appendix J. Investigations performed for the PIRT parameters are useful because they complement the many assessments performed regarding the PTS parameters of interest.

Table 4-4. Abbreviated PIRT for the Current PTS Thermal-Hydraulic Analyses

Importance Rank	Phenomenon/Boundary Condition	Type
1	HPI flow	boundary condition
2	Accumulator injection temperature	boundary condition
3	HPI temperature	boundary condition
4	Decay heat	boundary condition
5	HPI flow control	boundary condition
6	Feedwater temperature	boundary condition
7	Feedwater control	boundary condition
8	HPI asymmetry	boundary condition
9	Timing of RCP trip	boundary condition
10	Secondary pressure control	boundary condition
<hr style="border-top: 1px dashed black;"/>		
1	Accumulator injection rate	phenomenon
2	Break flow/break size	phenomenon
3	Reactor vessel wall heat conduction	phenomenon
4	Jet behavior, flow distribution and mixing in downcomer	phenomenon
5	Jet behavior, flow distribution and mixing in cold leg	phenomenon
6	Wall-fluid heat transfer in downcomer	phenomenon
7	Natural circulation flow and loop flow resistance	phenomenon
8	Downcomer-upper plenum bypass	phenomenon
9	Upper head heat transfer	phenomenon
10	Liquid/vapor interface in upper downcomer	phenomenon
11	Steam generator heat transfer	phenomenon
N.R.	Condensation during ECC injection	phenomenon
N.R.	Condensation during repressurization	phenomenon

4.8.2 Use of Thermal-Hydraulic Uncertainties in Developing Event Sequence Bins

An investigation into thermal-hydraulic uncertainties in PTS was carried out considering the various categories of accident scenarios, the most important boundary conditions, operator actions and physical models identified in the PIRT. This investigation is done in order to define sequence sub-bins that may be characterized using single RELAP5 runs. For each event sequence bin, RELAP5 runs were performed varying the important parameters and the output of the runs was used to develop a probability density function for the event sequence bin. From the probability density function, a cumulative density distribution was created, which allows dividing the sequence bin into sub-bins. Complete RELAP5 calculations were performed to characterize the behavior for each sub-bin.

An illustrative example of the binning process for the Oconee small-break LOCA bin is provided in Appendix K.

4.9 Assessment Conclusions

Assessments of RELAP5 capabilities were performed using test data from a variety of full-scale and scaled experimental facilities representing the configurations of all three U.S. PWR designs. The tests selected for assessment cover the range of behavior included in the dominant-risk PTS event sequences. The assessments concentrated on the PTS thermal-hydraulic parameters of interest (i.e., the reactor vessel downcomer pressure and fluid temperature and the vessel wall inside-surface heat transfer coefficient). RELAP5 nodalizations for models of the facilities employed in the assessments were consistent with RELAP5 model nodalizations used for the plant calculations in the PTS study.

The uncertainty in the RELAP5-calculated fluid pressure is characterized by an average bias (calculated pressure minus measured pressure) of -0.093 MPa (-13 psi) and an average $1\text{-}\sigma$ standard deviation of 0.32 MPa (46 psi). This pressure uncertainty is small with respect to the normal operation vessel stress and is not expected to significantly affect the outcome of fracture mechanics analyses.

The uncertainty in the RELAP5-calculated reactor vessel downcomer fluid temperature is characterized by an average bias (calculated temperature minus measured temperature) of -1 °C (-2 °F) and an average 1σ standard deviation of 10 °C (18 °F). The RELAP5-calculated fluid temperatures therefore contain effectively no average bias. The influence of the temperature deviation needs to be considered for its effect on the fracture mechanics analysis.

The assessment of RELAP5 predictive capabilities for the vessel wall heat transfer coefficient is not as straightforward as for the pressure and fluid temperature because direct measurements of heat transfer coefficient are not available. The heat transfer coefficient is affected by the fluid velocities in the downcomer and the temperatures of the wall and fluid. The prediction of the heat transfer coefficient is judged most important when its value is relatively low, when the wall heat transfer process is dominated by wall-to-fluid convection heat transfer and not by heat conduction within the vessel wall. For situations during PTS accident scenarios when RCPs are operating, when coolant loop flow is robust, or when the fluid on the vessel wall is boiling, the wall-to-fluid heat transfer coefficient is very large and the overall heat transfer process is conduction-dominated. The situations most pertinent for the assessment of heat transfer coefficient prediction capability are those where coolant loop natural circulation is at a slow rate or has been interrupted entirely. In these cases, the downcomer flow is not highly-turbulent and the wall-to-fluid heat transfer is attributable to either forced-convection or free-convection processes. These situations are encountered during LOCA sequences when tripping of the RCPs and draining of the upper regions of the RCS lead to slowdown and termination of the coolant loop circulation flows. The assessment for vessel wall heat transfer coefficient therefore concentrated on the downcomer behavior and conditions present for this stagnant-coolant-loop situation, when cold water from the ECC systems enters the vessel through the cold legs.

Direct and indirect downcomer fluid velocity experimental data in the UPTF, APEX-CE, and Creare facilities indicate that the cold ECC water entering the downcomer sets up buoyancy-driven circulations within the downcomer. These circulations result in downcomer velocities that are enhanced by a factor of ~20 over the superficial downcomer velocities (those that would result from the ECC alone flowing downward through the downcomer). Assessments for UPTF and APEX-CE indicate that to a first order RELAP5 well predicts the downcomer flow velocities. A comparison of RELAP5-calculated and COMMIX-calculated flow patterns for this situation indicates that the RELAP5 solution agrees with the overall flow pattern, while missing the finer-scale eddy flow behavior seen in the CFD solution. The RELAP5 and COMMIX flow velocities are similar.

Downcomer fluid temperature and wall temperature data from the UPTF and APEX-CE facilities were used to assess RELAP5 capabilities for predicting the vessel wall heat transfer coefficient. The experimental wall temperature responses were used as indications of wall-to-fluid heat flux and the difference between the experimental wall inside surface temperatures and fluid temperatures were used along with the heat flux to develop indications of the experimental wall-to-fluid heat transfer coefficients. The RELAP5 simulations for these tests were performed using two-dimensional nodalizations of the downcomer region and the calculated and measured heat transfer coefficient responses were compared. The assessment comparisons indicate that RELAP5 heat transfer coefficient predictions are in good agreement with the test data (within ~15%) for downcomer regions not directly below cold leg nozzles through which the ECC water enters the vessel. The assessment comparisons indicate that RELAP5 over predicts the heat transfer coefficients from the tests by a factor of ~2 for downcomer regions directly below cold leg nozzles through which ECC enters the vessel.

A study was performed using the FAVOR probabilistic fracture mechanics analysis code to evaluate the sensitivity of the vessel failure probability to variations in the downcomer fluid temperature and vessel wall inside-surface heat transfer coefficient. This study found that the CPF is much more sensitive to variations in the rate and extent of fluid cooldown than it is to variations in the wall-to-fluid heat transfer coefficient.

The conclusion from the assessments is that RELAP5 can well predict the PTS thermal-hydraulic parameters of interest, including the reactor vessel downcomer pressure and fluid temperature, as well as the vessel wall inside-surface heat transfer coefficient.

5. UNCERTAINTY EFFECTS OF THERMAL-HYDRAULIC BOUNDARY CONDITIONS

5.1 Objective

This chapter summarizes the uncertainties in the thermal-hydraulic boundary conditions,

$$T_{dc}(t), P(t), h_{dc}(t)$$

and relates them to their impact on the CPF of the reactor vessel, as well as uncertainties in PRA event frequencies. The PTS analysis employed probabilistic methods to address uncertainties, including probabilistic fracture mechanics, PRA, and thermal-hydraulics. The FAVOR probabilistic fracture mechanics analysis code incorporates distributions of materials parameters important to the analysis (e.g., fluence, chemistry, flaw size, flaw orientation, flaw location, etc.). The PRA frequency estimates also have a distribution.

In contrast, the thermal-hydraulic input to the combined analysis was a set of deterministic RELAP5 calculations to supply the boundary conditions $T_{dc}(t)$, $P(t)$, $h_{dc}(t)$ to the FAVOR code. Unlike the other parameters used by FAVOR, these three thermal-hydraulic boundary conditions cannot be input as probabilistic distributions, rather, they must be deterministic time histories. The entire thermal time history of the fluid is required to generate a temperature distribution in the vessel wall as a function of time.

The thermal-hydraulic uncertainty method used was, in effect, a combined PRA-thermal-hydraulic approach. It consisted of characterizing the behavior of various PRA bins by sets of RELAP5 calculations that represented the range of plant thermal-hydraulic behavior within the given bins. These deterministic RELAP5 calculations incorporated both uncertainties in the boundary conditions and thermal-hydraulic physical models. The latter are the constitutive relations that comprise the RELAP5 code. The sets of RELAP5 calculations were analyzed by FAVOR, along with the event frequencies determined for the subdivided bins. Risk-of-failure numbers were generated according to,

$$risk = \sum_i (f_i \times CPF_i)$$

where f_i is the event frequency and
 CPF_i is the conditional probability of failure of the reactor vessel.

This was the method used to incorporate thermal-hydraulic uncertainty into the overall PTS uncertainty analysis. However, a question with respect to the thermal-hydraulic analyses was,
If treated separately, what is the impact of thermal-hydraulic epistemic uncertainties on CPF or risk.

That is, how sensitive were the bottom risk line numbers to epistemic contributions to the uncertainties in $T_{dc}(t)$, $P(t)$, $h_{dc}(t)$, as compared to the method used to evaluate combined PRA-thermal-hydraulic uncertainties that treated aleatory and epistemic uncertainties together. Another way of posing the question was:

How good does RELAP5 need to be?

Before answering that question, it was necessary to first validate the application of RELAP5 to perform PTS analysis. That is, the accuracy of the model (RELAP5) must first be determined before attempting to assess the impact of the uncertainty in its predictions on the bottom line numbers of probability of vessel failure by addressing the following considerations:

- (1) Code Accuracy. Is RELAP5 best-estimate in its predictions, or does it have any systematic biases?
- (2) Code Uncertainty. To answer the question of how good RELAP5 needs to be, we formulated the following objectives:
 - (a) RELAP5's epistemic uncertainty should not dominate the overall determination of uncertainties in the determination of risk, as compared to the two other sources PRA (event frequency), and probabilistic fracture mechanics (distributions of important materials parameters).
 - (b) RELAP5's epistemic uncertainty should be small compared to the aleatory uncertainty of the PRA binning process. The code's uncertainty in predicting $T_{dc}(t)$, $P(t)$, $h_{dc}(t)$ should be small compared to the range in plant response that falls within a bin. This is the **binning process** uncertainty, or the variability in the severity of different sequences within a bin.

If RELAP5 meets these objectives, the credibility of its application to PTS analysis is substantiated.

5.2 Results

Based on the results presented in previous Chapters and details contained in Appendices, we RELAP5 has only a slightly conservative bias in the predictions of temperature and pressure, while there is a conservative bias in the code's calculation of heat transfer. This leads us to conclude that RELAP5 is, in fact, best-estimate, without systematic biases.

While RELAP5 provides accurate predictions of $T_{dc}(t)$, $P(t)$, $h_{dc}(t)$, its calculations of these three quantities have epistemic uncertainties whose impact should be defined and compared to other sources of uncertainty described immediately above. Figure 5-1 presents an illustration of the thermal-hydraulic and PRA contributions to uncertainty. The left histogram represents the uncertainty in event frequencies f . The evaluation of this uncertainty has been recently updated for LOCAs, and Table 5-1 shows the latest available published results [22]. Table 5-2 compares these to prior estimates documented in NUREG/CR-5750 [23]. The following is the range in probabilities between the 5th and 95th percentile estimates:

Small breaks	(>1.625 inch)	5 th to 95 th range = factor of 123
Medium breaks	(> 3 inch)	5 th to 95 th range = factor of 388
Large breaks	(>7 inch)	5 th to 95 th range = factor of 480

The uncertainty in the event frequency is more than two orders of magnitude. This provides one objective for the epistemic uncertainty of RELAP5 predictions. In other words, the uncertainty associated with physical models in RELAP5 (epistemic) should be small compared to the uncertainty associated with the analysis boundary conditions (aleatory). RELAP5 sensitivity studies to evaluate epistemic uncertainty will be discussed below with this in mind.

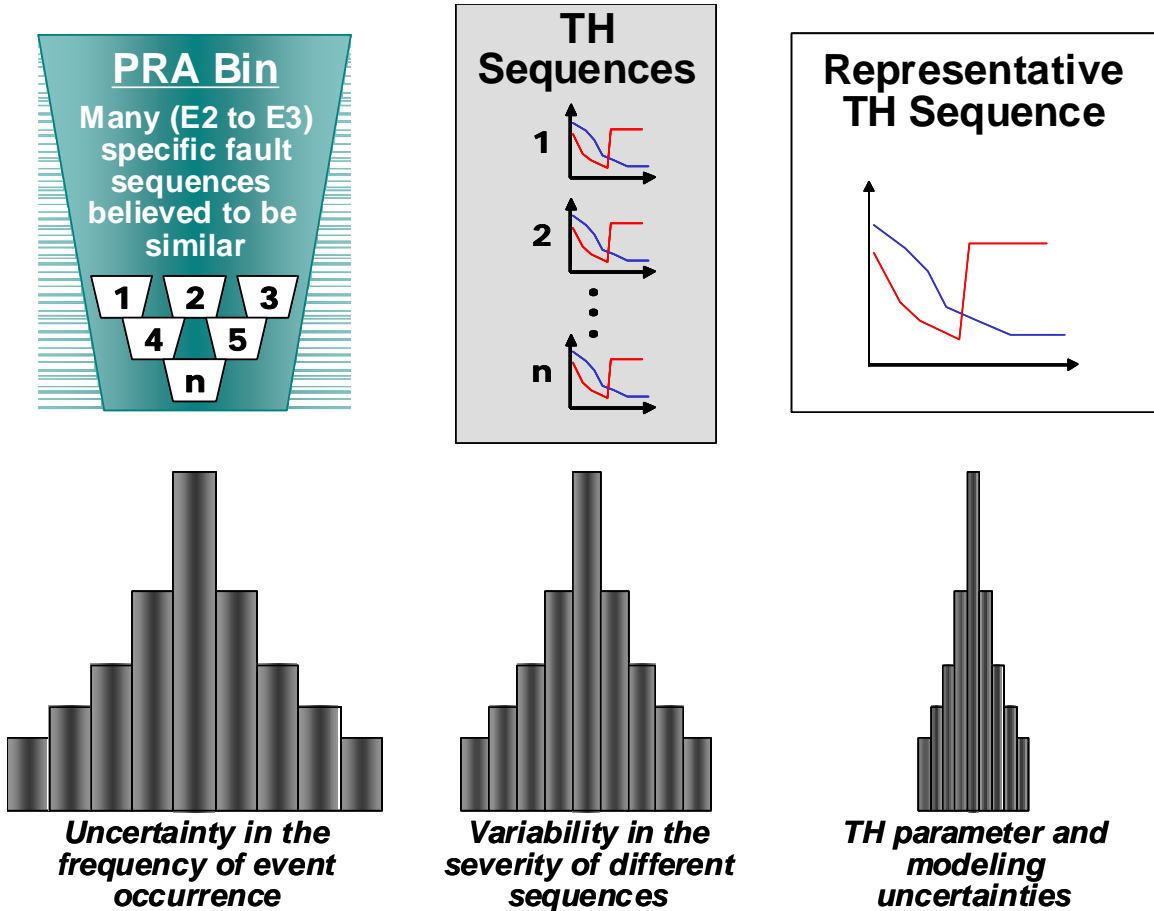


Figure 5-1. Relationship between PRA (event frequency) uncertainty, binning process uncertainty, and thermal-hydraulic epistemic uncertainty.

Table 5-1. PWR LOCA Frequencies (SECY-04-0060) [22]

Category	Break size, gpm	Break size, in	25-year average operation			40-year average operation		
			5%	Mean	95%	5%	Mean	95%
2	> 1,500	1.625	6.9 E-6	2.3 E-4	8.5 E-4	4.9 E-6	2.5 E-4	9.3 E-4
3	> 5,000	3	1.6 E-7	1.6 E-5	6.2 E-5	3.1 E-7	1.8 E-5	7.0 E-5
4	> 25,000	7	1.1 E-8	2.3 E-6	8.8 E-6	6.0 E-8	2.5 E-6	9.6 E-6

Note: LOCA category 1 includes frequency LOCA categories 2 - 6 as well, and so on
Probability of a single stuck-open pressurizer SRV = $1.6 \times 10^{-3}/\text{yr}$

Table 5-2. Comparison of LOCA Frequencies

SECY-04-0060 [22]		NUREG/CR-5750 [23]		
LOCA Category	Mean Frequency (yr ⁻¹)	LOCA Size	Mean Frequency (yr ⁻¹)	Ratio
1	6.2 E-03	SB	7.4 E-03	1.2
2	2.3 E-04	MB	3.0 E-05	0.1
3	1.6 E-05	LB	4.0 E-06	0.2
4	2.3 E-06	LB	4.0 E-06	1.7

A single thermal-hydraulic sequence is selected to represent a family of similar sequences in a particular PRA bin for purpose of input to the probabilistic fracture mechanics analysis. The physical modeling uncertainties associated with RELAP5 constitutive relations are small relative to the uncertainty associated with the initiating event frequency for a bin, and sequence-to-sequence uncertainty within a bin. These uncertainties are subsumed into the range of variation within a bin, enabling a deterministic treatment of P(t), T(t), and h(t) by FAVOR for a particular sequence.

The middle histogram in Figure 5-1 represents the variations in plant response that results from the grouping of some ~ 10² event sequences in a single bin. This variability in plant response was characterized by using RELAP5 to calculate a family of scenarios that fell within specific PRA bins. One of the key observations from the current PTS study regards the determination of thermal-hydraulic uncertainties. Namely, the boundary conditions (aleatory) to the analysis are the important determinants to the outcome, relative to the physical modeling uncertainties (epistemic) in RELAP5.

Table 5-3 shows the results from sets of RELAP5 calculations used to characterize risk-significant bins. Figures 5-2 to 5-10 plot the RELAP5 calculations for the various bins from which Table 5-3 was derived. This is the **binning process** (aleatory) uncertainty. **Typical variations in T_{dc,f} within bins are 100C.** According to the confidence criteria, the right hand histogram in Figure 5-1, which is RELAP5 epistemic uncertainty in temperature predictions, should be small compared to this value, which is the case as discussed below.

Table 5-3. Range of Temperature and Pressure Variation Within Bins

Bin	T Range	P Range
Palisades SBLOCA	100C	5 MPa
Palisades MBLOCA	60C	1 MPa
Oconee SBLOCA	150C	4 MPa
Oconee MBLOCA	50 C	1 MPa
Beaver Valley SBLOCA	150 C	4 MPa
Beaver Valley MBLOCA	40C	1 MPa
Oconee SRV (full-power)	125C	15 MPa
Oconee SRV (low-power)	125C	15 MPa
Beaver Valley SRV (1 valve)	180C	
Beaver Valley SRV (2 valves)	75C	

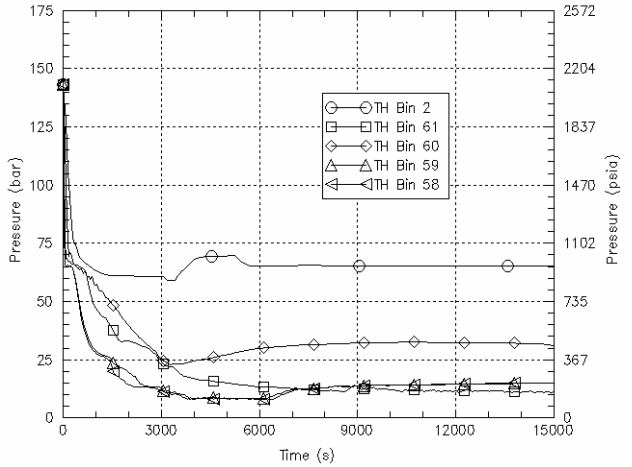
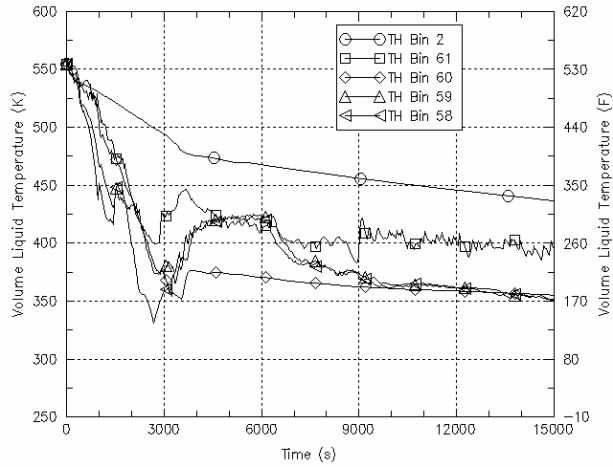


Figure 5-2. Palisades Small-Break LOCA Bin

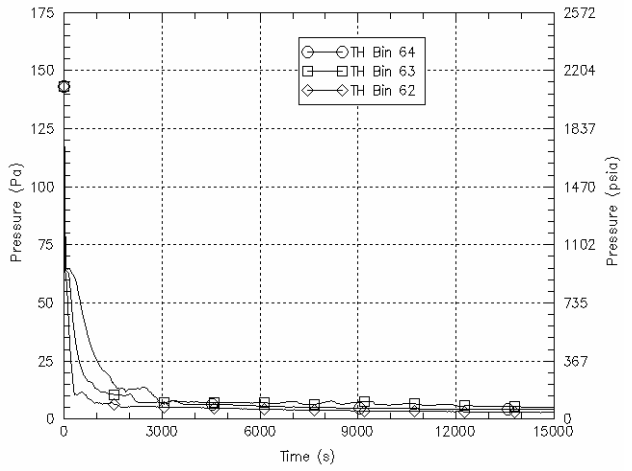
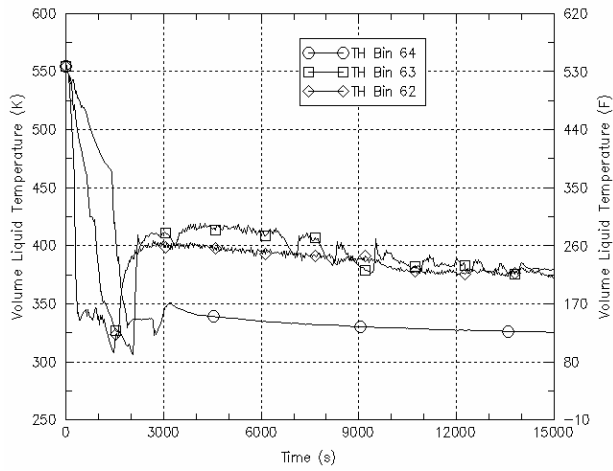


Figure 5-3. Palisades Medium-Break LOCA Bin

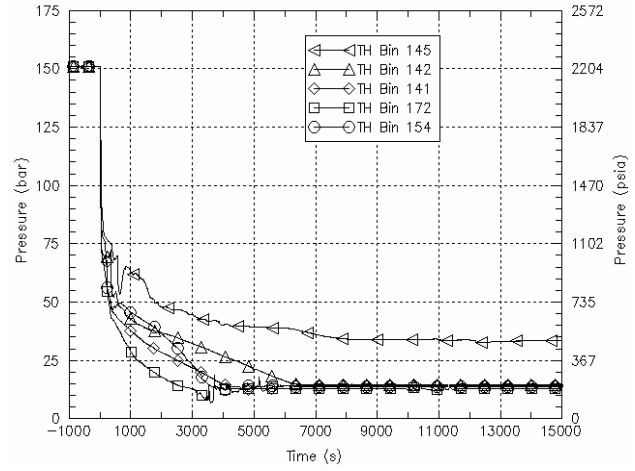
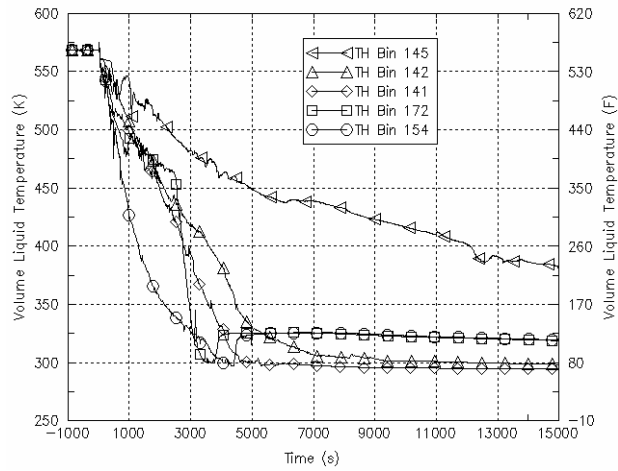


Figure 5-4. Oconee Small-Break LOCA Bin

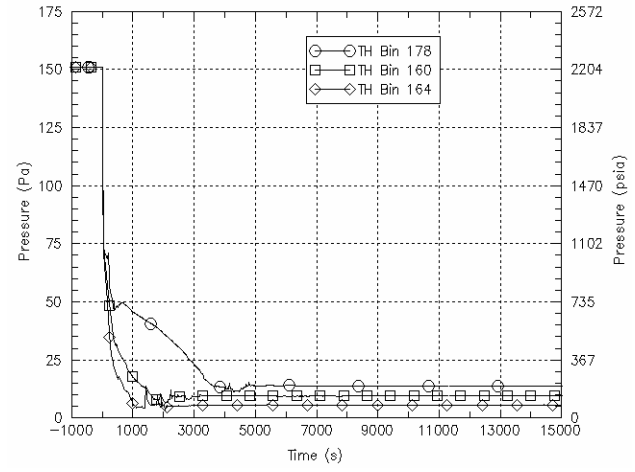
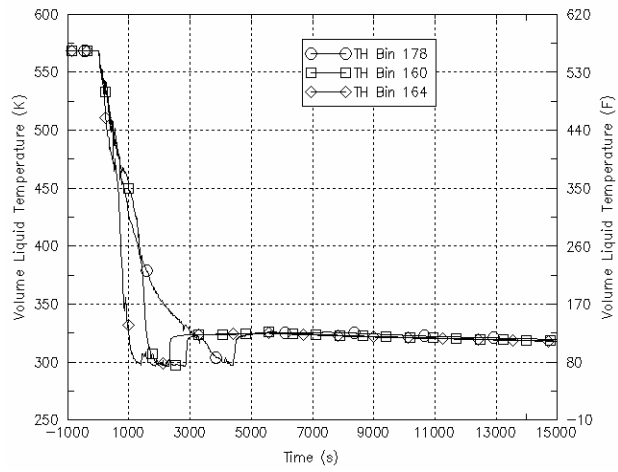


Figure 5-5. Oconee Medium-Break LOCA Bin

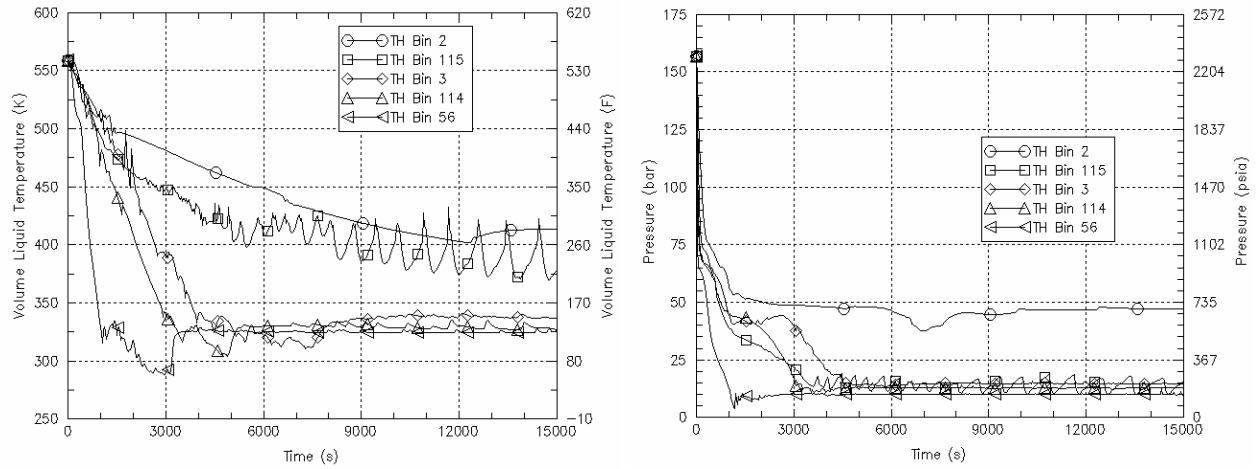


Figure 5-6. Beaver Valley Small-Break LOCA Bin

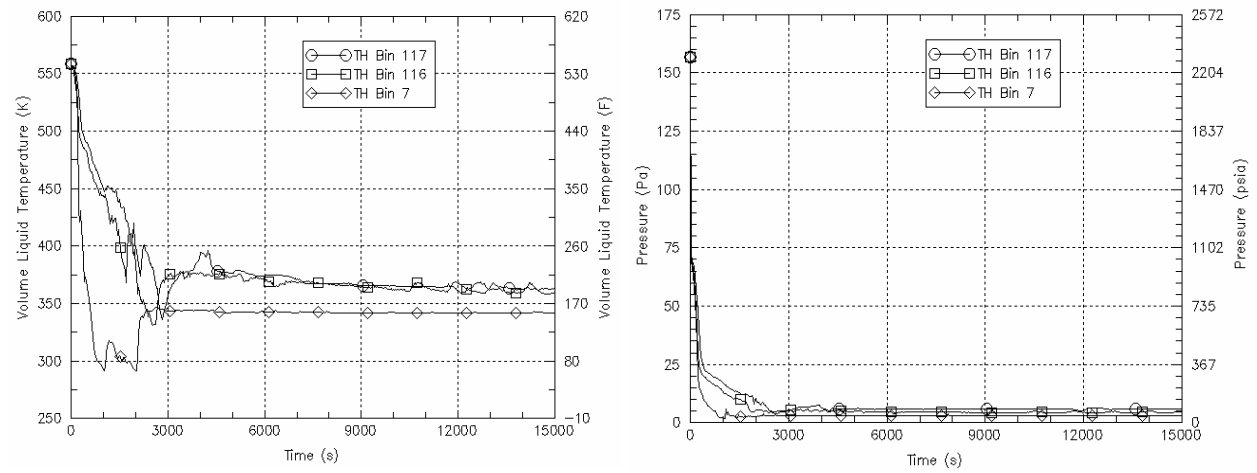


Figure 5-7. Beaver Valley Medium-Break LOCA Bin

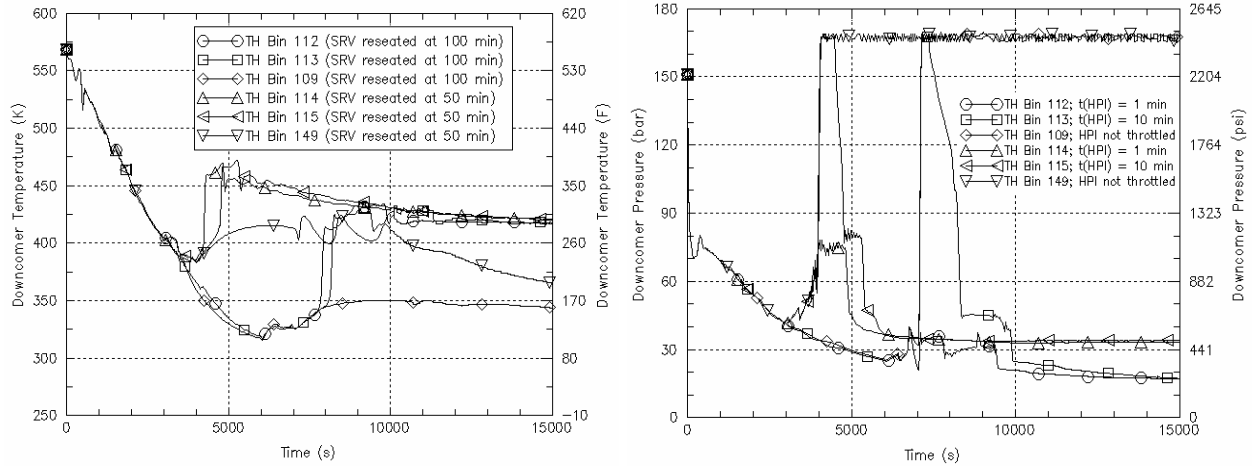


Figure 5-8. Ocone Stuck-Open SRV Bin (Full-Power)

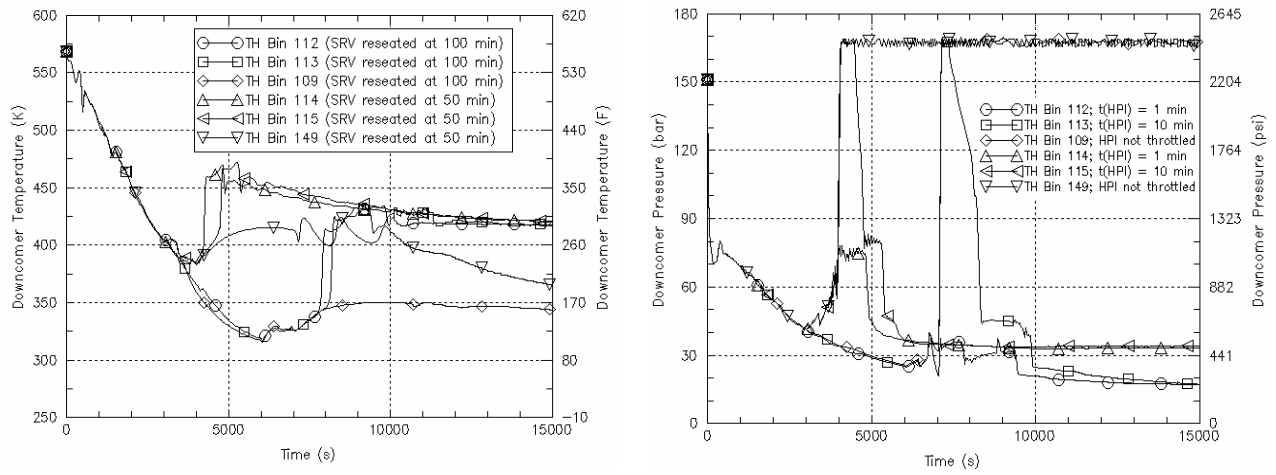


Figure 5-9. Ocone Stuck-Open SRV Bin (Low-Power)

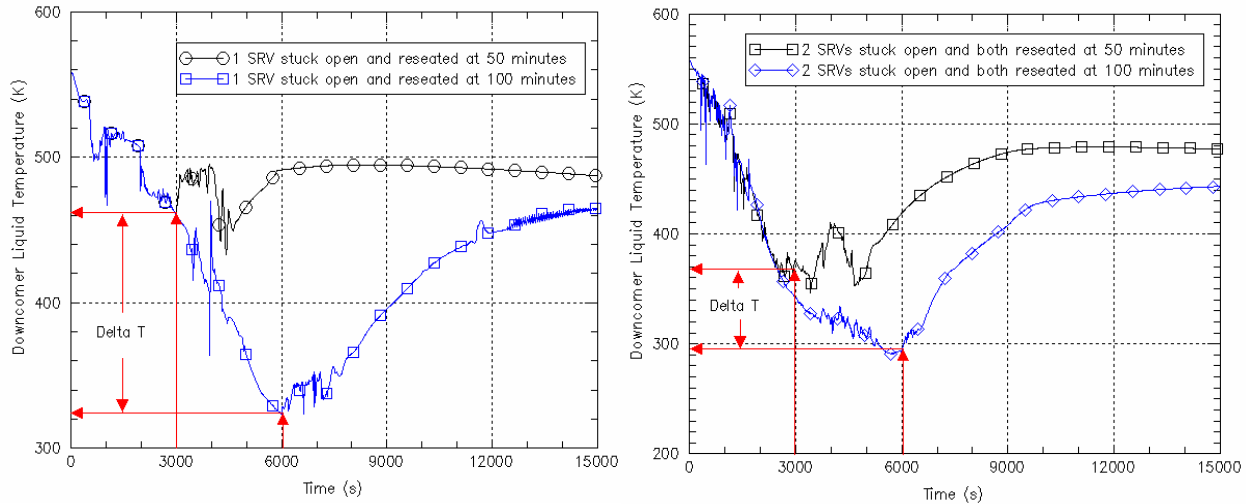


Figure 5-10. Beaver Valley Stuck-Open SRV Bin (1 and 2 valves)

5.3 Impact of Uncertainties in Calculated Boundary Conditions

For each plant, we analyzed (after binning and screening) between 30 and 100 different events for their PTS significance. The bottom line is the conditional probability of failure associated with an overall plant analysis, rather than a single particular transient.

There are two important thermal-hydraulic boundary conditions in the combined fluid-structural analysis performed by RELAP5-FAVOR that determines the probability of vessel failure. One is RCS pressure. The second is heat flux (q''). Heat flux is a function of downcomer fluid temperature and convective heat transfer coefficient.

$$q''_{dc}(t) = f [T_{dc}(t), h_{dc}(t)] = h_{dc}(t) (T_w(t) - T_{dc}(t))$$

The epistemic uncertainties in RELAP5 predictions of $T_{dc}(t)$, $P(t)$, $h_{dc}(t)$ were defined through assessment, as discussed in detail in Chapter 5 and the Appendices. The two parameters, $T_{dc}(t)$ and $P(t)$, are integral measures of RCS energy and inventory. The calculation of these two quantities by RELAP5 is a function of the entire set of physical models and the numerical methods employed by the code.

The assessment of RELAP5 to determine its uncertainty included several different integral system test facilities, whose designs were based on different scaling approaches. In all the integral system tests, geometric similitude was generally maintained. The facilities all shared a common governing scaling principal for LOCAs. Specifically, they maintained a power-to-volume scaling ratio of 1:1. This is the scaling parameter of first order importance to assess the integral quantities of energy and inventory (temperature and pressure). Therefore, the integral system tests may be expected to provide energy/inventory similitude to the full scale prototype. The experiments selected from these integral system facilities to assess RELAP5 covered a range of scenarios similar to the risk-dominant PTS transients.

5.3.1 Pressure

RELAP5 can predict pressure very accurately compared to the accuracy required for the combined fluid-structure analysis. Specifically, the assessment results for pressure (see Chapter 6) show the following:

$$\begin{aligned}\text{Bias (RELAP5-experiment)} &= -0.093 \text{ MPa } (-13 \text{ psi}) \\ \text{Standard deviation } (1\sigma) &= 0.32 \text{ MPa } (46 \text{ psi})\end{aligned}$$

RELAP5 has a small conservative *bias* in pressure. The RELAP5 *uncertainty* in pressure predictions is 2% of normal operating RCS pressure, which translates into an uncertainty in vessel wall stress of < 1% of vessel yield stress. Furthermore, for LOCAs, RCS pressure is low (i.e., < 2 MPa) and does not contribute significantly to wall stress. For stuck-open pressurizer SRV scenarios, pressure is high, but there is no thermal-hydraulic uncertainty in its determination. Rather, RCS pressure is determined by the SRV opening setpoint. Therefore:

The uncertainty in the RELAP5 prediction of pressure has a negligible bottom line impact on CPF.

5.3.2 Heat Flux

It is not possible to assess the impact of the uncertainty in RELAP5's predictions of q'' directly, since the entire time history of the quantity is important. Uncertainty in heat flux cannot be input to FAVOR as a distribution. The impact of the uncertainty in heat flux [$T_{dc,f}(t)$, $h_{dc}(t)$] varies depending on the transient. For a specific transient, uncertainty in heat flux calculated by RELAP5 can in some cases be significant, that is, it could affect CPF by an order of magnitude. That is a reflection of the sensitivity of the fracture toughness of vessel material to temperature.

If RELAP5 predicted values of q'' were systematically low, then true vessel wall temperatures would be higher than predicted. In turn, true fracture toughness would be higher and thermal stress would be lower, so failure probability would be under predicted.

We show that RELAP5 is realistic in predicting heat flux, neither systematically high nor low. The fact that the uncertainty in code predictions may be sometimes high and sometimes low, gives a reasonable degree of confidence, that having a large family of different events have been analyzed for which the heat flux predictions are sometimes high with respect to "reality and sometimes low, that on average the results are a reasonable representation of "reality." Although RELAP5 is not **biased** in its prediction of heat flux, the question remains, "*What is the impact on CPF of the uncertainty in the calculation of heat flux from the wall surface to the fluid?*" Whether an uncertainty in q'' is large or small is determined by its impact on CPF.

Temperature, $T_{dc}(t)$

From the assessment of RELAP5 against integral system experimental data, we found (Chapter 5 and Appendix E) the accuracy and uncertainty of RELAP5 predictions of $T_{dc}(t)$ to be:

$$\begin{aligned}\text{Bias (RELAP5-experiment)} &= -1\text{C } (-2\text{F}) \\ \text{Standard deviation } (1\sigma) &= 10\text{C } (18\text{F})\end{aligned}$$

The 1σ uncertainty in RELAP5 prediction of $T_{dc,i}(t)$ is 10C. This number is an uncertainty, not a bias. For any given transient, the RELAP5 prediction may be expected to be sometimes high and sometimes low, but not systematically biased. Comparing the 10C uncertainty to the temperature variations within bins of $\sim 100\text{C}$ (Table 5-1), the epistemic uncertainty in RELAP5 is small compared to the aleatory uncertainty of the binning process, which meets the second of the two credibility criteria:

The epistemic uncertainty in RELAP5 prediction is small compared to the aleatory uncertainty of variations within bins.

Heat Transfer, $h_{dc}(t)$

The effect of uncertainty in $h_{dc}(t)$ is similar to the uncertainty in temperature. These two parameters are part of one and the same question of the impact of the uncertainty in q'' ,

$$q''_{dc}(t) = h_{dc} (T_w - T_f)$$

Comparisons of RELAP5 with integral experimental data from UPTF and APEX-CE under conditions of loop flow stagnation show the code's prediction of $h_{dc}(t)$ to be realistic or conservative (Chapter 5 and Appendices E, F, G, and H). No nonconservatisms were identified.

One of the surprising observations from the system level experiments used to assess RELAP5 for PTS is that the coarse nodalization of the downcomer gave a good representation of the downcomer velocity. RELAP5, therefore, gives a good representation of $h_{dc}(t)$. These experiments were performed in UPTF and APEX-CE. Both of these experiments operated at reduced temperature, with the highest temperature around 200 °C rather than 285 °C in the PWR downcomer. UPTF was full scale, while the APEX-CE downcomer was reduced by about a factor of 4, but with the correct downcomer aspect ratio.

The details of the flow as it enters the downcomer from the cold leg are complex. Additional complexity is added by the mixing behavior of flows in the ECC injection line, the cold leg, and the downcomer and lower plenum, and from in-vessel circulation. To provide information on these flows, in the past a number of scaled separate effects test facilities were constructed and experiments run [24] with the view of capturing jet dynamics. The picture in the minds of the designers of these experiments was a complicated buoyant free jet discharging into a sector of the annular downcomer. What these experiments did not model was the induced secondary flow caused by the negatively buoyant jet in the annulus. The mixing of the entire jet was inadequately simulated, and the large scale flow induced by the somewhat denser fluid under the cold leg sinking to the lower plenum was missed.

In fact, the jet is confined and the mixing in the entrance region is quite good. The warm water entrained in the descending jet is replaced by rising warmer water from the lower downcomer and lower plenum, which sets up convection cells that decrease in strength over time. With two-dimensional nodalization, RELAP5 is able to capture this flow pattern in the downcomer on a first order basis. While UPTF and APEX-CE operated at reduced temperature initial conditions such that the initial density ratio was $\sim 1/2$ prototypic, the experimental evidence shows that at full scale initial conditions, the induced circulations in the downcomer would be greater. In any event, the velocity range measured in the downcomer of 0.3 to 1.5 m/s is comparable to that calculated by RELAP5.

The uncertainty in the heat transfer models used in RELAP5 is ~20% based on the large amount of data of basic experiments from which they were developed and assessed [25]. However, these models are employed in an integral setting in the code, and are applied in an integral setting when performing plant calculations. The resulting uncertainty in the RELAP5 prediction of $h_{dc}(t)$ is less well defined than $T_{dc}(t)$ and $P(t)$, as a result of a more limited integral system experimental data base, but is within a factor of two. The larger uncertainty stems mainly from the fact that the velocity field in the downcomer varies over time and space. The heat transfer from the vessel to the fluid is a conduction controlled process, meaning the resistance of the vessel wall (l/k) is high compared to the resistance of the fluid convection ($1/h$). Therefore, the impact of uncertainty in $h_{dc}(t)$ on uncertainty in q is highly damped (see Section 4.7.1)

5.4 Sensitivity Studies on the Impact of Heat Flux

5.4.1 Effect of h on Wall-to-Fluid ΔT

The effect of heat transfer uncertainty is shown in a study performed for this purpose. The twelve risk dominant Palisades transients, listed in Table 5-4, were calculated while varying h as follows:

- (1) Base case, no heat transfer modifications
- (2) Factor of 2 applied to h
- (3) Factor of 10 applied to h

The set of Palisades calculations with the factor of two applied to h was intended to evaluate the effect of introducing a **bias** in heat transfer that bounds the uncertainty in h ($\pm 20\%$ in heat transfer correlations, entrance effects, and velocity distribution). The study showed the effect of h on the quantity,

$$\Delta T = T_w - T_f$$

A summary of the results is shown in Table 5-5, while Table 5-6 provides additional detail. The values of ΔT are the average from the start of the transient until the time vessel failure is predicted. As seen in Table 5-5, transients can be grouped into *slow* and *fast*. Fast transients have a larger ΔT than slow transients. The dividing line between the two categories is a break diameter of ~5 to 6 inches. For slow transients the effect of increasing h by a factor of two is equivalent to a decrease in $T_{dc,f}$ by 4 °C. If h were made infinite, then

$$T_w = T_{dc,f} \quad \text{wall surface temperature equals fluid temperature}$$

The effect of perfect convective heat transfer ($h = \infty$) for slow transients (small breaks) would be equivalent to a decrease in $T_{dc,f}$ of 10 °C. This is equal to the 1σ uncertainty in RELAP5 prediction of $T_{dc,f}$.

Table 5-4. Palisades Transients Used as Basis for Sensitivity Studies

#	Transient	f
19	1 SG atmospheric dump valve (ADV) stuck open	2.3 E-3
40	16-inch HL LOCA	3.2 E-5
52	1 SG ADV stuck open	6.4 E-4
54	MSLB	4.3 E-6
55	2 SG ADVs stuck open	2.7 E-4
58	4-inch CL LOCA (winter)	2.7 E-4
59	4-inch CL LOCA (summer)	2.1 E-4
60	2-inch HL LOCA (winter)	2.1 E-4
62	8-inch CL LOCA (winter)	7.1 E-6
63	5.7-inch CL LOCA (winter)	6.1 E-6
64	4-inch HL LOCA (summer)	7.1 E-6
65	SRV recloses @ 6000s	1.2 E-4

Table 5-5. Summary of Effect of h on ΔT

Difference in ΔT	Slow Transients	Fast Transients
	(19, 52, 55, 65, 60, 59, 58, 64)	(63, 54, 62, 40)
Ave ΔT (base)	10 °C	34 °C
Ave ΔT (2 x h)	6 °C	19 °C
$\Delta T(h) - \Delta T(2 \text{ x h})$	4 °C	15 °C
Ave ΔT (10 x h)	3 °C	4 °C
$\Delta T(h) - \Delta T(10 \text{ x h})$	7 °C	30 °C

Table 5-6. Effect of h on ΔT

#	Transient	~ failure time, s	Average $T_w - T_f$, C		
			Base	2 x h	10 x h
19	1 SG ADV stuck open	5,400	1	0.6	0.1
52	1 SG ADV stuck open, both SGs unisolated	6,000	1	0.6	0.1
55	2 SG ADVs stuck open	4,800	2	1	0.2
65	SRV recloses @ 6000s	7,000	10	6	1
60	2-inch HL LOCA (winter)	2,800	15	8	2
59	4-inch CL LOCA (summer)	2,800	16	9	2
58	4-inch CL LOCA (winter)	2,800	18	10	3
64	4-inch HL LOCA (summer)	2,000	15	12	6
63	5.7-inch CL LOCA (winter)	1,600	19	15	7
54	MSLB	1,000	22	12	3
62	8-inch CL LOCA (winter)	800	34	16	6
40	16-inch HL LOCA	400	62	33	11

For fast transients (large LOCAs, MSLB), as seen in Tables 5-5 and 5-6, applying a factor of two bias to h is equivalent to decreasing $T_{dc,f}$ by 15 °C, which is within the 2σ uncertainty in RELAP5 prediction of $T_{dc,f}$ of 20 °C.

If a factor of two bias were applied to h , the effect on q would fall within the RELAP5 uncertainty in predicting $T_{dc,f}$.

5.4.2 Sensitivity Study on $h_{dc}(t)$

Sensitivity studies based on introducing a bias are not the same as introducing an uncertainty.

Introducing a bias is more severe than evaluating an uncertainty in heat transfer, which is not possible.

A bias is not the same as uncertainty. To calculate a bias, all values are altered in one direction. To calculate an uncertainty, half the values fall on one side of the best-estimate and half on the other. The consequences of using a bias are more severe than an uncertainty. Sensitivity studies were performed to assess the impact of a bias in downcomer temperature and a bias in heat transfer. These two sensitivity studies are part of one and the same question of the impact of uncertainty in heat flux. The same set of risk-significant Palisades transients listed in Table 5-4 were calculated with a factor of two applied to h . The intent was to evaluate the effect of introducing a ***bias*** in heat transfer that bounds the uncertainty in h .

The RELAP5 sensitivity study boundary conditions results were applied as boundary conditions to FAVOR in the usual manner. The analyses performed with FAVOR used the Palisades vessel at an embrittlement corresponding to 60 effective full-power years (EFPY). The vessel failure probability determined by FAVOR was used as the figure of merit for determining the effect.

The integrated results for the 12 dominant Palisades transients at 60 EFPY show an increase of 1.6×10^{-8} to 2.4×10^{-7} in through-wall cracking frequency (TWCF), a factor of 15 increase when the factor of two bias was applied to h . The risk is dominated by larger break LOCAs (5.7 inches and above) as shown in Table 5-7.

5.4.3 Sensitivity Study Varying Both $T_{dc}(t)$ and $h_{dc}(t)$

A sensitivity study was performed with respect to downcomer fluid cooldown rate ($T_{dc}(t)$), and heat transfer coefficient ($h_{dc}(t)$) [26]. The RELAP5 sensitivity study boundary conditions results were applied as boundary conditions to FAVOR in the usual manner. The analyses performed with FAVOR used the Palisades vessel at an embrittlement corresponding to 60 EFPY. The CPF determined by FAVOR was used as the figure of merit to determine the effects of the two variables.

For this study, a Palisades stuck-open SRV transient was selected, for analysis with RELAP5 (case 65). A simple exponential decay function was then fitted to the RELAP5 calculation of downcomer temperature ($T_{dc}(t)$). Then, the decay rate was varied using the exponential function.

$$T_{dc}(t) = T_{ECC} + (T_0 - T_{ECC}) e^{-t/\tau}$$

where T_{ECC} was 57 °C (136 °F)

T_0 was the temperature at the beginning of the transient, 278 °C (532 °F)

τ is the time constant

As T decreases, the cooldown becomes faster. Figure 5-11 shows the cooldown rates examined ($\beta=1/\tau$). The RELAP5 calculation falls in the middle of the family of curves. The same RELAP5 calculated values for P were used as boundary conditions for all of the calculations. Multipliers on heat transfer coefficient were explored as well as cooldown rate. The multipliers to h were applied to the base case $h_{dc}(t)$ time history calculated by RELAP5.

The base case RELAP5 calculation corresponds to the decay curve $\beta = 2.9 \times 10^{-4}$ ($\tau = 3450s$), whose value was selected as a visual fit to the RELAP5 temperature trace. β was then varied about this value in the positive and negative directions, over a range of two, according to the values in the table shown on the right of Figure 5-11. This gave a spread in temperatures of approximately 40 °C (75 °F) at 6000s, which is less than the spread in temperatures in any of the PRA bins (typically ~100 °C), and more than the RELAP5 uncertainty (10 °C). This family of curves all fall into the category of a small-break LOCA (slow transient).

Table 5-8 shows the results obtained in terms of CPF. The CPF from the RELAP5 calculation matched that obtained for $\beta = 2.9 \times 10^{-4}$, which shows that the selection of $\beta = 2.9 \times 10^{-4}$ was appropriate. More significantly, it supports the notion that the cooldown of the RCS as a whole, and the greater downcomer region in particular, closely resembles a simple exponential decay, which is also characteristic of a back-mixed (i.e., ideally mixed, mixing cup) volume.

Table 5-7. Percent Contribution of Individual Transients to TWCF and CPF (60 EFPY)

#	Transient	f	Base Case		2 x h		10 x h	
			CPF	% total	CPF	% total	CPF	% total
19	1 SG ADV stuck open	2.3 E-3	6.2 E-8	0.1	3.2 E-8	0.0	3.2 E-8	0.0
52	1 SG ADV stuck open	6.4 E-4	1.0 E-7	0.0	1.3 E-7	0.0	1.4 E-7	0.0
55	2 SG ADVs stuck open	2.7 E-4	2.4 E-7	0.3	1.1 E-7	0.0	1.2 E-7	0.0
65	SRV recloses @ 6000s	1.2 E-4	7.1 E-5	0.1	1.2 E-4	0.0	1.3 E-4	0.0
60	2-inch HL LOCA (winter)	2.1 E-4	1.8 E-7	0.2	7.0 E-5	4.4	1.2 E-5	0.2
59	4-inch CL LOCA (summer)	2.1 E-4	1.0 E-6	0.0	5.8 E-11	0.0	1.1 E-5	0.0
58	4-inch CL LOCA (winter)	2.7 E-4	1.1 E-5	0.0	2.0 E-4	0.0	7.5 E-3	0.2
64	4-inch HL LOCA (summer)	7.1 E-6	8.2 E-5	1.0	9.4 E-4	0.8	4.6 E-3	0.8
63	5.7-inch CL LOCA (winter)	6.1 E-6	8.5 E-5	13.7	2.7 E-3	28.8	2.0 E-3	4.8
54	MSLB	4.3 E-6	3.0 E-5	1.4	8.8 E-5	0.3	2.6 E-4	0.2
62	8-inch CL LOCA (winter)	7.1 E-6	2.2 E-5	53.7	2.1 E-4	33.3	9.5 E-4	33.2
40	16-inch HL LOCA	3.2 E-5	4.2 E-5	29.7	7.0 E-4	32.4	6.1 E-3	60.6

Table 5-8. Sensitivity Analysis for Exponential Temperature Decay Transients Solution

h = 1		h = 0.7		h = 1.56	
β	CPF	CPF	CPF/CPF _{base}	CPF	CPF/CPF _{base}
2.1×10^{-4}	2.3×10^{-5}	1.4×10^{-5}	0.61	3.4×10^{-5}	1.48
2.5×10^{-4}	5.5×10^{-5}	3.4×10^{-5}	0.62	8.2×10^{-5}	1.49
2.9×10^{-4}	1.0×10^{-4}	6.6×10^{-5}	0.66	1.5×10^{-4}	1.50
3.3×10^{-4}	1.6×10^{-4}	1.1×10^{-4}	0.69	2.2×10^{-4}	1.38
3.7×10^{-4}	2.2×10^{-4}	1.5×10^{-4}	0.68	2.9×10^{-4}	1.32
4.1×10^{-4}	2.6×10^{-4}	1.9×10^{-4}	0.73	3.5×10^{-4}	1.35
Ave	8.2×10^{-4}	5.5×10^{-4}	0.67	11.3×10^{-4}	1.42

The results showed the expected sensitivity of CPF to cooldown rate; the faster the cooldown, the higher the CPF value. Although the family of cooldown curves do not represent a large spread, CPF varied by an order of magnitude for the range of cooldown rates examined, regardless of the HTC multiplier.

Variations of h_{dc} were then applied to the same set of cooldown curves. Multipliers of 0.7 and 1.56 were used, but the overall effect of h_{dc} on CPF was not pronounced. For the two sets of cases where h_{dc} was reduced and increased, the impact on CPF was approximately 1.5.

$$\frac{CPF_{0.7h}}{CPF_{1.0h}} = 0.67 \qquad \frac{CPF_{1.56h}}{CPF_{1.0h}} = 1.42$$

Comparison of the $T_{dc}(t)$ sensitivity to the h_{dc} sensitivity show a much greater CPF sensitivity to the rate and degree of cooldown than to the heat transfer coefficient. This is consistent with expectation for the parameter variations used in this study, which used the cooldown rate for a stuck-open SRV scenario (Case 65). The effect of the variation in h by a factor of ~2 (1.56/0.7) for this family of curves is ~4 °C, compared to the 40 °C spread in temperatures represented by the different cooldown rates. The effect of varying h is similar to the results shown in previous Chapters. There, Case 65 (the same transient), shows the following consistent result:

$$\frac{CPF_{2h}}{CPF_{1.0h}} = 1.71$$

Therefore, the SRV bins, which account for ~ ½ the total PTS risk are insensitive to uncertainty in h. We, therefore, draw the following conclusions:

- ***For LOCAs, the impact of uncertainties in heat flux on risk was found to be small (one order of magnitude) compared to uncertainty in event frequency (two orders of magnitude).***
- ***For SRV scenarios, the impact of uncertainty in h on risk is negligible.***
- ***The impact of uncertainty in heat flux on risk (CPF's) is small compared to bin variations.***
- ***The boundary conditions to the analyses are the main source of overall thermal-hydraulic uncertainty. The variation within a bin is roughly an order of magnitude greater than the uncertainty in RELAP5 calculations of temperature and pressure.***

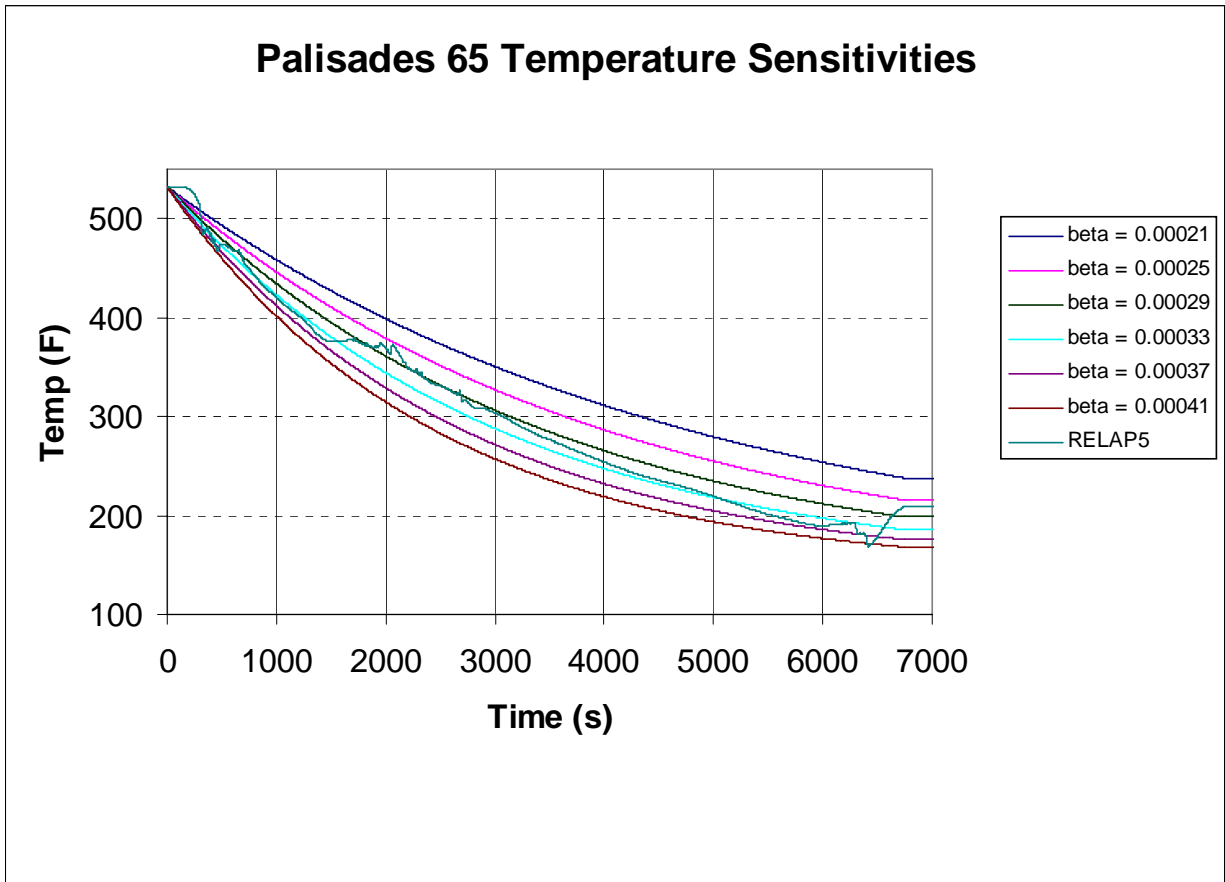


Figure 5-11. Cooldown Transients for Palisades

5.5 Sensitivity of Probabilistic Fracture Mechanics Analysis Results to Imposed Thermal Plumes in the Downcomer

Sensitivity studies were performed prior to the start of the current PTS re-evaluation to explore the importance of possible plumes [27]. The fracture mechanics analyses were performed using an early version of FAVOR (94.1). The applicability of these FAVOR 94.1 results to current analyses using the most recent version of FAVOR (04.1) is discussed in Appendix N.

In the FAVOR model, the plume had no effect on axially oriented flaws. It was assumed that 30% of the upper circumferential weld was subject to the lower centerline plume temperature. Plate material was not subject to the plumes. The affected region contained 2% of the total number of beltline flaws in the vessel model used. The effects on CPF apply to embrittlement levels (as quantified by RT_{PTS} for the circumferential weld) ranging from 228F to 305F, that is, to embrittlement levels that exceed the PTS screening limits defined in 10CFR50.61.

The base case calculation for the studies was a RELAP5 calculation of a 2-inch hot leg break LOCA in H.B. Robinson (similar to Beaver Valley), with averaged temperature applied throughout the downcomer. In addition to a base case calculation, three plume sensitivity cases were run, as listed in Table 5-9.

To obtain a nominal plume, a REMIX-calculated plume was superimposed upon the RELAP5 calculation of the 2-inch hot leg break in H.B. Robinson. The REMIX-calculated plume, illustrated in Figure 5-12, had a maximum strength at the beginning of the transient of ~40C (70F). The plume strength decreased as the transient proceeded due to the general cooldown of the entire downcomer.

Also investigated were the effects on vessel failure probability of plumes of magnified strength (twice nominal) run as case 5, and of diminished strength (half nominal) as case 6. Comparison of these analyzed plume strengths with those measured in integral system tests (Table 5-10) indicates that, at worst, the effects of plumes on vessel failure probability is best represented by the results for the diminished plume strength analysis.

The results of the FAVOR calculations were expressed in terms of Conditional Probability of Failure (CPF). Figure 5-13 and Table 5-9 gives the results. The effect of the plume on CPF was small, with essentially no difference between the nominal plume and the base case with no plume. Even at twice the REMIX-calculated plume strength, the difference from the base case with no plume was marginal. This study lent support to the use of a uniform temperature distribution in the downcomer.

Table 5-9 Sensitivity Studies on Plumes

#	h	plume	Maximum Plume Strength	Effect on CPF
1	nominal	none	0	NA
2	nominal	nominal	40C	~ no change
5	nominal	twice nominal	80C	increased by 30%
6	nominal	½ nominal	20C	~ no change

Table 5-10 Plume Strengths Observed in Experimental Facilities (see Appendix B for details).

Section of this Report	Facility	Maximum Observed Plume Strength
B3	Creare ½ Scale	20C (36F)
B4	APEX-CE	8C (14F)
B5	ROSA	None
B6	LOFT	None

The results suggest that plumes of the magnitude expected to exist in plant service (as evidenced by the integral systems tests summarized in Appendix B) are not expected to have any significant effect on the vessel failure probability. This sensitivity study supported the methods used in the current PTS reevaluation to make the simplifying assumption of using averaged downcomer temperature in the probabilistic fracture mechanics calculations, and validates the appropriateness of the axisymmetric stress models adopted in FAVOR. Therefore, we conclude

- ***If plumes did exist, they would have a negligible small effect on the conditional probability of vessel failure.***

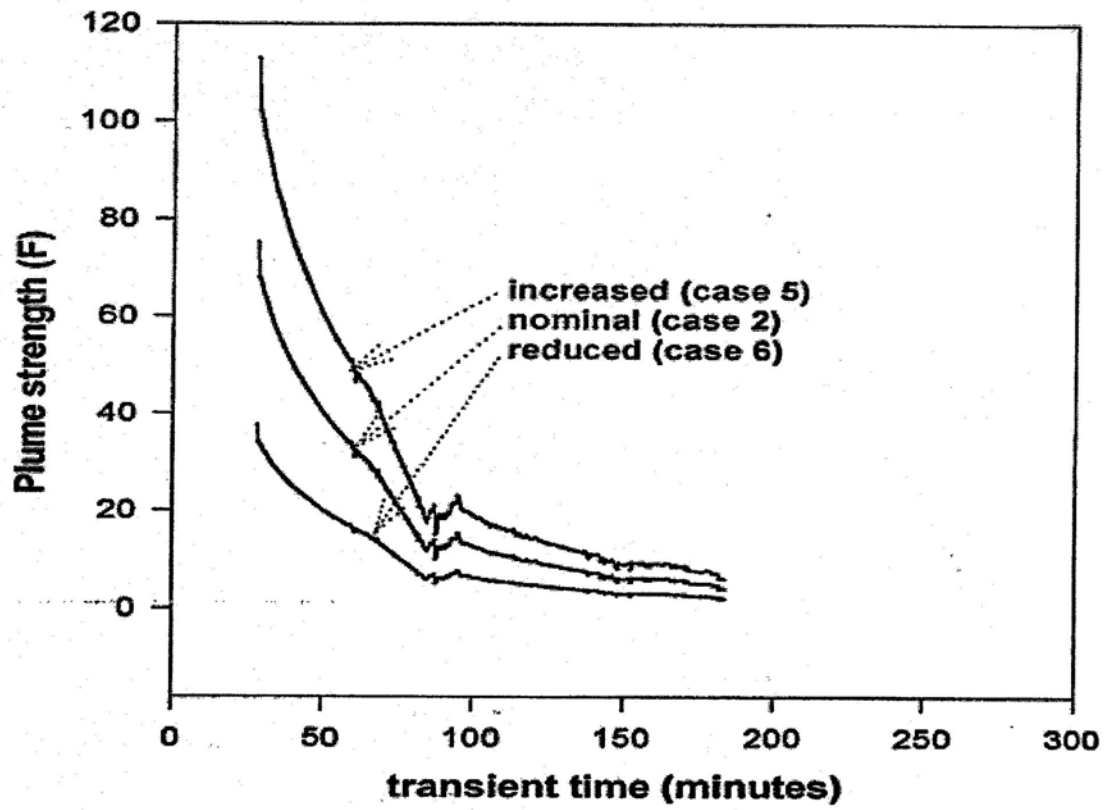


Figure 5-12 Plume Strengths Used in Sensitivity Study

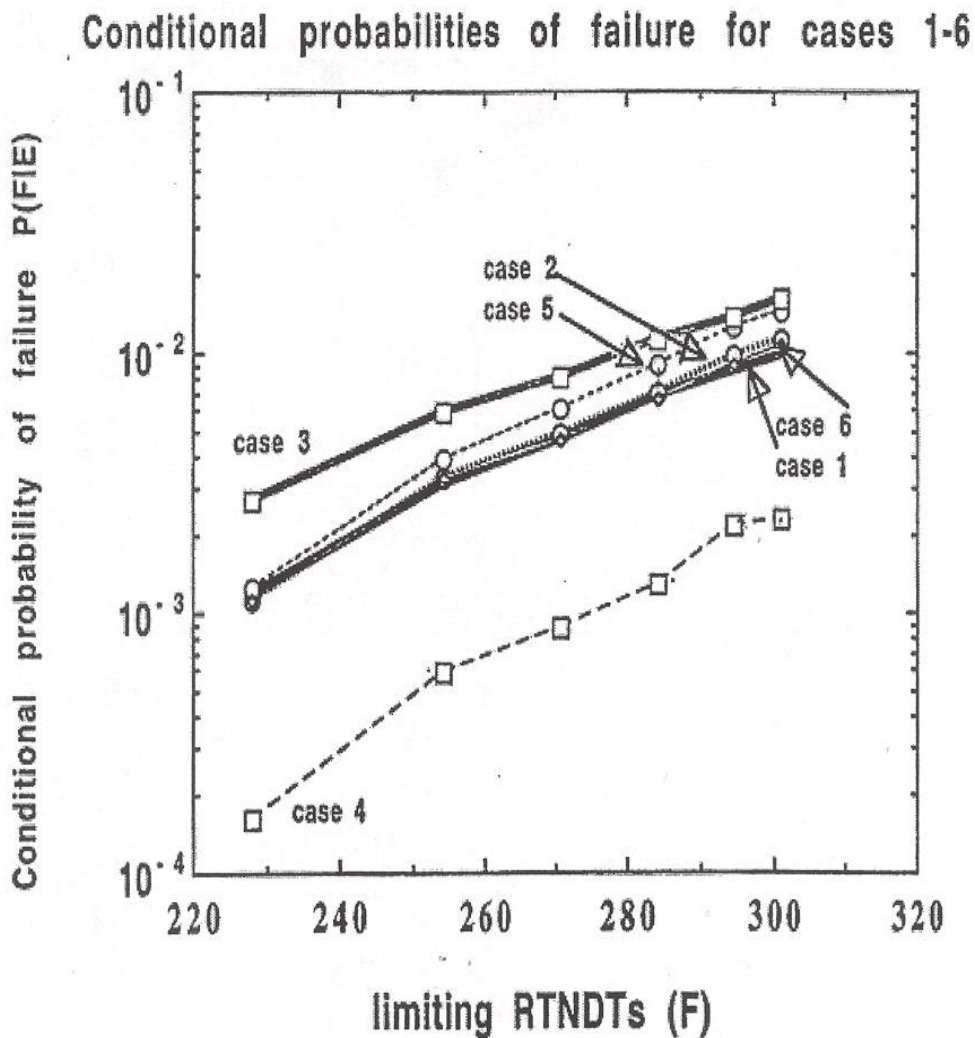


Figure 5-13 Effect of Plumes on Conditional Probability of Vessel Failure

- Case 1 is base case with no plume
- Case 2 is nominal plume
- Case 5 is twice nominal plume strength
- Case 6 is ½ nominal plume strength

The nominal value for heat transfer coefficient (h) was that calculated by RELAP5 for the plume sensitivity studies. Cases 3 and 4 were heat transfer sensitivity studies run with no plumes. The nominal value of h was increased by a factor of two for case 3, and decreased by a factor of two for case 4. The highest CPF was found for case 3, with no plume but increased h. For this case, the CPF increased by approximately a factor of 3.

6. CONCLUSIONS

Since the completion of the 1984 Integrated Pressurized Thermal Shock (IPTS) study, new information has resulted in an improved analytical capability to evaluate PTS events. This includes improved embrittlement correlations, improved estimates of flaw density, size, orientation, and distribution, and refinement of the probabilistic fracture mechanics code. The intervening years brought advances in probabilistic risk assessment and thermal-hydraulics, such as improved understanding of criteria for flow interruption and flow stagnation, and fluid mixing behavior in the downcomer. The current work is intended to provide a technical basis to support revision of the PTS Rule set forth in Title 10, Section 50.61, of the Code of Federal Regulations (10 CFR 50.61).

One of the main thermal-hydraulics tasks was to provide the downcomer boundary conditions for the fracture mechanics analysis. The boundary conditions of interest are time-dependent system pressure, fluid temperature in the downcomer, and the convective heat transfer coefficient from the fluid to the wall. The thermal-hydraulic activities can be divided into three main parts:

- (1) Thermal-hydraulic boundary conditions (downcomer fluid temperature, reactor system pressure, and downcomer fluid to wall heat transfer coefficient) were generated by ISL, Inc. and transmitted to Oak Ridge National Laboratory (ORNL) to serve as part of boundary conditions to the FAVOR code [5]. To support this application of RELAP5, PTS-specific assessment of the code was performed [12].
- (2) Estimates of the uncertainties were required for the calculated parameters of temperature, pressure, and heat transfer. The uncertainty evaluation of the thermal-hydraulics calculations was done by the University of Maryland [2].
- (3) The Oregon State University APEX-CE facility was used to generate PTS-specific experimental data [3,4]. This was a new experimental program to generate both integral and separate effects data in an integral test facility. The information generated on loop flow stagnation, cold leg stratification, and downcomer mixing, allowed better justification of the treatment of downcomer flows by a systems code such as RELAP5.

Five reports were generated by these three tasks [2-5, 12]. It is necessary to consider the above five reports, as well as the current report, to get a complete picture of the thermal-hydraulic work. This report describes the applicability and uncertainty of RELAP5 for performing PTS analyses. In particular, it shows that RELAP5 can predict the boundary conditions required by the fracture mechanics analysis, namely temperature, pressure, and heat transfer coefficient.

The overall project results are found in, "Technical Basis for Revision of the Pressurized Thermal Shock (PTS) Screening Limit in the PTS Rule (10 CFR 50.61) Summary Report," NUREG-1806 [1].

At the most basic level, the thermal-hydraulic analysis to support the PTS reevaluation was straightforward. It consisted of a methodical application of the RELAP5 code to characterize a large number of potential PTS scenarios identified by PRA, in order to supply boundary conditions to the fracture mechanics analyses. The challenge, however, rested with establishing the applicability and uncertainty of RELAP5 for calculating downcomer conditions for a very broad spectrum of postulated scenarios. This was in distinct contrast to past studies which have been scenario-specific.

The range of PTS scenarios analyzed was large and varied, and encompassed a very broad range of plant conditions. More than 500 different scenarios were calculated for the three plants under the current study. The 500 completed runs, simulating various PTS events, provide confidence that an unidentified scenario leading to vessel rupture is exceedingly unlikely. The RELAP5 code is highly flexible, and is designed to be applicable to the entire spectrum of postulated scenarios to which it was applied. However, questions about the specific applicability and uncertainty of RELAP5 calculations had to be considered, keeping in mind the established, accepted methodology for such studies. This study led to the following four key analysis results:

- (1) Event sequence selection uncertainty dominates the calculation of vessel failure probabilities.
- (2) The methodology used for event sequence selection is sound.
- (3) Thermal-hydraulic code calculations predict PTS conditions within an acceptable band of uncertainty and are realistic in nature.
- (4) Data used to benchmark thermal-hydraulic codes for PTS are extensive, appropriate, and of high quality.

Event sequence selection uncertainty dominates the calculation of vessel failure probabilities

The University of Maryland performed an uncertainty evaluation of the RELAP5 calculations [2] to derive the required uncertainty estimates for the calculated parameters of temperature, pressure, and heat transfer. The range of thermal-hydraulic conditions in a given bin is much larger than the RELAP5 physical modeling uncertainty. That is, the aleatory part of the problem dominates over the epistemic. The boundary conditions (aleatory), such as break flow, therefore, are the principal source of uncertainty. For example, the factor of 10 range in break size within a given bin overwhelms other sources of uncertainty contributed by physical models in RELAP5 (epistemic). Many uncertainties in the thermal-hydraulic phenomena, which were initially thought to be important in their effect on PTS (based on PIRT analyses), have turned out not to matter. These phenomena include stratification in the cold leg, mixing in the cold leg and upper downcomer, flow stagnation in the loops external to the vessel, and jet penetration in the downcomer immediately below the cold leg. The challenge in this problem, therefore, was not in the thermal-hydraulic modeling of the system, rather, it was in selecting the transients and boundary conditions that cover all the possibilities that can lead to failure of the vessel.

The methodology used for event sequence selection is sound

Plant behavior is adequately resolved from the number of thermal-hydraulic calculations and corresponding bins defined by the PRA. A close relationship between the PRA binning process and thermal-hydraulic uncertainty analysis was maintained throughout this study. The definition of bins was achieved through an interactive feedback between PRA and thermal-hydraulics analysts.

Thermal-hydraulic code calculations predict PTS conditions within an acceptable band of uncertainty and are realistic in nature

RELAP5 was able to adequately predict downcomer fluid temperature, pressure, and heat transfer coefficient based on comparisons between code results and facility data. The comparisons of RELAP5 with data yielded the following findings:

Pressure:	bias (RELAP5 - Experiment) = -0.093 MPa (-13 psi)
	standard deviation (1σ) = 0.32 MPa (46 psi)
Temperature:	bias (RELAP5 - Experiment) = -1 °C (2 °F)
	standard deviation (1σ) = 10 °C (18 °F)
HTC:	bias (RELAP5 - Experiment) = 1114 W/m ² -K
	standard deviation (1σ) = 1389 W/m ² -K

Since RELAP5 was developed and validated for use in thermal-hydraulic accident scenarios involving rapid primary system cooldown such as a LOCA, it was well suited for use to analyze potential PTS scenarios. Pressurized thermal shock is most likely to be initiated by a LOCA or similar transient such as a main steam line break. RELAP5 and its supporting experimental data base were design for analyses under the conditions found in LOCAs. Because of the nature of the PTS transients, the uncertainties found in typical LOCA analysis of peak cladding temperature are larger than those found in PTS transients. This is largely because the conditions in the downcomer are basically single phase for the most part of the PTS transient and these conditions are far easier to predict.

The RELAP5 models, which used two-dimensional downcomer nodalization was found appropriate for modeling the downcomer behavior. Consistent nodalization was used for the three plant models, as well as the various experimental facilities used to assess RELAP5, which included the Upper Plenum Test Facility (UPTF), Loss-of-Fluid Test (LOFT) Facility, Rig of Safety Assessment (ROSA), Advanced Plant Experiment Facility (APEX), and Creare.

Based on the uncertainty in the RELAP5 prediction of nominal downcomer temperature, we defined a plume as a temperature variation of greater than 10 °C (20 °F), which was the 1σ uncertainty in RELAP5. Temperature variations (circumferentially or axially) of less than this number are not significant to the analysis because they fall within the nominal predictive capability of RELAP5. That is, such temperature variations are less than the standard deviation of RELAP5 comparisons with experimental data. Review of integral system test data showed no temperature variations (i.e., variations <10 °C), either axially or azimuthally, in the downcomer that exceeded the predictive capability of RELAP5. Integral test facilities exhibit additional driving forces for mixing that are not present in separate effects tests. In addition, sensitivity studies performed with stronger plumes showed little impact on the probability of vessel failure.

Data used to benchmark thermal-hydraulic codes for PTS are extensive, appropriate, and of high quality

RELAP5 was assessed against a wide variety of integral system test data from UPTF, LOFT, ROSA, APEX, and the Multi-Loop Integral System Test (MIST). The APEX facility at Oregon State University was used to generate PTS-specific experimental data [3, 4]. This was a new experimental program to generate both integral and separate effects data in an integral facility. The information generated on loop flow stagnation, cold leg stratification, and downcomer mixing allowed better justification of the treatment of downcomer flows using RELAP5. The UPTF, LOFT, ROSA, APEX, and MIST facilities are geometrically similar to the three PWR vendor designs analyzed in this study. Power-to-volume scaling of 1:1 was used for all the integral test facilities. The geometric similitude and the energy/inventory (power-to-volume) scaling ensured that the experiments provided prototypic data for PTS. This ensured that the experiments provided prototypic data for PTS applications. A set of experiments was chosen that include scenarios similar to the risk-dominant PTS sequences.

The experiments consistently show large thermal stratification in the cold leg, however, these temperature differences do not carry over into the downcomer. Strong mixing occurs as the flow enters the downcomer from the cold leg as a result of buoyancy-driven flows in the downcomer. Based on data from three different facilities (UPTF, APEX-CE, and Create), downcomer mass flows exceed ECC injection flows by a factor of 20. The flows calculated by RELAP5 for UPTF and APEX-CE are consistent with the experimental data. The heat transfer coefficients that RELAP5 calculated for these two facilities either agree with those derived from the experimental data, or are conservative with respect to the data.

7. REFERENCES

1. EricksonKirk, M., Arcieri, W., Bass, B., Beaton, R., Bessette, D., Dickson, T., Fletcher, C., Junge, M., Kolaczowski, A., Malik, S., Mintz, T., Pugh, C., Simonen, F., Whitehead, D., Williams, P., Woods, R., and Yin, S., "Technical Basis for Revision of the Pressurized Thermal Shock (PTS) Screening Limit in the PTS Rule (10CFR50.61): Summary Report," NUREG-1806, United States Nuclear Regulatory Commission.
2. Chang, Y.H., Almenas, K., Mosleh, A., Pour-Gol, M., Bessette, D.E., "Thermal Hydraulic Uncertainty Analysis in Pressurized Thermal Shock Risk Assessment," University of Maryland, March 2004.
3. Reyes, J.N., et. al., "Final Report for the OSU APEX-CE Integral Test Facility," NUREG/C-6856, October 2004.
4. Reyes, J.N., "Scaling Analysis for the OSU APEX-CE Integral Test Facility," NUREG/CR-6731
5. Arcieri, W.C., Beaton, R.M., Fletcher, C.D., Bessette, D.E., "RELAP5 Thermal Hydraulic Analysis to Support PTS Evaluations for the Oconee-1, Beaver Valley-1, and Palisades Nuclear Power Plants," ISL, Inc., NUREG/CR-6858, October 2004.
6. Zuber, N, et al, "Quantifying Reactor Safety Margins," NUREG/CR-5249, December 1989.
7. Wulff, W, Cheng, H.S., Mallen, A.N., Johnson, G.W., "Uncertainty Analysis of Suppression Pool Heating During an ATWS in a BWR-5 Plant," NUREG/CR-6200, March 1994.
8. Ortiz, M.G. and L. S. Ghan, "Uncertainty Analysis of Minimum Vessel Liquid Inventory During a Small-Break LOCA in a B&W Plant: An Application of the CSAU Methodology Using the RELAP5/MOD3 Computer Code," NUREG/CR-5818, December 1992.
9. Zuber, N., et. al., "An Integrated Structure and Scaling Methodology for Severe Accident Technical Resolution," NUREG/CR-5809, November 1991.
10. Dunn, B.M., "Status Report on Return to Criticality Following Small Break Loss of Coolant Accident," Framatome Technologies, Inc., 47-5001748-00, June 1988.
11. Bessette, D.E., "A Simplified Safety Analysis Method for Small Break LOCAs," 6th International Conference on Nuclear Engineering, 1998.
12. Fletcher, C.D., Prelewicz, D.A., Arcieri, W.C., "RELAP5/MOD3.2.2y Assessment for Pressurized Thermal Shock Applications," NUREG/CR-6857, ISL Inc., October 2004.
13. Yonomoto, T., et al., "Summary Report ROSA-AP600 Program," JAERI-memo 13-009, 2001.
14. Gloudemans, J.R., "Multi-loop Integral System Test (MIST) Final Report," NUREG/CR-5395 Volumes 1 to 11, 1989.

15. Nalezny, C.L., "Summary of Nuclear Regulatory Commission's LOFT Program Experiments," NUREG/CR-3214, July 1983.
16. Damerell, P.S., Simons, J.W., "2D/3D Program Work Summary Report," Nuclear Regulatory Commission, Japan Atomic Energy Research Institute, Gesellschaft fur Reaktor Sicherheit, Los Alamos National Laboratory, MPR Associates Inc., NUREG/IA-0126, June 1993.
17. "2D/3D Program Upper Plenum Test Facility Test No. 1 Fluid-Fluid Mixing Test," Kraftwerk Union, R 515/87/09, UPTF Team, April 1987.
18. Erickson, L., et al., "The Marviken Full-Scale Critical Flow Tests Interim Report: Results from Test 22," MXC-222, March 1979.
19. Erickson, L., et al., "The Marviken Full-Scale Critical Flow Tests Interim Report: Results from Test 24," MXC-224, May 1979.
20. Wulff, W., Rohatgi, U.S., "System Scaling for the Westinghouse AP600 Pressurized Water Reactor and Related Test Facilities," NUREG/CR-5541, September 1999.
21. Banerjee, S., Ortiz, M.G., Larson, T.K., Reeder, D.L., "Top-Down Scaling Analyses Methodology for AP600 Integral Tests," INEL-96/0040, May 1997.
22. Travers, W.D., "Loss-of-Coolant Accident Break Frequencies for the Option III Risk-Informed Reevaluation of 10 CFR 50.46, Appdendix K to 10 CFR PART 50, and General Design Criteria (GDC) 35," Nuclear Regulatory Commission, SECY-04-0060, April 13, 2004.
23. "Rates of Initiating Events at U.S. Nuclear Power Plants: 1987 – 1995," NUREG/CR-5750, Idaho National Engineering and Environmental Laboratory, INEEL/EXT-98-00401, February 1999.
24. Theofanous, T.G., "A Unified Interpretation of One Fifth to Full Scale Thermal Mixing Experiments Related to Pressurized Thermal Shock." University of California Santa Barbara, NUREG/CR-5677, April 1991.
25. "RELAP5/MOD3.3 Code Manual, Volume IV: Models and Correlations," NUREG/CR-5535 Rev.1, December 2001.
26. Bessette, D.E., "RELAP5 Thermal-Hydraulics Sensitivity Studies for PTS", October 2004.
27. Dickson, T., "Sensitivity of Probabilistic Fracture Mechanics Analysis Results to Thermal-Hydraulic Variations," Letter to Chris Boyd, Nuclear Regulatory Commission, March 24, 1997.
28. "Preliminary Development of an Integrated Approach to the Evaluation of Pressurized Thermal Shock as Applied to the Oconee Unit 1 Nuclear Power Plant," NUREG/CR-3770, May 1984.

29. Fletcher, C. D., et. al., RELAP5 Thermal-Hydraulic Analyses of Pressurized Thermal Shock Sequences for the Oconee-1 Pressurized-Water Reactor, NUREG/CR-3761, June 1984.
30. Fletcher, C.D., et. al., "RELAP5 Thermal Hydraulic Analyses of Pressurized Thermal Shock Sequences for the H.B. Robinson Unit 2 Pressurized Water Reactor," NUREG/CR-3977, April 1985.
31. Fletcher, C.D., Davis, C.B., Ogden, D.M., "Thermal-Hydraulic Analysis of Overcooling Sequences for the H.B. Robinson Unit 2 Pressurized Thermal Shock Study," NUREG/CR-3935, May 1985.
32. "Pressurized Thermal Shock Evaluation of the Calvert Cliffs Unit 1 Nuclear Power Plant," NUREG/CR-4022, September 1985.
33. Theofanous, T.G., La Chance, J.L., Williams, K.A., "The Thermal Hydraulics of SBLOCAs Relative to Pressurized Thermal Shock," NUREG/CR-5135, October 1988.
34. Theofanous, T.G., La Chance, J.L., Williams, K.A., "The Thermal Hydraulics of SBLOCAs Relative to Pressurized Thermal Shock," NUREG/CR-5135, October 1988.
35. Janke, Mark, Beaver Valley Unit 1 RELAP Input Deck for PTS Analysis, Westinghouse Calculation CN-LIS-00-180, Rev. 0, March 2001.
36. Consumers Energy Company, Palisades Cycle 16 Principal Plant Parameters, EA-PPD-00-01, Revision 0, November 2000.
37. Final Safety Analysis Report, Palisades Nuclear Power Plant, Revision 22.
38. Theofanous, T.G., Iyer, K., Shabana, E., "Scaling of Thermal Mixing Phenomena from $1/5$ to Full-Scale Test Facilities," Proceedings of the 14th Water Reactor Safety Information Meeting, Gaithersburg, MD, October 27-31, 1986, pp. 363-386.
39. Theofanous, T.G., Iyer, K., "Mixing Phenomena of Interest to SBLOCAs," Nuclear Engineering and Design, 102, pp. 91-103, 1987.
40. Iyer, K., Theofanous, T.G., "Decay of Buoyancy-Driven Stratified Layers with Applications to Pressurized Thermal Shock: Reactor Predictions," Nuclear Science and Engineering, 108, pp. 184-197, June 1991.
41. Theofanous, T.G., Nourbakhsh, "PWR Downcomer Fluid Temperature Transients Due to High-Pressure Injection at Stagnated Loop Flow," Proceedings of Joint NRC/ANS Meeting on Basic Thermal-Hydraulic Mechanisms in LWR Analysis, NUREG/CP-0043, pp. 583-613, September 14-15, 1982.
42. Theofanous, T.G., Angelini, S., Yan, H., "Universal Treatment of Plumes and Stresses for Pressurized Thermal Shock Evaluations," Nuclear Engineering and Design, 146, pp. 1-14, 1994.

43. Theofanous, T.G., Iyer, K., Nourbakhsh, H.P., Gherson, P., "Buoyancy Effects in Overcooling Transients Calculated for the NRC Pressurized Thermal Shock Study," NUREG/CR-3702, May 1986.
44. Iyer, K., Theofanous, T.G., "Flooding-limited Thermal Mixing: the Case of High Froude Number Injection," Proceedings of the Third International Topical Meeting on Nuclear Reactor Thermal-Hydraulics, Newport, RI, October 15-18, 1985, Paper 13.E.
45. Nourbakhsh, H.P., Theofanous, T.G., "A Criterion for Predicting Thermal Stratification Due to High-Pressure Injection in a Circulating Reactor Loop," Nuclear Science and Engineering, 94, p. 77-79, 1986.
46. Valenzuela, J.A., Dolan, F.X., "Thermal and Fluid Mixing in 1/2 Scale Test Facility," NUREG/CR-3426 Volumes 1 and 2, 1985.
47. Iyer, K., Nourbakhsh, H.P., Theofanous, T.G., "REMIX: A Computer Program for Temperature Transients Due to High-Pressure Injection After Interruption of Natural Circulation," NUREG/CR-3701, May 1986.
48. Nourbakhsh, H.P., Lin, H.C., "A User's Manual for the Computer Code REMIX97." NUREG/CR-6568 (to be published).
49. "RELAP5/MOD3.3 Code Manual, Volume VI: Numerics," NUREG/CR-5535 Rev.1, December 2001.
50. Dittus, F.W., Boelter, L.K.M., "Heat Transfer in Automobile Radiators of the Tubular Type." University of California Berkeley, Publications in Engineering, Vol. 2, p. 443, 1930.
51. S. W. Churchill and H. H. S. Chu. "Correlating Equations for Laminar and Turbulent Free Convection From a Vertical Plate." International Journal of Heat and Mass Transfer. 18. pp. 1323-1329, 1975.
52. Petukhov, B.S., Kirillov, V.V., "The Problem of Heat Exchange in the Turbulent Flow of Fluid in Tubes," Teploenergetika, No. 4, pp. 63-68, 1958.
53. Filonenko, G.K., "Hydraulic Resistance in Pipes," Teploenergetika, Vol. 1, No. 4, pp. 40 - 44, 1954.
54. Gnielinski, V., Int. Journal of Chemical Engineering, Vol. 16, 359, 1976.
55. Swanson, L.W., Catton, I., "PWR Annulus Thermal Hydraulics Important to Analysis of Pressurized Thermal Shock," Nuclear Engineering and Design, 102, p. 105-114, 1987.
56. Catton, I, Swanson, L., "Mixed Turbulent Convective Heat Transfer in Vertical Ducts," EPRI NP-5916, July 1988.
57. Boyd, C.F., Dickson, T., "The Impact of the Heat Transfer Coefficient on Pressurized Thermal Shock," NUREG-1667, December 1988.

58. Palmrose, D. "Demonstration of Pressurized Thermal Shock Thermal Hydraulic Analysis with Uncertainty," NUREG/CR-5452, March 1999.
59. Roth, P.A., Palmrose, D.E., Ghan, L.S., Fisher, J.E., Berta, V.T., Naff, S.A., "A Preliminary Study of Pressurized Thermal Shock Thermal Hydraulic Issues in the Yankee Rowe Nuclear Power Plant," SAN-12-92, Idaho National Engineering Laboratory, July 16, 1992.
60. "Decay Heat In Light Water Reactors," American Nuclear Society, ANS/ANSI-5.1-1994, August 23, 1994.
61. R. E. Henry and H. K. Fauske. "The Two-Phase Critical Flow of One-Component Mixtures in Nozzles, Orifices, and Short Tubes." *Transactions of ASME, Journal of Heat Transfer*. 93. 1971, pp. 179-187.
62. Bass, B.R., Dickson, T.L., Williams, P.T., Phan, A.-V., Kruse, K.L., "Verification and Validation of FAVOR Code for Deterministic Load Variables," ORNL/NRC/LTR-04/11, Oak Ridge National Laboratory, March 22, 2004.
63. EricksonKirk, M., Bass, B.R., Dickson, T., Pugh, C., Santos, T., and Williams, P., "Probabilistic Fracture Mechanics: Models, Parameters, and Uncertainty Treatment Used in FAVOR Version 04.1," NUREG-1807, United States Nuclear Regulatory Commission, 2005.
64. Dickson, T.L. "The Inclusion of Thermal Streaming in Fracture Analyses of Reactor Pressure Vessels Subjected to Pressurized Thermal Shock," ASME PVP Vol. 251, Reliability and Risk in Pressure Vessels and Piping, 1993, pages 91-99.
65. Selby, D.L. et al., "Pressurized Thermal Shock Evaluation of the H.B. Robinson Unit 2 Nuclear Power Plant," NUREG/CR-4183, Vols. 1 & 2, United States Nuclear Regulatory Commission, September 1985.
66. Geiß, M., "Verification of OCA-P and VISA-II on Behalf of Strains and Stresses Induced During HDR-TEMB Thermal Mixing Tests," Proceedings of the 9th SMiRT, Rotterdam, August 1987.
67. Kordish, H., "Analysis of Initiation and Growth of a Circumferential Crack in the HDR-RPV Cylinder Under Pressurized Thermal Shock," Proceedings of the 10th SMiRT Post-Conference No. 2, Monterey CA, August 1989.
68. Neubrech, G.E., et al., "Crack Initiation and Crack Growth During Thermal Shock Tests in the Reactor Pressure Vessel of the HDR Under Corrosive Medium Conditions," International Journal of Pressure Vessels and Piping, Vol. 34, pp. 187-207 (1988).
69. Wolf, L., Schygulla, U., "Design Report Thermal Mixing Experiments in Cole Leg Downcomer, HDR-Test Group TEMB T32, PHDR Working Report No 3.340/84 (September 1985).

70. Wolf, L., et al., "Application of Engineering and Multi-Dimensional Finite Difference Codes to HDR Thermal Mixing Experiments," Nuclear Engineering and Design, Vol. 108. pp 137-165 (1988).
71. Stevens, D.L., et al., "VISA: A Computer Code for Predicting the Probability of Reactor Pressure Vessel Failure," NUREG/CR-3384, September 1983.
72. Simonen, F.A., Doctor, S.R., Schuster, G.J., Heasler, P.G., "A Generalized Procedure for Generating Flaw Related Inputs for the FAVOR Code," NUREG/CR-6817 Rev. 1, October 2003.
73. Dickson, T.L. and Simonen, F.A., "The Sensitivity of Pressurized Thermal Shock Results to Alternative Models for Weld Flaw Distributions," Proceedings of the ASME Pressure Vessel and Piping Conference, Cleveland, Ohio, 2002.

APPENDIX A. RELAP5 MODELING FOR PTS ANALYSIS

A.1 Summary

This Chapter describes the RELAP5 models developed for the Oconee-1, Beaver Valley Unit 1 and the Palisades plants. The thermal-hydraulic analysis methodology was essentially the same for the three plants. RELAP5/MOD3.2.2y was used to analyze all the PTS transients. In each case, the best available RELAP5 input model was used as the starting point to expedite the model development process.

For Oconee, the base model was developed originally for the IPTS study [29] and which was used in the small break CSAU study [8]. For Beaver Valley, the base model was the H.B. Robinson 2 model first developed and used in the original PTS study in the early 1980s [30, 31]. This model was revised by Westinghouse to reflect the Beaver Valley plant configuration. For Palisades, the base model was obtained from Nuclear Management Corporation, the operators of the Palisades plant. This model was originally developed and documented by Siemens Power Corporation to support analysis of the loss of electrical load event for Palisades. Palisades is similar to Calvert Cliffs, which was part of the IPTS study [32].

The RELAP5 models for the Oconee, Beaver Valley and Palisades plants are detailed representations of the power plants and include all major components for both the primary and secondary plant systems. RELAP5 heat structures are used throughout the models to represent structures such as the fuel, vessel wall, vessel internals and steam generator tubes. The reactor vessel nodalization includes the downcomer, lower plenum, core inlet, core, core bypass, upper plenum and upper head regions. Plant-specific features, such as the reactor vessel vent valves, are included as appropriate.

The downcomer model used in each plant utilizes a two-dimensional nodalization. The downcomer is divided into six azimuthal regions for each plant. This approach was used to allow two-dimensional flows to be modeled in the downcomer. RELAP5 was assessed against experimental data using both one-dimensional and two-dimensional downcomer models [12]. We found the two-dimensional downcomer nodalization was required to obtain better agreement with the experimental results. This is similar to other studies [33].

The safety injection systems modeled for Oconee, Palisades, and Beaver Valley include high pressure injection (HPI), low pressure injection (LPI), accumulators (also called core flood tanks or safety injection tanks), and makeup/letdown as appropriate.

The secondary coolant system models included steam generators, main and auxiliary feedwater (also called emergency feedwater), steam lines, safety valves, main steam isolation valves (as appropriate), and turbine bypass and stop valves.

Each of the models was updated to reflect the current plant configuration including updating system set points (to best estimate values) and modifying control logic to reflect current operating procedures. Other changes to the models include the addition of control blocks to calculate parameters for convenience or information only (e.g., minimum downcomer temperature). The Oconee, Beaver Valley and Palisades models were then initialized to simulate hot full power (HFP) and hot zero power (HZIP) steady plant operation for the purpose of establishing satisfactory steady state conditions from which the PTS transient event sequence calculations are started.

In the following sections, plant specific RELAP5 modeling features important to the Oconee, Beaver Valley and Palisades plants are discussed. A tabulation of the key parameters for these plants relevant to PTS is presented in Table A-1.

A.2 Oconee RELAP5 Model Description

The Oconee-1 Nuclear Power Station is a Babcock and Wilcox (B&W) designed pressurized water reactor with a rated power of 2568 MWt. The RCS consists of the reactor vessel with two cooling loops connected in parallel, designated as loops 'A' and 'B'. Each cooling loop consists of a hot leg, a once-through steam generator (OTSG), and a pair of parallel cold legs each with a reactor coolant pump (RCP). The pressurizer and pressurizer surge line are connected to the hot leg in loop A.

Water flow in the reactor coolant system is from the reactor core through the hot legs to the OTSG. From the steam generator, the primary system water flows to the reactor coolant pump suction and then back to the reactor vessel. The pressurizer, which is electrically heated, provides pressure control to the reactor coolant system. Oconee is a lowered-loop design with the lowest part of the cold leg about six feet lower than the bottom of the reactor vessel. The RCPs are located such that the center line of the discharge is about 1 meter (3.5 feet) above the center line of the cold leg nozzle. A section of the cold leg is sloped at 45 degrees towards the vessel compensate for the difference in elevation.

The Oconee-1 RELAP5 model is a detailed representation of the plant and includes all major components for both the primary and secondary systems. The noding diagrams are illustrated in Figures A-1 to A-5. RELAP5 heat structures are used throughout the model to represent structures such as the fuel, vessel wall, vessel internals and steam generators.

The reactor vessel nodalization includes the downcomer, lower plenum, core inlet, core, core bypass, and the upper plenum and upper head region, as shown in Figure A-1. A two-dimensional nodalization of the downcomer region in the reactor vessel was used. The downcomer adjacent to the core was divided into five axial and six azimuthal regions as shown in Figure A-1. Six azimuthal regions were used to permit one channel for each of the four cold legs, and two more for the two core flood tank/LPI injection points. This noding extends the axial length of the downcomer. Momentum flux model was disabled in the downcomer to avoid the possibility of numerically driven flows.

Eight vent valves connect the upper plenum to the upper downcomer above the hot and cold leg nozzles. Each valve consists of a hinged disk and valve body that remains closed during normal operation. The eight reactor vessel vent valves were represented by six RELAP5 servo valves, which connect from the upper plenum to each of the six sectors in the upper portion of the downcomer annulus as shown in Figure A-1. Adjustments were made to the valve flow area to compensate for the difference between the actual number of vent valves (8) and the number modeled (6).

Table A-1 Summary of Plant Parameters Relevant to the PTS Evaluation

Description	Oconee	Beaver Valley	Palisades
Power	2568 MWt	2660 MWt	2530 MWt
SRV opening pressure	17.34 MPa (2515 psia)	17.27 MPa (2505 psia)	Three valves with staggered opening set points of 17.24, 17.51 and 17.79 MPa (2500, 2540 and 2580 psia).
SRV capacity	Two valves each capacity 43.47 kg/s (345,000 lb/hr) at 16.89 MPa (2450 psia).	Three valves each capacity of 62.77 kg/s (498,206 lb/hr) at 17.24 MPa (2500 psia).	Three valves each capacity 29.0 kg/s (230,000 lb/hr) at 17.75 MPa (2575 psia)
Pressurizer PORV opening pressure	17.0 MPa (2465 psia)	First PORV controlled by a compensated error signal. Error (0 setpoint = pressurizer P 15.51 MPa (2250 psia)) is processed with proportional-integral controller. PORV begins to open when compensated error is ≥ 0.69 MPa (100 psi) and closes when compensated pressure error < 0.62 MPa (90 psi). Second and third PORVs open when pressurizer P ≥ 16.2 MPa (2350 psia) and close when P < 16.1 MPa (2340 psia).	Two valves, both with an opening setpoint pressure of 16.55 MPa (2400 psia). Note that closed block valves prevent the function of pressure relief through these valves during normal plant operation.
PORV capacity	Estimated flow rate is 16.03 kg/s (127,000 lb/hr) at 16.9 MPa (2450 psia).	Three valves each capacity of 26.46 kg/s (210,000 lb/hr) at 16.2 MPa (2350 psia)	Two valves each with a capacity of 61.5 kg/s (487,800 lb/hr) at 16.55 MPa (2400 psia).
LPI injection actuation setpoint	3.89 MPa (550 psig).	SI signal: pressurizer P ≤ 12.72 MPa (1845 psia), high steamline DP (steamline P $<$ header P by 0.69 MPa (100 psi) or more), or steamline P ≤ 3.47 MPa (503 psia).	Pressurizer P < 10.98 MPa (1593 psia) with a 27 second time delay.
LPI shutoff head	1.48 MPa (214 psia)	1.48 MPa (214.7 psia)	1.501 MPa (217.7 psia).
LPI pump runoff flow	505 kg/s (1110 lb/s) total for two pumps.	313.4 kg/s (690.84 lb/s) total for the three loops.	433.5 kg/s (955.7 lb/s) total for the four loops.

Description	Oconee	Beaver Valley	Palisades
HPI injection actuation setpoint	11.1 MPa (1605 psia)	SI signal: pressurizer P \leq 12.72 MPa (1845 psia), high steamline DP (steamline P < header P by 0.69 MPa (100 psi) or more), or steamline P \leq 3.47 MPa (503 psia).	Pressurizer P less than 10.98 MPa (1593 psia) with a 27 second time delay.
HPI shutoff head	>18.61 MPa (2700 psia)	>17.93 MPa (2600 psia)	8.91 MPa (1292 psia).
HPI pump runout flow	81 kg/s (178 lb/s) total for the four loops.	61.1 kg/s (134.7 lb/s) total for the three loops.	87 kg/s (191 lb/s) total for the four loops.
Reactor coolant pump trip setpoint	No automatic trips on RCPs. Operator assumed to trip RCPs at 0.28K (0.5F) subcooling.	No automatic trips on RCPs. Operator assumed to trip RCPs when DP between RCS and highest SG pressure was less than 2.59 MPa (375 psia).	No automatic RCP trip. Trip two RCPs (one in each loop) if pressurizer P < 8.96 MPa (1300 psia). Trip all RCPs if hot leg subcooling < 14K (25F) or if containment P > 0.127 MPa (18 psia).
SG SRVs opening P	Lowest MS SRV setpoint 6.76 MPa (980 psia).	Lowest MS SRV setpoint 7.51 MPa (1090 psig).	Lowest MS SRV setpoint 7.10 MPa (1029 psia).
SG atmospheric steam dumps opening criteria	Not included in the RELAP5 model.	Opening pressure 7.24 MPa (1050 psia).	Control the RCS T _{av} to 551K (532F)
Number of MSIVs	None.	One per steam line.	One per steam line.
Steamline flow restrictors	None.	Located in SG outlet nozzles.	Located in SG outlet nozzles.
Isolation of turbine-driven AFW pump during MSLB	Isolated during MSLB by isolation circuitry	Requires manual operator action and would be done if needed to maintain SG level	Requires manual operator action and would be done if needed to maintain SG level.
Analyzed range of ECC water temperature	Base case HPI, LPI 294K (70F) Acc 300K (80F). Sensitivity cases Summer HPI, LPI 303K (85F) Acc 311K (100F) Winter HPI, LPI 278K (40F) Acc 294K (70F)	Base case HPI, LPI 283K (50F). Acc 305K (90F). Sensitivity cases Summer HPI, LPI 286K (55F) Acc 313.7K (105F)	Base case HPI and LPI 304K (88F). Acc 311K (100F). Sensitivity cases Summer HPI, LPI 311K (100F) Acc 305K (90F) Winter HPI, LPI 278K (40F) Acc 289K (60F)
RWST volume	327,000 gallons	Useable volume 1628 to 1669 m ³ (430,000 to 441,000 gal).	890 m ³ (235,000 gallons)

Description	Oconee	Beaver Valley	Palisades
Containment spray actuation setpoint and flow rate	Total flow rate 3000 gpm (1500 gpm/pump)	Total flow rate 334 kg/s (5300 gpm)	Actuated on high containment pressure 0.127 MPa (18.4 psia). Total flow rate 230 kg/s (3643 gpm).
Accumulator water volume	2, each with water volume 28,579 liters (7550 gallons)	3, each with liquid volume 29,299 liters (7740 gallons)	4, each with water volume 29,450 liters (7780 gallons).
Acc. pressure	4.07 MPa (590 psia)	4.47 MPa (648 psia)	1.48 MPa (215 psia)

The vent valves open if the pressure drop across the core barrel reverses, a situation that can exist when natural circulation and/or flow stagnation occurs. The vent valves allow in-vessel natural circulation. Steam and/or water can also flow from the upper plenum through the downcomer to the break in the event of a cold leg break. Flow from the vent valves enhances mixing of the ECCS flow in the downcomer.

RCS loop nodalization included the hot legs (one per loop) and cold legs (two per loop), the reactor coolant pumps (two per loop), and the OTSG tubes, as shown in Figure A-2. Loop A components were numbered as 100 series while loop B components were numbered as 200-series. The RELAP5 default pump flow curves were used for the RCPs. The rated flow of each RCP is 4147Kg/s (88,000 gpm).

The HPI system connects to each cold leg and is modeled as a time dependent volume-junction combination. HPI actuates if the pressurizer pressure falls below 11.1 MPa (1605 psia), as listed in Table A-1. The LPI system and the accumulators inject directly into the vessel downcomer and hence are part of the reactor vessel nodalization. There are two injection nozzles for both the LPI and accumulators on opposite sides of the vessel. The LPI was modeled as a time-dependent volume-junction pair. The RELAP5 accumulator component models was used.

The pressurizer is connected to the riser section of the Loop A hot leg as shown in Figure A-2. The pressurizer system nodalization included the pressurizer, pressurizer spray line, power operated relief valve (PORV) and pressurizer SRVs, as shown in Figure A-3. The pressurizer spray system connects to the cold leg downstream of the reactor coolant pump in Loop A2. The SRVs and the PORV were modeled as trip valves. The discharge of these valves was connected to time-dependent volumes representing the quench tank in the containment. The pressurizer spray system was also represented in the Oconee-1 model. The spray valve was included as a RELAP5 trip valve.

Secondary side components included the hot well pump, condensate booster pump, two main feedwater pumps, startup and main feed regulation valves, steam generator secondary side and the connecting piping. The steam generator secondary side nodalization is shown in Figures A-4 and A-5 feedwater system was connected to the topmost node of the stack of nodes with the smaller flow area.

The turbine bypass valve, safety valves, and turbine stop valves are modeled as servo valve-time dependent volume pairs, where the time dependent volumes represent the condenser, atmosphere, and turbine-generator, respectively. These valves are connected to the main steam line at various

locations as shown in Figure A-4.

Modeling of the feedwater train from the high pressure feedwater header to the steam generator downcomers is shown in Figure A-4. This figure also shows the modeling of the turbine driven and motor driven emergency feedwater systems. The startup and main feedwater control valves for each steam generator are modeled as a pair of servo valves. The main feedwater crossover to the emergency feedwater lines is shown as components 850 to 852 on the 'A' side and components 950 to 952 on the 'B' side.

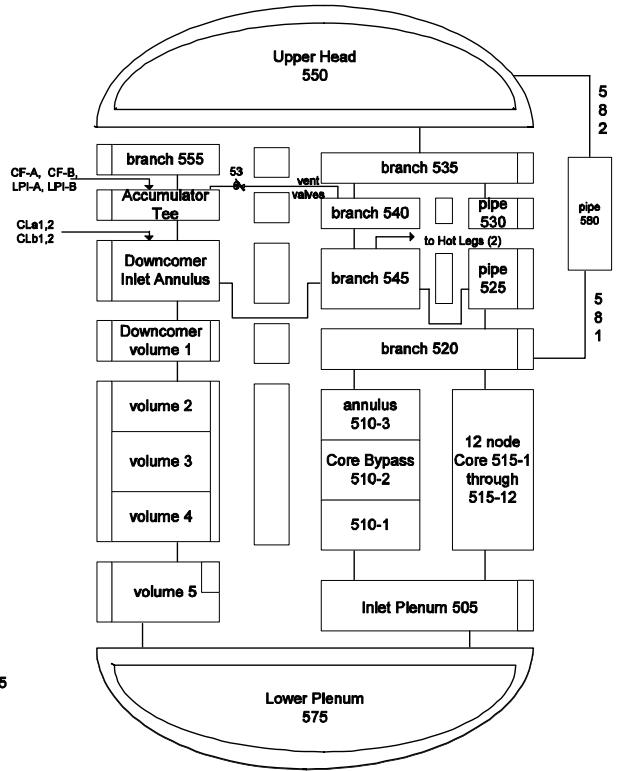
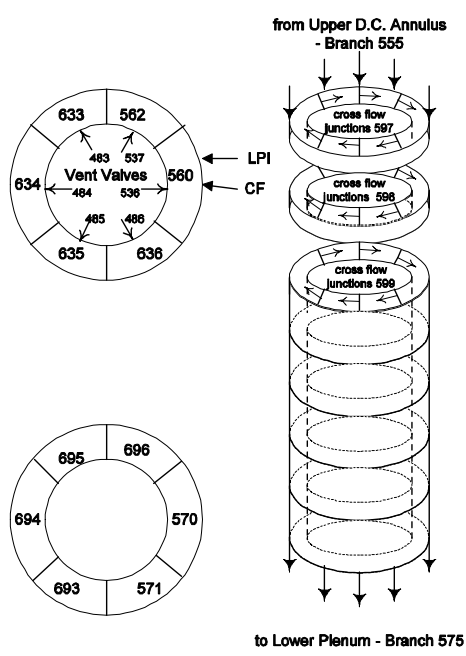
The turbine and motor driven emergency feedwater systems are modeled as time-dependent junction volume pairs. Valve components 775 and 777 are the feedwater isolation valves for the 'A' and 'B' trains, respectively. Modeling of the main feedwater train from the hot well to the startup and main feed valves is shown in Figure A-5. The main feedwater pumps (components 754 and 760) discharge to the main feedwater pump header (component 763). From this header, flow is through nodes representing high pressure feedwater heater trains (components 764 and 766) to the high pressure feedwater header (component 768).

Control system models were included for emergency feedwater control, turbine bypass valve control, and main feedwater control. The models used were originally developed for the IPTS study performed by INEL. The OTSG has two ranges of level indication that are used during plant operation: startup range and operating range. The startup range indication is used to monitor steam generator level during plant startup at power levels ≤ 15 percent of full power. The range of indication is 0 to 6.35 m (0 to 250 in) measured from the upper surface of the lower tube sheet.

Normal startup level is 0.76 m (30 in) above the tube sheet when the reactor coolant pumps are operating and 6.1 m (240 in) when they are tripped. The operating range indication is used during normal plant operation and is an input to the Integrated Control System (ICS). The operating range indication is monitored by the ICS for the purpose of limiting feedwater flow to prevent flooding of the aspirating ports.

The Main Steam Line Break (MSLB) detection and feedwater isolation circuitry is designed to mitigate containment over pressurization by isolating feedwater to both steam generators during a MSLB event. This circuitry is designed to trip the main feedwater pumps, to inhibit/stop the turbine-driven emergency feedwater pump, and to isolate main feedwater and startup feedwater systems. The MSLB circuitry was added in response to I&E bulletin 80-04 to prevent overfeed and rapid reactor cooldown and return to power. Section 7.9 of the Oconee FSAR [34] provides additional details on the MSLB circuitry.

Steady-state calculations simulating hot full power and HZP plant operation were performed with the Oconee RELAP5 model in order to establish model initial conditions from which to begin transient calculations. All subsequent transient analyses were started using the steady state hot full power or HZP model as appropriate.



	CF-B				CF-A	
	LPI-B				LPI-A	
	↓	↓			↓	↓
633	634	635	636	560	562	
643	CLb1	644	CLa1	645	646	561
						CLa2
673	674	675	676	565	567	CLb2
683	684	685	686	566	568	
693-1	694-1	695-1	696-1	570-1	571-1	
693-2	694-2	695-2	696-2	570-2	571-2	
693-3	694-3	695-3	696-3	570-3	571-3	
693-4	694-4	695-4	696-4	570-4	571-4	
693-5	694-5	695-5	696-5	570-5	571-5	

Accumulator Tee
 Downcomer Inlet Annulus
 Downcomer volume 1
 volume 2
 volume 3
 volume 4
 volume 5

Key:
 CF-A - Core Flood Tank (CMP 700)
 CF-B - Core Flood Tank (CMP 900)
 CLa1 - Cold Leg a1 (CMP 181)
 CLa2 - Cold Leg a2 (CMP 151)
 CLb1 - Cold Leg b1 (CMP 281)
 CLb2 - Cold Leg b2 (CMP 251)
 LPI-A - Low Pressure Injection (CMP 728)
 LPI-B - Low Pressure Injection (CMP 717, 718)

Unwrapped Downcomer Sectors

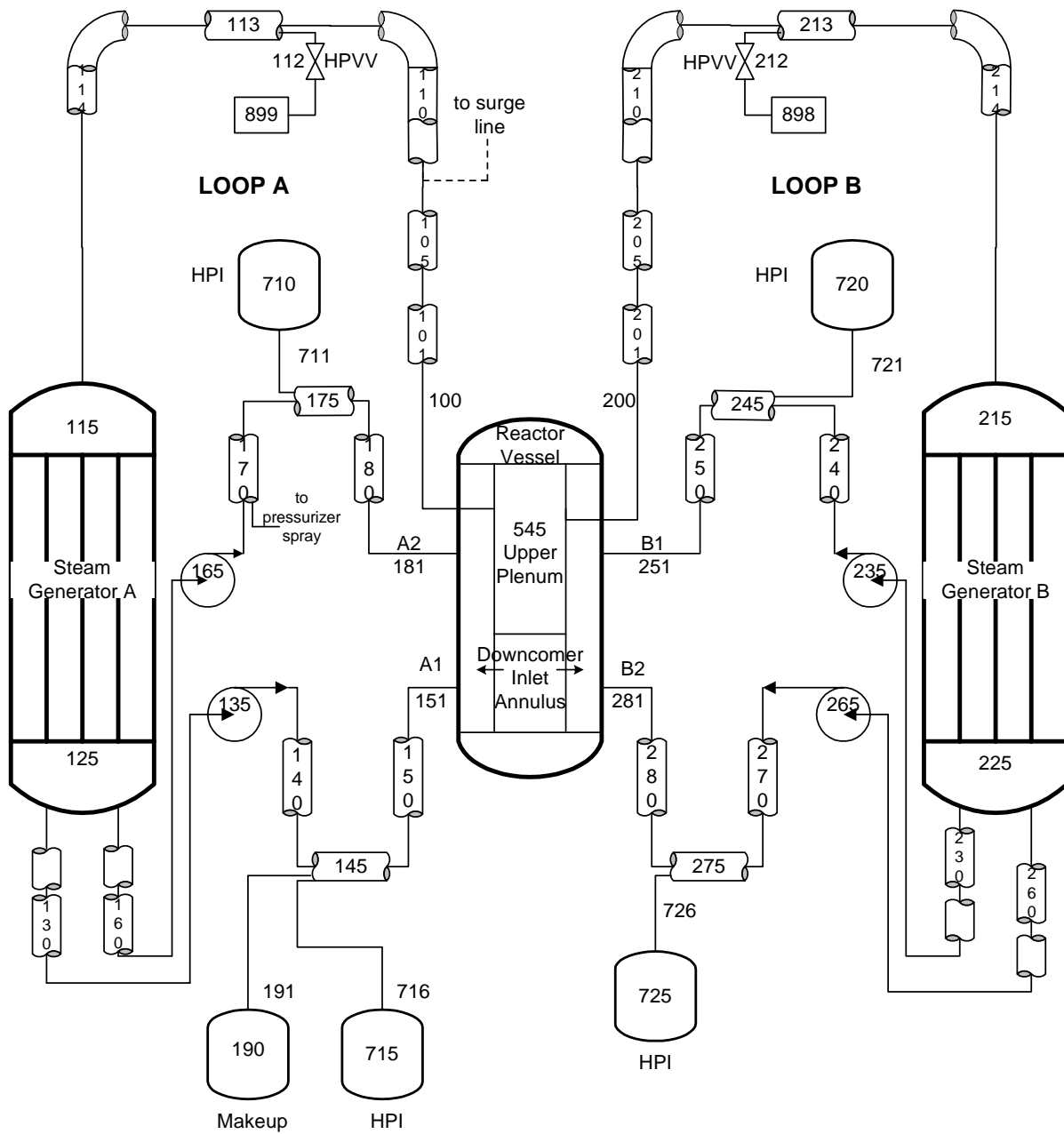


Figure A-2 Oconee Reactor Coolant System RELAP5 Nodalization

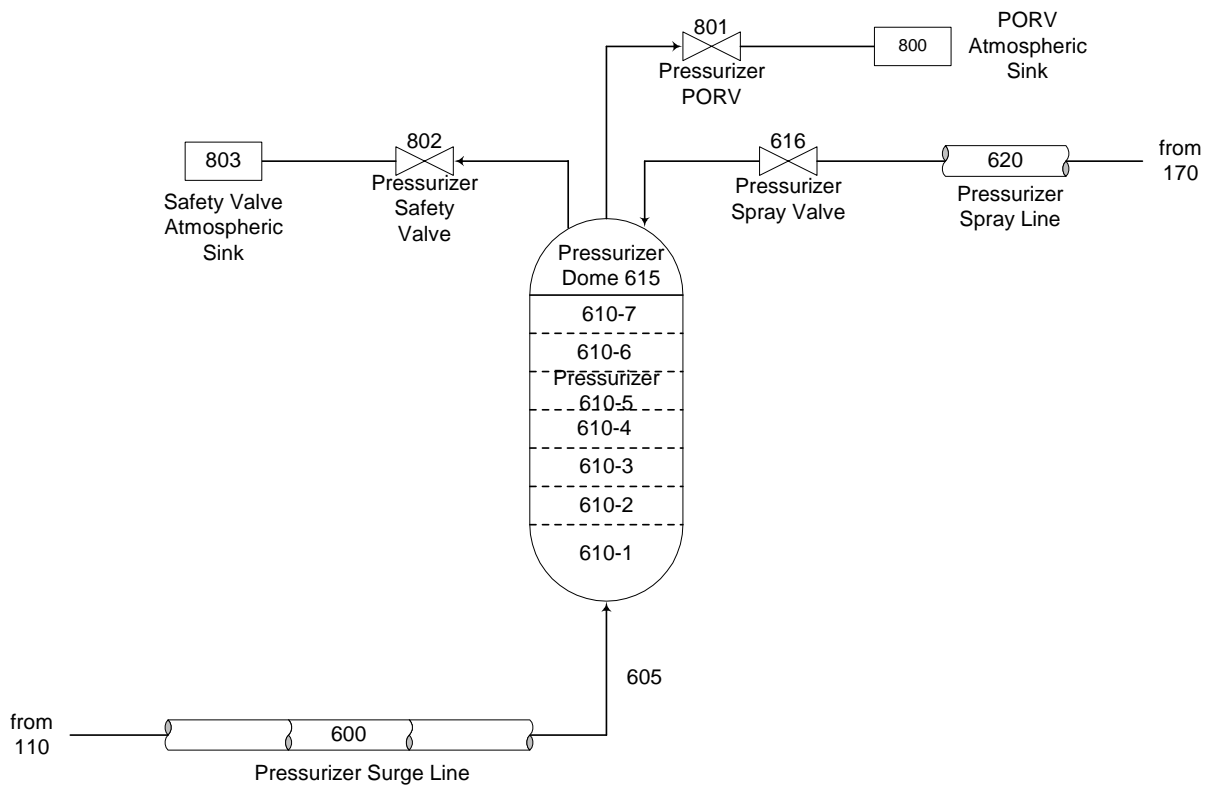


Figure A-3 Oconee Pressurizer System Nodalization

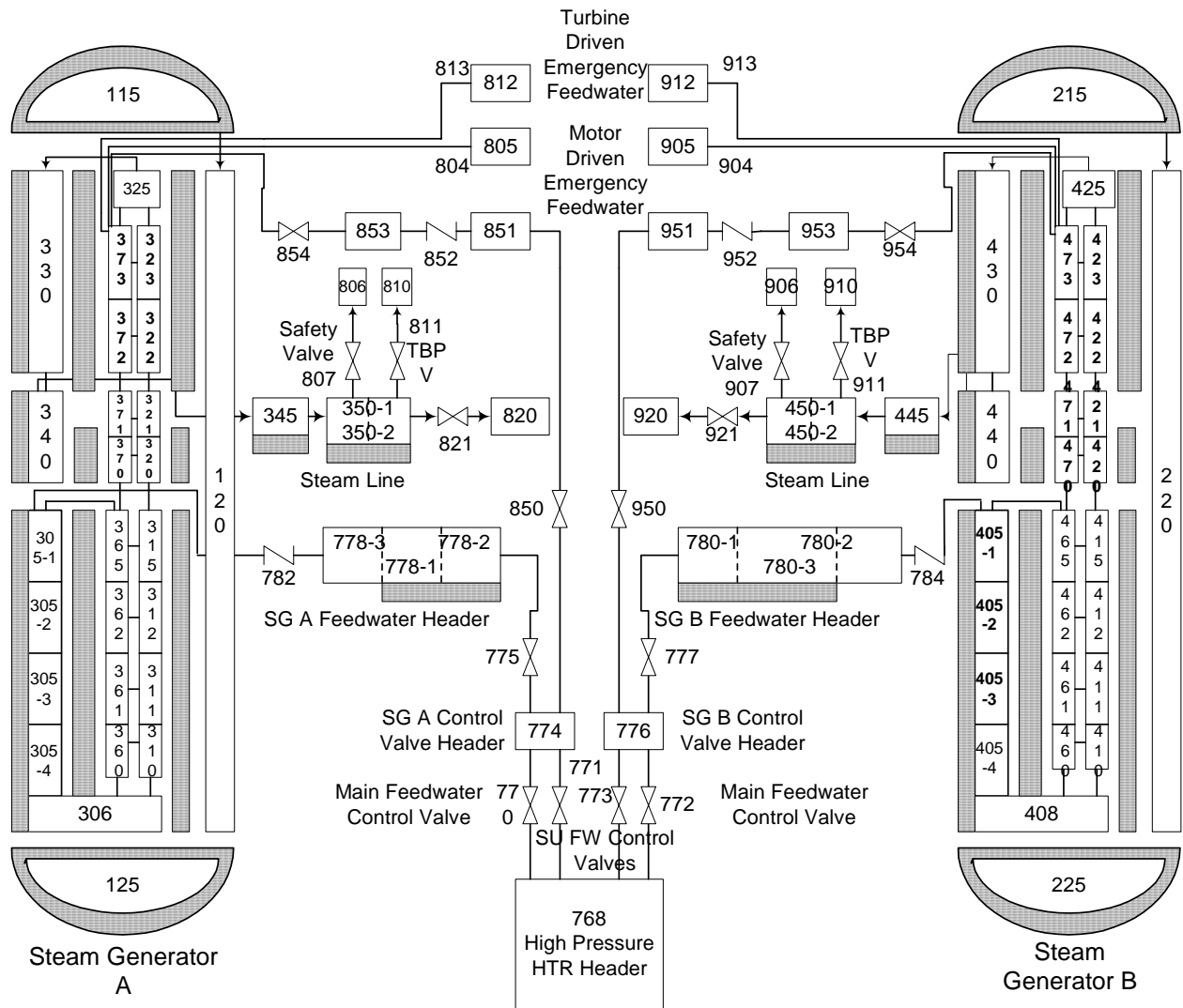


Figure A-4 Oconee Steam Generator Secondary Side Nodalization

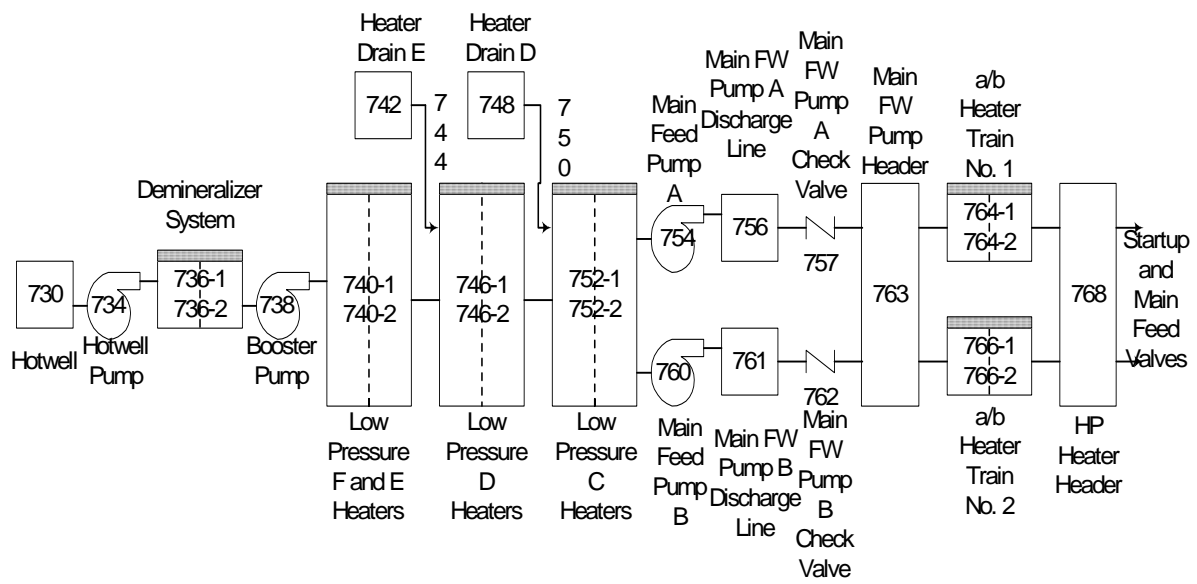


Figure A-5 Oconee Main Feedwater Train RELAP5 Nodalization

A.3 Beaver Valley RELAP5 Model Description

Beaver Valley Unit 1 is a Westinghouse three loop PWR, operated by First Energy Nuclear Operating Co., with a rated thermal power of 2660 MW (821 MWe). In early 2001, Westinghouse Electric Company created a RELAP5 input model of the Beaver Valley plant [35], which was based on the INEL H.B. Robinson RELAP5 model. ISL used the Westinghouse Beaver Valley model as the starting point for this analysis. ISL revised the Westinghouse model to include setpoint changes, additional control/trip logic, corrections to the original model, and addition of control blocks to calculate parameters for information only (i.e., items such as minimum downcomer temperature, etc.).

The RELAP5 Beaver Valley model is a detailed representation of the plant. The model describes all the major flow paths for both primary and secondary systems, including the main steam and feed systems, main feedwater, and auxiliary feedwater. It also models the ECCS (HPI, LPI, accumulators) and primary and secondary side safety/relief valves. The model contains 281 volumes, 377 junctions, and 353 heat structures. Noding diagrams of the model are shown in Figures A-6 through A-12.

The RELAP5 model represents all three primary coolant loops. The loops are designated as A, B, and C. Each coolant loop contains a hot leg, U-tube steam generator, pump suction, RCP, and cold leg as shown in Figure A-6. The pressurizer is attached to the C loop and the pressurizer spray lines are connected to the A and B loops.

Attached to each cold leg is a line that contains all three ECC sources, HPI, LPI, and accumulators. One-third of the total ECC flow is delivered to each loop. The RELAP5 model used time-dependent volume/junction pairs to model the ECCS. Also attached to the B loop is the chemical and volume control system (CVCS). The CVCS was modeled with a single time dependent volume-junction pair. Heat structures were connected to primary loop volumes to represent the metal mass of the piping and steam generator tubes. Heat structures were also used to represent the pressurizer heaters.

The reactor vessel noding is shown in Figures A-7 and A-8. The RELAP5 model represented the downcomer, downcomer bypass, lower plenum, core, upper plenum, and upper head. Similar to Oconee, the downcomer was divided into six azimuthal sectors. One channel was associated with each cold leg, with the remaining three channels interspersed. This allowed the representation of circulating cells in the downcomer.

The following leakage paths were represented in the model: downcomer to upper plenum, downcomer to downcomer bypass, downcomer bypass to lower plenum, cold leg inlet annulus to upper plenum, and upper plenum to the upper head by way of the guide tubes. Heat structures represented both external and internal metal mass of the vessel as well as the core (fuel rods). Decay heat was assumed to be at the ANS standard rate.

The secondary side of the RELAP5 model is shown in Figures A-9 through A-12. The steam generator secondary model represents the major flow paths in the secondary and includes the downcomer, boiler region, separator and dryer region, and the steam dome.

The major flow paths from the steam generator to the turbine control valves were modeled and are

shown in Figure A-12. Each steam line from the steam generators to the common header was modeled individually and include a main steam isolation valve, a check valve, atmospheric steam dump and safety relief valves. A single volume was used to model the piping run from the common steam header to the turbine control valve. The steam dump valves were modeled with a single RELAP5 valve component, with appropriate control logic capable of opening individual valves as required.

The major flow paths of the main feedwater system were modeled, and are shown in Figure A-12. The feedwater model begins at the main feedwater header just upstream of the main feedwater pumps. The conditions in the main feedwater header were held at a constant temperature. Downstream of the main feed pumps, the high pressure heaters were modeled as well as the main feedwater pump bypass line. The control valves which regulate main feedwater flow were also modeled. The auxiliary feedwater system was modeled included both the motor and steam driven systems.

Heat structures were used in the secondary side to include both internal and external metal mass of the steam generators, as well as the metal mass of the piping for both the steam and feedwater systems.

Steady-state calculations simulating hot full power and HZP plant operation were performed with the Beaver Valley RELAP5 model in order to establish model initial conditions from which to begin transient calculations. All subsequent transient analyses were started using the steady state hot full power or HZP model as appropriate.

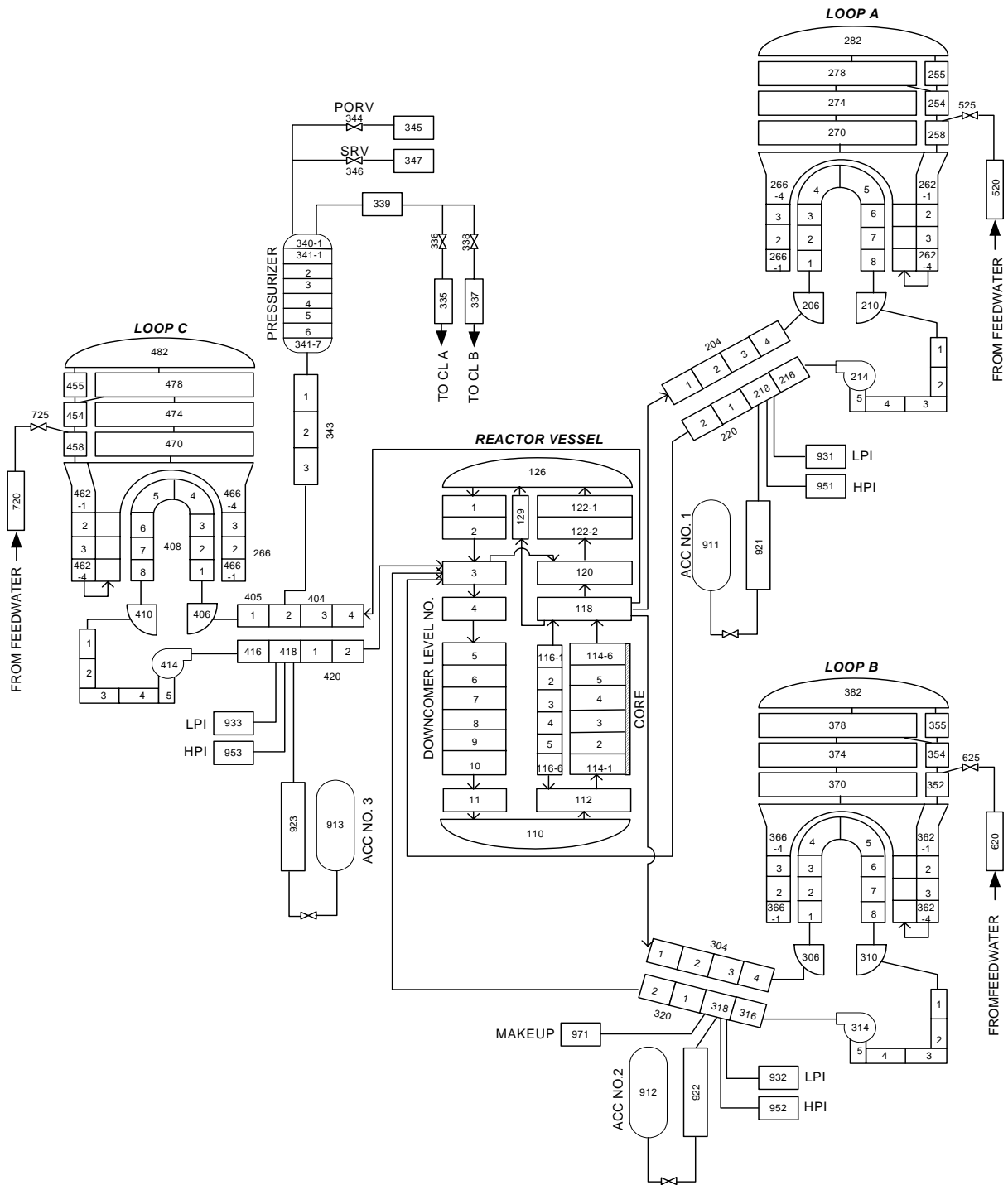


Figure A-6 Beaver Valley Reactor System Nodalization

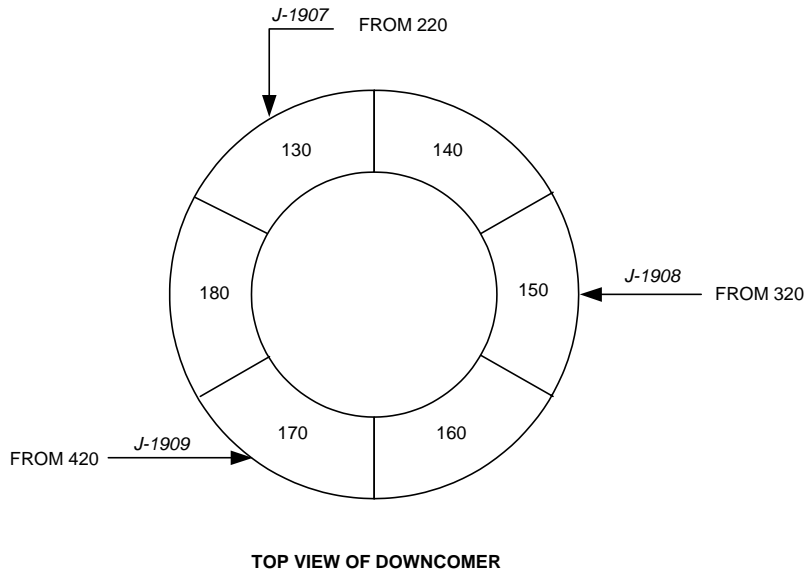
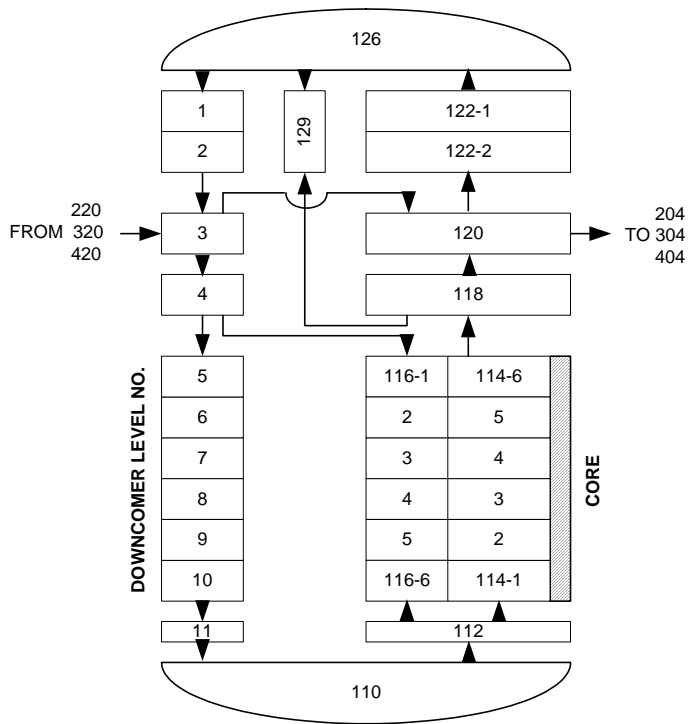


Figure A-7 Beaver Valley Reactor Vessel Nodalization

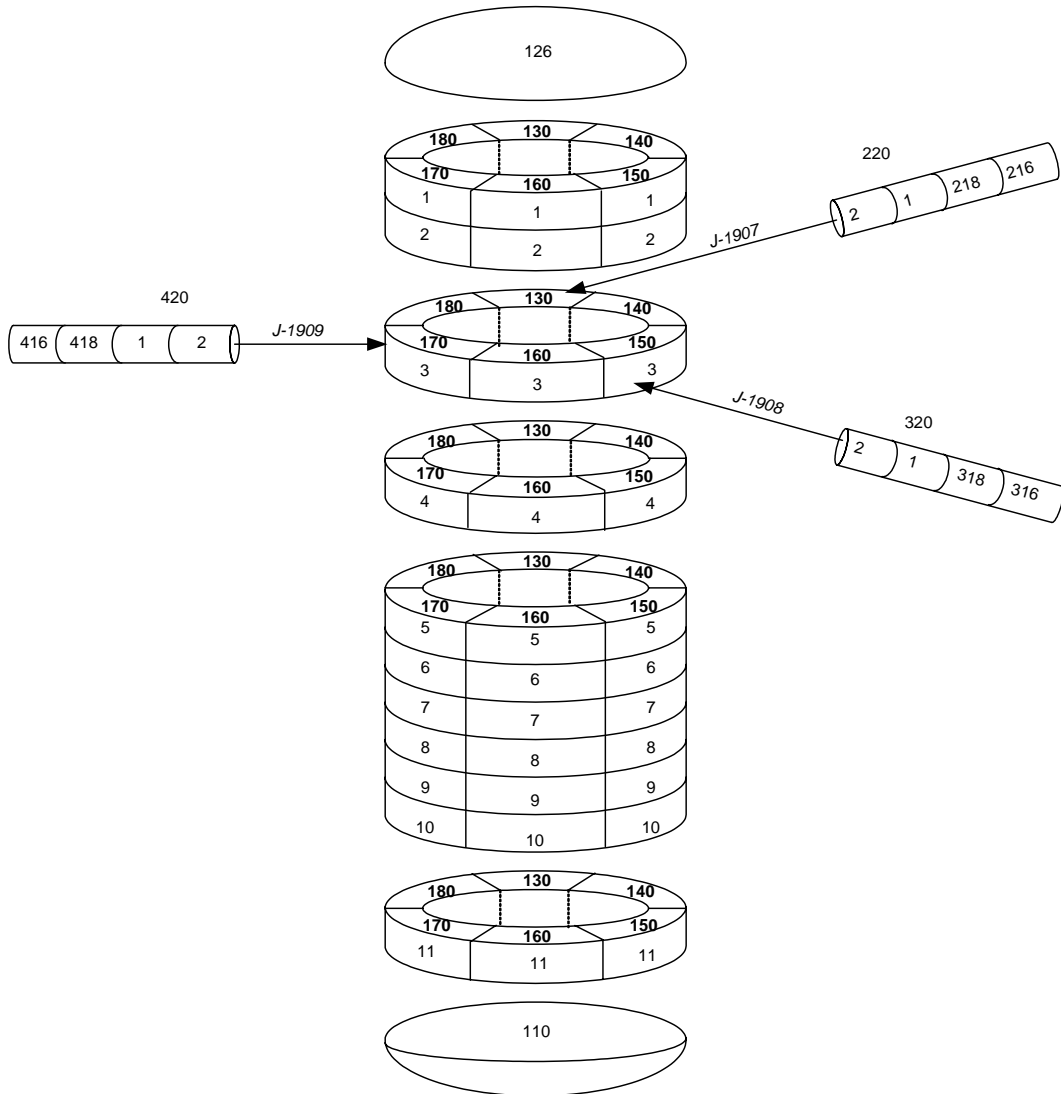


Figure A-8 Beaver Valley 2-Dimensional Downcomer Nodalization

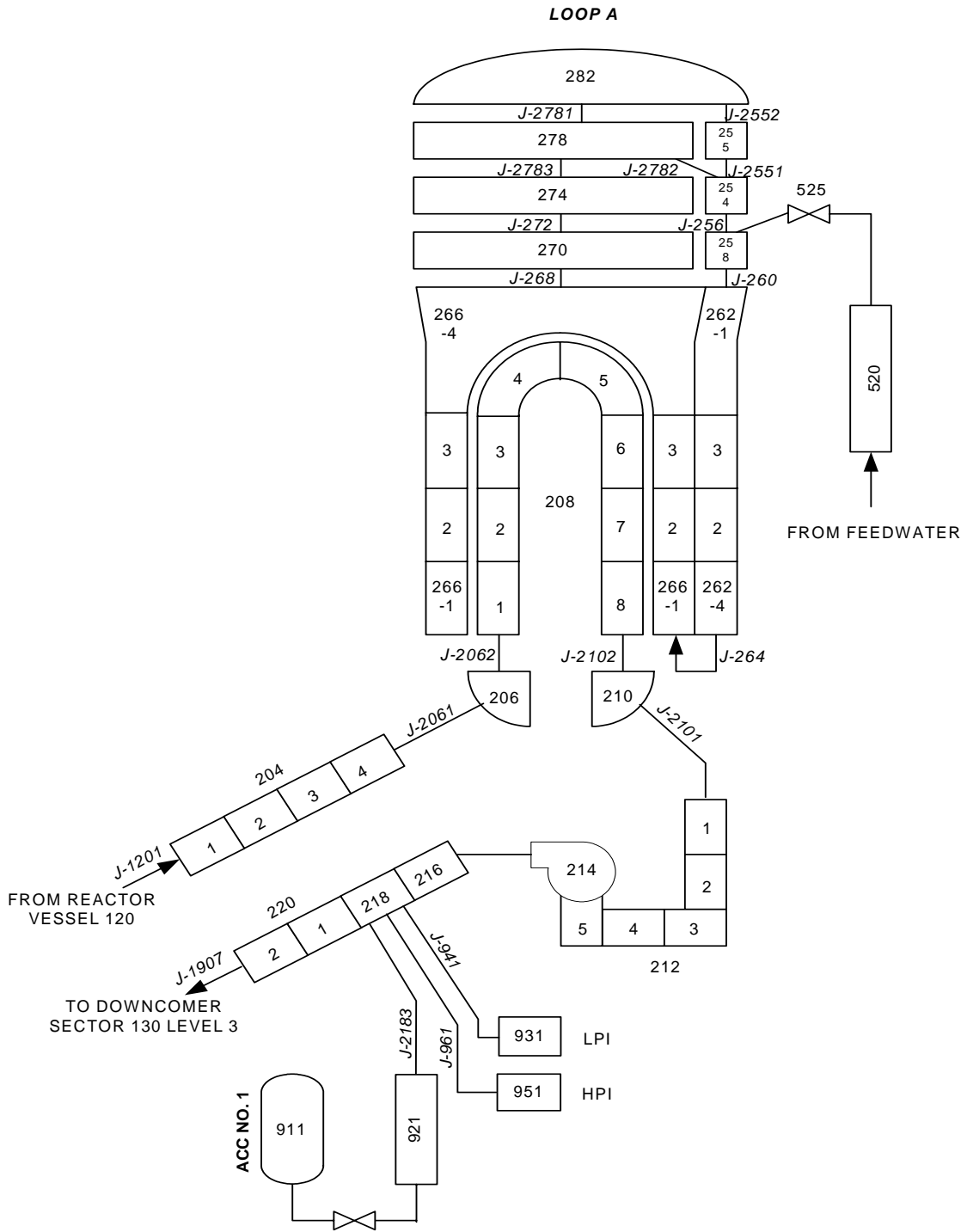


Figure A-9 Beaver Valley Loop A Nodalization

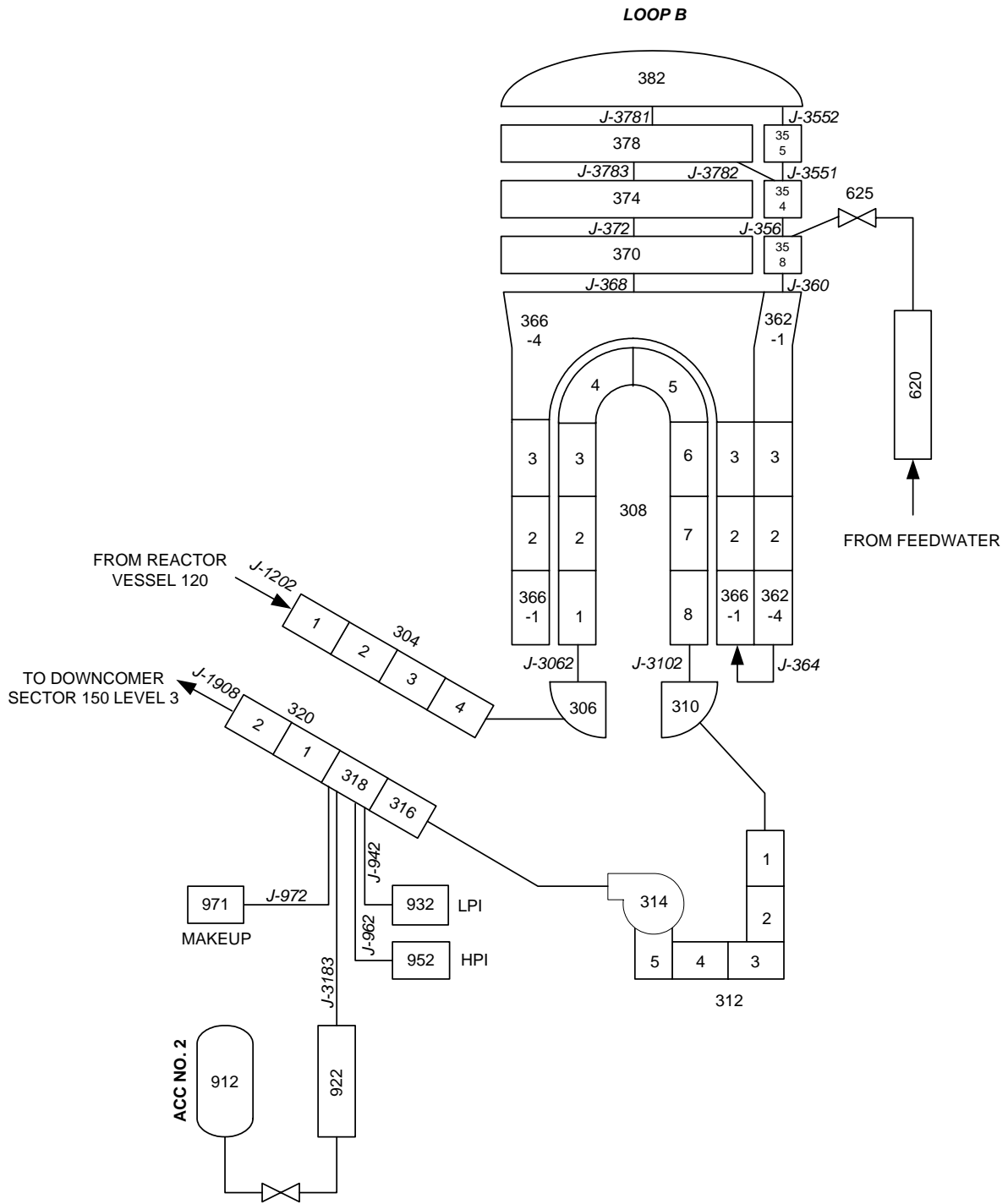


Figure A-10 Beaver Valley Loop B Nodalization

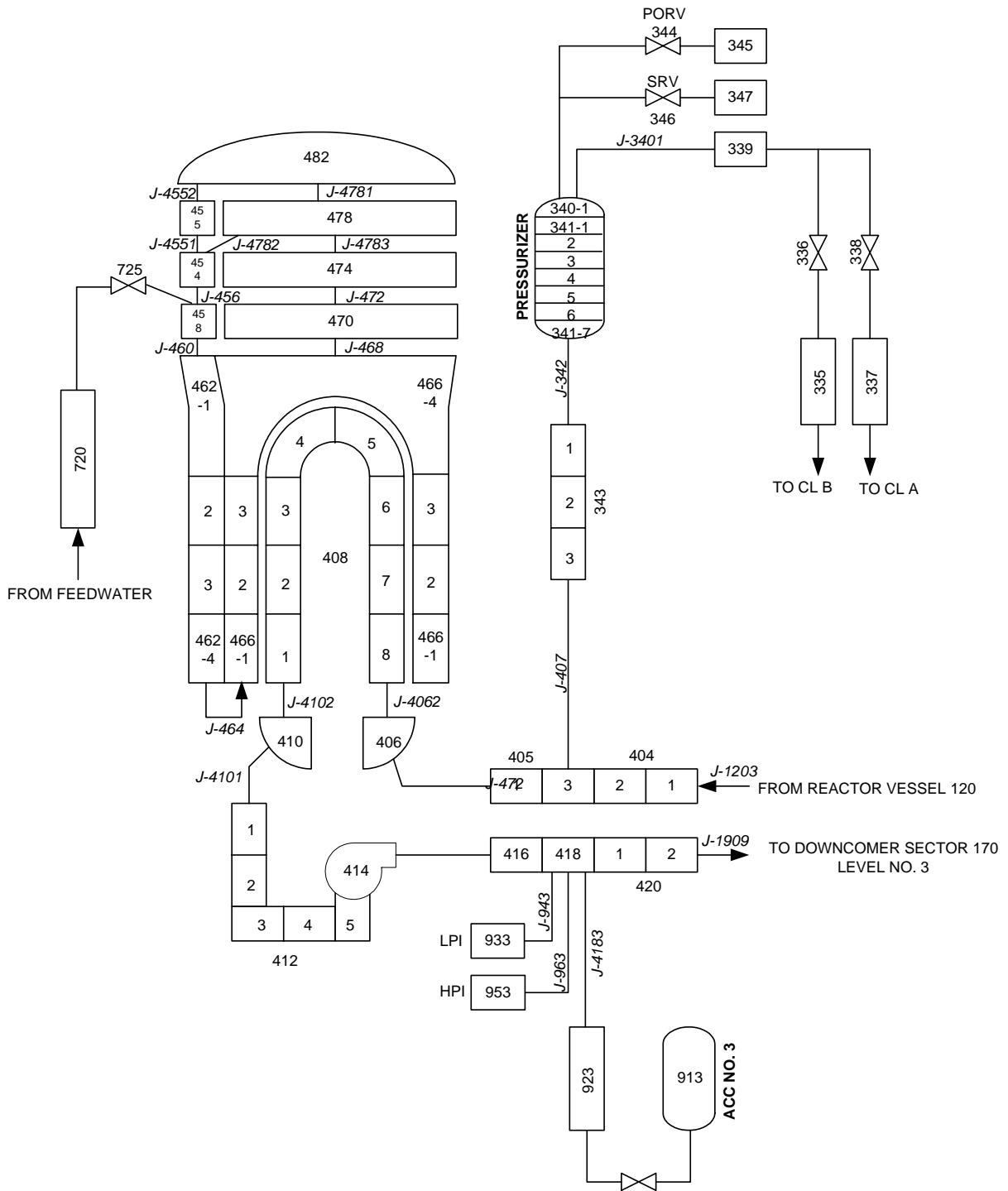


Figure A-11 Beaver Valley Loop C Nodalization

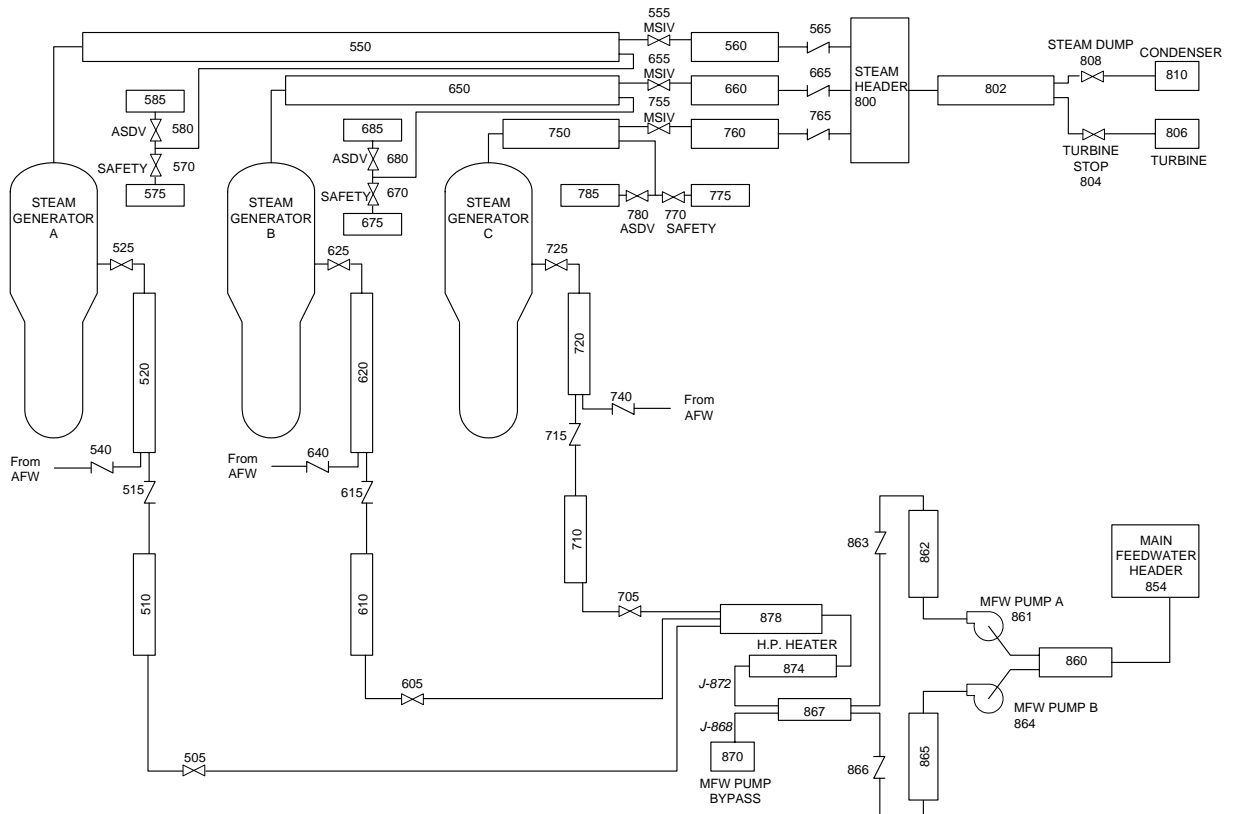


Figure A-12 Beaver Valley Secondary Side Nodalization

A.4 Palisades RELAP5 Model Description

Palisades is a PWR of Combustion Engineering design with a rated thermal power of 2530 MW. The Palisades reactor coolant system consists of a reactor vessel and two coolant loops connected in parallel and designated as Loops 1 and 2. Each coolant loop includes hot leg piping, an inverted U-tube type steam generator, and two sets of reactor coolant pumps and cold leg piping. The cold legs and reactor coolant pumps on each loop are designated as A and B.

The normal coolant flow on each loop is from the reactor vessel outlet nozzle, through the hot leg, steam generator, reactor coolant pumps and cold legs to the reactor vessel inlet nozzle. A pressurizer is connected via a surge line to the hot leg on Loop 1. The electrically-heated pressurizer provides pressure control for the reactor coolant system. Two pressurizer spray lines are routed from one of the pump-discharge cold legs on each loop, through control valves, to a spray nozzle in the pressurizer upper dome. Reactor coolant system over pressure protection is provided by SRVs atop the pressurizer (the plant also employs PORVs, but they are blocked closed during normal plant operation).

ECCS consists of HPI, LPI, and accumulators, which are connected to each of the four pump-discharge cold legs. A charging/letdown system provides RCS water chemistry control and pressurizer level control. Decay heat removal capability is provided by motor-driven and turbine-driven auxiliary feedwater systems that feed into the steam generator downcomers. The maximum auxiliary feedwater flow that may be delivered to each steam generator is automatically limited.

Steam generator secondary system over pressure protection is provided by safety relief valves, atmospheric dump valves, located on the main steam lines, and by turbine bypass valves. Main steam isolation valves are located in each of the two steam lines, limiting the influence that a break in one of the steam generator secondary systems would have on the other.

The Palisades RELAP5 model is a detailed thermal-hydraulic representation of the Palisades plant [36, 37]. It includes all major components of the primary and secondary coolant systems, as well as the plant control systems pertinent for simulating the PTS transient event sequences. Nodalization diagrams for the Palisades RELAP5 model are illustrated in Figures A-13 through A-15.

The reactor vessel model nodalization is shown in Figure A-13. Similar to Oconee and Beaver Valley, two-dimensional nodalization was used in the downcomer with seven axial and six azimuthal nodes. Four channels were associated with the four cold legs, while the other two were located in the remaining downcomer regions between Loops 1 and 2.

During preliminary RELAP5 calculations of LOCA sequences with break diameters of 10.2-cm (4-in) diameter and larger, nonphysical numerically driven circulations among the six reactor vessel downcomer internal channels of the model (Components 500 through 505 in Figure A-13) were observed. A variety of methods were tried in an attempt to suppress or remove these circulations from the calculations. However, the only modeling approach which successfully eliminated them was to disable momentum flux in all internal reactor vessel downcomer junctions. Since the downcomer flow pattern can be of significance for the PTS analysis, the Palisades transient LOCA cases with break diameters of 10.16 cm (4 in) and larger were run with momentum flux disabled in all internal downcomer junctions. More information is provided in Appendix B.

The reactor core region was modeled using six axial nodes. Additional nodes were used to represent the lower plenum, upper plenum, core bypass, control rod guide tube and upper head regions of the reactor vessel.

A constant reactor power is modeled until the reactor trip time using a table; afterward a reactor power decay is specified as a function of time after trip. The model includes control system logic that monitors various plant parameters during transient calculations and trips the reactor based on any of the following conditions: high containment pressure, low pressure in either steam generator, high pressurizer pressure, or exceeding the thermal margin/low pressure trip limit (the criterion varies as a function of several plant variables).

The reactor coolant loop region nodalization is shown in Figure A-14. The speed of the reactor coolant pump models is held constant to deliver the normal-operation flow rate unless the pumps are tripped by operator action (based on indications of low reactor coolant system pressure or low subcooling). Once tripped, the reactor coolant pump speed coasts down based on rotational inertia effects.

Charging flow is injected into the Loop 1A and 2A pump-discharge cold leg piping and letdown flow is withdrawn from the Loop 2B pump-suction cold leg piping. The charging flow is controlled so as to maintain a desired pressurizer setpoint level, which is specified as a function of average reactor coolant system temperature. The letdown flow is isolated upon receipt of a safety injection actuation signal, which results from a low pressurizer pressure condition. The operation of the pressurizer heater power and spray valve flow area are specified so as to maintain the pressurizer pressure within the desired range.

The safety injection tanks are modeled on each of the four pump-discharge cold legs using RELAP5 accumulator components. Safety injection tank flow occurs whenever the cold leg pressure is below the tank pressure. The high and low pressure injection systems are represented using RELAP5 time dependent volume and junction component pairs on each of the four pump-discharge cold legs.

The injection characteristics of these centrifugal pump systems are modeled with the flow delivered specified as a function of the cold leg pressure; flow is initiated after a time delay following the occurrence of a safety injection actuation signal. Control logic is included such that operator throttling of high pressure injection (based on pressurizer level and subcooling criteria) can be represented for event sequences specified to include that operator function. Control logic also is included to monitor the inventory status of the refueling water storage tank (that is first used as the source of emergency core coolant). This tank supplies water for the charging, high pressure injection, low pressure injection and containment spray systems. When the inventory of the tank has been expended, the model includes features that represent the actions taken in the plant (termination of the charging and low pressure injections and switching the suction of the high pressure injection system to the containment sump). Following this switch, the high pressure injection system flow characteristics are changed and the injected water temperature increases.

The main feedwater flow is adjusted so as to control the steam generator levels at the setpoint level and to match the feedwater and steam flow rates in each steam generator. After turbine trip, the main feedwater flow stops and the auxiliary feedwater flow is delivered to control steam generator levels within a specified range.

The main steam system nodalization is shown in Figure A-14. The model represents the steam line from each steam generator to the common turbine inlet header. A valve component is used to represent the turbine stop valves, which close upon receipt of a turbine trip signal. Over pressure protection is modeled by the main steam safety relief valve components on each steam line. Steam pressure control for post-turbine trip operating conditions is provided by a turbine bypass valve component located on the turbine inlet header. Primary coolant system average temperature control is provided by an atmospheric dump valve component on each of the steam lines. Main steam isolation valves connect each steam line to the turbine inlet header. These valves close if a low pressure condition is sensed in either steam generator or if a containment high pressure condition is sensed.

Steady-state calculations simulating hot full power and HZP plant operation were performed with the Palisades RELAP5 model in order to establish model initial conditions from which to begin transient accident calculations. All subsequent transient analyses were started using the steady state hot full power or HZP model as appropriate.

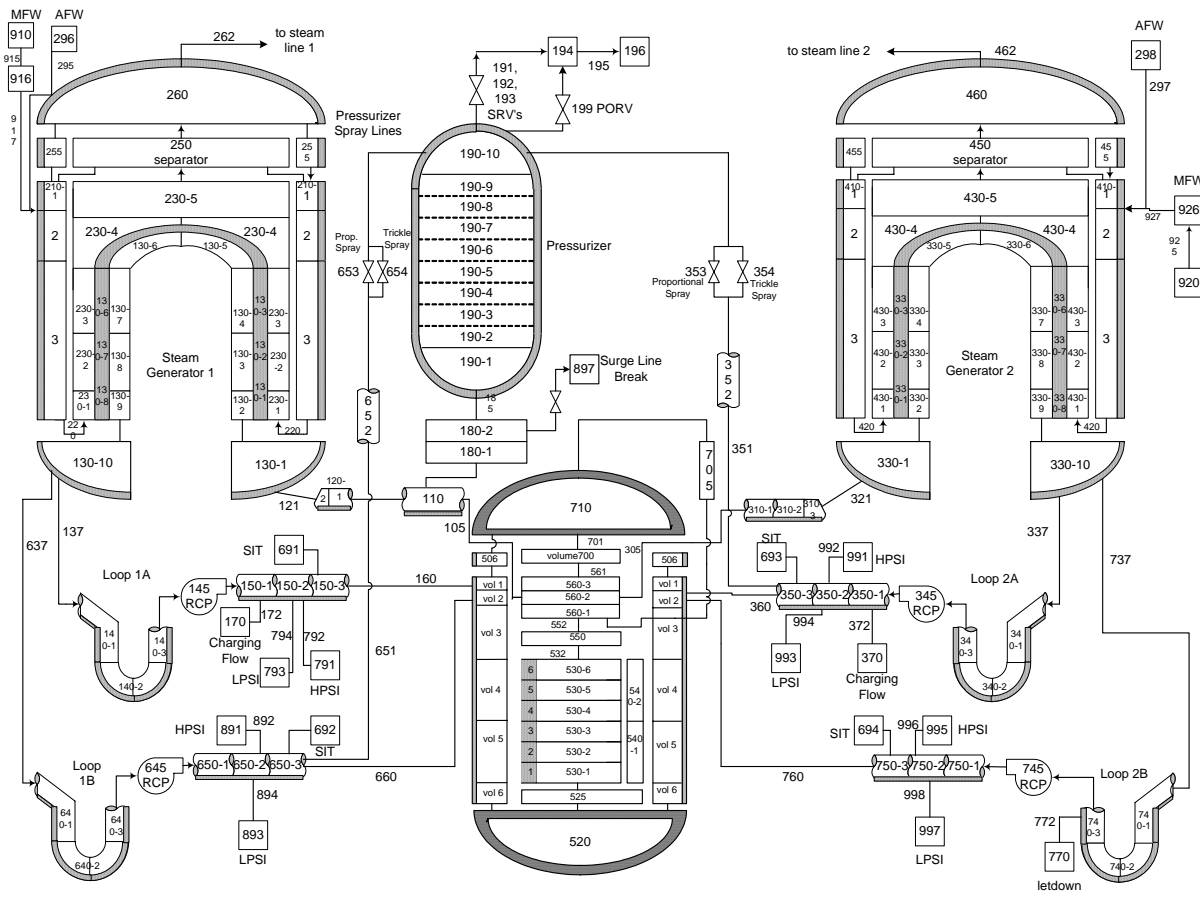


Figure A-14 Palisades Coolant Loops Nodalization

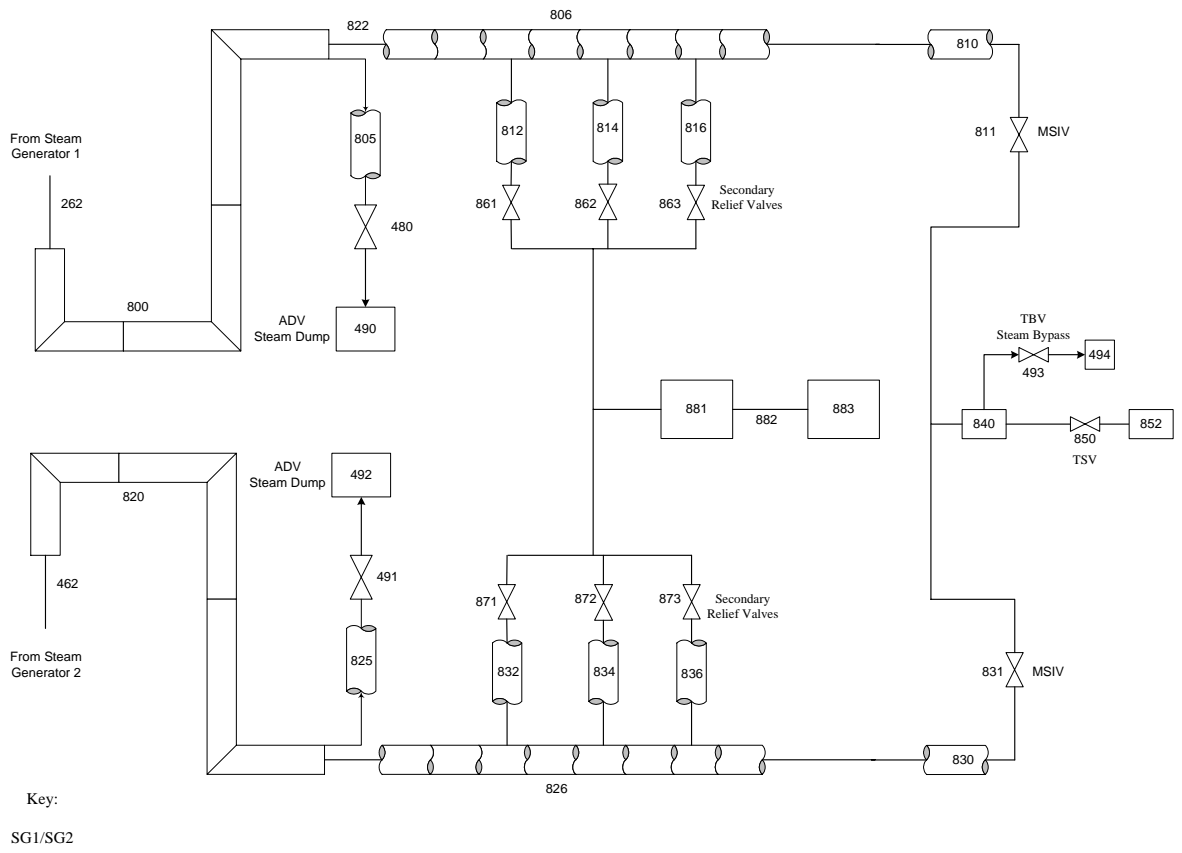


Figure A-15 Palisades Main Steam System Nodalization

A.5 Summary of the Oconee, Beaver Valley and Palisades Results

Tables A-2, A-3, and A-4 present a summary of the reactor vessel downcomer temperature and primary system pressure for the transient sequences discussed in Section 3 for the Oconee, Beaver Valley and Palisades Plants, respectively. This summary is presented to facilitate comparison of the results of the cases analyzed. Direct comparisons of downcomer temperature and system pressure results for many of the sequences analyzed among the plants show similar results. In other instances, direct comparisons are more difficult because of plant design differences and differences in sequence modeling assumptions.

The LOCA analyses for the Oconee, Beaver Valley and Palisades plants show similar results, as might be expected. Minor differences exist in the time that the minimum temperature is reached. For example, the 40.64 cm (16 in) break from hot full power (HFP) initial conditions,

Plant	Minimum T	ECC T	Time of min.
Oconee	298K (76F)	300K (80F)	1721s
Beaver Valley	291K (64F)	283K (5F)	960s
Palisades	308K (94F)	304K (88F)	1260s

The difference in minimum temperature is principally driven by the ECC injection temperature (Table A-1). Plant design differences may have some impact on the time that the minimum temperature occurs, but do not have much impact on the minimum temperature results in the case of a LOCA of this size. For smaller breaks, the minimum temperature is also dependent on the ECC injection temperature, although the time that the minimum temperature is reached is later since the blowdown time and time that the ECC systems inject is longer. Also, plant differences in ECCS flow capability and shutoff head can lead to differences in results. In general, the downcomer temperature decrease towards the injection temperature because the ECC systems continue to inject cold water into the reactor coolant RCS. The time that the minimum is reached is a function of the break size.

Scenarios involving stuck open pressurizer SRVs are not as directly comparable because of differences in valve sizes and sequence definitions, although portions of the transients are comparable. For example, the downcomer temperature for the Oconee case where a stuck open pressurizer SRV valve occurs during HZP operation and recloses at 3,000 s (Case 124) is 360K (188F). In this analysis, the operator is assumed to throttle HPI to maintain 28K (50F) subcooling, but throttling does not occur until after the valve recloses. In comparison, Case 97 for Beaver Valley, which is also a stuck open pressurizer SRV with reclosure at 3,000 s during HZP operation, results in a downcomer temperature of 321K (118F) at 3,000 s.

The comparison of the first part of the transient until the SRV recloses is of interest. The Beaver Valley downcomer temperature is lower because of several factors; the SRV has a somewhat larger capacity at Beaver Valley than Oconee (Table A-1) and the injection temperature at Beaver Valley is colder. A third factor relates to the vessel vent valves which are part of the Oconee plant design but are not in Beaver Valley or Palisades. The vent valves connect the vessel upper plenum to the upper part of the downcomer and open on small pressure differences to vent steam from the upper plenum to the downcomer and out the break during a LOCA. Warm water from the upper plenum can flow to the downcomer, resulting in higher temperatures than would otherwise be the case.

For MSLBs, the downcomer temperature results for the three plants are similar despite differences in assumptions for operator actions for HPI throttling, break location inside and outside containment, and timing of AFW isolation to the affected steam generator.

For example, Beaver Valley Case 102 is a MSLB from HFP, where AFW continues to feed the affected steam generator for 30 minutes and the operator controls HPI 30 minutes after allowed. In this case, the minimum downcomer temperature is 373K (212F) at 3,990 s. In comparison, Palisades Case 54, is a MSLB that occurs inside containment and where the AFW continues to feed the affected steam generator and the operator does not throttle HPI flow, results in a minimum downcomer temperature of 377K (219F) at 4,110 s. The difference is only 4K (7F) despite the scenario differences.

One reason is that the RCS remains nearly full during MSLBs. Loop natural circulation (and forced circulation in some cases) continuing throughout the event sequences. This circulation keeps the RCS fluid well mixed, so that the downcomer temperature does not drop to the ECCS injection temperature. Instead, the downcomer temperature tends to approach 373K (212F) (plus a small delta), which is the saturation temperature at the atmospheric pressure present in the affected steam generator secondary side. In contrast to LOCAs where the temperature of ECCS injection drives the downcomer temperature, MSLBs remove heat from the reactor coolant RCS uniformly, so that minimum downcomer temperatures is normally higher. This is why secondary side transients are less significant than LOCAs and stuck open pressurizer SRVs.

Some generic conclusions regarding classes of sequences that have been evaluated in this analysis are presented below:

- Larger break LOCAs cause RCS temperatures to fall rapidly, with a corresponding rapid drop in primary RCS pressure. There is no possibility of RCS repressurization. Downcomer temperatures will approach the ECCS injection temperature with the timing dependent principally on the break size.
- Smaller break LOCAs (includes stuck open primary relief valves) cause the downcomer temperature to drop to intermediate temperatures and RCS pressures. The value are break-size dependent. Plant-specific complexities are added, that are caused by different design parameters such as initial accumulator pressures, HPI and shutoff head, HPI throttling criteria.
- Stuck open primary SRV cases are an important subcategory of small break LOCAs with the potential for RCS repressurization should the valves later reclose.
- MSLBs cause the downcomer temperature to decrease to values somewhat higher than the small break LOCA. The RCS may repressurize unless operators throttle HPI. The saturation temperature of the secondary side of the broken steam generator provide a floor for the downcomer temperature. If the break is outside containment, this floor is ~377K (220F). If the break is inside containment, the floor is higher due to the containment back pressure, and is ~395K (250F). These floor temperatures limit the probability that a through wall crack in the vessel may develop.
- The thermal hydraulic analysis discussed in this report is a part of an overall risk analysis

where the risk of vessel failure due to a PTS event is determined by sequence probabilities that define the sequences analyzed and the fracture mechanics analysis that, combined with the sequence probabilities and thermal hydraulic results, determine the risk.

Table A-2 Summary of Oconee Thermal Hydraulic Results

#	Description	Minimum Downcomer Fluid Temperature	Corresponding Primary RCS Pressure
27	MSLB from hot full power. Both turbine driven and auxiliary driven feedwater are assumed to be operating. Operator throttles HPI (Note 2)	380 K (224F) at 4,400 s.	1.8 MPa (261 psia). No repressurization.
101	MSLB from HZP. Both turbine driven and auxiliary driven feedwater continue operating. Operator throttles HPI (Note 2)	377K (219F) at 2,600 s.	1.8 MPa (261 psia). No repressurization.
109	Stuck open pressurizer SRV recloses at 6,000 s, hot full power. No HPI throttling by the operator.	350K (170F) at 6,010 s.	2.3 MPa (330 psia). RCS repressurizes to 17 MPa (2,465 psia)
113	Stuck open pressurizer SRV recloses at 6,000 s from hot full power conditions. Operator throttles HPI (Note 1)	350K (170F) at 6,030 s.	2.3 MPa (330 psia). RCS repressurizes to 17 MPa (2,465 psia)
115	Stuck open pressurizer SRV recloses at 3,000 s from hot full power conditions. Operator throttles HPI.	433K (320F) at 3,010 s.	3.7 MPa (537 psia). RCS repressurizes to 17 MPa (2,465 psia)
122	Stuck open pressurizer SRV recloses at 6,000 s from HZP conditions. Operator throttles HPI.	307K (93F) at 6,010 s	1.7 MPa (249 psia). RCS repressurizes to 17 MPa (2,465 psia)
124	Stuck open pressurizer SRV recloses at 3,000 s from HZP conditions. Operator throttles HPI.	360K (188F) at 4,000 s.	2.8 MPa (406 psia). RCS repressurizes to 17 MPa (2,465 psia)
156	40.64 cm (16 in) break in the hot leg from hot full power	300K (80F) at 600 s	0.18 MPa (26 psia). No repressurization.
160	14.37 cm (5.656 in) surge line break from hot full power	299K (78F) at 2,300 s	0.9 MPa (130 psia). No repressurization.
164	20.32 cm (8 in) surge line break from hot full power	300K (80F) at 1,200 s	0.56 MPa (80 psia). No repressurization.
165	Stuck open pressurizer SRV recloses at 6,000 s from HZP conditions. No operator actions.	306K (91F) at 6,010 s	1.8 MPa (261 psia). Repressurizes to 17 MPa (2,465 psia)
172	10.16 cm (4 in) cold leg break from hot full power	355K (180F) at 2,700 s	1.1 MPa (160 psia). No repressurization
1.	Operator throttles HPI 10 minutes after 2.7K (5F) subcooling and 2.54 m (100 in) pressurizer level is reached. The throttling criteria is 28K (50F) subcooling.		
2.	Operator throttles HPI to maintain 28K (50F) subcooling.		

Table A-3 Summary of Beaver Valley Thermal Hydraulic Results

#	Description	Min T _{dc,f}	RCS P at T _{dc,min}
7	20 cm (8.0 in) diameter surge line break. Hot full power	291K (64F)	0.21 MPa (30 psia). No RCS at ~1,000 s repressurization.
9	40.64 cm (16.0 in) diameter hot leg break. Hot full power	291K (64F)	0.097 MPa (14 psia). No RCS at ~1,000 s repressurization.
56	10.16 cm (4.0 in) diameter surge line break. HZP	289K (60F)	0.917 MPa (133 psia). No RCS at ~2,975 s. repressurization.
60	One stuck open pressurizer SRV, recloses at 6,000 s. Hot full power	330K (134F) at 6,000 s	2.62 MPa (380 psia). RCS repressurizes to 16.2 MPa (2,350 psia)
71	One stuck open pressurizer SRV, recloses at 6,000 s, HZP	295K (71F) at 15,000 s	16.3 MPa (2,371 psia)
97	Stuck open pressurizer SRV which recloses (at 3,000 s) from HZP	321K (118F) at 3000 s	1.62 MPa (235 psia). RCS repressurizes to 16.2 MPa (2,350 psia)
102	MSLB with AFW continuing to feed affected SG for 30 minutes and operator controls HPI 30 minutes after allowed. Hot full power	373K (212F) at 3990 s	16.2 MPa (2,350 psia). RCS depressurizes due to HPI control, repressurizes due to heat up.
103	MSLB with AFW continuing to feed affected SG for 30 minutes and operator controls HPI 30 minutes after allowed. HZP	362K (192F) at 3420 s	16.2 MPa (2,350 psia). RCS depressurizes to 4.69 MPa (680 psia) by 15,000 s due to HPI control.
104	MSLB with AFW continuing to feed affected SG for 30 minutes and operator controls HPI 60 minutes after allowed. Hot full power	370K (206F) at 5820 s	16.2 MPa (2,350 psia). RCS depressurizes due to HPI control, repressurizes due to heat up.
105	MSLB with AFW continuing to feed affected SG for 30 minutes and operator controls HPI 60 minutes after allowed. HZP	355K (179F) at 5220 s	16.2 MPa (2,350 psia). RCS depressurizes to 4.27 MPa (620 psia) by 15,000 s due to HPI control.
108	Small SLB with AFW continuing to affected SG for 30 minutes. Operator controls HPI 30 minutes after allowed. Hot full power	395K (252F) at 3600 s	16.2 MPa (2,350 psia). RCS depressurizes due to HPI control, repressurizes due to heat up.
114	7,184 cm (2.828 in) surge line break from hot full power. Summer ECC T. Heat transfer to passive structures increased by 30%	304K (88F) at 4,890 s	1.34 MPa (195 psia). No RCS repressurization
126	One stuck open pressurizer SRV recloses at 6,000 s. Hot full power. Operator controls HPI (10 minute delay)	338K (148F) at 6,354 s	2.64 MPa (383 psia) RCS repressurizes to 16.2 MPa (2,350 psia)

#	Description	Min T _{dc,f}	RCS P at T _{dc,min}
130	One stuck open pressurizer SRV recloses at 3,000 s. Operator controls HPI (10 minute delay).	316K (110F) at 3,026 s	1.52 MPa (221 psia). RCS repressurizes to 16.2 MPa (2,350 psia)

Table A-4 Summary of Palisades Thermal Hydraulic Results

#	Description	Min T _{dc,f}	RCS P at T _{dc,min}
19	One stuck-open ADV on SG-A, HZP. Operator does not isolate AFW to SG-A and does not throttle HPI.	423K (301F) at 15,000 s.	17.24 MPa (2500 psia)
40	40.64 cm (16 in) hot leg break. HFP. Operator does not throttle HPI.	308K (94F) at 1,260 s.	0.14 MPa (21 psia).
52	One stuck-open ADV on SG-A with failure of both MSIVs to close. HZP. Operator does not isolate AFW to SG-A and does not throttle HPI.	425K (305F) at 15,000 s.	17.24 MPa (2500 psia)
54	MSLB on SG-A inside containment with failure of both MSIVs to close. HFP operation. Operator does not isolate AFW to SG-A and does not throttle HPI.	377K (219F) at 4,110 s	9.61 MPa (1395 psia). RCS repressurizes to 17.24 MPa (2500 psia) due to heat up.
55	Two stuck-open ADVs on SG A. HFP. Flow controller failure and operator action to start second motor-driven AFW pump, resulting in the delivery of two-pump AFW flow.	437K (328F) at 4,320 s	17.24 MPa (2500 psia).
58	10.14 cm (4 in) break in the pump-discharge cold leg from HFP. Operator does not throttle HPI. Winter conditions assumed for the ECCS injection water temperatures.	331K (136F) at 2,700 s	1.32 MPa (191 psia).
59	10.14 cm (4 in) break in the pump-discharge cold leg from HFP. Operator does not throttle HPI flow. Summer ECC temperatures.	351K (171F) at 14,940 s	1.53 MPa (222 psia).
60	5.08 cm (2 in) surge line. HFP. Operator does not throttle HPI. Winter ECC temperatures.	351K (173F) at 3,540 s	2.30 MPa (334 psia)
62	20.32 cm (8 in) break in the pump-discharge cold leg from HFP. Operator does not throttle HPI flow. Winter ECC temperatures.	308K (95F) at 1,470 s	0.72 MPa (104 psia)
63	14.37 cm (5.656 in) break in the pump-discharge cold leg from HFP. Operator is assumed not to throttle HPI flow. Winter ECC temperatures.	306K (92F) at 2,070 s	1.07 MPa (155 psia)
64	10.14 cm (4 in) break in pressurizer surge line. HFP. Operator does not throttle HPI. Summer ECC temperatures.	323K (121F) at 2,730 s	1.06 MPa (154 psia).
65	One stuck-open pressurizer SRV recloses at 6,000 s. HZP. Operator does not throttle HPI flow.	366K (199F) at 6,570 s	10.55 MPa (1530 psia). RCS repressurizes to 17.51 MPa (2540 psia) due to heat up.

APPENDIX B. FLUID TEMPERATURE DISTRIBUTION IN THE DOWNCOMER

B.1 Introduction

The fluid temperature distribution in the downcomer is one of the thermal hydraulic issues considered in the analysis of PTS. Since the IPTS study in the early 1980s, there has been continued interest in possible temperature nonuniformities in the downcomer and their possible effects. Both the IPTS study and the current PTS reevaluation adopted the simplifying assumption of uniform temperatures in the downcomer, in the region adjacent to the core. It is only in this region that the vessel adjacent to the is embrittled. The top of the core is approximately 5 feet below the cold leg. This distance provides a mixing zone for cold fluid entering the downcomer from the cold legs before it reaches the embrittled zone of the reactor vessel. The uniform temperature distribution allows the fracture mechanics analysis to be treated with a one dimensional assumption regarding vessel wall temperature distribution. This greatly simplifies the fracture mechanics calculations.

It was the task of thermal hydraulics to justify the uniform temperature distribution. At the start of the IPTS program, it was expected that the cold ECC injection flow would stratify in the cold legs, and from there flow into the downcomer, where it could form strong plumes. This could result in highly nonuniform temperatures. A number of separate effects experimental programs were conducted in the 1980s to study the phenomena of fluid-fluid mixing, stratification, plume formation, and plume decay, as summarized in Table B-1.

Table B-1 Separate Effects Mixing Data Base Developed for IPTS Study

Facility	Scale	Sponsor
Creare	1:5	EPRI
Creare	1:2	EPRI, NRC
Imatran Voima Oy (IVO) (Finland)	2:5	NRC, IVO
Purdue University	1:2	NRC
HDR (Germany)	1:1	Germany
UPTF (Germany)	1:1	NRC, Germany, Japan

In addition to the experimental programs, the NRC sponsored the development of the REMIX code [38, 39, 40]. REMIX is a fundamentally-oriented, lumped zonal approach, that integrates local mixing behavior into a system response. The code models mixing in the downcomer as an idealized free plume decay. Jet mixing at the injection location is modeled, as well as mixing and stratification in the cold leg. The mixing zone approach in REMIX is illustrated in Figure B-1.

The IPTS study took the approach of using TRAC and RELAP to calculate system behavior. At the time, it was concluded that only weak plumes may exist, based on separate effects mixing experiments and REMIX calculations. Therefore, it was concluded that use of a uniform temperature distribution for the fracture mechanics calculations was appropriate.

The basic thermal hydraulic phenomena involve cold ECC injection through the ECC line into each cold leg. Depending on the injection flow rate, backflow from the cold leg into the ECC line can

occur. Westinghouse (W) and Combustion Engineering (CE) plants have low injection flow velocities for HPI flow. Back flow and mixing in the ECC injection line is expected with HPI flow rates for W and CE plants, based on Froude number analysis (discussed below). Babcock and Wilcox designs have small injection lines for HPI, with concurrent high velocities that preclude back flow. At higher flow rates characteristic of accumulator and LPI in W and CE plants, back flow is precluded.

For W and CE plants the ECC water enters the cold leg as a weak jet (MR1 in Figure B-1), and falls to the bottom of the pipe, where it flows along in both directions, towards the loop seal and the reactor vessel. Warm water flows countercurrent from the upper downcomer into the cold legs. Some mixing between occurs between the two countercurrent flow streams.

As the colder ECC flow enters the downcomer, it turns 90° (MR3 in Figure B-1). Depending on the flow velocity, it may tend to jump the gap and impact the core barrel. Plumes may be formed in the downcomer below each cold leg (MR4 in Figure B-1). In-vessel natural circulation greatly affects the flows and mixing in the downcomer. Physically, the mixing in the downcomer is due to large scale secondary flow which is induced by the slightly colder water below the cold legs. Circulation cells are established in the downcomer, with upflow from the lower downcomer and lower plenum, as warm water is displaced by colder water.

The experimental evidence shows stratification in the cold legs during ECC injection is certainly present, but largely disappears by the time the injected ECC enters the downcomer, impacts the core barrel, and is deflected so that it flows down the downcomer. By the time that the plume, such as it is, makes it to the top-of-core elevation, the mixing has practically eliminated the evidence of a cold plume or jet. The water temperature, locally, is less than 10C below the local ambient water temperature.

The velocity levels and forced convection heat transfer coefficients in the downcomer at the core elevation are large enough so that the presence or absence of additional circulation in the loops external to the vessel doesn't have a significant effect on the vessel cooling rate. After the first few minutes of the transient, the conduction in the vessel metal dominates the heat transfer.

RELAP5 conserves mass and energy and will predict mixed mean temperature in tank volumes subject in inflow and outflow. Such is the case of the reactor vessel with inflow from ECC injection and outflow from a break. This was apparent from the temperature comparisons with integral system test data from ROSA, APEX, LOFT, UPTF, and MIST.

Systems codes such as RELAP5 employ a one dimensional formulation of flow in pipes precludes treatment of two fluid temperatures of the same phase, such as thermal stratification.

RELAP5 calculates an averaged fluid temperature for each node. The code cannot model plumes. Instead of calculating the Navier-Stokes equations, it employs nodal average behavior with constitutive relations for viscosity, wall boundaries, and interphase relations.

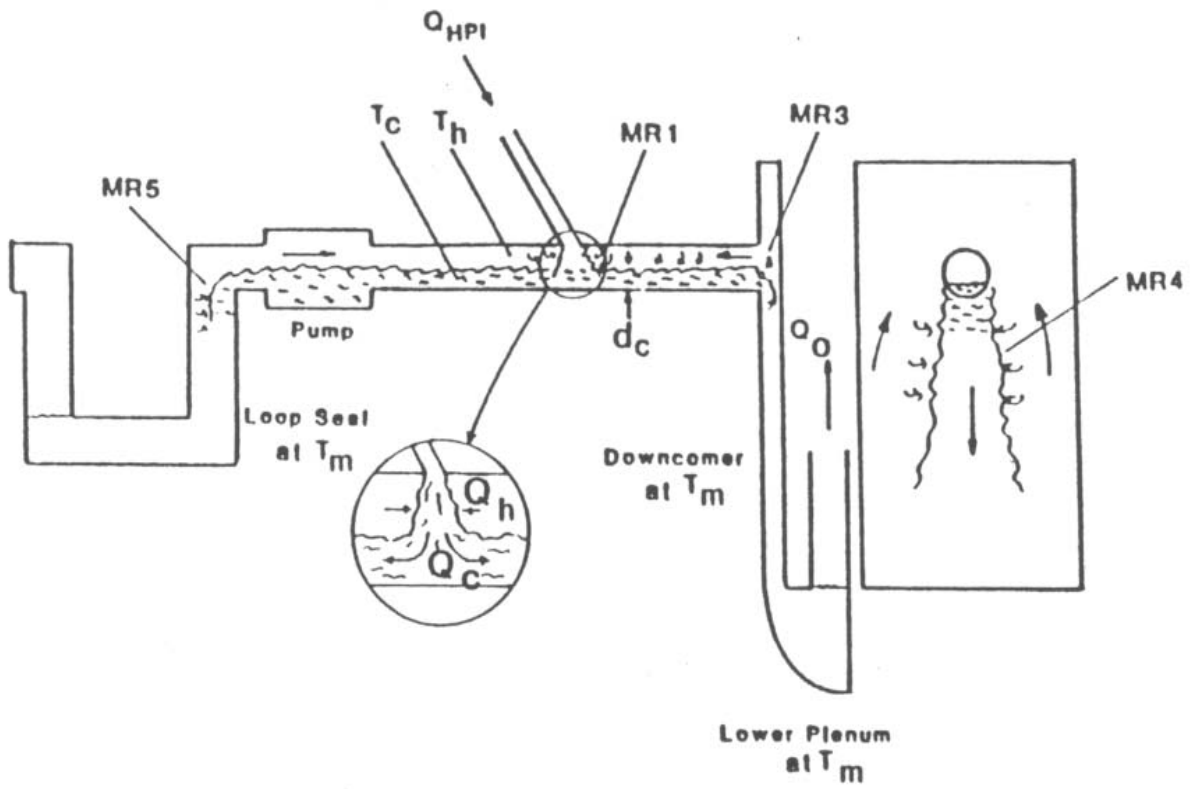


Figure B-1 Mixing Region During Loop Flow Stagnation

RELAP5 has the capability to predict natural circulation from buoyancy driven flows in a two dimensional geometry. The downcomer in the current PTS reevaluation was modeled with RELAP5 using six parallel channels. The two-dimensional temperature distribution in the downcomer calculated by RELAP5 was subject to question as to the predictive capability. The downcomer temperature distribution calculated had little axial or azimuthal nonuniformity, typically ~5C. The combination of coarse nodalization and numerical mixing resulted in a well-mixed downcomer. The temperature distribution predicted by RELAP5 is, in fact, similar to that seen in integral system experiments. Both are well mixed. The details of the circulation cells pattern in the whole downcomer are not captured by RELAP5, but the velocities are about right so the calculated values for h are about right too.

The purpose of this discussion is to show that RELAP5 provides a reasonable approximation of the averaged physical behavior. We will discuss the relevant integral system and separate effects tests experimental data, REMIX calculations, and computational fluid dynamics results. We will show that distributions, or variations, in temperature, in the downcomer region adjacent to the core are a second order effect. This is because the physical processes produce extensive mixing. RELAP5 is found to provide reasonable calculations of downcomer flows.

We summarize research performed to understand and model temperature distributions in the downcomer. The summary includes separate effects tests that investigated planar plume development in the reactor vessel downcomer and turbulent buoyant jet and plume mixing in the primary system cold legs. We consider temperature distribution from the perspective of

- Integral system tests of representative risk-dominant PTS sequences with representative downcomer scaling and instrumented to measure downcomer fluid temperature distributions. These included LOCAs, stuck open pressurizer power operated relief valves, and steam line breaks. These sequences correspond to the transients found by the current PTS analysis of greatest PTS risk significance. Integral system results are given in Sections B.4, B.5, and B.6 for APEX-CE, ROSA, and LOFT, respectively.
- Separate effects tests whose purpose was to evaluate fluid-fluid mixing phenomena in the cold leg and downcomer. These experiments investigated the degree of nonuniformity of temperatures in the downcomer in the elevations adjacent to the core. Fluid mixing patterns were evaluated during HPI flow into the cold legs for PWR geometries. Measurements were made of loop flow and HPI flow conditions that produce thermal stratification in the cold legs, as well as the plume temperature decay in the downcomer. Creare ½ scale results are described in Section B.3, while UPTF results are provided in Section B.7.
- Modeling of downcomer temperatures using REMIX. (Section B.8)

Mixing is most pronounced at changes in flow geometry. Using the terminology first developed by Theofanous and Nourbakhsh [41], mixing region 1 (MR1) is where the ECC injection jet enters the cold leg and stratifies (see Figure B-1). Mixing region 3 (MR3) is the transition from horizontally stratified flow in the cold leg to the vertical planer plume development in the downcomer. Mixing region 5 is at the entrance to the reactor coolant pump and loop seal. Mixing region 2 (MR2) is the cold leg itself. Mixing region 4 (MR4) is the downcomer plume decay.

An additional mixing region should be defined associated with the ECC injection line upstream of the cold leg. While substantial mixing occurs in the ECC injection line and the cold leg, the

experimental data shows the majority of the mixing to occur as the flow enters the downcomer from the cold leg (MR3).

There were several limitations to the earlier PTS Separate Effects Research.

- (1) The data base was comprised of separate effects tests and did not include integral system behavior.
- (2) The use of a single cold leg, except for the IVO facility, precluded interactions between multiple plumes.
- (3) The tests did not include effect of in-vessel natural circulation driven in part by core decay heat.
- (4) The tests were not transient in nature since they did not include break flow and depressurization.
- (5) The effect of wall heat transfer on mixing was not included in the salt water tests, and was less than prototypic in the fewer available thermal tests.

B.2 Scaling

The nature of scaling prevents complete similitude between all thermal hydraulic processes in the prototype and scaled facilities. A scaling analysis must be performed for each of the modes of operation specified by the experimental objectives. The objective of scaling is to simulate the processes most important to PTS to:

- (1) Identify the important phenomena and processes for which similitude must be maintained,
- (2) Prioritize the phenomena and processes,
- (3) Establish the similarity groups for the important phenomena and processes,
- (4) Identify the characteristic geometric scale ratios for the facility,
- (5) Establish the geometric similarity between the facility and the prototype, and
- (6) Identify limitations and biases due to scaling distortions.

The scaling of experimental facilities must be established with respect to the full scale prototype. A PIRT is used to identify the key thermal hydraulic phenomena and processes to be simulated and scaled in the context of PTS transients. If a specific transfer process is to have the same effect in the prototype, then the characteristic time ratios must be preserved. Because of differences in geometrical scale and fluid properties, it is not possible in general to match all of the time ratios of the full-scale prototype in a reduced scale model. It may be possible, however, to preserve a subset of time ratios that characterize the processes of greatest importance.

Mixing experiments with cold leg and downcomer geometries have been carried out in Creare 1:5 linear scale, Creare ½ linear scale, Purdue 1:2 linear scale, Imatran Voima Oy (IVO) 2:5 linear

scale, HDR full scale, and UPTF full scale [42, 43]. Data from these facilities were used to assess REMIX. Integral system tests were performed in ROSA, LOFT and APEX. The data indicated that HPI injection resulted in thermal stratification of the cold leg fluid whenever primary loop flow was low.

B.2.1 Mixing and Stratification

Dimensional analysis yield the following groups

$$Fr_{CL} = \frac{u_{CL}}{\left(g D_{CL} \frac{\rho_{ECC} - \rho_{CL}}{\rho_{ECC}} \right)^{1/2}} \quad \tau = \frac{V}{Q_{ECC}} \quad \frac{Q_L}{Q_{ECC}} \quad D^* = \frac{D_{CL}}{D_{ECC}} \quad \frac{L_{CL}}{D_{CL}}$$

$$aspect\ ratio\ axial = \frac{L_{axial}}{D_{H-dc}} \quad aspect\ ratio\ circumferential = \frac{L_{circ}}{D_{H-dc}}$$

where Fr is the Froude Number
u is the velocity
g is the gravitational constant
ρ is the fluid density
τ is a time constant
V is the volume
Q is the volumetric flow rate
L is length
D_H is the hydraulic diameter

subscripts

CL is the cold leg
ECC is the injected flow
dc is downcomer
axial is distance from the bottom of the core elevation to the cold leg centerline (C_L-CL)
circ is the circumference of the downcomer

The boundary between stratified and mixed is expressed by

$$Fr = 1,$$

Fr < 1 indicates the tendency for stratification while Fr > 1 would tend to indicate mixed conditions. The more general condition for two parallel flowing layers of different density is

$$Fr_1^2 = Fr_2^2 = 1$$

The Reynolds number indicates the degree of turbulence in the flow and is indicative of the propensity for mixing, which increases with increasing turbulence.

$$Re = \frac{\rho u D}{\mu}$$

where μ is the dynamic viscosity

B.2.2 Fluid Time Constant

The fluid time constant for LOCAs were estimated by considering the volumetric flow rate of ECC flow and the control volume. Characteristic ECC flows are

HPI 60 kg/s, 0.06 m³/s

Accumulator 1000 kg/s, 1 m³/s

LPI 360 kg/s, 0.36 m³/s

The control volume taken as the volume available for mixing. This consists of the volume up to the loop elevation and includes the vessel downcomer, lower plenum, cold legs, RCPs, and loop seals. This volume is approximately 100 m³. The fluid time constants are

$$\tau_{HPI} = 1300s, \quad \tau_{ACC} = 300s, \quad \tau_{LPI} = 300s$$

Flow stagnation conditions are of most interest to PTS, where

$$\frac{Q_L}{Q_{ECC}} = 0$$

For Palisades,

$$D^* = 2.8, \quad \frac{A_{ECC}}{A_{CL}} = 0.1285$$

$$Fr_{CL} = \frac{u_{CL}}{\left(g D_{CL} \frac{\rho_{ECC} - \rho_{CL}}{\rho_{ECC}} \right)^{1/2}} = 0.05 \text{ to } 0.25$$

where

$$u_{CL} = \frac{Q_{HPI}}{A_{CL}}$$

B.2.3 ECC Injection Line

For $Fr < 1$, back flow of warm water from the cold leg into the injection line may occur. From the Froude numbers shown in Table B-3, stratification and backflow may be expected in the ECC injection line for HPI flow rates. For LPI and accumulator flows, no stratification is expected. This is the case for CE and Westinghouse reactors, and has been found in practice in Purdue University [44, 45] and APEX-CE experiments [3]. Typical Froude and Reynolds numbers in the ECC injection line are,

$$\begin{aligned} Fr_{HPI} & 0.3 \text{ to } 0.5 \\ Re_{HPI} & 60,000 \text{ to } 90,000 \end{aligned}$$

Table B-3 Froude Numbers ECC Injection Line (W and CE)

T, C	ECC kg/s	u_{ECC} , m/s	Fr	ECC kg/s	u_{ECC} , m/s	Fr	ECC kg/s	u_{ECC} , m/s	Fr
285	50	0.22	0.30	100	0.43	0.58	200	0.86	1.2
250	50	0.22	0.36	100	0.43	0.71	200	0.86	1.4
200	50	0.22	0.46	100	0.43	0.91	200	0.86	1.8
150	50	0.22	0.65	100	0.43	1.3	200	0.86	2.5
100	50	0.22	1.2	100	0.43	2.4	200	0.86	4.8

Note: Because of high HPI injection velocities in B&W designs, $Fr \gg 1$
HPI injection rate up to 60 kg/s total, 15 kg/s per cold leg
LPI injection rate up to 360 kg/s total, 90 kg/s per cold leg

B.2.4 Cold Leg

The cold leg should stratify under loop flow stagnation or natural circulation conditions. Table B-3 shows the Reynolds and Froude numbers expected in the cold legs. Table B-4 shows important dimensions from Palisades used in various parts of the analysis.

B.2.5 Downcomer

The downcomer flow velocity based on natural circulation flow rate of 3% of rated flow is ~ 0.2 m/s based on a loop natural circulation flow rate of 3% (Figure 2-4). This is less than the flow velocity seen under flow stagnation conditions, therefore, downcomer recirculation may occur under these conditions as well. Based on velocities obtained from experimental data of 0.5 to 1.5 m/s, the following Re numbers are characteristic of downcomer flows during loop flow stagnation or natural circulation (Table B-5).

Table B-3 Cold Leg Froude and Reynolds Numbers

T _{CL} , C ↓ flow ⇒	Reynolds Number Cold Leg				Froude Number Cold Leg			
	Total ECC	50 kg/s	100 kg/s	200 kg/s	400 kg/s	50 kg/s	100 kg/s	200 kg/s
250	200,000	400,000	800,000	1,590,000	0.03	0.05	0.11	0.22
200	157,000	315,000	629,000	1,260,000	0.03	0.06	0.13	0.27
150	115,000	231,000	462,000	924,000	0.04	0.08	0.17	0.34
100	74,000	149,000	298,000	596,000	0.06	0.12	0.24	0.48
50	38,000	77,000	154,000	307,000	0.11	0.22	0.45	0.90

Note: HPI injection rate up to 60 kg/s total, 15 kg/s per cold leg
LPI injection rate up to 360 kg/s total, 90 kg/s per cold leg

Table B-4 Palisades Dimensions

Attribute	Dimension
Primary System Volume, m ³	347
Reactor Vessel Volume, m ³	131.7
Cold Leg Volume, m ³	2.777
Loop Seal Volume, m ³	4.064
Downcomer Volume, m ³	31.58
Downcomer Flow Area, m ²	3.38
Downcomer Gap, m	0.26
D _{CL} /D _H downcomer	1.34
Downcomer Circumference, m	14.71
Lower Plenum Volume, m ³	29.62
Vessel Diameter, m	4.794
Vessel wall thickness, m	0.22
Bottom of core, m	0
Top of core, m	3.66
D _H -DC CL-C _L to top of core	3
D _H -DC CL-C _L to bottom of core	10
DC aspect ratio axial	10
DC aspect ratio azimuthal	28.3
Cold leg Centerline, m	5.238
Cold Leg Diameter, m	0.698
Cold leg area, m ²	0.3825
Bottom of Lower Plenum, m	-1.259
CL-Top of Core L/R _{CL}	4.6
ECC nozzle to vessel, m	3.86
ECC nozzle to vessel L/D _{ECC}	14.5
ECC nozzle to vessel L/D _{CL}	5.5
ECC ID, cm	27.3
ECC nozzle area, cm ²	585.1

Table B-5 Reynolds Number Downcomer

T, C	0.5 m/s	1.0 m/s
250	185,0000	3,700,000
150	3,110,000	5,500,000
50	430,000	870,000

The Froude number calculation for the downcomer is uncertain. The relative velocity between the upflow and downflow regions based on experimental data is ~1 to 3 m/s. On this basis, and taking typical values from experiments for the extent of stratification in the cold leg (100C to 150C) yields downcomer Fr numbers of 1 to 6.

The high Re numbers and Fr numbers supports the extent of mixing observed in the experiments.

B.3 Creare ½ Scale

Creare was a 1:2 linear scale facility of a 1:4 sector (90⁰) of a PWR downcomer, with one of four cold legs. The Creare 1:2 scale mixing data are included in this summary since the facility measurements included flow velocity in the downcomer. The flow velocity measurements in Creare, together with similar velocity measurements in UPTF, provide key experimental data on downcomer flow conditions. The data from these two facilities show that during conditions of loop flow stagnation with HPI injection, downcomer flows are driven by buoyancy forces, with resultant mass flow rates and order of magnitude greater than the superficial ECC injection flow. This flow result in considerable mixing of the HPI flow shortly upon entering the downcomer.

The scaling for Creare included [46]

- (1) Geometric similarity,
- (2) Kinematic boundary condition similarity,
- (3) Froude and Reynolds numbers, and
- (4) Thermal similarity.

Linear dimensions were scaled to approximately one-half the prototypical PWR. The test facility was designed for operating at 1.38 MPa (200 psia) and 200C, with loop flows and HPI flow covering the range of interest for PTS. This temperature and pressure range is similar to UPTF. The downcomer represented a 90⁰ degree sector, and included one cold leg nozzle. The downcomer was unwrapped into a slab geometry. The downcomer length that was represented extended to the bottom of the core barrel. It included the blockage representation of ½ of a hot leg. The downcomer gap (0.1372 m) was scaled to ½ and was without step changes in width, as may occur in a B&W plant. It included a thermal shield spanning the full width of the downcomer and was sized and located to preserve the ratios of important dimensions.

The downcomer vessel and core barrel walls were made from carbon steel plate having a nominal thickness of 7 cm (2.75"). Flow exited the lower plenum upwards through a horizontal perforated plate. In the prototype the metal structures represent about ½ the total thermal capacity of the system while in Creare the value is about 1/3. The thermal time constant of the metal structures

in the prototype is approximately 13 times that of Creare, so the heat flux in Creare was greater than the prototype. The fluid time constants were similar. The cold leg diameter (0.364 m) was ½ the prototype.

Test measurements included flow rates, temperatures and pressures at the boundary locations, with measurements of temperature, flow velocity, and wall-to-fluid heat transfer. The facility included 261 thermocouple measurements in the cold leg, downcomer, and lower plenum. The cold leg was instrumented with four thermocouple rakes at different distances from the reactor vessel. The rakes measured temperatures at up to 10 elevations across the cold leg.

The downcomer was instrumented with thermocouples at 86 locations. At 40 of these, temperatures were measured in the mid-gap, about 1/3 of the distance from the vessel wall, and on the vessel wall. Temperatures at the two gap locations were similar. Temperatures were measured at 1 Hz.

The experiments were performed with prototypic Fr numbers, while the Re numbers were a factor of 6.5 lower than the prototype. Nine tests were run altogether (original plan called for 75). Variables included cold leg and downcomer geometry, loop, vent, and HPI flow rates, HPI Froude number, and loop/HPI density difference.

Two NRC tests (MAY105 and MAY106) were conducted [46]. The test conditions were similar with the exception of HPI flow rate, which was 50% higher in MAY105 than in MAY106. The results were similar for the two tests. The Creare test conditions were similar to UPTF (discussed in B.7). The basic test parameters were

Density ratio $\Delta\rho/\rho = 12.4\%$; full temperature $\Delta\rho/\rho = 35\%$
 $T_{ECC}, 14\text{C (58F)}$,
 Initial loop temp $T_0, 190\text{C (375F)}$; full temperature = 285C
 $T_0 - T_{ECC}, 186\text{C (317F)}$,

The density ratio $\Delta\rho/\rho$ was ~35% of the density ratio at full temperature initial conditions. The data are plotted in terms of

$$T^* = \frac{T(t) - T_{ECC}}{T_0 - T_{ECC}}$$

A value of $T^* = 0$ corresponded to local temperature equal to the ECC temperature (no mixing), while $T^* = 1$ means the local temperature equals the initial loop temperature.

Figure B-2 shows the cooldown transient obtained by Creare compared to an ideally mixed transient. The data were taken near the flow exit of the facility. The two tests, MAY105 and MAY106 had characteristic cooldown time constants (τ) of 666s and 987s respectively. The data compares closely to the ideally mixed condition.

If a plume is present, its temperature variation is imposed on the bulk cooldown of the downcomer. Early in the transient, the presence or absence of a plume is not important, because the minimum temperature in the downcomer is well into the temperature range in which the vessel material toughness is still high because its temperature is still high. The possible effects of temperature

nonuniformities becomes more significant later in time as the ambient downcomer temperature drops below ~140C.

Figure B-3 plots temperature traces for the two experiments at three locations. Trace A represents a well mixed lower plenum temperature (the flow exit temperature in the case of the present experiments. Trace B is in the annulus near the vessel wall below the cold leg. Trace C is in the annulus near the core barrel below the cold leg. The axial location of Traces A and B was at the top of the thermal shield. The traces represent the maximum temperature variations seen in the downcomer. The temperature data are normalized (1 = initial temperature, 190C; 0 = ECC injection temperature). The time scale is normalized according to the characteristic cooldown time. Measurements show the flow from the cold leg tended to jump the gap away from the vessel wall towards the core barrel. The vessel-side temperature, therefore, is warmer than the core barrel side, which was the case for all of the Creare experiments.

Figure B-4 shows the horizontal temperature profile across the downcomer (azimuthal direction), 1.5 D_H-DC (0.4 m) below the cold leg, for MAY105. This elevation corresponds to midway between the cold leg and the top of the core in the plant. In the prototype, the distance from the cold leg to the top of the core is 3 D_H. The figure shows the nondimensional temperature profile at 5 points in time. Time zero is the top of the plot while the end of the test is near the bottom. The data (Table B-6) show a maximum plume strength of ~12% T* (~20C) just below the cold leg.

Table B-6 Cold Leg Stratification and Plume at Top of Downcomer

τ	Cold Leg Stratification	Plume Strength	
0.3	125C	12%	20C
0.7	140C	12%	20C
1.4	30C	8%	14C
3.5	5C	0%	0C

Figure B-5 show the horizontal temperature profile across the downcomer (azimuthal direction), 5.5 D_H-DC (1.5 m) below the cold leg, for MAY105. This elevation corresponds to the core region in the plant. The figure shows the nondimensional temperature profile at the same 5 points in time $\tau = 0, 0.3, 0.7, 1.4,$ and 3.5. No plume can be seen.

Figure B-6 shows the axial temperature profile in the downcomer, and indicates the absence of vertical stratification.

Creare reported velocity measurements and flow rates based on Pitot tube measurements at four locations in the downcomer, two below the cold leg nozzle and two in the lower downcomer. Based on the measurements in the downcomer, Creare found an enhancement in mass flow of a factor of >20, as indicated in the following table reproduced from [46].

Test	Superficial Velocity	Measured	Ratio
MAY105	0.032 m/s	0.675 m/s	21
MAY106	0.022 m/s	0.616 m/s	28

In summary, the following are the main observations from the Creare data.

- ***The maximum plume strength of ~20C, which diminished with time during the course of the transient, was similar to UPTF. No plumes were detected at the core elevation.***
- ***The enhancement of downcomer flow rate by a factor of ~20 over the ECC injection flow rate was similar to UPTF.***

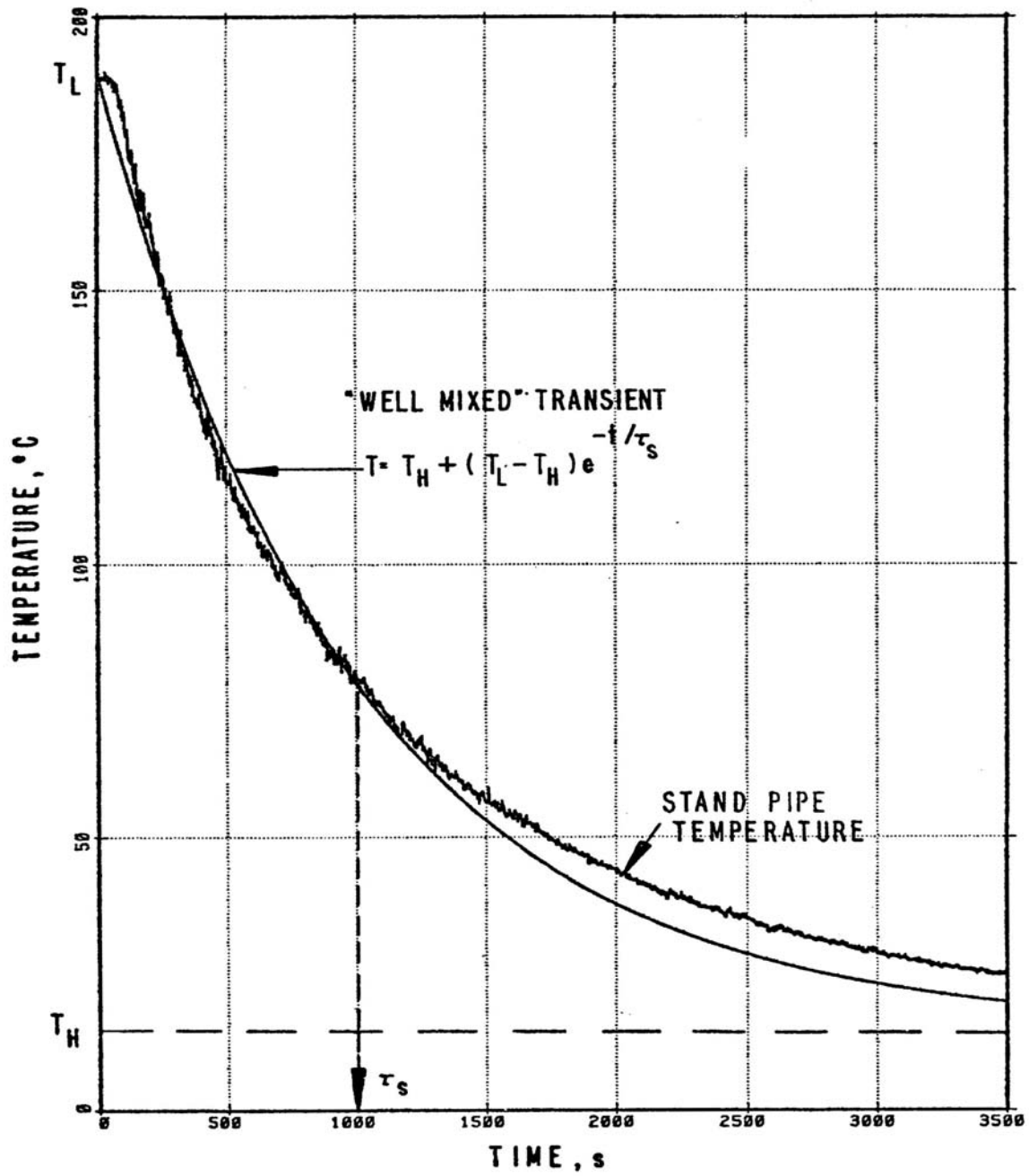


Figure B-2 Creare Downcomer Cooldown Transient

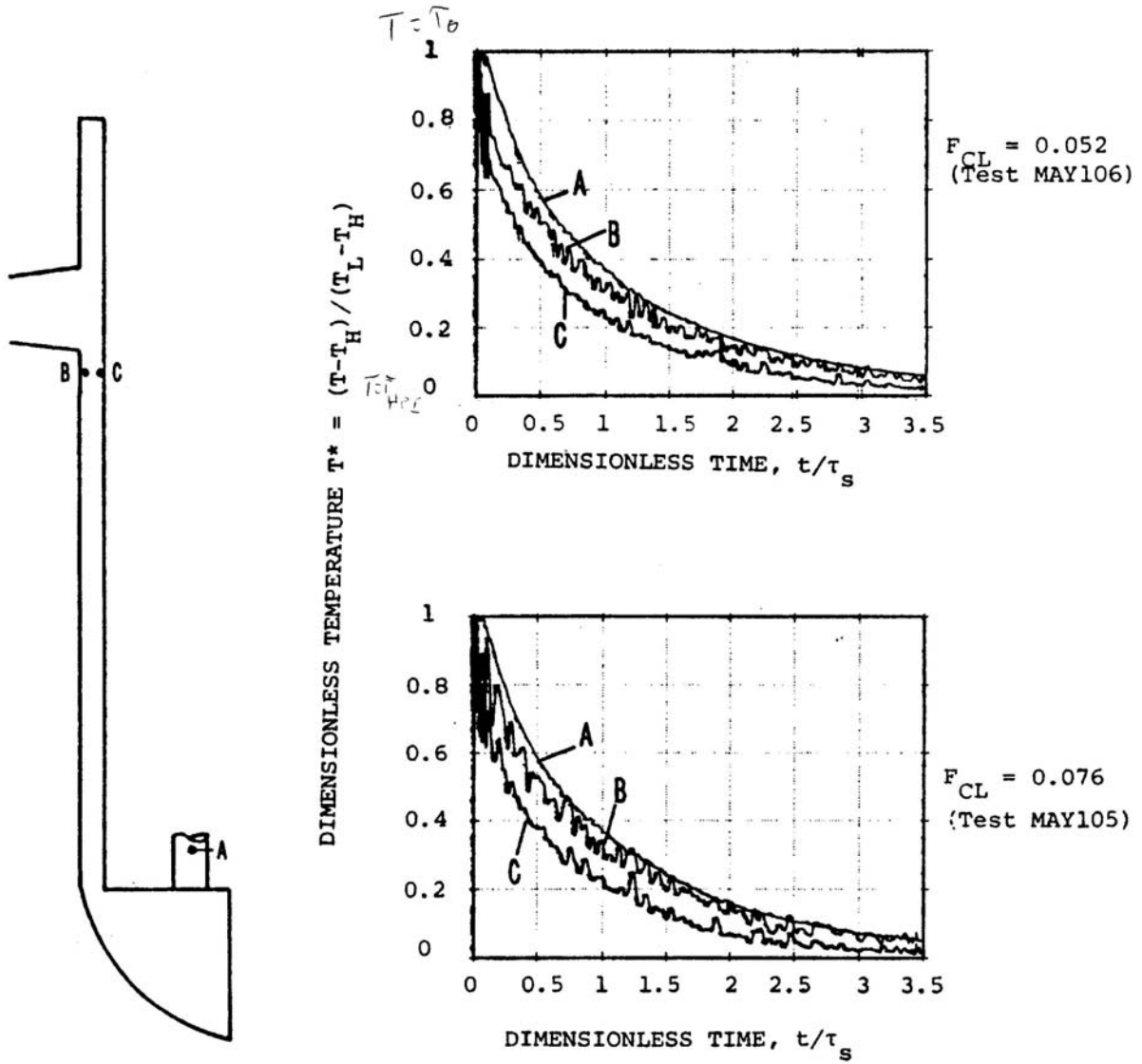


Figure B-3 Downcomer Temperatures Near Vessel Wall and Core Barrel

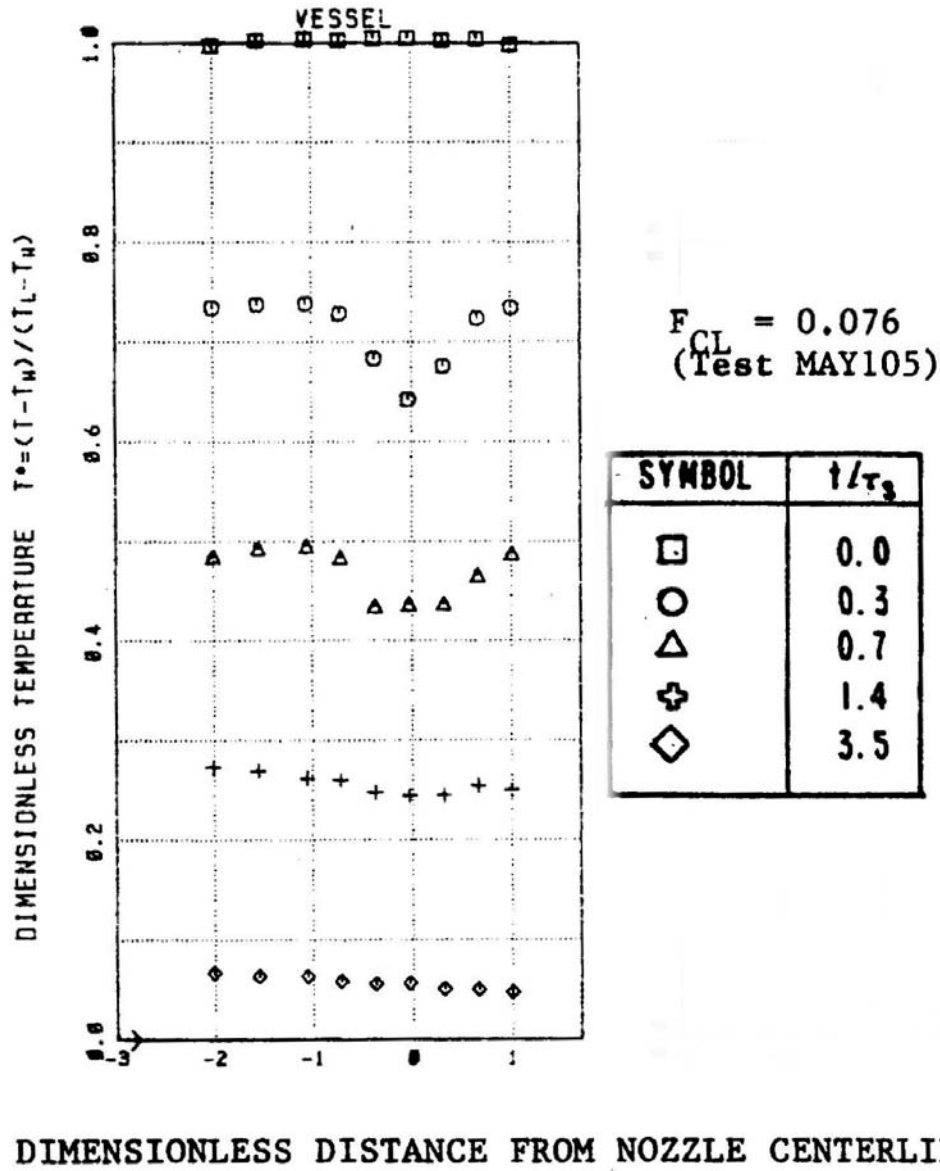
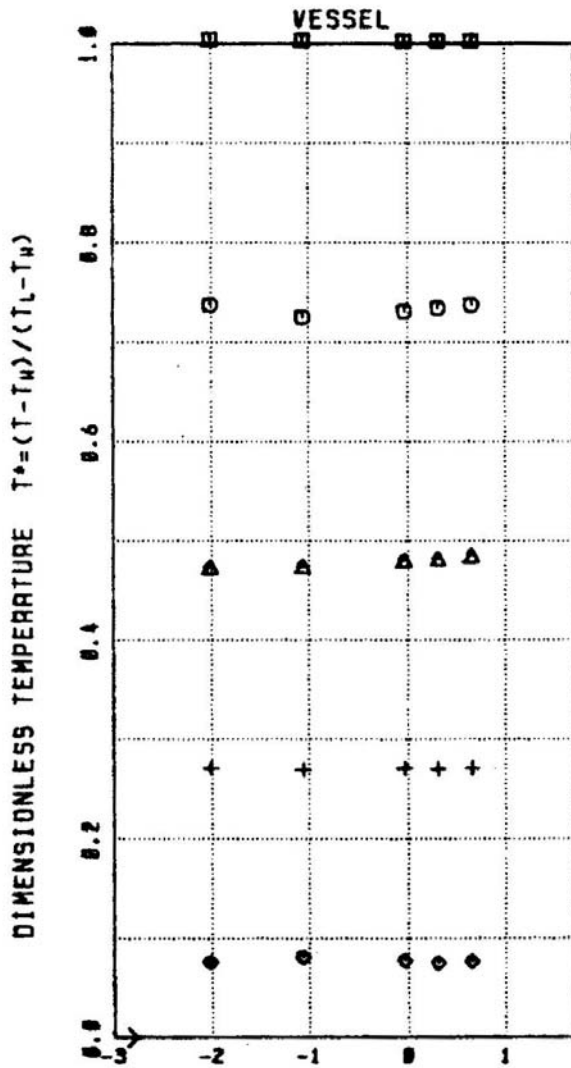


Figure B-4 Create 1:2 Scale Downcomer Temperature Distribution 0.4 m Below Cold Leg Nozzle Test MAY105

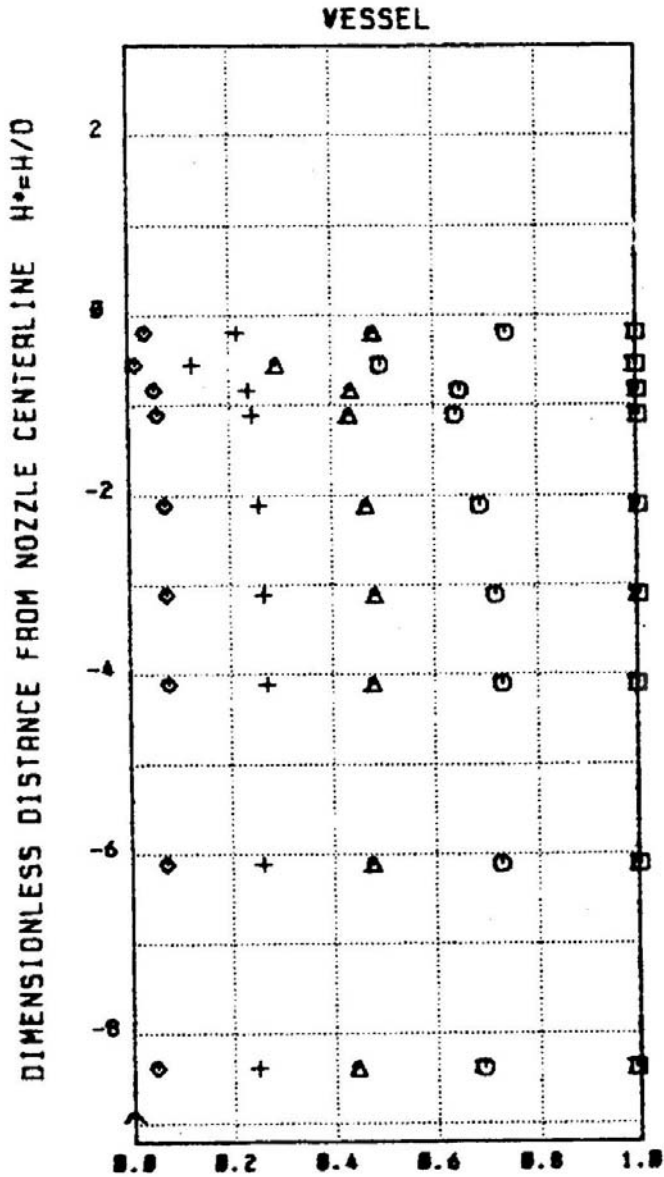


$F_{CL} = 0.076$
(Test MAY105)

SYMBOL	t/τ_3
□	0.0
○	0.3
△	0.7
+	1.4
◇	3.5

DIMENSIONLESS DISTANCE FROM NOZZLE CENTERLINE $X^* = X/D$

Figure B-5 Create 1:2 Scale Downcomer Temperature Distribution 1.5 m Below Cold Leg Nozzle Test MAY105



$F_{CL} = 0.076$
(Test MAY105)

SYMBOL	t/τ_s
□	0.0
○	0.3
△	0.7
+	1.4
◇	3.5

DIMENSIONLESS TEMPERATURE $T^* = (T-T_H)/(T_L-T_H)$

Figure B-6 Vertical Downcomer Temperature Profile Test MAY105

B.4 APEX-CE

As part of the PTS research, an experimental program was performed in the APEX facility at Oregon State University [3, 4]. APEX was originally build as a scaled model of AP-600. Its basic configuration and scale are, however, similar to the other CE plants; Calvert Cliffs I and II, Fort Calhoun, Palisades, St Lucie, and Waterford-2. Figure B-7 shows the facility layout.

The purpose was to generate experimental results of system effects to evaluate the dominant phenomena/processes. The objectives also included providing data to assess codes to be used for PTS analysis including RELAP5 and fluid-fluid mixing codes (CFD and REMIX). The phenomena of interest included fluid-fluid mixing in the cold legs and downcomer. Detailed temperature measurements and cooldown rates in the downcomer were obtained. Two types of tests were performed:

- Integral system tests of representative risk-dominant PTS sequences, including LOCAs, stuck open pressurizer power operated relief valves, and steam line breaks. The sequences corresponded to the transients found by the current PTS analysis to be most important to risk.
- Separate effects tests to study thermal fluid mixing, stratification in the cold legs, and plume development and interaction in the downcomer.

A scaling study was carried out on APEX using Palisades as the reference plant for comparison (NUREG/CR-6731). The scaling analyses determined whether the PIRT thermal hydraulic phenomena could be simulated in APEX-CE. The scaling analysis addressed:

- Geometric similitude,
- Parametric similitude,
- Depressurization,
- Single and two phase loop natural circulation flow,
- Interruption of loop flow and onset of primary loop stagnation,
- Fluid-fluid mixing and thermal stratification in the cold leg during ECC injection,
- Downcomer plume mixing and dissipation, and
- Mixing of ECC in the injection line.

The results of this scaling analysis were used in modifying APEX for the APEX-CE program. Phenomena involving integral RCS interactions, such as primary system depressurization or loop natural circulation, were examined at the "system" level. Phenomena, such as steam generator heat transfer, were examined at the "subsystem" level. Interactions between the steam-liquid mixture and metal structures were treated at the constituent level.

The scaling analysis assessed the similarity between cold leg and downcomer thermal fluid mixing

and heat transfer between APEX-CE and Palisades. The results of this analysis were used to specify the HPI nozzle diameter, the cold leg diameter and the HPI fluid temperature in APEX-CE. The top down scaling analysis was performed for a control volume that consisted of the cold leg and a portion of the downcomer, as depicted in Figure B-1. The global similarity criteria were closed using bottom-up scaling analysis to assess local phenomena such as the onset of thermal stratification in the cold legs, downcomer plume velocities and downcomer wall heat transfer.

The modifications made to APEX to produce the APEX-CE facility included the addition of:

- Cold leg loop seals,
- Horizontally mounted safety injection, and
- Approximately 50 thermocouples in the downcomer, shown in Figure B-8.

Similar to Palisades, each cold leg included a weir wall that limits backflow of HPI fluid towards the loop seals. All of the primary system components were designed to 2.75 MPa (400 psia). The maximum core power was 650 kW. The two steam generators each contained 133 tubes. The facility was operated on a one-to-one time scale. To preserve the time scale of 1:1 (isochronicity), power-to-volume was maintained, therefore, the core power and natural circulation mass flow rates scaled as the volume (i.e. 1:276). The aspect ratio of the downcomer was well-scaled at ~1:1.

The elevation difference in the thermal centers of the core and steam generators scaled as 1/3.2, which means that the APEX-CE facility was somewhat taller than the desired elevation scale ratio of 1/3.67. This is of interest with respect to natural circulation. This small elevation distortion was easily compensated for by the density difference and loop resistance terms so that the net effect on flow rate was maintained.

A comparison of the Palisades and APEX-CE geometries indicates that the scale ratios for the piping lengths, volumes, flow areas and elevations are relatively constant around the loop. Thus the minimum scaling requirement of geometric similarity for the test facility was established. Table B-7 presents the characteristic geometric scale ratios.

The twenty experiments that were performed are listed in Table B-8.

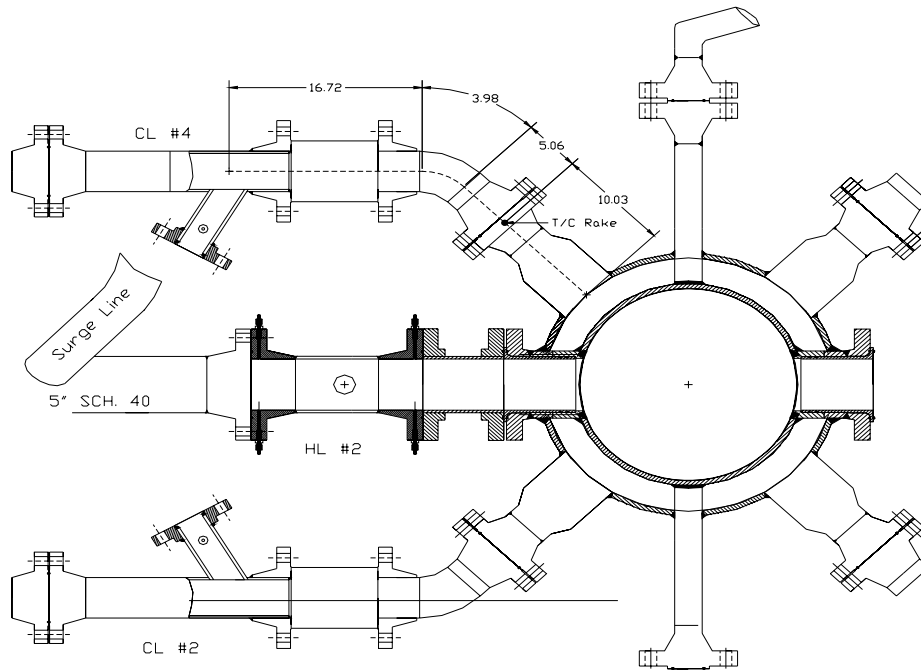


Figure B-7 APEX-CE Loop Configuration

Table B-7 Summary of APEX-CE Scaling Ratios

Attribute	Ratio
Flow Area	1:70
Lengths	1:3.
Volumes	1:276
Power	1:276
Power/Volume	1:1
Elevations	1:3.45
Natural Circulation Mass Flow Rate	1:276
Fluid Velocities	1:3.7
Diameter	1:8.5
Time	1:1
Cold leg/loop seal mixing volume	1:273

Attribute	Plant	APEX-CE	Ratio
Vessel Wall Thickness, m	0.2223	0.0126	17.6
Vessel ID, m	4.369	0.635	6.9
Core Barrel OD, m	3.88	0.508	7.6
Downcomer gap, m	0.244	0.064	3.5
Downcomer length, m	5.275	1.537	3.4
Downcomer volume, m ³	16.71	0.18	93
Downcomer aspect ratio (axial)	21.62	24.01	0.9
Cold leg ID, m	0.762	0.0901	8.5
Cold leg volume, m ³	4.78	0.019	252
Loop seal volume, m ³	3.5	0.01	350
ECC injection line, m	0.2889	0.0338	8.5

Table B-8 APEX-CE Test Matrix

#	Objective	Min DC T, C, (T- sat)	P at min T, MPa
1	Single phase natural circulation, power vs flow test		
2	Two-phase NC, stepped inventory reduction to characterize mass flow as a function of inventory. Coolant drained in a step wise manner, with steady state loop flow conditions established at each step. Power and secondary side conditions held constant at each step. Test continued until cold leg loop flow was below measurement capability, which corresponds to the onset of reflux condensation.		
3	Natural circulation parametric study to determine combination of HPI and CL flow rates at which thermal stratification occurs. Counterpart to the CREARE 1/5 scale test.		
4	HPI injection in one cold leg (CL-4). HPI flow at full scale 26 kg/s (scaled value 5.68 kg/min).		
5	HPI injection in all four cold legs. HPI flow at full scale 26 kg/s (5.68 kg/min) per leg.		
6	Flow stagnation, HPI injection in all four cold legs. HPI flow at full scale 13 kg/s (2.8 kg/min) per leg.		
7	1.4-inch HL Break	106(180)	1
8	2-inch HL Break	81(159)	0.6
9	Stuck-Open SRV	149 (198)	1.5
10	Stuck-Open SRV and SG ADV	97 (161)	0.63
11	MSLB in SG-1 with continued AFW, low power, 13.5-inch break. AFW remained on for 600s.	115(224)	2.51
12	MSLB with continued AFW, full power Integral System Test, Break in SG-2. 13.5-inch break. AFW remained on for 600s.	131(222)	2.4
13	Stuck-Open SRV that recloses	192(213)	2.05
14	Flow stagnation, injection in two adjacent cold legs (2, 4). HPI flow at full scale 26 kg/s (5.68 kg/min) per leg.		
15	Flow stagnation, injection in 2 opposite CLs (1, 4). HPI flow at full scale 26 kg/s (5.68 kg/min) per leg.		
16	Flow stagnation, injection in 3 CLs (1, 3, 4). HPI flow at full scale 26 kg/s (5.68 kg/min) per leg.		
17	Flow stagnation, injection in CL-4. HPI flow at full scale 26 kg/s (scaled value 5.68 kg/min). Upper-plenum/DC bypass open. Counterpart to CE-4.		
18	Flow stagnation, injection in 4 CLs. HPI flow at full scale 26 kg/s (scaled value 5.68 kg/min). Upper-plenum/DC bypass open. Counterpart to CE-5.		
19	2-inch HL break, Upper-plenum/DC bypass open. Counterpart to CE-8	75	0.55
20	Condensation during ECC injection, water level at bottom of hot leg,		

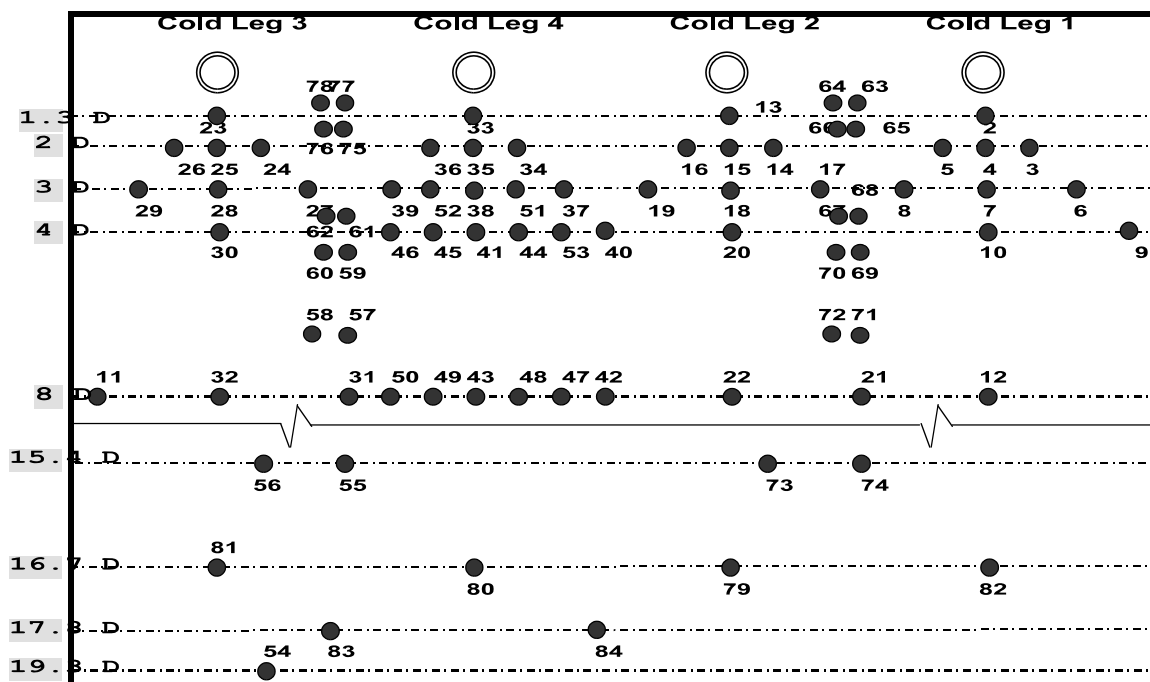


Figure B-8 APEX-CE Downcomer Thermocouple Map

B.4.1 Main Steam Line Break

A minimum downcomer temperature of 115C was reached in the steam line break tests during CE-11, which was run with low decay heat. This is consistent with the observation in the many RELAP5 calculations of MSLB scenarios in full scale plants. The RELAP5 calculation of two Palisades steam line break scenarios (P-50 and P-54) had minimum downcomer temperatures of 104C. These two transients were similar to CE-11 and CE-12, respectively, with no throttling of HPI or AFW to the broken steam generator. The only difference was that one was run from high decay heat conditions while the other had low decay heat conditions.

B.4.2 Upper Plenum - Downcomer Bypass

CE and Westinghouse plants have a flow path between the upper downcomer and the upper plenum. B&W plants have a larger flow path between the upper downcomer and the upper plenum due to vent valves. This flow path permits the establishment of an in-vessel natural circulation flow loop. The area of this path is generally not characterized precisely in power plants, but amounts to 1.54% of the RCS flow in Palisades. This translates to an approximate area of 0.3 m² (10-inch diameter equivalent).

To determine the effect of bypass flow on downcomer temperature, CE-17, 18, and 19 were run with the bypass holes open. For all other APEX-CE tests the bypass holes were plugged. There are 10 bypass holes with a diameter of 0.203 inch for a total flow area of 2.09 cm². This translates to 0.144 m² at full scale, about ½ the plant value.

Test CE-17 was a counterpart to CE-4. Both were separate effects tests with loop flow stagnation and HPI injection into a single cold leg. The downcomer temperature was approximately 2C (4F) warmer with the bypass open.

Test CE-18 was a counterpart to CE-5. Both were separate effects tests with loop stagnation and HPI injection into all four cold legs. The downcomer temperature was approximately 2C warmer with the bypass open.

Test CE-19 was a counterpart to CE-8. Both experiments were 2-inch hot leg breaks. The downcomer temperature was approximately 2C warmer with the bypass open. The minimum downcomer temperature with the bypass open was 75C compared to 81C with bypass closed.

The conclusion from these tests is that a small but noticeable warming of the downcomer occurs from the in-vessel natural circulation flow loop. The extent of warming was consistent with RELAP5 calculations of Oconee varying vent valve position, and the smaller bypass area in CE and Westinghouse designs compared with the B&W vent valve design.

B.4.3 Plumes

The data show temperature gradients (vertical) in the cold legs up to 120C (215F) due to HPI injection and thermal stratification. This was out of a maximum possible gradient of ~200C, which indicate mixing upstream of the downcomer in the cold leg of up to ~40% of ideal mixing.

In the downcomer, however, the maximum gradients are normally a few degrees, and never exceed 8C in the azimuthal and axial directions. The data indicate the presence of large scale circulation

cells that tend to keep the downcomer well mixed. Taken together, the APEX-CE data show no appreciable axial or azimuthal temperature gradients in the downcomer.

The maximum plume strengths were seen in the two MSLB tests (CE-11, CE-12). The maximum azimuthal temperature variation was approximately 8C. In these tests, AFW was continued to the broken steam generator for 600s (10 minutes). The plume was present between the two cold legs that connected to the broken steam generator. The data show the plumes from the two cold legs merged. Following dry out of the broken steam generator, the plume disappeared.

The second most pronounced plume appeared in CE-14. This was a loop stagnation separate effects test, with HPI injection into two adjacent cold legs. The plume from the two adjacent cold legs merged. This merging of adjacent plumes was observed in IVO experiments as well. The maximum plume strength was approximately 5C. None of the tests had axial gradients of more than 5C.

B.4.4 CE-5

This test will be used to illustrate the general results obtained from the APEX-CE tests. The purpose of CE-5 was to obtain baseline mixing data for stagnant coolant loop conditions. The initial pressure was 2.65 MPa (385 psia). The initial hot and cold leg temperatures were 217C (423F) while the ECCS injection temperature was 12C (54F). This gave an initial density ratio $\Delta\rho/\rho$ of 1.20, compared to 1.35 at full temperature scale.

Figure B-9 shows the cold leg temperature profile during the experiment. Stratification of up to 140C was observed. This compares to a maximum possible value of 205C, which indicates ~32% of total (ideal) mixing in the cold leg.

The top of the core was at 6 cold leg diameters (D) below the cold leg centerline, and the bottom of the core at was at 16D diameters. Thermocouples were arrayed around the azimuth at 2D, 3D, 4D and 8D below the cold leg centerline.

Figure B-10 shows downcomer temperatures at 0, 1.3D and 8D beneath each cold leg. Figure B-11 shows fluid temperatures at 8D below cold leg 4 at different azimuthal orientations. Figure B-12 is the same plot but with an expanded y-axis. The figures show no evidence of axial or azimuthal variations in temperature.

All of the APEX-CE experiments were examined with respect to fluid temperatures in the cold leg and downcomer. They show a consistent pattern of a large degree of thermal stratification in the cold leg. The downcomer temperatures are in all instances, however, nearly uniform. Table B-9 summarizes the maximum variations observed in downcomer temperatures. Since the data fit the definition of no plumes if the variation in temperatures is less than 10C, it is concluded that:

- ***No downcomer plumes occurred in the APEX-CE testing.***

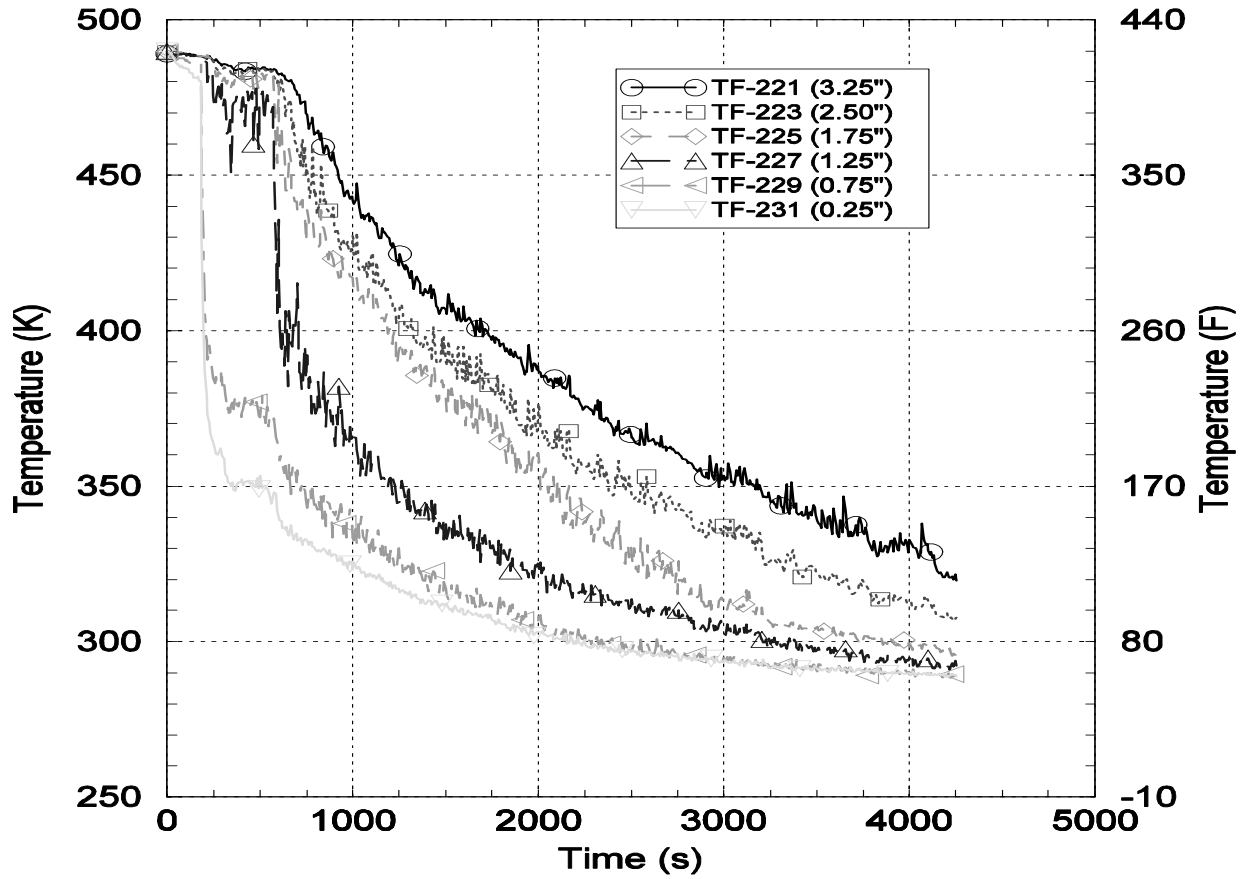


Figure B-9 Cold Leg Thermal Stratification During CE-5

Table B-9 APEX-CE Downcomer Temperature Gradients

Test	CL gradient, C (F)	Azimuthal variation, C	Vertical gradient, C
CE-4	80 - 120 (145 - 215)	1 - 4	0 - 5
CE-5	50 - 110 (90 - 200)	0 - 1	2 - 3
CE-6	50 - 120 (90 - 215)	0 - 2	1 - 2
CE-8	60 - 120 (110 - 215)	0 - 2	2 - 5
CE-12	60 - 120 C (110 - 215)	4 - 8	2 - 5
CE-14	20 - 110 (35 - 200)	3 - 5	0 - 1
CE-15	20 - 110 (35 - 200)	0 - 2	0 - 1
CE-20	5 - 50 (10 - 90)	0 - 3	1 - 3

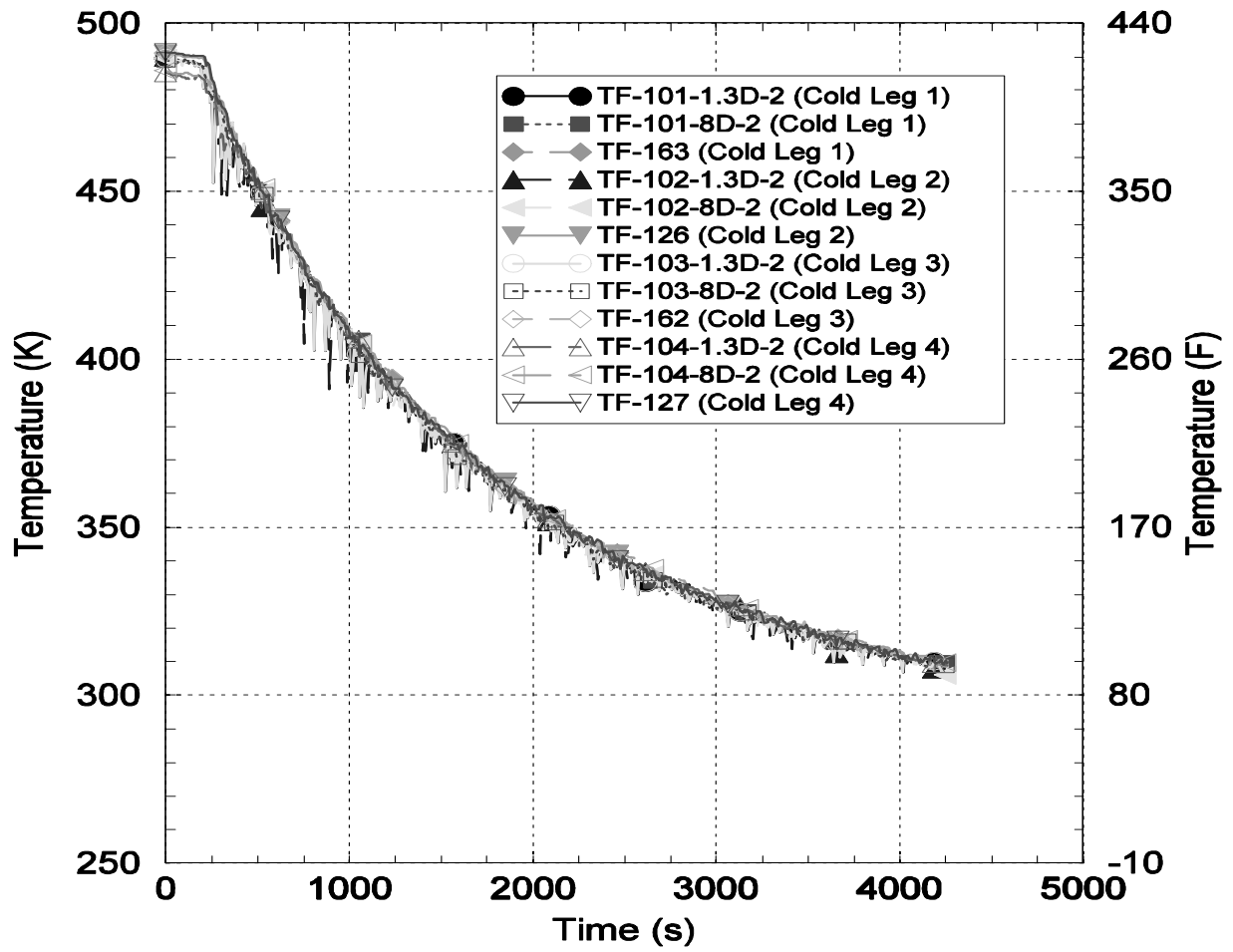


Figure B-10 Downcomer Temperatures at 0, 1.3 and 8 Cold Leg Diameters Beneath Each Cold Leg

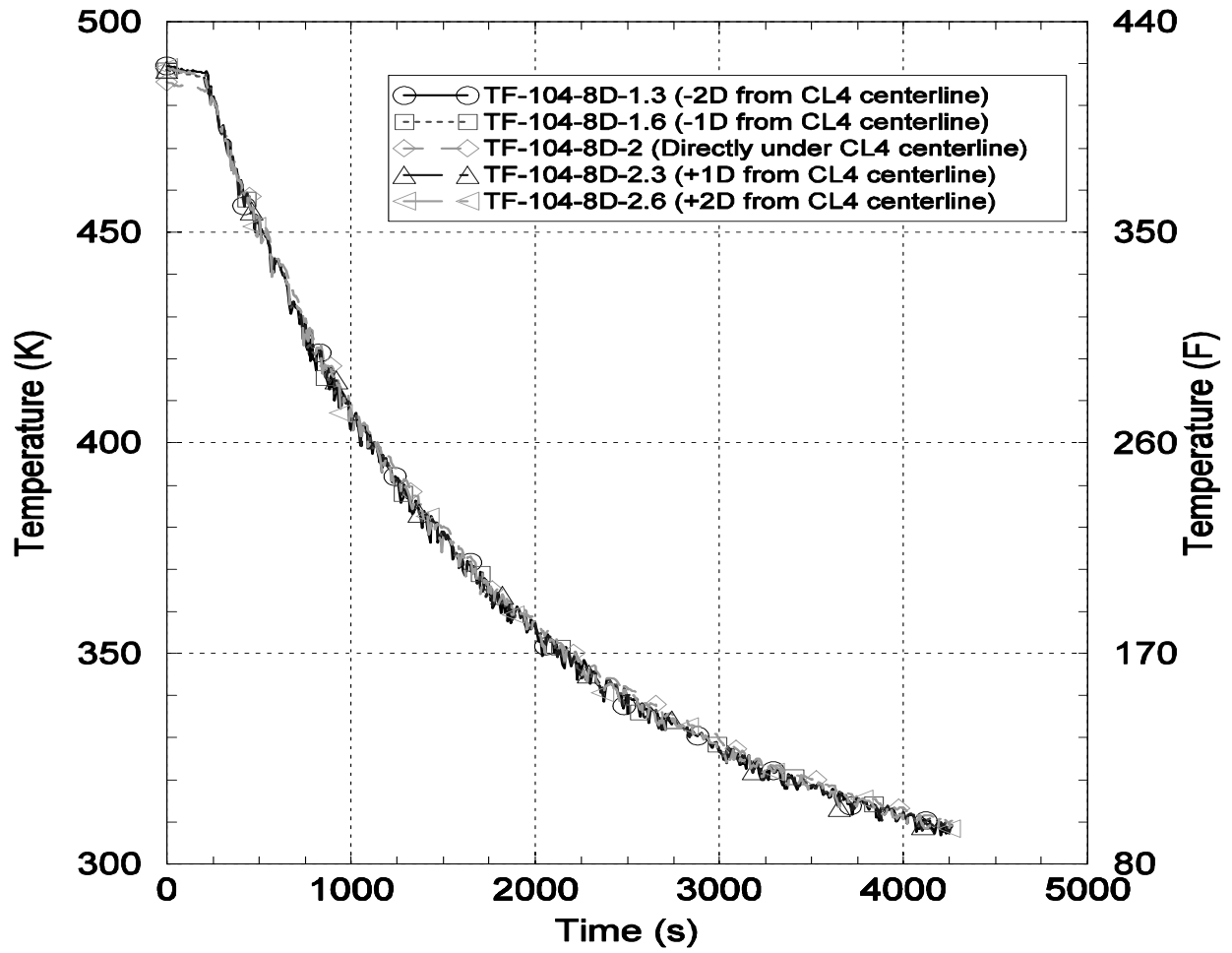


Figure B-11 Fluid Temperatures at 8 Cold Leg Diameters Below Cold Leg 4 at Different Azimuthal Orientations

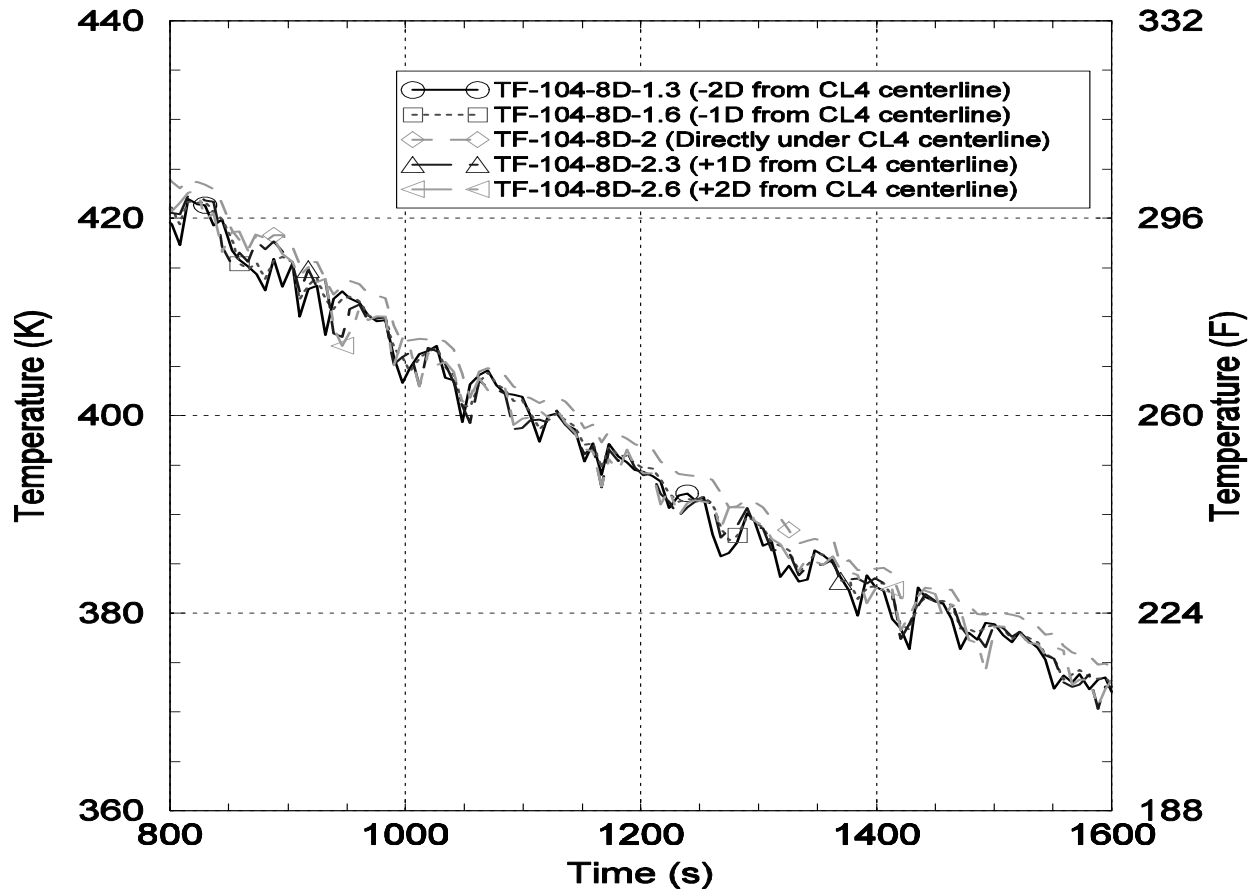


Figure B-12 Fluid temperatures at 8 Cold Leg Diameters Below Cold Leg 4 at Different Azimuthal Orientations Expanded Temperature Scale

B.5 ROSA

ROSA-IV was a full height, full pressure and temperature facility [13]. Table B-10 compares the facility to the full scale prototype. The volume scale was 1:48 with respect to a Westinghouse 4-loop plant. ROSA had a two loop configuration with the cold legs located 180° apart. The nominal aspect ratio of the facility compared to the prototype was 1:7. The azimuthal aspect ratio in the downcomer was slightly greater than the prototype, 1.3:1. In the axial direction, it was ~1:6. The effective mixing length was representative for azimuthal mixing, and greater for axial mixing. Therefore, the mixing lengths in the facility should tend to be similar azimuthally and greater axially. ROSA/AP600 experiments had direct vessel injection of ECC while ROSA-IV tests had cold leg injection. For the current discussion, this is an important difference between the two facility configurations.

ROSA-IV had four thermocouple stalks in the downcomer, located 90° apart. Table B-11 lists the downcomer temperature measurements and locations. The same four thermocouple stalks were in place for the ROSA-AP600 tests. With respect to the two cold legs and two Direct Vessel Injection (DVI) lines they are:

- 1.2 D_H (20°) from DVI-B; 2.4 D_H (40°) from CL-B
- 1.2 D_H (20°) from DVI-A; 2.4 D_H (40°) from CL-A
- 4.2 D_H (70°) from DVI-B; 3.0 D_H (50°) from CL-A
- 4.2 D_H (70°) from DVI-A; 3.0 D_H (50°) from CL-A

The downcomer thermocouples were located at four elevations, the bottom of the core, the mid-plane of the core, the top of the core, and the cold leg. The distance from the CL centerline to the top of the core (D_H -DC) was 20 D_H in ROSA, compared to 3 D_H in the plant.

In the AP600 configuration, there are three possible plumes that could form in the ROSA downcomer. One is beneath the A-loop cold leg, which contained the Passive Residual Heat Removal (PRHR) System return flow. The PRHR mass flow rate at full scale was approximately 75 kg/s, which is similar to full HPI flow, but which flowed through a single cold leg in ROSA-AP600.

The other two possible plums are associated with the two Direct Vessel Injection (DVI) lines. These two lines are located 180° apart, and are separated from the cold legs by 20°. The DVI lines enter the vessel 1.29 m (51-inches) below the cold leg and 0.67 m (27-inches) above the top of the core. The distance was 6.6 D_H . These aspect ratios allows ample distance for plume spreading so that the plume would be detectable at the thermocouple located at the top-of-core elevation. Plumes, if they existed, should have been apparent in the four azimuthal thermocouples located at the top-of-core elevation.

The two ROSA-AP600 tests included in the evaluation of downcomer temperatures had direct vessel injection so that there was no opportunity for mixing of ECC flows in the cold legs prior to entry into the downcomer. Similar to the AP-600, the DVI nozzle had an elbow in the downcomer so that the flow was directed downwards. This essentially eliminated the mixing zone at the entrance to the downcomer (MR3) and left only MR4 among the six mixing regions in the Theofanous model (Figure B-1).

Four ROSA tests were analyzed, two from the ROSA-IV facility and two from the ROSA/AP600

facility.

ROSA/AP600 CL-03 1-inch cold leg break in cold leg B; becomes hot leg break at 3500s when ADS opens

Figure B-13 shows the cold leg temperature profile for cold leg A, the PRHR loop. Figure B-14 gives the temperature profile in cold leg B, the CMT loop. The stratification in the A-loop is the result of operation of the PRHR. The stratification in the B-loop is the result of back flow into the leg from the downcomer. Flow is drawn from the top of cold leg C into the pressure balance lines and to the Core Makeup Tanks (CMTs). The onset of cold leg thermal stratification starts around 400s, somewhat before loop flow stagnation which begins about 300s later.

The data show a maximum of as much as 180C (325F) thermal stratification across the 20 cm diameter cold leg, with the bottom of the cold leg at ~75C and the top at its initial temperature of ~275C. The cold water flow in the cold leg is the result of PRHR flow. The PRHR mass flow rate scaled to full scale is ~75 kg/s which is similar to total HPI flow. The flow rate from each CMT scaled to full scale is approximately 20 kg/s, making it similar to the injection flow from HPI into each cold leg. Therefore, the plume mass flow from a DVI line is essentially the same as the plume mass flow from a cold leg. However, the *cold water is delivered directly to the downcomer as a downwards facing jet, without prior mixing in the ECC line and cold leg.*

The DVI line flow in ROSA/AP600 has the following attributes

$$Ri = 0.8$$

$$Re = 15,000$$

Therefore, there should not be mixing upstream of the vessel within the DVI line.

The cold leg flow in the PRHR loop shows the following

$$Ri \sim 50 \text{ to } 100$$

$$Re \sim 100,000$$

For the prototype the Richardson number is approximately 1.7 times greater because the cold leg diameter is a factor of 3.4 larger, however, the flow velocity in each cold leg is ~40% larger in the plant than ROSA. Each ROSA cold leg was larger than a scaled diameter of a single cold leg, because four cold legs in the plant were combined into two in ROSA. The plant cold leg Reynolds number is about a factor of 5 larger than ROSA. Therefore, the plant and ROSA cold leg behavior should be similar.

$$\text{Plant } Ri \sim 85 \text{ to } 170$$

$$Re \sim 500,000$$

Therefore, the cold leg should be stratified in ROSA, which agrees with the cold leg temperature data.

As noted, three downcomer plumes may be possible in the ROSA-AP600 configuration. Figure B-15 shows the downcomer fluid temperature at the top-of-core elevation near DVI-A, while Figure B-16 plots the downcomer temperatures near DVI-B at the top-of-core elevation. It can be seen that at 2000s, for example, the downcomer temperature (~100C) corresponds to the temperature in the lower part of the cold leg (see the lowest three of the five thermocouples (TE090C, D and E). This indicates that coolant flows through roughly the lower half of the cold leg to the downcomer. The DVI injection temperature equals the initial temperature of the CMTs, which was ~300K. While there are fluctuations in the downcomer temperature measurements of 10C to 20C reflecting the passing of eddies, there is no indication of plumes.

ROSA/AP600 CL-09 1-inch cold leg break in loop B. No core makeup tank injection.

As a ROSA/AP600 experiment, three plumes are possible, one associated with the P loop cold leg and two with the DVI lines. The DVI injection precludes prior mixing and ensure the jet temperature as it enters the downcomer is ~300K.

Figure B-17 shows the temperature profile in the P-loop cold leg that has the PRHR return flow. The stratification in the P-loop is the result of operation of the PRHR. The temperature difference across the 20 cm P-loop cold leg is as much as 200C (360F). Figures B-18 and B-19 show downcomer temperatures at the top-of-core elevation near DVI-B and DVI-A, respectively. No evidence is seen of plume effects. Figure B-20 shows downcomer temperature at the bottom-of-core elevation. No evidence is seen of axial gradients in the downcomer.

ROSA-IV HL-06: 2-inch hot leg break, in loop B (non pressurizer loop). No HPI and AFW. PORV opened at 5800s. Accumulator injection began at 6425s.

Because there was no HPI in the experiment, the downcomer temperatures stayed at saturation corresponding to the steam generator secondary temperature until approximately 5800s, when the PORV was opened. Following opening of the PORV, RCS pressure decreased and accumulator injection began at 6425s. Figure B-21 shows downcomer fluid temperatures at the top and bottom of core elevations in the downcomer. The data indicate the downcomer is well mixed axially following accumulator injection. The azimuthal temperature distribution is similar to the other ROSA experiments.

ROSA-IV CL-18 6-inch cold leg break. No HPI and AFW. Accumulator injection flow began at 455s.

Figure B-22 shows downcomer fluid temperatures at the top and bottom of core elevations in the downcomer. The downcomer is seen to be well mixed axially both before and after the start of accumulator injection at 455s, with no discernable difference between the two elevations. Because of the absence of HPI, plumes would not be expected prior to accumulator injection at 455s. No evidence of axial gradients is seen. The azimuthal temperature distribution is similar to the other ROSA experiments.

Table B-10 Comparison of ROSA-IV LSTF to Westinghouse 4-Loop Plant

Attribute	LSTF	Plant	Ratio
Primary System Volume, m ³	7.83	347	1:44
Reactor Vessel Volume	2.667	131.7	1:49
Cold Leg Volume	0.1157	2.777	1:24
Loop Seal Volume	0.2122	4.064	1:19
Downcomer Volume	0.6926	31.58	1:46
Downcomer Flow Area, m ²	0.858	3.38	1:39
Downcomer Gap, m	0.046	0.26	1:5.7
D _{CL} /D _H downcomer	2.25	1.34	1:1.7
Downcomer Circumference, m	1.98	14.71	1:7.4
Lower Plenum Volume, m ³	0.57	29.62	1:52
Vessel Diameter, m	0.64	4.794	1:7.5
Vessel wall thickness, m	0.058	0.22	1:3.8
Bottom of core, m	0	0	1:1
Top of core, m	3.66	3.66	1:1
D _H -DC CL-C _L to top of core	20	3	7
D _H -DC CL-C _L to bottom of core	60	10	6
DC aspect ratio axial	60	10	6
DC aspect ratio azimuthal	21.5	28.3	1:1.3
Cold leg Centerline, m	5.503	5.238	1:0.95
Cold Leg Diameter, m	0.207	0.698	1:3.37
Cold leg area, m ²	0.03364	0.3825	1:11
Bottom of Lower Plenum, m	-1.259	-1.259	1:1
DVI Elevation, m	4.27	NA	NA
DVI Nozzle ID, m	0.0428	NA	NA
D _H -DC DVI to top of core	6.6	NA	NA
D _H -DC DVI to bottom of core	46	NA	NA
D _{DVI} /D _H -DC	0.46	NA	NA
DVI-Top of Core L/D _{DVI}	14.25	NA	NA
CL-Top of Core L/R _{CL}	17.8	4.6	3.9:1
ECC nozzle A to vessel, m	2.072	3.86	1:1.9
ECC nozzle B to vessel, m	3.434	3.86	1:1.1
ECC nozzle A to vessel L/D _{ECC}	48	14.5	3.3
ECC nozzle B to vessel L/D _{ECC}	80	14.5	5.5
ECC nozzle A to vessel L/D _{CL}	10	5.5	2
ECC nozzle B to vessel L/D _{CL}	17	5.5	3
ECC ID, cm	4.28	27.3	1:6.4
ECC nozzle area, cm ²	14.38	585.1	1:41

North = 0°; Hot leg A = 200°; Cold leg A = 140°; Hot leg B = 20°; Cold leg B = 320°; DVI A = 200°; DVI B = 20°; # Ratio of azimuthal distance over gap width

Table B-11 ROSA Downcomer Temperatures Measurements

Thermocouple	Height	Position	Position m	$x D_H$	Position	Position m	$x D_H$
TE-N000C-DC	0.0 m	40° from CL-B	0.22	2.4	20° from DVI-B	0.11	1.2
TE-S000C-DC	0.0 m	40° from CL-A	0.22	2.4	20° from DVI-A	0.11	1.2
TE-E000C-DC	0.0 m	50° from CL-A	0.275	3	70° from DVI-B	0.385	4.2
TE-W000C-DC	0.0 m	50° from CL-B	0.275	3	70° from DVI-A	0.385	4.2
TE-N018C-DC	1.8 m	40° from CL-B	0.22	2.4	20° from DVI-B	0.11	1.2
TE-S018C-DC	1.8 m	40° from CL-A	0.22	2.4	20° from DVI-A	0.11	1.2
TE-E018C-DC	1.8 m	50° from CL-A	0.275	3	70° from DVI-B	0.385	4.2
TE-W018C-DC	1.8 m	50° from CL-B	0.275	3	70° from DVI-A	0.385	4.2
TE-N036C-DC	3.6 m	40° from CL-B	0.22	2.4	20° from DVI-B	0.11	1.2
TE-S036C-DC	3.6 m	40° from CL-A	0.22	2.4	20° from DVI-A	0.11	1.2
TE-E036C-DC	3.6 m	50° from CL-A	0.275	3	70° from DVI-B	0.385	4.2
TE-W036C-DC	3.6 m	50° from CL-B	0.275	3	70° from DVI-A	0.385	4.2
TE-N060C-DC	6.0 m	40° from CL-B	0.22	2.4	20° from DVI-B	0.11	1.2
TE-S060C-DC	6.0 m	40° from CL-A	0.22	2.4	20° from DVI-A	0.11	1.2
TE-E060C-DC	6.0 m	50° from CL-A	0.275	2.4	70° from DVI-B	0.385	4.2
TE-W060C-DC	6.0 m	50° from CL-B	0.275	2.4	70° from DVI-A	0.385	4.2
TE-N055C-DC	5.5 m	40° from CL-B	0.22	2.4	20° from DVI-B	0.11	1.2
TE-S055C-DC	5.5 m	40° from CL-A	0.22	2.4	20° from DVI-A	0.11	1.2

Downcomer thermocouple stalks located at 0°, 90°, 180°, and 270°
 0.0 m = bottom of core, 3.6 m = top of core

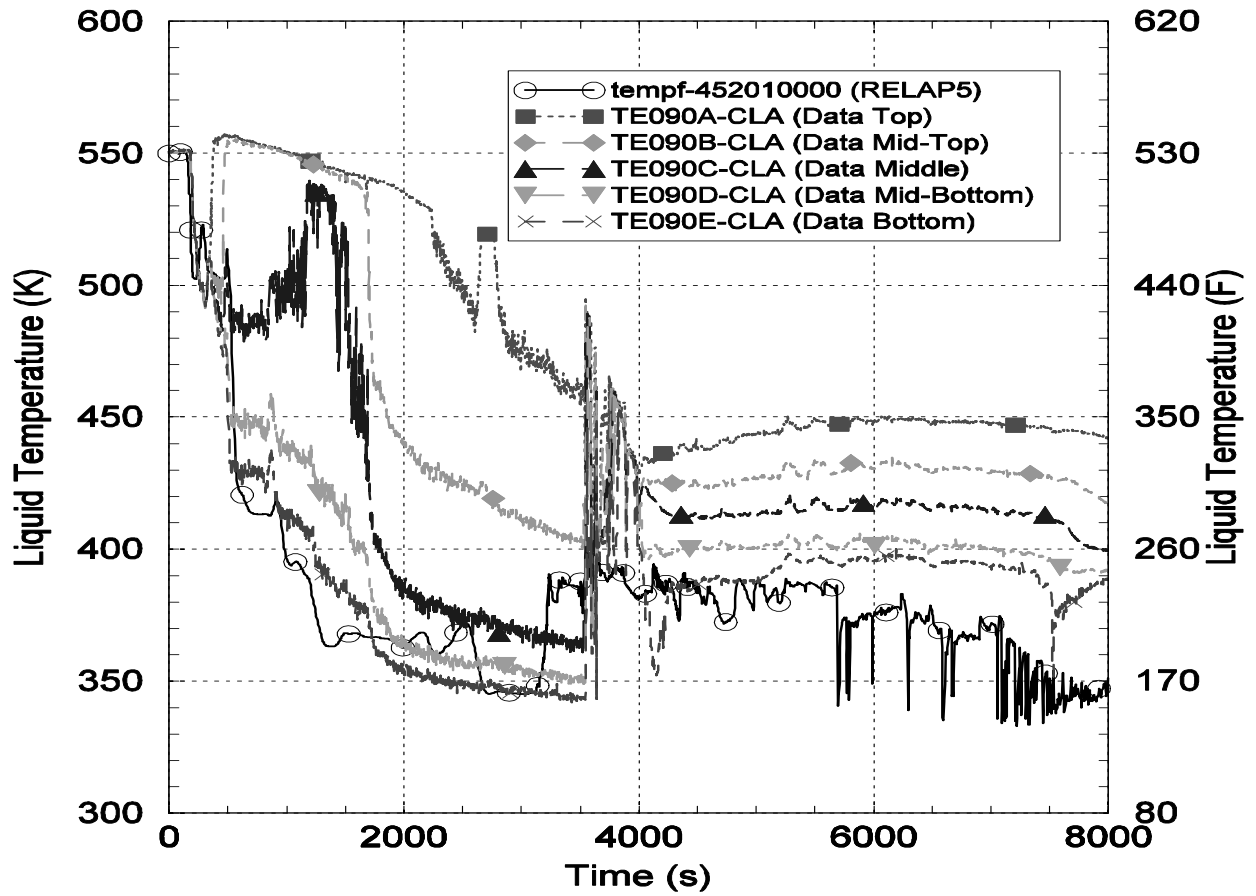


Figure B-13 ROSA/AP600 AP-CL-03 P-Loop Cold Leg Temperature Profile

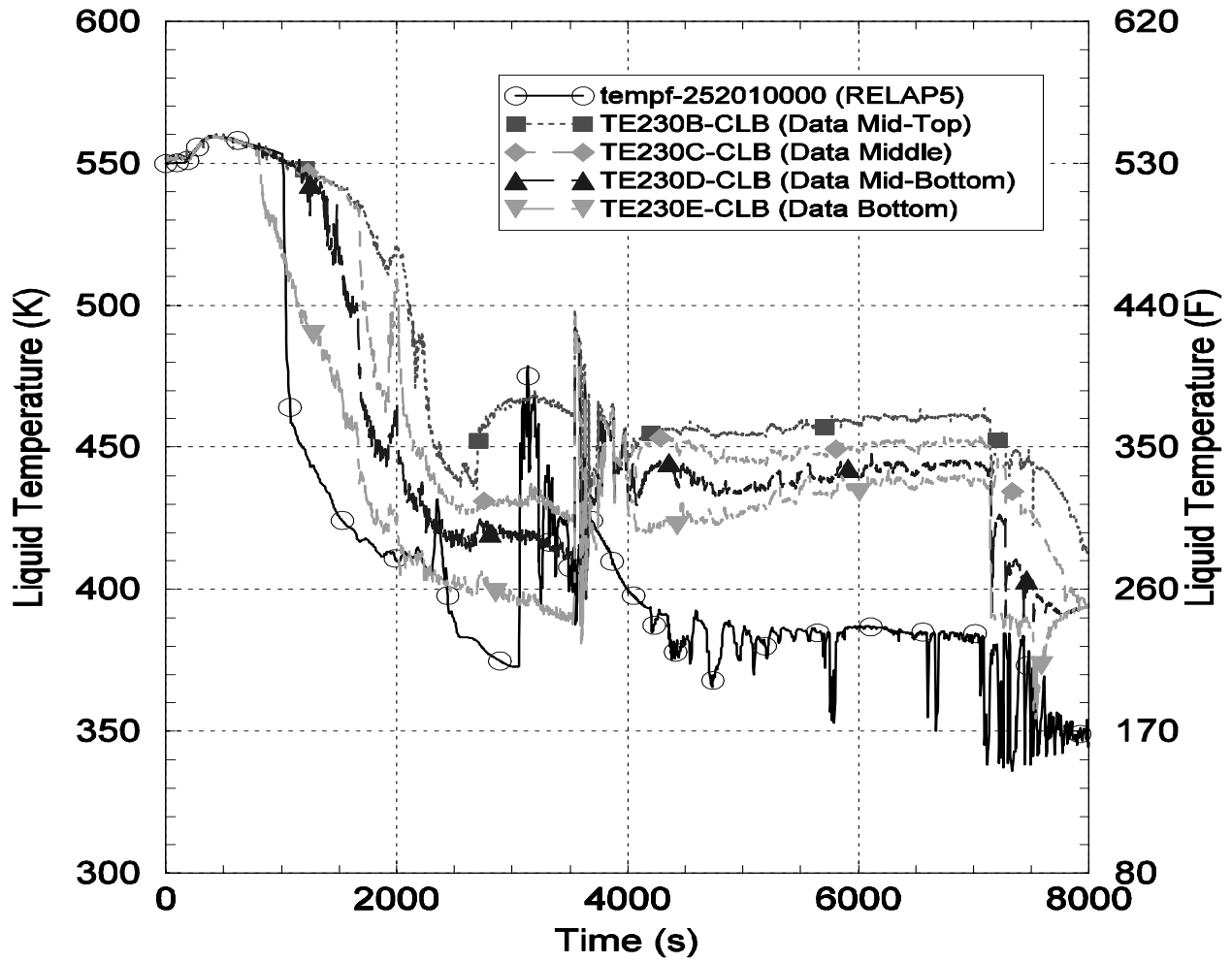


Figure B-14 ROSA/AP600 AP-CL-03 C-Loop Cold Leg Temperature Profile

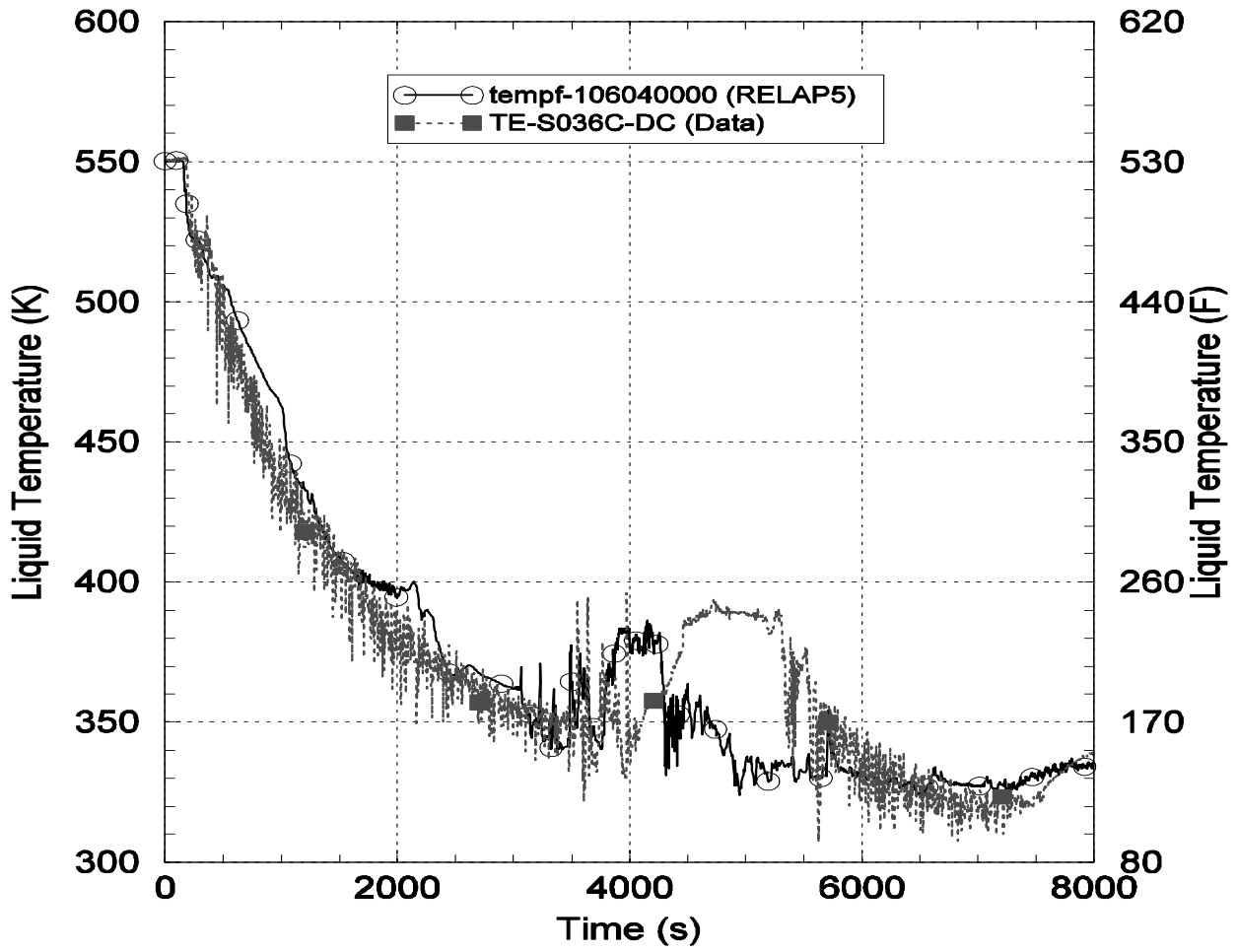


Figure B-15 ROSA/AP600 AP-CL-03 Downcomer Temperature at Top-of-Core Elevation Near DVI-A

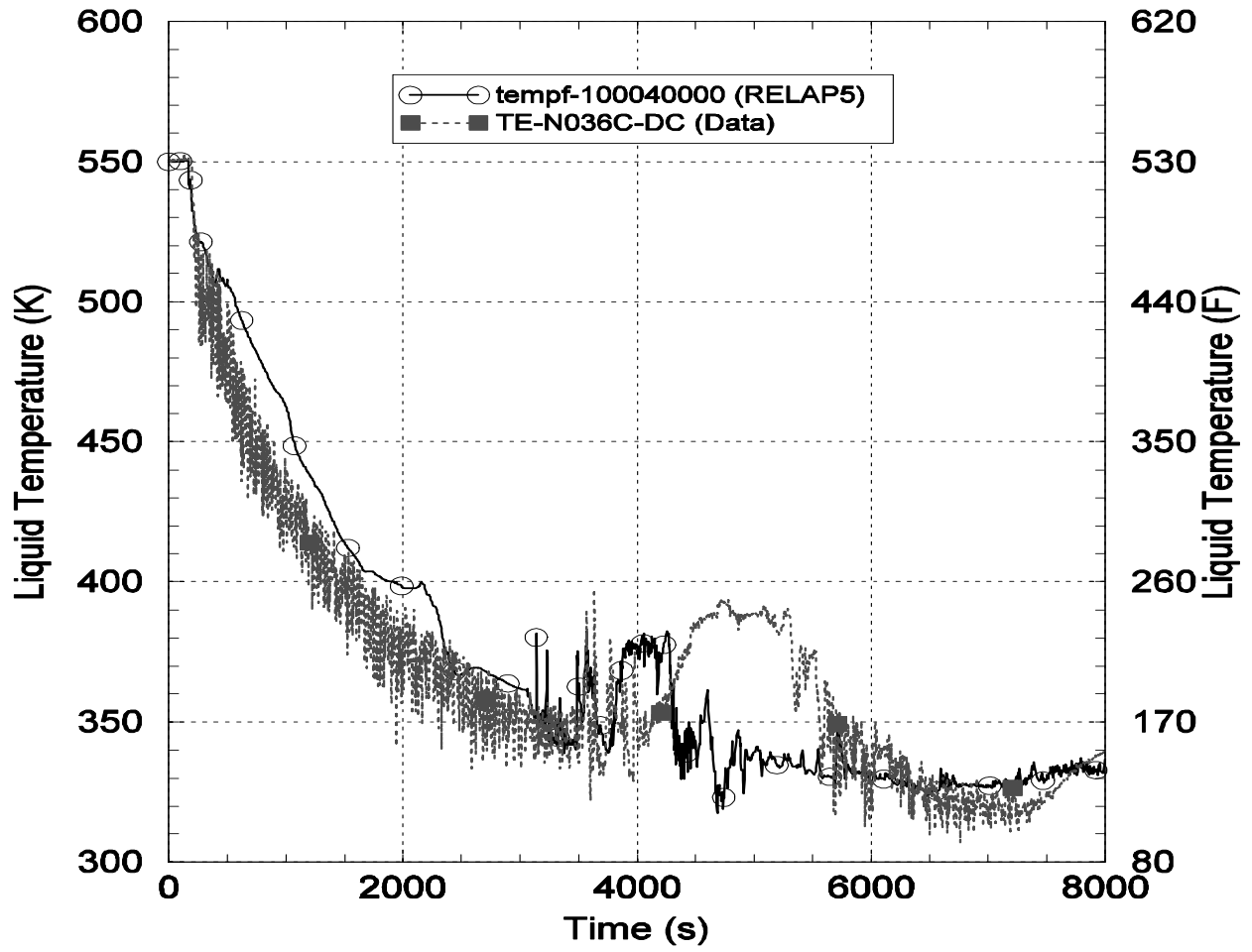


Figure B-16 ROSA/AP600 AP-CL-03 Downcomer Temperature at Top-of-Core Elevation Near DVI-B

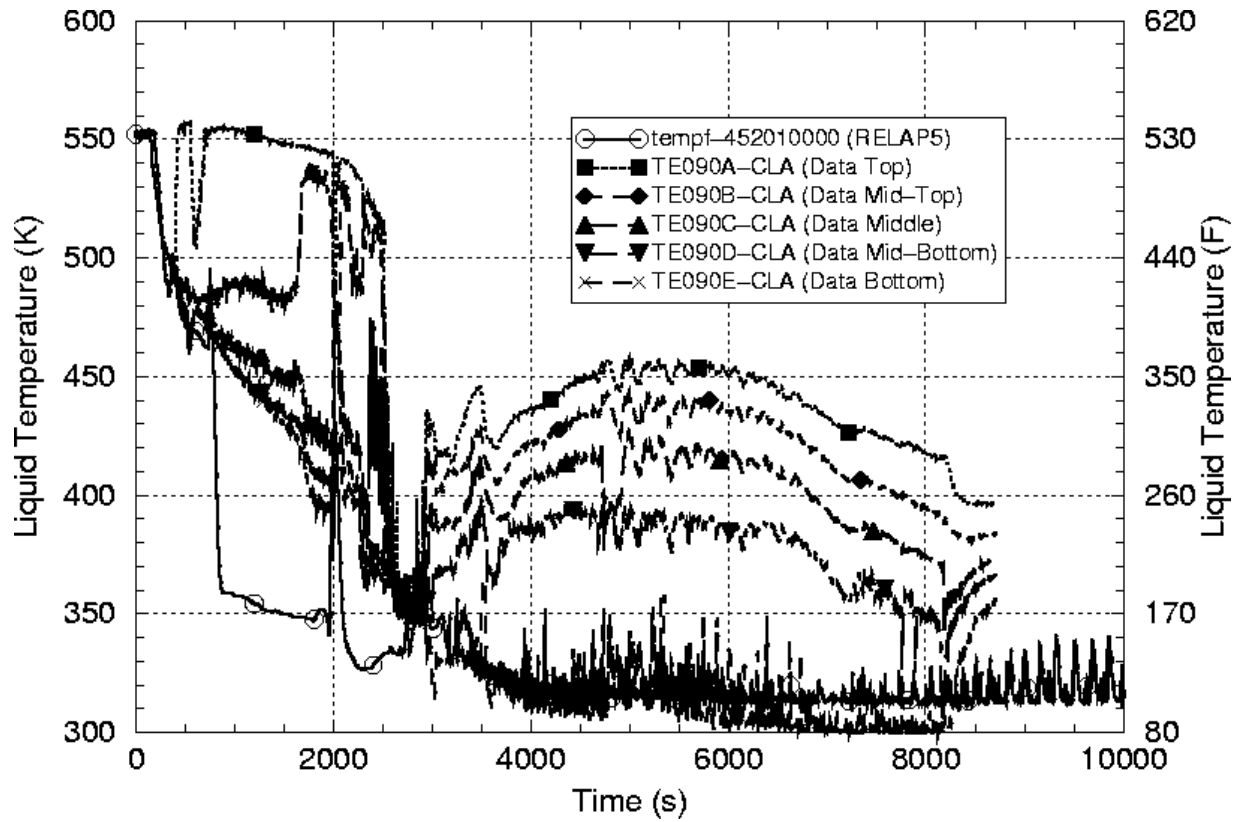


Figure B-17 ROSA/AP600 AP-CL-09 Cold Leg Temperature Profile in PRHR Loop

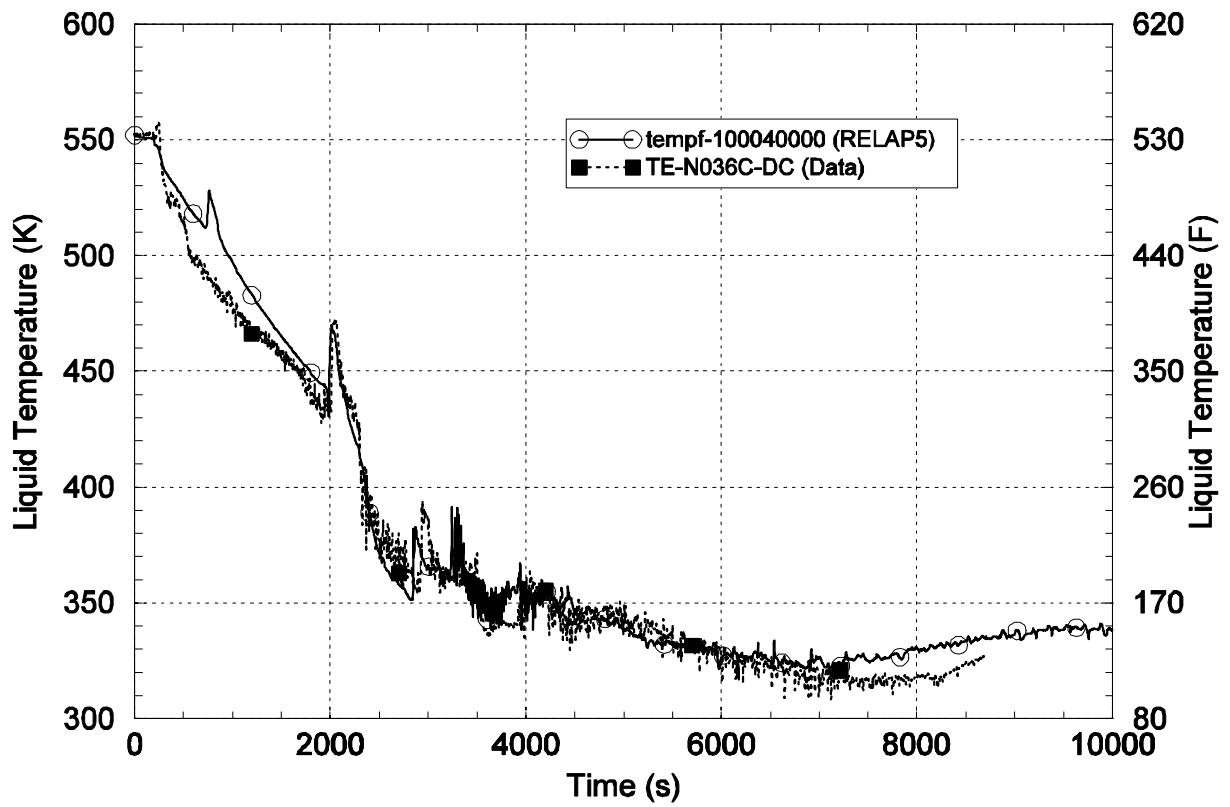


Figure B-18 ROSA/AP600 AP-CL-09 Downcomer Temperature at Top-of-Core Elevation Near DVI-B

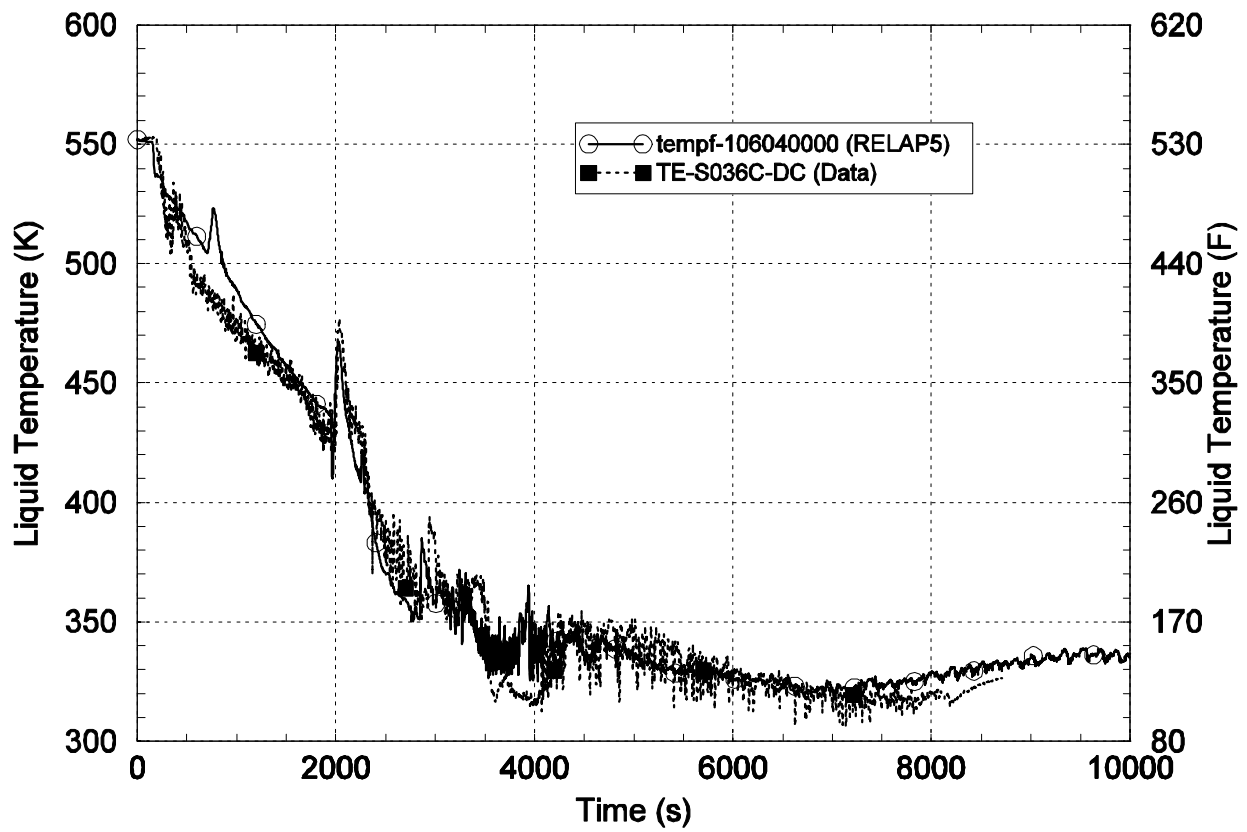


Figure B-19 ROSA/AP600 AP-CL-09 Downcomer Temperature at Top-of-Core Elevation Near DVI-A

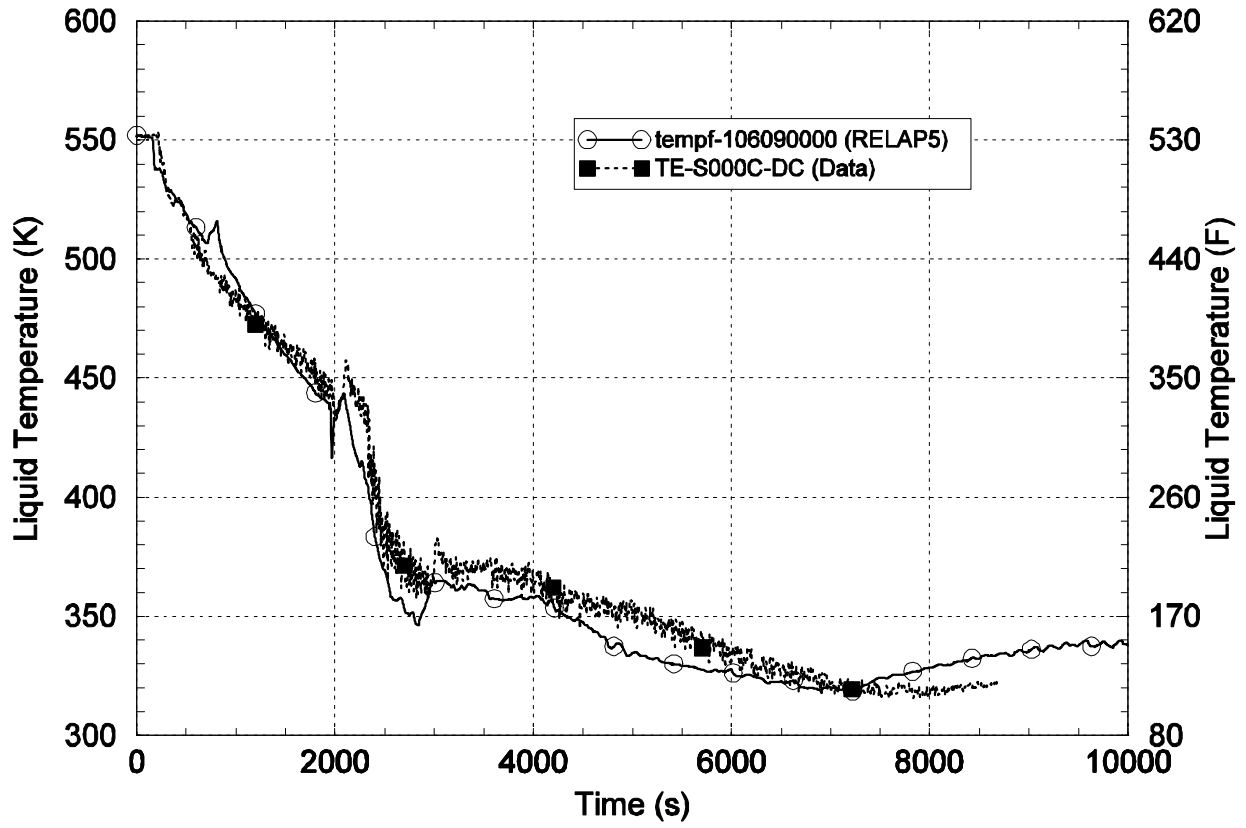


Figure B-20 ROSA/AP600 AP-CL-09 Downcomer Temperature at Bottom-of-Core Elevation

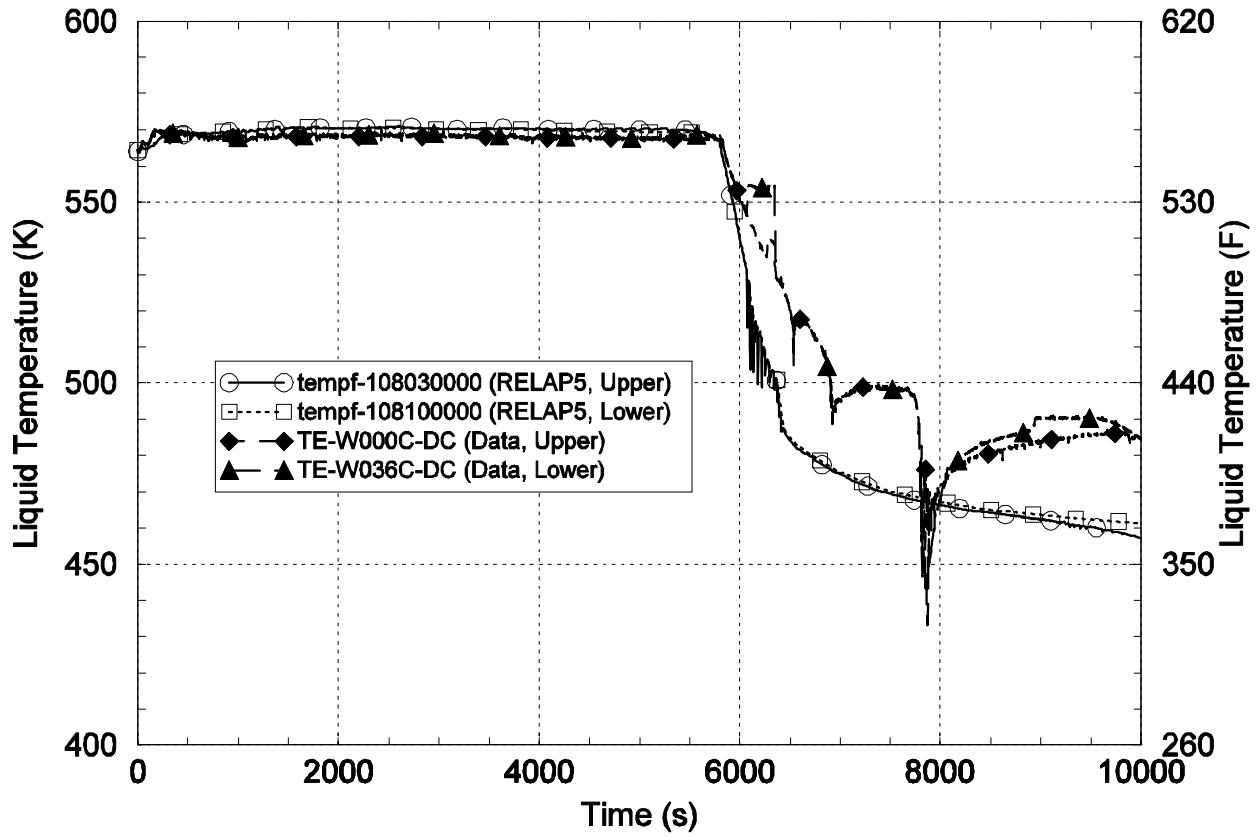


Figure B-21 ROSA-IV HL-06 Downcomer Temperature Comparing Top and Bottom of Core Elevations

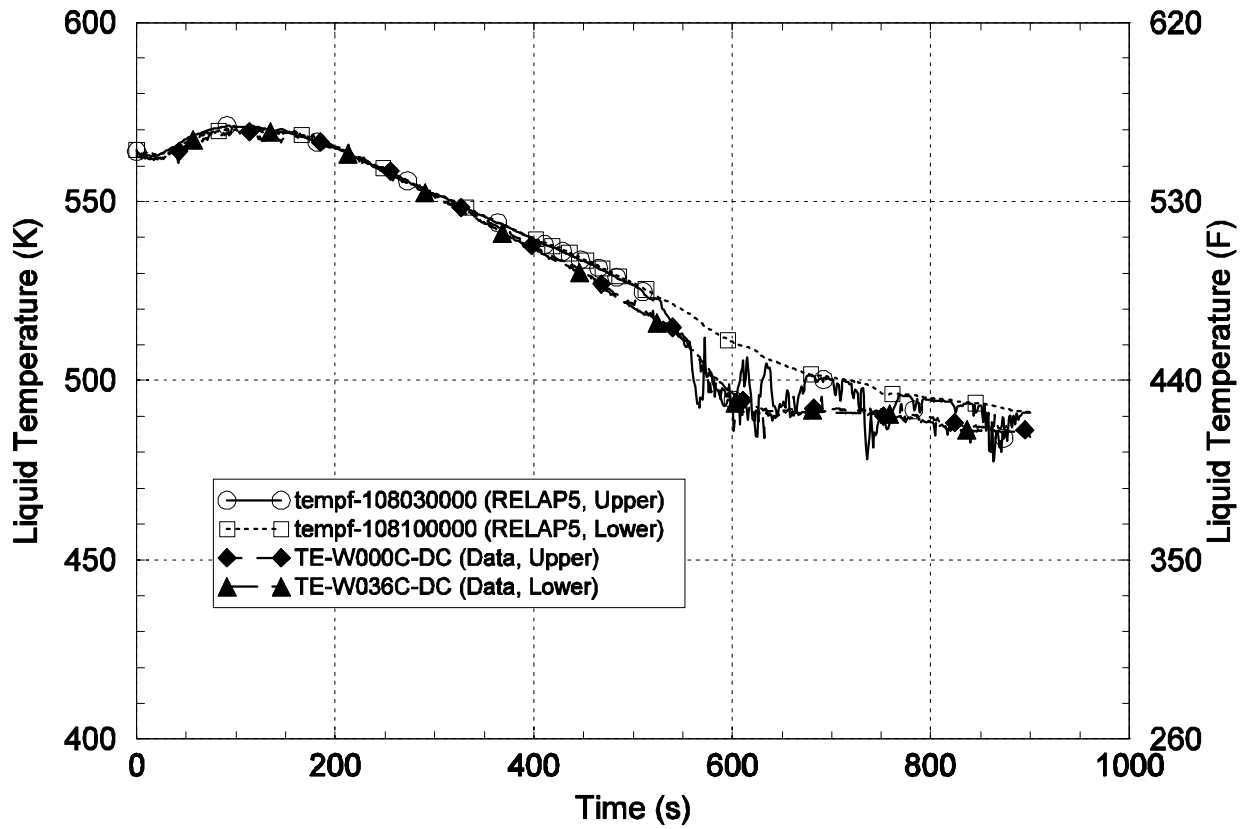


Figure B-22 ROSA-IV CL-18 Downcomer Temperature Comparing Top and Bottom of Core Elevations

B.6 LOFT

LOFT was a full pressure, full temperature, 1:50 volume scale facility [15]. The power-to-volume ratio was maintained at 1:1. The major design attributes of interest are listed in Table B-12, in comparison to the full scale prototype.

LOFT had two loops, one of which was the intact loop, which was sized to represent three loops in a Westinghouse 4-loop plant. The intact cold leg diameter was 0.28 m (11-inch). The second loop was the broken loop, sized to represent one loop in a Westinghouse 4-loop plant. ECC injection was into the intact loop; the injection rate represented 3/4 of total ECC injection in the plant. Breaks were located in the broken loop.

Comparing LOFT to the prototype, the axial aspect ratio of the downcomer was 3.7:1, meaning the downcomer was “elongated” with respect to the plant. The circumferential aspect ratio was 1:1, which indicates that the extent of azimuthal mixing should be similar.

LOFT had two downcomer thermocouple stalks, one located near the intact cold leg, and the other located near the broken cold leg (Table B-13). Stalk 1 was at 110° and the broken loop cold leg was at 136°. Stalk 2 was at 290° and the intact loop cold leg was at 316°. The stalks, therefore, were 26° from the cold legs, which in azimuthal distance was 0.20 m (8-inches). This is equal to two D_H -DC, that is, the stalks were located two downcomer hydraulic diameters away from being directly below the center of the cold leg. Elevation 2 (TE-1ST-2, TE-2ST-2) was approximately eight D_H -DC below the cold leg, compared to 3 D_H -DC in the prototype. At eight diameters down and two diameters laterally, if a plume existed it should have been recorded at this location.

Three LOFT tests were examined to assess RELAP5 to predict RCS pressure and downcomer temperature, representing a small break, medium break, and large break.

- L3-7 was a 1-inch cold leg break in which the RCPs were tripped at 36s. HPI flow began at 63 s, was shut off at 1800 s, and reinstated at 5975 s.
- L3-1 was a 4-inch cold leg break.
- L2-5 was a 200% cold leg break

These three experiments were included in the set used to establish the accuracy and uncertainty for RELAP5 to predict nominal downcomer temperature and RCS pressure. Figure B-23 compares RELAP5 calculated downcomer temperature to the experimental data for L3-7 (one-inch break). The temperature data shown are from two elevations, just below the cold leg (2 D_H -DC) and near the middle of the downcomer (26 D_H -DC). Both azimuthal locations are shown. The maximum temperature variation is within 5C, showing the downcomer to be well mixed.

Figure B-24 shows the cold leg temperatures for L3-1, a 4-inch cold leg break. The cold leg thermocouple rake is located between the injection nozzle and the reactor vessel. The data show up to 200C temperature gradient across the 28 cm (11-inch) diameter cold leg. The maximum possible gradient is ~265C. Despite the temperature gradient, the downcomer is seen to have a uniform temperature distribution. This shows that cold leg stratification is not indicative of downcomer nonuniformities. The degree of cold leg stratification is quite similar to that seen in ROSA.

Figure B-25 shows downcomer axial and azimuthal temperature distribution for L3-1 (4-inch cold leg break) at three elevations: just below the cold leg, near the middle of the downcomer, and near the bottom of the downcomer. Both azimuthal locations are shown. The data show the downcomer to be well mixed, with maximum temperature variations of ~2C.

Figure B-26 shows downcomer fluid temperatures for L2-5 (large cold leg break). The data shown are from the stalk located near the broken cold leg, at three elevations: just below the cold leg, near the middle of the downcomer, and near the bottom of the downcomer. The data show the downcomer to have a uniform axial temperature distribution.

To conclude

- ***LOFT data are consistent with ROSA and APEX. Large temperature gradients occur in the cold leg, but no significant axial or azimuthal temperature variations were observed in the downcomer.***

Table B-12 Comparison of LOFT to Westinghouse 4-Loop Plant

Attribute	LOFT	Plant	Ratio
Primary System Volume, m ³	7.896	347	1:44
Vessel Volume	2.943	131.7	1:45
Downcomer Volume	0.564	31.58	1:56
Cold Leg Volume	0.333	2.777	1:8.3
Loop Seal+ RCP Volume	0.535	4.064	1:7.6
Downcomer Flow Area, m ²	0.225	3.38	1:15
Downcomer Gap, m	0.051	0.26	1:5.2
D _{CL} /D _{H-DC} (downcomer)	2.79	1.34	2.1:1
Downcomer Circumference, m	2.795	14.71	1:5.3
Lower Plenum Volume, m ³	0.564	29.62	1:53
DC aspect ratio axial	36.6	10	1:0.27
DC aspect ratio azimuthal	27.4	28.3	1:1.3
ECC nozzle to vessel, m	1.01	3.86	1:3.8
ECC nozzle to vessel L/D _{ECC}	11.6	14.5	1:1.3
ECC nozzle to vessel L/D _{CL}	3.6	5.5	1:1.5
ECC ID, cm	8.73	27.3	1:3
ECC area, cm ²	59.83	585.1	1:10
Vessel Inner Diameter, m	1.457	4.794	1:3.3
Vessel wall thickness, m		0.22	
Bottom of core, m	0	0	NA
D _{H-DC} CL-C _L to bottom of core	37	10	4:1
Top of core, m	1.68	3.66	1:2.2
D _{H-DC} CL-C _L to top of core	20	3	7:1
CL-Top of Core L/R _{CL}	14.5	4.6	3:1
Cold leg Centerline, m	3.735	5.238	1:1.4
Cold Leg Area, m ²	0.0634	0.3825	1:6
Cold Leg Diameter, m	0.2842	0.698	1:2.5
Bottom of Lower Plenum, m	-1.248	-1.259	1:1

cold leg area ratio based on 3 cold legs in prototype

Table B-13 LOFT Downcomer Temperature Measurements

DC Stalk 1	DC Stalk 2	Elevation	$x D_H$ -DC
TE-1ST-1	TE-2ST-1	3.560 m	1.7
TE-1ST-2	TE-2ST-2	2.951 m	7.7
TE-1ST-3	TE-2ST-3	2.341 m	14
TE-1ST-4	TE-2ST-4	1.731 m	20
TE-1ST-5	TE-2ST-5	1.122 m	26
TE-1ST-6	TE-2ST-6	0.512 m	
TE-1ST-7	TE-2ST-7	-0.402 m	
TE-1ST-8	TE-2ST-8	-0.504 m	
TE-1ST-9	TE-2ST-9	-0.605 m	
TE-1ST-10	TE-2ST-10	-0.707 m	

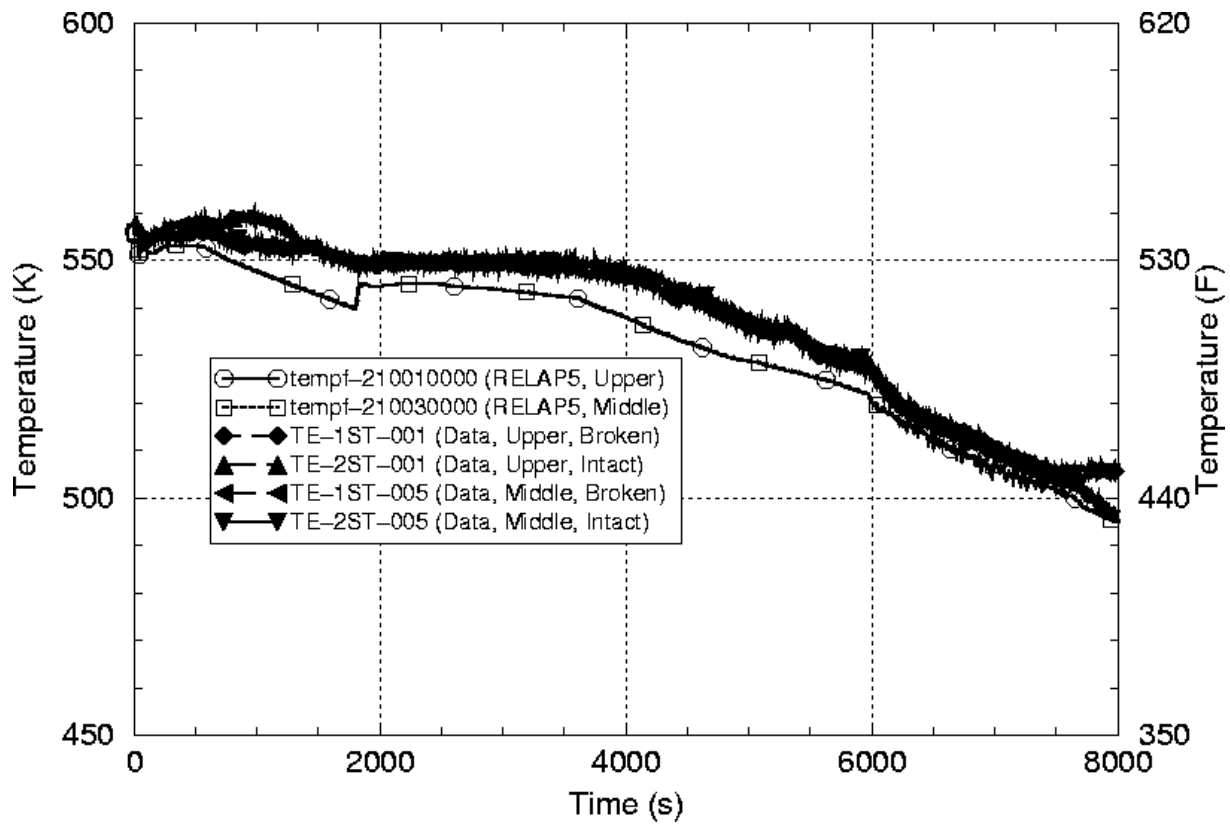


Figure B-23 LOFT L3-7 Azimuthal and Axial Downcomer Temperatures: Elevations Just Below Cold Leg (ST-1) and at Middle of Downcomer (ST-5)

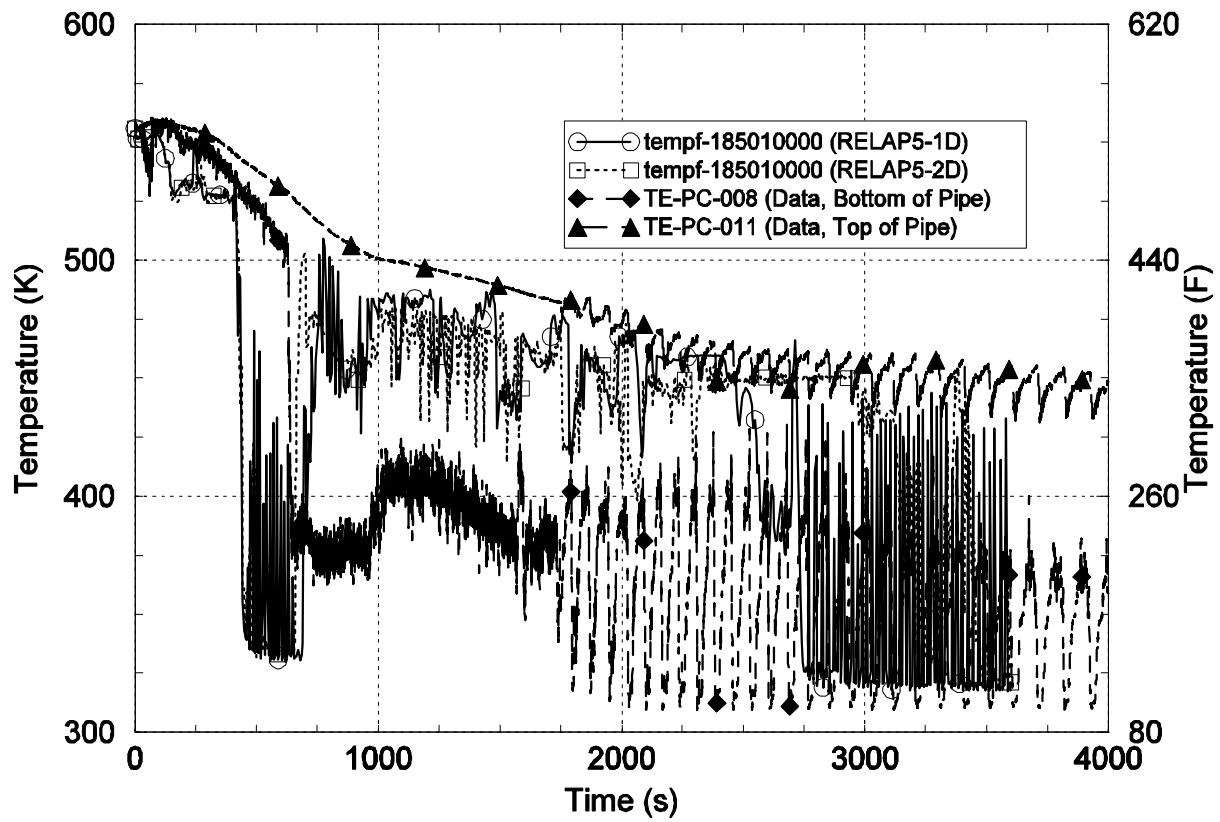


Figure B-24 LOFT L3-1 Cold Leg Temperature Profile

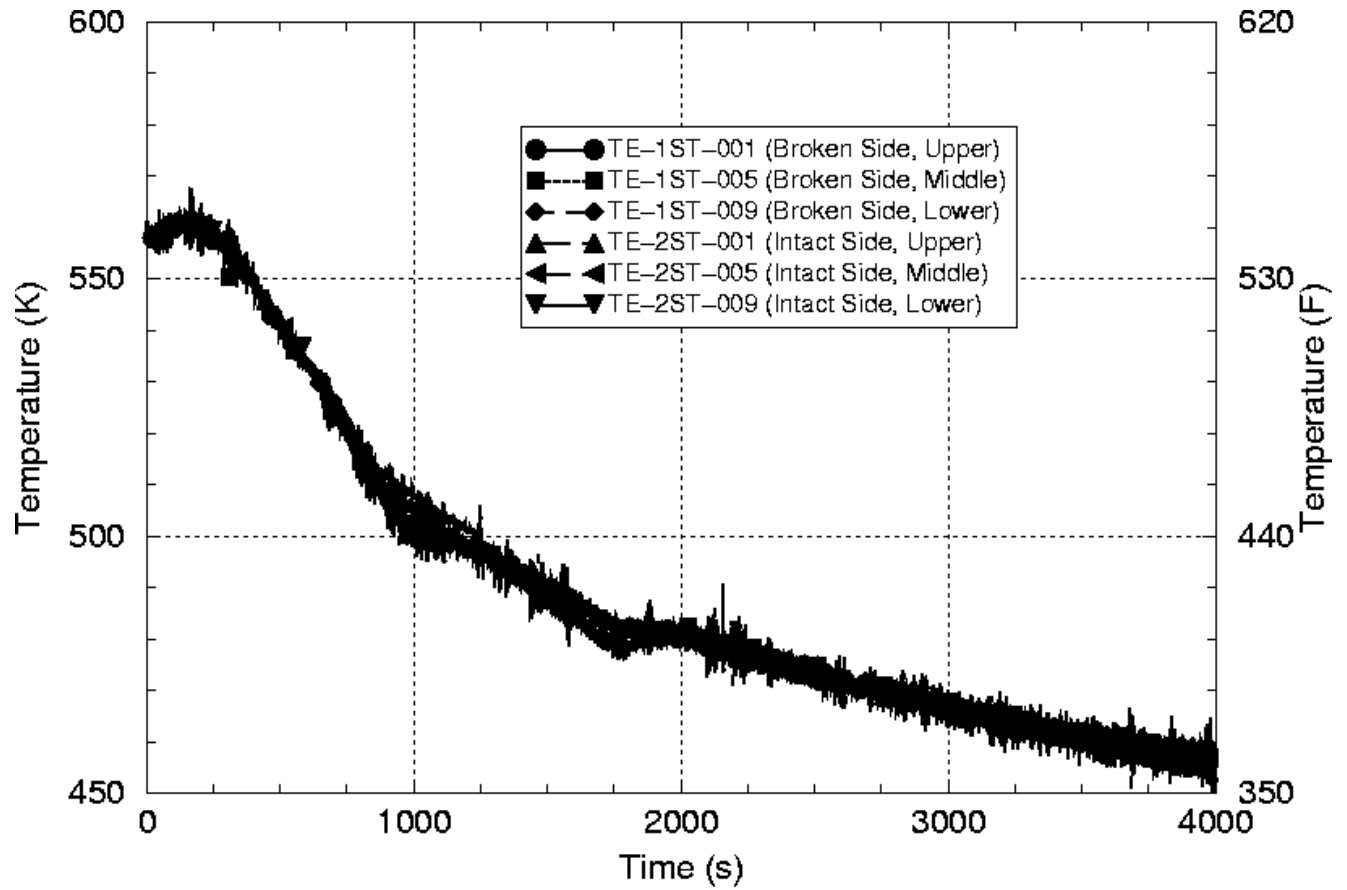


Figure B-25 LOFT L3-1 Downcomer Temperatures Axial and Azimuthal Distribution

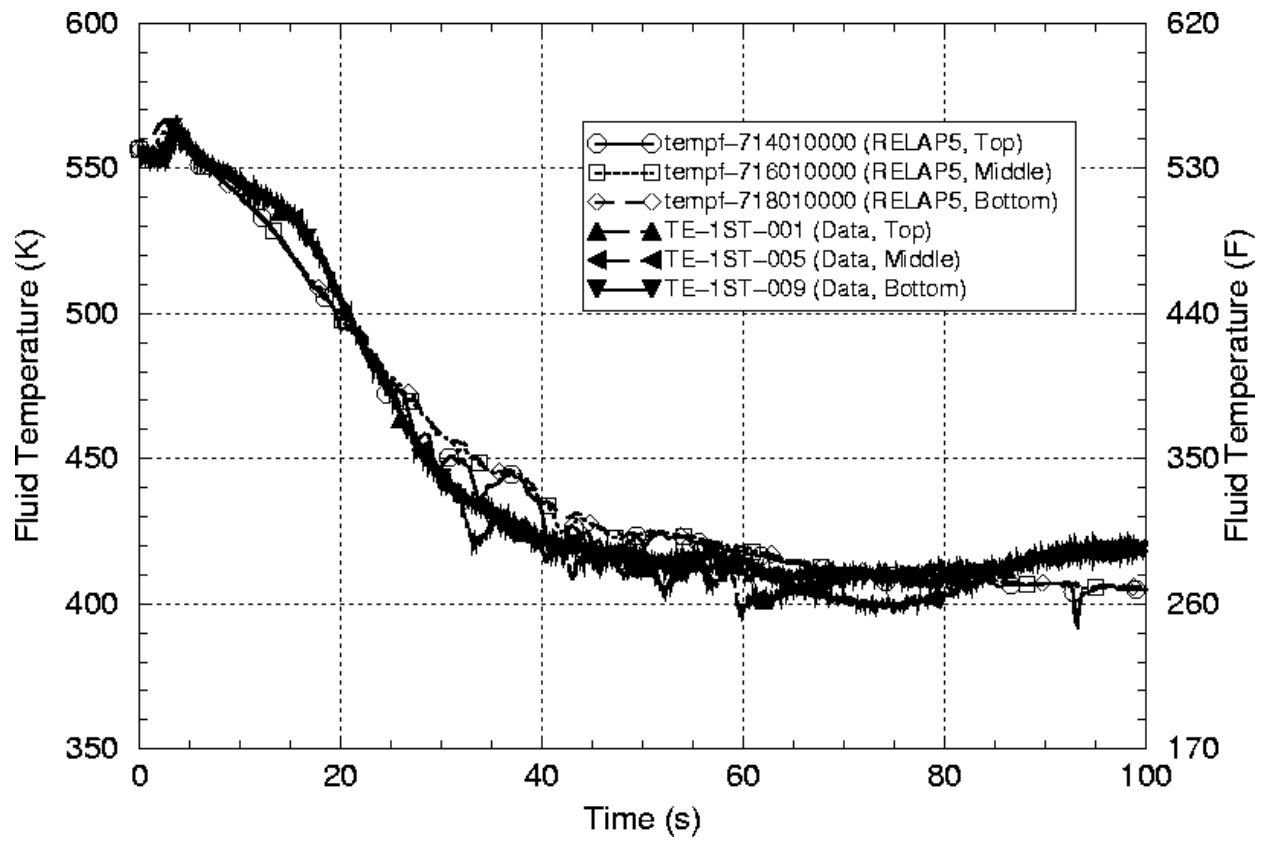


Figure B-26 LOFT L2-5 Axial Downcomer Temperatures; Data from Near Top, Middle, and Bottom of Downcomer

B.7 Upper Plenum Test Facility

The Upper Plenum Test Facility (UPTF) was a full scale model of the RCS of a KWU 1300 MWe PWR, operated as part of the 2D/3D program [16, 17]. UPTF had four hot legs and four cold legs. The core was simulated with a controlled injection of steam and water supplied from external sources. The facility operated at a maximum pressure of 1.8 MPa (265 psi), and corresponding temperature of 207C. These temperatures and pressures are less than prototypic, and are similar to the Creare ½ scale test facility. Table B-14 compares UPTF to Palisades for some key dimensions.

Eight thermocouple rakes were located in the downcomer, one below each hot and cold leg. Downcomer temperatures were measured at 11 axial elevations and the eight azimuthal locations. The frequency of data recording was 2 Hz.

One experiment, Test 1, was devoted to the study of fluid mixing under PTS conditions. The objective was to obtain data on the fluid mixing of a cold stream of injected emergency core coolant (ECC) with the hot primary fluid. No core heat was supplied during the experiments. All four cold legs are blanked off where the RCPs would normally be located, so the loop seal mixing volume was not available during the tests. The injection took place in a single cold leg. The vessel and loops were filled initially with stagnant hot water. The injection was into cold leg 2. The test conduct was similar to the Creare test MAY105 and MAY106, and to APEX-CE test 5, which were discussed above.

UPTF Test 1 actually consisted of five experiments, in which five ECC injection rates were used as listed below:

Test	HPI Injection, kg/s	u_{ECC}
Run 23	5	0.25
Run 26	10	0.50
Run 25	20	1.0
Run 21	40	2.0
Run 20	70	3.5

Because of the orientation of the HPI nozzle in UPTF, there is no possibility of buoyancy induced back flow and mixing in the HPI line. For the same injection rate, the HPI liquid velocity was 2.9 times greater in UPTF than Palisades because of the smaller nozzle flow area. The range of injection velocities expected in Palisades (and Beaver Valley) is 0.2 to 0.35 m/s, corresponding to injection flows of 10 to 20 kg/s per cold leg.

As expected, the experiments showed a high mixing zone at the injection location and the development of stratification in the cold leg. The colder water flowed along the bottom of the pipe towards the reactor vessel, while the warmer water flowed in the counter direction along the top of the pipe. By the time the flow reached the thermocouple rake in the cold leg nearest the vessel, the temperature was between 150C to 180C for the run 23. Therefore, of the order of 50% mixing was achieved in the cold leg, which is greater than observed in the other facilities.

The maximum plume strength seen in the Run 21 was ~20C in the early part of the transient. By 1500s it had decreased to ~10C, which is the definition of the threshold for considering a temperature variation in the downcomer to qualify as a plume.

Because there was only one plume, there are two zones in the downcomer to consider; (1) beneath cold leg 2, and (2) the balance of the downcomer. Figure B-27 shows the downcomer vessel inside wall temperature at the top-of-core elevation, representative of the balance of the downcomer. Figure B-28 is the vessel inside wall temperature below cold leg 2, which had the ECC injection. Wall temperatures track fluid temperatures. The injection started at 243s. The data show that there a sharp drop in downcomer temperature of ~20C upon the start of ECC injection. There is evidently a period of time required to build up a buoyancy force and to overcome the inertia of the stagnant fluid.

The maximum temperature difference occurred early in the experiment following the start of HPI injection. The initial plume strength was ~20C, which is similar to that observed in the Creare tests.

The plume strength diminishes as the transient proceeds as the ambient downcomer temperature decreases. After ~1000s it is down to ~10C, which is the definition of the minimum temperature difference to be considered a plume.

Table B-14 Comparison of UPTF to Palisades

Attribute	UPTF	Palisades	Ratio UPTF/Palisades
HPI injection line ID	0.159 m	0.271 m	0.59
Cold leg ID	0.750 m	0.7576 m	0.99
Downcomer gap	0.250 m	0.243 m	1.03
Vessel ID	4.870 m	5.202 m	0.94
Vessel wall thickness	5.8 cm	20 cm	0.29
Cold leg center to top of core	1.633 m	1.836 m (2.42 CLD)	0.89
Initial temperature	195C (374F)	285C	0.42 (density)
Injection temperature	33C	20C	

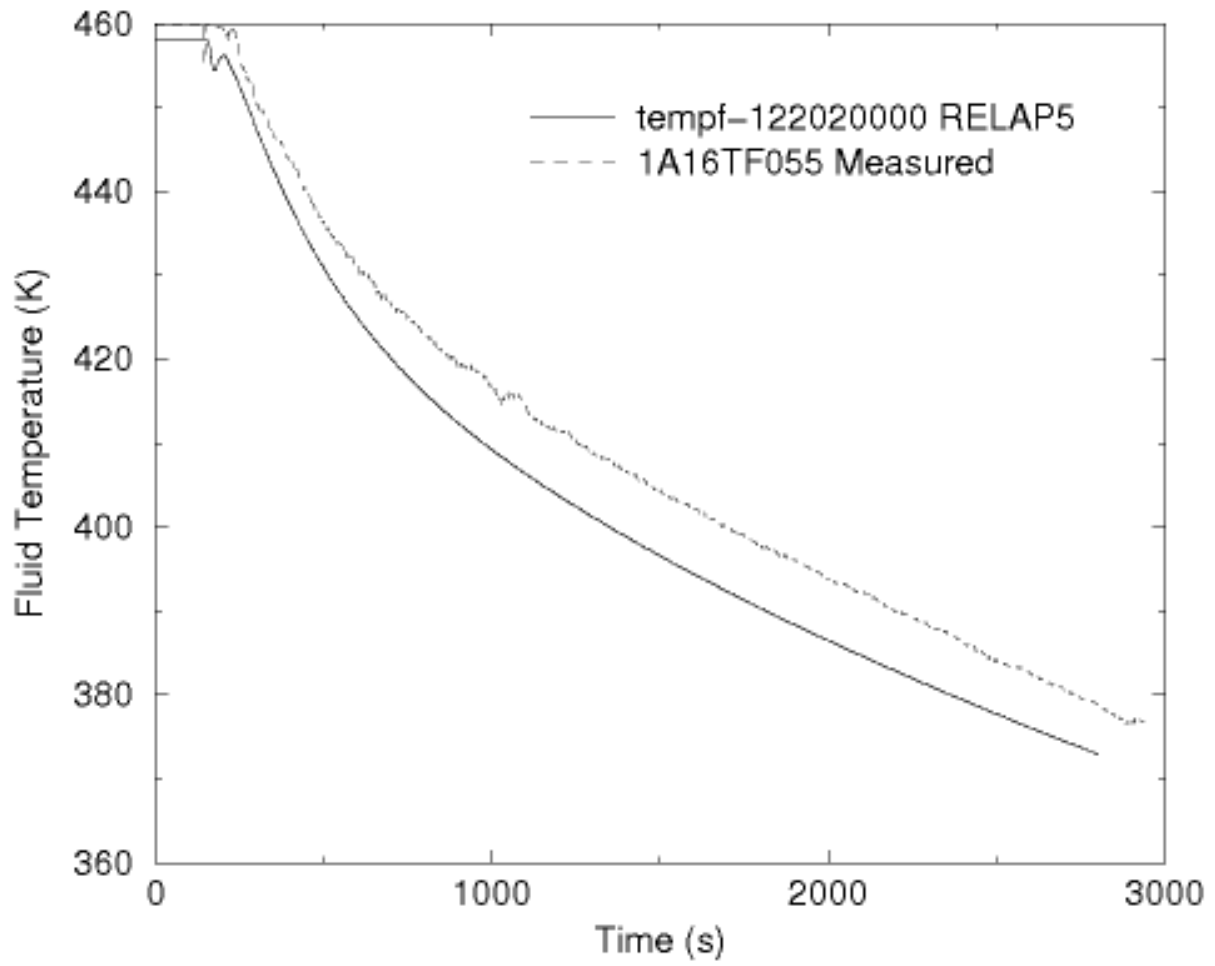


Figure B-27 UPTF 1-21 Downcomer Fluid Temperatures, Core-Top Elevation, Orientation in Direction of Hot Leg 2

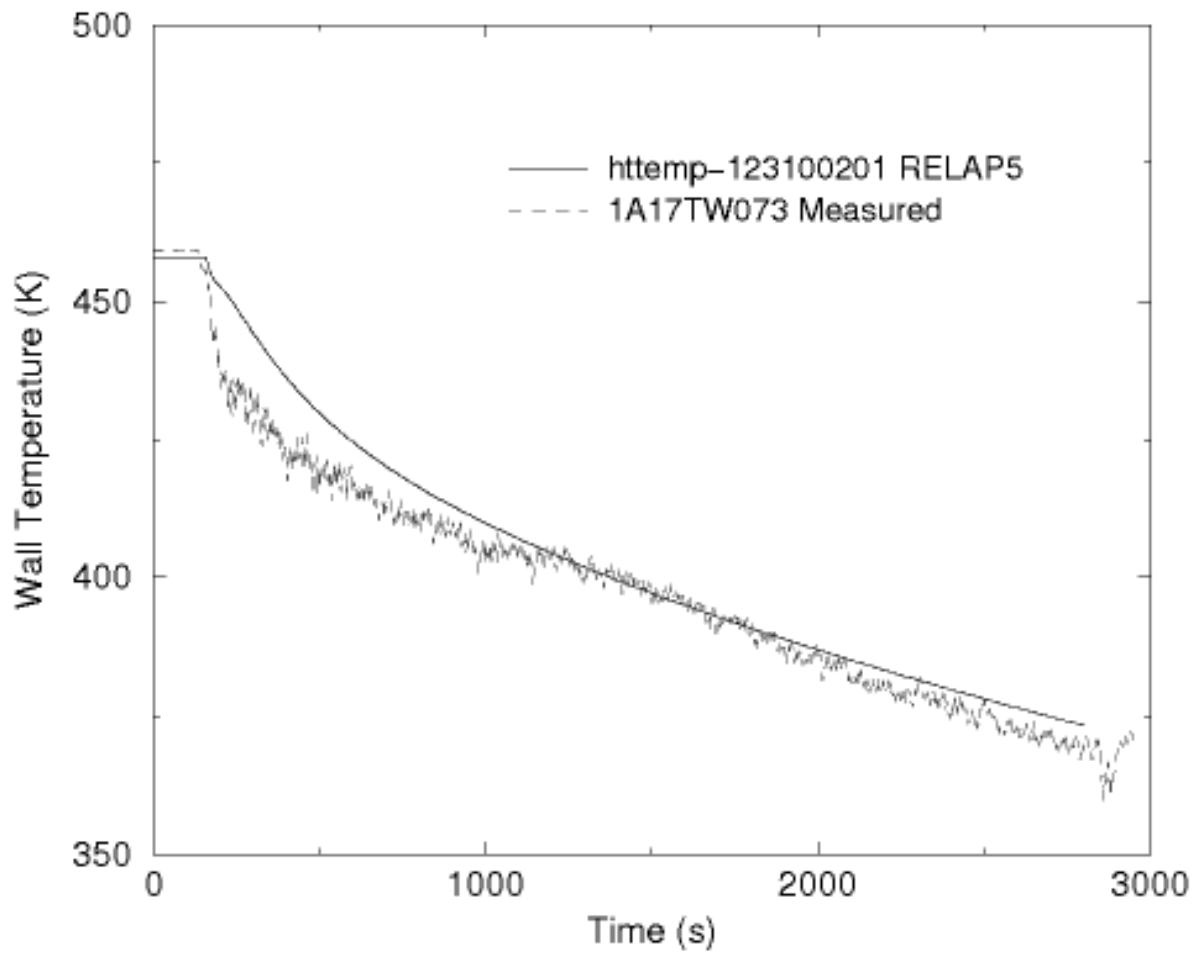


Figure B-28 UPTF 1-21 DC Inside Wall Surface Temperatures Core-Top Elevation, Orientation in Direction of Cold Leg 2

B.8 REMIX

REMIX, which was developed by Theofanous and Nourbakhsh [47, 48], is intended to calculate thermal mixing of water injected into the cold leg following loop flow stagnation. REMIX employs a control volume approach dividing the relevant part of the primary system, shown in Figure B-1, into mixing zones consisting of the cold leg, loop seal, and downcomer. with models for jet mixing at the ECC injection location. Below the cold leg, a free plume decay model is used.

A complicated three dimensional mixing region exists where the flow enters the downcomer from the cold leg. A simple mixing assumption is used at the junction between the cold leg and the downcomer, where the cold leg flow with an equal volume of fluid from the downcomer. This provides the initial planer plume temperature to the downcomer plume. The length scale for the planer plume in the downcomer is the cold leg diameter. The planer plume has an initial width of D_{CL} and $Fr = 1$. This gives an initial velocity of 2.5 m/s. The plume adjusts itself so that it has a $Fr = 0.5$ as it forms a planer plume in the downcomer. REMIX was not designed to take into account the effect due to interaction/merging of multiple plumes.

REMIX has been successfully benchmarked against fluid mixing data for separate effects tests from Creare, Purdue, HDR, IVO, and UPTF [24, 44]. REMIX was found to be conservative with respect to comparisons with data.

REMIX was used to model APEX-CE tests 4, 5 and 6. The results indicated that REMIX significantly under predicted the downcomer temperatures. This conservative effect was attributed to the selection of the wall heat transfer coefficient model in REMIX.

REMIX was used to calculate downcomer temperatures for Palisades. Some results are shown in Figures B-29 to B-31. The predictions are shown for the downcomer at an elevation of 5 feet below the cold leg, which is just above the top of the core. The initial conditions for the calculations were 285C (545F). Three comparisons are shown:

- Low temperature (40F) HPI injection, low loop flow (Figure B-29)
- Low temperature (40F) HPI injection, loop flow equal to HPI flow (Figure B-30)
- High temperature (140F) HPI injection, low loop flow (Figure B-31)

The REMIX calculations indicate a maximum plume strength of $\sim 20C$ ($\sim 40F$). This is similar to the maximum plume strengths seen in separate effects tests in UPTF and Creare. In integral system tests in APEX-CE, ROSA, and LOFT, no plumes were found.

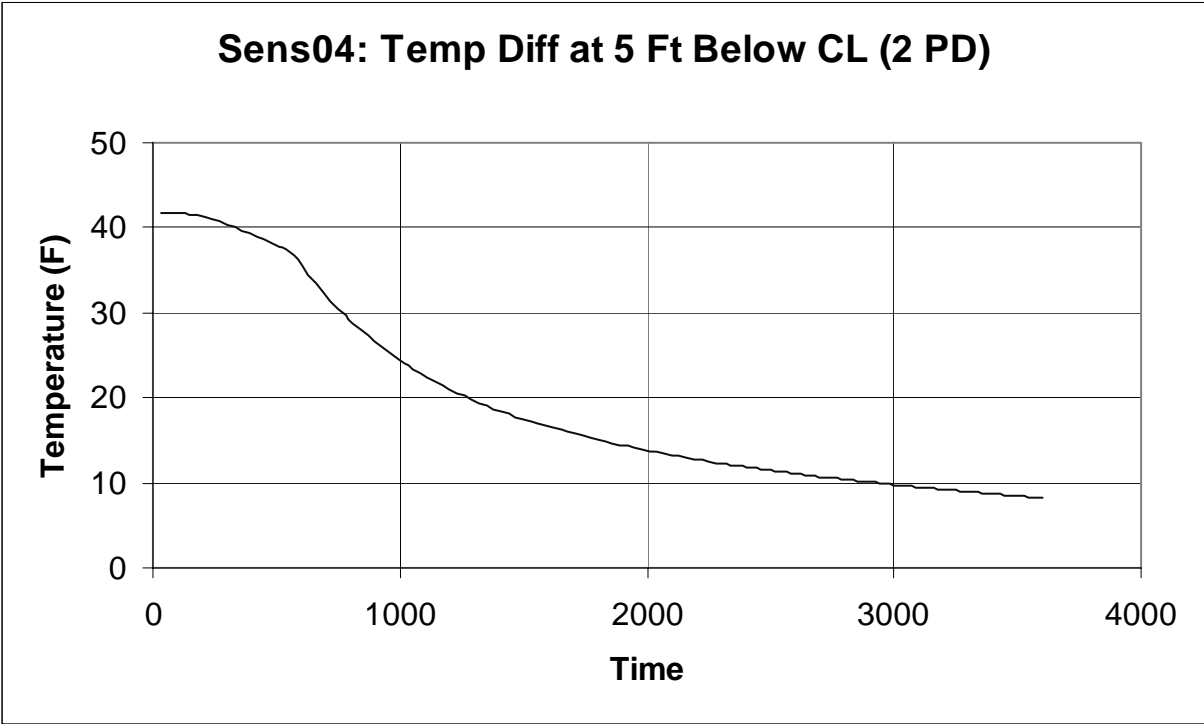


Figure B-29 REMIX Calculation of Palisades , HPI Flow 17 kg/s, Loop Flow: 4.4 kg/s, HPI Temp 5C (40F)

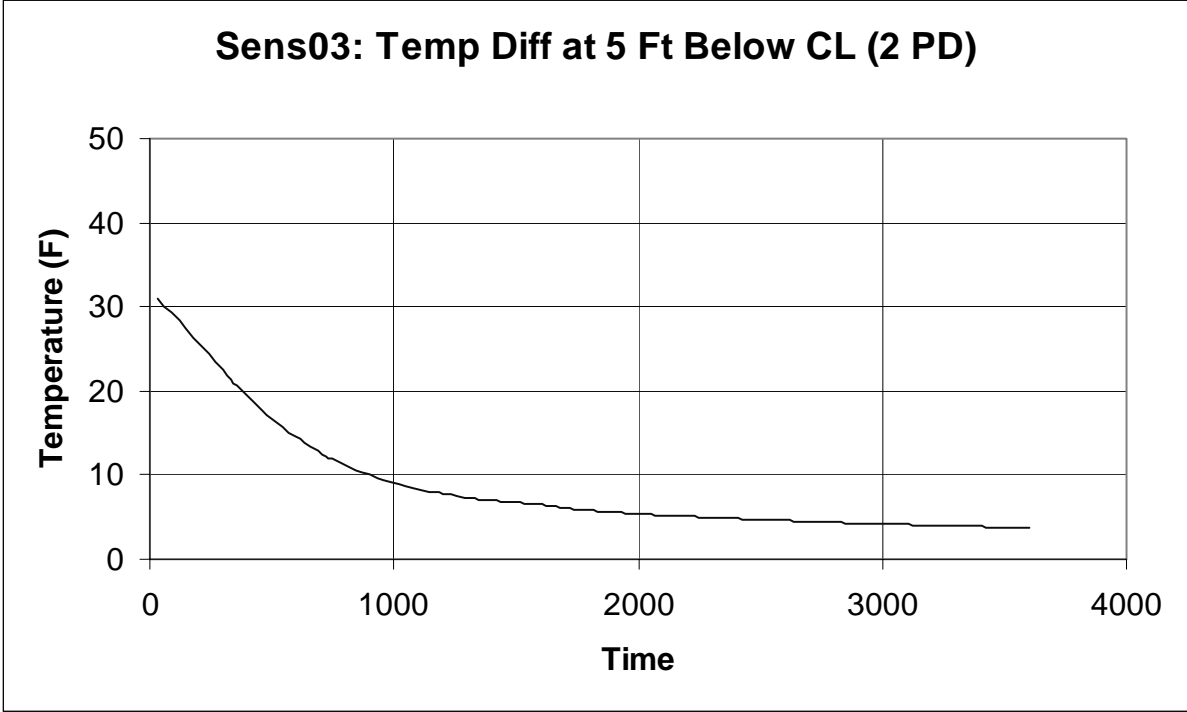


Figure B-30 REMIX Calculation of Palisades, HPI Flow = 7 kg/s, Loop Flow = 17 kg/s, HPI Temp = C (40F)

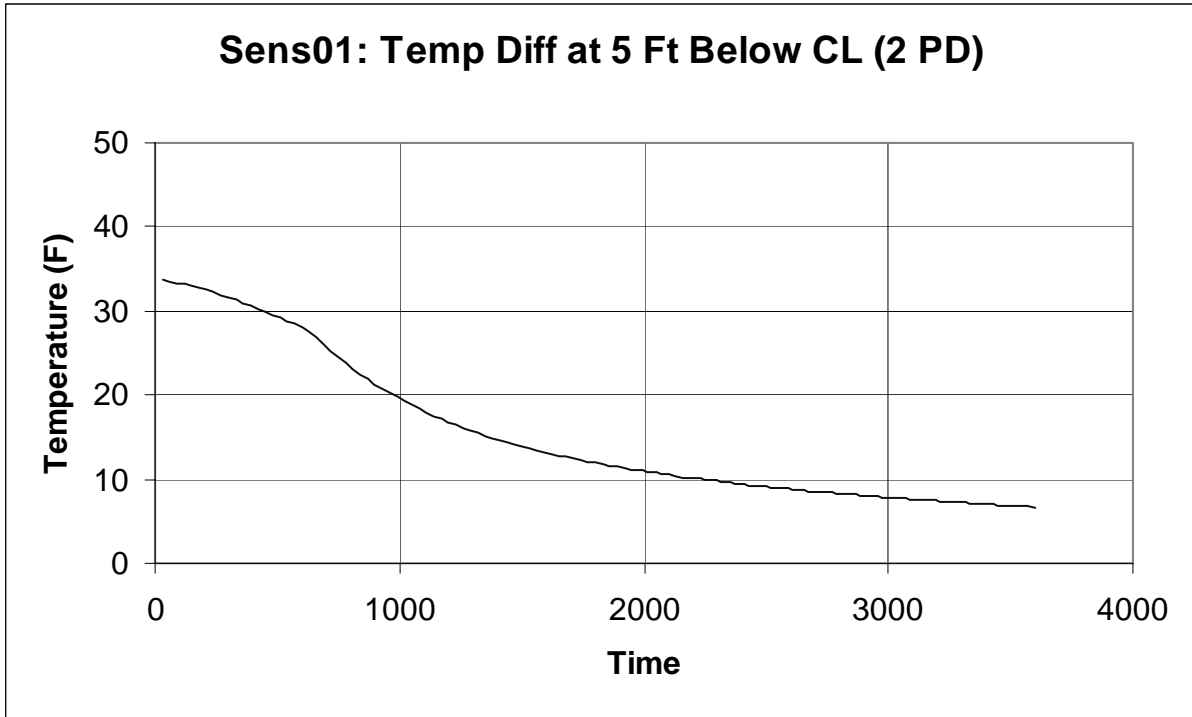


Figure B-31 REMIX Calculation of Palisades, HPI Flow 17 kg/s, Loop Flow 4.4 kg/s, HPI Temp 60C (140F)

APPENDIX C. NUMERICS

Two separate numerical circulation issues were observed in the RELAP5 simulations for PTS sequences. One related to circulations within relatively open regions that are nodalized using a multidimensional scheme (i.e. the downcomer). Separate but related is RELAP5's neglect of momentum flux in the cross flow direction in a two dimensional nodalization.

The other issue related to circulating flows through identical, parallel pipes within a flow network. The issue arose in RELAP5 simulations of LOCA event sequences for Oconee and Palisades. When the reactor coolant pumps are tripped and the loss of primary coolant system inventory is sufficient to interrupt coolant loop natural circulation flow, circulating flow was observed between the two cold legs on the same coolant loop. Note that both the Oconee and Palisades plants have a "2x4" configuration with two cold legs and one hot leg in each coolant loop. In contrast, the Beaver Valley plant has a single hot and cold leg per coolant loop and this type of circulating flow is not possible.

The circulation mixes coolant in the reactor vessel downcomer, cold leg and SG outlet plenum regions. When the circulation is present the calculated reactor vessel downcomer fluid temperature benefits from the warming effects created by mixing the cold HPI fluid with the warm steam generator outlet plenum fluid. When the circulation is not present the calculated reactor vessel downcomer fluid temperature more directly feels the influence of the cold HPI fluid. This mixing is not entirely unphysical. Certainly, the cold leg loop seal volumes are part of the mixing region under these circumstances, as modeled by the REMIX code, and illustrated in Figure B-1.

These two issues are discussed below. The numerical methods used in RELAP5 are documented in [49].

C.1 Circulation Within Open Regions Nodalized Using a Multidimensional Scheme

RELAP5 cross-flow modeling has been used at various times for various studies, going back to the 1970s when RELAP4 was in use. One recent major study was for AP600 analyses. The two dimensional modeling was used in several regions where two-dimensional flow were expected to be important, including the core and upper plenum, the In-Containment Refueling Water Storage Tank, and the downcomer.

Nonphysical recirculating single-phase and two-phase flows resulted. The nodalizations were converted to a one-dimensional scheme, with the exception of the downcomer. As a short term solution to reduce the development of circulating flows, the momentum flux terms for cross-flow between parallel channels were set to zero in the downcomer. This reduced the flow circulation by a factor of about 10,000. Three root causes for the circulation were identified in order of importance:

- (1) The manner in which the downward velocity was computed for inclusion in the momentum flux terms;
- (2) The value of the distribution coefficient (c_0) in the drift flux model and its values for special cases that include low flow and single-phase liquid; and

(3) Very large coefficients in the difference momentum equation for single-phase flow.

Fixes for the three root causes were developed, and evaluated with a number of test problems, including specific AP600 applications in which the problems were observed. These evaluations indicated that the three fixes were effective in preventing the circulations for those specific cases.

Flow circulation emerged again during the current PTS analyses. The particular problem was in the downcomer when a two-phase mixture level existed following the blowdown during large break LOCAs. Similar to AP600, the fix was to turn off momentum flux in the downcomer.

C.1.1 One Dimensional Versus Two Dimensional Downcomer

The PTS studies, and the related RELAP5 assessments, used two dimensional noding schemes in the downcomer. Questions were raised concerning the two dimensional representation of the downcomer in the RELAP5 plant models used in the PTS analyses. In particular, the one dimensional formulation does not include terms for cross-flow of momentum. An argument was advanced that the TRAC code might provide a better representation of downcomer flows, however, the TRAC code (like RELAP5) does not represent fluid-fluid shear forces between adjacent fluid nodes.

In the IPTS study of the early 1980s, the RELAP5 model of Calvert Cliffs used a one dimensional downcomer. It was observed that injection of HPI caused oscillations in flows. The effect was diminished when the downcomer was changed to a 2D representation, and disappeared when the HPI injection was changed to the downcomer. The two dimensional downcomer presents a degree of freedom to the flow.

These oscillations, on the average did not affect the downcomer temperature. The downcomer temperature oscillated in phase with the cold leg oscillations, however, if the mean was used, this value compared well with the calculation that employed a 2-D downcomer and direct vessel injection. When a mean value was drawn through the flow oscillations, it tended to represent a reasonable calculation of the "real" mass flow rate.

In the current study, thermal hydraulic sensitivity studies were performed using RELAP5 with respect to downcomer nodalization and downcomer momentum flux. The twelve risk dominant transients for Palisades, listed in Table C-1, served as the basis for comparisons. The fracture mechanics analyses were performed with FAVOR using the Palisades vessel, at an embrittlement corresponding to 60 EFPY. The RELAP5 sensitivity studies were supplied as boundary conditions to FAVOR, in the usual manner. The conditional probability of vessel failure (CPF) determined by FAVOR was used as the figure of merit for determining the effect of the different variables.

Table C-1 Palisades Transients Used as Basis for Sensitivity Studies

Case	Transient	Initiating frequency
19	1 SG ADV stuck open	2.3 E-3
40	16-inch HL LOCA	3.2 E-5
52	1 SG ADV stuck open	6.4 E-4
54	MSLB	4.3 E-6
55	2 SG ADVs stuck open	2.7 E-4
58	4-inch CL LOCA winter	2.7 E-4
59	4-inch CL LOCA summer	2.1 E-4
60	2-inch HL LOCA winter	2.1 E-4
62	8-inch CL LOCA winter	7.1 E-6
63	5.7 inch CL LOCA winter	6.1 E-6
64	4-inch HL LOCA summer	7.1 E-6
65	SRV recloses @ 6000s	1.2 E-4

The effect of downcomer nodalization was investigated to compare the 2-dimensional (2D) approach adopted for the PTS studies, with a single channel 1-dimensional (1D) approach. The overall CPF decreased by a factor of 1.4 when a 1D downcomer was used, as compared to the base case 2D downcomer. For hot leg breaks, little difference was seen between the two nodalizations. For cold leg break LOCAs, however, the difference was significant. Using a 1D downcomer, cold leg breaks decreased in importance. This was due to increased bypass of ECC injected flow towards the break, which is favored when a 1D downcomer is used. The 2D downcomer is physically more realistic because it allows a degree of freedom for flow between the cold legs and the lower plenum.

The largest variations observed among all of the cases were between the original and 1D calculations for the cold leg breaks (2, 2.8, and 4-inch breaks). For hot leg breaks, the ECC water flows into and through the downcomer and core to reach the break. With the cold leg breaks, the flow that goes out the break does not actually flow through the core. The hydraulic effects of this difference are significant because with the hot leg breaks the ECC continually flows through the downcomer and core and out the break while with the cold leg breaks the ECC mainly flows out the break (with only a little of the ECC water finding its way into the downcomer and core).

The flow pattern between the downcomer and the lower plenum/core region for the 1D calculation is noisier relative to the flow from the 2D calculation. It is this behavior difference that appears to cause the differences in many parameters between the original and 1D cases. The 2D nodalization exhibited a circulating well-mixed downcomer region. The 1D case causes an oscillating manometer flow situation to develop, with numerical mixing during oscillations into and out of the core. Downcomer temperatures for the 1D case show the downcomer heats up significantly during the time periods when the manometer oscillations are the greatest and vice versa.

Downcomer flows may be downwards near the intact cold legs, and upwards near the broken cold leg. Such flow patterns were commonly observed in large cold leg break experiments in UPTF. Naturally, use of a 1D downcomer precludes two dimensional flows. As a result, the 1D downcomer nodalization produced an average CPF for cold leg breaks that was more than a factor of 1000 lower than for the 2D downcomer.

Table C-2 shows the effect on the conditional probability of vessel failure for the individual transients. Taking into account the event frequencies, the overall calculated risk decreased by a factor of 1.4 when a 1D downcomer was used, as compared to the base case 2D downcomer. For hot leg breaks and secondary side breaks, the outcome is unchanged. The ratio of the conditional probability of vessel failure between the 2D and 1D cases was,

$$\frac{CPF_{2D}}{CPF_{1D}} = 0.93$$

For cold leg breaks, the one-dimensional nodalization results in considerably lower probability of vessel failure,

$$\frac{CPF_{2D}}{CPF_{1D}} = 7E6$$

Table C-2 Comparison 1D and 2D Downcomer Models Used in RELAP5

#	Transient	Mean event frequency	CPF 2D	CPF 1D	CPF _{2D} /CPF _{1D}
19	ADV stuck open	2.3 x 10 ⁻³	1.4 x 10 ⁻⁷	1.1 x 10 ⁻⁷	1.2
40	16-inch HL LOCA	3.2 x 10 ⁻⁵	5.2 x 10 ⁻⁵	3.0 x 10 ⁻⁵	1.7
52	ADV stuck open	6.4 x 10 ⁻⁴	1.4 x 10 ⁻⁷	2.1 x 10 ⁻⁷	0.7
54	MSLB	4.3 x 10 ⁻⁶	6.7 x 10 ⁻⁵	4.4 x 10 ⁻⁵	1.5
55	2 ADVs stuck open	2.7 x 10 ⁻⁴	4.2 x 10 ⁻⁷	4.8 x 10 ⁻⁷	0.9
58	4-inch CL LOCA winter	2.7 x 10 ⁻⁴	7.5 x 10 ⁻⁵	2.2 x 10 ⁻⁹	3.4 x 10 ⁴
59	4-inch CL LOCA summer	2.1 x 10 ⁻⁴	3.2 x 10 ⁻⁷	2.4 x 10 ⁻⁹	135
60	2-inch HL LOCA winter	2.1 x 10 ⁻⁴	2.7 x 10 ⁻⁶	9.3 x 10 ⁻⁶	0.3
62	8-inch CL LOCA winter	7.1 x 10 ⁻⁶	3.9 x 10 ⁻⁵	1.8 x 10 ⁻⁷	220
63	5.7 inch CL LOCA winter	6.1 x 10 ⁻⁶	1.5 x 10 ⁻⁴	5.4 x 10 ⁻¹¹	2.8 x 10 ⁷
64	4-inch HL LOCA summer	7.1 x 10 ⁻⁶	5.6 x 10 ⁻⁵	1.6 x 10 ⁻⁴	0.4
65	SRV reclose 6000s	1.2 x 10 ⁻⁴	6.8 x 10 ⁻⁵	9.7 x 10 ⁻⁵	0.7

Cold leg break LOCAs should not be analyzed using a one-dimensional downcomer nodalization. (It is interesting to note that studies conducted by Sandia National Laboratory for NRR in the 1980 time frame using RELAP4/MOD5 reached the same conclusion). Such a formulation means that the cold ECC injected flow is bypassed to the break through the upper downcomer instead of being allowed to flow to the lower downcomer. The downcomer temperatures, therefore, remain significantly warmer when a 1D model is used.

C.1.2 Momentum Flux

The PTS studies were performed with momentum flux off in the downcomer. While unphysical flow recirculation generally did not occur with momentum flux on, to ensure that it did not occur the calculations were mostly performed with momentum flux off. It should be noted that the flow recirculation in the downcomer is a **physically real phenomena**, as seen in the experiments. The characteristic downcomer velocities during loop flow stagnation are typically in the range of 0.3 m/s

to 1.5 m/s. The intent was to avoid situations where numerical effects outweighed the physical forces being calculated by the code.

To assess the use of the 2D downcomer, sensitivity studies were run with respect to momentum flux. The sensitivity study was based on the entire set of 75 Oconee PTS scenarios, which were calculated in two ways: (1) with ordinary flux of momentum in the downcomer nodes; and (2) with momentum flux disabled. Table C-3 shows results for the risk-significant scenarios.

Table C-3 Downcomer Momentum Flux Sensitivity Study Comparison of CPF

#	Transient	CPF		
		MF on	MF off	MF off/on
110	2-inch HL, no HPI, open TBV @ 900s	2.2×10^{-11}	1.7×10^{-7}	7748
122	SRV reclose @ 6000s, throttle HPI @ 10 min, HZP	1.3×10^{-5}	8.9×10^{-6}	0.68
124	SRV reclose @ 3000s, throttle HPI @ 10 min, HZP	3.5×10^{-7}	2.0×10^{-7}	0.57
141	3.22-inch HL	8.2×10^{-9}	3.2×10^{-10}	0.04
156	16-inch HL	5.4×10^{-5}	7.2×10^{-9}	1.3×10^{-4}
160	5.656-inch HL	7.1×10^{-7}	9.5×10^{-8}	0.13
164	8-inch HL	5.1×10^{-8}	1.9×10^{-8}	0.37
165	SRV reclose @ 6000s, HZP	1.5×10^{-5}	1.0×10^{-5}	0.67
168	SRV reclose @ 3000s, HZP	5.1×10^{-7}	4.5×10^{-7}	0.88
169	SRV valve size -30%, RVVV closed, summer, HZP	7.5×10^{-10}	9.5×10^{-10}	1.27
172	4-inch CL,	2.6×10^{-7}	2.0×10^{-7}	0.77
	Total CPF	8.7×10^{-5}	2.0×10^{-5}	0.23

MF Momentum Flux

Most transients were not significantly affected, with overall CPF reduced by 1/3 when momentum flux was disabled in the downcomer. The difference was attributable to one specific transient, a 16-inch hot leg break LOCA.

Most of the transients showed similar behavior, with the general trend being towards lower CPFs with momentum flux off compared to on. This is to be expected since disabling momentum flux removes a potential numerical driving "force." Discounting two transients that experienced a large change in CPF (156, 110), the CPF for the remaining transients is 1/3 higher with momentum flux on compared to off.

$$\frac{CPF_{MF\ on}}{CPF_{MF\ off}} = 1.5$$

Overall, the CPF was a factor of four higher with momentum flux on.

$$\frac{CPF_{MF\ on}}{CPF_{MF\ off}} = 4.3$$

As noted, two transients experienced a large change in CPF (O-156 and O-110). O-156 is a large break (16-inch) LOCA, for which the CPF was a factor of 1000 lower with momentum flux off. This was the one transient in particular that had exhibited excessive downcomer circulation when momentum flux was on, which was the impetus for the study.

Oconee 110 was a 2-inch surge line break with HPI failure. After 900s, the operator opened the two steam dump valves to lower primary system pressure and initiate accumulator and low pressure injection. The two sensitivity calculations compared very closely for this transient, with almost no noticeable differences. At approximately 1830s, however, in the case with momentum flux off, the RCS pressure decreased slightly more than the case with momentum flux on. The slight difference in pressure occurred when RCS pressure was ~200 psi for both calculations. The small difference was enough, however, to allow substantial LPI injection in one case but not the other (LPI shutoff head = 200 psi). The difference in LPI injection flows caused a significant difference in downcomer temperature, which caused the difference in CPF.

- ***This particular transient is an excellent example of divergent, nearly bifurcating behavior that can occur as a results of plant design feature such as: relief valve set points, level control, pressure control, pump shutoff heads, accumulator pressure, and so on.***

In summary, most transients were not affected significantly by whether momentum flux was on or off in the downcomer, indicating that the numerical effect was generally absent for a wide range of transients. The only exception was the large break LOCA.

The second case affected (O-110) was the result of a small difference that resulted in divergent response due to the LPI shutoff head. This is an example of amplification that can occur in analyses, and which reflects true reality in plant behavior. The remainder of the 75 Oconee PTS scenarios were unaffected.

C.2 Circulation Through Identical, Parallel, Vertical Pipes within a Flow Network

The second circulation problem concerns flow through identical, liquid-filled, parallel paths in a piping network. For the current PTS analysis, the relevance of this problem is the modeling of the cold leg regions of plants with two hot legs and four cold legs, namely plants of B&W and CE designs.

The cold leg flow circulation was identified at least as far back as 1984 in the Oconee analysis of the original IPTS study [29, pp. 88-90]. The code version at the time was RELAP5/MOD1.5. It is reasonable to presume, and routinely observed, that physically real differences exist in any flow network which can, given the right circumstances, result in physical flow instability. In a code model, this is not the case because the two cold legs are identical. Numerics, therefore, was suspected as the genesis of the temperature imbalance. The original Oconee PTS study concluded the circulation was initiated by numerics, but sustained by physical driving forces.

During preliminary calculations for the current PTS study, cold leg flow circulation were observed in RELAP5 calculations of Palisades (CE) and Oconee (B&W). Both the RELAP5 and TRAC-M codes predicted a similar flow pattern in the reactor cold legs for the 2-in surge-line break transient (see Figures C-1 and C-2). In these figures the loops are designated A and B and the cold legs as 1 and 2.

The flow began following draining of the steam generator. When the draining flows ended, there were no driving forces other than the ECC injection flows. The pair of cold legs attached to the same steam generator began to flow in a circular loop.

The flows bring the loop seals and lower parts of the steam generator into a common mixing volume with the cold legs, downcomer and lower plenum. In addition, the HPI water in the cold legs with negative flow is entirely entrained towards the steam generators. The circulating flow promotes mixing and leads to higher downcomer temperatures.

The numerical flows only appear when physical driving forces become very small. They may appear any time parallel flow paths are attached on either end to a common plenum. In this situation, the pressure and buoyancy driving forces are equal for both flow paths. Such forces are also small or nonexistent under the circumstances. Numerical flows may be induced and, once, begun, become amplified by physical forces.

The computed flow rates in the cold legs were sufficiently high that, when compared to a relevant criterion for thermal stratification, the occurrence of a thermally stratified flow in the cold legs was precluded. The effect, therefore, was to introduce a possible non-conservative bias into the calculations.

Figure C-3 shows the effect on downcomer temperature by comparing calculations with and without cold leg circulating flows. The case shown is a RELAP5 calculation of a 2-inch surge line break in Oconee. Oconee is a 2 x 4 plant with two hot legs and four cold legs. Compared to the CE design, the B&W loop seal volume is a factor of 10 greater, because it encompassed the lower ~1/3 of the steam generator. In contrast, in CE plants the lower end of the steam generator is above the loop elevation. In the sensitivity study, (labeled "high RCPs rev. flow resis."), the reverse flow K-factor of the RCPs was increased substantially over its standard value (labeled "No RCPs rev. flow resis. *enhancement*"). The forward flow RCP K-factor was unchanged. The difference in downcomer temperature in this instance was 50K.

Figure C-4 plots the flows for two adjacent cold legs on one side of the reactor vessel. Similar flows occur for the same RELAP5 calculation for the opposite side of the reactor vessel. A TRAC-M calculation of the same Oconee 2-inch break case showed the same results. A base case and a sensitivity case study are shown. The plots show that the flow is from the steam generator towards the reactor vessel in one cold leg, and opposite in the other cold leg (from the reactor vessel towards the steam generator). The magnitude of the flow rate, ~200 kg/s, is a factor of 10 larger than the HPI injection flow rate (~15 kg/s per cold leg).

Given the necessary precondition of loop flow stagnation, the physical mechanism begins with the injection of cold water into both cold legs between the RCPs and reactor vessel. When the cold leg flow circulates, mixing of the cold leg fluids can occur both in the reactor vessel downcomer and in the steam generator outlet plenum that is shared by the two cold legs. Because the cold legs are liquid filled, an incipient asymmetry in the numerical solution can cause an imbalance in otherwise equal cold legs. The force balance may grow until flow reverses in one cold leg. In this situation, the fluid temperatures in the vertical sections of the cold legs are different, creating a buoyancy driving head that can sustain the circulating flow.

A necessary condition for a physical circulating flow to be developed and sustained is the existence of a gravitational head in the cold leg flow path. There are two ways this can happen. For B&W designs (Oconee), the steam generator outlet plenum is considerably lower (5 m) than the vessel entrance. In the CE design, the same condition is fulfilled by the loop seal geometry.

Either geometry can develop a *thermal center of cooling* that is higher than *thermal center of heating*. The *thermal center of cooling* is where the cold water from high pressure injection is mixed with the cold leg fluid. The *thermal center of heating* is where the flows of the two cold legs are mixed in the steam generator outlet plenum. The elevation of the steam generator outlet plenum is considerably lower than the elevation where the high pressure injection flow enters the cold legs. The density difference creates a physical, gravitational driving head to drive circulating flow around the loop.

Since the original PTS study, the problem of circulation through identical vertical flow paths connected at their tops and bottoms has been studied further. The direction of flow circulation was observed to reverse when the nodalization numbering scheme for the two pipes was reversed. In one particular comparison of RELAP5 and TRAC calculations, one code spun the flow clockwise, while the other spun it counterclockwise.

This confirmed the numerical nature of the circulation initiator. Further investigation into the numerical initiator indicated that flow first begins due to round-off errors (in the last digitally-stored significant digits) in the pressure solutions at the ends of the identical pipes.

- ***The numerical initiator is judged to be unavoidable when using a digital thermal hydraulic systems code.***

Because the flow circulation initiator was judged to be numerical and because situations where apparent non-physical numerical driving heads are present, for the current PTS study it was elected to prevent this cold leg circulating flow. This was accomplished by placing large reverse flow loss coefficients at the reactor coolant pump of the RELAP5 models for Palisades and Oconee. Forward flow was unaffected. This provided sufficient damping to prevent the establishment of numerical flows. This resistance only acts to prevent flows that tend to be unphysical to begin with. That is, there are no pressure or buoyancy driving forces that can produce such flows under the given circumstances.

On the other hand, this precludes the RELAP5 calculations from the benefit of fluid-fluid mixing in the loop seals. The loop seal volume is part of the mixing volume treated by the REMIX code. The use of the reverse flow damping in the RELAP5 models errs on the side of conservatism.

The conclusions are:

1. Circulating flows are not a new problem, and occurred in the original IPTS study.
 2. Circulating flows occurs in both TRAC and RELAP5
 3. Circulating flows may occur whenever the input model has a parallel flow path, and, the physical forces are small. That is, whenever natural circulation or flow stagnation exists.
 4. The output should be examined for numerical flows whenever the conditions in #3 exist.
- ***For all cases that are PTS significant and forced circulation is stopped, high RCP reverse flow resistance was used to suppress cold leg circulation. This is a conservative approach to prevent a source of mixing that may not be physically***

justifiable. To a degree, however, the mixing that occurs with cold leg circulation has a physical basis.

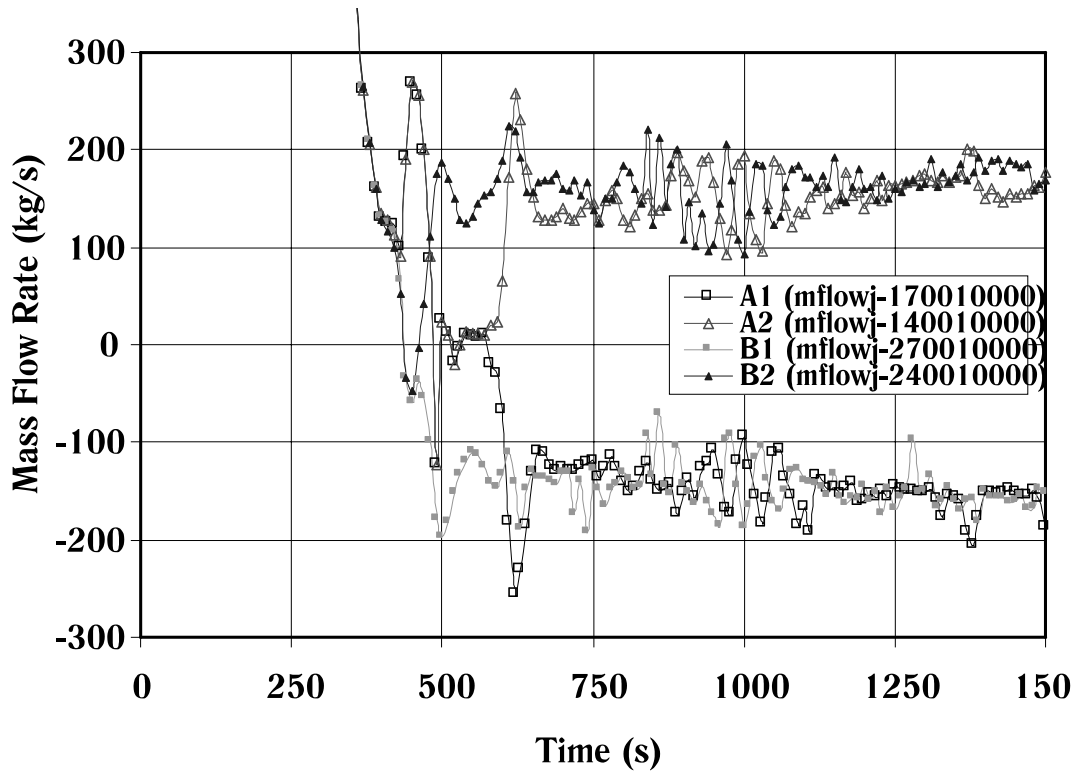


Figure C-1 RELAP5 Cold Leg Flow Rates in Both Loops Showing Circulation

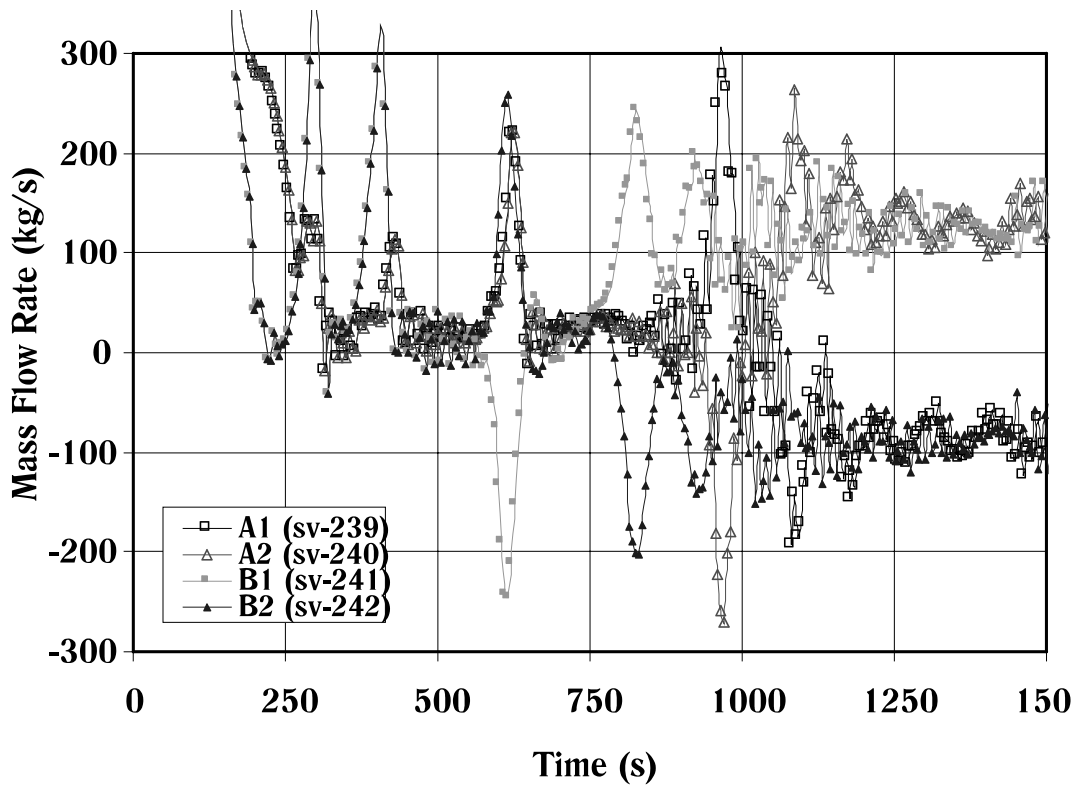


Figure C-2 TRAC-M Cold Leg Flow Rates in Both Loops Showing Circulation

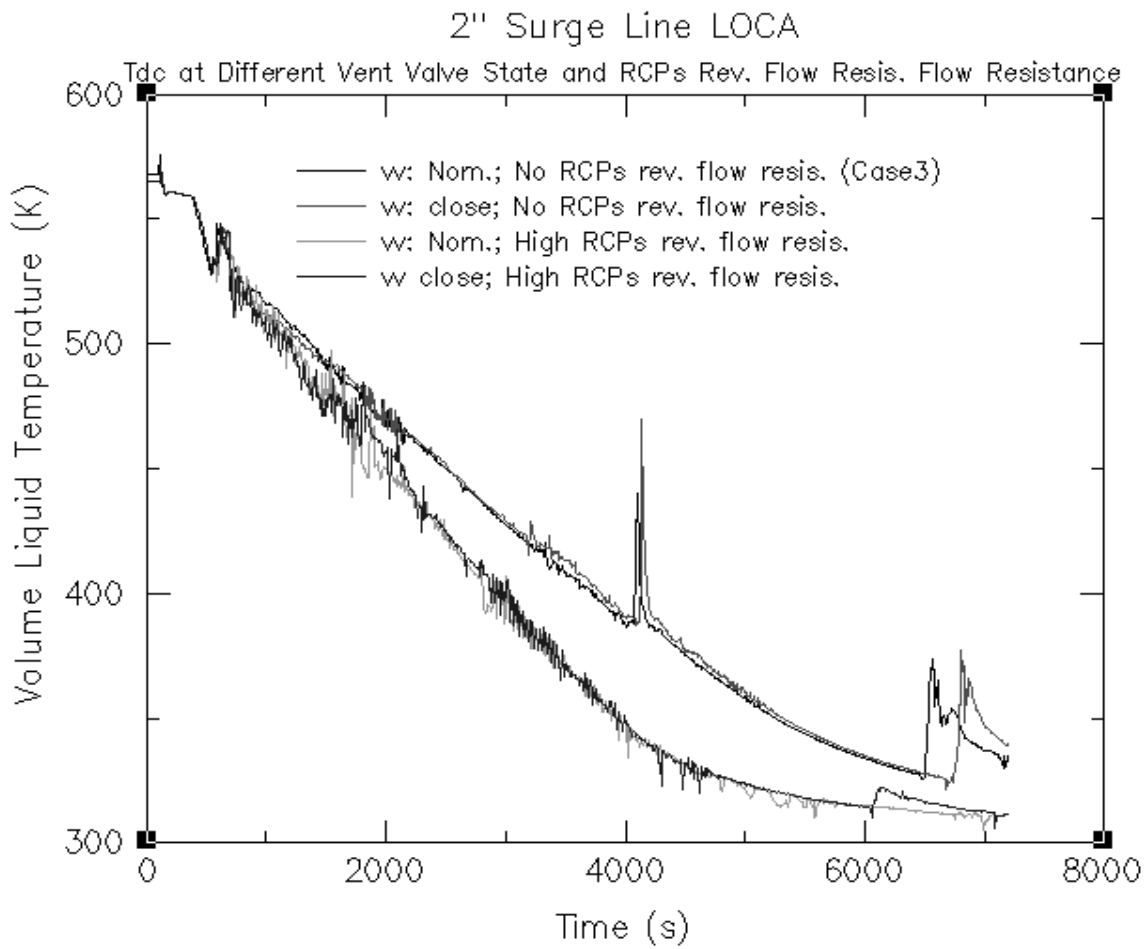


Figure C-3 Effect of Cold Leg Circulation on Downcomer Temperature

- Downcomer up to 50K colder when cold leg damping applied compared to no damping

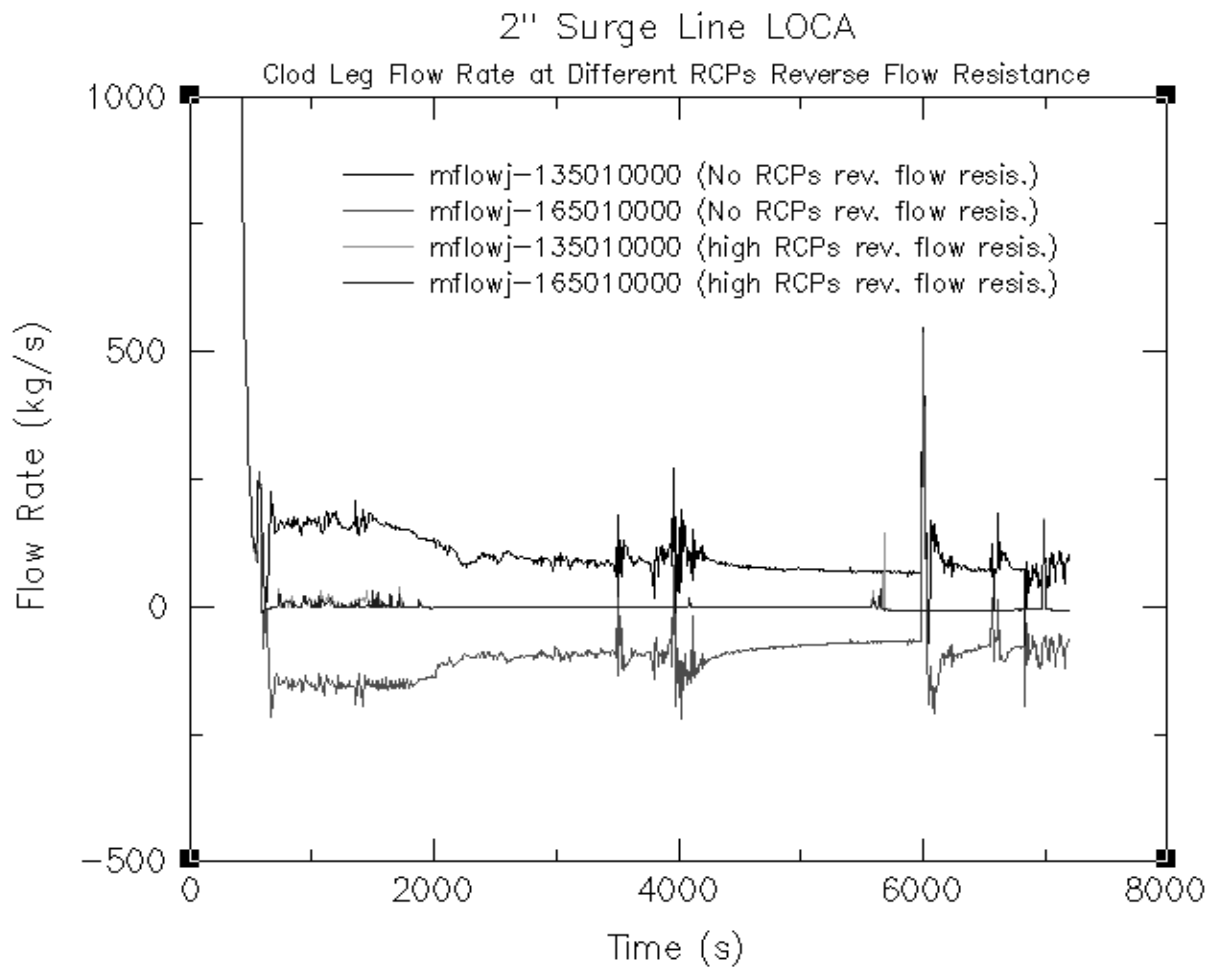


Figure C-4 Cold Leg Flow Rates With and Without Reverse Flow Damping

- Flow rates ~0 with damping applied, 200 to 300 kg/s without damping

APPENDIX D. QUALITATIVE ASSESSMENT CRITERIA

Judgements regarding RELAP5 accuracy for predicting physical phenomena are given based on criteria adopted by RES for this purpose and applied for various programs such as 2D/3D and AP600. While qualitative, the criteria have proven effective in achieving a level of standardization in communicating results of code qualifications. The criteria, which provide a useful perspective beyond the quantified comparison of time-averaged data, are

Excellent Code exhibits no deficiencies in modeling a given behavior. Major and minor phenomena and trends are predicted correctly. Calculated results agree closely with data. The calculation, with few exceptions, lies within uncertainty bands of the data. Code may be used with confidence in similar applications.

Major phenomena are those that influence key parameters, that is, high ranked PIRT phenomena. Minor phenomena are PIRT phenomena ranked medium or low.

Major trends means the prediction reproduces significant features of the data. Significant features means in turn the magnitude of a given parameter throughout the transient, including slopes (rates of change) and inflections points.

Reasonable Code exhibits minor deficiencies, but overall provides an acceptable prediction. Major phenomena and trends are predicted correctly. Differences between calculated results and data are greater than required for excellent agreement. Calculated results frequently lie outside but near the uncertainty bands of the data. Correct conclusions about phenomena and trends will be reached when the code is used in similar applications. Relevant physical models in the code as well as the input model for the experimental facility should be reviewed to see if improvements can be made.

Minimal Code exhibits significant deficiencies. Overall the code provides a prediction that is only conditionally acceptable. Some major phenomena and trends are not predicted correctly. Some calculated results lie considerably outside the uncertainty bands of the data. Incorrect conclusions about phenomena and trends may be reached when the code is used in similar applications. Relevant physical models in the code as well as the input model for the experimental facility must be reviewed and improvements made before the code can be used with confidence in similar applications.

Insufficient Code exhibits major deficiencies. The code provides an unacceptable prediction of the experiment. Major phenomena and trends are not predicted correctly. Most calculated results lie considerably outside the uncertainty bands of the data. Incorrect conclusions about phenomena and trends are probable when the code is used in similar applications. Relevant physical models in the code as well as the input model for the experimental facility must be reviewed and improvements made before the code can be used with confidence in similar applications.

APPENDIX E. RELAP5 ASSESSMENT COMPARISONS FOR REACTOR VESSEL DOWNCOMER PRESSURE AND FLUID TEMPERATURE

Figures E-1 through E-12 compare RELAP5 predictions of pressure and downcomer temperature for the experiments listed in Tables 4-2 and 4-3, used to determine statistical measures of RELAP5 bias and uncertainty. More complete information is found in [12], from which these results were taken.

Using the qualitative judgment criteria in Appendix D, the overall RELAP5 assessment results for reactor vessel downcomer pressure and fluid temperature are generally considered **excellent**. In certain time intervals, agreement for some phenomena may be considered **reasonable**. Differences between the code and the experimental data, where they occur, are attributed to the following:

- Facility input model: In some cases the magnitude and distribution of facility heat losses are not well known, or are suspect.
- Break flow: Generally break flow is predicted well. In a few cases there were discrepancies, due to uncertainties arising from upstream conditions. In some cases the break flow data are no longer available or are uncertain.
- Condensation during ECC injection. Larger break LOCAs generally result in condensation in the cold leg during ECC injection. The prediction of condensation under these circumstances is generally difficult, since several parameters are involved, most importantly, interfacial area.
- Experimental data uncertainty: Data are sometimes not available or are suspect. In such cases, the exact root cause of discrepancies remains in question.

ROSA-IV SB-CL-18

Figure E-1 plots results from ROSA-IV test SB-CL-18, a 6-inch diameter equivalent cold leg break with failure of HPI. The left hand plot compares downcomer temperatures from the experiment and RELAP5 results at the top and bottom core elevations. The right hand plot compares RCS pressure. Transition from natural circulation to loop flow stagnation was at 180 s in the experiment compared to 170 s in the RELAP5 calculation, which is good agreement.

Accumulator injection flow began at 455 s in the experiment compared to 470 s in RELAP5. Upon accumulator injection, the experimental data show a greater drop in downcomer temperature than RELAP5, due to more condensation during ECC injection in the experiment than was calculated by the code. This lowered the RCS pressure which caused more still more accumulator flow in the experiment. This demonstrates the feedback amplification effect that exists between condensation and the ECC injection flow rate.

For this experiment, RELAP5 had a bias of 2C in temperature with a standard deviation of 4C. RELAP5 had a bias of 0.14 MPa in pressure with a standard deviation of 0.27 MPa. The key

differences in the comparison of RELAP5 versus experiment for this test were due to: 1) the calculation of break flow; and 2) condensation during ECC injection.

ROSA-IV SB-HL-06

Figure E-2 plots results from ROSA-IV test SB-HL-06, a 2-inch diameter equivalent hot leg break with failure of HPI. The left plot compares downcomer temperatures from the experiment and RELAP5 results at the top and bottom core elevations. The right hand plot compares RCS pressure.

The gradual decrease in natural circulation flow was predicted well by RELAP5. The code predicted slightly earlier draining of the steam generator tubes, which resulted from an over prediction of break flow.

The PORV was opened at 5800 s in the experiment. The PORV size was scaled to 1.86-inches in diameter, so when it opened, the total break size was nearly doubled. This accounts for the decrease in temperature and pressure at that time. Previously, the RCS pressure was steady at the steam generator secondary side pressure. RELAP5 calculated a more rapid and larger decrease in RCS pressure than in the test upon opening of the PORV. This in turn caused more accumulator injection in the RELAP5 calculation. The difference in behavior originated because RELAP5 over predicted the break flow. This led to lower RCS inventory in the calculation. Therefore, when the PORV was opened the PORV flow was higher quality in the calculation, leading to the greater depressurization.

The sharp drop in downcomer temperature seen in the experiment at ~7800 s is due to condensation in the cold legs during ECC injection. There is a corresponding drop in pressure at this time. RELAP5 did not capture these phenomena.

For this experiment, RELAP5 had a bias of -9C in temperature with a standard deviation of 14C. RELAP5 had a bias of -0.38 MPa in pressure with a standard deviation of 0.66 MPa. The key differences in the comparison of RELAP5 versus experiment for this test were due to: 1) the calculation of break flow; and 2) condensation during ECC injection.

ROSA/AP600 AP-CL-03

Figure E-3 plots results from ROSA-AP600 Test AP-CL-03, a 1-inch diameter equivalent cold leg break. The left plot compares downcomer temperatures from the experiment and RELAP5 results at the top-of-core elevation. The right hand plot compares RCS pressure. This was a ROSA/AP600 experiment, so the test facility included the Passive Residual Heat Removal (PRHR), Core Makeup Tank (CMT), and Automatic Depressurization (ADS) system components.

During the early part of the transient, the downcomer is slightly colder in the test than in the calculation, due to colder PRHR return flow in the experiment. This in turn was due to lack of stratification modeling in the IRWST. Accumulator injection flow began at essentially the same time (1,900 s) in the calculation as in the experiment, since RCS pressure was in excellent agreement to that point. CMT draining began at the same time as well (2,200 s). CMT draining proceeded somewhat more rapidly in RELAP5 than in the experiment.

RELAP5 had an earlier opening of ADS1 (3,000 s) than the experiment (3,500 s) due to faster draining of the CMTs. This speeded up the progression of the transient in the calculation compared to the experiment. The discrepancy in temperatures beginning at ~3,800 s is due to the earlier opening of ADS4 in RELAP5 (3,850 s) compared to the experiment (4,450 s), which was due to somewhat faster draining of CMTs in the calculation. This led in turn to earlier IRWST injection in the calculation (4,250 s) than in the experiment (4,975 s). The same trends, however, are seen in the calculation and the experiment between 3,800 s and 5,500 s.

For this experiment, RELAP5 had a bias in temperature of 2C with a standard deviation of 25C. RELAP5 had a bias of 0.26 MPa in pressure with a standard deviation of 0.61 MPa. The key differences in the comparison of RELAP5 versus experiment for this test were due to calculation of the CMT draining rate, which in turn caused differences in the timing of ADS actuation.

ROSA/AP600 AP-CL-09

Figure E-4 plots results from ROSA/AP600 Test AP-CL-09, a 1-inch diameter equivalent cold leg break with failure of the CMTs and ½ of the ADS. The left plot compares downcomer temperatures from the experiment and RELAP5 results at the top-of-core elevation. The right hand plot compares RCS pressure.

The downcomer is slightly colder in the test than in the calculation, due to colder PRHR return flow in the experiment. This in turn was due to lack of stratification modeling in the RELAP5 model of the IRWST which caused the bottom of the tank to become warmer. The spike in temperature at 2000 s is due to opening of the ADS1 valve, which causes a surge in flow towards the pressurizer and a redistribution of inventory in the loops.

For this experiment, RELAP5 had a bias of 1C in temperature with a standard deviation of 9C. RELAP5 had a bias of 0.07 MPa in pressure with a standard deviation of 0.28 MPa. There were no significant discrepancies between the RELAP5 calculation and the data for this test.

APEX-CE-13

Figure E-5 plots results from APEX-CE Test 13, which simulated a stuck-open pressurizer safety relief valve that reclosed at 3,600 s. The temperature comparison on the left is for downcomer at the core mid-plane elevation. The RCS pressure comparison is on the right.

During the first ~1,000 s of the transient, the downcomer temperature is somewhat lower in the experiment than in the calculation. This is due to pressure being higher in the calculation, causing less HPI injection than in the experiment. After 1,300 s the situation begins to reverse. This pressure/temperature behavior is caused by differences between the code and experiment with respect to the steam generator secondary side. The differences in the secondary side calculation appear to be due to modeling limitations in the RELAP5 input deck for the APEX facility.

For this experiment, RELAP5 had a bias of -2C in temperature with a standard deviation of 8C. RELAP5 had a bias of -0.04 MPa in pressure with a standard deviation of 0.17 MPa.

APEX-CE-5

Figure E-6 plots results from APEX-CE Test 5, which simulates the cooldown of the reactor vessel due to HPI injection into a stagnant RCS. The temperature comparison on the left is for the downcomer at the mid-core elevation. The RCS pressure comparison is on the right.

There is good agreement in downcomer temperatures until ~2,200 s, at which time the RELAP5 temperature begins to fall below the measured temperature. The difference afterward results because RELAP5 cannot model the fluid-fluid mixing in the loop seal volumes. Therefore, the RELAP5 temperature becomes colder than the experiment. When large reverse flow losses were added to the RELAP5 model to limit loop recirculation, the magnitude of the RELAP5 downcomer temperature under prediction increased after 2,200 s. This indicates that the use of cold leg reverse flow damping in RELAP5 models is conservative. Doing so eliminates the loop seal as a mixing volume, leading to lower reactor vessel downcomer temperatures than are seen in the test.

For this experiment, RELAP5 had a bias of -5C in temperature with a standard deviation of 7C. RELAP5 had a bias of -0.15 MPa with a standard deviation of 0.05 MPa. The small differences between the code and data are believed to be due to loop seal behavior, including the inability to model fluid-fluid mixing. Since this degree of freedom does not exist in the code, there is a tendency for the code to calculate loop recirculation instead. When this recirculation is suppressed, the downcomer is somewhat cooler as a result.

LOFT L3-7

Figure E-7 plots results from LOFT Test L3-7, a 1-inch diameter equivalent cold leg break. HPI and AFW were stopped at 1,800 s; steam generator cooldown was begun at 3,600 s; HPI was restarted at 6,000 s. The temperature comparison is given on the left for two elevations in the downcomer. The RCS pressure comparison is on the right.

For this experiment, RELAP5 had a bias of -8C in temperature with a standard deviation of 4C. RELAP5 had a bias of -0.43 MPa in pressure with a standard deviation of 0.50 MPa. The temperature and pressure bias in this test are consistent. The differences between RELAP5 and the data appear to be due to modeling of the steam generator secondary side. RELAP5 appears to be giving too high a heat loss, which is a facility modeling issue for long transient tests such as this. The actual heat loss information for LOFT is not known with confidence.

LOFT L2-5

Figure E-8 plots results from LOFT Test L2-5, a large cold leg break LOCA. Temperature comparisons for three elevations in the downcomer are shown on the left. The RCS pressure comparison is on the right.

RELAP5 over predicted the depressurization rate between 10 s and 20 s. This was due to over prediction of the break flow quality. The difference in break flow quality is believed to be due to differences in upstream conditions of the break. That is, there was more upstream phase separation in the RELAP5 calculation than in the experiment, which caused the break flow to be higher quality, which therefore increased the energy removal from the RCS. The faster depressurization caused accumulator injection to start earlier in the calculation than in the test. This caused downcomer temperature to be a little low in the calculation from 10 s to 20 s, and a little high afterwards. This is a good example of the cascade effect that can occur in integral system calculations.

For this experiment, RELAP5 had a bias of 2C in temperature with a standard deviation of 9C. RELAP5 had a bias of -0.11 MPa in pressure with a standard deviation of 0.30 MPa. Overall, the code-data agreement for this test is considered excellent.

LOFT L3-1

Figure E-9 plots results from LOFT test L3-1, a 4-inch diameter equivalent cold leg break LOCA. Temperature comparisons in the upper downcomer region are shown on the left. The RCS pressure comparison is on the right.

The depressurization is somewhat faster in the experiment than in the RELAP5 calculation. This appears to be caused by lower reverse heat transfer from the steam generator to the RCS in the experiment after 400s. The result of the faster depressurization is that accumulator injection proceeds somewhat faster in the experiment than in the calculation.

The five large oscillations in downcomer temperature seen in the RELAP5 calculation from ~800 s to ~2,200 s are due to fluctuations in the accumulator injection rate. The accumulator injection behavior is due in turn to the interaction between the condensation due to ECC injection, RCS pressure, and accumulator pressure. When condensation increases, RCS pressure decreases, and accumulator injection increases, which leads to more condensation, and a surge of injection. The cycle interrupts when condensation stops, so RCS depressurization stops, which causes accumulator flow to stop. Overall, during the period from 600 s to ~2,200 s, there was more condensation during accumulator injection in the calculation than in the test. This caused more subcooling in the downcomer in the calculation. RELAP5 prediction of downcomer temperature was, therefore, conservative.

For this experiment, RELAP5 had a bias of -12C in temperature with a standard deviation of 9C. RELAP5 had a bias of 0.04 MPa in pressure with a standard deviation of 0.18 MPa.

MIST 360499

Figure E-10 plots results from MIST Test 360499. The temperature comparison in the downcomer is on the left. The RCS pressure comparison is on the right. The test simulated a primary-side feed-and-bleed cooling operation, which is the same scenario as a stuck open PORV. Although RELAP5 did not predict the interruption of loop flow correctly, the calculation of downcomer temperature agreed reasonably well with the test data. The differences between the code and data are believed to be due to the heat loss modeling for the MIST facility. Because of the small size of MIST test rig, the experimental results tended to be influenced by facility heat losses and the operation of the guard heaters. There was insufficient information from the facility to adequately qualify the input model heat loss.

For this test, RELAP5 had a bias of 4C in temperature with a standard deviation of 4C. RELAP5 had a bias of 0.03 MPa with a standard deviation of 0.40 MPa.

MIST 3109AA

Figure E-11 plots results from MIST Test 3109AA, a 1.4-inch diameter equivalent cold leg LOCA. The temperature comparison for the upper downcomer region is on the left. The RCS pressure comparison is on the right.

RELAP over predicted RCS pressure slightly. This caused HPI flow to be slightly less in the calculation than in the experiment, which in turn caused the downcomer temperature to be slightly higher in the calculation. The RELAP5 model for the MIST facility may underestimate heat loss, since the break flow comparison was found to be good. Because of the small size of MIST, the calculated results are sensitive to accurate modeling of heat loss. Actual information on distributed heat loss is generally not available from the facilities.

For this test, RELAP5 had a bias of 10C in temperature with a standard deviation of 6C. RELAP5 had a bias of 0.47 MPa in pressure with a standard deviation of 0.46 MPa.

MIST 4100B2

Figure E-12 plots results from MIST Test 4100B2, a 4.4-inch diameter equivalent cold leg break LOCA. The temperature comparison for the upper downcomer region is on the left. The RCS pressure comparison is on the right.

RELAP5 is in excellent agreement with the test data until ~2,600 s to ~3,400 s. Then the pressure in the calculation trended low, apparently due to break modeling effects.

For this test, RELAP5 had no bias (0C) in temperature with a standard deviation of 12C. RELAP5 had a bias of -0.25 MPa in pressure with a standard deviation of 0.26 MPa.

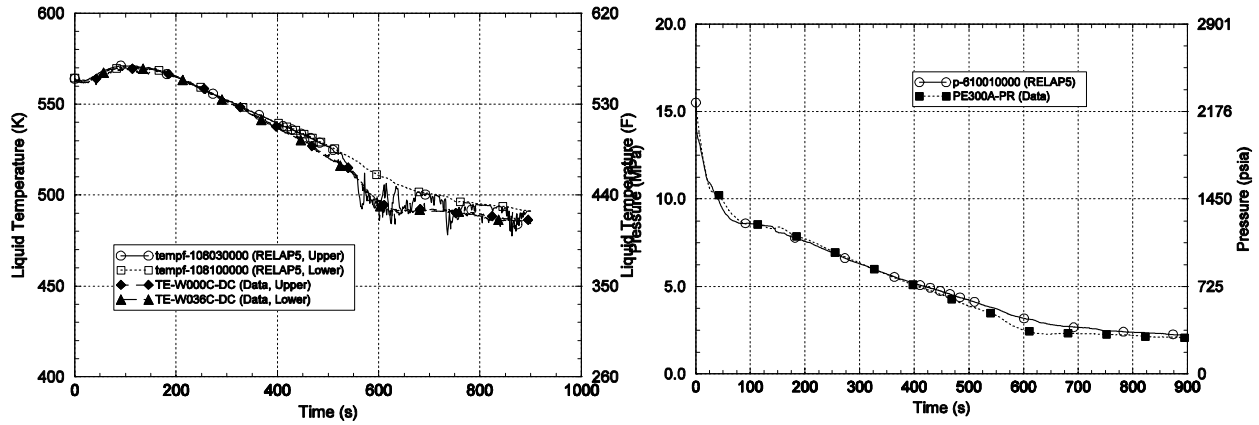


Figure E-1 ROSA-IV SB-CL-18, 6-inch Cold Leg Break (Side Orientation) with Failure of HPI

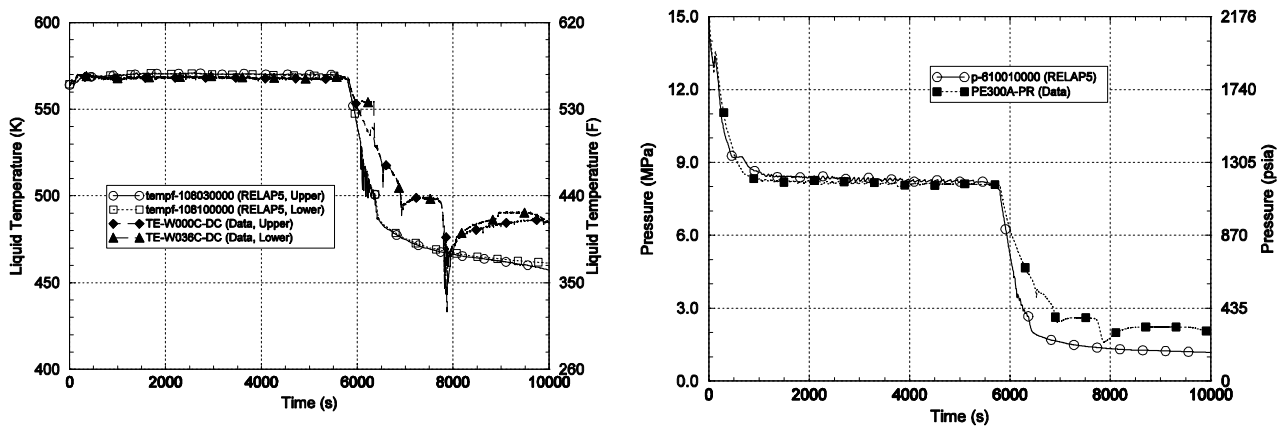


Figure E-2 ROSA-IV SB-HL-06, 2-inch Hot Leg Break (Top Orientation) with Failure of HPI

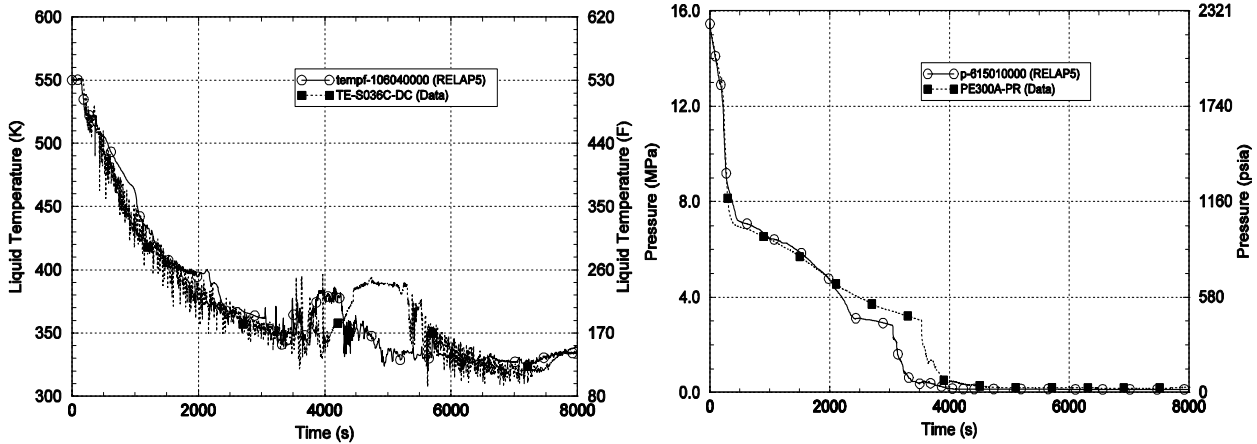


Figure E-3 ROSA/AP600 AP-CL-03, 1-inch Cold Leg Break (Bottom Break Orientation)

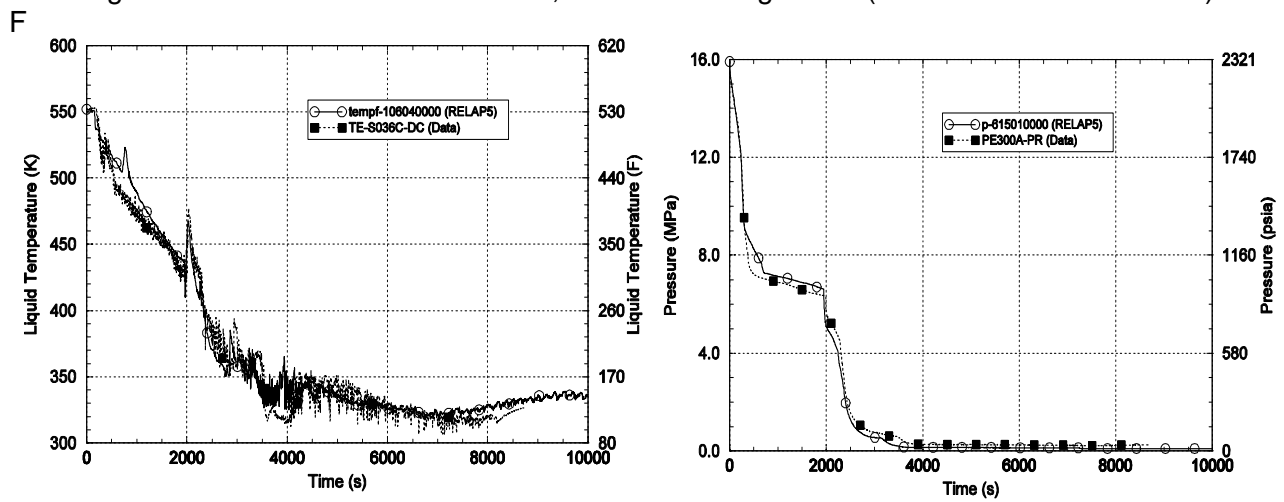


Figure E-4 ROSA/AP600 AP-CL-09, 1-inch Cold Leg Break (Bottom Break Orientation) with Failure of CMTs and 1/2 ADS

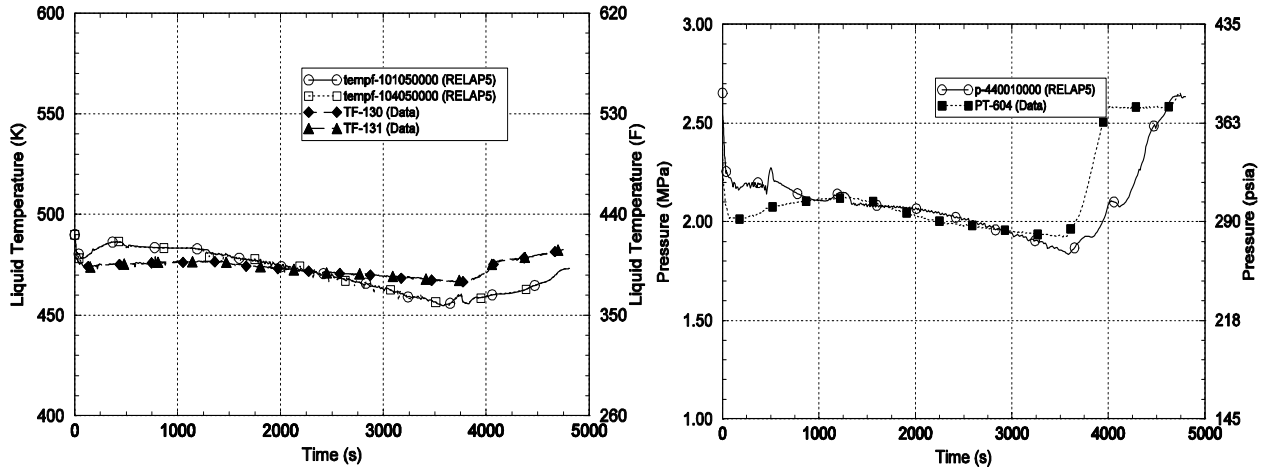


Figure E-5 APEX-CE-13, Stuck Open Pressurizer SRV That Recloses at 3600s

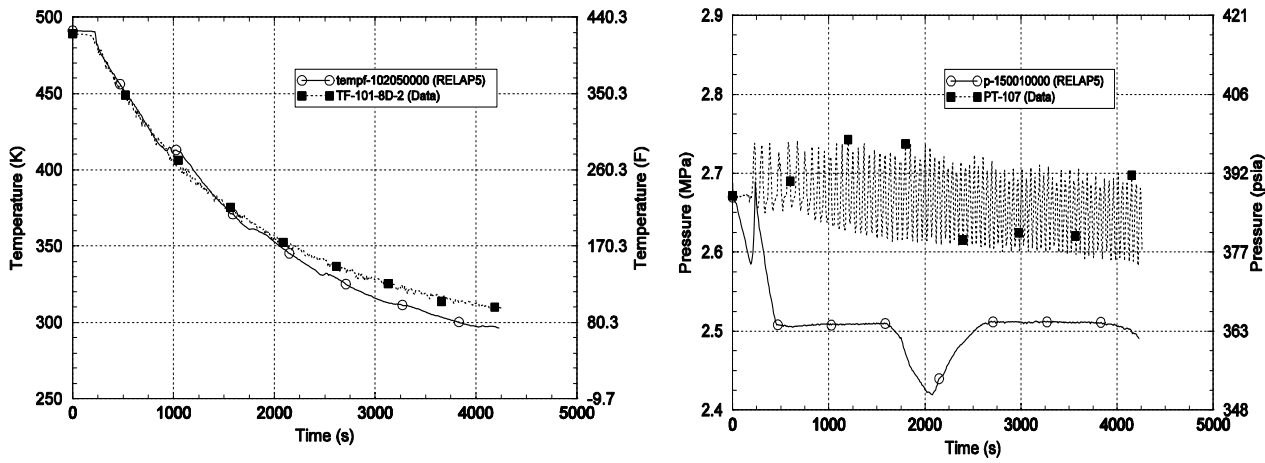


Figure E-6 APEX-CE-5, Loop Flow Stagnation, Cooldown Due to HPI Injection

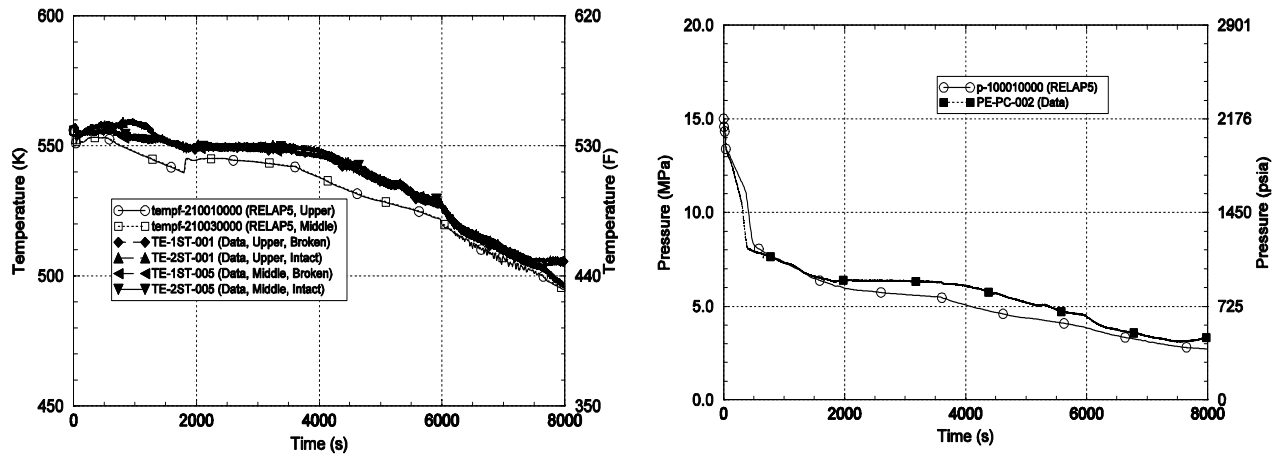


Figure E-7 LOFT L3-7, 1-inch Cold Leg Break LOCA

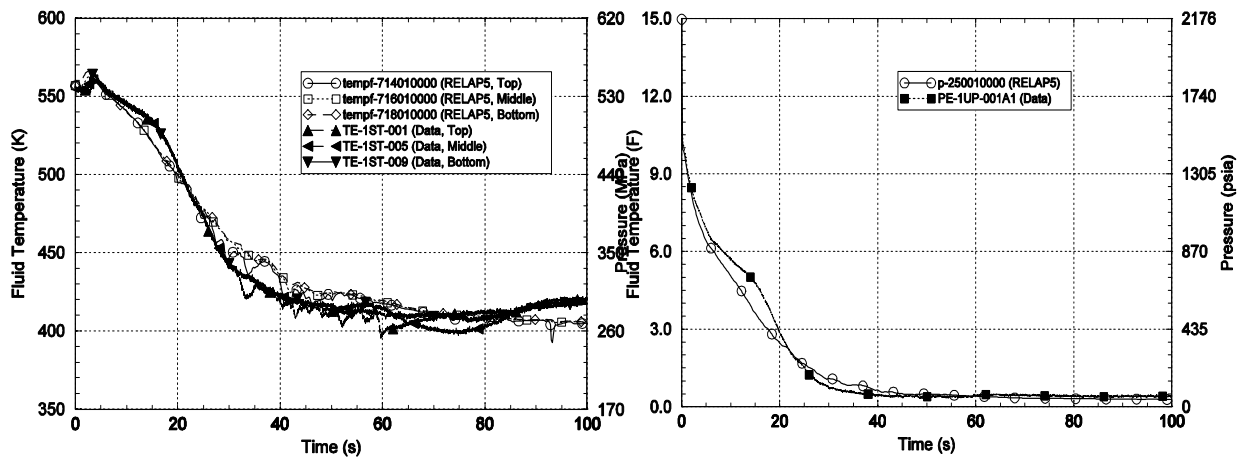


Figure E-8 LOFT L2-5, Large Break LOCA

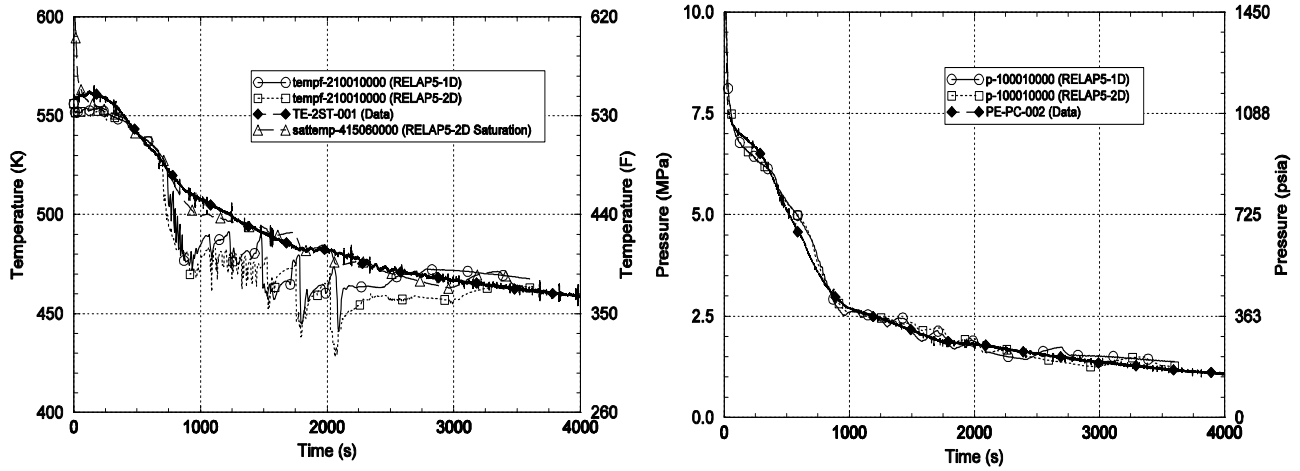


Figure E-9 LOFT L3-1, 4-inch Cold Leg Break LOCA

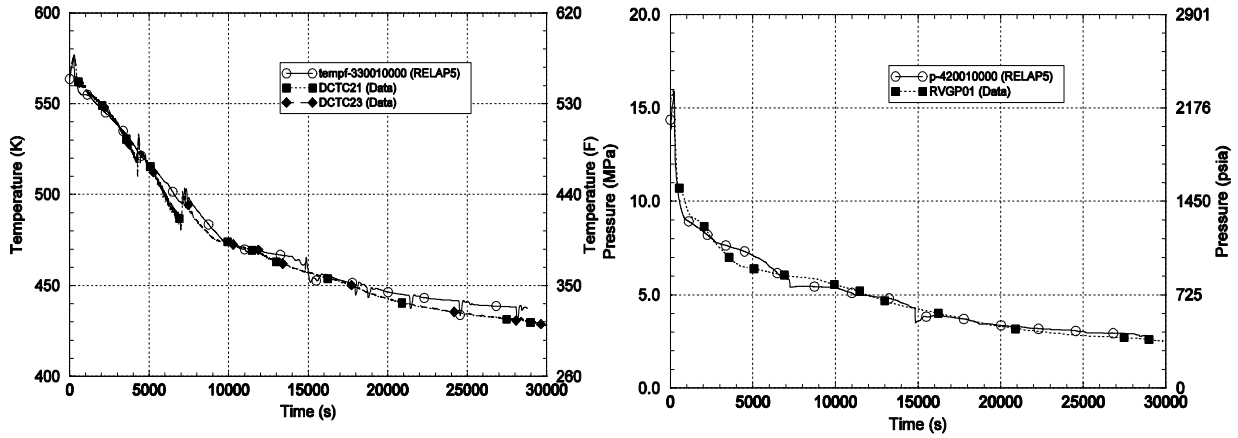


Figure E-10 MIST Test 360499, Feed and Bleed

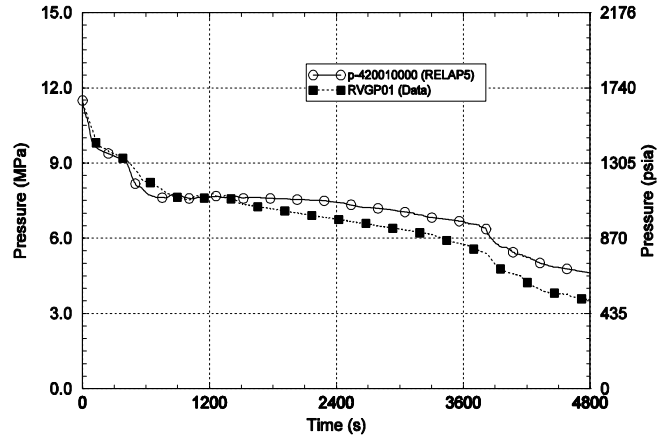
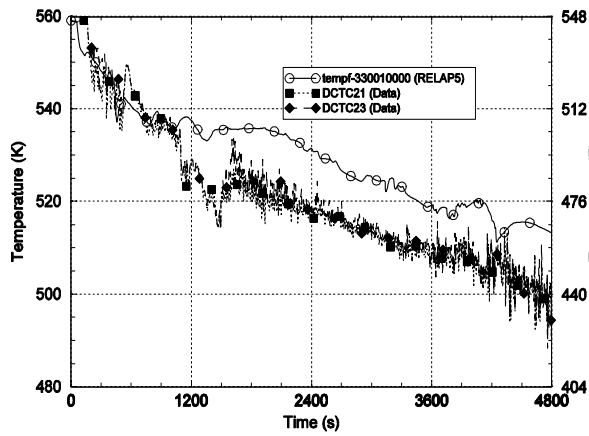


Figure E-11 MIST Test 3109AA, 1.4-inch Cold Leg Break LOCA

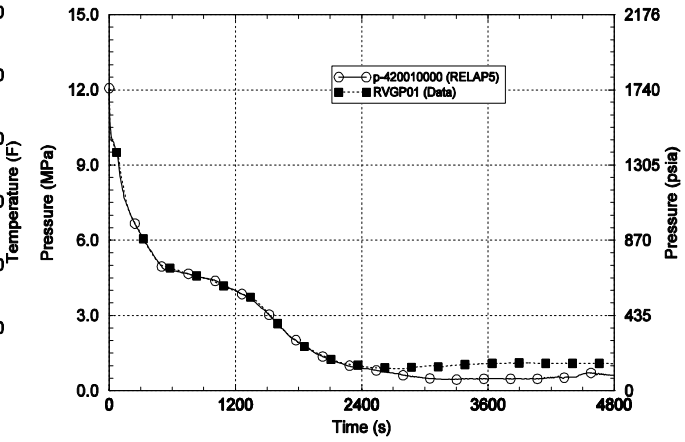
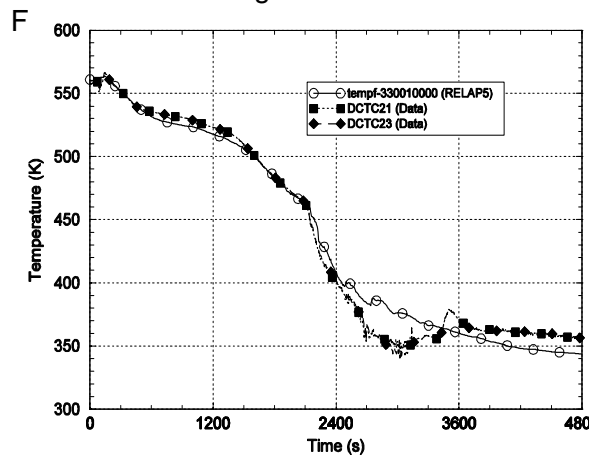


Figure E-12 MIST Test 4100B2, 4.4-inch Cold Leg Break LOCA

APPENDIX F. WALL HEAT TRANSFER MODELING IN RELAP5

Since the IPTS study in the early 1980s, the question of the relative importance of the convective heat transfer in the downcomer has been of considerable interest. While we conclude from an order of magnitude approach that its uncertainty is less important to PTS analysis than the other two figures of merit, temperature and pressure, nevertheless, its effect must be considered.

The heat transfer coefficient is a derived variable from the various heat transfer correlations used in the code. In general, the modeling of wall-to-fluid heat transfer in the code has considerable complexity, since the heat transfer package must cover the complete spectrum of possibilities. However, only a small subset of conditions are of significance under the current circumstances, due to the systematic similarities of the risk significant PTS events. The heat transfer in the downcomer is generally turbulent convection to a subcooled liquid at Reynolds numbers 500,000 to 3,000,000.

Heat flux is nearly always controlled, and generally dominated by, the downcomer fluid temperature $T_f(t)$, that is, the rate of change and absolute value of T_f . For a given h , the faster the transient, the larger the magnitude of $T_w - T_f$. Normally, this should make variation in h more important, however, for fast transients (large breaks) it is the *rate of change in T_f that dominates*. For slower transients (small breaks), T_w remains closer to T_f . The slower time scale of the conduction process requires more time to allow the wall temperature to track the fluid temperature, which renders variations in h relatively less important. Still, one expects to find more sensitivity in K_R to uncertainties in heat transfer coefficient for large LOCAs than for small LOCAs.

The RELAP5 heat transfer package is based on fully developed, steady state flow. Additionally, the one dimensional nature of the field equations in RELAP5 precludes direct simulation of effects that depend upon transverse gradients of any physical parameter, such as velocity or energy. Consequently, such effects must be accounted for through algebraic terms added to the conservation equations. These terms utilize equations that combine physical principles with correlating coefficients deduced from experimental data.

PTS scenarios all involve natural circulation or loop flow stagnation. The Reynolds numbers in the downcomer are well into the turbulent region. Experimental data indicate that the flow velocities in the downcomer fall in the range ~ 0.5 m/s to ~ 1.5 m/s under flow stagnation conditions. The downcomer flow velocity based on a natural circulation flow rate of 3% of rated flow is 0.2 m/s. During natural circulation, therefore, there should be downcomer recirculation.

RELAP5 modeled the downcomer as an internal, vertical flow field in a pipe geometry. In the RELAP5 nomenclature, Mode 2 is defined as single phase liquid convection at subcritical pressure, with a subcooled wall. Under these conditions, the DITTUS subroutine is called. This subroutine calculates heat transfer using both Dittus-Boelter [50] for forced turbulent convection, and Churchill-Chu [51] for free convection, and takes the maximum of the two,

$$Nu = \max (Nu_{\text{forced}}, Nu_{\text{free}}).$$

For high Reynolds number turbulent flow, Dittus-Boelter produces a higher number for h , while for lower Reynolds number turbulent flow it is Churchill-Chu.

Forced Convection (high Reynolds number turbulent flow)

The turbulent forced convection cooling of a wall by a fluid is described by the Dittus-Boelter equation

$$Nu_D = 0.023 Re_D^{0.8} Pr^{0.4}$$

where

$$Nu = \frac{hD_H}{k_f} \quad \text{surface temperature gradient}$$

$$Re = \frac{\rho u D_H}{\mu} \quad \frac{\text{inertial force}}{\text{viscous force}}$$

$$Pr = \frac{\nu}{\alpha} = \frac{\mu C_p}{k_f} \quad \frac{\text{momentum diffusivity}}{\text{thermal diffusivity}}$$

and

- h is the convective heat transfer coefficient
- D_H is the hydraulic diameter
- k_f is the conductivity of the fluid
- ρ is the density of the fluid
- u is the velocity
- μ is the dynamic viscosity
- C_p is the heat capacity of the fluid

The range of applicability is

$$\begin{aligned} 0.7 < Pr < 160 \\ Re > 10,000 \\ L/D > 10 \end{aligned}$$

Calculation of the Nusselt number requires the liquid thermophysical properties, which are temperature dependent, and the liquid velocity to determine the Reynolds number. RELAP5 evaluates the physical properties at the bulk fluid temperature. In addition to the temperature dependent thermophysical properties, the key to correct prediction of the heat transfer coefficient is calculation of liquid velocity.

The range of interest of downcomer temperatures extends from the initial conditions, 285C to the lower bounds of final conditions, 20C. The upper boundary is determined by the cold leg temperature under normal operating condition and post scram, or hot standby conditions. The lower bound is determined by the ECC injection temperature, which is nominally ~20C.

As discussed above, the boundary region for the Reynolds number is defined by the flow velocities under flow stagnation conditions for primary-side induced cool downs (LOCAs) and by natural circulation for secondary-side induced cool downs (MSLBs).

The Pr number is nearly equal to one for the range of fluid temperatures of interest as shown in Table F-1.

Table F-1 Prandtl Numbers for Water

T	Pr	Pr ^{0.4}
100C	1.76	1.25
200C	0.91	0.96
300C	0.95	0.98

Therefore, for a given fluid temperature, the heat transfer is determined by the fluid velocity. If RELAP5 calculates fluid velocity correctly, the code will calculate turbulent forced convection heat transfer correctly.

Free Convection (low Reynolds number turbulent flow)

When equality of the Grashof (Gr) number and Re² exists, the buoyancy forces and drag forces affecting the velocity profile are of the same order of magnitude. The transition encompasses a significant range in Gr and Re for various geometries. The Grashof number is used to evaluate buoyancy driven flow.

$$Gr = \frac{g\beta(T_w - T_f)D_H^3}{\nu^2} \quad \text{ratio of buoyancy to viscous forces}$$

where g is the gravitational constant
 β is the bulk coefficient of expansion
 ν is the kinematic viscosity

Whether heat transfer is predominantly free or forced convection can be determined by evaluating the ratio of Grashof Number to Reynolds Number. If

$$\frac{Gr}{Re^2} = \frac{g\beta(T_w - T_f)D_H}{u^2} \ll 1$$

then the heat transfer is governed by forced convection. If

$$\frac{Gr}{Re^2} \gg 1$$

then the flow and heat transfer are governed by free convection. Substituting the numbers and solving for u,

$$Nu_{p-C} = Nu_{p-K} + Nu_{p-K} 0.9 \left[\ln \left(\frac{Gr}{Re^2} + 1 \right) \right]^{1.39}$$

u > ~ 0.75 m/s	Gr/Re ² < 0.1
Forced Convection	
Free Convection	u < ~ 0.075 m/s
Mixed Convection	Gr/Re ² > 10
	Gr/Re ² = 1

Pumped flow is well into the forced convection region, while downcomer velocities characteristic of natural circulation or loop flow stagnation tend towards free convection.

For the Churchill-Chu model free convection flow model,

$$Nu = \left(0.825 + \frac{0.387(Ra_L)^{1/6}}{\left[1 + \left(\frac{0.492}{Pr} \right)^{9/16} \right]^{8/27}} \right)^2$$

where $Ra = Gr Pr$

Churchill-Chu was developed for free convection with a vertical flat plate, over the full laminar and turbulent Rayleigh number range. The fluid properties are evaluated in RELAP5 at the bulk fluid temperature. The length term is determined by the user. If not specified it defaults to the hydraulic diameter.

The effects of combined free and forced convection are different for opposing flow and result in changes in the value of the heat transfer coefficient. The opposing flow situation is characterized either by down flow of cooler liquid past a heated wall, or upflow of warmer liquid past a cooled wall. Swanson-Catton developed a heat transfer enhancement factor to account for buoyancy opposed mixed convection. The Reynolds numbers in those experiments were 6,000 to 20,000, which is one to two orders of magnitude below the downcomer conditions. The Swanson-Catton mixed convection experimental conditions were

$$Re \sim 10,000$$

$$Gr \sim 2 E8$$

$$Gr/Re^2 \sim 0.6 \text{ to } 2$$

$$Nu \sim 300$$

Catton-Swanson developed an enhancement factor model that was applied to Petukhov-Kirillov

where Nu_{p-K} is obtained from the Petukhov-Kirillov model [52],

$$Nu_{p-K} = \frac{\frac{C_f}{2} Re Pr}{1.07 + 12.7 \left(\frac{C_f}{2} \right)^{1/2} (Pr^{2/3} - 1)}$$

where C_f is the Fanning friction factor, which is determined from the Filonenko [53] correlation

$$C_f = \frac{f}{4} = \frac{1}{(3.64 \log_{10} Re - 3.28)^2}$$

The Petukhov-Gnielinski [54] version differs slightly from Petukhov-Kirillov. It extends the applicability into the turbulence transition region ($Re = 3,000$ to $10,000$),

$$Nu = \frac{\frac{C_f}{2} (Re-1000) Pr}{1 + 12.7 \left(\frac{C_f}{2} \right)^{1/2} (Pr^{2/3} - 1)}$$

RELAP5 provides the user an option to model the downcomer wall heat transfer using the Petukhov-Gnielinski instead of the Dittus-Boelter correlation. When that option is selected RELAP5 then takes the maximum of Churchill-Chu and Petukhov-Gnielinski (replacing Dittus-Boelter). Coding was also implemented to invoke the Catton modifier on Petukhov-Gnielinski over the range of $Gr/Re^2 < 30$, the range of applicability recommended by Catton [55, 56]. As Gr/Re^2 goes to zero, the multiplier goes to one. The code version with these optional models incorporated has not been assessed.

Sensitivity studies investigating the effects of variations in the heat transfer coefficient on the wall heat flux were performed and are discussed in Section 3.4.2 and Appendix G.

APPENDIX G. EFFECT OF HEAT TRANSFER COEFFICIENT ON WALL HEAT FLUX

Prior to the start of the current PTS program, a study was performed of the sensitivity of the wall heat flux to changes in the wall-to-fluid heat transfer coefficient [57]. The study evaluated the effect of varying the heat transfer coefficient over the range from 850 W/m²-C to 10,000 W/m²-C. This bounds the range of conditions from flow stagnation to beyond natural circulation, and into the forced flow regime. In fact, the range of interest for flow stagnation and natural circulation is generally within approximately 1,000 to 3,000 W/m²-C. In comparison, for forced circulation with the reactor coolant pumps on, the heat transfer coefficient is approximately 27,000 W/m²-C. Consider the conduction-convection equation,

$$k(T, t) \frac{dT_w(t)}{dx} = h(t)[(T_w(t) - T_f(t))]$$

where k is the conductivity (of the vessel wall)
 h is the convective heat transfer coefficient
 T is temperature
subscripts w and f refer to wall and fluid, respectively

From the Biot number, we know whether the heat transfer process (i.e. heat flux) is conduction controlled or convection controlled. The two terms, convective heat transfer coefficient (h) and wall-to-fluid temperature difference ($T_w - T_f$) cannot be varied independently. As h increases, $T_w - T_f$ decreases, and vice-versa.

To evaluate the coupled solution for the above equation, a finite difference code was written. Idealized cooldown transients were evaluated with four different exponential cooldown rates, whereby the time constants τ were varied from 900 s to 5,400 s. The time constant was determined according to

$$T^* = \frac{T - T_{ECC}}{T_0 - T_{ECC}} = e^{-t/\tau}$$

where τ is the characteristic time of the fluid transient. This equation also provides a dimensionless temperature for comparing experiments at different temperature ranges, and to express the degree of mixing that has occurred. This expression describes the cooldown of an ideally mixed (back-mixed, mixing cup) volume. The characteristic time T is determined by

$$\tau = \frac{V}{Q_{ECC}}$$

where V is the effective mixing volume (of the reactor coolant system)
 Q_{ECC} is the ECC injection flow rate

The time constants T chosen for the simple exponential cooldown are closely related to RELAP5 calculations of actual PTS LOCA sequences. In fact, the cooldown curves used in the analysis are simplified approximations of actual PTS transients calculated by RELAP5, as follows:

Table G-1 Correspondence Between Cooldown Time and Plant Scenario

τ , s	PTS Transient
900	~3-inch LOCA
1,800	~2-inch LOCA
3,600	~1.72-inch LOCA
5,400	~1.5-inch LOCA (SRV)

Figure G-1 is a plot of $T_f(t)$ for the four cooldown rates analyzed, as indicated in Table G-1. For each of the four cooldown transients, the convective heat transfer coefficient was varied over the range from 850 to 10,000 W/m²-C.

Using the cool-down rate (τ) of 1,800 s as an example, five values of h were used to analyze the thermal transient. The fluid temperature was determined by the cooldown calculation. The wall temperatures were determined from a conduction solution with an adiabatic outer boundary condition and the inner wall temperature determined from the convective boundary condition

Table G-2 shows how the temperature difference ($T_w - T_f$) and the heat flux (q'') change as a function of h . Five values of h , shown in the first column, were used to analyze the thermal transient. The table was developed for the time during the transient at which $T_w - T_f$ was at its maximum value. As seen in the second column, and shown in detail in Figure G-2, the wall temperature is driven toward the fluid temperature as the convection coefficient increases.

Since the heat flux is conduction-controlled, the effects of uncertainties in h are damped. If h were infinite, the wall surface temperature would track the fluid temperature exactly. If k were infinite, the heat flux would be completely controlled by h . When the heat transfer coefficient was changed by 1200%, the heat flux changed by only 22%. The range of interest for flow stagnation and natural circulation is approximately 1,000 to 3,000 W/m²-C. The temperature difference between the fluid and the wall ($T_f - T_w$), therefore, lay in the range of 7C to 20C. The difference between low heat transfer (1,000 W/m²-C) and high heat transfer (3,000 W/m²-C) was equivalent to a difference of 13C in fluid temperature.

Table G-2 Heat Flux From Wall to Fluid for Several h Values

T = 1800s, time = 1500s			
h , W/m ² -C	$(T_w - T_f)$, C	q_w'' W/m ²	q_w % change
850	23.5	20,000	22
1,700	13.4	22,800	10
3,400	7.2	24,500	4
5,100	4.9	25,024	2
10,214	2.5	25,535	0

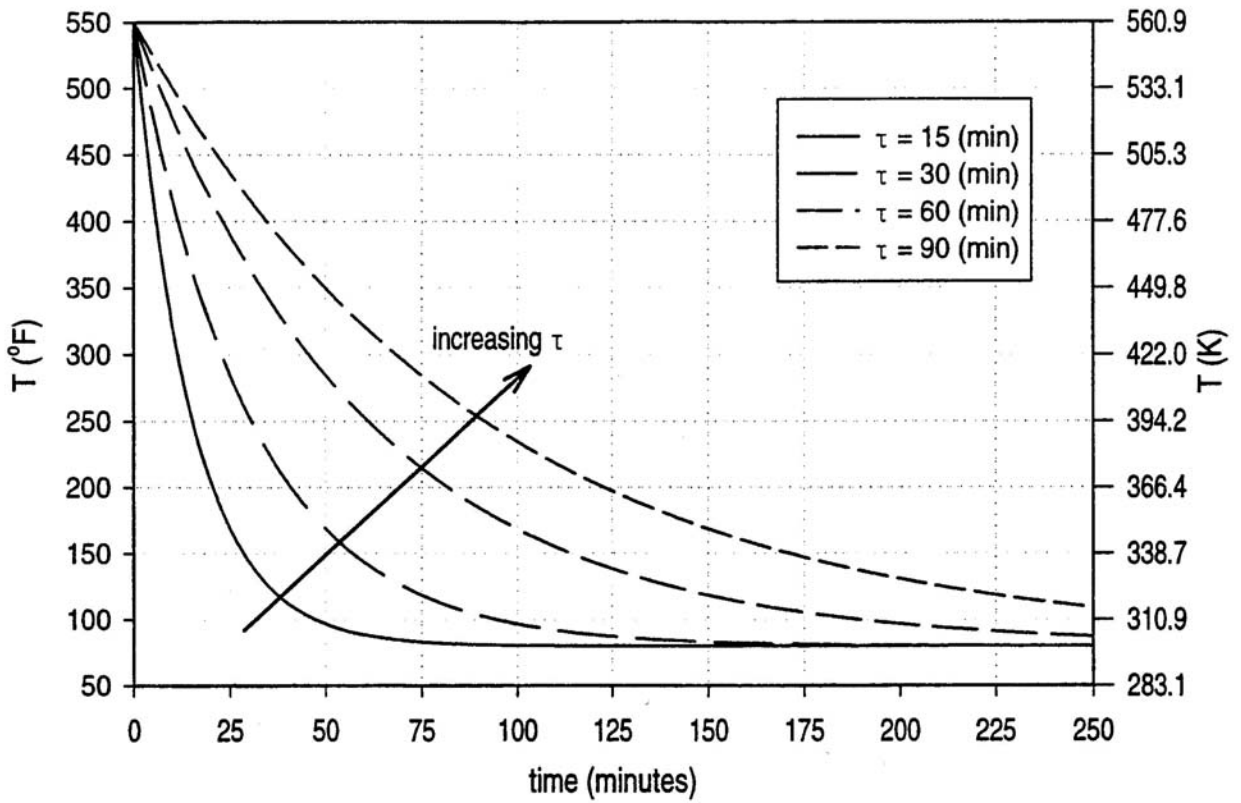


Figure G-1 Downcomer Fluid Temperature Transient for Several Time Constants

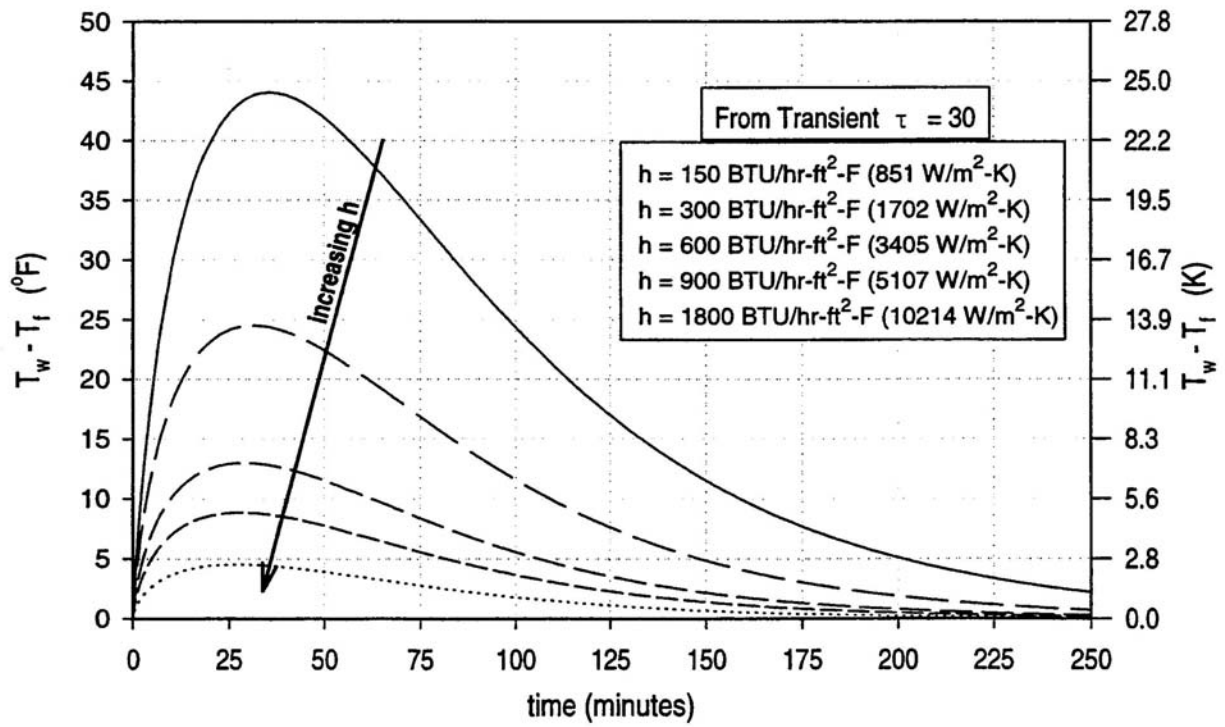


Figure G-2 Effect of Convective Heat Transfer Coefficient on Wall-to-Fluid Temperature Difference

The heat transfer coefficient effect was an order of magnitude less than the absolute change in fluid temperatures (~200C) routinely calculated during PTS scenarios. The 1 σ uncertainty in temperature prediction by RELAP5 is 10C. Therefore, the fidelity of RELAP5 to predict average fluid temperature in the downcomer was of the same magnitude as changing h by a factor of three. The change in wall temperature over the total range from 850 W/m²-C to infinite h is 23.5C, which is close to the 2 σ uncertainty for RELAP5 of 20C. In those terms, the uncertainty in temperature prediction may be comparable to a substantial variation in heat transfer coefficient, but the dominant factor remains the absolute change in temperature.

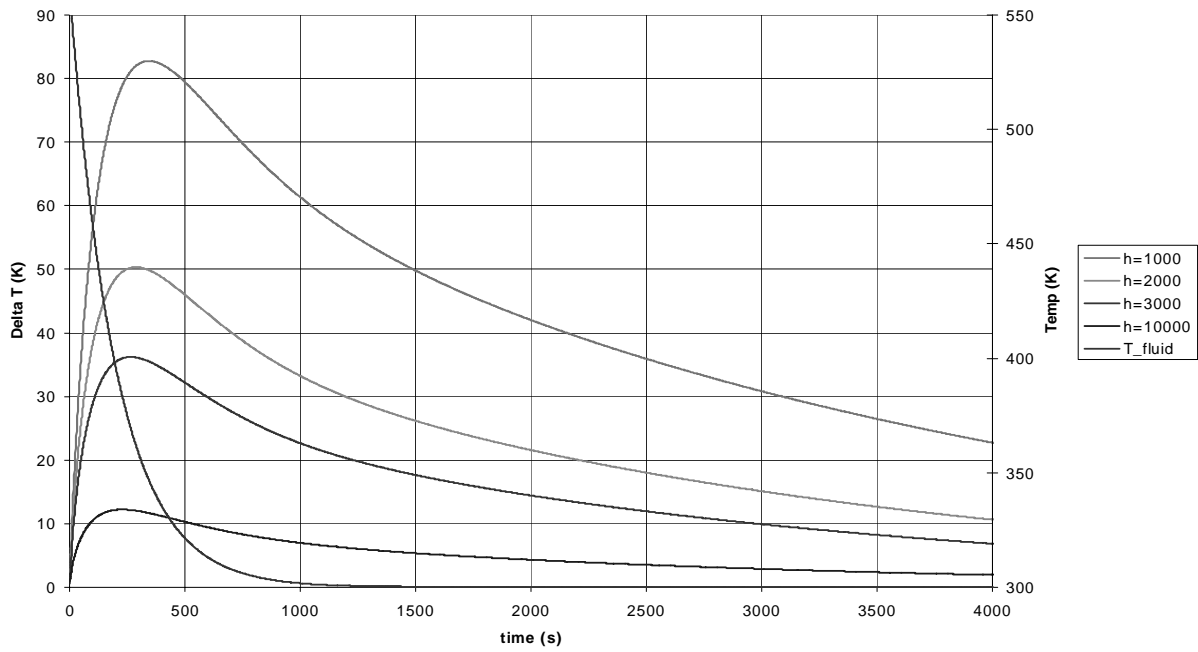
The maximum wall-to-fluid temperature difference arises under conditions when the cooldown rate is the most rapid. The faster the cool down of the fluid in the downcomer, the larger the temperature difference between the wall and the fluid ($T_w - T_f$). Fast cool down is characteristic of large break LOCAs and MSLBs. For a given value of h, fast cool down (small τ) yields larger values for the term ($T_w - T_f$) than slow cool down, therefore, the calculated heat flux, q'' , is more sensitive to h.

Conversely, slow cool downs (large τ) yield small differences in the term ($T_w - T_f$) because there is time for the wall temperature to track the fluid temperature. Variations in h are less important since the slower the transient, the smaller the magnitude of q'' . Small breaks have smaller temperature differences between the wall and fluid for a given value of h. The fluid time constant is comparable to the vessel wall time constant. These effects are illustrated in Table G-3, and Figures G-3 through G-6.

Table G-3 Maximum ΔT as a Function of Cooldown Rate and Heat Transfer Coefficient

h, W/m ² -C	T, s			
	200 s	500 s	1000 s	2000 s
1,000	83 C	62 C	49 C	37 C
2,000	50 C	37 C	28 C	20 C
3,000	36 C	26 C	19 C	14 C
10,000	12 C	8 C	6 C	4 C
Maximum Range	71 C	54 C	43 C	33 C
Range @3,000 s	28 C	31 C	30 C	30 C

Fluid Temperature & Temperature Difference at tau=200s



Temperature Profile, tau=200s at 500 s

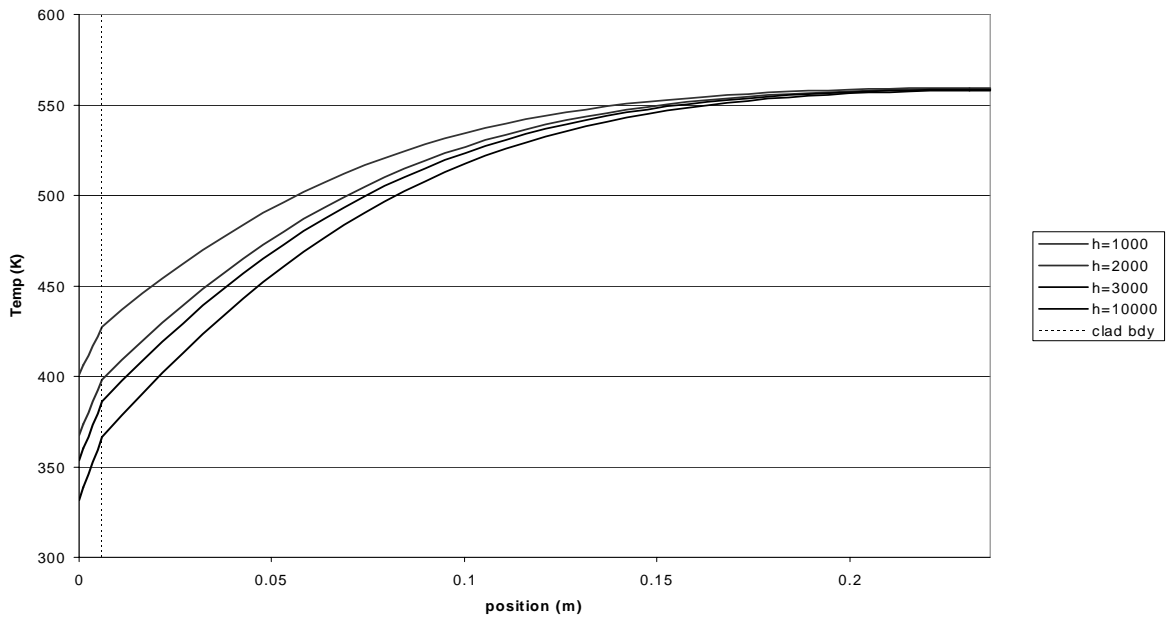


Figure G-3 Wall-to Fluid ΔT for Cooldown Transient $\tau = 200$ s, and Resulting Temperature Profile Across Vessel Wall, for Different Values of h

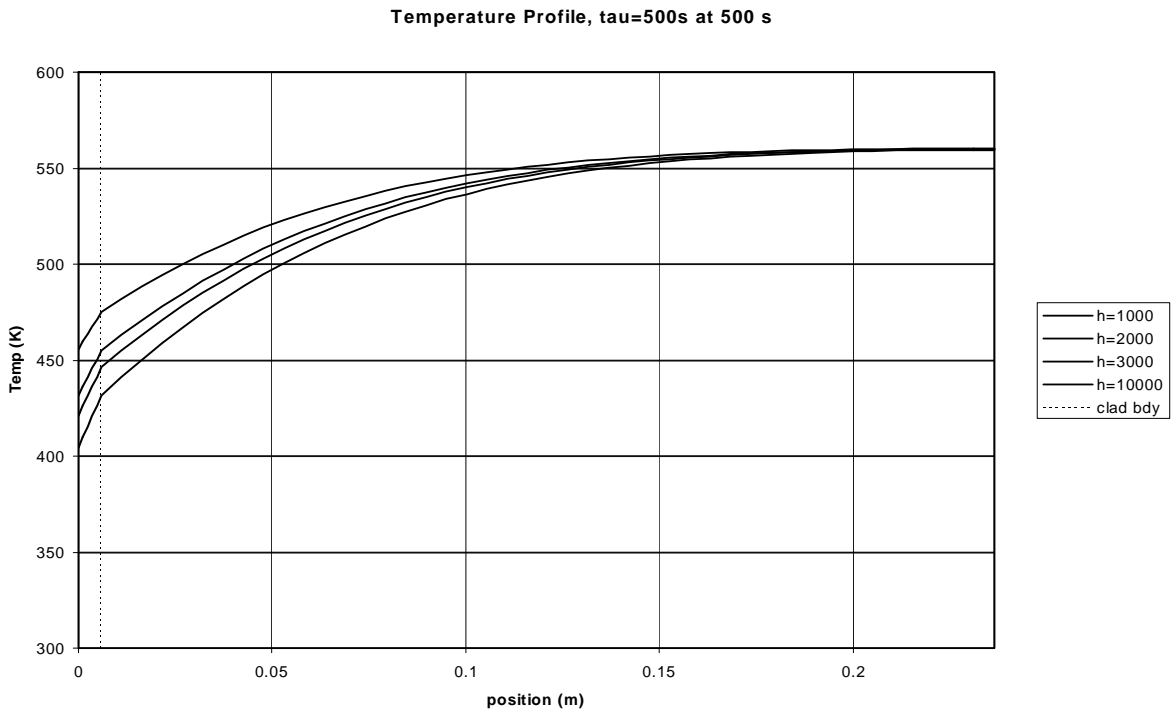
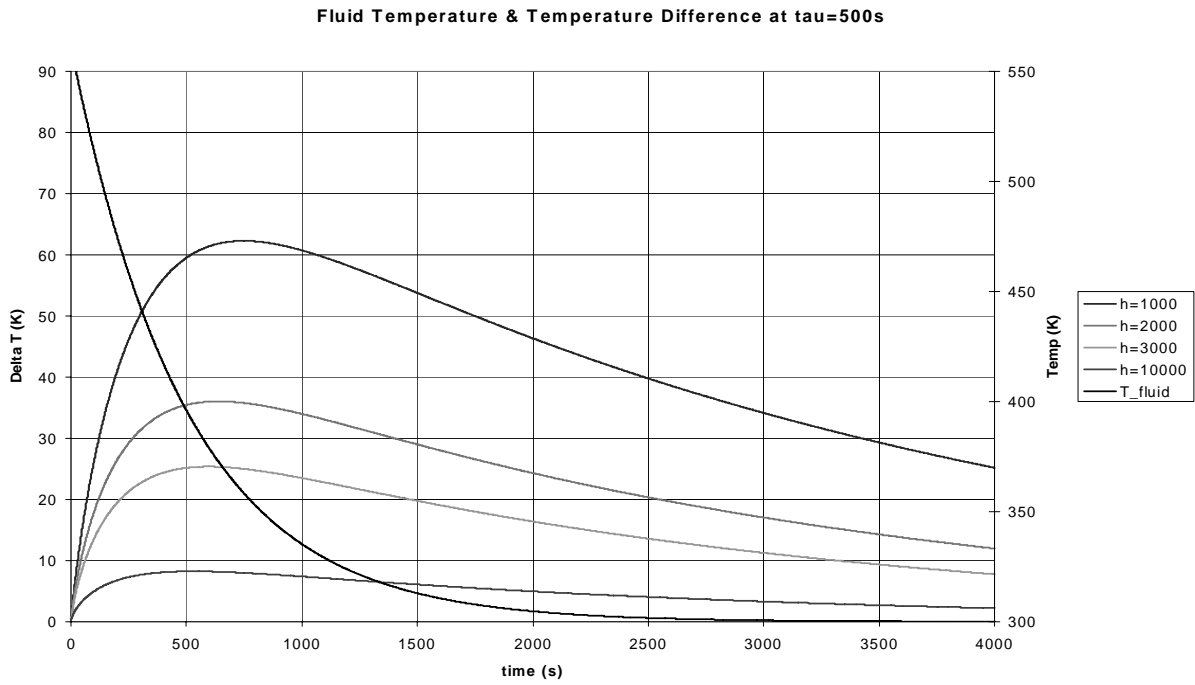


Figure G-4 Wall-to Fluid ΔT for Cooldown Transient $\tau = 500$ s, and Resulting Temperature Profile Across Vessel Wall, for Different Values of h

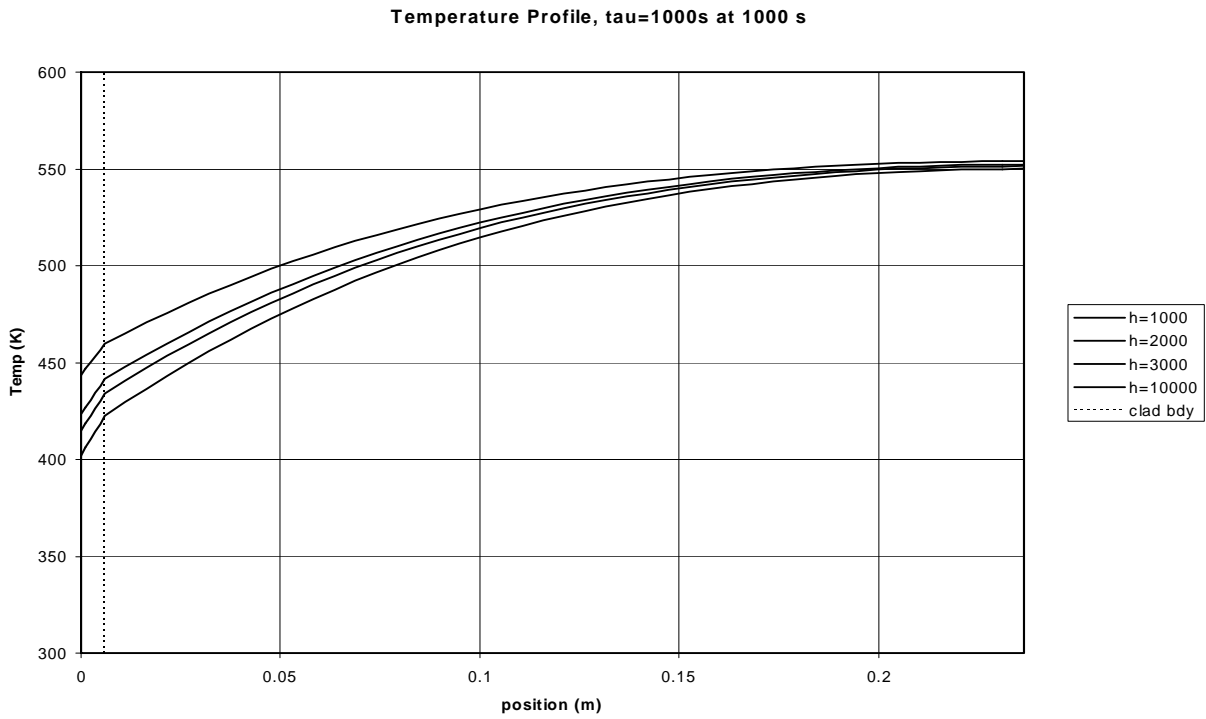
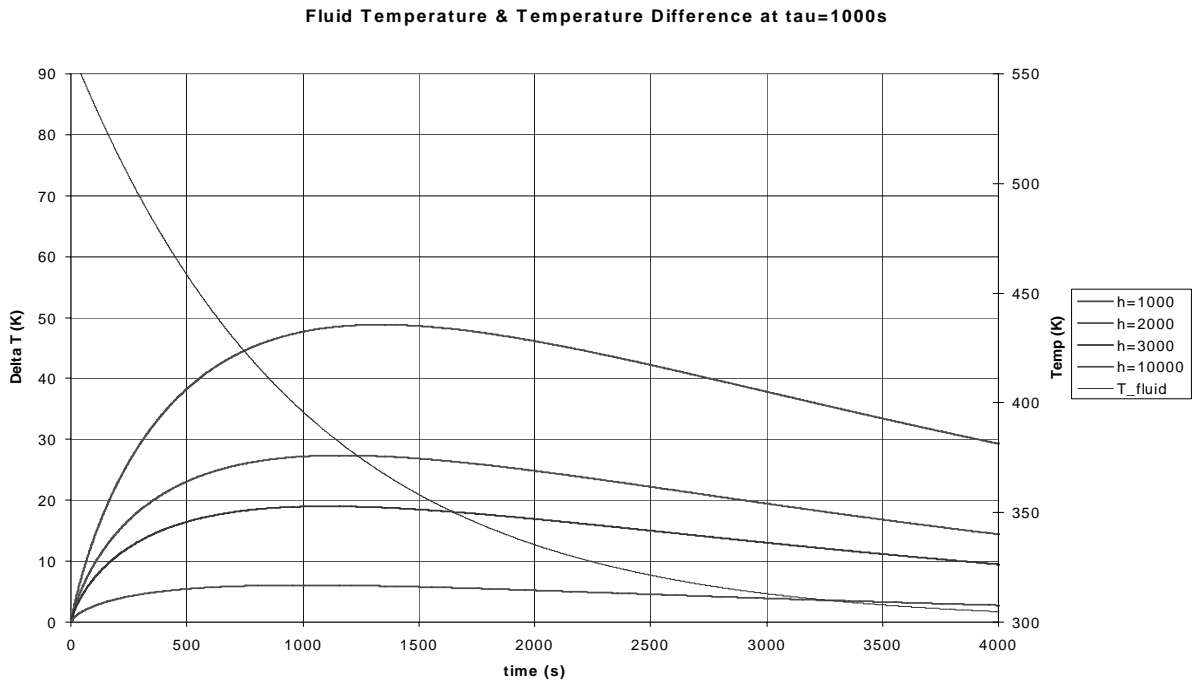
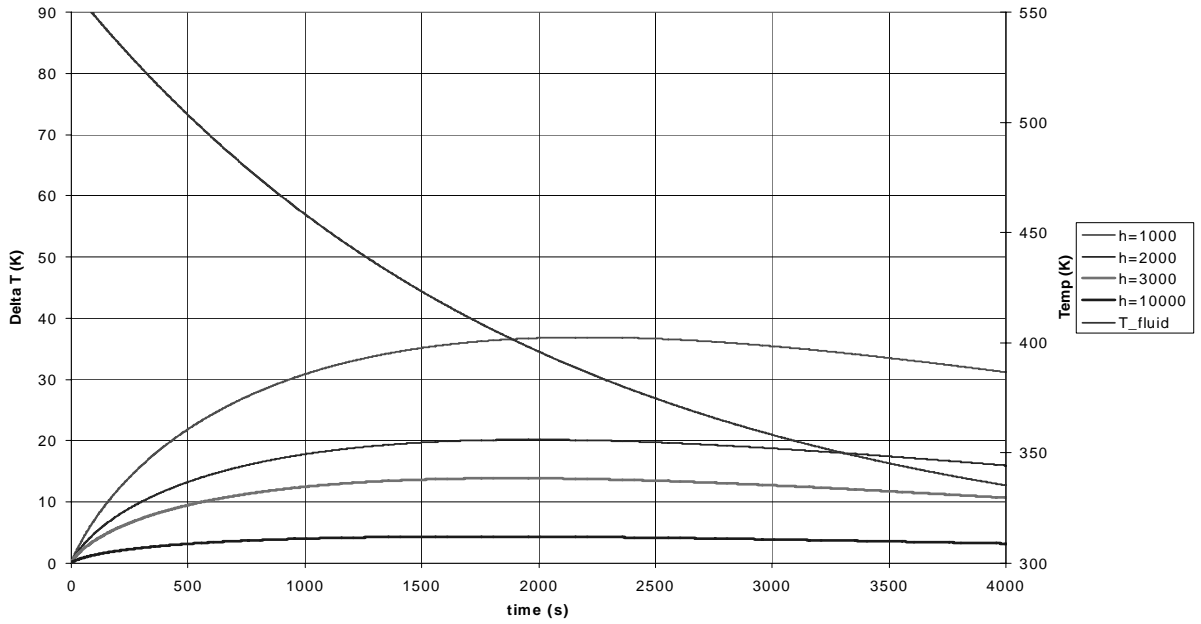


Figure G-5 Wall-to Fluid ΔT for Cooldown Transient $\tau = 1000$ s and Resulting Temperature Profile Across Vessel Wall, for Different Values of h

Fluid Temperature & Temperature Difference at tau=2000s



Temperature Profile, tau=2000s at 1000 s

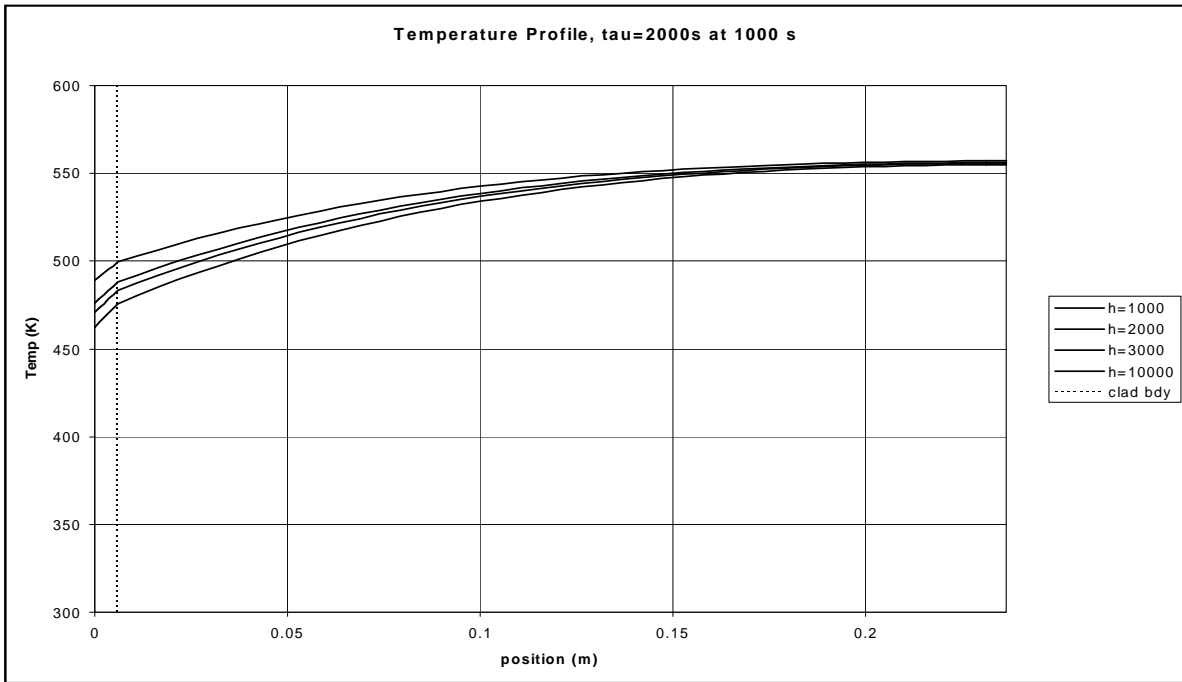


Figure G-6 Wall-to Fluid ΔT for Cooldown Transient $\tau = 2000$ s, and Resulting Temperature Profile Across Vessel Wall, for Different Values of h

PTS combines thermal hydraulics with fracture mechanics and material properties to determine the probability of vessel failure. The thermal analysis must be a combined fluid-structure analysis to determine whether the magnitude and uncertainty in h is of significance. Therefore, while uncertainty studies based on fluid thermal hydraulics alone are revealing, they are but an interim step. The actual uncertainty analysis must be part of a combined fluid-structure analysis. Whether a change in h is significant depends on the PTS figure of merit, namely, K_R , which is an integral measure of the loading (thermal plus pressure) normalized by the fracture toughness.

To investigate the sensitivity of vessel fracture to heat transfer coefficient, calculations were performed using an early version of FAVOR. The analyses utilized a fixed set of material and fracture mechanics assumptions. The results were not sensitive to the RT_{NDT} value of the material or the analysis location within the flaw. The geometry and material properties used for this analysis were typical of U. S. PWRs. The analysis considered only thermal stress. Pressure was not a variable.

Figure G-7 is a plot of K_I and K_{IC} for different values of h for $\tau = 1800$ s (30 minutes). Increasing h increased the calculated K_I . Since thermal stress is a strong function of thermal gradient, the K_I curves are very similar in form to plots of the wall temperature gradient near the inner surface. K_{IC} is a measure of the fracture toughness, which is a function of the temperature of the material. Lower temperatures result in lower fracture toughness.

The ratio, K_I/K_{IC} , determines the importance of two parameters. K_R accounts for all of the thermal effects in a single parameter. The ratio measures the thermal loading normalized by the fracture toughness. If the ratio is greater than one, the failure probability becomes non-zero. The higher the value of K_R above 1, the greater the probability of vessel failure. K_R is plotted in Figure G-8 for several values of h applied to the $\tau = 1800$ s (30 minutes) transient.

Additional studies of the sensitivity of the fracture mechanics results to variations in the downcomer fluid temperature and vessel wall heat transfer coefficient are discussed in Section 4.7.4 and Appendix I.

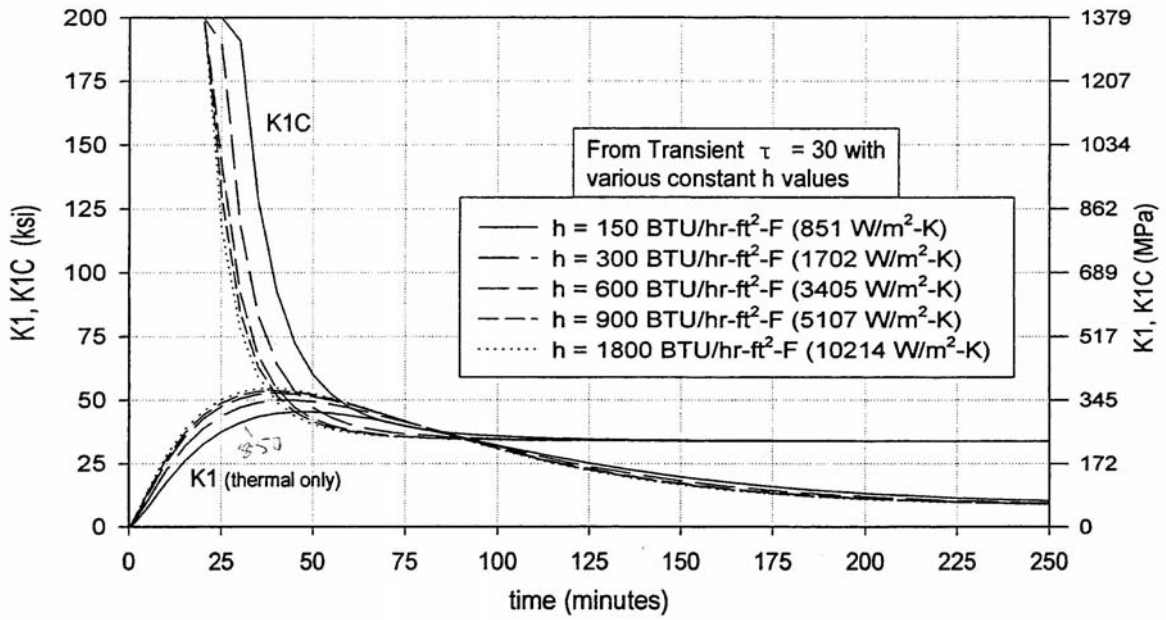


Figure G-7 K_1 and K_{1C} for Cooldown Transient ($\tau = 30$ minutes) for a range of values of h

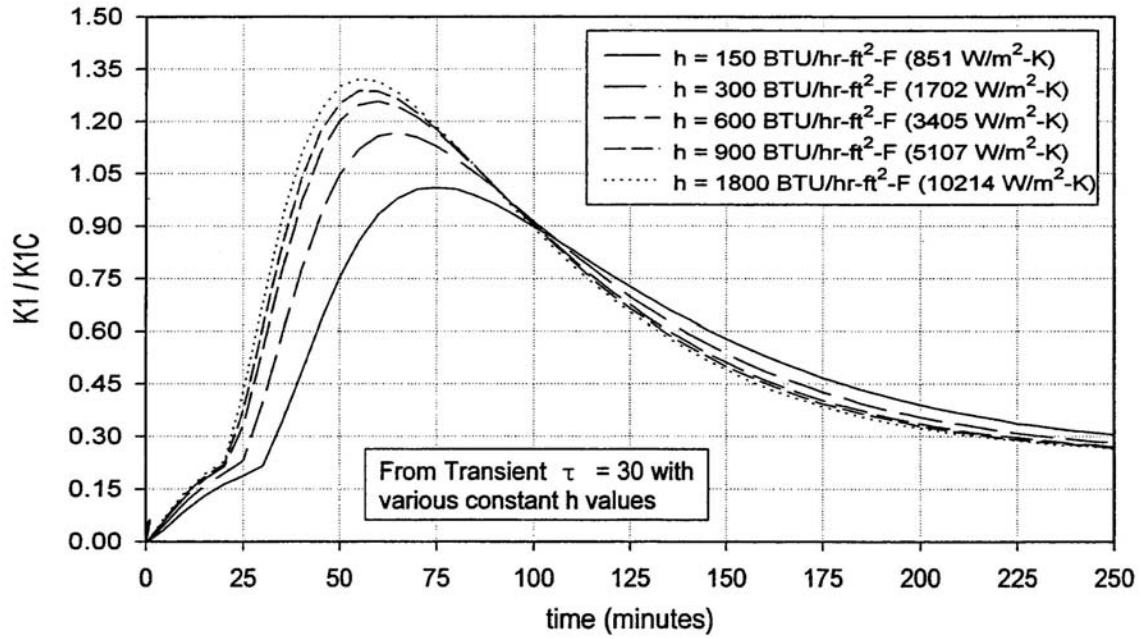


Figure G-8 K_R for Cooldown Transient ($\tau = 30$ minutes) for a Range of Values of h

APPENDIX H. COMPARISON OF MEASURED AND RELAP5-CALCULATED REACTOR VESSEL WALL HEAT TRANSFER

This section compares RELAP5 calculations of downcomer heat transfer with experimental data from UPTF and APEX-CE. Downcomer fluid temperature and adjacent wall temperature measurements, as well as downcomer fluid velocity measurements, were available from these two facilities enabling an integrated assessment to be performed. Additionally, data from Creare are shown. Creare had fluid and wall temperature measurements, and fluid velocity measurements as well, which allowed an experimental determination of h .

Based on velocities measured or determined from the experimental facilities, the flows in the downcomer are considerably greater than those resulting from ECC injection and break flow alone. Typical velocities in the downcomer were found to be in the range of 0.5 m/s to 1 m/s. The corresponding Reynolds numbers in the downcomer, based on the hydraulic diameter of the downcomer (twice the gap width) were

Reynolds Number Downcomer		
T, C	0.5 m/s	1.0 m/s
250	1,850,000	3,700,000
150	2,750,000	5,500,000
50	430,000	870,000

This range of velocities is sufficiently high to avoid buoyancy opposed mixed convection enhancement to heat transfer.

H.1 UPTF

A comparison was made for UPTF Test 1 Run 21, which was one of a series of five fluid-fluid mixing experiments conducted in the facility as part of the 2D/3D program [17]. The objective was to compare measured and RELAP5-calculated data for parameters relevant to the reactor vessel wall inside-surface convective heat transfer behavior. The experiment consisted of injecting cold HPI water into one of the four cold legs (CL-2) of a system initially filled with hot pressurized water. The experimental conditions were similar to the loop flow stagnation cooldown situation for PWR LOCAs. No core heat was delivered during the experiment.

The UPTF downcomer azimuthal sectors oriented near CL-1, HL-2 and CL-2 were the best instrumented. This assessment concentrated on those three regions (out of eight) of the downcomer. Table H-1 summarizes comparisons of measured and calculated behavior for parameters pertinent for the vessel wall inside surface heat transfer coefficient for these three downcomer sectors.

The data showed a weak, plume under CL-2. RELAP5 was assessed against this test [12] with respect to its prediction of downcomer temperature. The code tended to over predict the water temperatures in the downcomer sector associated with CL-2, and under predicted it elsewhere in the downcomer. That is, RELAP5 tended to predict more mixing than seen in this experiment. The same experiment was used to assess RELAP5 for convective heat transfer in the downcomer.

Table H-1 Comparison of RELAP5 with UPTF 1-21 Data at the Top-of-Core Elevation

Temperature	Cold Leg 1	Hot Leg 1	Cold Leg 2
Fluid (T_f)	RELAP5 low by 8K	RELAP5 low by 8K	RELAP5 high by : 20 K (200-1,200 s) 9 K (1,200-2,790 s)
Wall Inside Surface (T_w)	RELAP5 low by 8K	RELAP5 low by 8K	RELAP5 high by: 18 K (200-1,200 s) 1 K (1,200-1,800 s) 4 K (1,800-2,790 s)
Wall 25 mm from Inside Surface (T_{w-25})	RELAP5 low by 8K	RELAP5 low by 8K	RELAP5 high by: 12 K (200-1,500 s) 1 K (1,500-1,800 s) 3 K (1,800-2,790 s)
$\Delta T (T_{w-surf} - T_f)$	RELAP5 within 10% of data	RELAP5 within 15% of data	RELAP5 low by factor of: 0.2 (200-1,200 s) 0.4 (1,200-2,790 s)

Figures H-1 through H-3 compare the calculated and measured downcomer fluid temperature behavior at the top-of-core elevation. HPI injection began at 126 s and continued until the end of the experiment at 2,790 s. These figures show that the code-calculated fluid temperatures were low by ~8 K away from CL-2, whereas below CL-2 the code-calculated temperatures were high by ~20 K during the period from about 200 s to 1,200 s. The over prediction decreased to ~9 K over the remainder of the test. This suggests the code calculated too much mixing in the downcomer. The fluctuations in the thermocouple data below CL-2 in Figure H-3 reflect the passage of eddy flows past the thermocouple.

Figures H-4 through H-6 compare the corresponding calculated and measured vessel inside wall surface temperatures at the same elevation. The calculated and measured wall surface temperature responses were similar to the fluid temperatures. RELAP5 under predicted the wall surface temperature by about 8 K away from CL-2, the same value of the under prediction of fluid temperature. The consistent temperature predictions indicates that RELAP5 provided an accurate calculation of heat transfer away from the weak plume below CL-2.

Below CL-2, RELAP5 over predicted wall surface temperature by ~18 K from 200 to 1,200 s, which was a little less than the ~20 K over prediction of fluid temperature during this time. From 1,200 s to 1,800 s, RELAP5 calculation of wall surface temperature was high by ~1K (compared to high by 8 K for fluid T). After 1800 s, RELAP5 was high by ~4 K (compared to high 8 K for fluid. The wall temperature over prediction was, therefore, ~ 1/2 of the fluid temperature over prediction over the later part of the test, which suggests that RELAP5 over predicted the heat transfer coefficient. This is consistent with RELAP5 tending to over predict mixing for this test.

To ensure that the wall surface temperature measurements were valid, the assessment included embedded thermocouples as well. At selected locations on the reactor vessel, thermocouples were embedded 25 mm (1 inch) beneath the inner surface of the vessel wall. Figures H-7 through H-9 compare the calculated and measured temperatures at the locations of the embedded thermocouples at the top-of-core elevation. Away from CL-2, RELAP5 under predicted wall temperature by ~8 K, which was the same as the wall surface temperature comparison. This

indicates that the surface thermocouple measurements were a reliable indication of true wall surface temperature.

Below CL-2, the over predictions at the embedded location are somewhat smaller than seen in the surface thermocouple comparison. This difference is likely caused by the rapid initial temperature drop that initially occurs below CL-2 when HPI flow first begins. The rapid initial temperature transient is delayed in time and damped as a result of the conduction process over the first 25 mm (1 inch) of the vessel wall.

Figures H-10 to H-12 compare the calculated and measured $\Delta T (T_w - T_f)$ for the three downcomer azimuthal locations. The comparisons show excellent agreement (within ~ 1 K) away from CL-2 (Figures H-10 and H-11).

Below CL-2, the ΔT data were noisy, reflecting the passage of eddies in the flow past the thermocouples locations (similar to the behavior in Figure H-3). For the purpose of comparison, the differential temperatures shown in Figure H-12 were smoothed by applying a 100 s running average to the data. The code under predicted ΔT throughout the test by a factor of three. This means that RELAP5 over predicted heat transfer in the plume region, which may indicate that fluid velocity was over predicted.

The wall-to-fluid heat transfer process is governed by the following equation,

$$Q = h A (T_w - T_f)$$

$$h = \frac{Q}{A(T_w - T_f)}$$

where Q is the wall surface heat transfer rate,
 h is the heat transfer coefficient,
 A is the wall surface area,
 T_w is the wall inside surface temperature and
 T_f is the fluid temperature.

Knowing T_w , T_f , and computing Q , h can be determined from the experimental data. Away from Cold Leg 2, the slopes of the measured and calculated wall temperature curves in Figures H-4, H-5, H-7 and H-8 compare well. Figures H-11 and H-12 plot ΔT in the regions away from Cold Leg 2, and show good agreement between RELAP5 and the data. If the slopes of the measured and calculated wall temperatures are the same, then the measured and calculated wall surface heat fluxes (Q/A) are also the same. Since the measured and calculated wall surface heat fluxes, and fluid-to-wall differential temperatures agree well, then the measured and calculated wall inside surface heat transfer coefficients must also agree well. Therefore, RELAP5 calculated h is in good agreement with the data away from CL-2.

The situation below CL-2 is more complex:

200 s to 1200 s: (ECC injection began at 126s) Figure H-12 shows the code under predicted ΔT by a factor of ~ 3 . Figures H-3 and H-6 show the measured fluid temperature and corresponding wall temperature dropped faster than the calculated values when HPI flow first began. RELAP5

did not capture the sharp initial drop in fluid temperature, therefore, the code under predicted wall heat flux early during the transient.

An estimate of the heat flux under prediction is made using the measured and calculated 25-mm wall temperatures at 600 s (Figure H-9). This time was selected because it is about when the calculated and measured temperatures stop diverging and start converging. From the start of HPI injection to 600s, the decline in the calculated temperature at 25 mm is 55% of the measured value. From this, it may be inferred that the average calculated wall heat flux is 55% of the actual wall heat flux.

If the code under predicted ΔT by a factor 3, and also under predicted wall surface heat flux by a factor of 0.55, then the code *over predicted* h by

$$\frac{0.55}{0.33} = 1.67$$

This comparison indicates RELAP5 over predicted heat transfer, which is conservative. The sharp drop in temperature below CL-2 when HPI arrives is probably due to the inertia of the fluid in the downcomer. Initially a strong (~40 K) plume develops that behaves initially like a free plume. Soon, however, the shear and buoyancy forces begin to establish a circulation cell in the downcomer, which limits the extent of temperature nonuniformity thereafter. RELAP5 is seen to miss this initial inertial effect.

1,200 s to end of test. Figure H-12 shows that the calculated wall-to-fluid ΔT remains ~1/3 the measured value. After 1,200 s the calculated wall temperatures show good agreement with the data, both at the surface (Figure H-6) and at 25 mm (Figure H-9). This indicates that the code is predicting surface heat flux well. Since ΔT is low by a factor of ~2, h must be high by a factor of ~2. This suggests that RELAP5 might be over predicting flow velocity below CL-2.

The UPTF downcomer is instrumented with eight turbine flow meters to measure flow velocity. These are regularly spaced around the circumference of the downcomer at an elevation near the bottom of the core. Figure H-13a shows the data channels from the eight turbine flow meters. Positive velocities represent the downward flow direction.

The turbine meter data is noisy reflecting turbulence in the flow past the meter, therefore for comparison purposes a 30 s running average was calculated and is shown in Figure H-13b show a 30 s running average. The one channel that shows positive flow is below CL-2. The measured velocity was 1 to 1.5 m/s. The remaining seven flow meter locations generally indicate no flow, or upflow. The turbine meters were designed to measure high velocity flows characteristic of large break LOCA phenomena. The range of the instruments was ± 25 m/s ± 0.5 m/s. The low flow cutoff is not known. The upflow velocities in the test away from CL-2 were generally too low to be measured accurately.

The superficial velocity associated with the 40 kg/s HPI injection flow through CL-2 (0.75-m diameter) was 0.091 m/s (3.6 inch/s). A flow velocity of 1.5 m/s in the downcomer is greater by a factor of,

$$\frac{1.5 \text{ m/s}}{0.091 \text{ m/s}} = 16$$

The downcomer flow data, therefore, show the flow to be driven primarily by buoyancy effects created by the cold water entering the downcomer inducing a circulation within the downcomer that results in a flow velocity at the core-bottom elevation that is 16 times the cold leg flow velocity. The flow enhancement should be greater near the top of the core. A simple plume decay would predict decreasing velocity with distance. As will be discussed in the next section, these flow data are consistent with APEX-CE and Creare experiments.

Figure H-14 shows the RELAP5-calculated downcomer flow velocities at the bottom of the core elevation for the same eight azimuth locations as the measured data in Figure H-13. The calculated flow velocities are smooth and, like the measured velocities, indicated downflow below CL-2 of ~ 0.75 m/s, which is $\sim 1/2$ the measured velocity.

Upflow regions away from CL-2 are present in both the test and the calculation, however, these sectors are different. Unlike the measured data, where upflow was seen in regions near CL-2, the upflow channels with RELAP5 are grouped together on the opposite side of the downcomer (CL-1, CL-4 and HL-4) from CL-2. The experimental data suggest upflow velocities of the order of 0.5 to 1 m/s (Figure H-13a). At $\sim 1/3$ m/s, the upflow velocities calculated by RELAP5 appear to be $\sim 1/2$ the measured velocities.

The RELAP5-calculated velocities, like the measured velocities, show a declining trend over the test period, consistent with a decrease in the buoyancy driving force as the whole downcomer gradually cools.

Figure H-15 shows the RELAP5-calculated fluid velocities at the top-of-core elevation (no measured data are available at elevations other than core-bottom). At this elevation only the channel with CL-2 is in downflow. The velocity in this channel is ~ 1.5 m/s early on and declines to ~ 1 m/s as the transient proceeds. The channels away from CL-2 flow upward with velocities ~ 0.2 m/s early on, declining to ~ 0.1 m/s later during the transient. The calculated velocities are, therefore, and as expected, higher at the top-of-core elevation than at the bottom-of-core elevation, by a factor of two.

Figure H-16 shows the RELAP5-calculated reactor vessel wall inside surface heat transfer coefficients below CL-2 and away from CL-2 at the top-of-core elevation. A hand calculation was performed using the conditions at 1,500 s to verify that RELAP5 was using the correct heat transfer correlations. At that time, the RELAP5 wall-to-fluid heat transfer coefficients below CL-2 and away from CL-2 are $4,380$ W/m²-K and $1,135$ W/m²-K, respectively.

RELAP5 calculates heat transfer coefficients separately using Dittus-Boelter and Churchill-Chu and then uses the maximum of the two. Below CL-2, the flow velocity is high enough for the turbulent forced convection heat transfer coefficient to be used. Hand calculations using Dittus-Boelter and the top-of-core elevation fluid conditions at 1,500 s resulted in a heat transfer coefficient of $4,357$ W/m²-K, which differs by a scant 0.53% from the RELAP5-calculated heat transfer coefficient.

Away from CL-2, the lower flow velocity results in the natural convection heat transfer coefficient exceeds the turbulent forced convection heat transfer coefficient. Hand calculations using Churchill-Chu and the top-of-core elevation fluid conditions at 1,500 s resulted in a heat transfer coefficient of $1,125$ W/m²-K which differs by a meager 0.89% from the RELAP5-calculated heat transfer coefficient.

In both the test and calculation, a predominant downward flow is seen in the downcomer sector into which the cold water enters. Lesser downward and upward flows are seen in the other sectors. At the core-bottom elevation (the only elevation at which flow measurements are available) RELAP5 under predicts the downcomer flow velocities in both affected and unaffected sectors by a factor of $\sim 1/2$.

Heat Transfer Statistics from UPTF

UPTF Tests 1-21 and 1-20 were used to generate comparisons between RELAP5 and the experimental data with respect to accuracy and uncertainty in the code's prediction of h . Vessel wall and fluid thermocouple test data at seven locations azimuthally around the downcomer, and at top, middle and bottom downcomer elevations. The transient was subdivided into periods of ~ 500 s. An experimental h was derived at each of the locations for each period. Then we statistically compared the experimental and RELAP5-calculated values of h .

UPTF 1-21

This test had HPI injection of 40 kg/s injection discussed immediately above. RELAP5 was within about 15% of the experimental h away from CL-2 and was a factor of ~ 2 high below CL-2. The statistics from the Test 1-21 comparison are:

$$\begin{aligned} \text{bias (RELAP5 - test data)} &= 1114 \text{ W/m}^2\text{-K,} \\ 1\sigma &= 1389 \text{ W/m}^2\text{-K.} \end{aligned}$$

RELAP5 over predicts h and is therefore, conservative.

UPTF 1-20

An additional assessment case was performed using data from the experiment that had the highest ECC injection rate, 70 kg/s. The downcomer flow velocities for this test are similar to Test 1-21. RELAP5 was found to moderately under predict the velocities which were measured at the bottom of the downcomer.

Also as with Test 1-21, RELAP5 significantly under predicted the wall-to-fluid differential temperature below CL-2.

For Test 1-20, RELAP5 under predicts both fluid and wall temperatures everywhere in the downcomer; whereas for Test 1-21, RELAP5 tended to slightly over predict the temperatures under the flowing cold leg and slightly under predict them elsewhere. At the higher injection rate in Test 1-20, RELAP5 significantly under predicted all of the temperatures.

Comparing the two experiments, evidently there is more mixing at the higher injection rate of Test 1-20 that is not being captured by RELAP5. The additional circulation in the experiment incorporates the cold legs into the mixing volume, which is not captured by the RELAP5 calculation. RELAP5 cannot capture "cold water under warm water" cold leg circulation and so in the calculation all of the cold water just goes into the vessel, leading to the over prediction of the downcomer cooldown rate. This is conservative for PTS.

For Test 1-20 RELAP5 consistently over predicts h by a factor of ~2 away from the flowing cold leg and by a factor of ~6 underneath the flowing cold leg. The h comparison statistics for Test 1-20 are:

$$\begin{aligned} \text{bias: (RELAP5 - test data)} &= 1067 \text{ W/m}^2\text{-K,} \\ \sigma &= 947 \text{ W/m}^2\text{-K.} \end{aligned}$$

The measured values of h are lower for the test with the higher injection rate. It may be that at the higher injection rate the cold leg flow from CL-2 jumps the downcomer gap and flows preferentially near the core barrel.

The quantified numerical values for the code-data comparison of h bias and standard deviations are remarkably similar for the two tests (although on a percentage basis they are larger for the test with the higher injection flow).

Comparison of UPTF Convective Heat Transfer Experimental Data to RELAP5 Prediction

As seen in measurements of downcomer flow velocity from UPTF (as well as Creare and APEX-CE), the absolute value of integrated mass flow in the downcomer is ~20 times the injected ECC flow. Therefore, instead of “nearly creeping” flow rates of ~1 in/s, the flow velocities are of the order of 1 m/s. RELAP5 predicts downcomer velocities consistent with these numbers.

RELAP5 calculates forced convection heat transfer using these velocities. The code applies the *maximum* of free convection and forced convection heat transfer. As the fluid velocity decreases to zero, therefore, h does not drop to zero. Rather, free convection provides a lower floor of heat transfer, which is rather substantial.

Figures H-17 and H-18 compare RELAP5 predicted heat transfer to UPTF data for two experiments, 1-21 and 1-20. We used vessel wall and fluid thermocouple test data at seven locations, scattered around the downcomer periphery and at top, middle and bottom downcomer elevations. We subdivided the transient into 500s periods and derived an experimental h at each of the locations for each period. Then we statistically compared the experimental and RELAP5-calculated values of h.

UPTF 1-21

This test had 40 kg/s injection into a single cold leg, CL-2. This injection rate is about twice that of normal HPI flow into a single leg, and ½ of total HPI flow of four loops. For this test, RELAP5 tended to slightly over predict the temperatures under the flowing cold leg and slightly under predict them elsewhere.

RELAP5 was within ~15% of the experimental h for regions away from CL-2 that had the ECC injection, whereas RELAP5 over predicted the experimental h underneath CL-2 (with the ECC injection) by a factor of ~2. Figure H-17 shows the results. About half of the points indicate very good agreement between the test and RELAP5, for the locations away from CL-2. The remaining points show that RELAP5 over predicts h underneath the CL-2.

The statistics from the Test 1-21 comparison are as follows:

- average difference (RELAP5 - test data) = 1114 W/m²-K,
- $\sigma = 1389$ W/m²-K.

UPTF 1-20

This test had a higher injection rate of 70 kg/s injection into CL-2, which is approaching the LPI injection rate into a single cold leg. RELAP5 moderately under predicted the experimental velocities in the downcomer. The downcomer flow velocity comparisons for this test are similar to those of Test 1-21.

RELAP5 under predicted (RELAP5 temperatures were too low, which is conservative) both the fluid and wall temperatures from the test everywhere in the downcomer. This is attributed to cold leg mixing in the experiment being more robust at the higher injection rate than it is at the lower rate. There is more circulation within the cold legs at the higher injection rate so more cold leg fluid volume participates in the mixing process. For test 1-20, RELAP5 may be under predicting in-vessel natural circulation as well, possibly due to incorrect upper plenum to downcomer bypass.

Figure H-18 shows that RELAP5 consistently over predicts h of this test by a factor of ~ 2 away from CL-2 with the ECC injection, and by a factor of ~ 6 below CL-2.

The h comparison statistics for Test 1-20 are

- average difference (RELAP5 - test data) = 1067 W/m²-K,
- $\sigma = 947$ W/m²-K.

The numerical values for the code-data h comparison differences and standard deviations are remarkably similar for the two tests (although on a percentage basis they are larger for the test with the higher ECC injection flow).

The flow patterns in the downcomer are not fixed. The downcomer flow is unsteady. This can be seen in Figures H-19 and H-20, which show downcomer velocity and fluid temperature data, respectively, from UPTF. The “noise” in the data reflects the unsteady flow.

If, for the sake of argument, the plant experienced fixed points of flow stagnation in the downcomer, the heat transfer at the stagnation points would be lower than the flowing parts of the downcomer. Such stagnation points would experience higher vessel wall temperatures and would, therefore, be less likely to fail. The RELAP5 calculations do not produce flow stagnation points. If there were significant temperature variations in the downcomer where there were colder temperatures due to incomplete mixing (plumes), previous study (see Section 5.5) showed that the impact on conditional probability of vessel failure is minimal.

In summary we conclude that,

- ***Based on two UPTF tests with different ECC injection rates, the RELAP5 predictions of h compared to the data were bias (RELAP5 - data) = ~ 1100 W/m²-K***

$$1\sigma = \sim 1150 \text{ W/m}^2\text{-K}$$

In over predicting h, RELAP5 was conservative .

- *The flow induced in the downcomer region by cold water entering through one cold leg is much larger (~16 times) than the HPI injection rate. The experimental data indicate velocities in the range ~0.5 m/s to 1.5 m/s.*
- *Hand calculation checks show that the code is using the intended heat transfer correlations and that the RELAP5-calculated heat transfer coefficients agree with the calculated fluid and wall conditions.*

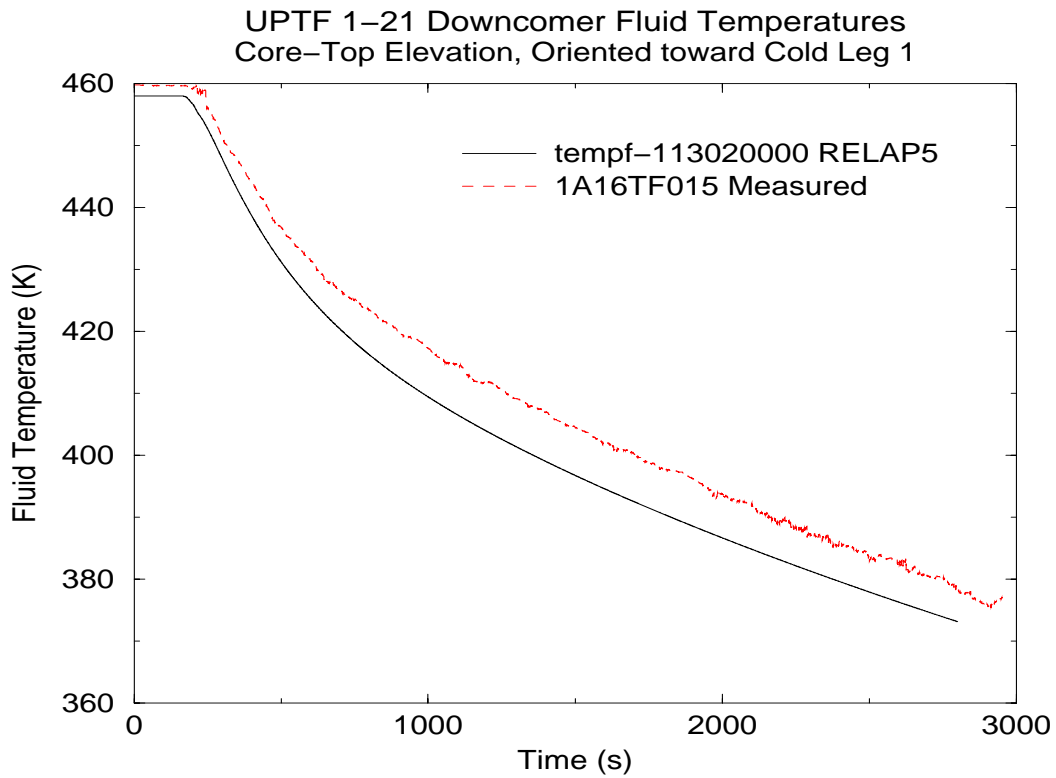


Figure H-1 UPTF 1-21 Downcomer Fluid Temperatures Core-Top Elevation, Oriented Toward Cold Leg 1

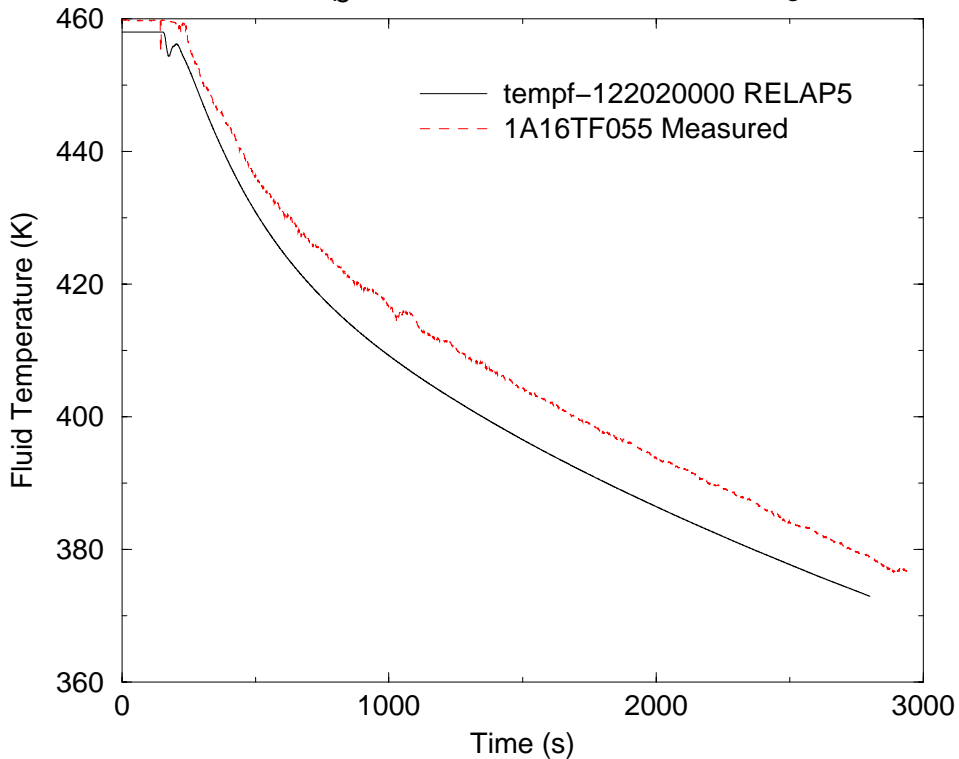


Figure H-2 UPTF 1-21 Downcomer Fluid Temperatures Core-Top Elevation, Oriented Toward Cold Leg 2

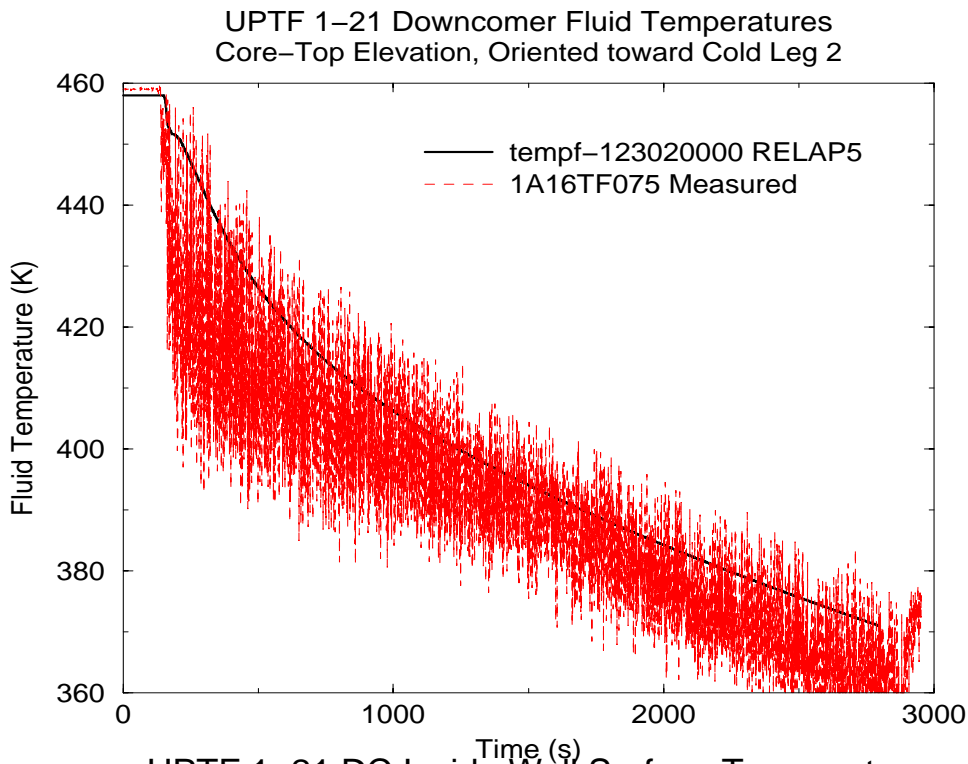


Figure H-3 UPTF 1-21 DC Inside Wall Surface Temperatures Core-Top Elevation, Oriented Toward Cold Leg 2

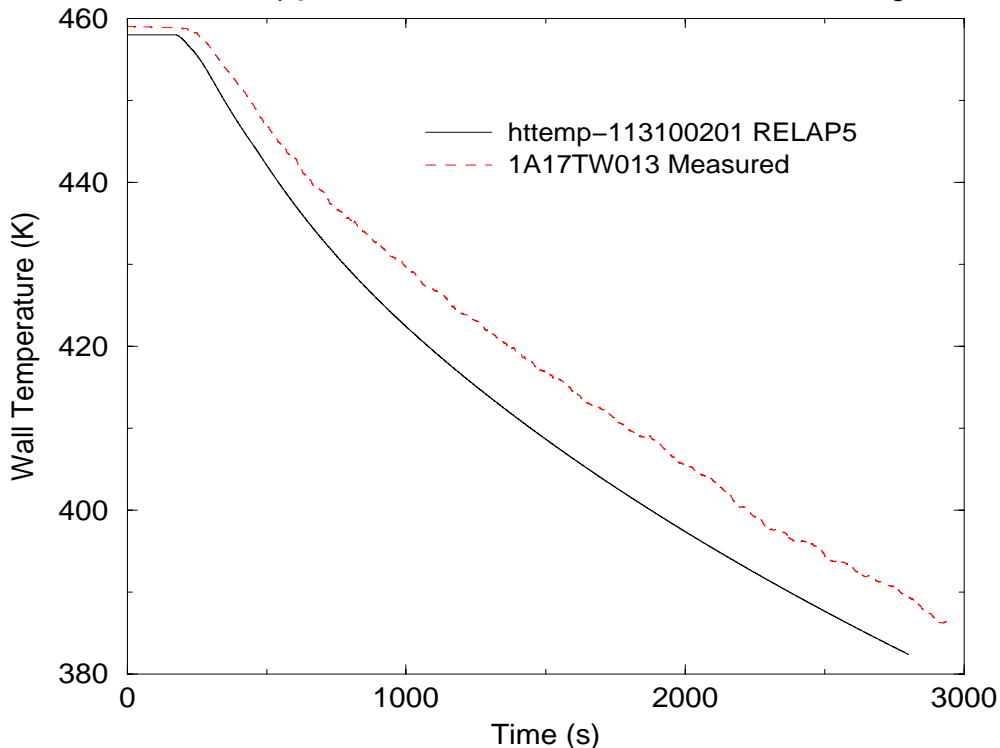


Figure H-4 UPTF 1-21 DC Inside Wall Surface Temperatures Core-Top Elevation, Orientation in Direction of Cold Leg 1

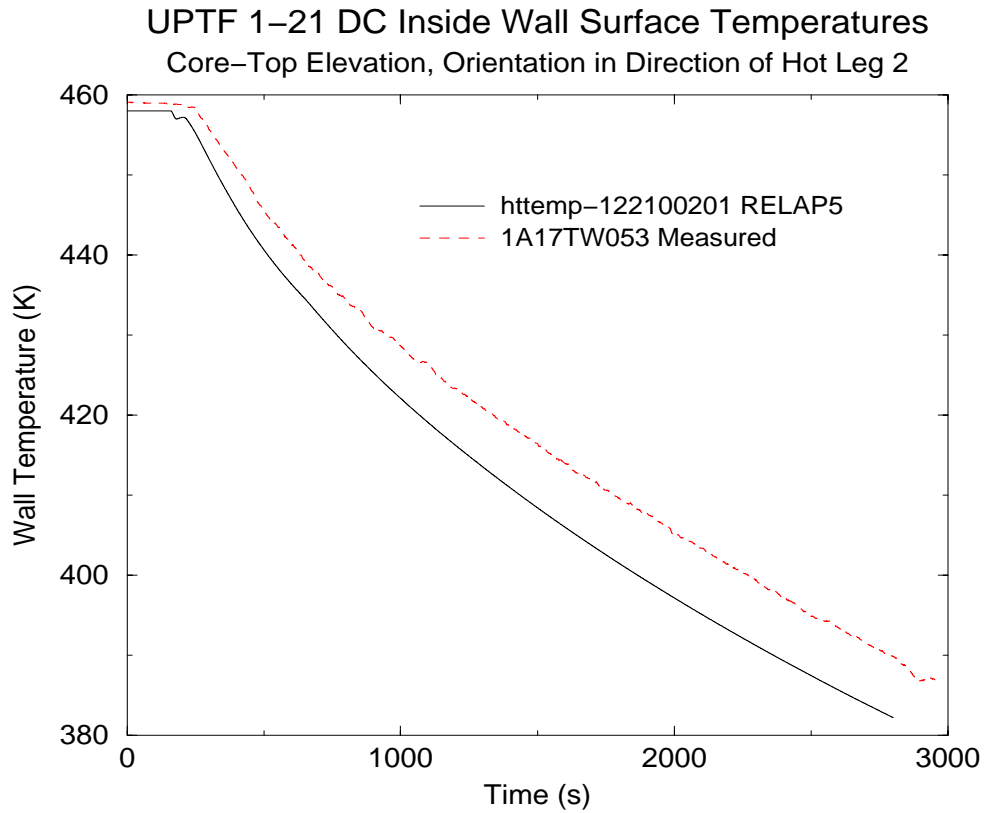


Figure H-5 UPTF 1-21 DC Inside Wall Surface Temperatures Core-Top Elevation, Orientation in Direction of Hot Leg 2

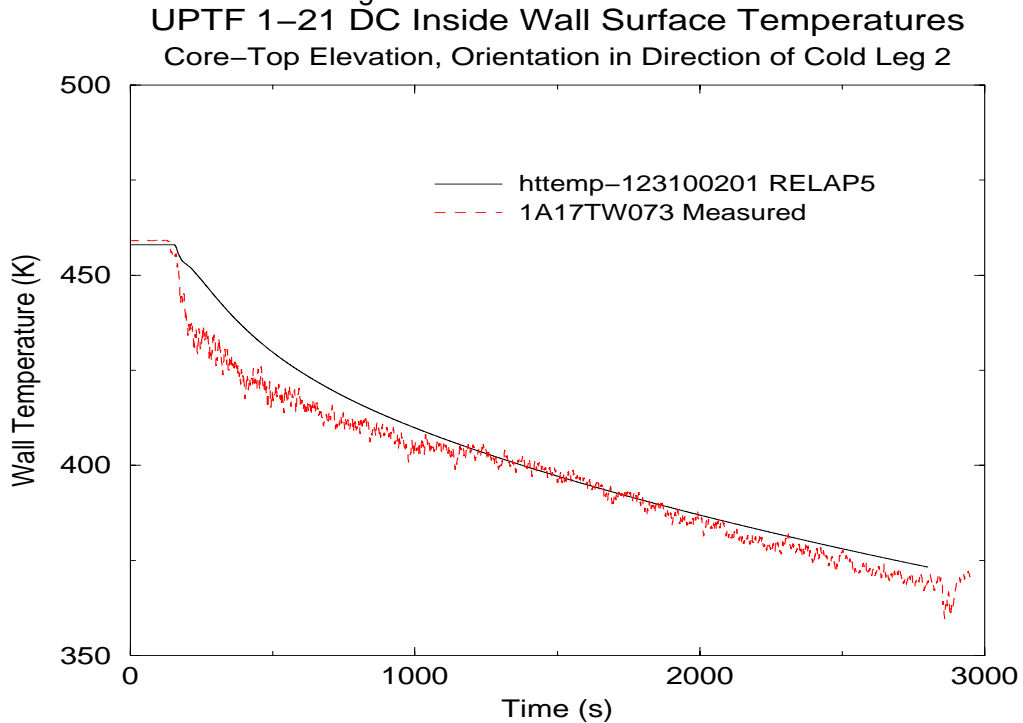


Figure H-6 UPTF 1-21 DC Inside Wall Surface Temperatures Core-Top Elevation, Orientation in Direction of Cold Leg 2

UPTF Test 1-21 Wall Temperatures at 25 mm Depth

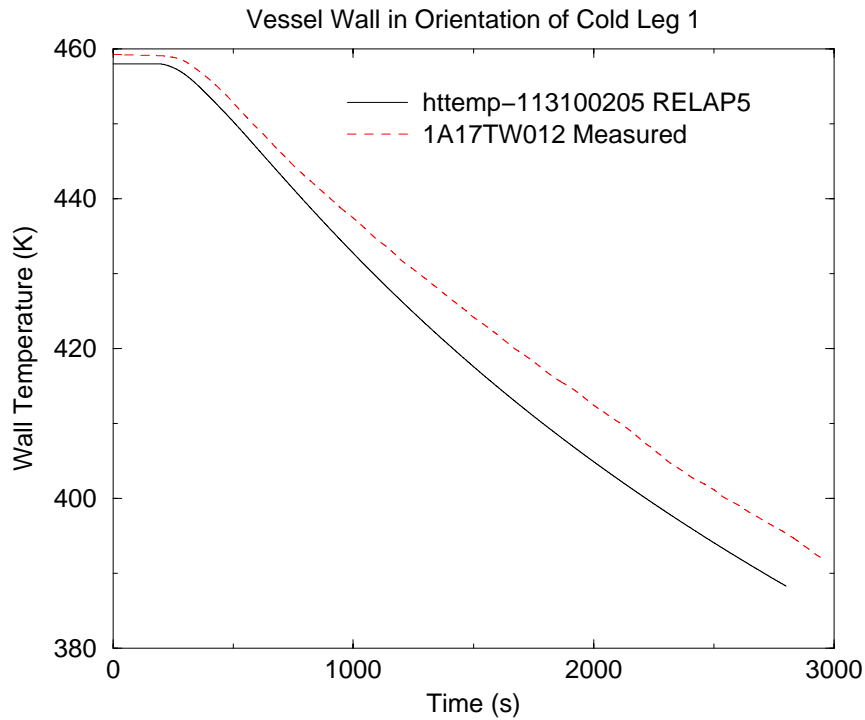


Figure H-7 UPTF 1-21 Wall Temperatures at 25 mm Depth Vessel Wall in Orientation of Cold Leg 1

UPTF Test 1-21 Wall Temperatures at 25 mm Depth

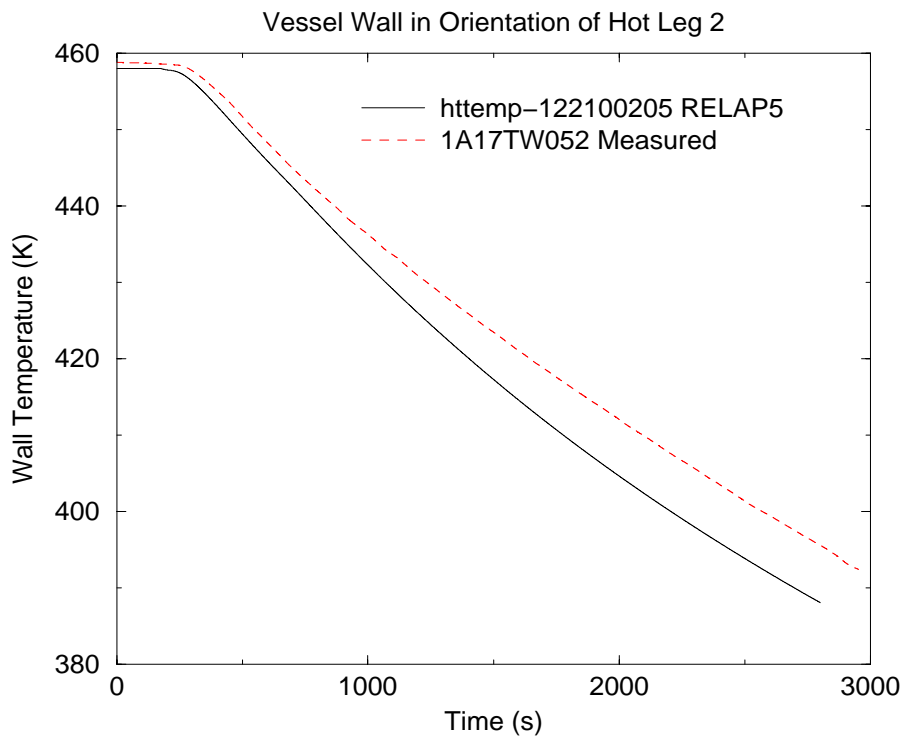


Figure H-8 UPTF Test 1-21 Wall Temperatures at 25 mm Depth Vessel Wall in Orientation of Hot Leg 2

UPTF Test 1-21 Wall Temperatures at 25 mm Depth

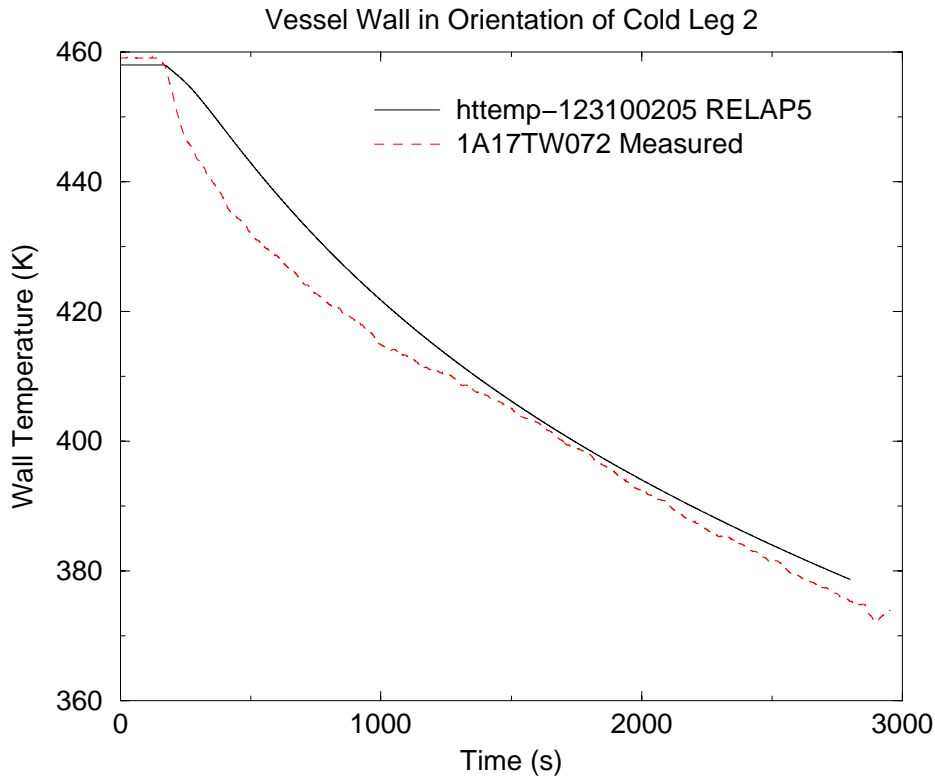


Figure H-9 UPTF Test 1-21 Wall Temperatures at 25 mm Depth Vessel Wall in Orientation of Cold Leg 2

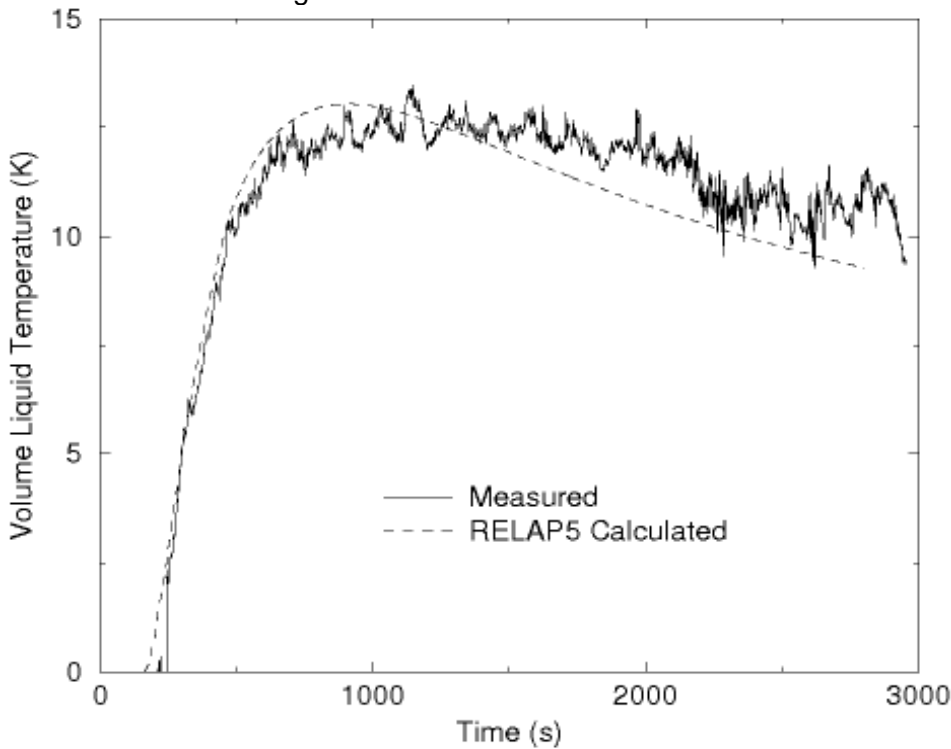


Figure H-10 UPTF 1-21 Inside Wall Temperature Minus Fluid Temperature Under Cold Leg 1 at Core-Top Elevation

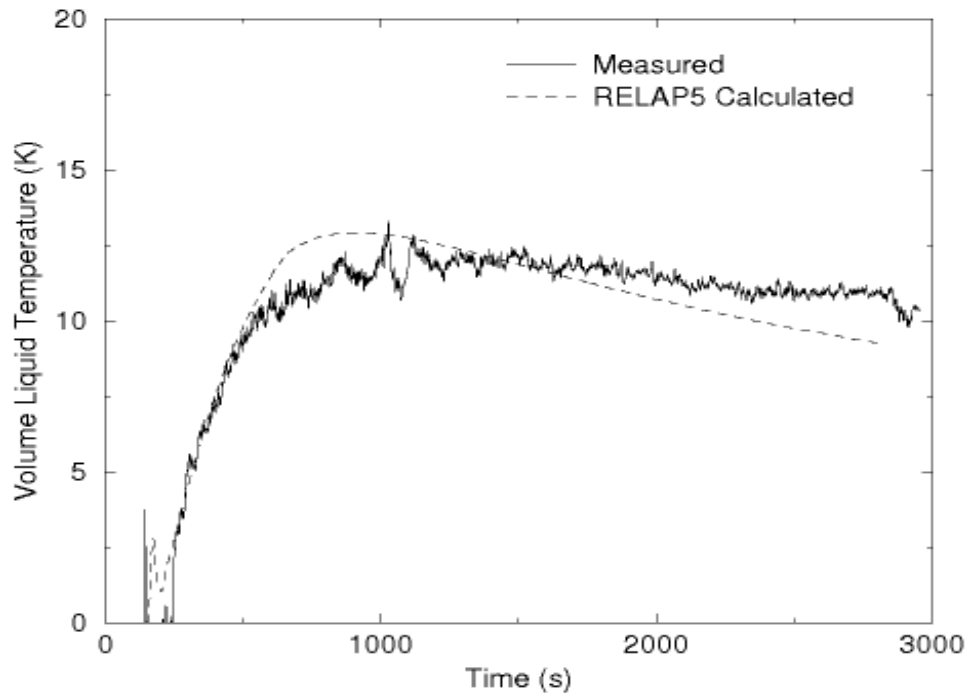


Figure H-11 UPTF 1-21 Inside Wall Temperature Minus Fluid Temperature Under Hot Leg 2 at Core-Top Elevation

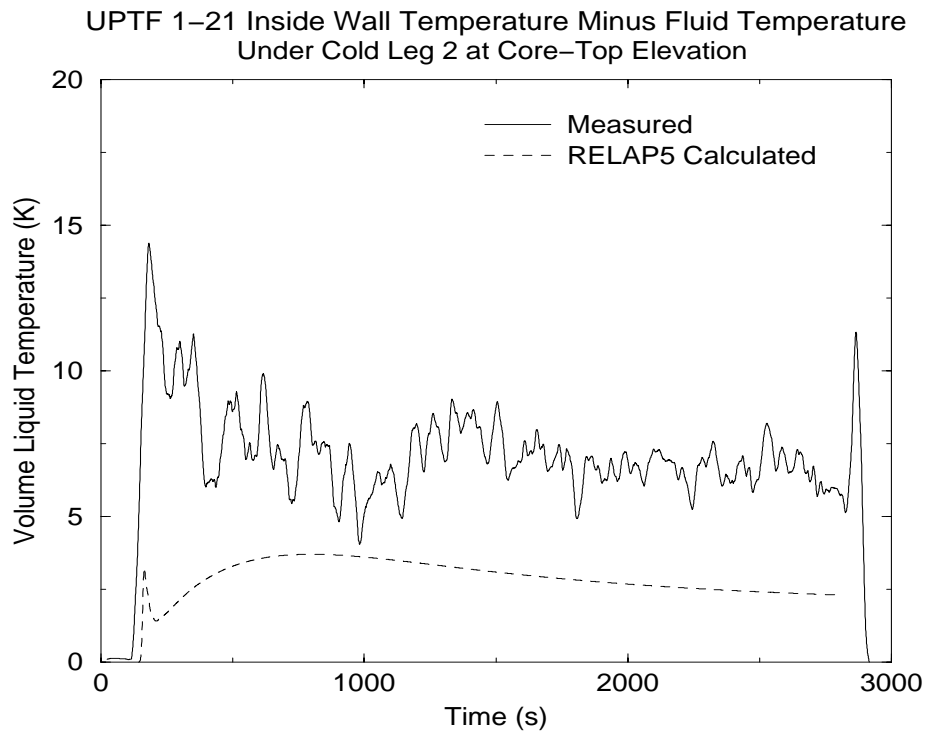


Figure H-12 UPTF 1-21 Wall Temperature Minus Fluid Temperature Under Cold Leg 2 at Core-Top Elevation

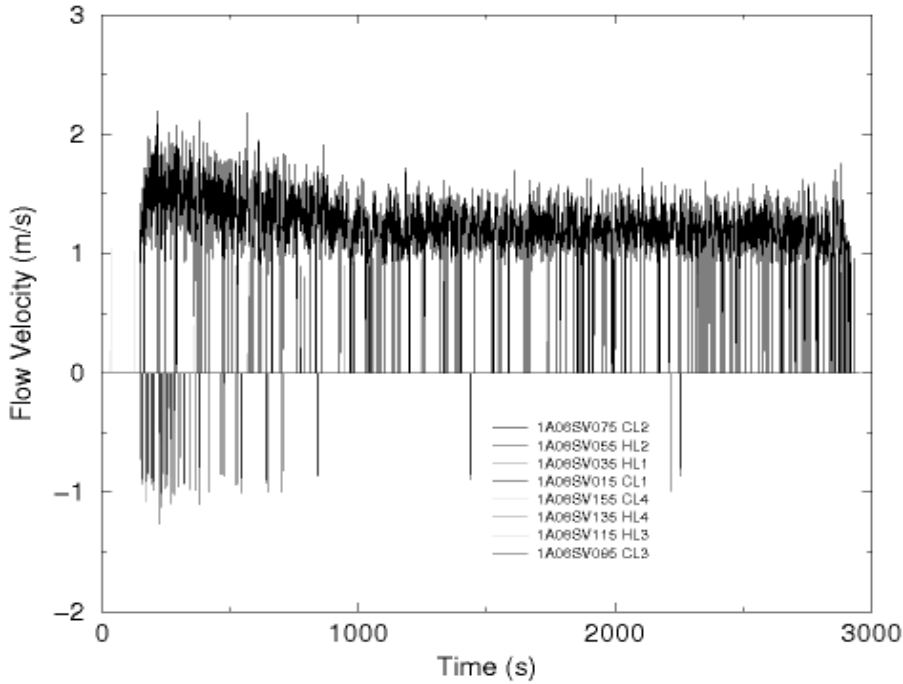


Figure H-13a UPTF 1-21 DC Velocities at Bottom-Core Elevation Measured, Turbine Meters, Clockwise from Cold Leg 2, Unfiltered

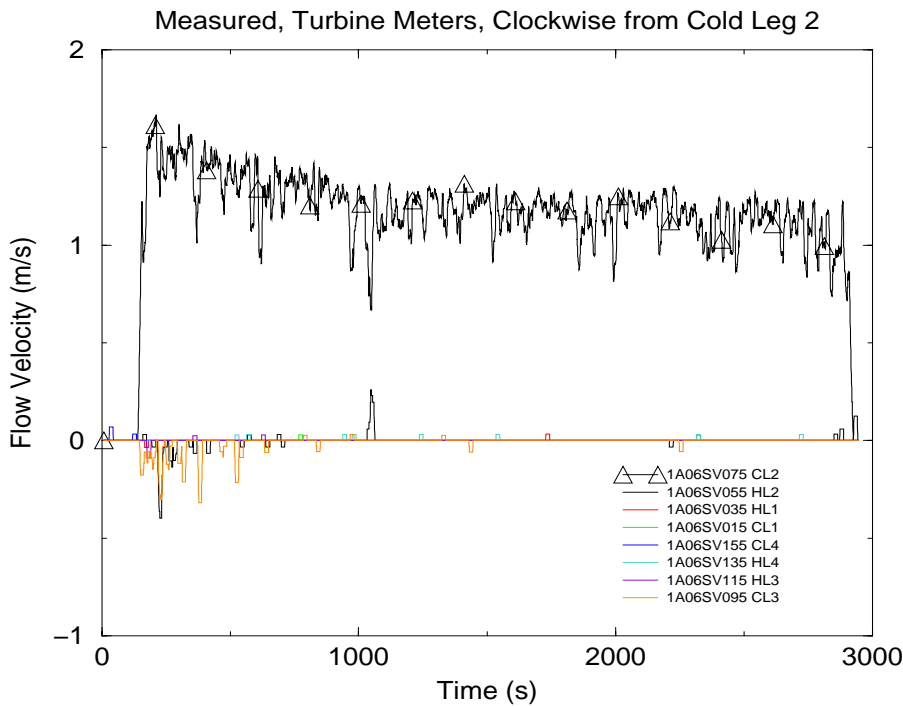


Figure H-13b UPTF 1-21 DC Velocities at Bottom-Core Elevation Measured, Turbine Meters, Clockwise from Cold Leg 2, Filtered

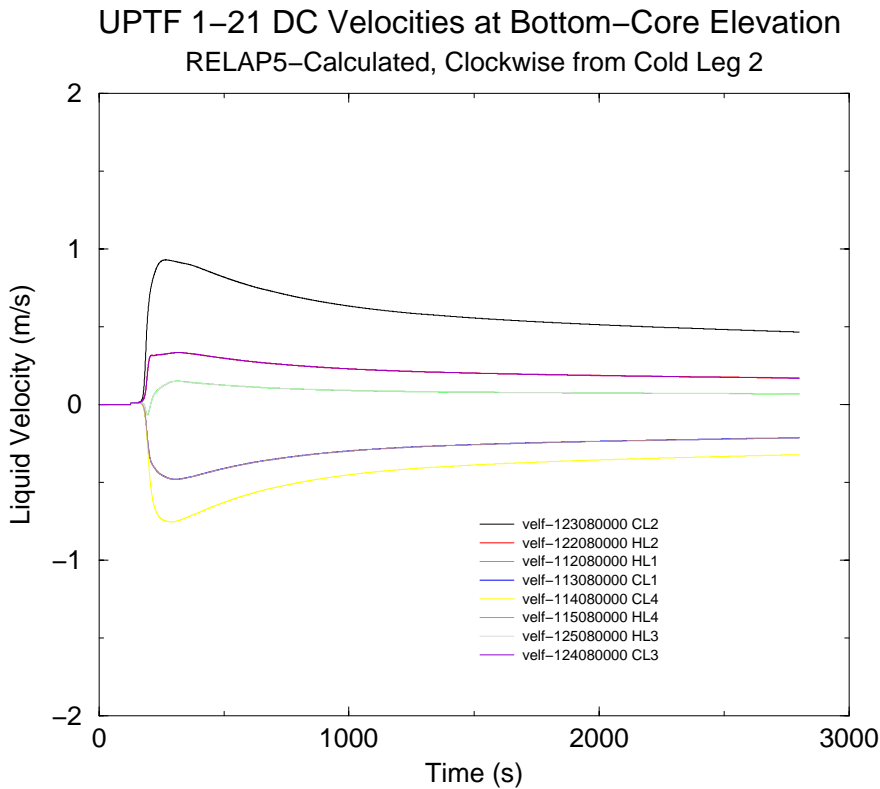


Figure H-14 UPTF 1-21 DC Velocities at Bottom-Core Elevation RELAP5-Calculated, Clockwise from Cold Leg 2

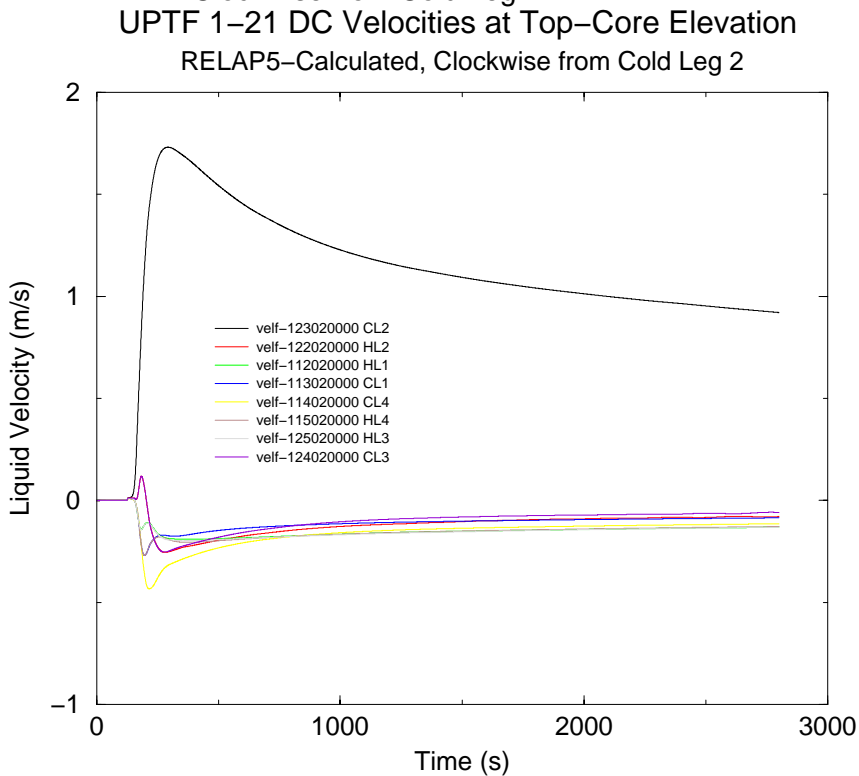


Figure H-15 UPTF 1-21 DC Velocities at Top-Core Elevation RELAP5-Calculated, Clockwise from Cold Leg 2

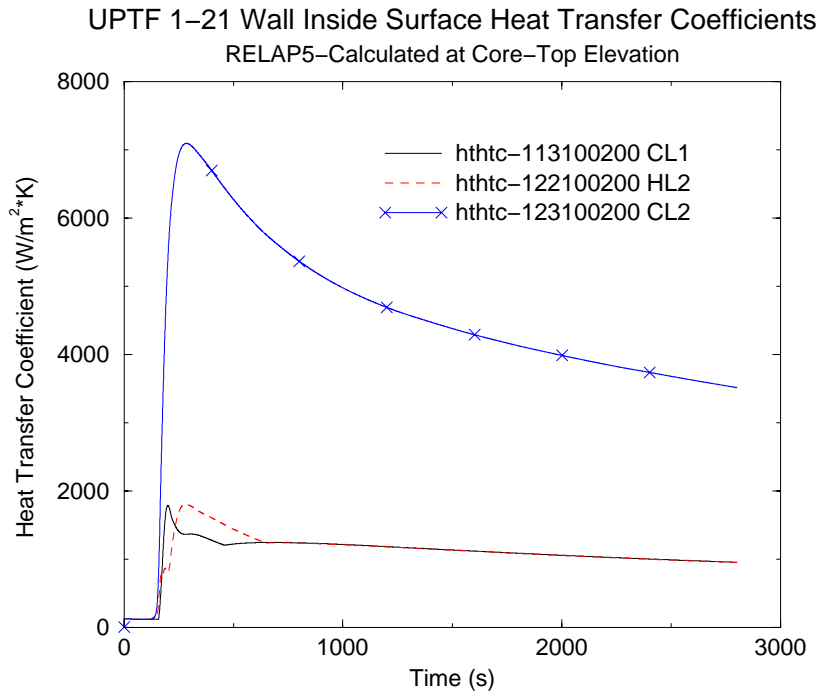


Figure H-16 UPTF 1-21 Wall Inside Surface Heat Transfer Coefficients RELAP5-Calculated at Core-Top Elevation

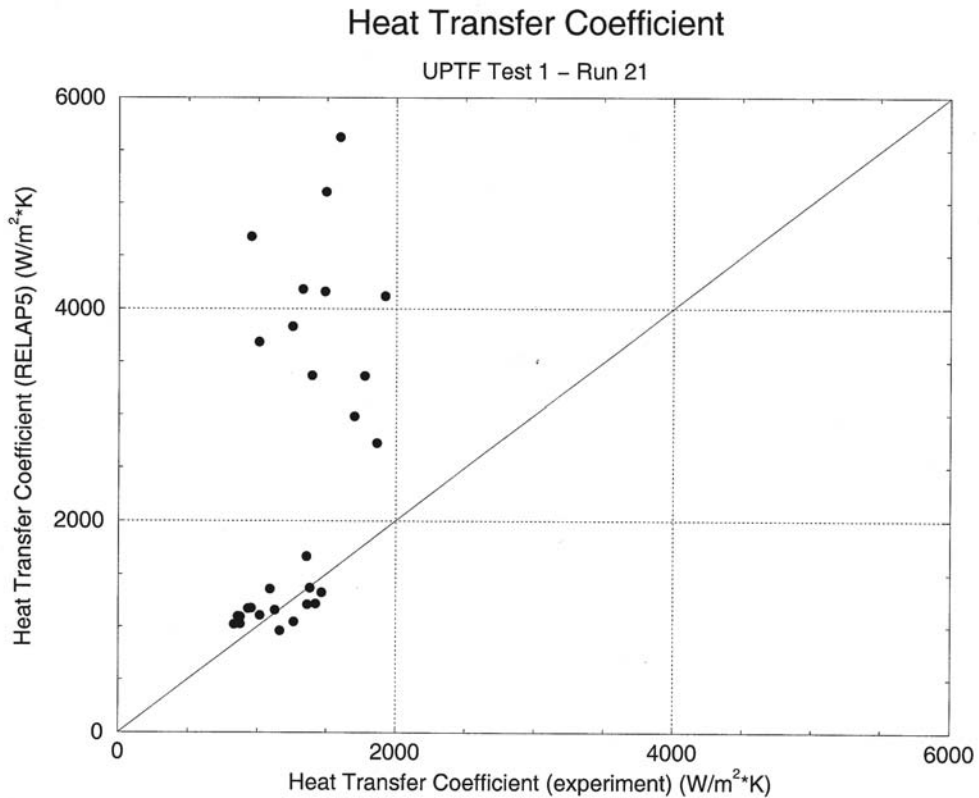


Figure H-17 Comparison of RELAP5 Predicted h with Data from UPTF 1-21

- RELAP5 is within ~15% for points away from CL-2 with ECC injection
- RELAP5 over predicts h by factor of 2 for points below CL-2 with ECC injection

The statistics from the Test 1-21 comparison are as follows:

- average difference (RELAP5 - test data) = 1114 W/m²·K (conservative)
- $\sigma = 1389$ W/m²·K

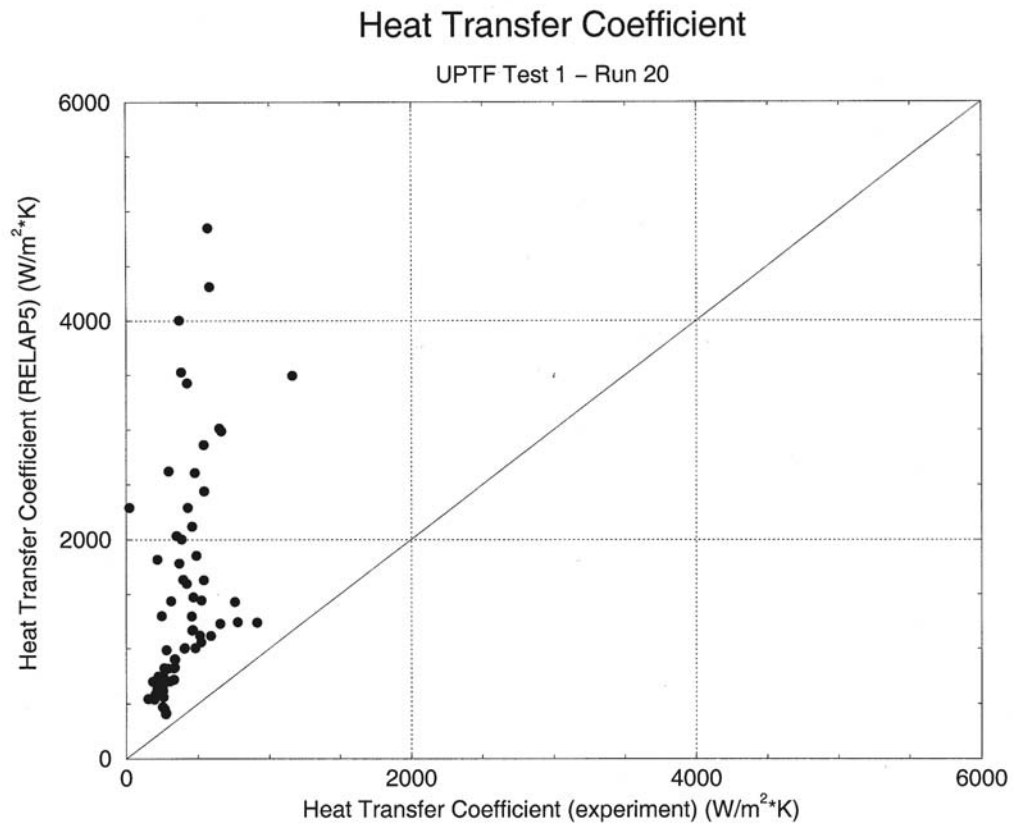


Figure H-18 Comparison of RELAP5 Predicted h with Data from UPTF 1-20

The h comparison statistics for Test 1-20 are

- average difference (RELAP5 - test data) = 1067 W/m²-K (conservative)
- $\sigma = 947$ W/m²-K

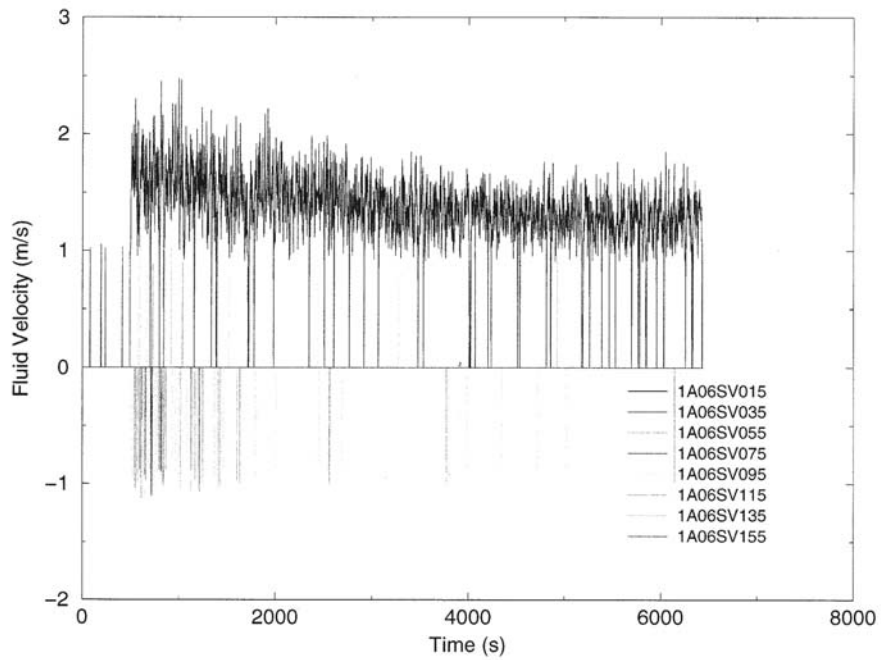


Figure H-19 Fluid Velocity Measurements at Bottom of Core Elevation in UPTF at 8 Azimuthal Locations in the Downcomer

The “noise” in the data reflect the real nature of the unsteady flow. The velocities are near the measurement threshold of the turbine flow meters of ~1 m/s. Where indicated velocities drop to zero reflect actual velocities <1 m/s.

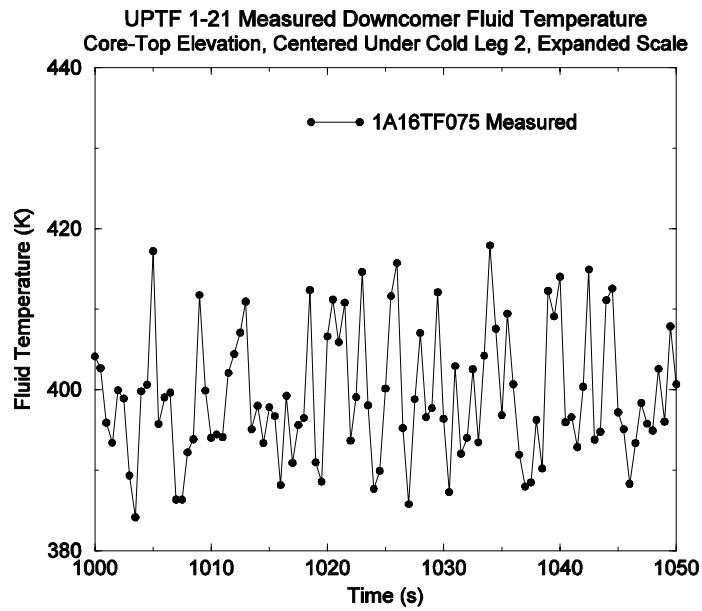


Figure H-20 UPTF 1-21 Downcomer Fluid Temperature at Top-of-Core Elevation Below CL-2 Showing Unsteady Nature of Flow

Time scale expanded to show individual data points

H.2 APEX-CE

Test APEX-CE-5 consisted of injecting cold HPI water through all four cold legs into a system that was initially filled with hot pressurized water. The cold water injection commenced at 186 s and the test was terminated at 4,229 s. This test was similar to the two UPTF tests discussed above, with the exception that APEX-CE-05 had injection into all four cold legs instead of one.

A basic assessment of RELAP5 capabilities using data from this test is documented in the RELAP5 PTS assessment report [12]. RELAP5 predicted the downcomer temperatures well for the first 1,700 s, and under predicted them slightly thereafter.

The APEX-CE facility had three vessel wall temperature measurements in the downcomer region below the CL-4 nozzle. The analysis concentrates on the region of the lowermost of these three thermocouples, which is centered below CL-4 at an elevation between the cold leg nozzle and the top of the core. While there were no fluid velocity measurements, estimates of velocity were obtained using thermocouple data.

Figures H-21 and H-22 compare the calculated and measured downcomer fluid temperature and vessel wall inside surface temperature, respectively. Both comparisons show good agreement between the calculated and measured data up to ~1,700 s. The good agreement between the slopes of the measured and calculated wall temperature curves in Figure H-22 also indicates that the code is also predicting the wall-to-fluid heat flux well during this period. The heat transfer coefficient analysis here concentrates on the test period up to 1,700 s.

After 1700 s, Figures H-21 and H-22 show that the code under predicts both the fluid and wall temperatures. In the basic assessment of RELAP5 for this test, these under predictions were attributed to the involvement of a greater volume of fluid in the mixing process in the experiment than in the calculation. This could be attributed to the code under predicting circulation of fluid from the cold leg loop seal regions into the vessel or under predicting the vessel upper head-to-downcomer region bypass flow.

Figure H-23 compares the measured fluid and vessel wall inside surface temperatures beneath CL-4. Figure H-24 compares the RELAP5-calculated values for the same parameters. RELAP5 shows a smaller ΔT than the data, which suggest that h is over predicted by RELAP5.

Figure H-25 plots ΔT for the data while Figure H-26 is the ΔT calculated by RELAP5. There was considerable noise in the fluid temperature, so the measured data were smoothed using a 50-s running average. The measured wall-to-fluid ΔT averaged 6 K over the first 1,700 s of the test. The calculated ΔT is ~1/2 the experimental value.

Similar to UPTF, the noise in the thermocouple data indicates the passage of eddy flows past the thermocouple.

As described in the [12], the code calculated discrete periods of circulating flows within the two cold legs on each coolant loop. During these circulation periods, flow moves toward the vessel through one of the cold legs and away from vessel in the other cold leg on the same coolant loop. Subsequently the flows decelerate and decay away.

Figure H-27 shows the RELAP5-calculated vessel wall inside surface heat transfer coefficient. The peaks in the heat transfer coefficient at about 400 s, 1100 s and 1,900 s reflect periods of high cold leg flow circulation. These cold leg circulations, along with variations in the RELAP5-calculated fluid temperature, are responsible for the large variations in the RELAP5-calculated wall-to-fluid ΔT seen in Figure H-26. Note that what appear (because of the y-axis scale) to be small variations in the calculated fluid temperature in Figure H-25, are actually 3 K in magnitude, which is large compared to the average ΔT (2.3K) over the course of the transient

This analysis shows that RELAP5 is predicting the wall surface heat flux (Q/A) well, but is significantly under predicting the wall-to-fluid differential temperature by a factor of

$$\frac{2.3K}{6.3K} = 0.37$$

over the first 1,700 s of the test period. It is, therefore, concluded that RELAP5 is over predicting the wall-to-fluid heat transfer coefficient by a factor of

$$\frac{1}{0.37} = 2.74$$

This over prediction by RELAP5 of h is similar to that obtained from the UPTF comparison.

The downcomer velocities were compared between the RELAP5 calculation and the data. There are no velocity measurements in APEX-CE, however, it is possible to determine velocity from thermocouples. The distance between two thermocouples is divided by time it takes a temperature wave to pass two thermocouple locations. In this manner, we obtained an estimate of 0.15 m/s (6 inches/s). RELAP5 calculations were examined at three elevations in the downcomer. The code calculated a velocity of 0.2-to-0.25 m/s during this time, which is in reasonable agreement with the value estimated from the data.

The superficial velocity from ECC flow in the downcomer was ~0.8 cm/s (0.3 inches/sec). Therefore, the velocity in the downcomer is ~20 times greater than the superficial velocity, which is very similar to the factor of 16 obtained in UPTF.

The height scaling of APEX-CE was 1:3.66. Since the downcomer flows are buoyancy driven, the driving force is

$$F = \Delta \rho g h$$

At full height, the elevation will be 3.66 times greater. The density ratio of APEX-CE and the prototype based on initial temperature are

$$\frac{\rho_{ECC}}{\rho_0} = 1.16 \quad \text{APEX - CE}$$

$$\frac{\rho_{ECC}}{\rho_0} = 1.35 \quad \text{prototype}$$

so the driving force will be 2.2×3.66 , or ~ 8 times greater at full scale. The APEX-CE velocity scaled up to the prototype should therefore be approximately

$$0.15 \sqrt{8} = 0.42 \text{ m / s}$$

Therefore, we conclude

- ***RELAP5 calculated flow velocities and fluid temperatures agree well with the data.***
- ***The code calculated heat flux agreed well with the data. The code calculated heat transfer coefficient is higher than the data.***
- ***APEX-CE data show a factor of 20 increase in downcomer flow over ECC flow. The experimental data suggest downcomer velocities at full scale of ~ 0.4 m/s.***

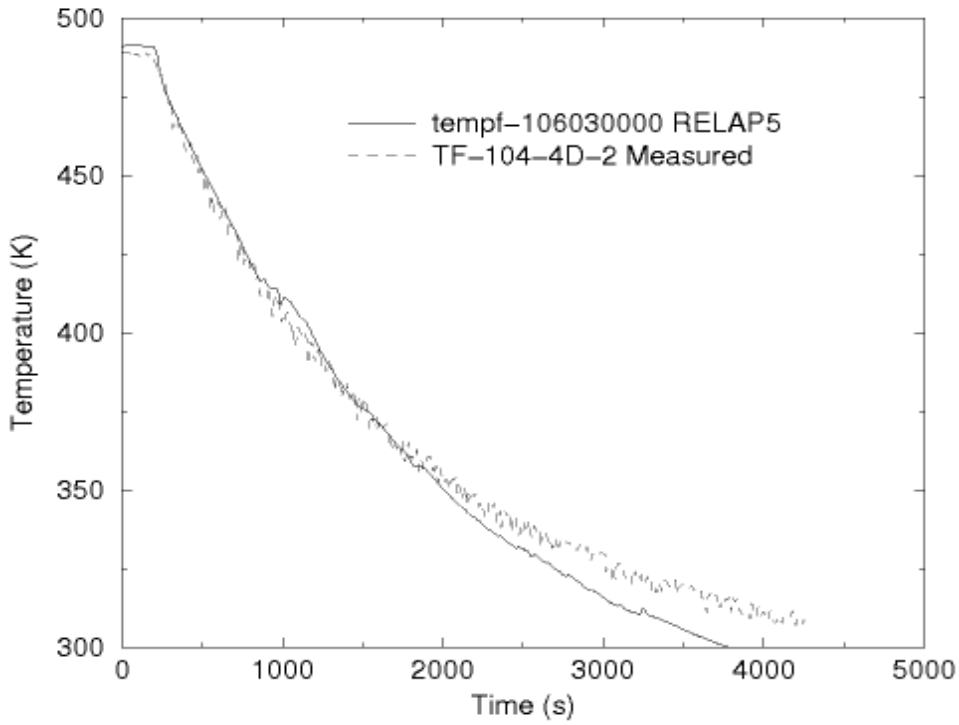


Figure H-21 APEX-CE-05 Measured and RELAP5 Fluid Temperatures 4D Below and Centered on the Cold Leg 4 Nozzle

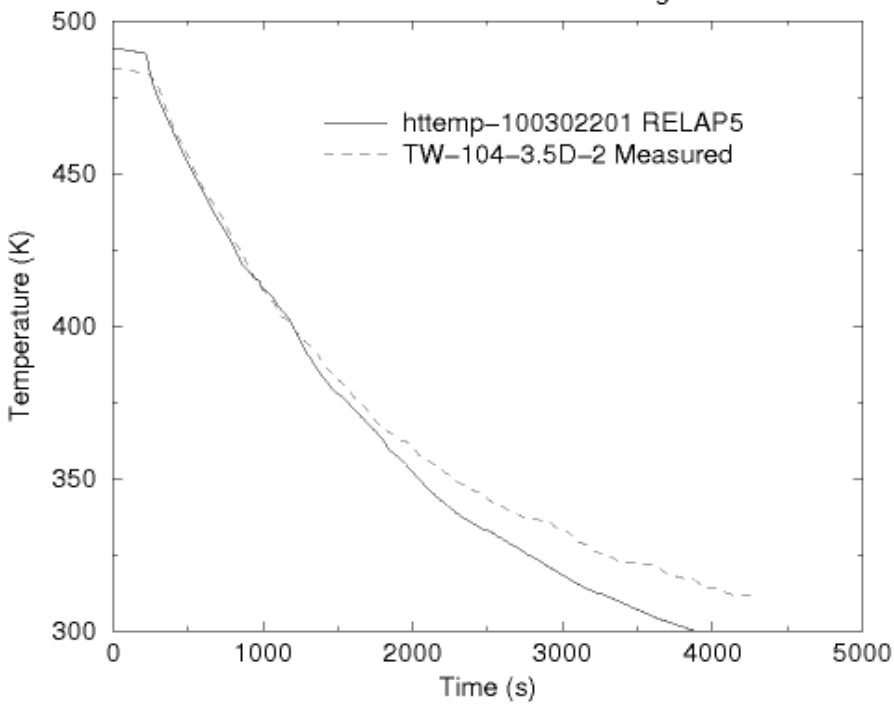


Figure H-22 APEX-CE-05 Measured and RELAP5 Wall Temperatures 4D Below and Centered on the Cold Leg 4 Nozzle

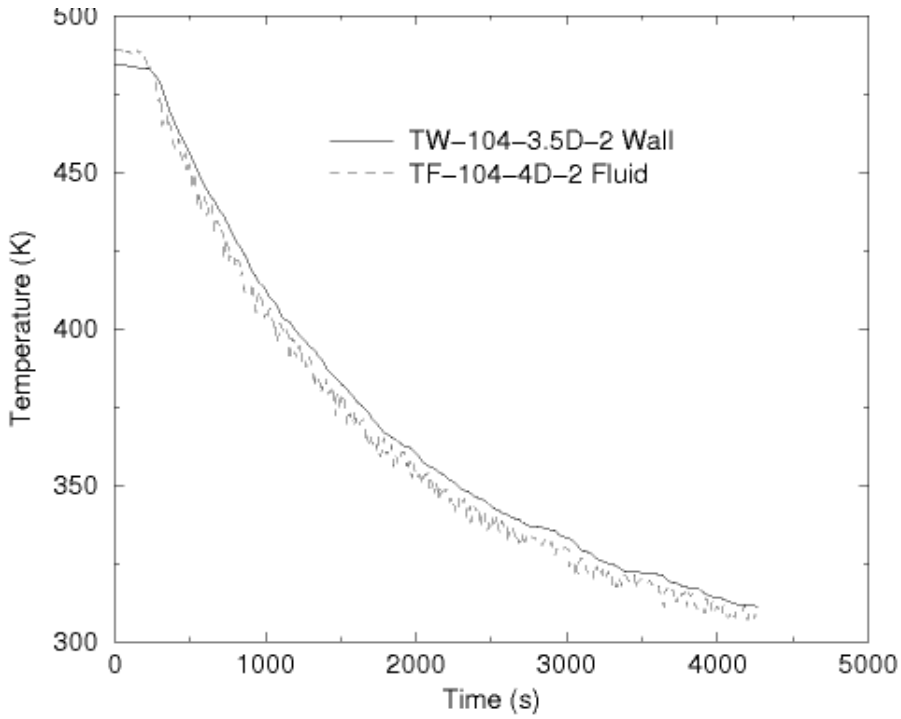


Figure H-23 APEX-CE-05 Measured Fluid and Inside Wall Surface Temperatures 4D Below and Centered on the Cold Leg 4 Nozzle

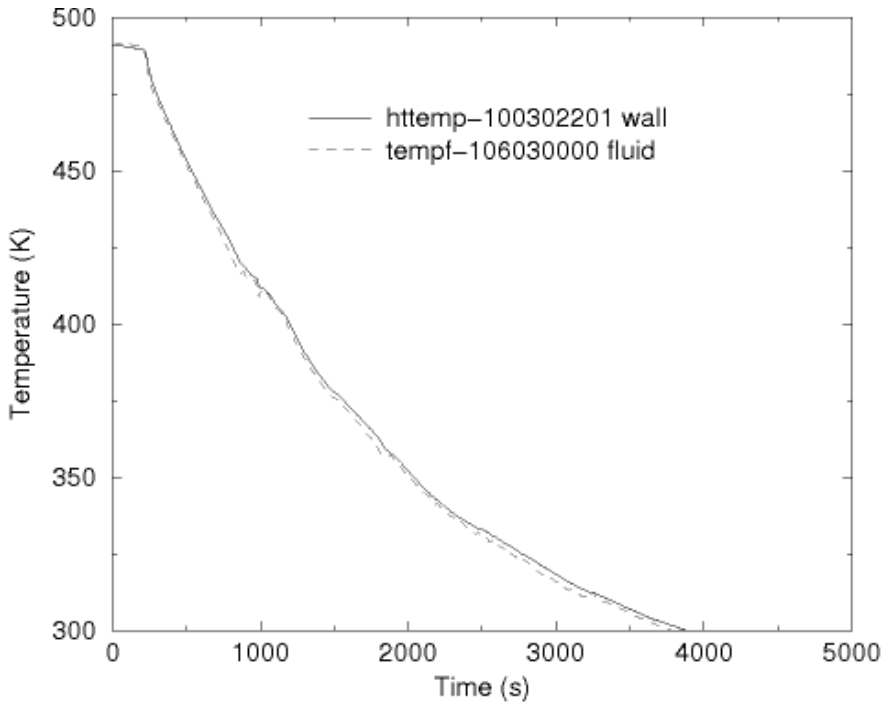


Figure H-24 APEX-CE-05 RELAP5-Calculated Wall and Fluid Temperatures Centered Below Cold Leg 4, Between Cold Leg and Top of Core

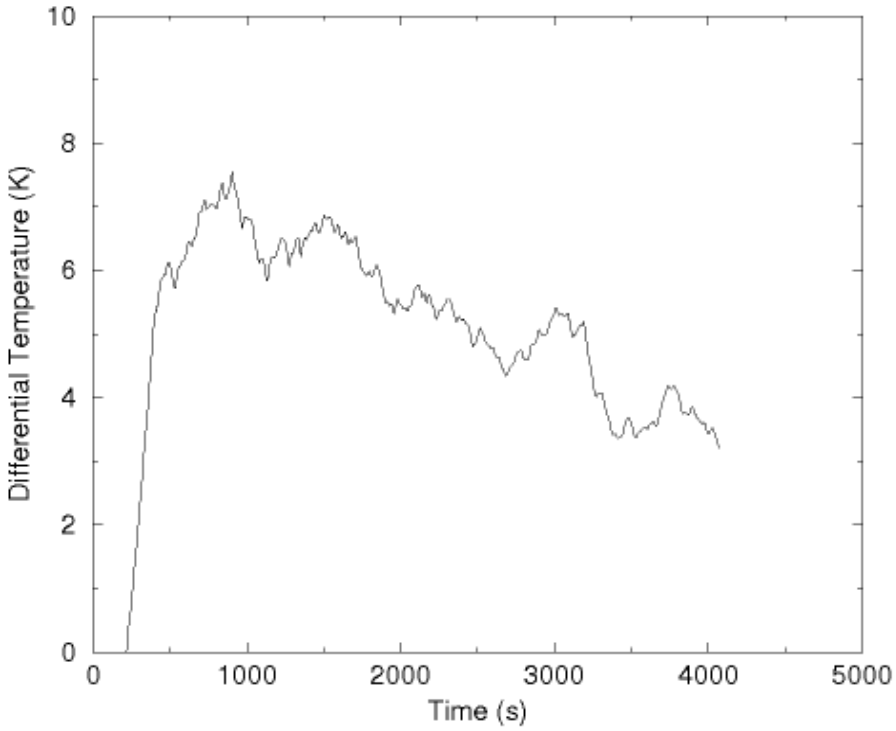


Figure H-25 APEX-CE-05 Measured Wall Temperature Minus Fluid Temperature 4D Below and Centered on the Cold Leg 4 Nozzle

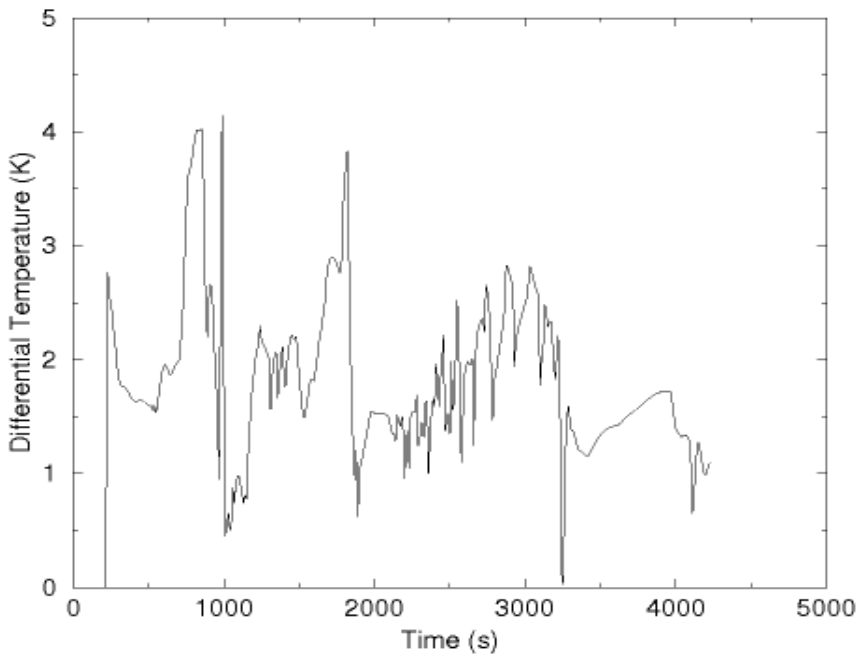


Figure H-26 APEX-CE-05 RELAP5-Calculated Wall Temperature Minus Fluid Temperature Centered Below Cold Leg 4, Between Cold Leg and Top of Core

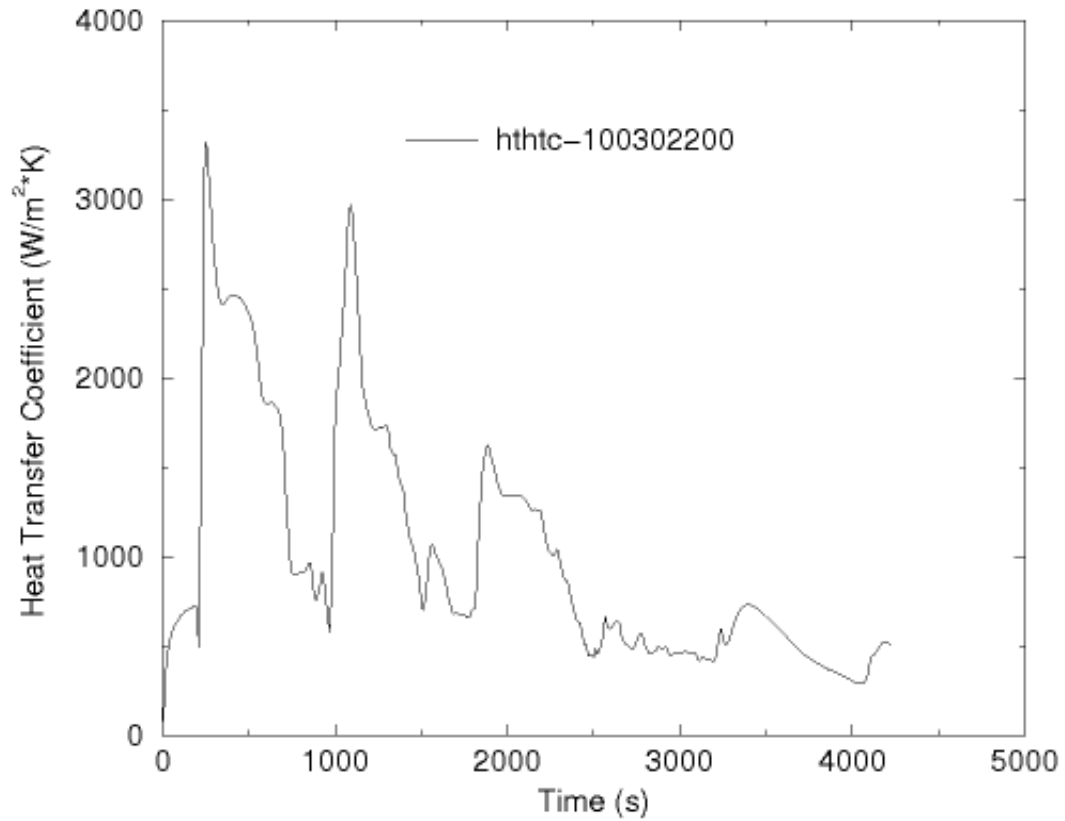


Figure H-27 APEX-CE-05 RELAP5-Calculated Wall Inside Surface HTC 4D Below and Centered on the Cold Leg 4 Nozzle

H.3 Creare

RELAP5 assessment was not performed against the Creare data. The use of the thermal shield in the downcomer of the Creare facility would have made the modeling of the facility more difficult since it divided the downcomer into an inner annulus and an outer annulus. As a result, a flow split is introduced into the downcomer flow. The Creare experiments, nevertheless, provide experimental data on downcomer mass flow and heat transfer.

Creare performed experiments in a 1:2 linear scale facility to investigate fluid mixing in a stagnant loop geometry. The Creare test facility modeled a single cold leg and one-fourth of the reactor vessel downcomer. All of the major linear dimensions were scaled to approximately one-half the dimensions of a prototypical PWR.

The cold leg diameter was 36 cm (14 inches). The downcomer was represented by a planar section having a width, height, and gap comparable to a 90° sector of a reactor downcomer. The downcomer had a thermal shield that spanned the full width of the downcomer, and which was sized and located to preserve the ratios of important dimensions. The downcomer walls were constructed of 7-cm (2.75-in) thick steel plate. The downcomer gap width was 13.7 cm (5.4 inches).

The two NRC tests (MAY105 and MAY106) were conducted with an initial loop (i.e., cold leg and downcomer) fluid temperature of 190C (375F) and an HPI fluid temperature of 15C (59F) at stagnant loop flow conditions. The difference between the two tests was the ECC injection rate, 5.2 kg/s (scaled from 166 kg/s) and 3.45 kg/s (scaled from 110 kg/s). The test conditions were similar to UPTF and APEX-CE-5.

The nominal cooldown transient is shown in Figure H-28. It displays the characteristic mixing cup exponential decay behavior.

Velocities were measured at two elevations in the downcomer; 0.4 m (16 inches) below the cold leg nozzle, and at the bottom of the thermal shield. Two instruments were located at the upper elevation, both directly below the cold leg, so they were within the plume region. One was on the vessel side of the thermal shield and the second on the core barrel side of the thermal shield. Comparing measured velocity to that of the HPI injection flow rate, Creare reported a velocity ratio for Test MAY105 of (measured velocity / superficial velocity =) 21. For Test MAY 106, the ratio was 26. The ratio gradually decreased over the duration of the tests as the buoyancy driving force decrease in the downcomer, towards a value of ~6. The actual downflow velocities measured were 0.7 m/s, decreasing to 0.2 m/s.

The values of upflow velocities were ~1/2 the downflow velocities. These results are consistent with the UPTF measurements. Considering the reduced temperature operation of Creare and its reduced height scaling, the buoyancy driving force scaled up from Creare to full scale is ~4 (height ratio = 2; density ratio = 2.5; velocity ratio = 2.23). Therefore, the Creare velocity measurements scaled up to full scale should scaled up would be ~1.5 m/s, decreasing over time as the RCS temperature dropped.

Creare found that the heat transfer coefficients in the downcomer were an order of magnitude greater than would be obtained from the superficial velocity from the HPI flow. This is consistent

with the enhanced flow measured in the downcomer. The downcomer flows were concluded to be buoyancy driven.

The downcomer flows were influenced by the presence of the thermal shield. Most of the flow from the cold leg jumped the gap and flowed down between the thermal shield and the core barrel. The flow was steady in this region. Some of the cold leg flow traveled down between the thermal shield and the vessel wall. In this region, the flow alternated between downflow and upflow.

The calculated values for h ranged from $1,700 \text{ W/m}^2\text{-C}$ to $6,000 \text{ W/m}^2\text{-C}$. This compares well with the range of $1,100 \text{ W/m}^2\text{-C}$ to $4,400 \text{ W/m}^2\text{-C}$ found for UPTF, which only injected into one cold leg, so overall flows were lower.

The Reynolds numbers in the downcomer for experiments ranged from 30,000 to 300,000. Creare reports that the Reynolds numbers for the prototype should be 6.5 times larger because of the scaling, which agrees with the estimates provide earlier of Reynolds numbers in the range 300,000 to 3,000,000 for the prototype. For their test conditions, Creare estimated the possible enhancement of heat transfer due to mixed convection to be ~5%. Because the Reynolds numbers at full scale are much higher, they concluded mixed convection effects can be neglected.

As shown in Figure H-29, the measured heat transfer coefficients were proportional to the Dittus-Boelter correlation. Creare observed a heat transfer enhancement over Dittus-Boelter of a factor of ~1.55 in correlating their data, which they attribute to entrance effects. The presence of the thermal shield in the Creare experiments introduced a change in geometry and, therefore, a new development length effect as the flow split and ran down either side. The measurement location for the data plotted was 18 cm (7 inches) downstream of the top of the thermal shield. The enhancement applies to the down flowing plume region. No enhancement was observed during upflow, which is illustrated in Figure H-30 by one data point (upward facing triangle) from a time of upflow along the vessel wall that falls slightly below the Dittus-Boelter prediction.

From the Creare data we conclude,

- ***Creare data show a factor of 21 to 26 increase in downcomer flow over ECC flow. The downcomer velocities measured in the experiments were 0.7 m/s, decreasing over the duration of the experiment as the buoyancy force decreased. The equivalent scaled up velocities are ~1.5 m/s. The enhancement in downcomer mass flow is similar to that observed in UPTF.***
- ***The Creare heat transfer data are consistent with Dittus-Boelter. Creare reported a possible entrance effect enhancement attributed to the location of the measurement. No enhancement was observed in a different location.***
- ***Creare reported that because of the buoyancy enhanced flow in the downcomer, mixed convection effects were negligible.***

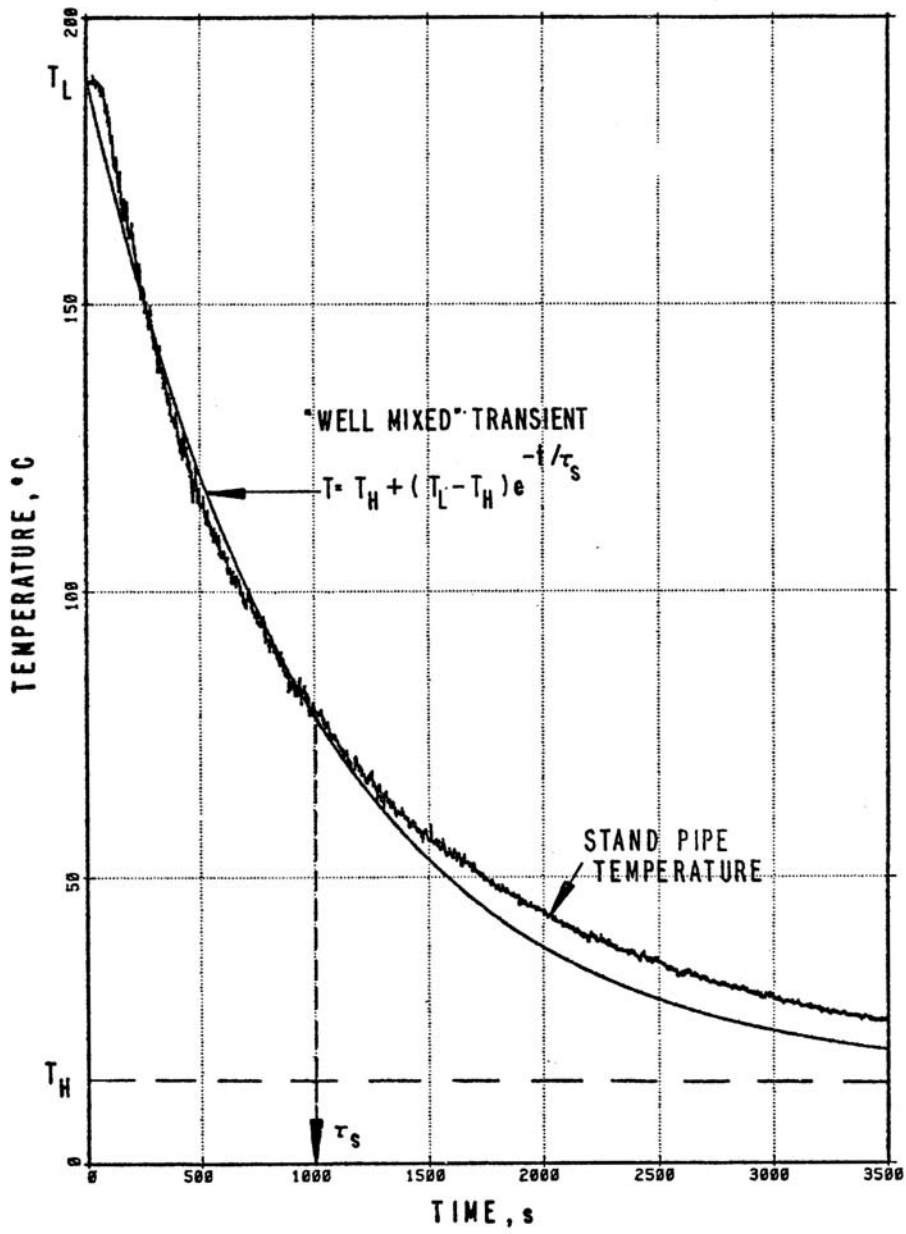


Figure H-28 Cooldown Transient for Creare Fluid Mixing Test

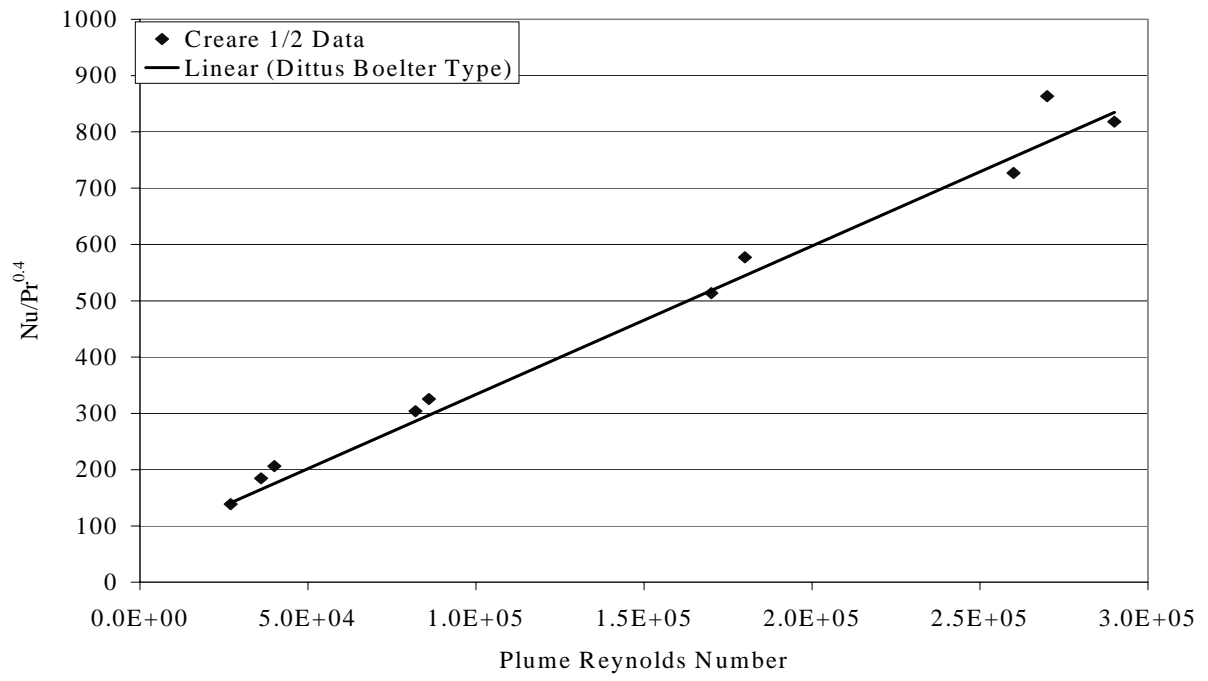


Figure H-29 Creare Data Correlated to Dittus-Boelter Relation

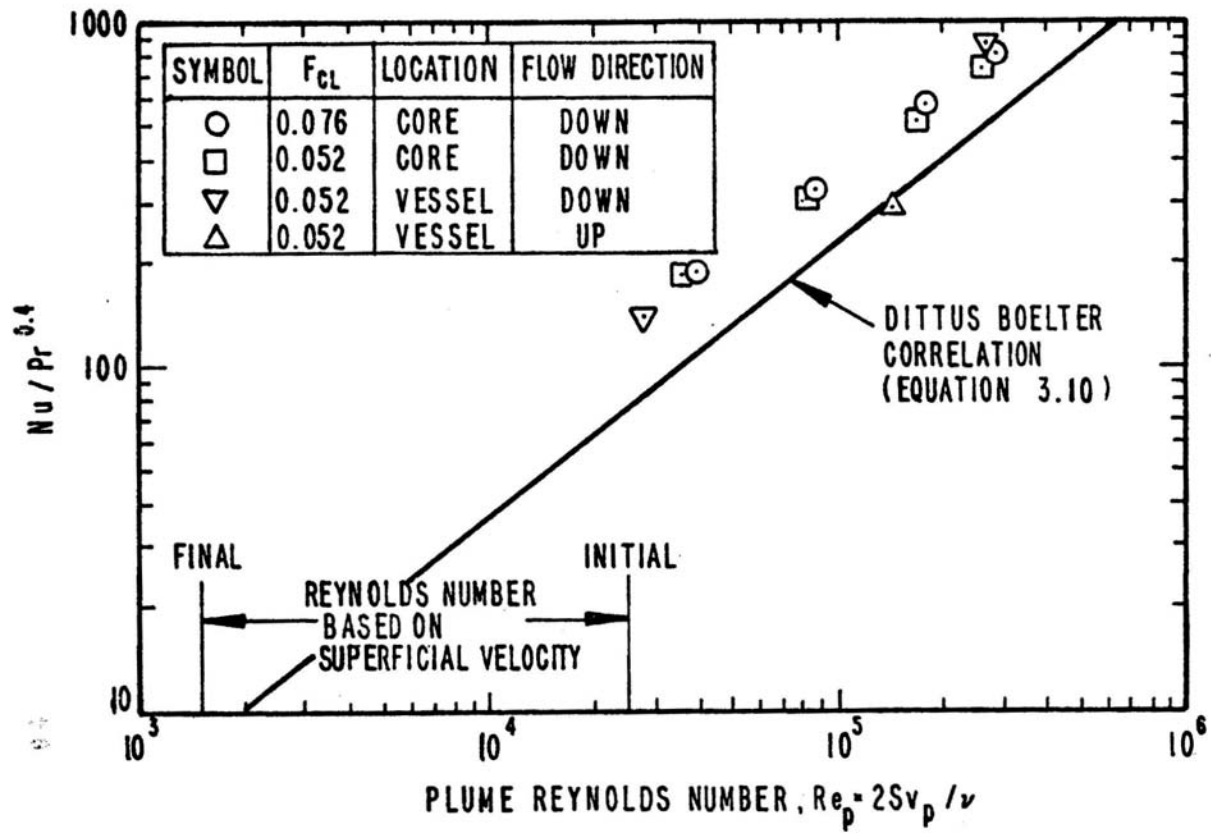


Figure H-30 Create Data Compared to Dittus-Boelter

APPENDIX I. COMPARISON OF RELAP5-CALCULATED AND CFD-CALCULATED DOWNCOMER FLOWS

As part of a prior PTS evaluation for H.B. Robinson, a CFD calculation of downcomer flows was performed using the COMMIX-1C code [58]. H.B. Robinson is a three loop Westinghouse plant similar to Beaver Valley. The calculation was performed to determine whether the RELAP5 modeling of the downcomer adequately captured the flow field. The transient boundary conditions to the COMMIX calculations were provided by a RELAP5 calculation of a 2-inch hot leg break in H.B. Robinson.

The RELAP5 model of H.B. Robinson utilized 6 azimuthal channels and 11 axial cells (66 nodes). This nodalization is similar to that used for the three plants in the current study. In the COMMIX model, the entire downcomer was modeled using ~4,000 nodes (6 nodes across the gap in the radial direction).

Figure I-1 shows the flow field results from the COMMIX calculation at 3,000 s. The flows are downwards below the cold legs and upwards between the cold legs, as to be expected. There was a tendency for the flows below Cold legs 2 and 3 to merge together. This behavior has been observed in experiments in APEX-CE and IVO and in CFD calculations performed by Oregon State University of the APEX-CE experiments [3]. Mixing between the downflow and upflow regions is seen in the form of the velocity vectors showing cross flow. Such cross flow is found between adjacent nodes in the RELAP5 calculation.

The study concluded that the RELAP5 calculations adequately captured the overall flow behavior in the downcomer but missed prediction of finer-scale eddy flows, as to be expected. The flow velocities in the COMMIX calculation were 0.5 to 1 m/s, which was similar to RELAP5 predictions.

RELAP5 Calculation of Beaver Valley Downcomer Flows

The RELAP5 calculation of a 2-inch surge line break in Beaver Valley is shown in Figure I-2. This provides a comparison to the COMMIX flow field: for the same 2-inch surge line break transient; in a three loop Westinghouse plant of the same design; at the same point in time of 3000 s. The flow velocities calculated by RELAP5 are similar in magnitude to COMMIX. The velocities shown in Figure I-2 are ~0.5 m/s. Earlier in the transient the calculated velocities are higher, and decrease with time, which is the same response seen in the experiments due to buoyancy effects. RELAP5 is seen to merge the downflow plumes together which results in one region of downflow (3 channels) and one region of upflow (3 channels).

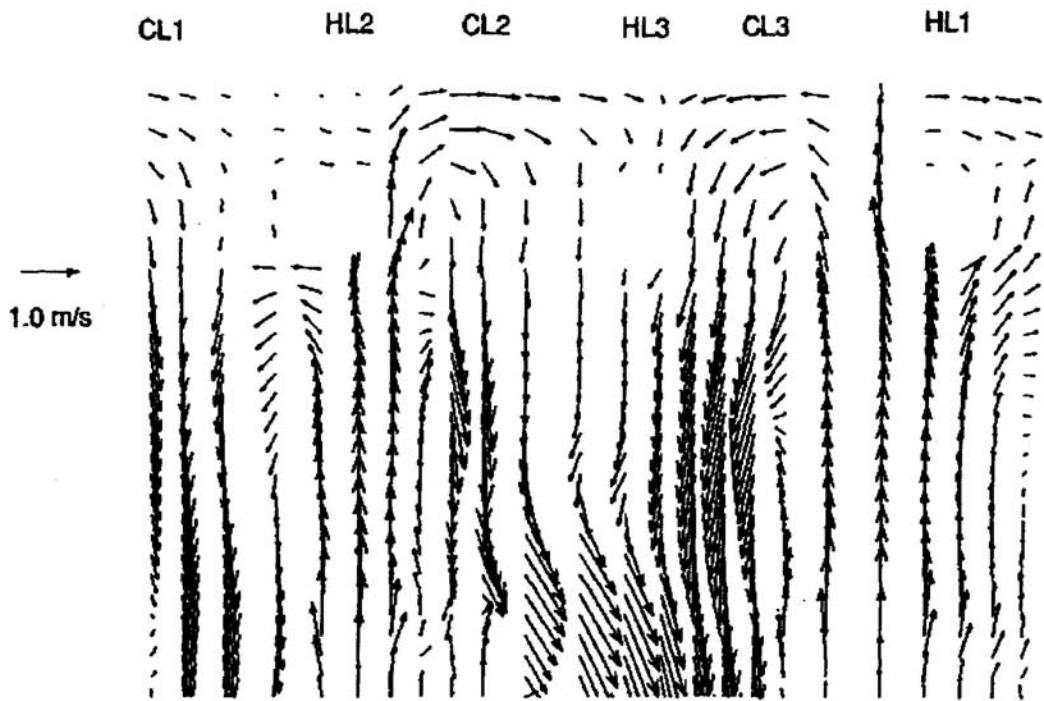


Figure I-1 COMMIX Calculation of Downcomer Flow Field at 3,000 s

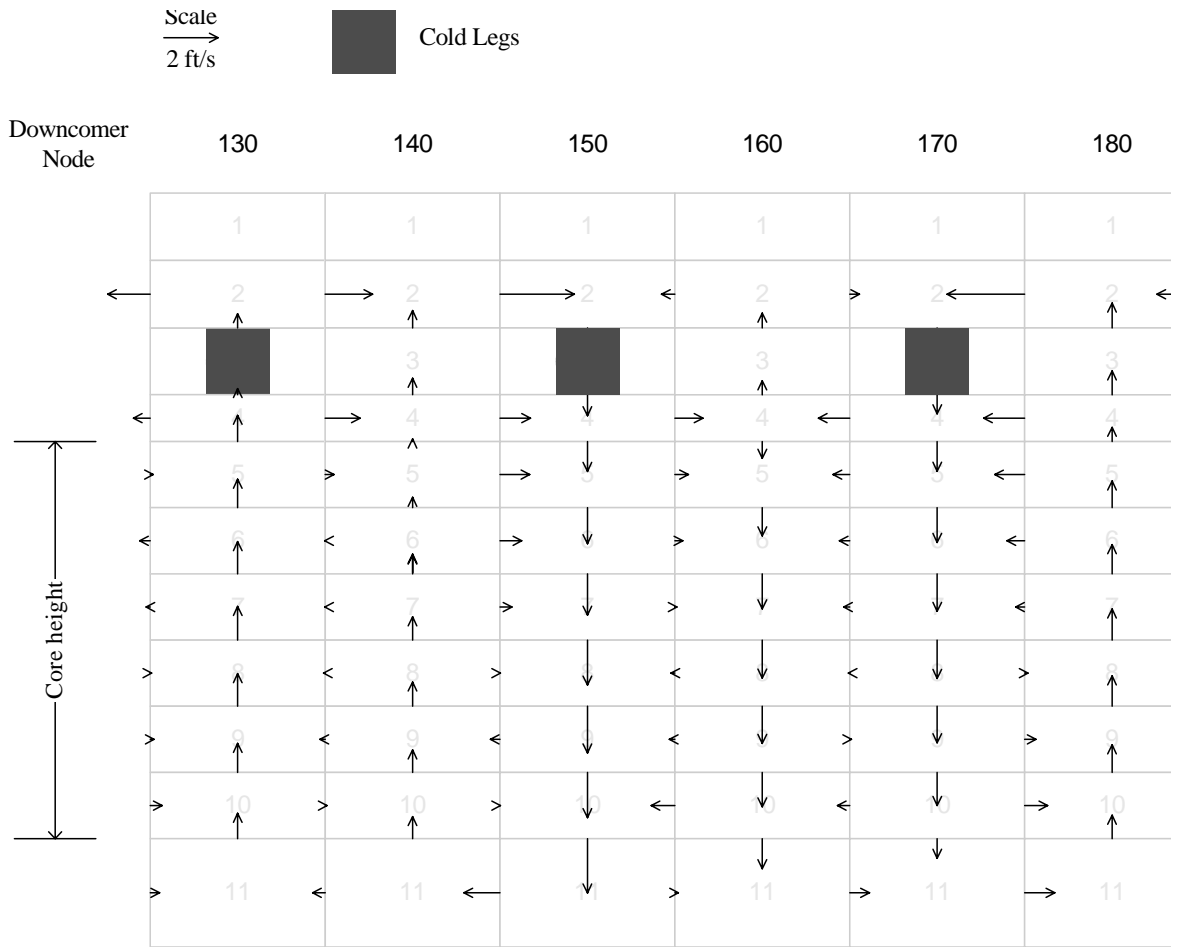


Figure I-2 RELAP5 Calculation of Downcomer Flow Field

APPENDIX J. SENSITIVITY OF FRACTURE MECHANICS RESULTS TO VARIATIONS IN THE FLUID COOLDOWN RATE AND HEAT TRANSFER COEFFICIENT

Thermal hydraulic sensitivity studies were performed using RELAP5 with respect to downcomer fluid cooldown rate ($T_{dc}(t)$), and heat transfer coefficient ($h_{dc}(t)$) [26]. The analyses were performed with FAVOR using the Palisades vessel, at an embrittlement corresponding to 60 EPFY. The RELAP5 sensitivity studies were fed to FAVOR as boundary conditions, in the usual manner. The conditional probability of vessel failure (CPF) determined by FAVOR was used as the figure of merit for determining the effect of the different variables.

For this study, a Palisades stuck-open SRV transient was selected, which was first calculated with RELAP5 (Case 65). A simple exponential decay function was then fitted to the RELAP5 calculation of downcomer temperature ($T_{dc}(t)$). Then, the decay rate was varied using the exponential function.

$$T_{dc}(t) = T_{ECC} + (T_0 - T_{ECC}) e^{-\beta t}$$

where T_{ECC} was 57C (136F)

T_0 was the temperature at the beginning of the transient, 278C (532F)

$\beta = 1/\tau$

Figure J-1 shows the cooldown rates examined. The RELAP5 calculation falls in the middle of the family of curves. The same RELAP5 calculated values for system pressure and heat transfer coefficient were used for all the calculations, with the exception that multipliers on heat transfer coefficient were explored as well.

The base case RELAP5 calculation corresponds to $\beta = 2.9 \times 10^{-4}$ ($\tau = 3450$ s), whose value was selected as a visual fit to the RELAP5 temperature trace. β was then varied about this value in the positive and negative directions, over a range of two, according to the values in the table shown on the right of the figure. This gave a spread in temperatures of approximately 45C (80 °F).

Table J-1 shows the results obtained in terms of CPF. The CPF from the RELAP5 calculation matched that obtained for $\beta = 2.9 \times 10^{-4}$, which shows that the selection of $\beta = 2.9 \times 10^{-4}$ was appropriate. More significantly, it supports the notion that the cooldown of the reactor coolant system as a whole, and the greater downcomer region in particular, closely resembles a simple exponential decay, which is also characteristic of a back-mixed (i.e. ideally mixed, mixing cup) volume.

The results showed the expected sensitivity of CPF to cooldown rate; the faster the cooldown, the higher the value of CPF. For the range of cooldown rates examined, CPF varied by an order of magnitude (columns 3, 6 and 9), regardless of the heat transfer coefficient multiplier.

Variations of h_{dc} were then applied to the same set of cooldown curves. Two multipliers were used: 0.7 and 1.56. The value of 0.7 reflects the typical uncertainty of +/- 30% applied to heat transfer correlations. The number 1.56, is a product of 1.3 times 1.2. The 1.3 is the same 30% uncertainty in heat transfer correlations. The factor of 1.2 was the estimated enhancement from *Excel* calculations from buoyancy-opposed mixed convection. The estimate of 1.2 was obtained

by comparing the Swanson-Catton model to Churchill-Chu. The comparisons were done over the range of temperatures 50C to 250C, and velocities 0.1 m/s to 1.0 m/s. The average heat transfer enhancement obtained from Swanson-Catton compared to Churchill-Chu by this method was ~20%.

Columns 6 and 7 show the results of applying the 0.7 multiplier to h, using the same six exponential temperature decay curves. The last two columns (9 and 10) show the results of applying the 1.56 multiplier to h, using the same six exponential temperature decay curves. When the heat transfer coefficient was increased, CPF increased as well, and vice-versa. The overall effect of h_{DC} on CPF was not, however, pronounced. For the two sets of cases where h_{DC} was reduced and increased, the impact on CPF was approximately 33%.

$$\frac{CPF_{0.7h}}{CPF_{1.0h}} = 0.67 \qquad \frac{CPF_{1.56h}}{CPF_{1.0h}} = 1.38$$

Comparison of the $T_{dc}(t)$ sensitivity to the h_{DC} sensitivity show much greater CPF sensitivity to the rate and degree of cooldown than to the heat transfer coefficient.

Other heat transfer sensitivity studies for a range of transients showed that when h_{DC} was increased, the effect was greater for fast transients (large LOCAs, MSLBs) compared to slow transients (small LOCAs, SRVs). That is, higher heat transfer makes large breaks more important relative to smaller breaks and to stuck open pressurizer SRV that later reclose. This was consistent with the earlier discussion.

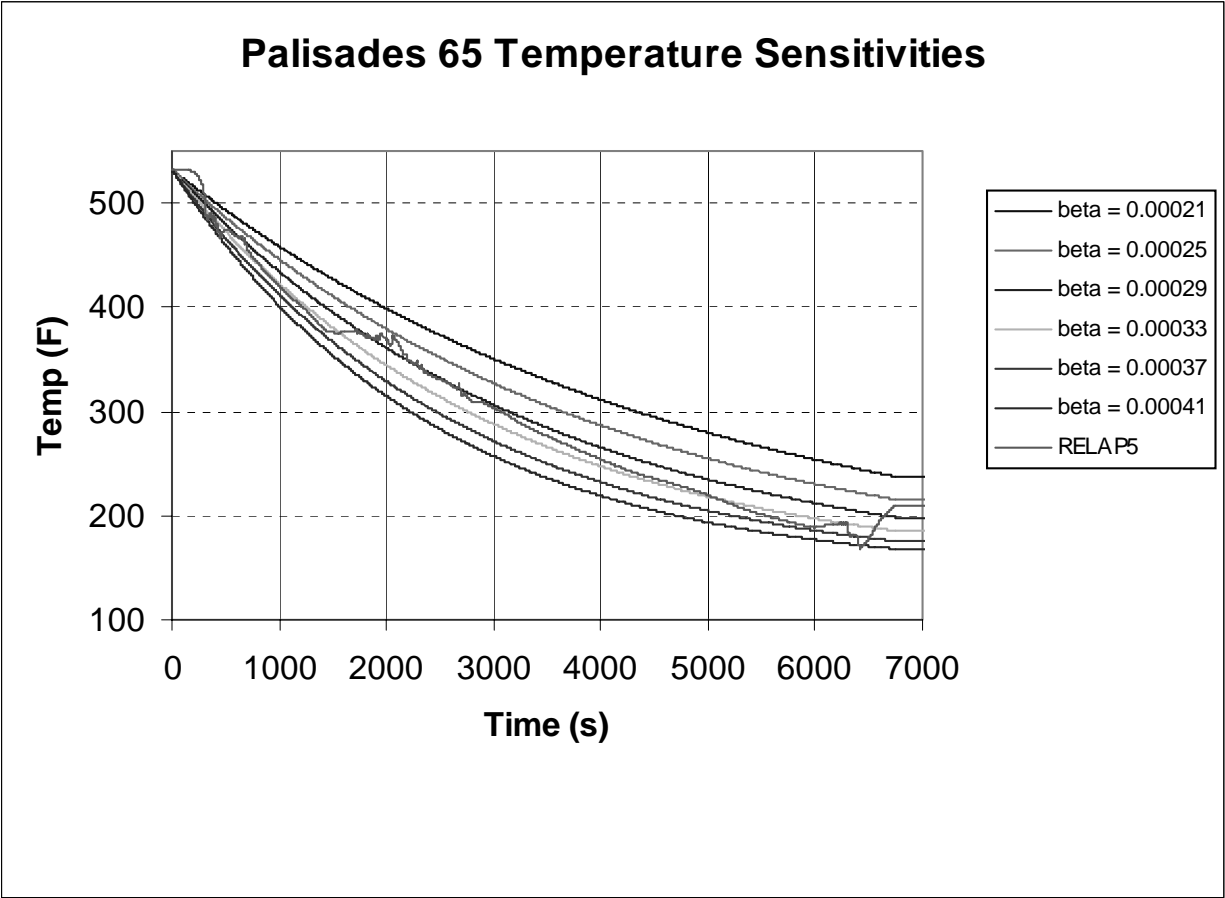


Figure J-1 Cooldown Transients for Palisades

Table J-1 Sensitivity Analysis for Exponential Temperature Decay Transients vs. RELAP5 Solution

1	2	3	4	5	6	7	8	9	10
β	h multiply	CPF	CPF/ CPF _{base}	h multiplier	CPF	CPF/ CPF _{base}	h multiplier	CPF	CPF/ CPF _{base}
RELAP	1.0	1.0×10^{-4}	1.00	1.0	1.0×10^{-4}	1.00	1.0	1.0×10^{-4}	1.0
2.1×10^{-4}	1.0	2.3×10^{-5}	0.22	0.7	1.4×10^{-5}	0.14	1.56	3.4×10^{-5}	0.3
2.5×10^{-4}	1.0	5.5×10^{-5}	0.54	0.7	3.4×10^{-5}	0.34	1.56	8.2×10^{-5}	0.8
2.9×10^{-4}	1.0	1.0×10^{-4}	1.02	0.7	6.6×10^{-5}	0.65	1.56	1.5×10^{-4}	1.5
3.3×10^{-4}	1.0	1.6×10^{-4}	1.57	0.7	1.1×10^{-4}	1.04	1.56	2.2×10^{-4}	2.2
3.7×10^{-4}	1.0	2.2×10^{-4}	2.12	0.7	1.5×10^{-4}	1.45	1.56	2.9×10^{-4}	2.9
4.1×10^{-4}	1.0	2.6×10^{-4}	2.60	0.7	1.9×10^{-4}	1.82	1.56	3.5×10^{-4}	3.4
Ave		8.2×10^{-4}			5.5×10^{-4}			11.3×10^{-4}	

APPENDIX K. PTS PHENOMENA IDENTIFICATION AND RANKING TABLE

The PTS PIRT defines a list of phenomena, processes, and boundary conditions important to the analysis of PTS. The objective of the PIRT is to identify and rank these three categories with respect to the three thermal hydraulic figures of merit: temperature, pressure, and heat transfer coefficient.

Prior to the current study, PTS PIRTs were developed on two occasions. The first was as part of a PTS analysis by RES of Yankee Rowe [59]. The Yankee Rowe PIRT was based on a 1.3-inch cold leg break. This size, scaled up from Yankee Rowe to the three current plants, is equivalent to approximately a 2.8-inch cold leg break. The second was for a PTS analysis by RES of H.B. Robinson [58]. The H.B. Robinson PIRT was based on a 2-inch hot leg break.

These two PIRTs were used in the current PTS reevaluation to

- (1) Direct the initial efforts on thermal hydraulic uncertainty evaluation [2],
- (2) Plan the separate effects assessment of RELAP5 as part of the code validation effort for PTS applications [12], and
- (3) Identify modeling issues/ This included phenomena not modeled in RELAP5 and showing that the missing models are not important to assuring the applicability of the code to PTS. For example, RELAP5 does not model “jet behavior, flow distribution, and mixing in the cold leg.” Appendix B showed that this modeling capability, while identified in the PIRT, was not needed.

As part of the current PTS reevaluation, the PTS PIRT was revisited and updated according to the improved knowledge resulting from the reevaluation. This work is described in [12]. The revised PIRT included additional influencing factors including: LPI temperature; stuck open pressurizer SRV reseating time, inter-cold legs flow circulation, and break location (i.e., hot leg, cold leg, pressurizer). The PTS reevaluation incorporated the revisions to the earlier PIRT shown in Table K-2.

The expert groups that prepared the two prior PIRTs are shown in Table K-1. The two PIRT efforts produced similar lists of phenomena/processes, and will be discussed together.

On both occasions, the tabulation of important phenomena/processes comprised entities that fall into two distinct categories:

- Processes that are modeled as part of the RELAP5 (or other code) input deck;
- Phenomena/processes that are represented by physical models within the code itself.

Table K-2 shows the PIRTs, classified according to the nature of the phenomena/process, along with their rankings. Each of items listed in the PIRT was considered with respect to the level of knowledge, or how well its is modeled in RELAP5, as well as how is the modeling uncertainty was addressed. For specific physical phenomena, in general, it is of limited value to attempt to quantify

the results of individual assessment cases. This is especially true as the complexity of the experiment increases, involving more and more physical models in the code. There are cases for which quantification is possible, but generally the value judgement agreements described in Appendix C are applied.

It is noteworthy that the PIRTs do not list pressure or downcomer temperature. These figures are system parameters. The rationale for their exclusion was that these are not phenomena/processes, but rather, are calculated state variables which follow from the calculation of break mass and enthalpy flow.

To the PIRT list, two additional phenomena were added as part of the RELAP5 assessment, namely condensation during ECC injection, and condensation during increase in pressure. Condensation during ECC injection was included since, in addition to the scenarios upon which the PIRTs were based, medium and large LOCAs were subsequently found to be a dominant contributor to PTS risk. For these larger break LOCAs, the possibility exists of significant direct contact condensation in the cold legs during ECC injection.

Table K-1 H.B. Robinson PIRT Panel

Member	Affiliation
Cliff Davis	Idaho National Engineering Laboratory
Prof. Marino di Marzo	University of Maryland
Prof. Peter Griffith	Massachusetts Institute of Technology
Prof. Yassin Hassan	Texas A&M University
Prof. Barclay Jones	University of Illinois
Dr. Marcos Ortiz	Idaho National Engineering Laboratory
Donald Palmrose	Idaho National Engineering Laboratory

Yankee Rowe PIRT Panel

Member	Affiliation
Prof. Marino di Marzo	University of Maryland
Prof. Peter Griffith	Massachusetts Institute of Technology
Dr. Gerald Lellouche	Saul Levy, Inc.
Prof. Sy Ostrach	Case Western Reserve
Prof. Ray Viskanta	Purdue University

Table K-2 PTS PIRT Used to Plan the Current PTS Thermal Hydraulic Analyses

#	Phenomena/Boundary Condition	Type	HBR Order	HBR Rank (1-10)	Y-R Rank Order
1	HPI injection flow	boundary condition	3	8.9	13
2	Accumulator injection temperature	boundary condition	5	5.6	N.R.
3	HPI injection temperature	boundary condition	7	5.2	13
4	Decay heat	boundary condition	9	4.4	12
5	HPI flow control	boundary condition	N.R.	NA	17
6	Feedwater temperature	boundary condition	18	1.0	14
7	Feedwater control	boundary condition	19	1.0	16
8	HPI asymmetry	boundary condition	N.R.	NA	5
9	Timing of reactor coolant pump trip	boundary condition	20	1.0	10
10	Secondary pressure control	boundary condition	N.R.	NA	18
1	Accumulator injection rate	phenomena/boundary condition	1	10.0	N.R.
2	Break flow/break size	phenomena/boundary condition	6	5.3	6
3	Reactor vessel wall heat conduction	phenomena	2	9.0	8
4	Jet behavior, flow distribution and mixing in downcomer	phenomena	4, 8	6.0	1, 3, 21
5	Jet behavior, flow distribution and mixing in cold leg	phenomena	8, 12, 13	4.4	2, 21
6	Wall-fluid heat transfer in downcomer	phenomena	10	3.2	7
7	Natural circulation flow and loop flow resistance	phenomena	11, 22	2.8	9
8	Downcomer-core inlet bypass	HBR plant-specific	14	1.2	N.A.
9	Downcomer-upper plenum bypass (includes B&W RVVVs)	phenomena	15	1.2	20
10	Upper head heat transfer	phenomena	16	1.2	19
11	Liquid/vapor interface in upper downcomer	phenomena	17	1.1	4
22	Steam generator heat transfer	phenomena	19	1.0	22
23	Check valve characteristics	Y-R plant-specific	NA	NA	11
24	Pump performance in two phase	Y-R plant-specific	NA	NA	1

Notes: *Downcomer-Core Inlet Bypass* was specific to H.B. Robinson, which was designed with a flow path to divert flow from the downcomer inside the core barrel, which then flowed downwards between the core barrel and core shroud.

Check valve characteristics was specific to Yankee Rowe, which had check valves in the cold legs.
Pump performance in two phase was specific to Yankee Rowe since at the time the reactor coolant pumps could remain operating during a LOCA.

The second condensation phenomenon is associated with stuck open SRV scenarios, which is the other significant class of scenarios contributing to PTS risk. These transients all involve refill and repressurization of the RCS following valve reclosure, until the system is water solid. Therefore, these transients all involve the compression of a volume of saturated steam. Prior to the RCS becoming water solid, condensation of the steam volume on walls and fluid surface determines system pressure.

The uncertainty analysis classifies the PIRT boundary conditions as aleatory. The uncertainties in these attributes are not amenable to further refinement from increasing knowledge. The uncertainties associated with physical models in RELAP5 are classed as epistemic. The following discusses each of the items listed in Table K-2. For completeness, all are addressed, even those which were ranked low. Section K.1 describes boundary conditions while Section K.2 describes physical models.

K.1 Boundary Conditions

(1) HPI Injection Flow

HPI and LPI flow rates are determined from the pump head curves obtained as design information from the respective plants. As an example, Table K-3 shows HPI flow rate as a function of pressure for Palisades. HPI was modeled as fully on for all transients for which a HPI signal was generated.

Sensitivity studies were performed to evaluate the effect of failing a HPI train [2]. Failures of one or more HPI pumps to operate lowered PTS consequences considerably because it results in warmer downcomer temperatures. Failures were not included in the sequences submitted for FAVOR analysis since such failures are low probability (1×10^{-2}) and consistent with the practice of not crediting opportune failure in risk analysis.

Additional sensitivity studies were performed varying HPI flow rate by +/- 10%. The effects were found to be small [2].

Similar to accumulator injection, the HPI and LPI flow rate depends on the reactor coolant system pressure, which is a global state parameter. There is, therefore, an aspect of the flow rate determination that involves RELAP5 calculation of physical phenomena that affect RCS pressure. Condensation is an example of a physical model that affects pressure, which in turn affects ECC injection.

Table K-3 HPI Flow as a Function of Primary System Pressure

RCS Pressure (psia)	Total HPI Flow Rate (lb/s)
15	191
90	186
140	183
180	181
216	178
615	144
1015	95
1190	59
1290	3
> 1290	0

(2) *Accumulator Injection Temperature*

Accumulator water temperature was an input boundary condition. Sensitivity studies were performed on accumulator temperature, whereby it was varied from 70 °F to 100 °F (nominal 80 °F) to account for the range of conditions in containment temperatures between winter and summer. The effects on downcomer temperature were found to have nearly a one-to-one correspondence [2].

(3) *HPI Injection Temperature*

The HPI temperature was an input boundary condition. For Palisades and Oconee, in addition to nominal conditions (60 °F), the values used in the calculations covered the expected temperature variations between winter (40 °F) and summer (100 °F). The exception was for Beaver Valley, which maintains its ECC water at a constant value of 50 °F by design.

(4) *Decay Heat*

Two sets of analyses were performed. One set were transients originating from full power operation. For these RELAP5 calculations, the 1994 ANS decay heat standard was used [60]. The standard assuming infinite operating time at full power. For the time scale of interest, decay heat ranged from ~3% (value at 37 s) to 1% (value at 10,000 s). Over this same time scale, the uncertainty (2σ) in the decay heat predictions of the ANS standard ranges from 4% (at 37 s) to 1.2% (at 10,000 s). This is equivalent to an uncertainty in power of 3 MW to 0.3 MW.

The second set of calculations were transients originating from hot standby conditions. To bracket the range of possible decay heat conditions, we assumed decay heat at the end of a refueling outage; one month after shutdown with one third of the core replaced with fresh fuel. The decay heat for these calculations was 0.2%, or 5 MW.

The uncertainty in decay heat is small compared to the range of conditions examined.

(5) *HPI Flow Control*

This was something that was originally specific to Yankee Rowe, but it was retained for another reason. The PIRTs did not include repressurization scenarios, which are important to the current PTS re-analysis.

For transients involved either closure of a stuck open pressurizer SRV or main steam line breaks, the reactor coolant system may return to conditions for which operator procedures call for HPI to be throttled or terminated. SRV reclosure sequences accounted for approximately 1/2 of the total risk. The control of HPI was treated as distinct PRA sequences. For example, sequences were analyzed with RELAP5 consisting of: (1) control of HPI one minute after criteria are met; (2) control of HPI ten minutes after criteria are met; and (3) failure to control HPI.

The throttling criteria for HPI are as follows,

Palisades

For HPI to be throttled, the following three conditions must be met:

- Auxiliary feedwater is running.
- At least one steam generator has a wide range level that is greater than 84%
- Reactor coolant system subcooling is >25 °F.

If all three conditions are met, then HPI is throttled to maintain pressurizer level between 40% and 60%.

Beaver Valley

When the following conditions are met, the operator stops a single HPI pump:

- RCS subcooling (core exit) > 40 °F
- At least 1 steam generator narrow range level >6% (32% if adverse containment)
- Reactor coolant system pressure stable or rising
- Pressurizer level >5% (32% if adverse containment).

After the first HPI pump is tripped, the operator waits 5 minutes, then, if the conditions are still met, the second HPI pump is tripped. If at any time after the pumps have tripped, the criteria are not met, then both pumps are turned back on.

Oconee

When the following conditions are met, the operator throttles HPI flow:

- Subcooling >5 °F

- Pressurizer Level >100 inches

HPI flow is throttled to maintain a given condition. This condition varied in the Oconee PTS runs; sometimes HPI flow was throttled to maintain pressurizer level, sometimes subcooling, sometimes both.

(6) *Feedwater Temperature*

Feedwater temperature was an input boundary condition. Two characteristic feedwater temperature were used. One was associated with main feedwater and took account of stored energy in the feedwater heaters. Plant data were obtained from Oconee to use as input.

The second was for auxiliary feedwater temperature. In addition to nominal conditions (60 °F), the values used in the calculations covered a range of temperature variations between winter (40 °F) and summer (100 °F).

(7) *Feedwater Control*

Feedwater control was treated as a boundary condition that was defined by PRA event sequences. The scenarios included a complete spectrum of feedwater control scenarios ranging from:

- (A) Normal flow and steam generator level control; to
- (B) Failure of level control or operator error, resulting in filling of the steam generators until water entered the steam lines.

For the latter sequences, feedwater was assumed to be controlled once water entered the steam lines. The rationale is that steam would no longer be available to drive the turbine driven main feedwater pumps or the turbine driven auxiliary feedwater pump.

(8) *HPI Asymmetry*

This appeared in the Yankee Rowe PIRT to account for the HPI flow out the break, for those breaks occurring in the cold leg. This factor is taken into account through the range of breaks that were considered in the analyses, which included cold leg as well as hot leg breaks.

(9) *Timing of Reactor Coolant Pump Trip*

The timing of the reactor coolant pump trip was assumed to be according to operating procedures in all calculations. Failure to trip the reactor coolant pumps would result in less adverse PTS conditions since the reactor coolant system remains well mixed. Additionally the reactor coolant pumps add considerable heat to the fluid (~20 MW). No credit was taken for opportune errors.

For very small breaks, HPI is sufficient to compensate for break flow, and the reactor coolant system inventory and pressure control can be maintained sufficiently to avoid meeting the RCP trip criteria. The boundary region for break size will differ somewhat from plant to plant depending on the capacity of HPI and core power. Generally, it falls with the range of 1 to 1.5 inch equivalent-diameter break. Beyond this break size, subcooling is lost in the hot legs. Upon loss of

subcooling, operating procedures for all three PWR vendors call for tripping the RCPs. The criteria for pump trip differs somewhat from vendor to vendor, but the impact on the transient progression of these differences is minor. The specific trip criteria were,

Oconee: Operator trips RCPs when subcooling is lost. RELAP5 model assumed that subcooling is lost at 0.28 K (0.5 °F). In some of the hot zero power cases, RCPs were tripped at 7 °F since the sequence definition stated that pump trip occurred.

Beaver Valley: Operator trips RCPs when the differential pressure between the RCS and the highest steam generator pressure is less than 1.38 MPa (200 psia). This setpoint is different for “adverse containment conditions” (2.59 MPa (375 psia)).

Palisades: Operator trips one RCP in each loop if primary pressure < 8.96 MPa (1300 psia) and trips other two pumps if subcooling falls below 13.9 K (25 °F).

(10) *Secondary Pressure Control*

Steam generator pressure control was treated as a boundary condition, according to the specific PRA sequence definition. The scenarios analyzed included a complete spectrum of secondary side valve failures, including steam dump valves, steam generator safety/relief valves, and atmospheric release valves. The failures were combined in some instances with failure of feedwater control such that the open steam generator continued to be fed.

K.2 Phenomena

This section describes the physical phenomena listed in the PIRT. For each phenomena, we summarize the means by which RELAP5 models the phenomena, the assessment of RELAP5 for the phenomena, and the uncertainty treatment of each phenomena.

(1) *Accumulator Injection Rate*

Accumulator injection is important in that it supplies water at a much higher flow rate (i.e. factor of 10) than HPI. This high injection flow is able to quickly flood the downcomer with cold water. The accumulator injection may be viewed as either as a boundary condition or as a phenomena, or both. The injection rate is a function of primary system pressure and accumulator pressure. The differential pressure between the accumulator and the cold leg, along with the resistance of the injection line, determine the injection flow rate. The line resistance is an input and is known with little uncertainty. The injection is always single phase liquid until the accumulator is empty, when it becomes nitrogen.

RELAP5 calculates downstream pressure as a system parameter. The accumulator is pressurized with nitrogen, which is treated as an ideal gas. The accumulator pressure as a function of time depends on the volume expansion and temperature. As the accumulator empties, the temperature of the gas space drops. RELAP5 calculates the heat transfer from the accumulator wall to the gas as well as from the liquid surface to the gas.

The accumulator modeling has been assessed against LOFT data from the LOFT L3-1 accumulator blowdown [12]. This was a non-nuclear small break LOCA blowdown. The volume

scaling of the LOFT accumulator was ~1:20. Excellent agreement was obtained between RELAP5 and the experimental data.

While system pressure is global parameter indicative of the RCS as a whole, condensation in the cold leg during ECC injection can lower local pressure and increase the differential pressure driving accumulator injection. If accumulator injection occurs while the reactor coolant system inventory has decreased to the loop (cold leg) elevation or below, then there is potential for direct contact condensation in the cold legs. This results in significant steam condensation and mixing throughout much of the reactor coolant system.

Therefore, RELAP5 was assessed for condensation against UPTF Test 6 Run 131 [12]. The experiment was a full scale study of the injection of ECC liquid into steam flowing through a cold leg. Test 6 investigated blowdown conditions of a large cold leg break. The experiment was quasi steady state, with steam injected in the core region and ECC injected in the cold legs. The objective was to evaluate the amount of condensation in the cold leg and downcomer, as well as ECC bypass and downcomer. For the test, the RCS pressure was ~2 bar. The ECC water was ~80C subcooled. Steam was injected in the core region. Accumulator flows were injected in the three intact cold legs. Good agreement was obtained of condensation rate and liquid temperature entering the downcomer (Figure K-1).

The uncertainty analysis included treatment of accumulator injection. It considered both flow rate, injection timing, and accumulator water temperature. The effect of pressure on flow was examined by varying the initial accumulator pressure from 550 psia, 600 psia (nominal), and 650 psia. The differences were found to be insignificant.

The effect of temperature was evaluated by varying between winter conditions and summer conditions. While the accumulators are in the containment, the temperature can vary. Values of 70F were used for winter and 100F for summer. The results show an influence of injection temperature [2].

(2) *Break Flow/Break Size*

Break flow is the single most important factor in determining the cool down rate of the RCS. Since depressurization is a function of the break size, and since ECC injection rate is a function of RCS pressure, the break flow effect is amplified. As break flow increases with break size, so does the rate of ECC injection. Both the rate of energy removal and the rate of cold water addition increase together. Together with ECC injection flow, particularly accumulators and LPI, the break size dominates the outcome of LOCAs. The effect of break flow was treated both as a variable boundary condition, and as a physical modeling uncertainty

Variation in boundary conditions included the effect of break size and break location. A complete break size spectrum was performed for all three plants, increasing the break area by a factor of two sequentially as shown in Table K-4

Figure K-2 illustrates the results. The conditional probability of vessel failure increases sharply with increasing break size, before reaching an asymptotic maximum.

The effect of break location was explored by calculating both cold leg and hot leg breaks. The reactor coolant system in thermal hydraulic terms consists of a hot side and a cold side. For PTS

analyses, for a given break size, hot leg breaks are worse than cold leg breaks. The reason is that the break flow enthalpy is higher for a hot leg break than for the same size cold leg break. Therefore, the depressurization and cooldown rates are faster. In addition, for cold leg breaks, the ECC flow into the broken cold leg tends to flow out the break, therefore, less cold ECC water is delivered to the reactor coolant system and to the downcomer. In contrast, for hot leg breaks, all the ECC flows through the downcomer in order to reach the break. The two effects combine to increase downcomer temperatures for cold leg breaks relative to hot leg

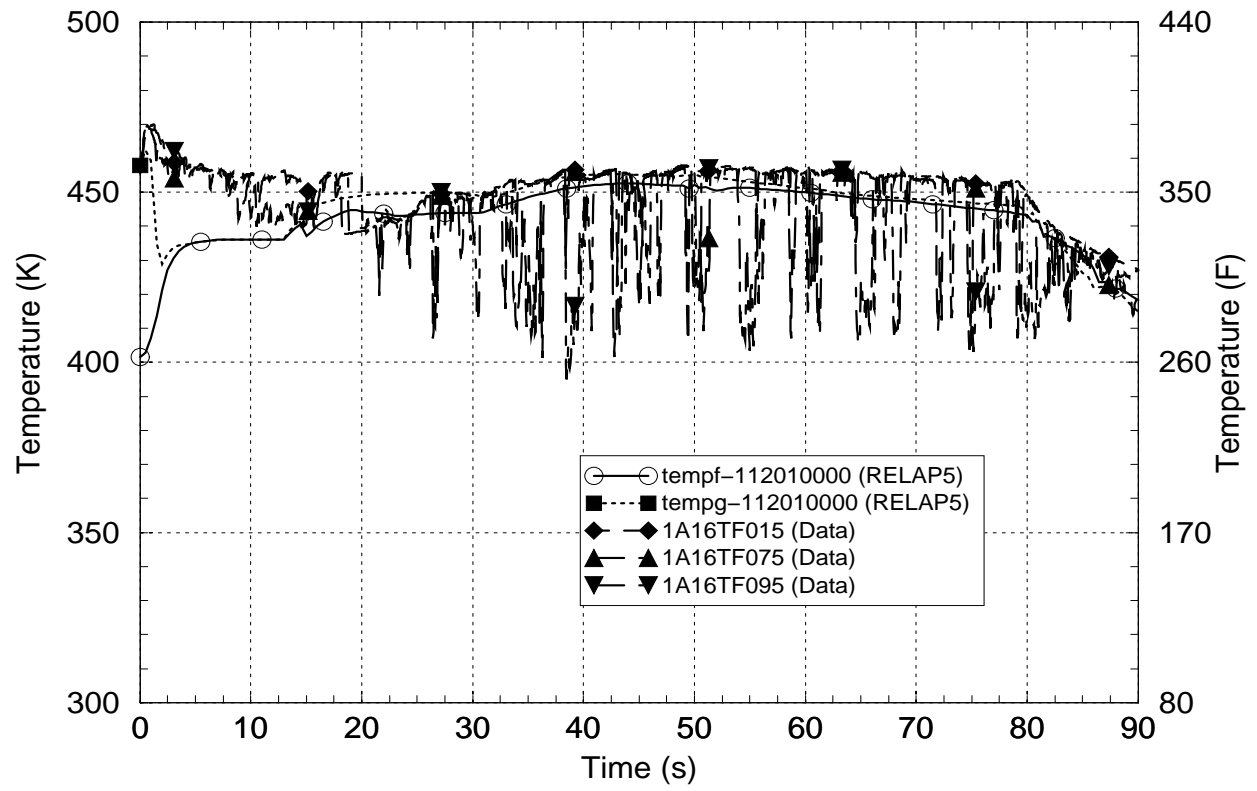


Figure K-1 Comparison of RELAP5 with UPTF Cold Leg Condensation Test-6

Table K-4 Break Size Spectrum Analyzed for Each Plant

Break size (diameter)

1-inch
1.414-inch
2-inch
2.828-inch
4-inch
5.656-inch
8-inch
11.312-inch
16-inch
22.624-inch

breaks. Figure K-2 demonstrates this by comparing hot leg to cold leg breaks, with respect to the averaged downcomer temperature and conditional probability of vessel failure, for a range of break sizes [2].

The calculation of break flow is determined by the break flow model and the upstream conditions. The break flow model used in all the analyses was Henry-Fauske [61], which was implemented in RELAP5 during AP600 analysis. This is a physically based model in which coefficients were adjusted to match ROSA/AP600 experimental data. The code was applied extensively to calculate experiments in ROSA, APEX, and SPES. The upstream conditions are based on the system effects of pressure and local quality.

Two assessment cases were run, MARVIKEN Tests 22 and 24. MARVIKEN was a operating boiling water reactor that operated briefly before being shut down. The facility was used for many experimental studies, among which were critical flow experiments. The MARVIKEN vessel is 420 m³, which makes in larger the a PWR RCS.

The initial test conditions for the two tests were similar. Initial vessel pressures were ~5 MPa (720 psia). The water at the upper portion of the vessel was saturated (264C) and the lower portion subcooled by ~32C (58F), making the fluid temperature variation similar to the temperature difference between the hot and cold legs of a PWR. Both tests used relatively low L/D, rounded-entrance nozzles with a 0.5 m (~20-inch) diameter. This break size is towards to high end of the LOCA sizes analyzed. The experiments used two different break nozzle L/D ratios, 1.5 for Test 22 and 0.33 for Test 24. The breaks were in the bottom of the vessel, so the inlet conditions were initially subcooled before becoming saturated.

Table K-5 shows a statistical comparison of RELAP5 to the two MARVIKEN experiments. The comparison is considered reasonable. Figures K-3 and K-4 compare RELAP5 to the experiments for break mass flow and pressure, respectively.

The uncertainty in the physical modeling of break flow by RELAP5 was considered [2]. Because the break area was varied by a factor of 500 from 1 inch to 22 inches diameter, to an extent the further consideration of the uncertainty in the physical modeling of break flow in RELAP5 is

superfluous. Nevertheless, its effect can be compared with other sources of uncertainty. The effects of break flow modeling uncertainty was evaluated by varying the flow by +/- 30%. This magnitude of variation is based on a large data base of comparisons of critical flow modeling with experimental data, as well as the results from the MARVIKEN assessments.

Table K-5 MARVIKEN Break Flow Comparisons

Test	Mean Mass Flow Error, (RELAP5 - Exp,)	σ	% Error
22	-190 kg/s	709 kg/s	20%
24	-180 kg/s	987 kg/s	20%

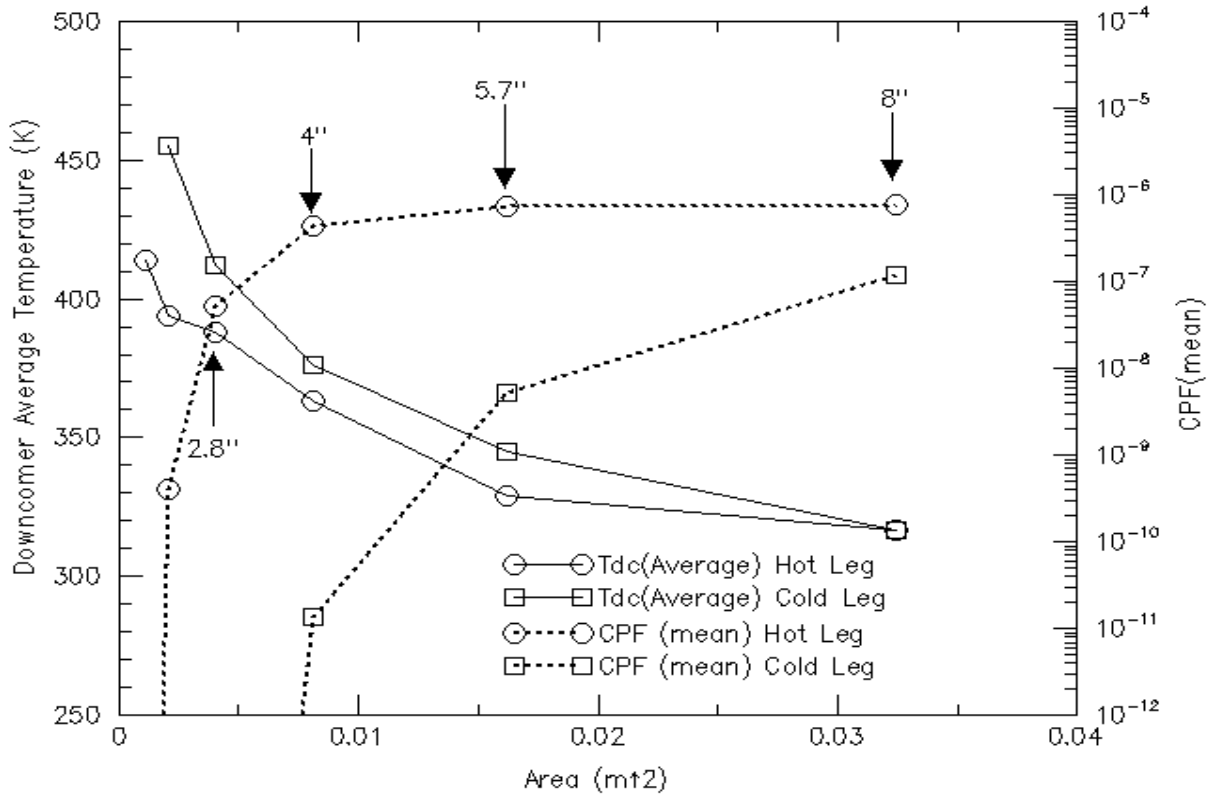


Figure K-2 Effect of Break Location on CPF and T-DC_{sen} for Oconee (60 EFPY)
Downcomer temperature averaged over 10,000s duration of the calculation

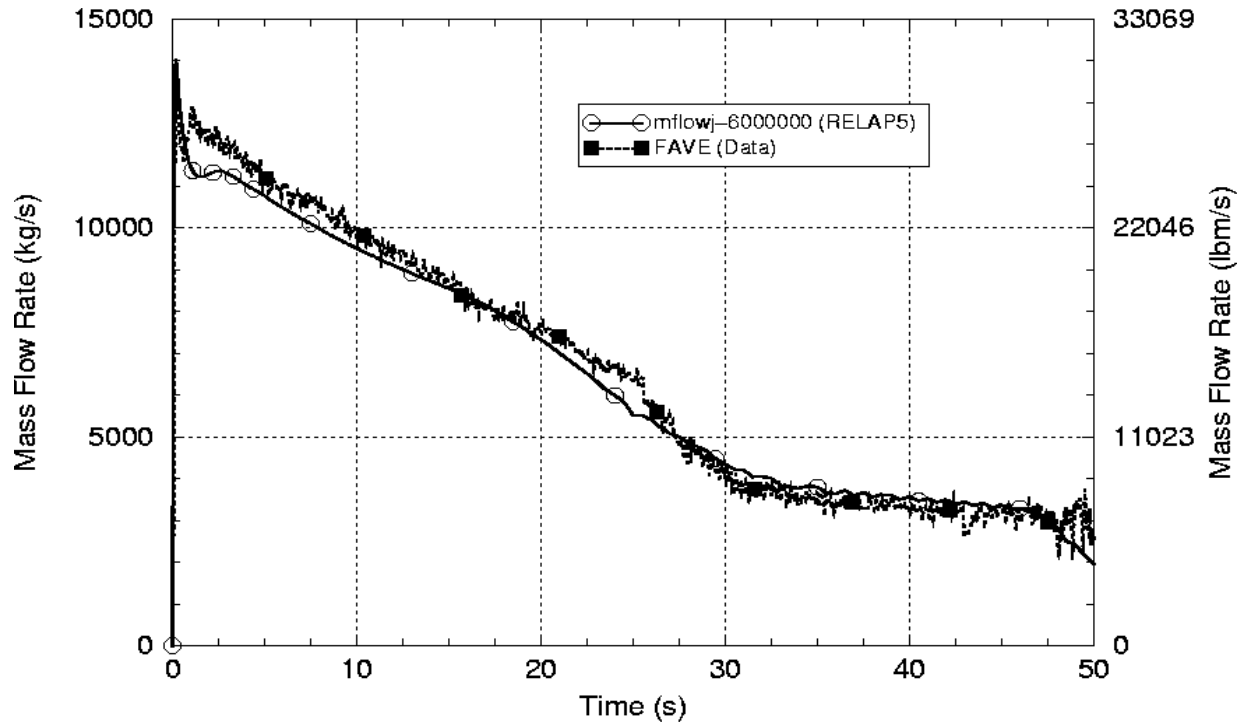


Figure K-3 MARVIKEN Critical Flow Test 24 Break Mass Flow Comparison to RELAP5

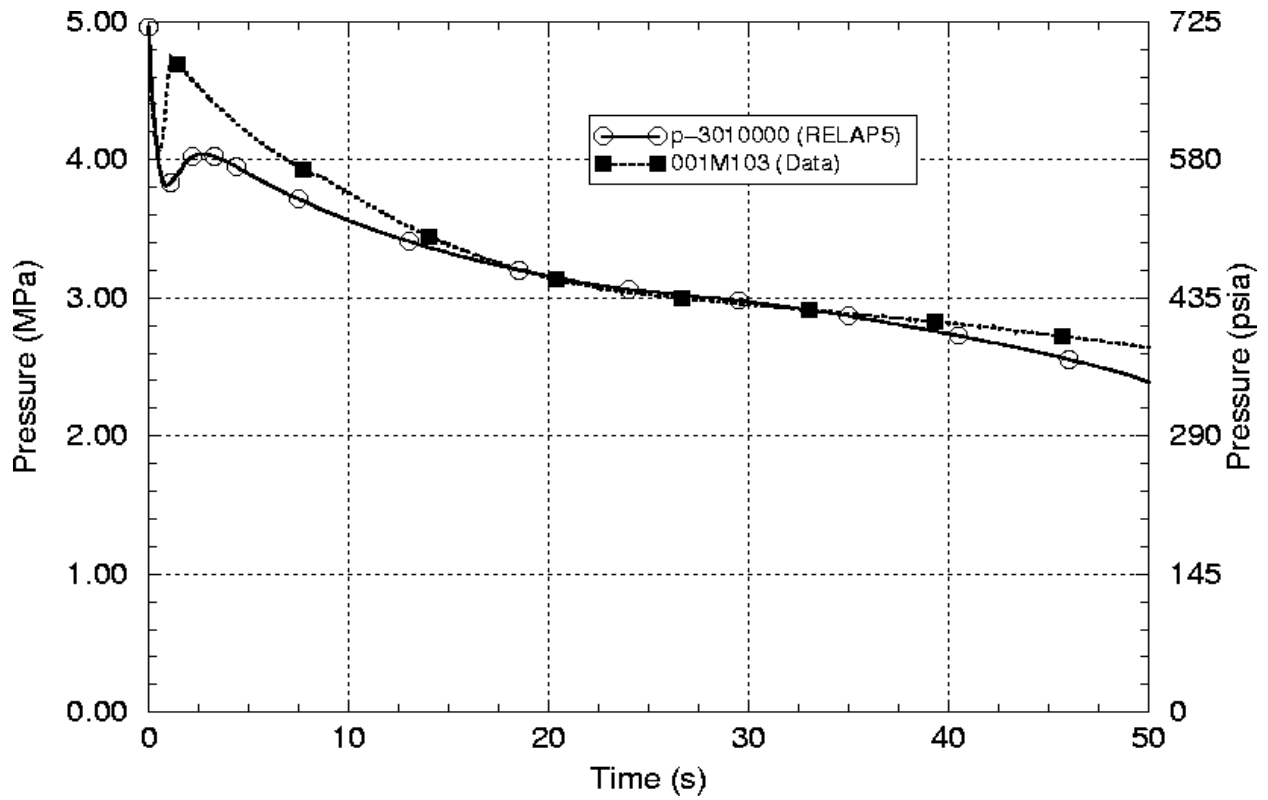


Figure K-4 MARVIKEN Test 24 Vessel Pressure Comparison

(3) *Reactor Vessel Wall Heat Conduction*

This phenomena was ranked high because it is essential to knowing the temperature distribution in the reactor vessel. Reactor vessel wall conduction is modeled in RELAP5, however, this information is not used directly since FAVOR performs its own conduction analysis. The FAVOR conduction solution has been compared with ABACUS with agreement to within 0.5% of the ABACUS value [62].

Vessel wall nodalization sensitivity studies were performed with RELAP5. This was done because under low flow conditions, the Churchill-Chu free convection model is invoked, and calculation of h depends on knowing the value,

$$T_w - T_f$$

While FAVOR does not use the RELAP5 wall conduction solution, in order to ensure that RELAP5 calculates h correctly, T_w must be calculated correctly. The conduction solution can affect the value of T_w , which is at the inner surface of the first (inner most) node of the vessel wall structure. We performed a nodalization sensitivity study to determine whether the noding in the existing plant models was adequate. As a result, the vessel wall nodalization was increased from its prior value, used in the IPTS study, of ~6 nodes, to ~80 nodes,

A sensitivity study was performed based on the 12 risk-important scenarios from Palisades to evaluate the effect of vessel wall nodalization [26]. The study assessed using 80 nodes in the RELAP5 vessel wall model as opposed to the base case of 8 nodes. The nodes were equally spaced. The coarse node size was 2.6 cm (1 inches) while the fine node size was 2.1 mm (0.1 inches). Wall nodalization had negligible overall effect. This indicates that the calculation of h by RELAP5, was not affected by the RELAP5 wall conduction solution.

$$\frac{CPF_{80node}}{CPF_{8node}} = 0.99$$

(4) *Jet Behavior, Flow Distribution and Mixing in Downcomer*

This includes several related phenomena under the heading of fluid-fluid thermal mixing: circulation cells in the downcomer, plume spreading or penetration, mixing as the flow enters from the downcomer and turns from horizontal to vertical, and plume decay.

As a one-dimensional code, RELAP5 cannot model fluid-fluid mixing phenomena. Each node has only a single temperature that applies to all liquid within the node. It was shown in Chapter 3 that RELAP5 provides excellent predictions of nominal downcomer temperatures (no bias, standard deviation of 10C). The experimental data on downcomer mixing are discussed in Section 5. The data show that a one-dimensional modeling approach is reasonable. The relative insensitivity of CPF to possible nonuniform distribution is addressed in Section 5 as well.

Based on integral system experimental data, the downcomer is well mixed, both axially and azimuthally. The nonuniform temperature distributions in the experimental data are within the absolute uncertainty of RELAP5 to predict bulk fluid temperature. Temperature variations seen in APEX-CE experiment are similar (5C) to RELAP5 predictions of plant transients. The small

magnitude of temperature nonuniformity in the downcomer is due to large eddy mixing occurring in the downcomer and the lower plenum.

(5) *Wall-Fluid Heat Transfer*

As discussed in Section 3, the wall to fluid heat transfer is one of the key thermal hydraulic parameters that serve as boundary conditions to the fracture analyses. The Biot number evaluation showed that the overall vessel temperature distribution is weakly affected by the convective heat transfer coefficient.

The near-surface region of the vessel, that is, the 1-to-2 cm near the inside wall, are where flaws may propagate to cause failure. This region can be sensitive to changes in h , though the effects of h remain relatively small compared to temperature and pressure effects.

Uncertainty in heat transfer was evaluated to determine the impact on the fluid temperature of the release of the initial stored energy in the structures [2]. RELAP5 employs a complex heat transfer package based on a combination of best-estimate models that treat the entire heat transfer regime. The nominal calculated value calculated by RELAP5 was varied by +/- 30%. This range is based on the typical uncertainty in heat transfer models. The variations were applied to all the heat structures to obtain a global effect on fluid temperature. The total heat transfer to the fluid from the wall is relatively insensitive to the value of the heat transfer coefficient. The heat flux from the vessel to the fluid does not have the required capacity to significantly modify the downcomer cool down rate.

Sensitivity studies were performed on convective heat transfer. They were focused specifically on the downcomer to evaluate the effect of heat transfer on heat flux from the vessel wall to the fluid, and in turn, on the probability of vessel failure. The standard version of RELAP5 used for the PTS analyses applies the maximum of heat transfer calculated using Dittus-Boelter and Churchill-Chu. For the conditions of interest to PTS, RELAP5 often applies Churchill-Chu free convection heat transfer modeling, not Dittus-Boelter since it predicts higher heat transfer under low flow conditions. Churchill-Chu is a best-estimate model based on free convection over a vertical flat plate, and extends from laminar to fully turbulent flow. The results of these studies were discussed in Section 4.7 and Appendix I.

(6) *Jet behavior, Flow Distribution and Mixing in Cold Leg*

This includes several related phenomena under the heading of fluid-fluid thermal mixing. It includes the mixing in the ECC injection line before the flow reaches the cold leg, mixing of the ECC jet where it enters the cold leg, stratification in the cold leg, mixing of the stratified flow within the cold leg as it moves towards the vessel, and back-flow of ECC liquid from the upper downcomer towards the RCP and loop seal. RELAP5 cannot model fluid-fluid mixing phenomena.

Applicable experimental data were reviewed from integral system test facilities, as will be discussed in Section 5. To summarize, the data show temperature gradients across the cold leg of up to 200C (360F). The large temperature gradients in the cold leg do not, however, translate to corresponding temperature variations in the downcomer. The downcomer temperature remains uniform, both axially and azimuthally. This appears to be due to large eddy mixing occurring in the downcomer which mixes the incoming flow from the cold leg soon after it enters the downcomer.

RELAP5 cannot calculate temperature gradients in the cold leg. In this situation, the code tends to predict an averaged behavior. The RELAP5 calculations of cold leg temperatures in ROSA generally fall within the temperature distribution measured in the cold leg.

(7) *Natural Circulation Flow and Loop Flow Resistance*

Natural circulation in the RCS is the dominant flow condition for secondary side breaks. For LOCAs, loop flow stagnation is the regime of importance. Under the single-phase conditions that persist in the RCS during secondary side breaks, the prediction of natural circulation flows is straightforward. Concerning loop flow resistance, generally adjustments are made to the input model values of form losses until agreement is obtained with measured pressure drop data.

Sensitivity studies were performed in which the flow resistance was increased by a factor of two. The magnitude of the variation chosen is large compared to the actual uncertainty in modeling loop flow resistance. Although this was a low ranked phenomena in the PIRT, it was investigated for completeness. While the natural circulation mode is important during secondary side PTS scenarios, the uncertainty in heat transfer and temperature distribution is small due to the overwhelming effect of the large heat transfer area in the core and the steam generator, compared to the low decay heat level. Little effect was seen [2].

The capability to calculate two-phase natural circulation, up to the conditions of reflux condensation conditions is important to assess. This type of assessment provides information relevant to the ability of the code to predict mass and energy distribution during LOCA scenarios.

RELAP5 comparisons were made to two-phase flow test series in SEMISCALE [12]. The tests were run as a series of steady states in which core power and steam generator conditions were held constant. This fixes the heat source and heat sink. Reactor coolant system inventory was decreased in a step wise manner and the two phase mass flow rates were measured. The assessment represented a substantial test of the combination of the flow regime and interfacial drag package in the code. The flows encompassed during the experiments include single-phase liquid, bubbly, slug/plug, stratified, and countercurrent, in both vertical and horizontal geometries. Therefore, they provide an overall indicator of the ability of the code to predict the range of flow conditions encountered.

Figure K-5 shows the results. The trends are similar. The agreement on the peak mass flow rate is similar but shifted towards a lower inventory in RELAP5. As the inventory is reduced, RELAP5 appear to over predict interphase drag. Overall, the agreement is reasonable.

Natural circulation is not an important phase of LOCA PTS scenarios. In contrast to secondary side breaks, for LOCAs the downcomer and vessel wall do not begin to cool until natural circulation ceases. The timing of interruption of loop flow is, therefore, a key turning point in LOCA transients. The ability of RELAP5 to predict the onset of loop flow stagnation is of interest, because this marks the start of cool down. In order to predict the timing of the interruption of natural circulation correctly, the key factor is determining when the primary system

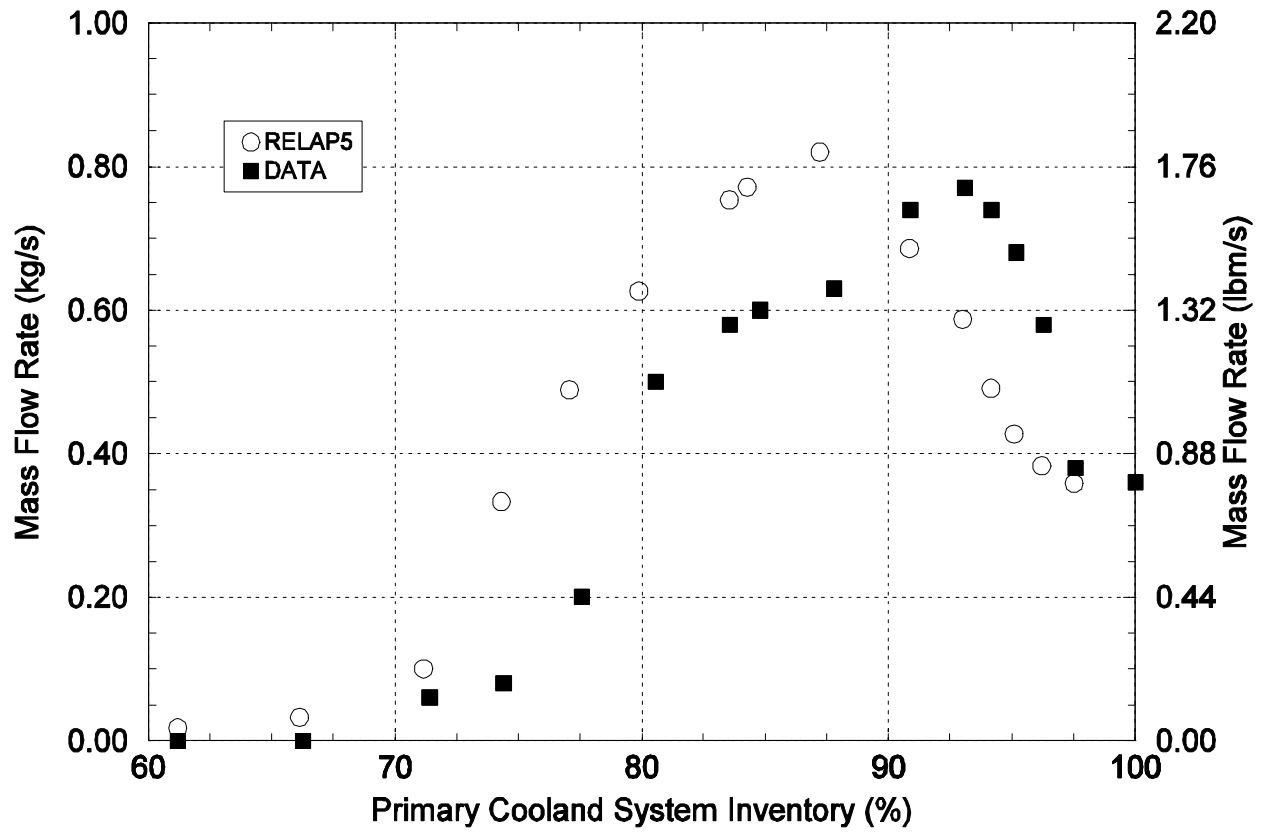


Figure K-5 Natural Circulation Flow vs Inventory Comparison for SEMISCALE S-NC-2

becomes cooler than the secondary system. This includes several factors, the most important of which is the correct prediction of break flow.

The assessment of RELAP5 to predict interruption of natural circulation was made against the integral system tests described in Sections 4.4, 4.5 and 4.6. The agreement was generally excellent with the exception of one MIST test, for which system heat loss modeling played an important role. Results from the assessments of the four ROSA tests are shown in Table K-6. The agreement is reasonable to excellent.

Table K-6 Interruption of Loop Flow in ROSA

Experiment	Break Size	Test	RELAP5
SB-CL-18	6-inch cold leg break	180 s	170 s
SB-HL-06	2-inch hot leg break w/o HPI	A - 1700 s; B - 1900 s	1700 s
AP-CL-03	1-inch cold leg break	A - 463 s; B - 1115 s	A - 470 s; B - 1080 s
AP-CL-09	1-inch cold leg break with failure of CMTs, ½ ADS1-4	A - 770 s; B - 1984 s	A - 1228 s; B - 1967 s

(8) *Downcomer-Upper Plenum Bypass*

During LOCAs, the possibility exists for in-vessel circulation flows that deliver water from the upper plenum region to the upper downcomer. Such flows would tend to warm the water in the upper downcomer and the cold legs. Experiments and CFD studies have shown that there is significant countercurrent flow of warm water from the upper downcomer into the cold legs, and energy exchange in the cold leg between the warm stream and the cold ECC injection. .

The vent valve design of B&W allows for the possibility of significant in-vessel circulation under flow stagnation conditions. While the RCPs are on, the vent valves are held shut by differential pressure. Table K-7 shows vent valve flows calculated by RELAP5 for four different LOCA break sizes in Oconee. Figure K-6 shows the results of sensitivity studies based on a 2.8-inch hot leg break in Oconee. For this break size, the vent valve operation had a significant effect on the downcomer temperature, ranking behind only HPI failures and decay heat level in importance. When the vent valves were held open, T_{sen} increased by 25C, while when the vent valves were held shut, T_{sen} decreased by 25C. T_{sen} is the downcomer temperature averaged over the duration of the calculation (10,000 s). All comparisons are with respect to the nominal base case calculation value.

While Westinghouse and CE plants do not have vent valves, there is still a bypass flow path between the upper downcomer and the upper plenum. The area of this path is generally not characterized precisely in power plants, but amounts to approximately 1.5% of the total flow during normal operation. This translates to an approximate area of 0.054 m² (10-inch diameter equivalent). This area is ~7% of the Oconee vent valve flow area (0.785 m²).

The RELAP5 results were reviewed to evaluate bypass flows, for a large number of Palisades and Beaver Valley transients. Typical upper plenum-downcomer bypass flows were 5-15 kg/s,

1	100% HPI fail
2	50% HPI fail
3	25% HPI fail
4	RVVVs Open
5	CL LOCA
6	90% HPI
7	130% h
8	Summer
9	P _{CET} - 50 psi
10	Nominal
11	P _{CET} + 50 psi
12	110% HPI
13	70% h
14	Winter
15	High CL rev. K
16	RVVV Closed
17	HZP

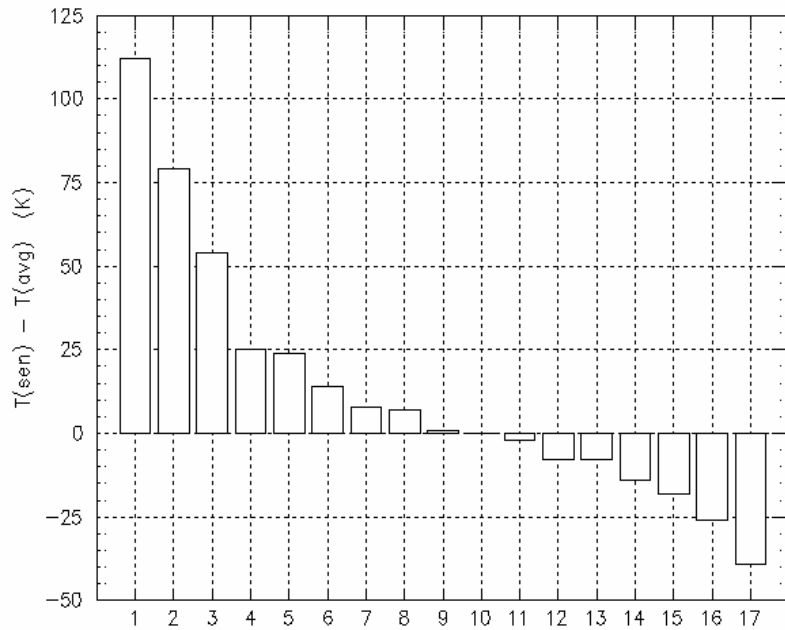


Figure K-6 Sensitivity Study Results for 2.8-inch Hot Leg Break in Oconee

Table K-7 Vent Valve Flows in Oconee

Case	Transient	Total RVVV Flow
156	16 in hot leg break.	180 kg/s
160	5.656 in surge line break	45 to 300 kg/s
172	4 in cold leg break	200 to 450 kg/s
164	8 inch surge line break	45 to 350 kg/s

which is ~10% to 20% of HPI flow. Considering the flow area ratio of 1:15 compared to Oconee, the bypass flows are consistent among the three plants. The effect on downcomer temperatures should be correspondingly less for Westinghouse and CE.

We performed counterpart experiments in APEX-CE with the bypass closed to examine the effect of bypass flow on downcomer temperature. Three tests that were run with the bypass path closed were repeated with the bypass path open. The effect on downcomer temperature was ~2C. When multiplied by the area ratio of 15, the effect is consistent with the calculated effect for Oconee of $T_{sen} = 25C$.

(9) *Upper Head Heat Transfer*

During LOCAs, the primary system will tend to stratify, with steam-water interfaces established in high points in the RCS. In particular, a steam bubble will form in the upper plenum-upper head region that occupies the elevation from the top of the hot leg to the top of the reactor vessel. This steam bubble exerts an influence on primary system pressure.

The physical phenomena involve heat exchange under stratified conditions between a steam volume and a liquid interface, and between the steam and the surrounding metal structure. Heat exchange between the phases is limited under these conditions.

While this phenomenon was ranked low in the two PTS PIRTs, it was of possible significance in the current analyses, since unlike the small break LOCA that formed the basis of the PIRTs, some sequences involved refill and repressurization of the RCS. Specifically, transients analyzed included stuck-open pressurizer SRVs that reclose. For these transients, steam bubbles form in the system early in the transient. Later, when HPI refills and repressurizes the RCS, the steam bubbles gradually condense and collapse by heat transfer from vapor-to-wall and vapor-to-fluid. For stuck-open SRV scenarios, the dominant uncertainty is the timing of HPI control by the operator. If the operator followed procedure in a timely manner, HPI is throttled before reaching high RCS pressures. If there is a delay, however, the RCS can become water solid. The latter events contribute ~1/2 of the total PTS risk.

RELAP5 models the heat exchange between the vapor and liquid phases using a number of different models depending on whether the liquid is superheated, the liquid is subcooled, the vapor is superheated, or the vapor is subcooled [25, pp 84-91]. In addition, there is energy exchange between the vapor and the vessel structures. The heat transfer package is too complicated to be summarized here.

To assess RELAP5 for these phenomena, we used the MIT pressurizer experiment. In the experiment, the tank was filled from the bottom, causing a steam bubble in the tank to be compressed. The experimental apparatus was a small tank of diameter 0.203 m (8 inches), height 1.14 m (45 inches), and thickness 0.82 cm (0.32 inches). The experiment involved compressing the vapor space in the tank by filling the tank from the bottom with water and measuring the pressure. The process is the same as refilling and depressurizing the reactor coolant system.

The initial level in the tank was 0.43 m, which was increased at ~1 cm/s over a 45-s period. This increased the level by 0.52 m for a final level of 0.95 m, which compressed the vapor space by a little under a factor of four. As pressure rose, the vessel walls became subcooled and film condensation occurred. Figure K-7 compares RELAP5 to the data for pressure, while Figure K-8

shows the temperature comparison. RELAP5 tended to under predict the pressure rise and over predict the pressure decay. This is believed to be because heat loss to the environment was not included in the RELAP5 model. Also, the RELAP5 tendency towards numerical diffusion reduces the thermal stratification and increases the condensation of steam to liquid.

The results show *reasonable* agreement between RELAP5 and the data. In any event, the outcome of repressurization scenarios is dominated by the RCS becoming water solid. In such circumstances, RCS pressure is determined by the SRV setpoint for opening, which is a well-defined number. Therefore, there is little uncertainty in RCS pressure.

(10) *Liquid/Vapor Interface in Upper Downcomer*

During LOCAs, the inherent response is for the liquid level in the reactor coolant system to fall until it reaches the elevation of the break. Thereafter, break flow and ECC injection flow equilibrate and the level remains the same. The break elevation is generally at the loop elevation, that is, the level of the hot and cold legs. The ECC injection is at the same elevation. This means that there is significant potential for direct contact condensation during ECC injection during LOCAs. The more condensation that occurs, the warmer the ECC liquid becomes. RELAP5 assessment for condensation was discussed above (see Figure K-1).

(11) *Steam Generator Heat Transfer*

Steam generator heat transfer was evaluated [2, Appendix C]. The heat transfer area of the steam generators is sized to exceed 100% power. All the PTS scenarios analyzed involve decay heat conditions, where the energy generation is approximately 1% of full power. Therefore, under conditions of forced circulation or natural circulation, the primary and secondary system are tightly coupled with temperature differences of the order of 1C. Under these circumstances, the initial stored energy of the steam generators is additive to the primary system initial energy.

Once the primary system temperature drops below the secondary side temperature, the two systems decouple. Reverse heat transfer may occur for some period of time while primary system inventory is dropping. However, this process tends to make the steam generators act like a pressurizer helping to force remaining water out of the tube region on the primary side.

Because the steam generator heat transfer is area dominated, its uncertainty was found to be small, and was not considered further.

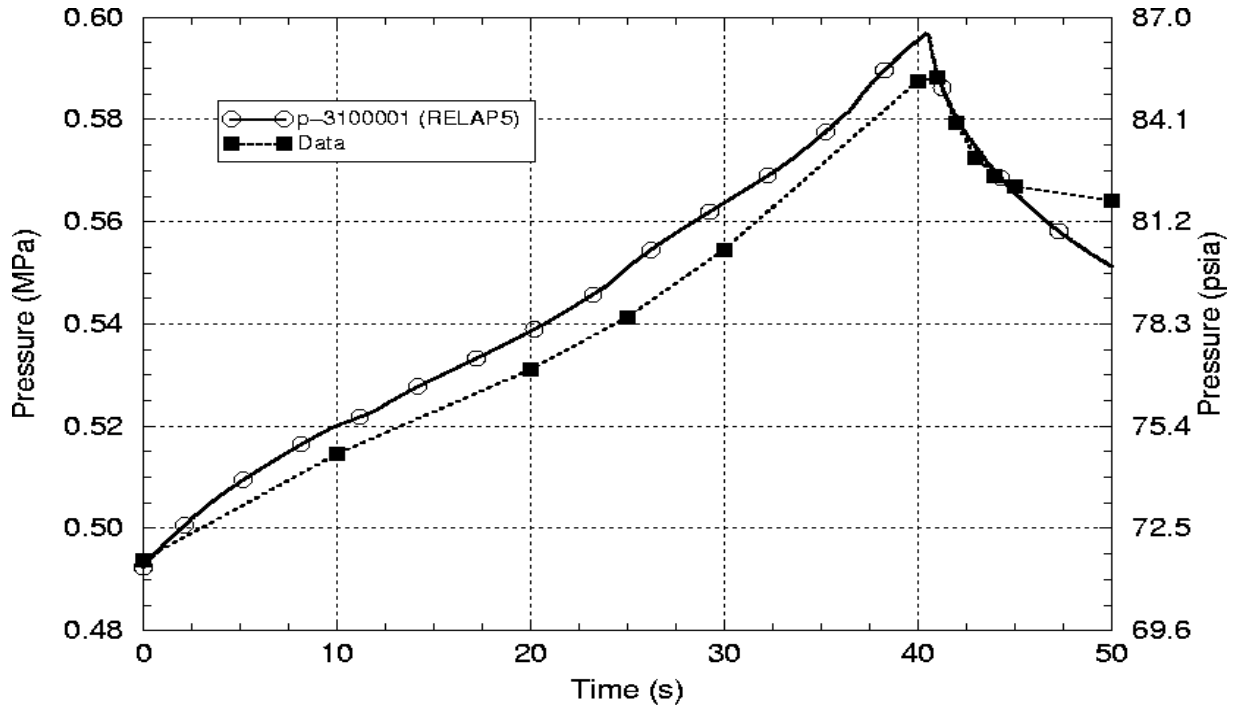


Figure K-7 Comparison of RELAP5 Pressure with MIT Pressurizer Test Data

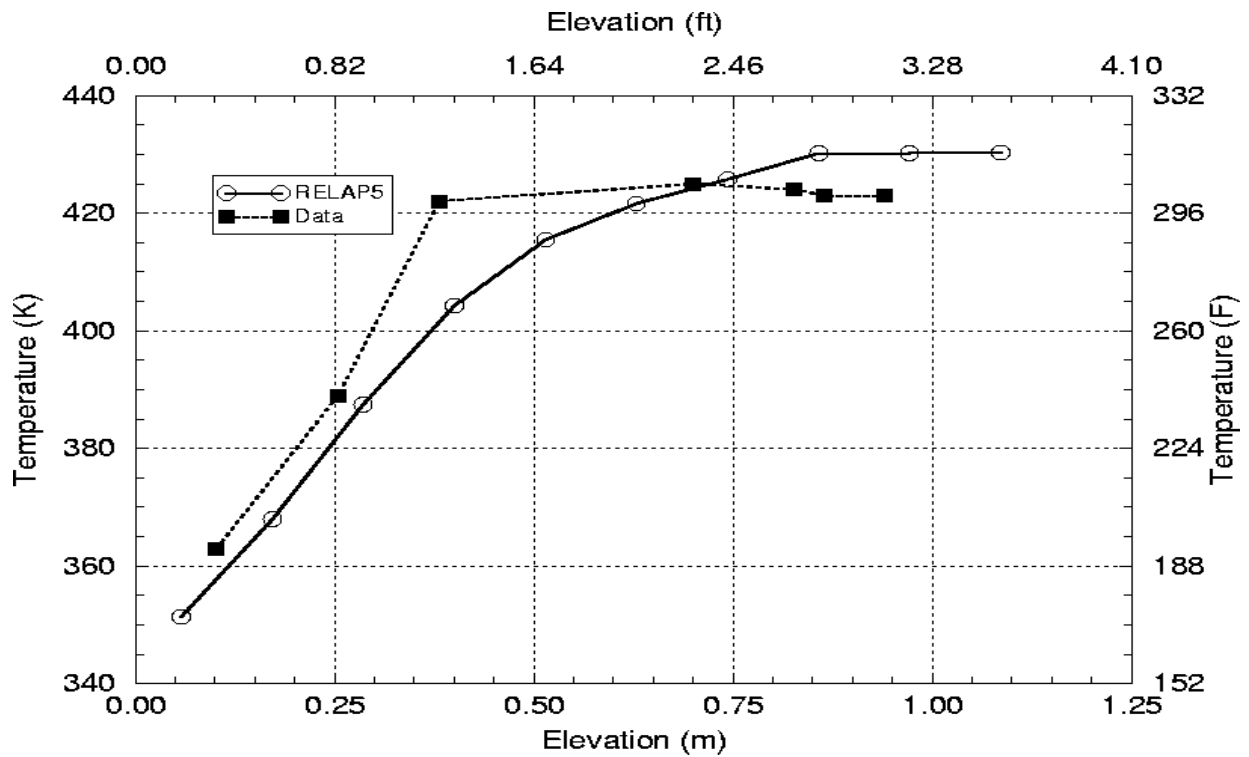


Figure K-8 Comparison of RELAP5 Temperature Distribution with MIT Pressurizer Test Data

APPENDIX L. USE OF THERMAL-HYDRAULIC UNCERTAINTIES IN DEVELOPING EVENT SEQUENCE BINS

The thermal hydraulic uncertainty analysis is described in detail in [2], along with supporting information and analyses. The purpose of this section is to provide a very brief summary of the approach. It was a collaborative effort among PRA, thermal hydraulic and fracture mechanics staff. The set of scenarios considered was extremely broad. The PRA sequence definition evolved from a bottom up approach, with a range of possible equipment malfunctions and operator errors considered. The resulting set of scenarios numbered of the order of 10^4 to 10^5 for each plant.

The thermal hydraulic uncertainty of each individual sequence cannot be addressed, nor would it be useful to do so. To develop a workable method, therefore, a top-down approach was mandatory. The current uncertainty effort is a departure from prior thermal hydraulic uncertainty analyses performed according to the CSAU methodology [7, 8, 9]. CSAU has aspects of a bottom-up approach. Additionally, however, it provides an overall systematic structure and possesses top-down features as well. The approach we following was entirely top-down in its evolution.

From a thermal hydraulic perspective, the only way to generate thermal shock is by overcooling. Overcooling can result from either a break on the secondary side or from a break on the primary side. From this a classification scheme was developed.

Cooldown Classification Hierarchy

- Primary Side Break
 - Large LOCA
 - Medium LOCA
 - Small LOCA
 - Unisolable Small LOCA - pipe break
 - Isoable LOCA - stuck open valve (SRV) that recloses
 - Timing of closure; 3000 s, 6000 s
 - Variations in HPI control; 1 min, 10 min, no control
- Secondary Side Break
 - Steam line - including pipe break, stuck open SRV, stuck open steam dump valves, stuck open atmospheric relief valve
 - Variations in feedwater control; 1 min, 10 min, no control
 - Feed line
- Combinations of primary side and secondary side breaks

From this classification scheme, individual accident sequences were quantified. Similar sequences were combined into preliminary thermal hydraulic bins. As the analysis proceeded, new thermal hydraulic bins were developed as necessary, as an iterative process. The process involved characterizing a bin through thermal hydraulic analysis and assessing its contribution to risk through FAVOR analysis, to generate a *conditional probability of failure* (CPF) times a PRA *frequency of the initiating event*.

The frequencies of all the thermal hydraulic bins were quantified with point-estimates. For each plant, approximately 150 transients were calculated using RELAP5, including base case and sensitivity studies. The principal bins that resulted included

- LOCA: small, medium, large. We examined the effect of out flow from breaks in the primary system by performing a break spectrum analysis ranging from 1-inch to 23-inch, a factor of 500 in break flow area.
- Overcooling with repressurization - Stuck open primary side valve (pressurizer safety/relief valve or power operated relief valve).
- Feed and bleed (similar to stuck open primary side valve).
- Stuck open secondary side valve (steam generator safety/relief valve, atmospheric release valve, steam dump system valve).
- Main steam line break - large and small.

The events were analyzed from normal full power initial conditions and from low power (low decay heat) initial conditions.

With respect to operator actions, for a given LOCA scenario, there is essentially nothing the operator can do to affect the risk significance. For the subset of LOCAs that are isolable, (i.e., SRV sequences) for a given scenario, the key operator action that is to prevent the reactor coolant system from going water solid. For secondary side breaks the key operator action is to terminate feedwater to the broken steam generator.

The sensitivity studies used downcomer fluid temperature as the focus, as the most important of the three thermal hydraulic figures of merit.

The uncertainty analysis was a combination of variation within a bin, as well as uncertainty in physical models in RELAP5. Uncertainties that related to sequence definition translated into specific variations in boundary and initial conditions used in RELAP5 input models. The uncertainties are represented in terms of discrete RELAP5 calculations to characterize the range of possibilities within a bin. This aspect of uncertainty is not an examination of physical models in RELAP5. Within a given bin, the code uncertainty can be seen as a subset of the total uncertainty.

The uncertainty evaluation included both mapping of the range of behavior within a bin through variations in *boundary conditions* and uncertainties stemming from *physical modeling uncertainties* in the code. The analyses considered both:

- (a) The code input model, which defines the boundary conditions to the problem. Input model variations were defined through close interaction with PRA.
- (b) The physical models and numerical solution methods that comprise the code itself.

Variations of boundary conditions have as much or greater impact on calculated results as the physical models that comprise the code. Both must be considered in any uncertainty evaluation.

Mapping the range of sequence variations within a bin was performed by varying the boundary conditions of the RELAP5 input model. Uncertainties arising from the PRA become uncertainties in the boundary and initial conditions used in RELAP5. The *variation within a bin* was determined by a number of different, discrete RELAP5 calculations to characterize a bin.

Each RELAP5 calculation is deterministic. In performing a mapping analysis, a family of curves is generated that provides a family of input boundary conditions of P, T, and h to FAVOR. This *range of thermal hydraulic inputs* translates into a range of outcomes, measured as a *range of CPFs* calculated by FAVOR.

The list of boundary conditions and physical phenomena described in the PIRT table (Table K-2) were categorized as follows:

Table L-1 Classification of Boundary Conditions and Physical Models

Aleatory (Boundary Conditions)	Epistemic (Physical Models)
Break size (1 to 22 inches diameter)	In-vessel recirculation, downcomer/upper plenum bypass
Break location (hot leg, cold leg)	Structure-fluid heat transfer
Decay heat level (full power, low power)	Flow resistance (loop flow)
HPI state (full, 50%)	Break flow model
HPI flow rate ($\pm 10\%$), temperature	
LPI, accumulator temperature	
Accumulator pressure (± 50 psi), temperature (70F,110F)	
Feedwater flow control, temperature	
Operator control of HPI, feedwater (1 min, 10 min, none)	

Sensitivity studies were performed with RELAP5 for each phenomena/process/boundary condition. This was done varying one factor at a time from its nominal value to an upper value and a lower value. For each plant approximately 150 sensitivity studies were performed using RELAP5.

The basis for measuring the effect of each sensitivity studies was the downcomer fluid temperature from the RELAP5 calculations averaged over the 10,000-s duration of the calculation (T_{sen}). Downcomer temperature was used since it is the most important of the three thermal hydraulic boundary conditions to the fracture analysis. This gave a downcomer temperature in terms of T_{sen} as an indication of the CPF magnitude of a unique scenario. The values of T_{sen} of the various scenarios within a bin were used to represent the uncertainty range of the bin.

Following the one-at-a time sensitivity studies, the individual contributions were combined considering all possibilities. A special purpose code was written to combine the one-factor-at-a time calculations from RELAP5, into all possible combinations of multiples. From this, a probability density function was generated, as shown in Figure L-1 for the example of the small break LOCA bin for Oconee.

From the probability density function, a cumulative distribution function was created, as shown in Figure L-2. The cumulative distribution was then subdivided into sub-bins. Each sub-bin was given a probability that was a fraction of the total probability of the bin. Thus, as illustrated in Figure L-2 for Oconee, five sub-bins were created for the category of small break LOCAs.

Each of the five sub-bins was then characterized by discrete RELAP5 calculations whose value of T_{sen} corresponded to that from the cumulative distribution function. In this way, each bin was represented by several RELAP5 calculations that described the uncertainty range of that bin. In this example, five RELAP5 calculations were performed to represent the uncertainty of the bin.

Each individual contribution of uncertainty was considered to be *linearly additive*. This hypothesis was tested by performing a number of additional RELAP5 calculations that combined multiple factors at a time. Figure L-3 shows one of these analyses, and indicates that the linearly additive assumption is reasonable.

Key observations of the uncertainty analyses were:

- For events with similar thermal hydraulic signatures, the effect of uncertainty in pressure (P) on PTS uncertainty were small compared with the impact of downcomer temperature (T_{dc}) uncertainty.
- The two categories of: 1) large LOCAs, and 2) pressurizer safety/relief valve (SRV) stuck open and later reclosed, are the most risk significant.
- For pressurizer SRV stuck open and later reclosed scenarios, the timing of SRV reclosure, and the timing of operator throttling HPI, both affect risk significantly.

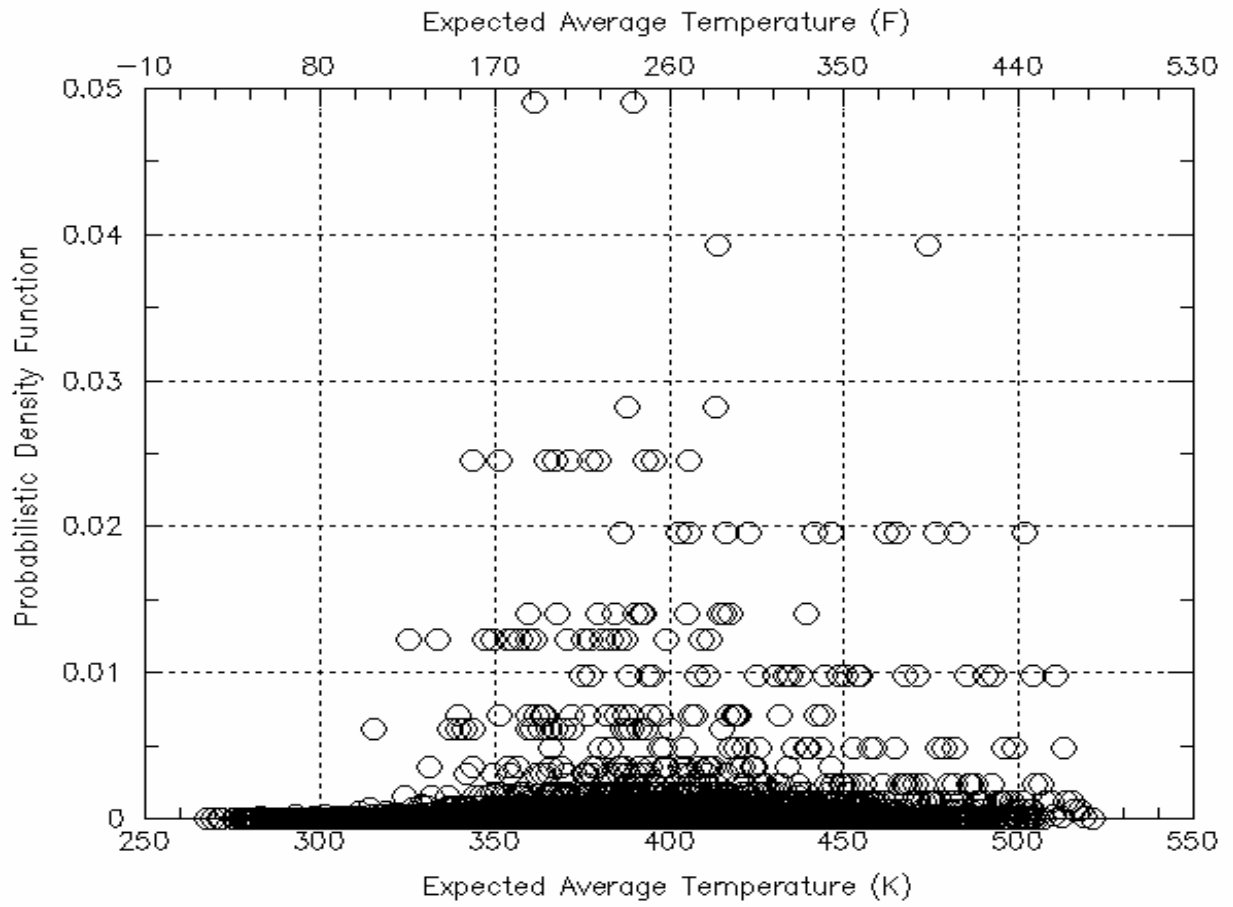


Figure L-1 Probability Density Function for Small Break LOCA Bin in Oconee

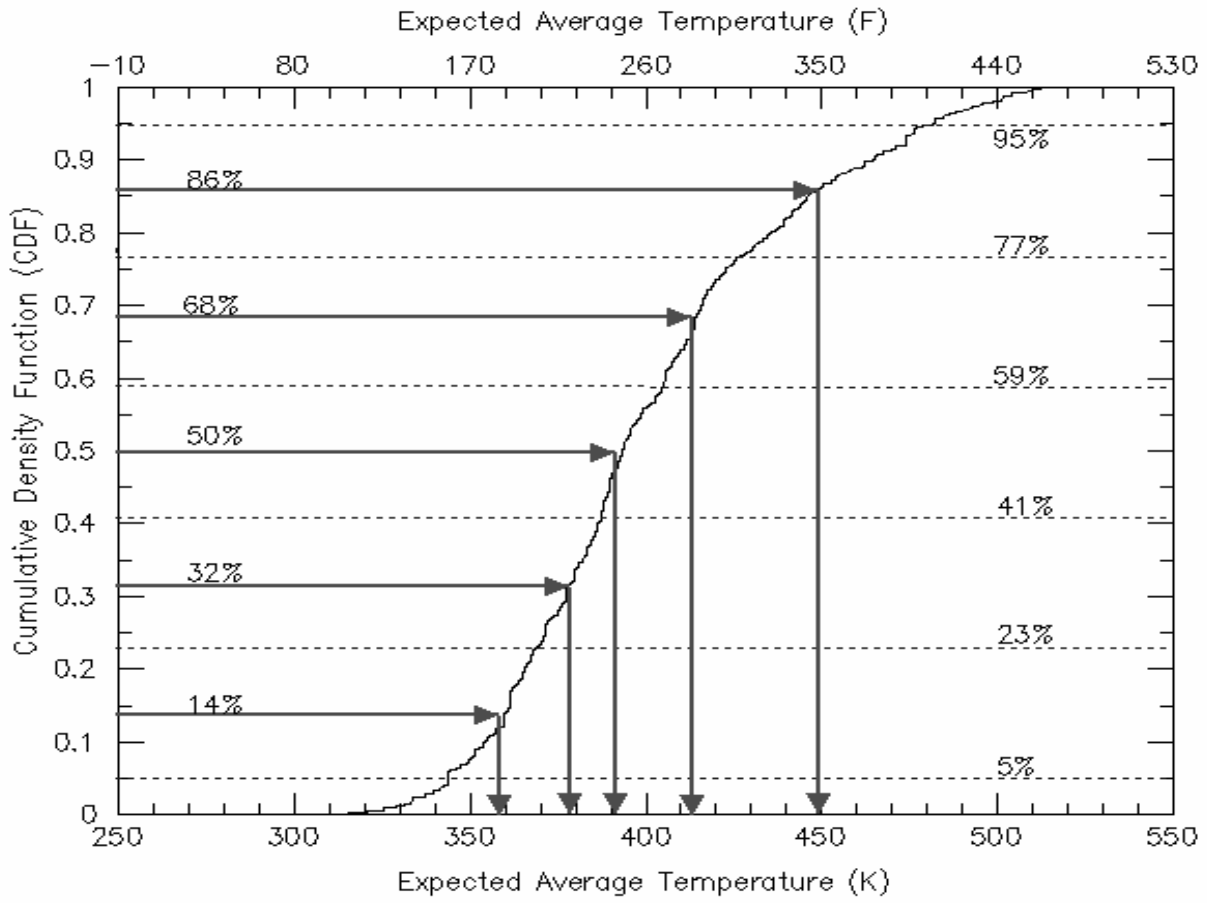


Figure L-2 Cumulative Density Function for Small Break LOCA Bin for Oconee-1

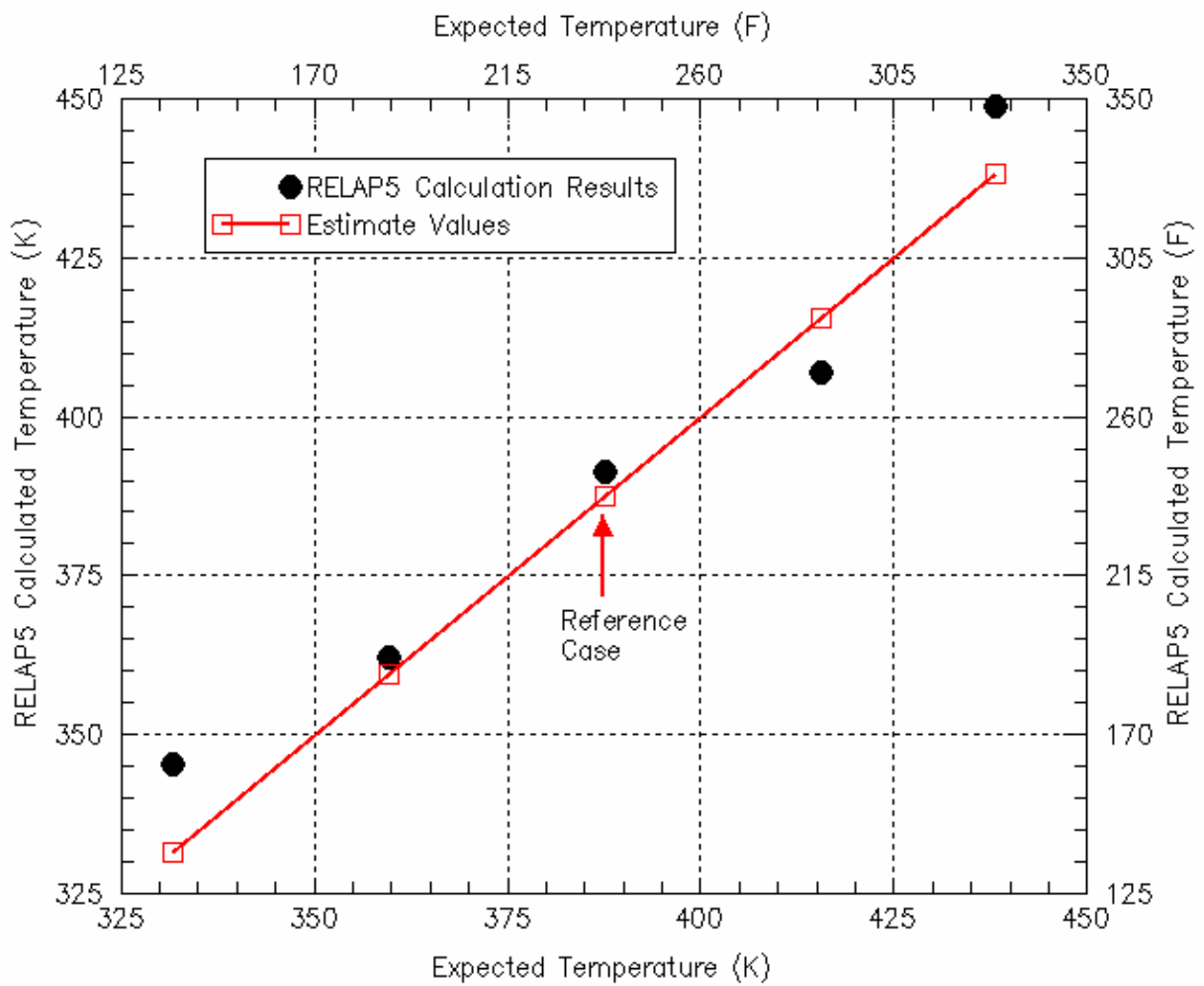


Figure L-3 Confirming the Linearly Additive Assumption Using RELAP5: 2.8 inch Surge Line Break LOCA

APPENDIX M. EXAMPLES OF COMBINED THERMAL-MECHANICAL RESULTS

Figures M-1 through M-4 illustrate for four main risk-significant bins the general relationship between the thermal hydraulic transient and the vessel response. Four risk-dominant PTS scenarios from Palisades are shown representative of risk-significant bins:

1. Large break LOCA (Figure M-1);
2. Small break LOCA (Figure M-2);
3. Stuck open SRV that recloses (Figure M-3); and
4. MSLB (Figure M-4).

These figures each plot:

- a. RCS pressure (in ksi)
- b. Downcomer temperature (in F/100)
- c. Downcomer convective heat transfer coefficient (in kW/m²-C)
- d. K_R (K/K_{min}). The vessel failure probability becomes non-zero when K_R exceeds one, and continues to increase until it reaches its maximum value.

P, T, and h are from RELAP5 calculations. The K-ratio (K_R) curves are from the FAVOR calculations, where the boundary conditions were supplied by RELAP5. K_R is the ratio of the applied stress intensity due to the transient to the minimum critical stress intensity for crack initiation K_{IC} . It is specific to a given flaw size and geometry. In contrast to the PTS analyses, for these calculations FAVOR was run in the deterministic mode. A fixed flaw geometry was used, along with fixed vessel properties representative of Palisades at 60 EFPY.

For the base PTS analysis, FAVOR is run in a probabilistic mode, with distributions of the important parameters, including K_{IC} . K_{IC} has some minimum value that is dependent on the shift in transition temperature below which the probability of initiation is zero, but that the probability of initiation increases as the applied K increases over the minimum K_{IC} , i.e., as $K_R > 1$. The probability of initiation can be computed from Eq 4-7 of NUREG-1807 (p. 61 in the draft). This probability is not just a function of K_R , rather, it also depends in the actual embrittlement of the material, but the dependence is weak and to first order the probability can be taken just as a function of K_R . Values for the probability of initiation as a function of K_R are given in the Table M-1.

From Fig 4-20 in NUREG-1809, as h increases by an order of magnitude, K_R increases from 1 to 1.33. From the table we see that a crack which was thought to have a very low probability of cracking (0) still has a low probability of cracking (2.3×10^{-3}) even if h increases by an order of magnitude. Note that this is for initiation. The crack may arrest so it gives a conservative estimate of the change in the probability of failure. This result is for a transient with a decay time of 30 min.

Figure M-5 is a plot of K_R for a 5.656-inch break in Palisades, which falls at the boundary between a fast transient and a slow transient. RCS pressure decreased to 200 psi by about 1000s, which

allowed the accumulators and LPI to inject. The injection rapidly cooled the downcomer, which reached a minimum temperature of 33C. At the same time, K_R increased sharply, before reaching a maximum at ~1500s.

Table M-1 Probability of Crack Initiation as a function of K_R

K_R	P initiation
1.00	0
1.01	1.98×10^{-9}
1.05	1.23×10^{-6}
1.10	1.98×10^{-5}
1.25	7.71×10^{-4}
1.33	2.34×10^{-3}
1.50	1.23×10^{-2}
2.00	0.179
2.50	0.632
3.00	0.958
3.50	1.000

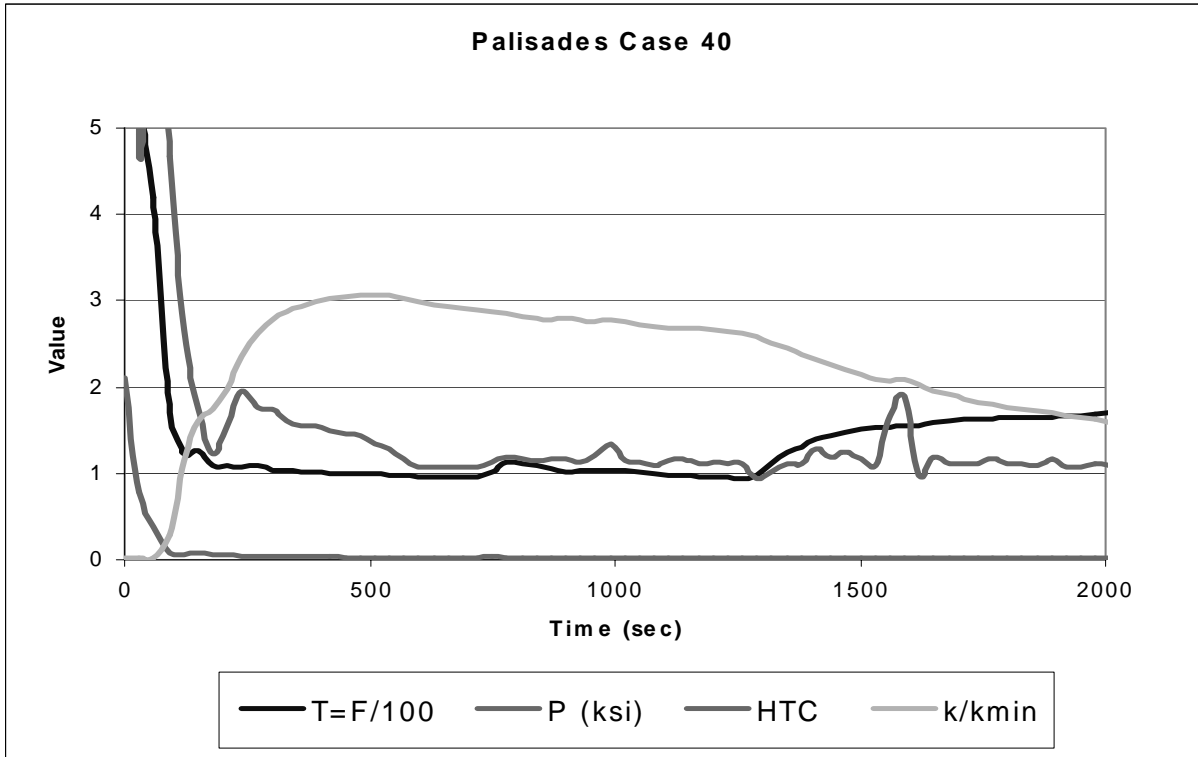


Figure M-1 Palisades Large Break LOCA (16-Inch Hot Leg) 21% of Total Palisades PTS Risk

Most probable failure time 300s (180s first failure, 600s last failure). The downcomer temperature is seen to fall quickly to a terminal value of 100F in about 100s. K_R rises from its initial value of zero, reaching a maximum of about 3 at 600s. Note that as seen in this figure, pressure does not contribute to vessel failure for large break LOCAs. This transient contributes 21% of the total probability of vessel failure for Palisades, with a through wall cracking frequency of $2 \times 10^{-9}/yr$. The heat transfer coefficient, which is plotted in terms of kW/m^2-C , lies between 1000 and 2000 W/m^2-C .

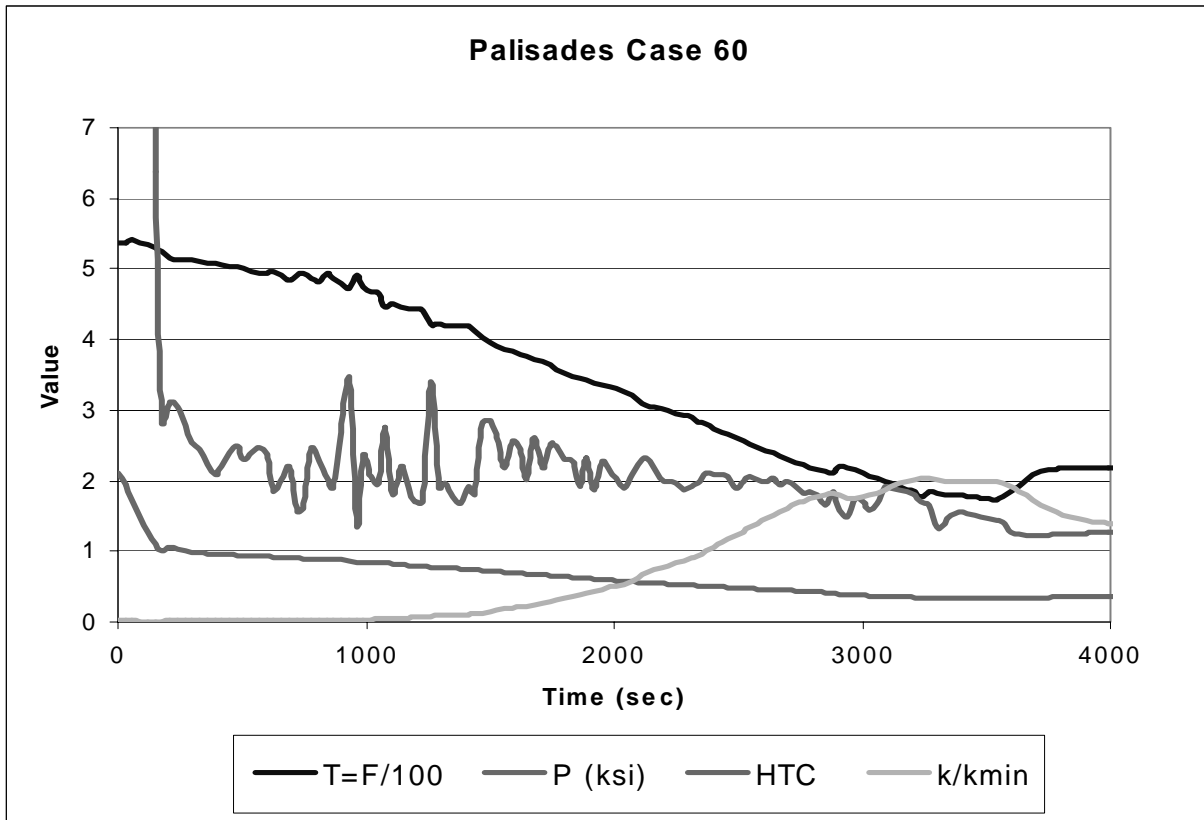


Figure M-2 Palisades Small Break LOCA (2-inch Hot Leg, Winter) 2% of Total Palisades Risk; Most Probable Failure Time 2820s (1800s first failure, 2820s last failure)

In contrast to the large break LOCA, the 2-inch small break LOCA exhibits a gradual cooldown with the downcomer temperature reaching 200F at ~3000s. The maximum value of K_R obtained is 2, compared with 3 for the large break. The through wall cracking frequency is 2×10^{-10} , a factor of 10 lower than the large break, which is consistent with the lower value of K_R . The heat transfer coefficient, which is plotted in terms of $\text{kW/m}^2\text{-C}$, generally lies between 2000 and 3000 $\text{W/m}^2\text{-C}$.

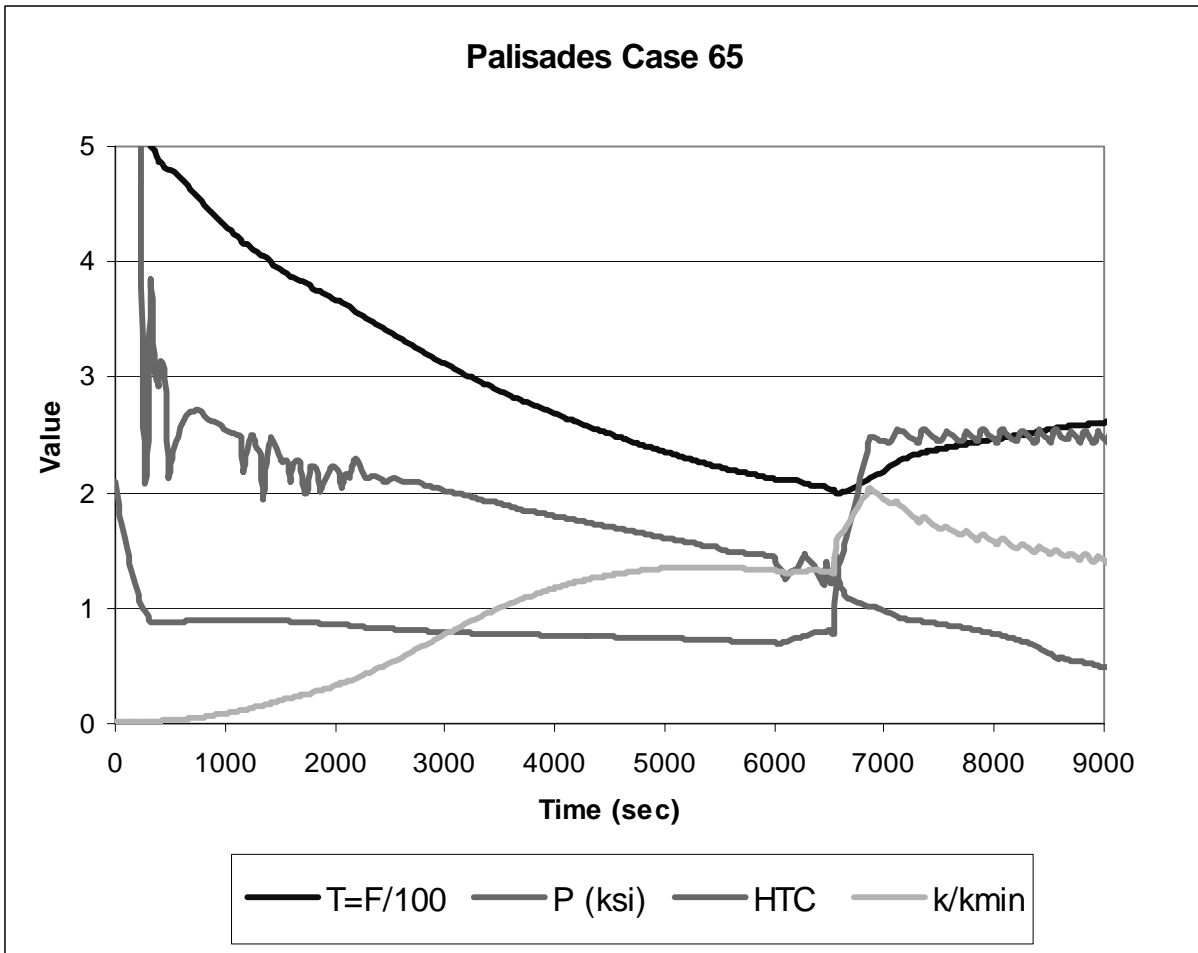


Figure M-3 Palisades Stuck Open Pressurizer SRV Recloses @ 6000s, Low Decay Heat 45% of Total PTS Risk; Most Probable Failure Time 6840s (2640s First Failure, 7140s Last Failure)

$T_{dc}(t)$ shows a more gradual decrease compared to the 2-inch break LOCA, since the SRV size is smaller. A minimum value of 200F is reached at ~6500s compared to ~3000s for the 2-inch break. The SRV is 1.425-inch equivalent diameter, which is about half the break area of the 2-inch break. The maximum K_R reaches 1.3 prior to the SRV reclosure, and climbs to 2.5 when the RCS pressure increased to 2400 psi. The through wall cracking frequency is 6×10^{-9} , a factor of 3 greater than the large break LOCA. This transient has a higher frequency of occurrence and a slightly lower CPF than the large break. The heat transfer coefficient falls gradually during the course of the transient. The break area of the valve falls at the boundary between very small and small breaks. The calculation indicates some natural circulation continuing up to ~2000s.

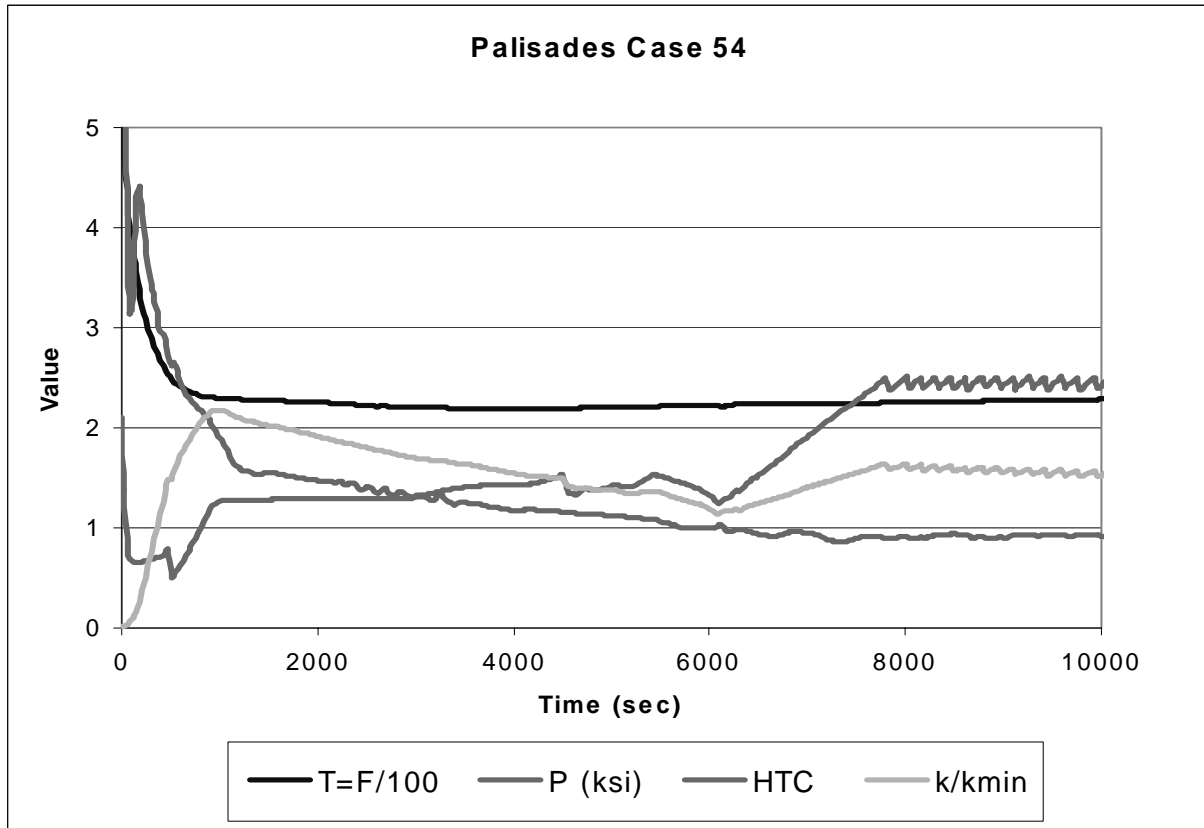


Figure M-4 Main Steam Line Break in Palisades, Failure of Both MSIVs to Close, with Continued Operation of HPI and AFW

2% of total Palisades PTS risk most probable time to failure 180s (first failure 840s, last failure 8000s)

This MSLB transient had the highest failure probability amongst the Palisades MSLB scenarios calculated. This scenario is the most severe cooldown induced by a secondary side fault that can be postulated. Following the initiating event, both MSIVs fail to close, resulting in blowdown of both steam generators. Auxiliary feedwater (AFW) is maintained, along with HPI. Continued operation of AFW ensures that the RCS cools down to ~220F.

K_R reaches a maximum of ~2.1 at 800s. The through wall cracking frequency is 3×10^{-10} , a factor of 10 less than the large break LOCA. The two transients have nearly the same CPF, but this MSLB scenario has 1/10 the frequency of occurrence compared to the large break LOCA.

Primary system pressure drops rapidly as the steam generators blowdown and the RCS inventory shrinks. Once the cooldown is complete, pressure begins to recover as HPI refills the RCS. Once primary pressure reaches ~1200 psi, the rate of repressurization decreases since the HPI pumps reach their shutoff head. Thereafter, charging flow continues filling the RCS at a low rate (9 kg/s, 150 gpm) until the SRV set point is reached at 8000s.

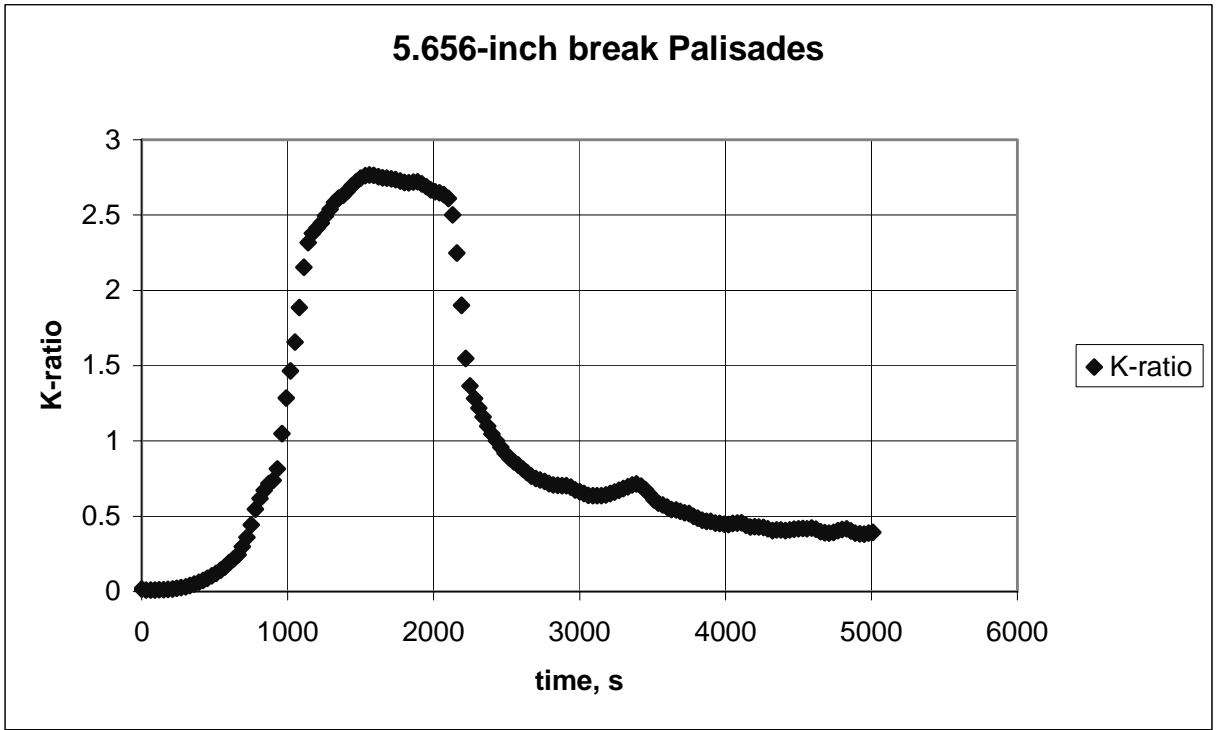


Figure M-5 K_R for Medium Break LOCA in Palisades

APPENDIX N. APPLICABILITY OF 1994 FAVOR RESULTS TO CURRENT PTS REEVALUATION

Section 5.5 described an assessment of the potential effects of thermal plumes on the probability of through wall cracking during a PTS transient [27]. The study used an early version of FAVOR (94.1) in contrast to that used in the current PTS study (04.1). In this appendix we review FAVOR 94.1 modeling compare it with FAVOR 04.1.

Aside from the modeling of plumes, the overall probabilistic fracture mechanics computational methodology differs considerably between FAVOR 94.1 and FAVOR 04.1. While the underlying principles of both codes is that of linear elastic fracture mechanics, a great majority of the sub-models and parameter inputs that make up the code were improved as part of the PTS re-evaluation effort [63]. It is beyond the scope of this appendix to perform a point-by-point comparison of the two code versions. Rather, the intent is to indicate if the any of the changes made between the 94.1 and 04.1 versions of FAVOR substantively alter the findings of the study of plume effects on vessel failure probability performed using FAVOR 94.1 [27].

FAVOR 94.1 Model of Thermal Plumes

Since its initial release in 1994, all versions of FAVOR have employed one-dimensional, axisymmetric, finite-element thermal and stress analyses to predict the time-dependent stresses associated with the applied pressures and radial variations in temperature that characterize different PTS transients.

FAVOR 94.1 used a simplified method to incorporate the multidimensional aspects of thermal plumes due to incomplete mixing of safety injection flow into the cold leg. The stresses and stress intensity factors (applied- K_I values) predicted by this method compared well with those predicted by more geometrically accurate two-dimensional finite element analyses [64]. Here we first describe thermal plumes in general, and their effect on the stresses in the vessel wall. We then present the FAVOR 94.1 approximate model of thermal plumes and compare the predictions of FAVOR 94.1 with those of two-dimensional finite element calculations. The information presented summarizes that found in [64].

The formation of a plume under a cold leg nozzle is postulated to occur due to incomplete mixing of the ECC water injected into the cold leg, with the coolant already in the downcomer [65]. The ECC water has a much lower temperature than the RCS coolant. Incomplete mixing can produce a thermal plume in the downcomer that varies in both space (circumferentially around the downcomer and axially below the cold leg) and time (the magnitude of the cold plume will reduce as the transient proceeds because the RCS as a whole, and the downcomer in particular, cools.

Finite element analyses and experimental investigations demonstrate that should a plume exist, it increases the axial stress in the vessel wall, but not the circumferential stress [66-70]. Specifically, [66] compares the stresses in the vessel wall produced by a plume in HDR [69] with the stresses estimated by the VISA-II code. VISA-II was a predecessor to FAVOR and used the same assumption of axisymmetric stress [71]. This comparison demonstrated that the axisymmetric assumption predicts circumferential stresses well compared to experiments, but can underestimate the axial stresses (by a factor of ~1.4 to 2) relative to those measured when a

plume was present. This additional axial stress increases the stress on *circumferentially* oriented flaws as compared to one-dimensional axisymmetric stress calculations. Conversely, the stress on axially oriented flaws is unaffected by plumes because plumes do not increase appreciably the circumferential stress in the vessel wall.

A plume can be characterized by a minimum temperature at its center and the temperature of the coolant in the downcomer away from the plume. The difference between these two temperatures is referred to as the “plume strength.” Experimental data indicate that once a plume is established, the plume strength decreases with time in the transient and with distance below the nozzle.

Plume strength expressed as a function of both time after transient initiation and of distance below the nozzle was, therefore, used to characterize plumes for analysis in FAVOR 94.1. FAVOR 94.1 represented the circumferential variation in temperature associated with a plume as a square wave of amplitude equal to the plume strength.

The following equation was used to estimate the additional axial stress in the vessel wall based on the plume strength and on the physical properties of the vessel steel:

$$\sigma_{z,plume}(z,t) = E \alpha \Delta T_{plume}(z,t)$$

where $\sigma_{z,plume}$ is additional axial stress generated by the plume
 z is distance below the cold leg,
 t is time,
 E is Young’s modulus,
 α is the coefficient of thermal expansion.
 ΔT_{plume} is the plume strength

This relationship assumes the region of the vessel outside the plume is infinitely rigid. This is a reasonable assumption when plumes occur at only one nozzle and tends to be conservative if plumes occur at more than one nozzle. In FAVOR 94.1, $\sigma_{z,plume}$ was assumed to be constant through the vessel wall thickness (a conservative assumption). The added stress was linearly superimposed on the time-dependent stresses caused by the combination of the temperature gradient across the wall and the pressure force. In addition to accounting for the higher axial stresses produced by plumes, FAVOR 94.1 also accounted for the reduction in fracture toughness caused by the lower temperatures in the region of the vessel affected by the plume. In [64] evidence is presented that the values of applied- K_I calculated by FAVOR 94.1 from $\sigma_{z,plume}$ conservatively approximates (overestimate) those estimated by a more rigorous two-dimensional stress analysis.

Comparison of FAVOR 94.1 to FAVOR 04.1 Methodology

As detailed in [63], FAVOR includes several components:

1. Models that establish the driving force to fracture produced by the thermal-hydraulic loading applied to the vessel;

2. Models that quantify the effect of irradiation damage and attenuation on the transition temperature of the vessel steel;
3. Models that establish the resistance of the vessel steel to crack initiation based on this transition temperature;
4. Models that establish the ability of the vessel steel to arrest a running cleavage crack based on this transition temperature; and
5. Models that establish the distribution of flaws throughout the vessel wall, including their location, their orientation, and their size.

Of these models, only those under item #1 have not changed substantially since FAVOR 94.1. Many aspects fracture toughness and irradiation damage modeling (#2 through #4) have changed. The combined effect of all of these models is to establish the fracture toughness for a given set of conditions. These conditions are characterized by the fracture toughness prior to irradiation, the degree of irradiation damage, and the chemical composition of the vessel steel.

Conclusions drawn using 94.1 based on only one level of fluence would, therefore, be suspect because, based on the new models, the same level of fluence could be associated with a much different level of toughness. Conversely, conclusions drawn from a range of fluence should be more robust because, while the numeric estimates of vessel failure probability will unquestionably have changed, the relative effects of specific changes made to the model (plumes vs. no plumes, for example) on the estimated probability of vessel failure should be reasonably similar between FAVOR 94.1 and FAVOR 04.1.

The one set of changes made to the PFM model that can be expected to influence the effect plumes have on the vessel failure probability are the changes made to the flaw model (#5). The new flaw model [72] differs from that used in FAVOR 94.1 in that:

- In FAVOR 94.1 all flaws were placed on the inner surface of the vessel. Based on [72] FAVOR 04.1 places few if any flaws on the inside surface, rather the great majority are fully embedded within the ferritic steel.
- FAVOR 04.1 uses a higher density of flaws than did FAVOR 94.1, but these flaws are almost all of smaller size than in FAVOR 94.1.

For axisymmetric calculations based on a variety of transients that, collectively, represent the complete PTS challenge to the plant, the vessel failure probabilities calculated using the flaw distributions in FAVOR 04.1 are lower than those used on FAVOR 94.1 by a factor of 20 to 70 [73]. Since plumes produces the largest increase in stress on the inner surface of the vessel, it is also reasonable to expect that the increase in vessel failure probability caused by plumes would be estimated to be less using the current flaw model [72] than the FAVOR 94.1 flaw model because of the lack of surface breaking flaws.

Finally, when considering the effect of the flaw model on plume analyses, plumes increase *only* the axial stress in the vessel. Therefore, a **plume only affects circumferentially oriented flaws**. As detailed in Section 8.4.1 of [1] **circumferential flaws contribute very little to vessel failure probability** because, for a cylindrical geometry, the symmetry of the circumferential flaw limits the

amount by which the applied- K_I can increase as the crack grows into the thickness. This produces a natural crack arrest mechanism for circumferential flaws that is not present for axial flaws.

In the context of a discussion of plume effects, this crack arrest mechanism provides confidence that the axial stresses produced by postulated plumes do not increase substantially the through wall cracking probability.

BIBLIOGRAPHIC DATA SHEET

(See instructions on the reverse)

NUREG-1809

2. TITLE AND SUBTITLE

Thermal-Hydraulic Evaluation of Pressurized Thermal Shock

3. DATE REPORT PUBLISHED

MONTH

YEAR

4. FIN OR GRANT NUMBER

5. AUTHOR(S)

D. E. Bessette, W. Arcieri, C. D. Fletcher, R. Beaton

6. TYPE OF REPORT

Technical

7. PERIOD COVERED (Inclusive Dates)

1/2000-6/2005

8. PERFORMING ORGANIZATION - NAME AND ADDRESS (If NRC, provide Division, Office or Region, U.S. Nuclear Regulatory Commission, and mailing address; if contractor, provide name and mailing address.)

U.S. Nuclear Regulatory Commission, Division of Systems Analysis and Regulatory Effectiveness,
Office of Nuclear Regulatory Research
Washington, DC 20555-0001
ISL, Inc., 11140 Rockville Pike, Rockville, MD 20852

9. SPONSORING ORGANIZATION - NAME AND ADDRESS (If NRC, type "Same as above"; if contractor, provide NRC Division, Office or Region, U.S. Nuclear Regulatory Commission, and mailing address.)

U.S. Nuclear Regulatory Commission, Division of Systems Analysis and Regulatory Effectiveness,
Office of Nuclear Regulatory Research
Washington, DC 20555-0001

10. SUPPLEMENTARY NOTES

D. E. Bessette, Technical Monitor

11. ABSTRACT (200 words or less)

In 2000, the U.S. Nuclear Regulatory Commission began a new research program to develop the technical basis for revising the Pressurized Thermal Shock (PTS) rule, set forth in Title 10, Section 50.61, of the Code of Federal Regulations (10 CFR 50.61). Since the first research program in the early 1980s, analytical methods have continued to improve allowing for more realistic analysis of PTS risk. The research program was coordinated among probabilistic fracture mechanics, probabilistic risk assessment, and thermal-hydraulics analysts. The thermal-hydraulic analysis was performed with the Fifth Version of the Reactor Excursion and Leak Analysis Program (RELAP5) code. Thermal-hydraulic information was supplied by RELAP5 as boundary conditions to the Fracture Analysis of Vessels: Oak Ridge (FAVOR) probabilistic fracture mechanics analysis code. An accompanying effort was made to demonstrate the applicability and uncertainty of RELAP5 to calculate a broad spectrum of transients of possible PTS significance. Assessment of RELAP5 to specific PTS applications was performed and showed the code to be applicable and to be reasonably accurate. Uncertainty in the code calculations was also quantified and the main source of uncertainty to the thermal-hydraulic analyses was from plant boundary conditions rather than from physical models in the code. This report demonstrates the applicability and uncertainty of RELAP5 for PTS applications.

12. KEY WORDS/DESCRIPTORS (List words or phrases that will assist researchers in locating the report.)

pressurized thermal shock, RELAP5, thermal-hydraulic, thermal hydraulic evaluation, fracture mechanics, FAVOR, probabilistic risk assessment

13. AVAILABILITY STATEMENT

unlimited

14. SECURITY CLASSIFICATION

(This Page)

unclassified

(This Report)

unclassified

15. NUMBER OF PAGES

16. PRICE